sprezzatura
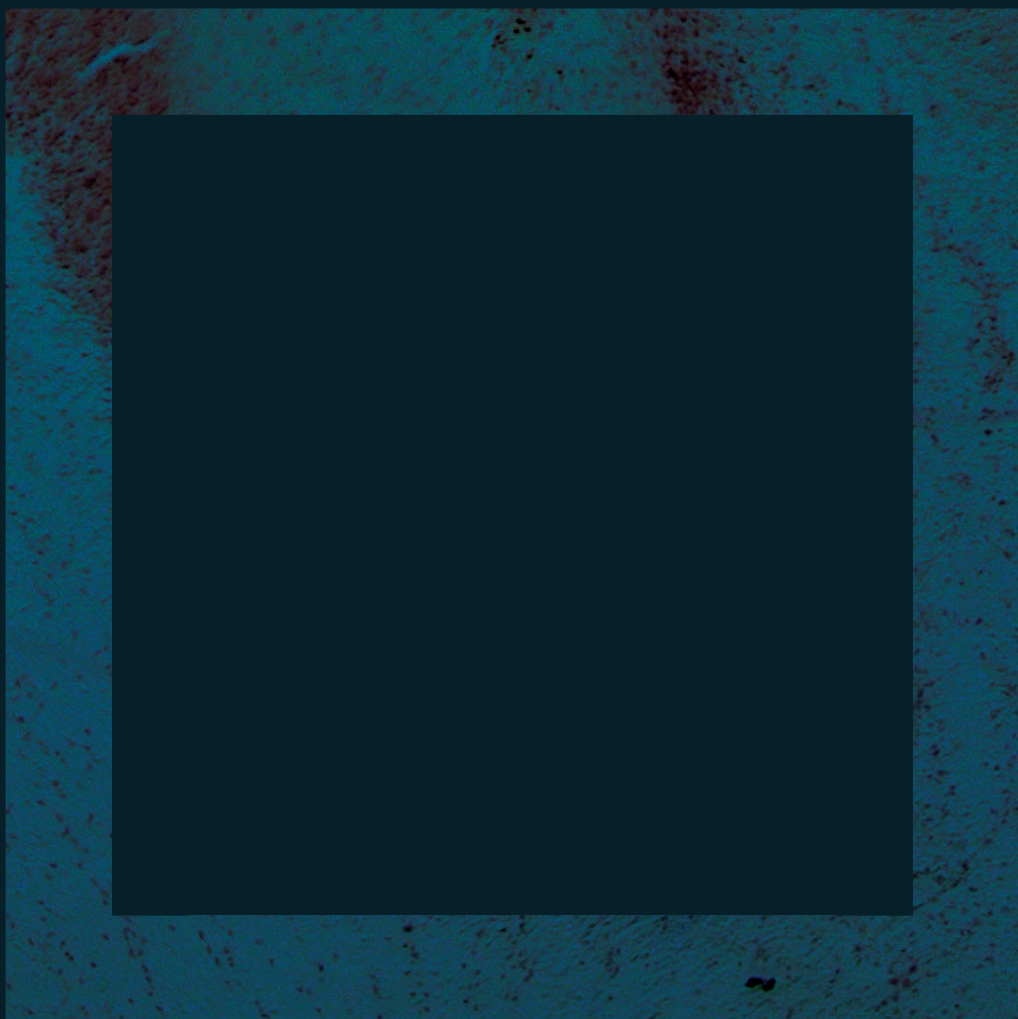
On Olivocerebellar Activity
and Function

Michiel M. ten Brinke

sprezzatura

On Olivocerebellar Activity and Function

Michiel M. ten Brinke

Sprezzatura

On Olivocerebellar Activity and Function

Proefschrift

ter verkrijging van de graad van doctor aan de
Erasmus Universiteit Rotterdam
op gezag van de
rector magnificus
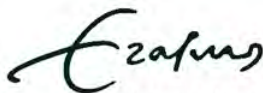
Prof.dr. H.A.P. Pols

en volgens besluit van het College voor Promoties.
De openbare verdediging zal plaatsvinden op

dinsdag 5 december 2017 om 9.30 uur
door

Michiel Manuel ten Brinke

geboren
te Kampen

Erasmus University Rotterdam

Promotiecommissie

Promotor: Prof.dr. C.I. De Zeeuw

Copromotor: Dr. H.J. Boele

Overige leden: Prof.dr. M.A. Frens
                     Prof.dr. S.A. Kushner
                     Prof.dr. R.A.H. Adan

Mamma, pappa, kijk!

Table of Contents

Preface

I came across this term a few years ago, reading a concert review. The writer used it to describe the laid-back effortlessness with which some saxophone player whipped up incredible improvisations. This paradoxical correlation between the great mastery of a complex skill and the ease of its performance underlines the fascinating nature of procedural learning. The exertion with which my seven-year-old niece Hannah wrote the cover title with her fledgling handwriting skill to me highlights the illusory nature of this effortlessness, just as Castigione's definition implies. Especially in the case of procedural learning, there's a great cost to effortlessness, and it lies in past toil. The olivocerebellar system, one of the major players in procedural learning, feeds on error. Each round of practice, it painstakingly chisels its way toward a neuronal response repertoire that enables errorless performance. What stands on the other side of that process, is like a soft sculpture. It is robust but malleable, and it is simply there, in its full intricate glory, requiring no other effort than just letting it be seen, and while it may weather, it will largely persist. This is just one imperfect interpretation of the olivocerebellar system, and the existing body of research on it is itself a sculpture in progress. Ideally, the work in the current thesis contributes to a deepening scientific understanding of how this system can facilitate procedural and associative learning. If it does not, let it be an homage to all the error and exertion underlying sprezzatura.

MtB

Chapter 1

General Introduction
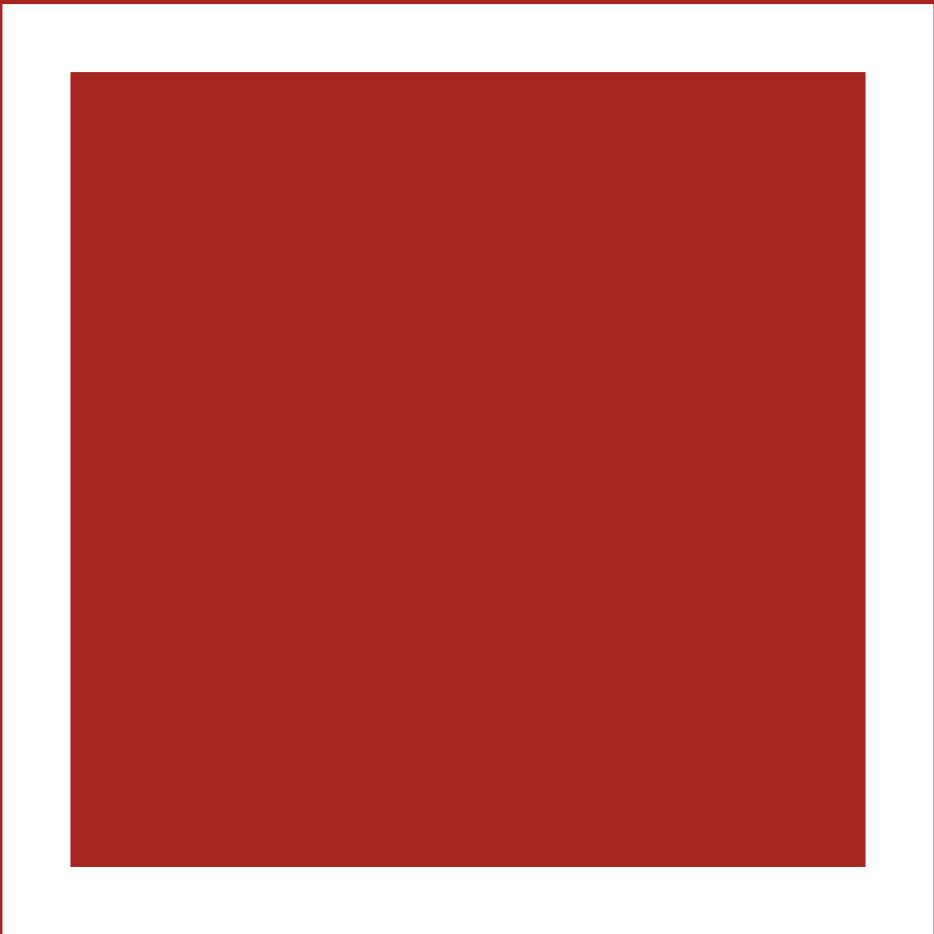
1 Cerebellar PR

I remember concluding as a child the cerebellum had to be special, because it looked so funky in the pictures. Such a characteristically grooved separate module just plopped on there at the lower back of the brain surely constitutes an enigmatic evolutionary add-on, and tremendous powers must surely lay dormant therein, I imagined. I knew telekinesis, mind-reading, or time-bending were a tall order, but I was a little disappointed when I read that they already knew what the cerebellum does, and that it *merely* ''helps coordinate movement''.
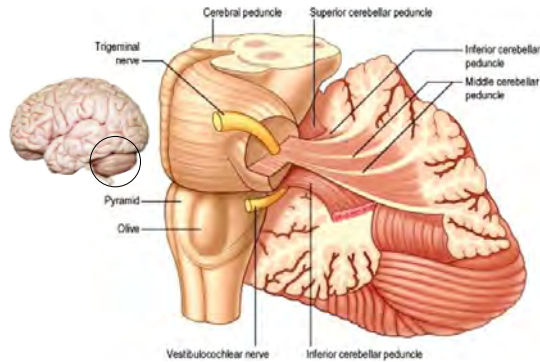
Figure 1 Cerebellar macroscopy.

A recent report on a 24-year old Chinese woman whose brain completely lacked a cerebellum (Yu et al., 2015) was heralded by the media as a testament to the flexibility of the human brain. As it turned out, the absence of this fist-sized chunk of tissue that contains a good majority of our roughly 85 billion brain cells, surprisingly resulted in ''only mild to moderate motor deficiency, dysarthria, and ataxia'' (Yu et al, 2015). Thus, one mainstream take-home message of the story became the impressive capacity of the brain to compensate for the absence of a cerebellum.

Figure 2 Brain scan showing a lack of a cerebellum, from the case described by Yu et al. (2015).

When that story came out I would have been doing cerebellar research for a couple of years already. If I hadn't, I imagine it could have led me to thoughtlessly dismiss the cerebellum as an underwhelming, non-essential, inexplicably overpopulated and apparently still replaceable brain area. If you had to shoot me in the brain, I'd probably have asked to put the bullet in the cerebellum (but see Holmes (1917) for a detailed account of clinical symptoms due to cerebellar gunshot injuries).

By now being acquainted with the unique and orderly structure of the cerebellum (Box 1), its relation to the cerebrum, and the fascinated scientists studying it, I am in a better position to see why the cerebellum does in fact hold tremendous powers, it is enigmatic, and its influence actually spans the entire cerebrum. I should thus like to invest some time on cerebellar PR, in case you the reader are as unaware as I was of the relevance of the olivocerebellar system central to this thesis.

As suggested by the story about the woman who lacked one, the cerebellum is not as essential for survival as many other regions are. Together with the inferior olivary nucleus in the brainstem, it forms a system that is a supreme example of an add-on, i.e. it is superimposed on other, more primary systems. In this sense, the olivocerebellar system is not more essential than its underlying systems, much like there's no use for a hat if you have no head.

However, it seems the conventional view fails to separate the non-essentiality of the olivocerebellar system from the magnitude of the added functionality it actually provides. To me, the predicate ''coordinates movement'' sounded like you'd take a little longer to put your pants on if you had no cerebellum. In reality, cerebellar disease does not just take the spring out of your step; it exhaustingly leaves you exerting substantial concentration to even pick up a glass, preempting the automatic execution of any meaningful movements associated with the word *skill* (Babinski, 1899, 1902; Holmes, 1917, 1939; Zackowski, Bastian, & Thatch, 2002). It breaks any flow to a sequence of movements in a way that I imagine to be as frustrating as what a slow internet connection does to an online video stream. There are actually some good YouTube videos of patients with spinocerebellar ataxia, which show just how reminiscent their movement can be of that of today's state-of-the-art robots; it somehow gets the job done, but completely lacks *sprezzatura*, i.e. an effortless smoothness and elegance. This *magic sauce* that the cerebellum adds to our ongoing actions and that enables complex skill execution constitutes a difficult hurdle in the field of artificial intelligence as it attempts to engineer procedural learning and memory, with cerebellum-inspired algorithms only beginning to be meaningfully integrated in robotics (e.g. Luque et al., 2011; Casellato et al., 2015).

One reason why it is hard to straightforwardly grasp and convey the relevance of the olivocerebellar system is that its function can get quite abstract. For instance, rather than for *seeing*, it would account for *facilitating seeing*, which is the case for the flocculus, a cerebellar region. When the head moves around, muscles controlling the eyes are compelled to counter these movements to keep whatever we're looking at in the center of our vision. The flocculus is implicated in this so-called vestibulo-ocular reflex (Robinson, 1976; Ito, 1982a; Van Alphen et al., 2002; Katoh et al., 2005), but its role is actually clearer in the adaptation of this reflex, i.e. when the strength of the compensatory eye movements needs to increase or decrease (Nagao, 1983, McElligott et al., 1998; Shutoh et al., 2006). This constitutes yet another level of abstraction: the flocculus allows for the adaptation of the strength of the eye movements that
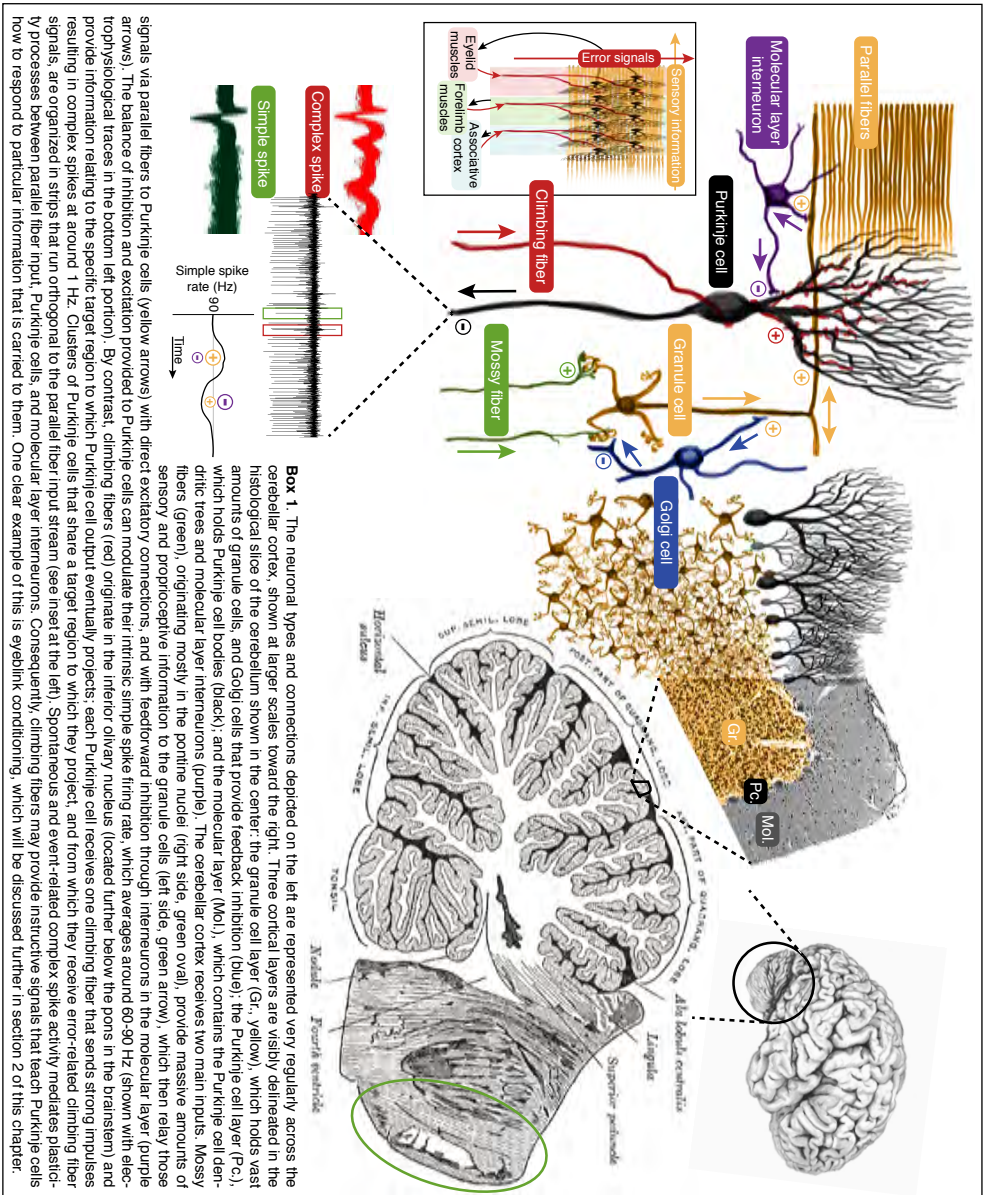
Box 1. The neuronal types and connections depicted on the left are represented very regularly across the cerebellar cortex, shown at larger scales toward the right. Three cortical layers are visibly delineated in the histological slice of the cerebellum shown in the center: the granule cell layer (Gr., yellow), which holds vast amounts of granule cells, and Golgi cells that provide feedback inhibition (blue); the Purkinje cell layer (Pc.), which holds Purkinje cell bodies (black); and the molecular layer (Mol.), which contains the Purkinje cell dendritic trees and molecular layer interneurons (purple). The cerebellar cortex receives two main inputs. Mossy fibers (green), originating mostly in the pontine nuclei (right side, green oval), provide massive amounts of sensory and proprioceptive information to the granule cells (left side, green arrow), which then relay those signals via parallel fibers to Purkinje cells (yellow arrows) with direct excitatory connections, and with feedforward inhibition through interneurons in the molecular layer (purple arrows). The balance of inhibition and excitation provided to Purkinje cells can modulate their intrinsic simple spike firing rate, which averages around 60-90 Hz (shown with electrophysiological traces in the bottom left portion). By contrast, climbing fibers (red) originate in the inferior olivary nucleus (located further below the pons in the brainstem) and provide information relating to the specific target region to which Purkinje cell output eventually projects; each Purkinje cell receives one climbing fiber that sends strong impulses resulting in complex spikes at around 1 Hz. Clusters of Purkinje cells that share a target region to which they project, and from which they receive error-related climbing fiber signals, are organized in strips that run orthogonal to the parallel fiber input stream (see inset at the left). Spontaneous and event-related complex spike activity mediates plasticity processes between parallel fiber input, Purkinje cells, and molecular layer interneurons. Consequently, climbing fibers may provide instructive signals that teach Purkinje cells how to respond to particular information that is carried to them. One clear example of this is eyeblink conditioning, which will be discussed further in section 2 of this chapter.

14

compensate for head movements to facilitate stable vision. Try to explain that to someone on the elevator. And yet the absence of this very subtle kind of functionality would have likely turned the formidable Mongolian horse archer into an embarrassing warfare experiment.

The structure of the cerebellar cortex is uniquely designed to allow for the dynamic coupling of vast amounts of different neural signals to specific output targets, with high temporal precision (Marr, 1969; Albus, 1971). Through experience, associations are formed between pieces of information that reliably co-occur on a sub-second times-pan, be they internal or external (Giovannucci et al., 2017), sensorimotor (Gormezano et al., 1962; Thompson, 1988) or even cognitive (Wagner et al., 2017) in nature. Based on what in the past has reliably followed ongoing signals, the cerebellum can learn to send real-time predictive information to the rest of the brain. Take a simple single association between a flash of light and an air puff to the eye a quarter second later; this constitutes a basic form of eyeblink conditioning, a central behavioral paradigm in this thesis (Gormezano, 1962; Chettih, 2011). By forging the association between light and air puff in the cerebellar cortex through many co-occurences, *light - 250 ms - puff … light - 250 ms - puff*, etc., the resulting cerebellar output facilitates a well-timed preemptive eyeblink in response to the light. The same principle holds for chains of associations between multi-jointed movements and multisensory information (Koeneke et al., 2004; Brown, Martinez, & Parsons, 2006; Hoogland et al., 2015), such as those etched out by a figure skater as she painstakingly practices her axel jump.

The absence of a cerebellum continuously feeding the brain a meticulously crafted stitch work of anticipatory signals would leave it much less prepared, constantly trying to catch balls it doesn't know from what direction they are coming. In the resulting neural disorientation, with a lack of internal models directing ongoing processes (Wolpert, Miall, & Kawato, 1998), you can imagine the virtual impossibility of sophisticated movement, of the figure skater, of the paintbrush, of the violin bow. Much of this functionality falls outside the scope of clinical enquiry, which cares about impairments to basic functioning; it is no surprise that from this angle, one would largely miss the fact that the cerebellum is also a neural basis for the effortless expression of mastery, refinement, and grace.

Outside the motor domain, the difficulty of grasping olivocerebellar functionality is further compounded by the elusive nature of internal, non-motor processes. Yet, a growing body of evidence suggests the cerebellum faithfully complements the cerebrum, offering its intricate one-of-a-kind functionality to each of many, if not all, neocortical regions, and subcortical regions (Buckner et al., 2011; Bostan, Dum, & Strick, 2013; Buckner, 2013). In fact, cerebellar connectivity with associative cortex in the cerebrum outstrips that with sensorimotor cortex (Buckner, 2013), leaving a majority of cerebellar activity at a more tantalizing distance from scientific understanding. The notion that motor dysfunction is simply the most immediately obvious of a substantially larger set of symptoms that come with cerebellar disease has been advocated for a while now (Schmahmann & Sherman, 1998; Thatch, 1998, 2007; Ito, 2008; Schmahmann, 2010), but moving off the treaded path proves to be a slow process, in academia and in the clinic, but most importantly in public perception, if my own experience is any indication.

Nevertheless, accounts of non-motor cerebellar effects accumulate, showing behavioral disinhibition (Tanaka et al., 2003), impairments in cognitive planning (Grafman

et al., 1992), visuospatial ability (Schmahmann & Sherman, 1998), language expression (Fabbro et al., 2004), and verbal working memory (Ravizza et al., 2005), and symptoms related to neuropsychiatric disorders like autism, psychosis, schizophrenia, and depression (Courchesne, 1991; Schmahmann, 2000; Hoppenbrouwers et al., 2008, D'Mello et al., 2015). These effects are found across patients with acquired (Schmahmann & Sherman, 1998; Levisohn et al., 2000; Riva & Giorgi, 2000) or congenital (Steinlin et al., 1999; Tavano et al., 2007) cerebellar pathology, and are summarized as *cerebellar cognitive affective syndrome* (CCAS) in Schmahmann and Sherman (1998), with cognitive effects linked more to posterior cerebellar hemispheres, and affective symptoms more to the cerebellar vermis.

The uniformity of the cerebellar architecture implies a roughly similar cerebellar computational process that is applied throughout the cerebellum, irrespective of the specific target of the resulting output, which as it seems could pretty much be anywhere in the brain. This notion of one *universal cerebellar transform* (Schmahmann, 2010) suggests that whatever the cerebellum is doing for movement, it is also doing for mental activity. This has been elaborately conceptualized in terms of the same type of internal models used for movement, here directing cognitive and affective processes (e.g. Ito, 2008), and *dysmetria* has been suggested as the root flaw underlying virtually all cross-domain symptomatology of cerebellar dysfunction (Andreasen, Paradiso, & O'Leary, 1998; Schmahmann, 1998). However, we are still a long way from a truly comprehensive understanding of the cerebellar operation. Importantly, differences in morphology and prevalence of different cell types across cerebellar regions (Eccles, Ito, & Szentagothai, 1967; Armstrong & Schild, 1970; Diño, Willard, & Mugaini, 1999), and differences in expression of various molecular markers (Cerminara et al., 2015) and neuronal activity (Zhou et al., 2014, Xiao et al., 2014) across zebra-stripe-like zones, suggest that a universal cerebellar transform may actually not exist (Cerminara et al., 2015), or should at least manifest in a number of flavors. Moreover, it is as of yet quite unclear how these core *transforms* emerge from the interplay across and within the different nodes in the olivocerebellar system (the olivary nuclei, the granule cell glomerulus, the Purkinje cell with its afferents, the cerebellar nuclei).

Pursuant of an understanding that flows ''continuously from molecules and cells through synapses and circuits to behavior without any grossly embarrassing gaps in the middle'' (Hansel et al., 2001), the field of cerebellar research is unraveling the secrets of perhaps the most elusive domain of learning, directed through perhaps the most sophisticated neuronal computation, in perhaps the most intricate part of perhaps the most advanced piece of biology. It should now be clear that the work that lies ahead, hopefully making use of the knowledge generated in this thesis, will help disentangle an indeed enigmatic, ubiquitous, and tremendously powerful functionality concealed in our brain. Having established a more thorough account of the relevance of the cerebellum than that suggested by the somewhat lackluster predicate ''coordinates movement'', let us now turn in more detail to procedural learning in the cerebellum, focusing specifically on eyeblink conditioning, a central behavioral paradigm in this thesis.

2 Classical conditioning of timed motor responses: neural coding in cerebellar cortex and cerebellar nuclei*

During delay classical conditioning of the eyelid response, which models both associative learning and motor learning, the essential memory is formed in the cerebellum. In this chapter we will discuss how the cerebellar cortex and cerebellar nuclei may synergistically interact in order to generate conditioned eyelid responses. For this, we will first describe some important behavioral aspects of eyeblink conditioning, including new data on the effects of CS durations that are either shorter or longer than the trained CS-US interval. Second, we will provide a systematic overview of the neuro-anatomical circuits involved in eyeblink conditioning. In the third part we will discuss the contribution of different forms of neural plasticity in the cerebellar cortex and cerebellar nuclei to the formation of a memory trace during eyeblink conditioning. Together, these parts allow us to synthesize an overview of putative encoding mechanisms underlying eyeblink conditioning.

Behavioral aspects of eyeblink conditioning

Soon after Pavlov's first description of classical conditioning of the salivation response at the beginning of the 20th century (Pavlov, 1927), other scientists, also motivated to develop objective methods for studying learning and memory formation and the underlying neural mechanisms, extended the study of classical conditioning to other responses. In 1922 Cason showed that the eyelid response in humans could be successfully conditioned (Cason, 1922). The first eyeblink conditioning studies in animals were done by Hilgard and Marquis in the 1930s, first in dogs and later in monkeys (Hilgard and Marquis, 1935; Hilgard and Marquis, 1936). In the 1960s, Gormezano and co-workers started fundamental work on the behavioral aspects of eyeblink conditioning in rabbits, measuring the movements of the nictitating membrane instead of the eyelid responses directly (Gormezano et al., 1962; Schneiderman and Gormezano, 1964). Today, also due to mouse transgenics, eyeblink conditioning is one of the most extensively studied forms of classical or Pavlovian conditioning. As a result, the neuro-anatomical circuits involved in eyeblink conditioning and the electrophysiological changes they exhibit are described at a relatively high level of detail. In a typical eyeblink conditioning experiment, the conditional stimulus (CS) consists of an auditory or visual stimulus and the unconditional stimulus (US) of a peri-ocular electrical stimulation or – in a more operant form of conditioning – a corneal air puff (for discussion of classical versus more operant forms of eyeblink conditioning, we refer to Longley and Yeo, 2014). In a delay paradigm, the CS onset precedes the US onset usually by a couple of hundreds of milliseconds and CS and US co-terminate. Repeated pairings of CS and US will gradually lead to an eyelid closure in response to the CS, which is called the conditioned response (CR). The behavioral similarities between nictitating membrane CRs and eyelid CRs allows the use of a common term for both: eyeblink CRs. Although the eyelid response is extremely simple compared to for instance complex limb movements, it can be identified as a motor response. Since fundamental features of a motor response, like timing and strength, can be

measured relatively easily and reliably in the nictitating membrane and/or eyelid response, eyeblink conditioning has become a popular model to investigate not only associative learning but also motor learning.

CS-US interval

The length of the interval between CS and US onset in an eyeblink conditioning delay paradigm greatly affects the rate of acquisition of eyeblink CRs. In rabbits, there is hardly any eyeblink conditioning possible when using CS-US intervals below 100 ms or above 4000 ms, and the best learning, in terms of percentage of trials showing CRs occurs with a CS-US interval between 250 and 500 ms (Schneiderman and Gormezano, 1964; Schneiderman, 1966; Smith, 1968). The same pattern has been reported for other species. Apart from some exceptions (for humans: Kimble, 1947; Woodruff-Pak and Finkbiner, 1995; Bolbecker et al., 2011), the overall trend seems to be that at intervals between about 150 and 1000 ms, the duration of the CS-US interval is negatively correlated with the rate of eyeblink CR acquisition; i.e. the longer the CS-US interval, the lower the rate of acquisition (for humans: McAllister, 1953; Boneau, 1958; Steinmetz et al., 2011; for rabbits: Schneiderman and Gormezano, 1964; Schneiderman, 1966; Smith, 1968; Solomon et al., 1991; Vogel et al., 2009; for mice: Chettih et al., 2011)

CR amplitude

Eyeblink CRs are not all-or-nothing responses in the sense that they suddenly pop-up during the conditioning process. Instead, they seem to be acquired gradually. Although there is substantial variability between subjects and between trials within one subject, one can observe in averaged data a clear rise in the amplitude of eyeblink CRs over training, starting with small ''hesitating'' eyeblink CRs at the beginning and ending with full eyelid closures at end of training (Smith, 1968; Gormezano and Kehoe, 1975; Mauk and Ruiz, 1992; Garcia et al., 2003 (for comparison between eyelid CR and nictitating membrane CR); Gallistel et al., 2004; Kehoe et al., 2008).

Latency to CR peak

Eyeblink CRs are perfectly timed responses of which the peak coincides with the time point at which the US is about to be delivered. For instance, when training occurs with a CS-US interval of 250 ms the eyeblink CR will reach its maximum amplitude at about 250 ms after CS onset. If a 500 ms CS-US interval were used instead, the CR would peak at 500 ms after CS onset (Figure 1) (Boneau, 1958; Ebel and Prokasy, 1963; Schneiderman and Gormezano, 1964; Smith, 1968; Mauk and Ruiz, 1992; Garcia et al., 2003; Koekkoek et al., 2003; Vogel et al., 2003; Welsh et al., 2005; Kehoe et al., 2008; Vogel et al., 2009; Chettih et al., 2011).

    After the peak around the US, the eyelid will open quickly again. This way, an eyeblink CR provides optimal protection against the aversive US while vision is disrupted for the shortest possible period. In contrast to CR amplitude, the latency to CR peak seems to be relatively constant during training. Although some initial studies report a slow migration of the (median) latency to CR peak towards either
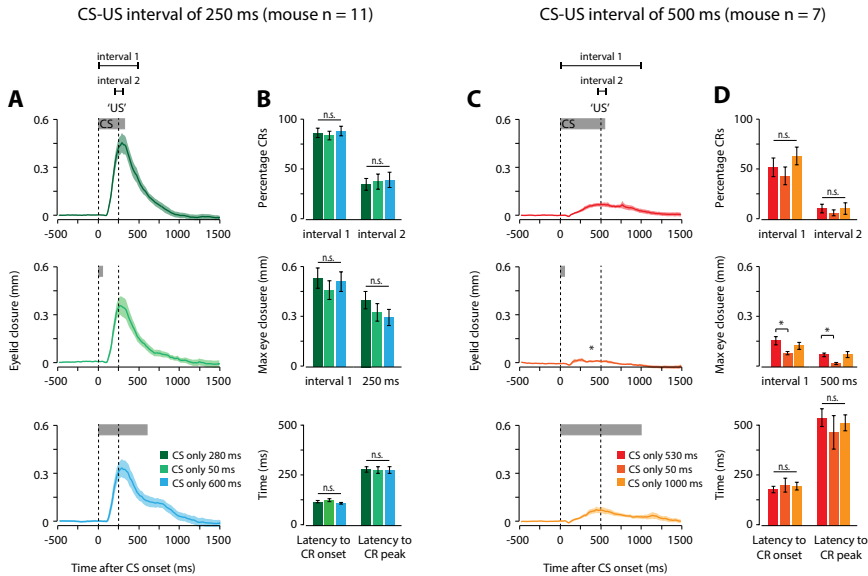
Figure 3 Eyeblink CRs in CS-only trials with various CS durations. (A) Averaged eyelid response traces (±SEM) of mice in a probe session consisting of paired CS-US trials (not depicted) intermingled with three types of CS-only trials: (i) normal CS-only trials with a duration of 280 ms (dark green), (ii) short CS-only trials with a duration of 50 ms (light green), and (iii) long CS-only trials with a duration of 600 ms (blue). Prior to this probe session, mice were trained in 10 consecutive daily acquisition sessions, each consisting of 100 paired CS-US trails with an ISI of 250 ms. **(B)** Between eyeblink CRs in the three types of CS-only trials, no significant differences were found for CR percentage (calculated for interval 1 (0-500 ms after CS onset) and interval 2 (200-300 ms after CS onset), maximum eyelid closure in interval 1 and maximum eyelid closure at expected US onset at 250 ms after CS onset, latency to CR onset, and latency to CR peak. **(C)** Averaged eyelid response traces (± SEM) of mice in a probe session consisting of paired CS-US trials (not depicted) intermingled with three types of CS-only trials: (i) normal CS-only trials with a duration of 530 ms (dark green), (ii) short CS-only trials with a duration of 50 ms (light green), and (iii) long CS-only trials with a duration of 1000 ms (blue). Prior to this probe session, mice were trained in 10 consecutive daily acquisition sessions, each consisting of 100 paired CS-US trails with an ISI of 500 ms. **(D)** No significant difference could be established between CR percentage (calculated for interval 1 (0-1000 ms after CS onset) and interval 2 (450-550 ms after CS onset), latency to CR onset, and latency to CR peak. Instead, maximum eyelid closure in interval 1 (0-1000 ms after CS onset) and maximum eyelid closure at expected US onset at 500 ms after CS onset were significantly smaller in trials with a short CS compared to eyelid responses in normal and long CS-only trials.

earlier (Schneiderman and Gormezano, 1964) or later portions of the CS-US interval (Boneau, 1958) during training, more recent work shows only very minimal migration within the CS-US interval. Both day-by-day analysis, in which each data point is computed by averaging all mean values for a particular day or session (Mauk and Ruiz, 1992; Garcia et al., 2003; Vogel et al., 2003; Kehoe et al., 2008), and trial-by-trial analysis, in which each data point is computed by averaging together all individual traces for a specific trial (Kehoe et al., 2008), show that the CR peak seems to be timed properly with respect to the US from the first moment they appear, i.e. from the moment they surpass a preset threshold (in rabbits: 0.2 or 0.5 mm movement of the nictitating membrane). In line with this ''non-migration phenomenon'' is the finding

that a sudden change in the CS-US interval during training does not lead to a gradual migration of the CR peak from the old US onset towards the new US onset but rather to a selective extinction of the CR for the old interval together with an acquisition of CRs to the new interval (Boneau, 1958; Yeo et al., 1997; Kehoe and Joscelyne, 2005). Previous studies reporting a gradual shift of the CR peak amplitude as a result of a switch in the CS-US interval, could be explained by the type of analysis, in which CRs with bimodal distributions were averaged over successive sessions (for humans: Ebel and Prokasy, 1963; Prokasy et al., 1963; for rabbits: Prokasy and Papsdorf, 1965; Leonard and Theios, 1967; Coleman and Gormezano, 1971; Salafia et al., 1979; for rats: Welsh et al., 2005 (report that ''the peak of the CRs shifted to a longer latency'')).

Latency to CR onset

Interestingly, the same absence of migration can be observed in the latency to CR onset during training. In rabbits, early reports again suggest a gradual migration of the latency to CR onset from just before US onset to earlier parts of the CS-US interval (Gormezano et al., 1983). Although at first glance some later studies suggest the similar trend, this migration to earlier portions of the CS-US interval appeared to be non-significant (Garcia et al., 2003; Kehoe et al., 2008). In rabbits, cats, ferrets, and humans the latency to CR onset is determined by the used CS-US interval, i.e. the longer the CS-US interval the longer the latency to CR onset (Mauk and Ruiz, 1992). However, in rats and mice it seems that the latency to CR onset seems to be rather independent of the used CS-US interval (Welsh et al., 2005; Chettih et al., 2011). In mice, it has been reported that regardless of the CS-US interval used, the latency to CR onset seems to be about 100 ms after CS onset (but compare this finding with Fig. 3B, D). Interestingly, in rabbits and ferrets the latency to CR onset may be changed by alterations in the intensity of the CS: CS intensities higher than the one used during acquisition training sessions appear to decrease the latency to onset of the CR (Frey, 1969; Svensson et al., 1997; Svensson et al., 2010). In mice this phenomenon has not been demonstrated so far, probably because mice exhibit, when using higher (auditory) CS intensities, more startle responses and fear short-latency responses (SLRs), which precede and easily mask eyeblink CR onsets (Boele et al., 2010; Chettih et al., 2011).

Test CS-only trials with CS durations shorter or longer than used CS-US interval

Interestingly, the duration of the CS seems to be rather dissociated from the kinetic profile of the eyeblink CR. It has been shown that the presentation of CS-only trials, in which the duration of the CS either extends beyond the used CS-US interval (Kehoe and Joscelyne, 2005) or is much shorter than the CS-US interval during training (Svensson and Ivarsson, 1999), results in normal eyeblink CRs. However, particularly for the short CS, it remains to be elucidated whether this result also holds for longer CS-US intervals and for more natural CSs instead of direct mossy fiber stimulation. We therefore trained 11 mice (C57Bl/6, male, aged 15-20 weeks) for 10 daily acquisition sessions (100 paired CS-US trials per daily session) in a delay paradigm with a CS-US interval of 250 ms (CS duration of 280 ms and US duration of 30 ms). After this training protocol we presented in a probe session (session 11) the same 100 paired

CS-US trials, but now intermingled with three different types of CS-only trials: 10 normal CS-only trials with a duration of 280 ms, 10 short CS-only trials with duration of 50 ms, and 10 long CS-only trials with a duration of 600 ms. For a second group of 7 mice (C57Bl/6, male, aged 15-20 weeks) we used the same training procedures except that these mice were trained with a CS-US interval of 500 ms (CS duration of 530 ms and US duration of 30 ms) and the probe session consisted of 100 paired CS-US trials intermingled with three different types of CS-only trials, 10 of which were normal CS-only trials with a duration of 530 ms, 10 short CS-only trials with duration of 50 ms, and 10 long CS-only trials with a duration of 1000 ms. For both groups the CS was a green LED light placed at $\pm$ 7 cm in front of the animal and the US a weak air puff applied to the cornea, which elicited a reflexive full eyelid closure. Animals were head-restrained but able to walk freely on a foam cylinder and eyelid movements were recorded with MDMT (for further details on experimental setup, MDMT, and training procedures, see Koekkoek et al., 2002; Chettih et al., 2011). For the CS-US interval of 250 ms, eyelid responses were considered significant if: a) CR amplitude was >5% from a full eyelid closure (UR = 100%), b) latency to CR onset was between 50-250 ms, and c) latency to CR peak amplitude was between 100-500 ms (interval 1) or 200-300 ms (interval 2: so called ''perfectly timed eyeblink CRs''). For the CS-US interval of 500 ms, eyelid responses were considered as significant if: a) CR amplitude was >5% from a full eyelid closure (UR = 100%), b) latency to CR onset was between 50-500 ms, and c) latency to CR peak was between 100-1000 ms (interval 1) or 450-550 ms (interval 2). When first comparing mice that were trained with a 250 ms CS-US interval versus mice trained with a 500 ms CS-US interval, we found that the averaged CR percentage and CR amplitude were both higher for animals trained with the shorter interval, which is in line with previous mouse work (Chettih et al., 2011) (CR percentage interval 1: $[F (1, 16) = 13.604, p = 0.002]$, averaged eye closure in interval 1 $[F (1, 16) = 23.309, p < 0.001]$, values were calculated in normal CS-only trails) (Fig. 3). In addition, we found a significant difference in the timing of eyeblink CRs: both the latency to CR onset and latency to CR peak time are shorter for animals, which were trained with a 250 ms CS-US interval (latency to CR onset: $[F (1, 16) = 18.973, p < 0.001]$, latency to CR peak time: $[F (1, 16) = 33.555, p < 0.001]$, values calculated in normal CS-only trials). This shorter latency to CR onset in mice trained with a 250 ms CS-US interval is in agreement with previous rabbit work (e.g. Mauk en Ruiz, 1992) but seems to be in contrast with the mouse work reported by Chettih et al. (2011). It can be explained by the fact that the longest CS-US interval used in the Chettih study was only 400 ms.

Second, for mice trained with a 250 ms CS-US interval, eyeblink CRs in all three types of CS-only trials were indistinguishable (Fig. 3A, B). No differences could be established between the averaged CR percentage (interval 1: $[F (2, 30) = 0.244, p = 0.785]$, interval 2: $[F (2, 30) = 0.103, p = 0.903]$), averaged eyelid closure in interval 1 $[F (2, 30) = 0.406, p = 0.670]$, averaged eyelid closure at 250 ms after CS onset $[F (2, 30) = 0.592, p = 0.559]$, latency to CR onset $[F (2, 30) = 1.761, p = 0.189]$ and latency to CR peak amplitude $[F (2, 30) = 0.010, p = 0.990]$. However, for mice that were trained with a 500 ms CS-US interval, things appear to be quite different. Although no significant differences were found between averaged CR percentage (interval 1: $[F (2, 18) = 1.223, p = 0.318]$, interval 2: $[F (2, 18) = 0.300, p = 0.744]$), latency to CR onset $[F (2, 17) = 0.242, p = 0.788]$, or latency to CR peak $[F (2, 17) = 0.421, p = 0.663]$,

averaged eyelid closures in interval 1 and at the expected US onset were undeniably smaller in the short 50 ms CS-only trials than in trials with a normal 500 ms CS or 1000 ms CS (interval 1: [$F_{(2, 18)}$ = 4.493, p = 0.026], Bonferroni post hoc: 50 vs. 500 p = 0.025, 50 vs. 1000 p = 0.22; eyelid closure at 500 ms after CS onset: [$F_{(2, 18)}$ = 6.192, p = 0.009], Bonferroni post hoc: 50 vs. 500 p = 0.023, 50 vs. 1000 p = 0.019) (Fig. 3C, D). This almost complete absence of eyeblink CRs in the short 50 ms CS-only trials might explain why the latency to CR peak was not significantly different from those in the normal 500 ms CS-only trails.

In short, a very brief CS does not seem to affect the kinetic profile of the eyeblink CRs when training occurs with a CS-US interval of 250 ms. Instead, for a 500 ms interval, the short CS seems to be insufficient to elicit proper CRs. In addition, a long CS that extends beyond the time point where the US would be delivered, does not significantly change the CR profile for both the 250 ms and 500 ms CS-US interval, although one can sometimes observe an extra hump that seems to be time locked to CS offset.

Neural circuits engaged during eyeblink conditioning

Where in the brain is the memory formed during eyeblink conditioning? Theoretically, such a brain locus should (i) receive converging inputs from CS and US, (ii) innervate the eyelid premotoneurons and (iii) be able to undergo plasticity as a result of CS-US pairings. Early lesion experiments, aimed to define the minimal brain tissue sufficient for normal conditioning, revealed that lesions of the cerebral hemispheres, hippocampus, or diencephalon could not prevent the acquisition and expression of eyeblink CRs (Oakley and Russell, 1972; Schmaltz and Theios, 1972; Norman et al., 1974; Oakley and Russell, 1975, 1976; Norman et al., 1977; Oakley and Russell, 1977), suggesting that the memory formation takes place at ''lower'' levels of the brainstem and/or cerebellum.

Lesions of cerebellar nuclei

In the early 1980's Desmond and Moore found that lesions of the superior cerebellar peduncle prevented both CR acquisition and CR expression without affecting the URs (Desmond and Moore, 1982). Around the same time McCormick and Thompson reported that lesions of the cerebellar nuclei permanently abolished eyeblink CRs (McCormick et al., 1981; McCormick et al., 1982), which was a little later delineated more precisely by Yeo et al. to the anterior interposed nucleus (AIN) (Yeo et al., 1985a). To date, many groups have replicated these initial findings in different species. In addition to a permanent eyeblink CR abolishment as a result of electrolytic or aspiration lesions of the AIN, eyeblink CRs could also be reversibly abolished by cooling of or lidocaine or muscimol infusions in the AIN (Chapman et al., 1990; Clark et al., 1992; Krupa et al., 1993; Nordholm et al., 1993; Bracha et al., 1994; Hardiman et al., 1996; Garcia and Mauk, 1998; Bracha et al., 2001; Aksenov et al., 2004; Freeman et al., 2005b). In addition, Delgado-Garcia and colleagues targeted the posterior interposed nucleus (PIN), instead of the AIN, as one of the main cerebellar nuclei involved in eyeblink conditioning in cats, serving a modulatory role (Jimenez-Diaz et al., 2002; Jimenez-Diaz et al., 2004; Delgado-Garcia and Gruart, 2006). Koekkoek

and colleagues (Koekkoek et al., 2003; Koekkoek et al., 2005) found that lesions of the AIN in mice affected their eyeblink responses in the CS-US interval in an incomplete fashion (see also Boele et al., 2010).

Lesions of cerebellar cortex

Yeo et al. (1985b) demonstrated that unilateral electrolytic lesions of the cerebellar cortical lobule HVI, sparing the cerebellar nuclei, *completely* abolished CRs. Lesions of other parts of the cerebellar cortex did not affect CRs (Yeo et al., 1985b). Attwell et al. (2001 and 2002) replicated these findings, showing that blocking Purkinje cell input to the AIN by infusions with PTX (picrotoxin; $GABA_A$ chloride channel blocker) or gabazine ($GABA_A$ receptor antagonist) completely abolished CRs; no remnant CRs with short-latency to onset and peak were observed, neither in the nictitating membrane response nor the eyelid response (Attwell et al., 2001; Attwell et al., 2002). Recently, Mostofi et al. showed in rabbits that extremely small infusions of CNQX (6-cyano-7-nitroquinoxaline-2,3-dione; non-NMDA ionotropic glutamate receptor antagonist) in the D0 zone of lobule HVI, the eyeblink controlling microzone, were sufficient to completely abolish eyeblink CRs (Mostofi et al., 2010). Other groups however initially reported that lesions of the cerebellar cortex would have *no effect* on eyeblink CRs (McCormick et al., 1981; McCormick et al., 1982; Clark et al., 1984; McCormick and Thompson, 1984), which might be explained by the fact that the lesioned areas in these studies spared the eyeblink controlling microzone. Instead, Lavond and colleagues found that both amplitude and timing of eyeblink CRs would be affected following lesions of the eyeblink controlling microzone, albeit in *incomplete* fashion (Lavond et al., 1987; Lavond and Steinmetz, 1989). In line with this latter finding, Mauk and coworkers reported that both permanent lesions of the cerebellar cortex and reversible disconnections of the AIN from the cerebellar cortex by PTX infusions in the AIN or muscimol infusions in the cerebellar cortex, mainly disrupted the learning-dependent timing of eyeblink CRs: after removing cortical inputs from the AIN rabbits still showed CRs but these residual CRs had an extremely short latency to onset and latency to peak, therefore called short-latency responses (SLRs) (Perrett et al., 1993; Garcia and Mauk, 1998; Medina et al., 2001; Bao et al., 2002; Ohyama et al., 2003; Ohyama et al., 2006). In short, inactivation of the IN generally severely affects eyeblink CRs, whereas inactivation of the cerebellar cortex leads to more conflicting results, with some groups reporting a full abolishment of eyeblink CRs and others reporting residual SLRs.

Unconditional stimulus and unconditioned response pathway

Sensory stimulation of the cornea, conjunctiva or peri-ocular region will normally elicit a reflexive eyeblink. This eyeblink consists of a rapid contraction of the external eyelids together with, in some animals, a passive lateral sweep of the nictitating membrane or third eyelid due to retraction of the eyeball in the orbita. The sensory information is relayed via the ophthalmic division of the trigeminal nerve to the trigeminal nucleus (N. V), which in turn innervates the oculomotor nucleus (N. III), the (accessory) abducens nucleus (N. VI) and the orbicularis oculi motor neurons of the facial nucleus (N. VII) (Fig. 4) (Holstege et al., 1986; Pellegrini et al., 1995; van
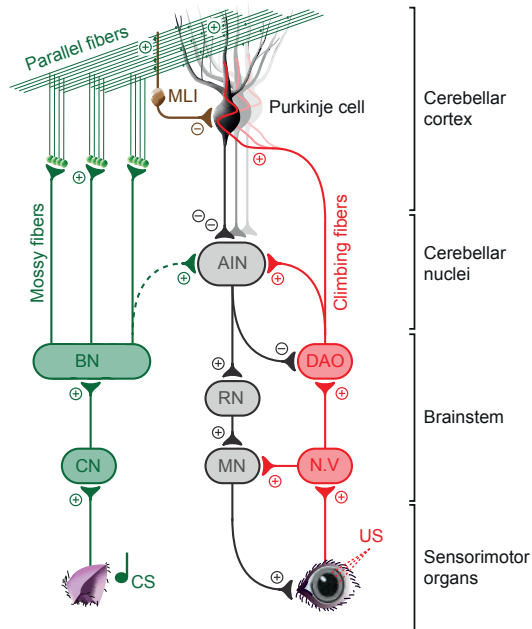
Figure 4 Neural circuits engaged during eyeblink conditioning. Purkinje cells in eyeblink controlling microzones receive climbing fiber input from the dorsal accessory olive, which relays sensory information from the peri-orbital facial region (US pathway in red). Additionally, the same Purkinje cells receive a continuous stream of virtually all sensory information from some two hundred thousand parallel fibers, originating from mossy fibers from various brainstem nuclei including the basilar pontine nuclei (CS pathway in green). The Purkinje cells project to the AIN, which in turn innervates, via the red nucleus, the motor neurons that control the eyeblink (CR pathway in gray). *Abbreviations: AIN anterior interposed nucleus, BN brainstem nuclei (e.g. basilar pontine nuclei, nucleus reticularis tegmentis pontis, lateral reticular nucleus), CN cochlear nucleus, DAO dorsal accessory olive, MLI molecular layer interneuron, MN motor neurons innervating the eyeblink muscles (oculomotor nucleus (III), accessory nucleus (VI), and facial nucleus (VII)), N.V trigeminal nucleus, RN red nucleus.*

Ham and Yeo, 1996a, b). The eyeblink is a result of simultaneous action of these three motor nuclei: the facial nucleus activates the orbicularis oculi muscle, the oculomotor nucleus de-activates the levator palpebrae muscle, and the oculomotor and abducens nuclei together retract the eyeball (van Ham and Yeo, 1996a, b; Trigo et al., 1999; Delgado-Garcia et al., 2002; Delgado-Garcia et al., 2003).

In addition to these eyeblink motoneurons, the trigeminal neurons also project to the medial part of the dorsal accessory inferior olive and dorsomedial group of the principal olive (De Zeeuw et al., 1996). These olivary regions provide the climbing fiber input via the inferior cerebellar peduncle to the eyeblink controlling microzones in the cerebellar cortex (Fig. 4). In cats, Hesslow identified four of these cortical microzones in the C1 and C3 zones of Lobule VI and VII, which showed complex spike responses with a short latency of about 10 ms on ipsilateral peri-orbital stimulation. Stimulation of these areas can produce eyeblink responses and micro-stimulation of

these areas during the CS-US interval in conditioned animals can completely abolish eyeblink CRs (Hesslow, 1994). The directly adjacent C2 regions also showed complex spikes on peri-orbital stimulation, but these complex spikes can be elicited by both ipsi- and contralateral stimulation and have longer latencies (ipsilateral $\pm$ 15 ms; contralateral $\pm$ 20 ms (Hesslow, 1994). Since microstimulation of these adjacent C2 areas does not produce an eyeblink response, they may not directly control the eyeblink CR. Hesslow's finding of multiple eyeblink controlling microzones is in agreement with the hypothesis that microzones themselves are part of a larger entity, called ''multizonal micro-complexes'' (Apps and Hawkes, 2009). In ferrets, a more or less similar cortical pattern of eyeblink controlling microzones can be found (Hesslow and Ivarsson, 1994). For rabbits an eyeblink controlling microzone has been found in the zebrin-negative D0 zone, which according to Sugihara's terminology represents zebrin band P5- (Voogd, 2003; Sugihara and Shinoda, 2004; Voogd and Ruigrok, 2004; Mostofi et al., 2010). For other species like rats and mice, evidence is now accumulating that this microzone in the depth of lobule VI is also controlling eyeblink responses (Van Der Giessen et al., 2008; Heiney et al., 2014; Steinmetz and Freeman, 2014).

Climbing fibers originating from the medial part of the dorsal accessory inferior olive and dorsomedial group of the principal olive do not only innervate Purkinje cells in the cerebellar cortex but also give off collaterals to the cerebellar nuclei, predominantly to the lateral AIN and its dorsolateral hump (DLH) (Pijpers et al., 2005), which are the nuclear parts of the eyeblink controlling zone. These climbing fiber collaterals are excitatory and seem to innervate particularly inhibitory glutamatic acid decarboxylase 67 (GAD67) positive cerebellar nuclei neurons (Uusisaari and Knopfel, 2011), but also GAD67-negative projection neurons (Fig. 5) (McCrea et al., 1978; Hoebeek et al., 2010).

As proposed by Marr (1969) and Albus (1971) climbing fibers indeed seem to transmit US or error information (Marr, 1969; Albus, 1971). Electrical stimulation of the inferior olive or climbing fibers directly can serve as an effective US during eyeblink conditioning and has been demonstrated to result in normal eyeblink CR acquisition (Yeo et al., 1985c; Mauk et al., 1986; Steinmetz et al., 1989; Yeo and Hardiman, 1992; Jirenhed et al., 2007; Rasmussen et al., 2013). Interestingly, only a train of several stimulus pulses can cause acquisition; a single climbing fiber pulse even causes extinction (Rasmussen et al., 2013). This finding is in line with behavioral work using a peri-ocular US which shows that a stronger US induces faster acquisition and a very weak US indeed leads to extinction of eyeblink CRs (Passey, 1948; Spence, 1953; Smith, 1968; Freeman et al., 1993; Kehoe and White, 2002; Najafi and Medina, 2013).

Lesions of the inferior olive severely impair CR acquisition (Welsh and Harvey, 1998), although data is less consistent on this point. Intuitively, one would expect that lesions of inferior olive after CR acquisition cause an extinction-like behavior during normal paired CS-US training. Since the US cannot be transmitted to the Purkinje cell, paired CS-US may be seen by the Purkinje cell as ''CS-only'' trials. Such extinction-like behavior has indeed been reported (McCormick et al., 1985; Welsh and Harvey, 1998). On the other hand, removal of climbing fiber input from the Purkinje cells is also known to increase simple spike firing of Purkinje cells within several minutes to exceptionally high levels and sustained climbing fiber inactivation

(30 min to 5 hours) will even lead to simple spike oscillations with high-frequency bursts (up to 150 Hz) with in between periods of complete spiking silence (Colin et al., 1980; Montarolo et al., 1982; Cerminara and Rawson, 2004). More in line with these robust changes in Purkinje cell physiology, other groups report an immediate abolishment of CR after removal of climbing fiber inputs (Yeo et al., 1986; Zbarska et al., 2007; Zbarska et al., 2008). Thus specific parts in the inferior olive receive peri-orbital sensory information and these olivary parts innervate with their climbing fibers Purkinje cells in specific eyeblink controlling zones in the cerebellar cortex and by means of collaterals neurons in the eyeblink controlling zones in the cerebellar nuclei. These climbing fibers transmit error information, or in classical conditioning terminology: the US, which elicits a short-latency complex spike in the Purkinje cells.

Conditional stimulus pathway

Mossy fibers transmit sensory information from many modalities, including auditory and visual, to the cerebellar cortex (Buchtel et al., 1972; Altman et al., 1976; Steinmetz et al., 1987; Freeman et al., 2007; Leergaard and Bjaalie, 2007; Freeman and Duffel, 2008; Halverson et al., 2008; Halverson and Freeman, 2009, 2010). These mossy fibers originate from various brainstem nuclei, including the basilar pontine nuclei. The basilar pontine nuclei receive a massive amount of sensory information from cortical and subcortical areas (Glickstein et al., 1972; Glickstein et al., 1980; Mower et al., 1980; Mihailoff et al., 1985; Kosinski et al., 1988; Legg et al., 1989; Mihailoff et al., 1989; Wells et al., 1989). Mossy fibers innervate granule cells, which in turn, with their massive parallel fiber projection, supply input to the Purkinje cells, including those in the eyeblink controlling microzone. In unconditioned animals, mossy fibers originating from the basilar pontine nuclei sparsely give off collaterals to the lateral cerebellar nuclei but do not project to the eyeblink controlling regions of the cerebellar nuclei, which would be the lateral AIN and the DLH (Dietrichs et al., 1983; Brodal et al., 1986; Parenti et al., 2002; Cicirata et al., 2005; Boele et al., 2013). For other mossy fiber sources, like the nucleus reticularis tegmentis pontis, the innervation of the AIN and DLH is probably slightly more pronounced. The sparse mossy fiber collaterals, which are just like climbing fiber collaterals excitatory, innervate mainly the large GAD67-negative projection neurons (Fig. 5; Uusisaari and Knopfel, 2011).

Electrical stimulation of mossy fiber origins like basilar pontine nuclei (Steinmetz et al., 1986; Tracy and Steinmetz, 1998; Freeman et al., 2005a), but also of mossy fibers directly in the middle cerebellar peduncle (Steinmetz et al., 1986; Svensson et al., 1997; Hesslow et al., 1999) can serve as CS and can result in robust conditioning. In addition, lesioning of the middle cerebellar peduncle prevents both CR acquisition and CR expression (Lewis et al., 1987). Thus, mossy fibers seem to transmit conditional or contextual information, in classical conditioning terminology the CS, out of many modalities via the granule cell - parallel fiber system to the Purkinje cells, including Purkinje cells in the eyeblink-controlling microzone.

Conditioned response pathway

Purkinje cells in cortical eyeblink controlling microzones form the ultimate point of convergence of climbing fibers transmitting the US and mossy fibers the CS informa-

tion. Temporal silencing of these Purkinje cells'simple spike firing by optogenetic stimulation of molecular layer interneurons can produce eyeblink responses (Heiney et al., 2014). In addition, electrical micro-stimulation of these areas during the CS-US interval in conditioned animals can completely abolish eyeblink CRs (Hesslow, 1994). Purkinje cells in eyeblink controlling microzones project to the lateral part of the AIN, including its DLH (Rosenfield and Moore, 1995). The cerebellar nuclei should not be treated as a simple relay nucleus with little neuronal diversity (Uusisaari and Knopfel, 2011). Evidence is accumulating that these nuclei act as the final, integrative processing unit in the cerebellar circuitry. In the cerebellar nuclei one can categorize at least four neuronal types based on electrophysiological properties and activity of the GAD67 and glycine transporter (GlyT2) promotors, which are often used as markers for GABAergic and glycinergic neurons, respectively. The cerebellar nuclei contain at least two excitatory neuron types, namely large GAD67-negative projection neurons and small GAD67-negative interneurons, and four inhibitory neuron types, namely GAD67-positive projection neurons and interneurons, and GlyT2 positive projection neurons and interneurons (Fig. 5) (for monkey: Chan-Palay, 1977; for cat: Palkovits et al., 1977; for rat: Aizenman et al., 2003; Knopfel and Uusisaari, 2008; Bagnall et al., 2009; Uusisaari and Knopfel, 2011). Purkinje cells have a strong inhibitory effect on both types of excitatory cerebellar nuclei neurons (large and small GAD67-negative neurons) and at least one type of inhibitory cerebellar nuclei neuron (GAD67-positive neurons) (Uusisaari and Knopfel, 2011). As mentioned, the AIN also receives excitatory inputs from climbing fiber collaterals transmitting the same US information, but in untrained animals, mossy fiber collaterals are, depending on their source and thus the CS modality, extremely sparse (Dietrichs et al., 1983; Brodal et al., 1986; Parenti et al., 2002; Cicirata et al., 2005; Boele et al., 2013).

Retrograde trans-synaptic tracing experiments using (pseudo-)rabies virus showed that the orbicularis oculi muscle is mainly innervated by the ipsilateral AIN, including its dorsolateral hump, and lobule HVI (Morcuende et al., 2002; Gonzalez-Joekes and Schreurs, 2012). Indeed, electrical stimulation of this AIN region can produce an eyelid closure (McCormick and Thompson, 1984; Freeman and Nicholson, 2000; Halverson et al., 2010). In addition, stimulation of the ''downstream'' magnocellular division of the red nucleus can induce eyeblink responses (Nowak et al., 1997), whereas lesions of the red nucleus completely abolish eyeblink CRs (Rosenfield and Moore, 1983, 1985; Ohyama et al., 2006). Thus, the CR pathway contains AIN projections to the magnocellular division of the red nucleus, which projects to the motor nuclei that innervate the eyelid muscles, including the facial nucleus (N. VII) to activate the orbicularis oculi muscle, the oculomotor nucleus (N. III) to de-activate the levator palpebrae muscle, and the oculomotor and abducens nuclei (N. VI), together ensuring retraction of the eyeball (van Ham and Yeo, 1996b; Trigo et al., 1999; Delgado-Garcia et al., 2002; Delgado-Garcia et al., 2003). It is important to note at this point that the reflexive eyeblink (UR) and the conditioned eyeblink (CR) differ from each other in kinematics because of differences in their neural control. For URs the eyeblink motor neurons (III, VI, VII) receive their main input from the trigeminal nucleus (N. V), whereas for CRs they receive their main input from the red nucleus. As a result, the temporal profile of the UR is determined by the US: a stronger stimulation leads to a bigger and faster eyeblink. The temporal profile of the CR instead is governed by the CS-US interval: the CR peaks just before the onset of the US.
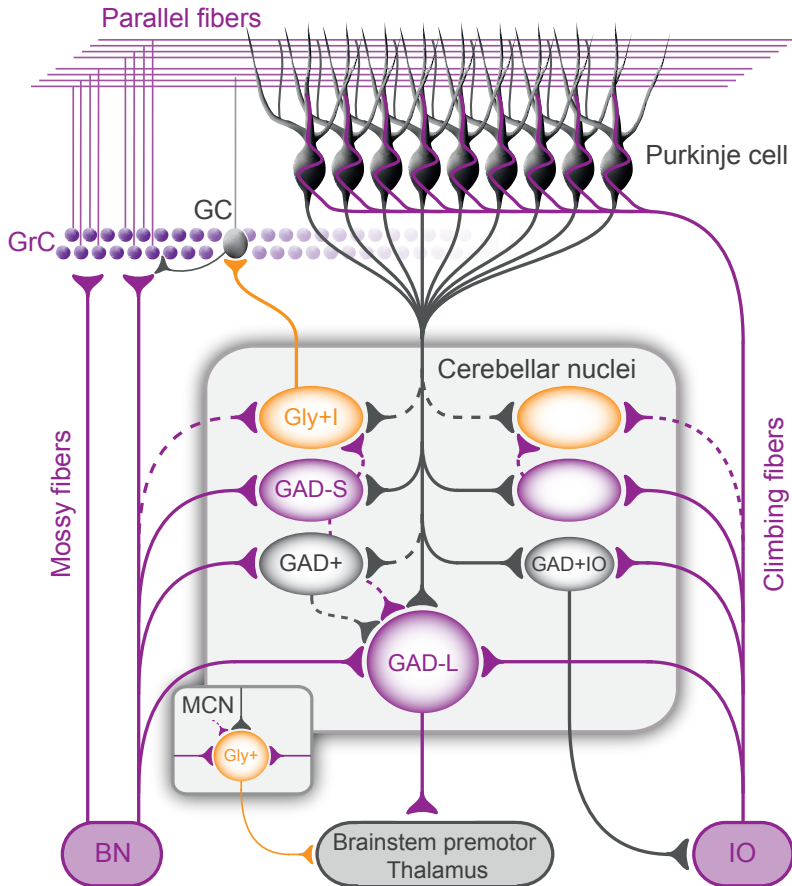
Figure 5 The cerebellar nuclei contain different cell types and form the final integrative processing unit in the cerebellum. In the cerebellar nuclei one can categorize at least six neuronal types based on electrophysiological properties and activity of the glutamatic acid decarboxylase (GAD67) and glycine transporter (GlyT2) promotors. The cerebellar nuclei contain at least two glutamatergic neuron types, namely large GAD67 negative projection (GAD-L) neurons and small GAD67 negative interneurons (GAD-S), two GABAergic neuron types, namely GAD67 positive projection neurons (GAD+IO, IO stands for Inferior Olive) and GAD67 positive interneurons (GAD+), and two glycinergic neuron types, namely GlyT2 positive projection neurons in the MCN (Gly+) and GlyT2 neurons (Gly+I, I stands for Inactive), which project back to the Golgi cells and Purkinje cells in the cerebellar cortex. In contrast to other cerebellar nuclei neurons, Gly+I neurons are not spontaneously active. Dashed lines denote connections of uncertain strength. Gray projections are GABAergic, purple are glutamatergic, and orange are glycinergic or mixed glycinergic/ GABAergic. (Figure based on Uusisaari and Knopfel, 2011, and Ankri et al., 2015). Since the focus of this figure is on the cerebellar nuclei neurons we did not depict all cortical neurons and projections. *Abbreviations: BN brainstem nuclei, GC Golgi cell, GrC granule cells, IO inferior olive, MCN medial cerebellar nucleus.*

Apart from the excitatory projection to the premotor neurons in the red nucleus provided by large glutamatergic projection neurons (large GAD67-negative), the cerebellar nuclei have an inhibitory projection back to the inferior olive, provided by small GAD67-positive neurons (de Zeeuw et al., 1988; de Zeeuw et al., 1989; Ruigrok and Voogd, 1990; Fredette and Mugnaini, 1991). In this GABAergic feedback loop, the cerebellar zonal arrangement is again preserved (Dietrichs and Walberg, 1981; Courville et al., 1983; Dietrichs and Walberg, 1986; de Zeeuw et al., 1989; Ruigrok, 2011) and thus the lateral AIN and DLH regions project back to the medial part of the dorsal accessory inferior olive and dorsomedial group of the principal olive. Since Purkinje cells innervate both excitatory and inhibitory neurons in the cerebellar nuclei, the excitatory cerebellar output system and the inhibitory feedback to the inferior olive are most probably controlled simultaneously (De Zeeuw and Berrebi, 1995; Teune et al., 1998; Uusisaari and Knopfel, 2011). Indeed, cerebellar nuclear recordings show that during acquisition inputs from the inferior olive are being suppressed, suggesting that the inferior olive becomes functionally inhibited by the cerebellum during the generation of an eyeblink CR (Andersson et al., 1988; Hesslow and Ivarsson, 1996; Kim et al., 1998; Medina et al., 2002), resulting in a decreased complex spike frequency within the CS-US interval (Rasmussen et al., 2008; Rasmussen and Hesslow, 2014; Rasmussen et al., 2014). Interestingly, early recordings from Purkinje cells during eyeblink conditioning seem to suggest the opposite: some cells would show an increase of complex spikes within the CS-US interval in conditioned animals (Berthier and Moore, 1986). These intuitively conflicting results might partly be explained by differences in experimental design and differences in data analysis. First, Rasmussen et al. conditioned the animals for several hours and looked particularly at the changes in complex spike frequency in the last 100 ms of the CS (CS and US co-terminate), whereas Berthier and Moore performed a longer training for several days and report increased complex spike frequencies for some Purkinje cells in the first 100 ms of the CS. Second, Rasmussen et al. recorded specifically from Purkinje cells in the eyeblink controlling microzone, whereas Berthier and Moore had a more global approach. Instead, manipulation of the nucleo-olivary pathway has provided more consistent results. Whereas blockade of nucleo-olivary feedback after acquisition prevents extinction of conditioned eyelid responses, blocking excitatory inputs to the inferior olive or stimulation of the nucleo-olivary feedback loop just before US presentation in a trained animal leads to extinction of eyeblink CRs (Medina et al., 2002; Bengtsson et al., 2007).

Contribution of extracerebellar structures

Numerous studies have focused on the contribution of extracerebellar structures like (medial) prefrontal cortex, hippocampus, thalamus, and amygdala to memory formation relating to delay eyeblink conditioning (mPFC: Leal-Campanario et al., 2007; Plakke et al., 2009; Wu et al., 2012; Hippocampus: Berger and Thompson, 1978; Hoehler and Thompson, 1980; Lee and Kim, 2004; Blankenship et al., 2005; Wu et al., 2013; Thalamus: Halverson et al., 2008; Halverson and Freeman, 2009; Halverson et al., 2009; Halverson and Freeman, 2010; Halverson et al., 2010; Ng and Freeman, 2012; Steinmetz et al., 2013; Amygdala: Neufeld and Mintz, 2001; Lee and Kim, 2004; Blankenship et al., 2005; Boele et al., 2010; Ng and Freeman, 2013). Especially

amygdala inactivation seems to have major effects on the acquisition of eyeblink CR, and we have suggested that in mice the particularly the amygdala contributes to the potentiation of startle or short-latency fear responses in the eyeblink trace (Boele et al., 2010). Since this book chapter focuses on cerebellar coding and the role of extracerebellar structures seems to be mainly limited to either a modulation of CS inputs to the cerebellum or the potentiation of fear components in the eyeblink trace, they will not be further discussed in here.

Neural plasticity in cerebellar cortex and cerebellar nuclei

Learning versus performance

As mentioned above, inactivation of the AIN can abolish eyeblink CRs. From the very beginning this finding was challenged by the argument that lesions of the AIN would produce a *performance* deficit rather than an impairment of *learning*. The first argument against the cerebellar learning hypothesis came from studies suggesting that AIN lesions simply block the expression but not the learning of eyeblink CRs (Welsh and Harvey, 1989, 1991; Welsh, 1992; Llinás and Welsh, 1993; Bracha et al., 1994). This issue has to a large extent been tackled in several temporal (or reversible) inactivation studies using the local anesthetic lidocaine or the GABA (γ-aminobutryc acid) agonist muscimol, with the rationale that inactivation of a brain region where memory formation takes place should result in no CRs during training and no CRs once the inactivation has been removed. In contrast, inactivation of a brain area that is not involved in memory storage but only in the expression of learning should result in no CRs during the inactivation but CRs should be expressed once the inactivation has been removed. Lidocaine or muscimol infusions in the eyeblink controlling parts of the cerebellar cortex and AIN prevent learning, reflected by the absence of CRs both during inactivation and after the removal of the inactivation (Krupa et al., 1993; Nordholm et al., 1993; Bracha et al., 1994; Hardiman et al., 1996; Attwell et al., 2001; Bracha et al., 2001; Aksenov et al., 2004). In contrast, inactivation of cerebellar premotor efferents, like the red nucleus, by the same drugs prevents the expression of CRs during the inactivation, but does not prevent learning in that after the washout of the drug CRs are present (Krupa and Thompson, 1995; Krupa et al., 1996; Ohyama et al., 2006). Thus, learning takes place upstream from the red nucleus in the CR pathway, which is the cerebellum.

   A second argument against the cerebellar learning hypothesis came from studies reporting that neurons in the interposed nucleus start firing about 20 ms after the onset of the eyeblink CR, suggesting that the interposed nuclei cannot initiate/generate the eyeblink CR (Gruart and Delgado-Garcia, 1994; Gruart et al., 1995; Gruart et al., 2000; Delgado-Garcia and Gruart, 2002, 2005, 2006; Sanchez-Campusano et al., 2011). According to this work also, the cerebellum is not involved in memory storage but rather in the timing of eyeblink CRs and dampening oscillations in the eyeblink. However, most of these recordings were made in the PIN, which is an area of the cerebellar nuclei that does not seem to be directly involved in the control of eyelid muscles as there are no major projections to the red nucleus (Ruigrok, 2004). In contrast, electrophysiological recordings from neurons in the AIN do exhibit a firing profile, which precedes the onset of the eyeblink CRs and is only observed in trials

wherein a CR is present and their activity models the timing and amplitude of these CRs (McCormick et al., 1982; McCormick and Thompson, 1984; Berthier and Moore, 1990; Gould and Steinmetz, 1996; Freeman and Nicholson, 2000; Nicholson and Freeman, 2002; Choi and Moore, 2003; Green and Arenos, 2007; Halverson et al., 2010). Together, these recordings suggest that the AIN is causally related to eyeblink CR by driving the premotor neurons that innervate the eyelid muscles and that the PIN might contribute to the motion trajectory of CRs once they started.

Cerebellar cortex versus cerebellar nuclei

It appeared to be much more challenging to tease apart the relative contributions of the cerebellar cortex and the cerebellar nuclei. Is the abolishment of CRs after AIN inactivation a result of disruption of the memory that is formed in the AIN itself or simply the effect of blocking the output of the memory that is formed ''upstream'' in the Purkinje cells? In other words, is the essential memory formed in the cerebellar nuclei or in the cerebellar cortex? Or maybe in both?

Learning in the cerebellar cortex

According to Marr's and Albus'theoretical work the essential learning would take place in the cerebellar cortex (Marr, 1969; Albus, 1971). They hypothesize that simultaneous activation of a set of parallel fibers with a climber fiber results in a change in the synaptic strength of this set of parallel fiber – Purkinje cell synapses. According to Albus this process should be regarded in a sense of classical conditioning: ''*It is now hypothesized that the inactivation response pause* [after a complex spike] *in Purkinje spike rate is an unconditioned response (UR) in a classical learning sense caused by the unconditioned stimulus (US) of a climbing fiber burst. It is further hypothesized that the mossy fiber activity pattern ongoing at the time of the climbing fiber burst is the conditioned stimulus (CS). If this is true, the effect of learning should be that eventually the particular mossy fiber pattern (CS) should elicit a pause (CR) in Purkinje cell activity similar to the inactivation response (UR) that previously had been elicited only by the climbing fiber burst (US)*'' (Albus, 1971). Thus, cerebellar learning requires context or conditional (CS) information from mossy fibers and an error or teaching signal (US) from climbing fibers. As a result of pairing the CS with the US, Purkinje cells in the cerebellar cortex eventually will pause their simple spike firing. Since Purkinje cells have a tonic inhibitory effect on the cerebellar nuclei, this simple spike suppression will disinhibit the cerebellar nuclei, which in turn should ultimately result in an increase of cerebellar output.

Thus, Purkinje cells in a cerebellar microzone receive on the one hand a massive amount of sensory information from many modalities (CS) and on the other hand sensory information from a very specific receptive field (US). Therefore, they appear well suited for associative learning (Harvey and Napper, 1991). The best evidence that Purkinje cells in the cerebellar cortex indeed can acquire pauses in their simple spike firing during eyeblink conditioning comes from Hesslow's lab. Their exact identification of eyeblink controlling microzones in the C1 and C3 regions and their decerebrated preparation makes it possible to study changes in Purkinje cell activity as it might occur during eyeblink conditioning. In a training paradigm, using peripheral forelimb or direct mossy fiber stimulation as CS paired with a peri-ocular or

direct climbing fiber stimulation as US, one could observe a gradual acquisition of a suppression and even complete silencing of Purkinje cell simple spike firing. This Purkinje cell pause or Purkinje cell CR is adaptively timed in that the response latency varies with the used interval between CS and US and the suppression is maximal, exactly just before the onset of the US (Fig. 6A-C) (Jirenhed et al., 2007; Rasmussen et al., 2008; Svensson et al., 2010; Jirenhed and Hesslow, 2011b). Moreover, many other known behavioral phenomena like extinction and rapid reacquisition (Fig. 6 D-I) (Jirenhed et al., 2007), adaptation of the timing of CRs after changing the CS-US interval (Jirenhed and Hesslow, 2011b), a minimal CS-US interval of about 100 ms (Wetmore et al., 2014), facilitating effects on the rate of conditioning by increasing the US intensity (Rasmussen et al., 2013), and a decreased CR onset after increasing the CS intensity (Svensson et al., 2010), can also be observed in the single Purkinje cell.

Together, these findings strongly suggest that the essential learning takes place in these Purkinje cells in the eyeblink controlling microzone. However, it is still unclear whether this Purkinje cell simple spike pause alone is sufficient to generate eyeblink CRs. First, in Hesslow's approach in the decerebrated ferret training occurs within a couple of hours and from behavioral experiments we know that, with a few exceptions, it is impossible to train an animal within this time window, even if the animal is used to spending long times in the experimental setup (observations by H.J. Boele, data not shown). Second, because of their preparation they do not record simultaneously from Purkinje cells and the conditioned external eyelids. However, other studies, which do perform simultaneous recordings, show that indeed a subpopulation of Purkinje cells can show a learning related inhibitory response of which the temporal profile corresponds with that of the eyelid CR (Hesslow and Ivarsson, 1994; Kotani et al., 2006). In addition, some Purkinje cells would instead increase their firing in the CS-US interval during conditioning (Berthier and Moore, 1986; Kotani et al., 2003; Green and Steinmetz, 2005; Kotani et al., 2006). However, these cells do not seem to control the eyeblink CR directly, since their firing profile does not seem to be correlated with the temporal profile of the eyeblink CR (Kotani et al., 2006). So far, a conclusive and quantitative study on the exact role and contributions of Purkinje cells controlling the overt eyeblink CR at different stages during the learning process is still lacking.

Plasticity mechanisms in the cerebellar cortex

What is the neural mechanism underlying this adaptively timed simple spike suppression of a Purkinje cell? Albus proposed that the main underlying mechanism would be a synaptic weakening of the parallel fiber – Purkinje cell synapse (pf-PC synapse) (Albus, 1971). A few years later Masao Ito provided the first experimental support for this learning mechanism by showing that Purkinje cells (in the flocculus) indeed showed a strong suppression (of about ten minutes) in their simple spike firing as a result of conjunctive mossy fiber and climbing fiber stimulation (Ito et al., 1982). This initial suppression was followed by a longer lasting (hour) slow suppression. In addition, this depression seemed to occur specifically at pf-PC synapses that are involved in the conjunctive stimulation. This long-term depression (LTD) was later confirmed in many other studies (Ekerot and Kano, 1985; Linden and Connor, 1991; Linden et al., 1991). Further strengthened by reports that LTD-deficient mouse mutants showed impaired eyeblink conditioning, LTD was increasingly considered as the
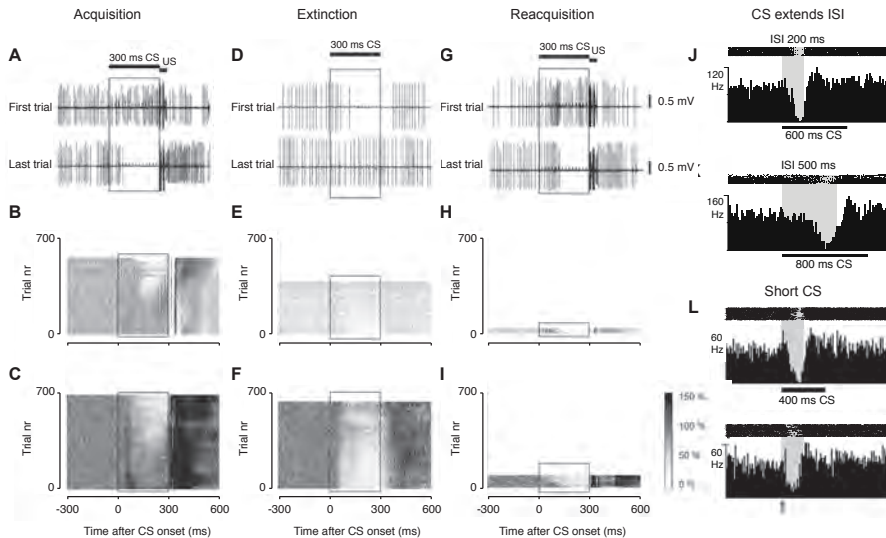
Figure 6 (A-C) Acquisition of Purkinje cell CR. **(A)** Two sample records from a Purkinje cell exposed to paired CS-US presentations (bars above graph), from trial 1 (top) and 640 trials later (bottom). The acquired Purkinje cell response had a latency relative to CS onset of $\pm$ 60 ms. **(B)** Raster plot of the simple spike activity recorded from the same cell during 640 trials of paired CS-US presentations. The inhibitory response during the CS period (framed) gradually developed as training progressed. **(C)** Average raster plot based on 11 Purkinje cell records during acquisition. The plot is built up of squares, the shadings of which indicate average firing rate across all cells. The light area that gradually appears represents the Purkinje cell CR, i.e., an inhibitory response with a firing rate below background level (100%). The darker areas indicate increased simple spike activity. **(D-F)** Purkinje cell activity during extinction. **(D)** Two example records from a Purkinje cell exposed to unpaired CS-US stimulation (bar above graph indicates the 300 ms CS period), from trial 1 (top) and 440 trials later (bottom). The Purkinje cell CR had a latency relative to CS onset of 60 ms and a duration of 300 ms. **(E)** Raster plot of simple spike activity recorded from the same cell as above during 440 trials of unpaired CS-US stimulation. The inhibitory response during the CS period (framed) gradually extinguished as training progressed. **(F)** Average raster plot of simple spikes recorded from nine Purkinje cells during paired CS-US stimulation. **(G-I)** Purkinje cell activity during reacquisition. **(G)** Two example records from a Purkinje cell reexposed to paired CS-US stimulation (bars above graph) after extinction of the CR. Trial 1 (top) and 40 trials later (bottom) are shown. **(H)** Raster plot of simple spike activity (recorded from the same cell as above) during 40 trials of reintroduced pairing of CS-US stimulation. Notice the savings in the rate of reacquisition compared with acquisition. After only four trials, the CR was reacquired. **(I)** Average raster plot based on five Purkinje cell records during paired CS-US stimulation. **(J,K)** Conditioned Purkinje cell responses on a CS that extends the CS-US interval. **(J)** Example raster plot and histogram of responses from a cell conditioned to a 200 ms CS-US interval (gray shading), using a CS of 600 ms duration (black bar below graph). **(K)** Example raster plot and histogram of responses from a cell conditioned to a 500 ms CS-US interval (gray shading), using a CS of 800 ms duration (black bar below graph). **(L)** Conditioned Purkinje cell response on a short CS displayed as raster plot and histogram. Upper panel shows the average response to CS-alone stimulation after conditioning with a 200 ms CS-US interval (gray shading) using a 400 ms duration CS (black bar below graph); the CS consisted of 400 ms pulse train (50 Hz) to the mossy fibers. Lower panel shows CRs from the same cell elicited with a short CS of only two pulses; each CS pulse is indicated by an arrow (interval between stimuli was 20 ms). For J, K, and L: each graph is based on 40 trials. The duration is 1.5 s. *(Figure and legend used with permission from Jirenhed et al., 2007; Jirenhed et al., 2011a, b.)*

main learning mechanism underlying eyeblink conditioning (De Zeeuw et al., 1998; Mauk et al., 1998; Hansel and Linden, 2000; Hansel et al., 2001; Mauk and Buonomano, 2004; Yeo, 2004; De Zeeuw and Yeo, 2005; Yamazaki and Tanaka, 2009; Freeman and Steinmetz, 2011). For instance, LTD and eyeblink conditioning are impaired in (i) Mutants lacking the metabotropic glutamate receptor mGluR1 in Purkinje cells (Aiba et al., 1994; Ichise et al., 2000; Kishimoto et al., 2002), (ii) Mutants lacking the glutamate receptor subunit delta2 (GluRΔ2) (Kishimoto et al., 2001), (iii) Mutants lacking glial fibrillary acidic protein (GFAP) (Shibuki et al., 1996), and (iv) Purkinje-cell specific mutants overexpressing Protein Kinase C inhibitor (PKC-I) (Koekkoek et al., 2003).

However, recent experimental and theoretical work has thrown some doubt on the essential role that pf-PC LTD would play in motor learning. First, Welsh et al. (2005) report that application of T-588, which blocks LTD by acutely reducing calcium release from intracellular stores, does not prevent adaptation of the eyeblink CR timing to a new CS-US interval (Welsh et al., 2005). Second, Schonewille et al. (2010) demonstrate that in three different types of mutant mice (PICK1 KO, GLuR2Δ7 KI, and GluRK882A KI) that selectively lack *expression* of cerebellar LTD eyeblink conditioning was not affected (Schonewille et al., 2011). In these mutants, the expression of pf-PC LTD is specifically targeted by modifications downstream of the molecular cytosolic pathways at the level of either the intermediary PICK1 between PKC activation and AMPA receptor internalization or even at the level of the cell membrane (GluR2Δ7 KI and GluR2K882A KI). In contrast, in previous mutants not only pf-PC LTD but also other forms of cerebellar plasticity are affected (Gao et al., 2012). For example, inhibition of PKC may affect the efficacy of $GABA_A$ receptors at the MLI to Purkinje cell synapse by influencing their surface density and sensitivity to positive allosteric modulators and/or by modifying chloride conductance (Song and Messing, 2005). Similarly, Purkinje cells also display intrinsic plasticity (Pedroarena and Schwarz, 2003), and protein kinases may well be required for persistent use-dependent modulation of one or more of the ion channels involved. Finally, the kinases might also play a role in presynaptic plasticity at the Purkinje cell to cerebellar nuclei neuron synapse (Belmeguenai et al., 2010) and/or postsynaptic plasticity at the mossy fiber or climbing fiber collateral to cerebellar nuclei neuron synapse (Zhang and Linden, 2006; Pugh and Raman, 2008). These more global effects might explain why in previous mutants with enzymatic deficits eyeblink conditioning was impaired and why in these improved and newer mutants with receptor-linked subtle deficits eyeblink conditioning is normal.

Third, LTD of the pf-PC synapse seems to be insufficient to explain the millisecond-precise timing of eyeblink CRs. The LTD hypothesis assumes that a specific CS will activate different sets of granule cells, which in response will fire with different latencies and durations. LTD then would occur specifically at those pf-PC synapses, which burst activity coincides with the climbing fiber input provided by the US. As a result of LTD simple spike firing will be suppressed in the CS-US interval and thus the eyelid will close in the CS-US interval. If this hypothesis were true, then one would expect that a change in duration of activity of specifically those parallel fibers, which underwent LTD at their synapses with the Purkinje cells, would result in a change in duration of simple spike suppression and thus a change in duration of the eyeblink CR. In other words, the CS duration would determine the length of the CR. However, it has been shown in Purkinje cell CR and eyeblink CRs that a long CS,

which extends beyond the used CS-US interval, results in normally shaped CRs (Fig. 3, 6J, K) (Jirenhed and Hesslow, 2011b). Thus, even if the CS outlasts the used CS-US interval by several hundreds of milliseconds, the CR is perfectly timed with its peak just at the point where the US is about to be delivered. Interestingly, after training with a CS-US interval of 250 ms, a very brief CS of only tens of milliseconds is also sufficient to elicit normal Purkinje cell and eyeblink CRs (Fig. 3A, B, 6L) (Svensson et al., 2010; Jirenhed and Hesslow, 2011a), but when training occurs with a longer CS-US interval of 500 ms, the brief CS seems to be insufficient to elicit proper CRs (Fig. 3C, D).

Together, these data together strongly suggest that the CR seems to be rather uncoupled from the CS duration and that for short CS-US intervals of about 250 ms especially the first tens of milliseconds contain crucial information for the Purkinje cell to suppress its firing which, in our view, cannot be merely explained by pf-PC LTD. At this point it is still unclear whether parallel fibers transmit a natural CS, for instance an auditory tone, during the full duration of the of the CS to the Purkinje cell, as in the approach with the mossy fiber stimulation as described above (cf. Jorntell and Ekerot, 2006; Ruigrok et al., 2011; van Beugen et al., 2013). Fourth, it appeared that LTD of the parallel fiber – Purkinje cell synapse cannot even be established after eyeblink conditioning (Jirenhed and Hesslow, 2011a). In an approach where animals were first being trained with a CS consisting of direct mossy fiber stimulation at 50 Hz for a duration of 800 ms and a US of direct climbing fiber stimulation at 500 Hz for 20 ms and starting at 200 ms after CS onset, they looked at the simple spike probability after single mossy fiber pulses in CS alone trials after training at different time points in the 800 ms CS period. They argue that, if LTD would take place, then one would expect a lower simple spike probability at each time point in 800 ms CS period, and thus a coupling of CS length and simple spike suppression. However, in conditioned Purkinje cells they could only establish a decreased simple spike probability within the CS-US interval and not in the 600 ms period wherein the CS outlasts the US, suggesting that LTD of the parallel fiber – Purkinje cell synapse has not taken place (Jirenhed and Hesslow, 2011a; Hesslow et al., 2013).

For further arguments against LTD as being the sole essential form of plasticity underlying eyeblink conditioning, we refer to Hesslow et al. (2013) and Gao et al. (2012) (Gao et al., 2012; Hesslow et al., 2013). Hesslow et al. (2013) argue that the conditions under which LTD is induced in vitro do not match those of behavioral eyeblink conditioning experiments. In the slice preparation, LTD can be induced within minutes and optimal LTD is obtained when the delay between ''CS'' and ''US'' would close to zero milliseconds, whereas during behavioral experiments, the acquisition of eyeblink CRs takes several hundreds of paired trials and the minimum interval in order to get proper conditioning is between CS and US is about 100 milliseconds. In contrast, Hansel and coworkers argue that LTD can also be successfully induced at longer intervals of hundreds of milliseconds (Piochon et al., 2012; Titley and Hansel, 2015). Further, since Purkinje cells have an intrinsic spike generating mechanism (Raman and Bean, 1997, 1999), removal of excitatory inputs from the Purkinje cell by the application of CNQX only has minor effects on simple spike firing rate (Cerminara and Rawson, 2004; Zhou et al., 2014) and granule cells are mostly silent to begin with (Isope and Barbour, 2002), LTD of the parallel fiber – Purkinje cell synapse alone cannot easily explain the complete silencing of Purkinje cell simple spike firing for

hundreds of milliseconds. In other words, removal of excitation seems unable to induce a complete pause in simple spike firing.

Which alternative plasticity mechanisms could potentially explain or contribute to timed simple spike pauses during eyeblink conditioning? First, Johansson et al., (2014) have demonstrated that Purkinje cells can be successfully conditioned by direct stimulation of parallel fibers as CS and direct climbing fiber stimulation as US up to CS-US intervals of at least as long as 300 ms. Moreover, application of the $GABA_A$-antagonist gabazine seems to have no effect on acquired simple spike pauses (Johansson et al., 2014). However, as the role of molecular layer interneurons can probably not be excluded completely because of the strong ephaptic inhibitory effects they have on Purkinje cells (Blot and Barbour, 2014), these data strongly suggest the existence of a cellular mechanism within the Purkinje cell which may suppress its simple spike firing for the duration of the CS-US interval (i.e. several hundreds of milliseconds). In other words, Purkinje cells seem to ''convert'' increases in parallel fiber input (by the CS) to decreased output. The exact nature of these cellular mechanisms remains to be elucidated, but group II and III metabotropic glutamate receptors are likely to play a role (Johansson et al., 2014; Dutar et al., 1999). Second, it should be noted that stellate and basket cells make strong inhibitory chemical but possibly also electrical synapses with Purkinje cells, as shown in lower vertebrates (Sotelo and Llinás, 1972). As a result, their activity may induce long simple spike pauses (Korn and Axelrad, 1980; Mittmann et al., 2005; Heiney et al., 2014) and thereby contribute to the CRs. However, how these cells contribute to the exact timing of CRs is unclear. Third, from a Purkinje cell's perspective, it seems unwise to decrease input strengths of relevant sets of parallel fibers transmitting CS information. If Purkinje cells indeed have an intrinsic mechanism to convert increases in parallel fiber input, caused by the CS, to a decreased output, then pf-PC LTP would be an effective mechanism to enhance the input strength of specific parallel fiber inputs transmitting CS. This pf-PC might enable the Purkinje cell to ''pick up'' more easily the relevant CS information. This optimization of input strength might explain why after conditioning a minimum of CS information, for instance a very brief CS, can be sufficient to elicit perfectly timed CRs (Fig. 3A, B, 6L) (Svensson et al., 2010; Jirenhed and Hesslow, 2011a). The importance of pf-PC LTP is further supported by the finding that eyeblink conditioning is severely impaired in L7-PP2B mice, which have a Purkinje cell-specific impairment in pf-PC LTP and cannot increase their intrinsic excitability (Belmeguenai and Hansel, 2005; Schonewille et al., 2010).

Plasticity in cerebellar nuclei

One of the main arguments for plasticity in the cerebellar nuclei during eyeblink conditioning, comes from studies showing inactivation of cortical eyeblink controlling zones could not completely abolish eyeblink CRs: after removal of cortical inputs from the AIN, animals would still display residual CRs with extremely short latency to onset and latency to peak, therefore called short-latency responses (SLRs) (Perrett et al., 1993; Garcia and Mauk, 1998; Medina et al., 2001; Bao et al., 2002; Ohyama et al., 2003; Ohyama et al., 2006). Since other groups do not find these SLRs, they have been a matter of big dispute (Yeo et al., 1985b; Attwell et al., 2001; Attwell et al., 2002). These conflicting results have been addressed extensively by Bracha and co-workers.

Initially, they report that PTX infusions in the AIN did not have any effect on eyeblink CRs and should even increase the amplitude of the eyelid responses (Bracha et al., 2001). However, later they show that the effects of PTX and gabazine injection in the AIN are at least partly determined by the used dosage: a low dose of gabazine or PTX results in SLRs whereas higher dosages result in a complete abolishment of CRs (Aksenov et al., 2004; Parker et al., 2009). In addition, they also report that the effects of the low dose PTX in similar AIN injections are surprisingly variable: some rabbits do show SLRs whereas others do not. Importantly, they also perform extracellular recordings before and after injection from AIN neurons, which are categorized into three groups based on resting firing frequency before injection of PTX. The main effect of low dose infusions (0.5 μL per side) of PTX in the AIN is an increased baseline firing frequency and diminished the modulation during the CS-US interval in all three categories of AIN neurons (mainly lateral parts of the AIN). A consecutive second injection (again 0.5 μL per side) further increases the baseline firing frequency and almost completely abolishes modulation during the CS-US interval. No SLRs could be observed in the firing profile of AIN neurons (Fig. 7). The behavioral results of PTX injections comprise increased tonic eyelid closures and increased UR amplitudes. According to the same group, blocking climbing and mossy fiber collateral input with DGG (gamma-d-glutamylglycine; glutamate receptor antagonist) does not abolish CR but has only minor effects on the CR latency (increase) and CR incidence (decrease) (Aksenov et al., 2005), a finding which is in line with Attwell et al. (Attwell et al., 2001; Attwell et al., 2002), suggesting that plasticity in the cerebellar nuclei only plays an accessory role in the expression of CRs.

Since, to our knowledge, SLRs have never been described for the firing profile of AIN neurons, it raises the question whether these SLRs indeed form the behavioral correlate of memory that has been formed in the cerebellar nuclei. Inactivation of the cerebellar cortex results in a tonic disinhibition of the cerebellar nuclei, which in turn results in an increased excitation of premotor areas innervating the eyelid motoneuron (N. III, VI, VII). As a result, sensory input from the trigeminal nucleus to these motoneurons could potentially increase their responsiveness. Indeed, it has been shown that removal of cortical inputs to the AIN results in stronger and bigger reflexive eyelid closures (Yeo and Hardiman, 1992; Parker et al., 2009). Similarly, the effect of other brain structures, which (in)directly innervate the eyelid motoneurons might become more evident after lesions of the cerebellar cortex. Therefore, we propose that it cannot be excluded that SLRs in rabbits are also a result of extra-cerebellar learning.

Plasticity mechanisms in the cerebellar nuclei

Plasticity in the AIN during eyeblink conditioning assumes convergence of CS and US at this site by mossy fibers and climbing fibers, respectively. But, as mentioned already, in untrained animals there is hardly any convergence of CS and US in the AIN. For climbing fibers, it is clear that they give off collaterals to the cerebellar nuclei (Pijpers et al., 2005), thus US signals are also sent to the AIN. However, in unconditioned animals mossy fiber projections from the basilar pontine nuclei to the cerebellar nuclei are sparse and mainly restricted to the lateral cerebellar nuclei. For other sources of mossy fibers, like the nucleus reticularis tegmentis pontis, projections
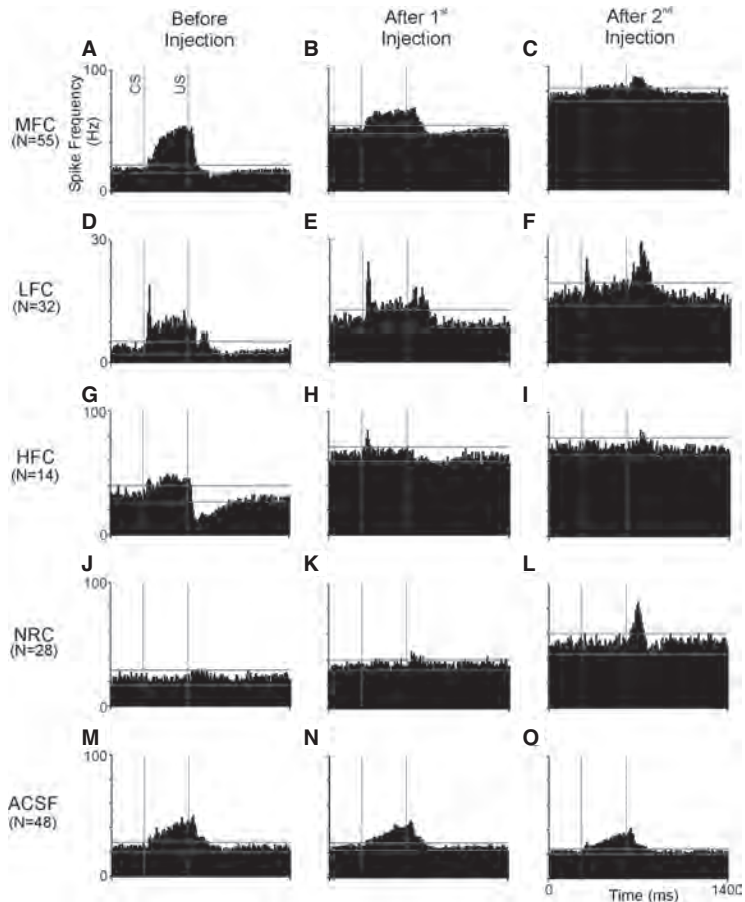
Figure 7 Extracellular recordings from cerebellar nuclei neurons during eyeblink conditioning. Effects of picrotoxin (PTX) and artificial cerebrospinal fluid (aCSF) injections on recorded populations of cells. Averaged peri-stimulus histograms are arranged in rows corresponding to cell types and in columns representing the activity before injection, after the first PTX injection, and after the second PTX injection. **(A-C)** Medium-frequency cells (MFC). **(D-F)** Low-frequency cells (LFC). **(G-I)** High-frequency cells (HFC). **(J-L)** Non-responding cells (NRC). **(M-O)** Cells recorded during control injections of vehicle aCSF. Note that the first injection of PTX increased baseline firing frequency and diminished the relative size of firing modulation in all cell types. The second injection further increased baseline activity and further reduced the depth of firing modulation. Also note the emerging response to the US in MFC, LFC, and NRC that becomes the most prominent response following the second PTX injection. Bin width 10 ms. Horizontal lines in each histogram represent tolerance limits, which were computed based on the statistical assumption that 99% of observations should not exceed this limit with a probability of 0.95. Abbreviations: aCSF artificial cerebrospinal fluid, CS conditioned stimulus onset, HFC High-frequency cells, LFC Low-frequency cells, MFC Medium-frequency cells, NRC Non-responding cells, US unconditioned stimulus onset. *(Figure and legend used with permission from Aksenov et al., 2004.)*

to the cerebellar nuclei seem to be more predominantly present, but are also mainly restricted to the lateral cerebellar nuclei (Dietrichs et al., 1983, Brodal et al., 1986; Parenti et al., 2002; Cicirata et al., 2005; Boele et al., 2013). Thus, there seems be an asymmetry in climbing fiber and mossy fiber projections to the AIN and the main neuronal pathway that would enable memory formation in the cerebellar nuclei, i.e. the projection from the basilar pontine nuclei to AIN, appears virtually absent following standard tracing experiments in naïve animals. Therefore, we tested the hypothesis that during eyeblink conditioning mossy fiber collaterals can grow to specific eyeblink controlling parts of the cerebellar nuclei thus enabling the CS to also terminate in the AIN and that as a consequence memory formation in the cerebellar nuclei can take place (Boele et al., 2013). Such reorganization of neuronal circuits by axonal growth and synaptogenesis has been recognized as a plausible mechanism for learning and memory formation for many decades (Holt, 1931), since it could robustly increase memory storage capacity of the brain (Wen et al., 2009). Yet, evidence for this learning mechanism still was missing.

We demonstrated first that in untrained mice mossy fiber collaterals originating from the lateral parts of the basilar pontine nuclei, which are considered to convey auditory information to the cerebellum, are sparse and limited to the lateral cerebellar nucleus and caudolateral PIN, which is in perfect agreement with previous findings obtained in other species (Dietrichs et al., 1983, Brodal et al., 1986; Parenti et al., 2002; Cicirata et al., 2005). Second, we demonstrated that these mossy fiber collaterals to the cerebellar nuclei could expand considerably following Pavlovian eyeblink conditioning to a tone, whereas no changes are observed following pseudo-conditioning to this tone (Fig. 8A-C). Because pseudo-conditioned animals show similar patterns of labeling as untrained animals, the data strongly suggest that the changed distribution and increased density of terminal labeling in the conditioned animals are specifically due to the paired presentation of CS and US rather than to the less specific aspects of the learning task, like habituation or sensitization to the CS and US. Third, no changes are observed in conditioned animals after labeling non-auditory mossy fibers from the medial part of the basilar pontine nuclei. Therefore, we conclude that the observed conditioning-induced neuronal outgrowth specifically involves basilar pontine nuclei neurons that transmit the tone CS to the cerebellar nuclei. Fourth, and this last observation maybe gives the most important clue for the role of these mossy fiber collaterals, we established a positive correlation between the amplitude of the eyeblink CRs after training and the amount of mossy fibers collaterals in the DLH region (Fig. 8D), which is the part of the AIN in mice receiving input from Purkinje cells known to be involved in controlling eyelid movements (Morcuende et al., 2002; Mostofi et al., 2010; Gonzalez-Joekes and Schreurs, 2012). We could not establish any correlations between CR timing and the amount of mossy fiber collaterals in this DLH region.

We propose that this new excitatory input to the DLH and adjacent lateral AIN interacts with the well-timed Purkinje cell disinhibition of the same DLH neurons (Medina et al., 2000; Witter et al., 2013) and results in a stronger output to the eyelid muscles than would happen with changes in the Purkinje cell input alone. In addition, it has been shown that excitatory mossy fiber input followed by inhibitory Purkinje cell input could induce LTP at the mossy fiber – cerebellar nuclei neuron synapse (Zhang and Linden, 2006, Pugh and Raman 2008). On the other hand, the AIN itself
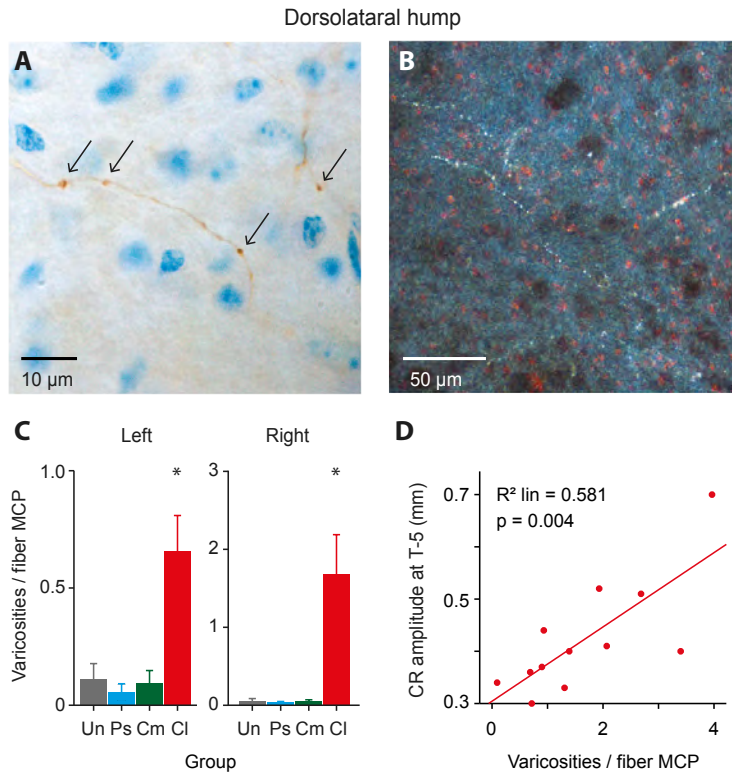
Dorsolataral hump

Figure 8 Labeled mossy fiber collaterals and varicosities in the dorsolateral hump (DLH) for each group. (A) Light microscopic image of a BDA labeled mossy fiber collateral with varicosities in the DLH region of a conditioned animal. Bar represents 10 μm, arrows indicate labeled varicosities. **(B)** Darkfield microscopic image of BDA labeled mossy fiber collaterals with varicosities in the DLH region of a conditioned animal. Bar represents 50 μm. **(C)** Total number of synapses in the DLH per labeled fiber in the middle cerebellar peduncle (MCP) for all four groups. Conditioned animals with BDA injection in lateral right basilar pontine nuclei (BPN) show a significant increase in their number of varicosities per MCP fiber. **(D)** Mean number of labeled varicosities in the DLH per labeled MCP mossy fiber plotted against the mean CR amplitude (mm) at the last training session for conditioned animals with BDA injected in the lateral BPN. In conditioned animals, the number of labeled varicosities in the DLH per MCP fiber correlates positively with the amplitude of the eyelid CRs in the last training sessions. Abbreviations: Cl = Conditoned with BDA injection in lateral right BPN, Cm = Conditioned with BDA injection in medial right BPN, MCP middle cerebellar peduncle, Ps = Pseudo-conditioned with BDA injected in lateral right BPN, Un = Untrained with BDA injected in lateral right BPN. *(Figure and legend used with permission from Boele et al., 2013.)*

does not seem to be the major driver of the eyeblink CRs, since blockade mossy fiber and climbing fiber inputs to the AIN with CNQX or DGG does only have very minor effects on CRs in trained animals (Attwell et al., 2001; Attwell et al., 2002; Aksenov et al., 2004).

Conclusions

Starting from the elegant models and work by Marr, Albus and Ito psychologists and cerebellar scientists have come a long way in understanding classical Pavlovian eyeblink conditioning. Even though the original concept of an interaction between the two main afferent pathways, i.e. the mossy fiber and climbing fiber system, still stand, it has become increasingly clear that there is not a single essential form of plasticity in any part of the cerebellum that is doing the job by itself under normal physiological circumstances. Instead the picture is emerging that the cerebellar cortex directly and constantly interacts with the cerebellar nuclei and inferior olive to facilitate the learning process and that the cellular processes within all of these areas entail not only synaptic depression or potentiation but also hard-wired plasticity. Indeed, one could state that the olivocerebellar system has evolved as a wonderful and diverse learning machine that can resist most mutations affecting single processes taking part in its computations required for memory formation.

3 Scope and aims

The research comprising this thesis spans the olivocerebellar system, and is divided across three parts. Overall, emphasis lies on the electrophysiological investigation of spike responses in individual neurons in the context of cerebellar motor learning. Additionally, transgenic mouse mutants are used to assess the relevance of particular components of the olivocerebellar network for proper neuronal and behavioral functioning.

In **Part I**, we are interested in the activity and function of neurons in the cerebellar cortex, Purkinje cells and molecular layer interneurons, in behaving mice. Particularly, want to address the following questions:

> **Chapter 2**: How do Purkinje cells and molecular layer interneurons modulate their spike activity during associative learning?

> **Chapter 3**: How may molecular layer interneuron to Purkinje cell inhibition in combination with long term depression (LTD) at the parallel fiber to Purkinje cell synapse, influence associative learning?

> **Chapter 4**: How may potentiation of Purkinje cell activity mediate adaptation of whisking behavior?

> **Chapter 5**: How does autism-related Shank2-mutation affect Purkinje cell activity, and to what extent may these effects contribute to autism-like behavior?

In **Part II**, our focus lies at the receiving end of the inhibitory output of the cerebellar cortex, the cerebellar nuclei. With a particular focus on the interpositus nucleus, we want to know:

> **Chapter 6**: How do cerebellar nuclear neurons integrate the conditioning-related input from their afferents during associative learning?

> **Chapter 7**: To what extent may recurrent input from the cerebellar nuclei to the cerebellar cortex carry a functional role in associative learning?

In **Part III**, we expand our scope to consider the olivocerebellar network in its entirety, and evaluate it in broader terms. Specifically, we ask:

> **Chapter 8**: How does olivary coupling influence the synchrony of their inputs to the cerebellar cortex?

> **Chapter 9**: What could be the origins and functions of conditioned climbing fiber responses in cerebellar cortex and nuclei?

> **Chapter 10**: How may different olivocerebellar modules use different encoding schemes to form and express their respective memories?

part I

Cerebellar Cortex

Chapter 2

Evolving models of Pavlovian conditioning:
cerebellar cortical dynamics
in awake behaving mice

Three decades of electrophysiological research on cerebellar cortical activity underlying Pavlovian conditioning have expanded our understanding of motor learning in the brain. Purkinje cell simple spike suppression is considered to be crucial in the expression of conditioned eyelid responses (CRs). However, trial-by-trial quantification of this link in awake behaving animals is lacking, and current hypotheses regarding the underlying plasticity mechanisms have diverged from the classical parallel-fiber to Purkinje cell synapse LTD-hypothesis. Here, we establish that acquired simple spike suppression, acquired conditioned stimulus (CS)-related complex spike responses, and molecular layer interneuron (MLI) activity predict the expression of CRs on a trial-by-trial basis, using awake behaving mice. Additionally, we show that two independent transgenic mouse mutants with impaired MLI function exhibit motor learning deficits. Our findings suggest multiple cerebellar cortical plasticity mechanisms underlying simple spike suppression and implicate the broader involvement of the olivocerebellar module within the interstimulus interval.

M.M. ten Brinke*, H.J. Boele*, J.K. Spanke*, J.W. Potters, K. Kornysheva, P. Wulff, A.C.H. Ypelaar, S.K.E. Koekkoek, & C.I. De Zeeuw (2015) **Cell Reports**

1 Introduction

The cerebellum offers the perfect neuronal territory within which to achieve an understanding of simple forms of learning and memory that flows ''*continuously from molecules and cells through synapses and circuits to behavior without any grossly embarrassing gaps in the middle*'' (Hansel et al., 2001). Pavlovian eyeblink conditioning illustrates this beautifully for an elementary building block in learning: the capacity to make associations (Gormezano et al., 1962). Imagine receiving an air puff on your eye a quarter second after seeing a green LED light turn on, over and over again. The air puff is an unconditional stimulus (US) in that it yields an unconditional blink response (UR). From the reflex loop underlying this blink, a signal is transmitted to the inferior olive and subsequently through climbing fibers to a subset of Purkinje cells in mainly the simplex lobule (HVI) of the cerebellar cortex (Fig. 1A; Jirenhed et al., 2007; Mostofi et al., 2010). This climbing fiber signal causes a complex spike in these Purkinje cells, whose activity moderates cerebellar nuclear cells that ultimately innervate the same eyelid musculature targeted by the reflex loop. The same Purkinje cells also receive massive sensory input through the mossy fiber-parallel fiber system, in large part originating in the pontine nuclei (Fig. 1A). Hidden within this sea of parallel fibers are signals encoding the green LED light, which by default is a neutral stimulus. Only on the condition that it is consistently paired with the air puff and only by virtue of the Purkinje cell's capacity to forge associations between parallel and climbing fiber signals, you will learn to perform a well-timed, conditioned blink response (CR) upon exposure to the light, which is thusly called the conditional stimulus (CS).

In tandem with lesion and stimulation research (Clark et al., 1984; Yeo et al., 1984, 1985a,b; McCormick & Thompson, 1984a; Yeo & Hesslow, 1998), electrophysiology studies of increasing sophistication have extended and solidified our understanding of eyeblink conditioning across behavioral, circuitry, and cellular levels (McCormick & Thompson, 1984b; Berthier & Moore, 1986; Hesslow & Ivarsson, 1994; Green & Steinmetz, 2005; Kotani et al., 2006; Jirenhed et al., 2007; Halverson et al., 2015). It is now established using peripheral stimuli as well as direct stimulation of nuclei and fibers that Purkinje cells can acquire various types of simple spike modulation within classical conditioning paradigms (Jirenhed et al., 2007; Tracy & Steinmetz, 1998; Kotani et al., 2006). Importantly, Hesslow and colleagues have shown in decerebrate ferrets that Purkinje cells with reliable short-latency complex spike responses to the ipsilateral US quite uniformly acquire suppressive simple spike responses with properties that are very similar to behavioral CRs (Hesslow & Ivarsson, 1994; Jirenhed et al. 2007; Wetmore et al. 2014). Additionally, recent work in rabbits has begun drawing confirmative cross-correlations between the kinematic profile of eyelid behavior and simple spike activity in awake rabbits (Halverson et al., 2015).

The simple spike suppression observed in eyelid-related Purkinje cells seems in good agreement with the classical hypothesis dominating the synaptic level of cerebellar learning theory. Long-term depression (LTD) occurs at parallel fiber to Purkinje cell synapses when their activation is linked to climbing fiber activation (Ito et al., 1982; Coesmans et al., 2004; Gao et al., 2012). This plasticity mechanism is posited to constitute learning by suppressing simple spike firing in Purkinje cells, which in turn disinhibits the cerebellar nuclei, increasing cerebellar output (Marr,
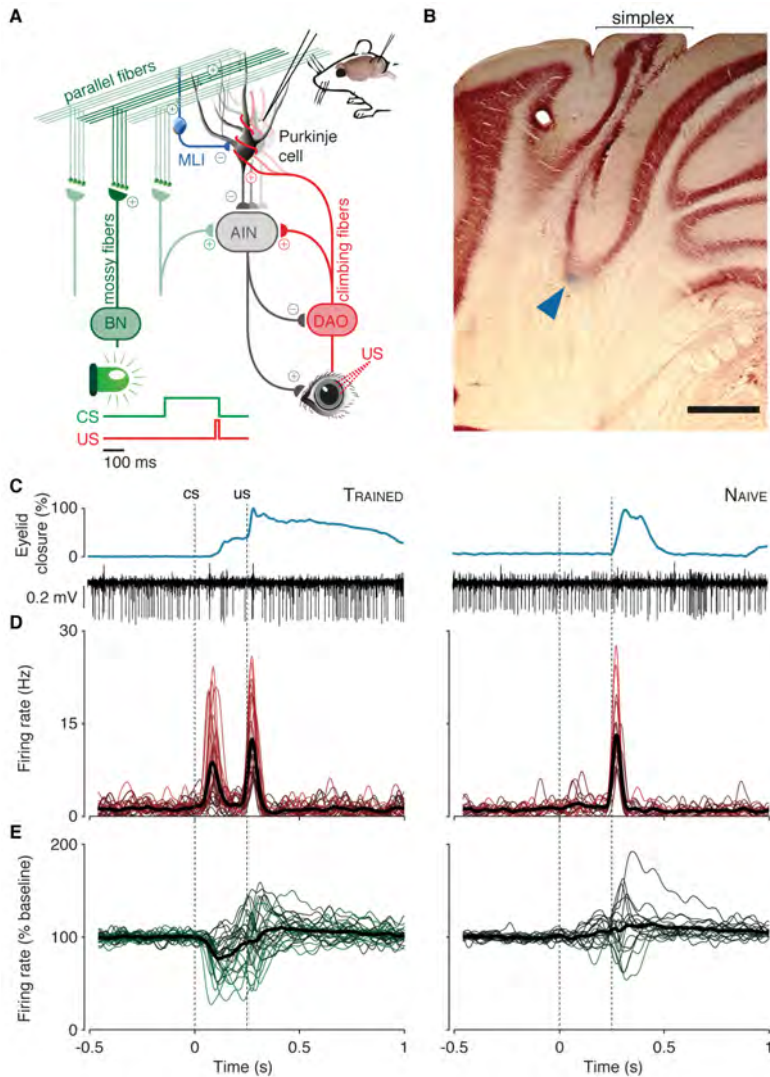
Figure 1 Purkinje cell characterization. (A) Purkinje cells in lobule HVI (zones C1/C3/D0) receive input from mossy fibers and climbing fibers, which carry CS and US signals, respectively. Simple spike suppression disinhibits the anterior interposed nuclei (AIN) which then drive CRs. Paired trials consisted of a 260 ms LED light CS, co-terminating with a 10 ms corneal air puff. **(B)** Coronal cerebellar section at -5.8 mm from bregma, blue arrow indicating staining of a typical extracellular recording site. The scale bar denotes 500 μm. **(C)** Example eyelid and Purkinje cell traces for eyelid-related cells in trained animals (left column, n = 28) and in naive animals (right column, n = 17). **(D)** Spike density functions of complex spikes for individual cells (strength of modulation relates to color brightness) and the mean for each set (thick black line). **(E)** Same, for simple spike density functions. *BN: brainstem nuclei; DAO: dorsal accessory olive; HVI: hemispheric lobule VI; MLI: molecular layer interneurons.*

1969; Albus 1971; Ito, 2001). However, LTD seems neither necessary nor sufficient for eyeblink conditioning, as selective genetic or pharmacological blockage of parallel fiber to Purkinje cell LTD expression does not significantly impair eyeblink conditioning (Welsh et al., 2005; Schonewille et al., 2011) and short interstimulus intervals (ISIs) increase rather than decrease simple spike firing, while presumably preserving LTD induction (Wetmore et al., 2008; Wetmore et al., 2014). In addition to Purkinje cells, parallel fiber activity encoding the CS reaches molecular layer interneurons (MLIs) through excitatory synapses, which can probably be strengthened through concomitant climbing fiber activity and thereby in principle contribute to eyeblink conditioning (Gao et al., 2012). However, having shown that conditioned Purkinje cell simple spike suppression seems to persist after blocking cerebellar cortical feed forward synaptic inhibition provided by MLIs, Hesslow and colleagues are now homing in on potential mechanisms intrinsic to Purkinje cells (Johansson et al., 2014).

In the pursuit of a seamless understanding of Pavlovian conditioning across levels of analysis, we wish to address three considerable gaps that exist in current understanding. First, it remains to be seen how eyelid-related Purkinje cells in awake mice behave within a functional, undamaged brain, as existing work has heavily relied on the decerebrate preparation. Especially complex spike activity may depend to a large degree on circuitry level factors, which are likely different between awake and decerebrated preparations. Second, the potential disqualification of MLIs as a main mechanism underlying Purkinje cell simple spike suppression (Johansson et al., 2014) raises the questions what role they do carry, if and how they modulate in an eyeblink conditioning paradigm, and to what extent their activity correlates with eyelid behavior. Finally, trial-by-trial quantification of simultaneously recorded conditioned eyelid behavior and cerebellar cortical activity in awake behaving animals is lacking so far. To bridge these gaps, we here present simultaneously recorded cerebellar cortical electrophysiology and eyelid behavior from awake behaving mice that were either naive or trained in an eyeblink conditioning paradigm. Additionally, we present behavioral data obtained from two independent transgenic mouse mutants in which MLI inhibition is impaired through different mechanisms (Wulff et al., 2009; Seja et al., 2012).

2   Results

Purkinje cell characterization

Our dataset comprises 57 Purkinje cells, 40 of which were recorded in trained mice, and 17 in mice that were not previously trained. Guided by former studies (Heiney et al., 2014; Mostofi et al., 2010), we centered our recording area on the floor of the primary fissure (Fig. 1B). We considered Purkinje cells to be eyelid-related when they exhibited a complex spike response within 60 ms after the periocular air puff US in at least 20% of paired trials, correcting for chance occurrence. In the trained dataset, this criterion adequately separated 28 cells showing this US-complex spike response (henceforth, Trained cells; Fig. 1C-E; Table 1) from 12 cells that did not (Supp. Fig. 1). The untrained dataset consists of only eyelid-related Purkinje cells (Naïve cells;

Fig. 1C, D) by virtue of meeting the US-complex spike criterion. Note that the latency of the consistent US-complex spike averaged 24.2 ms, but could range as far as 58 ms, which is why we used a 60 ms time range for the criterion. Although we refer to all conforming cells as eyelid-related, the lack of a clear distinction of those showing short-latency US-complex spikes and those exhibiting longer ones, presumably due to our use of an air puff US instead of electrical stimulation, means our dataset could possibly also contain cells from zone C2, deemed non-essential for eyeblink behavior (Mostofi et al., 2010; Hesslow, 1994; Heiney et al., 2014).

Acquired simple spike suppression and CS-related complex spikes

In line with existing work (e.g. Kotani et al., 2006; Jirenhed, 2007), we found a uniquely strong prevalence of simple spike suppression in the Trained cells (Fig. 1E). In 14 Trained cells, we found a clear prevalence of CS-related complex spike responses at a mean latency of 88.1 ms that occurred in at least 20% of trials (corrected for chance occurrence). One cell showed more than 20% complex spikes in the ISI, but at a much longer latency (189.7 ms; Table 1) and without the characteristically thin distribution found in the other cells (Fig. 1D), and was hence not considered a cell with a CS-complex spike response. In contrast, across the 17 Naive cells, only one cell showed a CS-complex spike response, and this was in a mouse that actually started showing small CRs already during a second experiment. The uniquely high prevalence of simple spike suppression and CS-complex spikes in the Trained group confirms that both phenomena developed over the course of conditioning.

Simple spike suppression correlates with conditioned eyelid behavior

Average significant simple spike suppression ranged from 7 to 42% across 20 Trained cells (mean = 20.5%). Between cells, the average magnitude of suppression did not relate to the average CR amplitude, onset, or prevalence (each p > 0.25) observed during the recordings. However, on a trial-by-trial basis, the percentage simple spike suppression showed clear correlations with conditioned behavior. First, simple spike suppression was on average 22% higher in trials with a CR compared to those without, in a linear mixed-effects regression (p < 0.0001; Supp. Table 1A; see Exp. Procedures). Moreover, simple spike suppression correlated to CR amplitude on a trial-by-trial basis, as apparent from eight individually significant Trained cells (Fig. 2B; Table 1), as well as a similar mixed-effects model with random intercepts and slopes for each cell (p < 0.0001; Fig. 2A; Supp. Table 1B; see Exp. Procedures), which estimated an increase in CR amplitude of 0.33 percentage points per unit increase of percentage simple spike suppression. This coefficient was 0.72 when just including the eight individually significant Trained cells. Post-hoc power analyses confirmed high statistical power for these and subsequent mixed models (Supp. Table 1). The incorporation of individual slopes per cell in the mixed model was based on likelihood ratio tests and implies that certain cells showed suppression across a large range but predicted rather small differences in CR amplitude, whereas others only mildly suppressed but predicted a large range of CR amplitudes. Even considering the possible inclusion of non-essential (C2) Purkinje cells in the dataset, this variation

was as apparent among just the most clearly correlating cells (Fig. 2B). Together with the lack of correlation between the averages, this observation juxtaposes the clear correlation between simple spike suppression and CR amplitude with a probable dissociation between their average magnitudes.

Having determined significant correlation between simple spike firing and CR expression, we next explored its temporal distribution across the ISI with the following descriptive methodology. Trial-by-trial correlations of concomitant mean instantaneous simple spike firing frequency and eyelid position in 20 ms windows were made with 5 ms steps, resulting in the diagonal elements denoting r-values in Fig. 2D. Next, we correlated simple spike activity with eyelid position at both earlier and later time-points, resulting in the lower and upper triangular parts of a correlation matrix (Fig. 2D, Supp. Fig. 2). This matrix shows for each temporal configuration the average negative correlation of 11 Trained cells that showed clear focal areas in the upper triangular part of the ISI range, i.e. negative correlations within the ISI between simple spike firing frequency and subsequent eyelid position (see Exp. Procedures; Supp. Fig. 2). Two observations stand out in this analysis. First, taking the net negative correlation within the ISI at each offset between spikes and behavior revealed that simple spike activity correlates most optimally to eyelid behavior 50 ms afterward. Second, there seem to be two focal areas of negative correlation shared between the 11 cells. While the diagonal area at the end of the ISI is completely in line with expectations, the distinct focal area at the 100 ms mark is more surprising. It is positioned right around the time the CS-complex spike happens to occur, and its vertical orientation suggests a relatively short (40 ms) window of reduced simple spike activity predicting the majority of the CR trajectory. The mean simple spike and eyelid traces for seven cells that showed these early focal areas (red) and four cells that did not (green) show latencies are in compelling agreement with this distinction (Fig. 2C,E). Although not significant cell-wise (n = 11, p = 0.35), the prevalence of CS-complex spikes was higher in the cells that showed early focal areas (median = 45.2%) than in those that did not (median = 22.4%).

CS-Complex spikes correlate with simple spike suppression and conditioned eyelid behavior

The occurrence of CS-complex spikes correlated to that of US-complex spikes between cells (n = 28, r = 0.57, p = 0.0015) and marginally to US-complex spike latency (r = -0.384, p = 0.0437). Among Trained cells, mean percentage simple spike suppression was intimately connected to the prevalence of CS-complex spikes (n = 28, r = 0.804, p < 0.0001; Fig. 3A). Additionally, a between-trial mixed-effects linear regression shows that suppression is on average 19.2% higher in trials with a CS-complex spike compared to those without (p < .0001; Supp. Table 1C). This translates to 9.2 ms of silence, a boost that could be sufficiently explained by the climbing fiber pause (mean: 16.5 ms).

As was the case with simple spike suppression, neither average CS-complex spike occurrence nor its average latency showed between-cell correlations to average CR properties (each p > 0.25), except for a small correlation between mean CS-complex spike latency and mean CR onset (n = 14, r = 0.567, p = 0.0346). However, on a

Table 1. Summary of Trained Purkinje Cell Recordings

Cell #	Simple spike frequency (Hz)	Complex spike frequency (Hz)	% CRs	Mean CR onset (ms)	Mean CR amplitude (%)	# Valid Trials	% Ssp suppression in last 200 ms ISI / baseline	SSp x CR amplitude r-value	% US-complex spikes (corrected)	Mean US-complex spike latency (ms)	% CS-complex spikes in ISI (corrected)	Mean CS-complex spike latency (ms)
1	62.5	1.08	91.3	134	26.9	23	11.6**	0.086	23.9	33.0	12.1	-
2	97.6	1.24	92.3	99.6	29.1	26	-3.5	0.031	23.3	41.0	15.2	-
3	78.9	1.11	89.5	154.6	48.4	39	5.8**	0.250	22.3	31.0	14.3	-
4	78.5	1.76	94.4	115.0	44.4	18	-2.2	0.029	22.7	30.0	-16.3	-
5	162.8	1.79	68.2	170.2	31.9	22	-1.3	0.060	89.2	13.0	9.7	102.3
6	69.3	1.69	46.2	159.4	30.9	26	3.7	-0.345	74.5	10.0	23.1	-
7	89.4	1.06	45.7	182.1	35.2	35	7.1**	-0.172	36.5	28.0	5.0	-
8	61.9	1.98	28.6	169.1	44.4	49	1.9	0.309	20.8	41.0	-0.6	-
9	95.8	1.40	47.5	171.8	36.2	40	18.4**	-0.218	69.1	13.0	54.9	96.3
10	78.3	1.60	71.4	171.6	37.4	42	19.1**	0.240	52.3	15.0	50.5	90.1
11	108.2	1.28	43.4	172.7	34.6	76	42.4**	0.348*	42.3	14.0	45.6	103.8
12	114.2	1.22	97.4	101.8	51.5	39	5.0*	-0.303	26.0	16.0	18.3	-
13	107.7	1.39	100.0	121.3	50.8	51	31.1**	0.444**	32.8	14.0	39.7	94.0
14	84.0	1.02	100.0	117.2	52.3	33	31.4**	0.065	27.2	20.0	29.1	(189.7)
15	146.7	0.71	76.5	94.0	62.1	17	12.0**	0.146	25.2	24.0	5.9	-
16	127.7	0.43	71.4	129.3	60.2	14	21.3**	-0.123	54.6	12.0	32.1	74.7
17	115.7	1.55	65.2	110.6	48.9	23	26.5**	0.073	77.7	25.0	52.7	67.8
18	130.7	0.84	92.9	87.6	58.7	14	30.0**	0.113	52.1	23.0	57.6	73.7
19	113.6	1.52	50.0	97.6	29.3	16	18.7**	0.093	65.9	18.0	49.4	71.1
20	85.2	1.69	94.7	130.8	50.1	19	14.1**	0.624**	26.7	58.0	15.6	97.6
21	104.2	1.41	40.0	157.3	26.9	50	8.9**	0.024	65.5	17.0	30.6	104.1
22	87.3	1.33	54.2	165.9	51.5	24	8.6**	-0.178	54.5	16.0	20.8	93.7
23	44.2	1.49	69.2	47.2	50.3	39	32.6**	0.626**	42.4	33.0	60.3	81.8
24	129.8	1.45	96.4	61.2	49.0	28	15.0**	0.415*	27.0	26.0	20.9	82.9
25	65.1	1.14	92.9	82.1	25.6	84	32.1**	0.451**	69.3	19.0	64.3	-
26	101.6	1.00	85.3	76.5	32.8	34	1.9	0.582***	20.6	20.0	-7.4	-
27	104.3	1.10	90.0	106.6	44.7	71	9.3**	0.410**	27.8	36.0	-0.1	-
28	62.3	1.50	43.9	113.3	22.9	23	3.0	-0.065	35.4	30.9	1.2	-
Mean	96.7	1.3	72.8	125	41.7	34.8	14.4	0.143	43.1	24.2	25.2	88.1

$* p < 0.05$, $** p < 0.01$
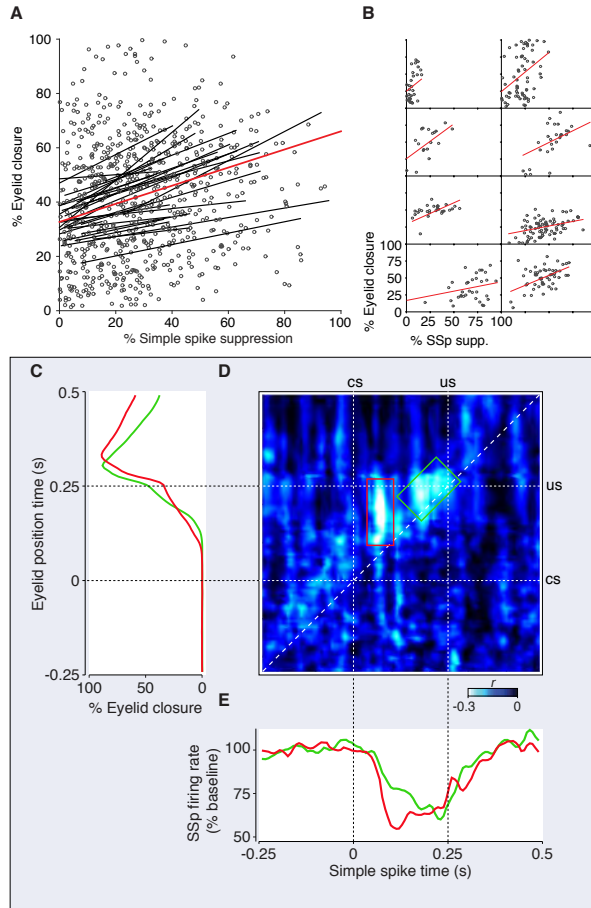
Figure 2 Simple spike suppression relates to CR expression. (A) Fit lines based on a linear mixed-effects regression, with random slopes and intercepts for each individual Trained cell and the red line showing the full model fit. Each circle denotes a trial. **(B)** Separated plots for eight Trained cells that individually showed significant correlation between simple spike suppression and CR peak amplitude. **(C)** Mean eyelid traces, rotated 90ř to fit the y-axis of the correlation matrix in D. Red corresponds to seven Trained cells showing correlation at the early focal area bound with a red box in D, green corresponds to four Trained cells that correlated most in the later focal area. **(D)** Averaged correlation matrix of 11 Trained cells, detailing the temporal distribution of the negative correlation between simple spike activity and conditioned behavior. The two focal areas within the ISI indicated by the red and green boxes show the early and late spiking periods that correlate most prominently to subsequent eyelid behavior. **(E)** Simple spike density functions for the same seven and four cells relating to the focal areas in the red and green boxes in D, respectively.

trial-by-trial basis, mixed-effects regression on the 14 cells with a clear CS-complex spike did show that CRs in trials with a CS-complex spike were on average 13.7% higher in amplitude than those without (p = 0.0194; Fig. 3B; Supp. Table 1D). Also, in a similar mixed model, CR amplitude related inversely to CS-complex spike latency,

with an average decrease in percentage eyelid closure of 0.26 percentage-points per ms increase of CS-complex spike latency (p = 0.0034; Supp. Table 1E). Conversely, CS-complex spike latency was 4.9 ms earlier in trials with a CR compared to those without (p < 0.0001; Fig. 3C; Supp. Table 1F). Together, these mild effects imply a modest contribution of CS-complex spikes to conditioned behavior on a trial-by-trial basis. The significance of the link between CS-complex spike occurrence and CR amplitude disappears when including simple spike suppression in the regression model (p = 0.16; Supp. Table 1G). This raises the possibility that CS-complex spikes affect conditioned behavior in part through their effect on simple spike suppression. Still, CS-complex spike latency retains some significance as a predictor of CR amplitude, even when including simple spikes in the model (p = 0.0083; Supp. Table 1H). This raises the possibility that climbing fiber signals and/or that of their collaterals in the nuclei directly contribute to the conditioned motor response.
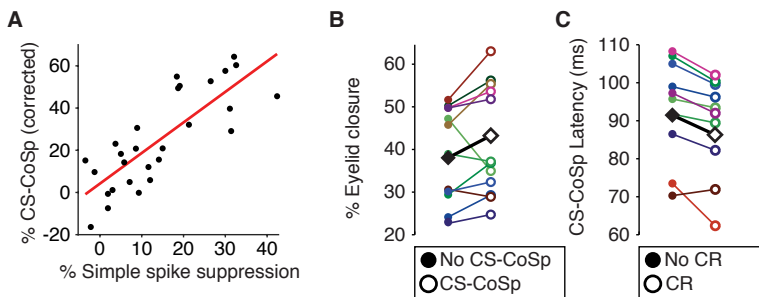
Figure 3 CS- and US-related complex spikes relate to CR expression. (A) Between Trained cells, the prevalence of CS-complex spikes correlated strongly to average percentage simple spike suppression (n = 28, r = 0.803, p < 0.0001). **(B)** Trials with CS-complex spikes tend to exhibit higher CR amplitudes compared to those without. The black squares indicate the overall estimate from the mixed model (p = 0.0194). **(C)** Conversely, latencies of CS-complex spikes for individual cells show that they tend to appear earlier in trials with a CR compared to those without (p < 0.0001).

Molecular layer interneuron activity correlates with conditioned eyelid behavior

Recent findings showed conditioned simple spike suppression in the absence of MLI feed forward inhibition by GABAergic neurotransmission (Johansson et al., 2014). Yet, the existence of conditioned CS-related complex spike responses reported here raises the possibility of conditioned CS-related MLI activation, either through glutamate-spillover (Jorntell & Ekerot, 2003; Szapiro & Barbour, 2007) or ephaptic inhibition (Blot & Barbour, 2014). During the current experiments we recorded a set of 13 interneurons in the molecular layer (see Exp. Procedures; Ruigrok et al. 2011; Badura et al., 2013), all of which showed significant increases in their firing frequency in the ISI (Fig. 4A, B, Supp. Table 2). Cell-wise, mean onset of modulation correlated with the mean CR onset (n = 13, r = 0.582, p = 0.03675). Within the dataset, six MLIs individually showed

significant positive trial-by-trial correlations between firing frequency in the ISI and CR amplitude; two cells showed significant negative correlations to CR amplitude (despite an overall increase in firing frequency in the ISI; Supp. Table 2). In one case, we were able to record a block of paired trials during the recording of an MLI immediately adjacent to a Purkinje cell from which we also recorded a block of paired trials. The latencies of the modulation of these cells were complementary (Fig. 4C), as were their correlations to behavior (Fig. 4D). Using the same correlation matrix approach explained above, the six positively correlating MLIs showed focal areas that complement those found in the Purkinje cell simple spike correlation matrix (Fig. 2D), with a diagonal area focused near the end of the ISI and centered at an offset of approximately 50 ms between spikes and subsequent eyelid position, and again an early vertically oriented focal area. Here too, mean spike and eyelid traces for cells split on whether they showed this early focal area or not were in line with this distinction (Fig. 4E). The two negatively correlating MLIs showed only a focal area near the end of the ISI (Fig. 4F).

To investigate whether impairments in MLI function actually leads to any behavioral deficits, we subjected two independent cell-specific mouse lines, in which MLI function is impaired via a completely different strategy, to behavioral eyeblink conditioning; these included the L7-$\Delta\gamma$2 mouse mutant, which lacks the $\Delta\gamma$2-subunit of the GABAA receptor in Purkinje cells (Wulff et al., 2009), and the L7-KCC2 mouse mutant, which lacks the potassium-chloride co-transporter KCC2 in Purkinje cells (Seja et al., 2012). In line with our expectations, and despite potential developmental compensation, deficits in conditioned eyelid responses were found in both the L7-$\Delta\gamma$2 (p = 0.0039, Fig. 4G) and L7-KCC2 (p = 0.0029, Fig. 4H) mutants. Together with the fact that MLIs modulate in the ISI and even strongly correlate to behavior, these behavioral findings in two different knock out lines assert partial involvement of MLIs in the establishment of conditioned eyeblink behavior.

Figure 4 MLIs modulate in the ISI and correlate to CRs. (A) Example eyelid and electrophysiology trace during a paired trial while recording a molecular layer interneuron (MLI). **(B)** Spike density functions (SDFs), standardized to baseline, for 13 MLIs (thick black line denotes mean trace). **(C)** Overlay of the SDFs of a Purkinje cell recording (green) and an MLI recording (blue) adjacent to it, encountered immediately afterward. **(D)** The activity of the MLI and Purkinje cell in panel C show opposite significant correlations to CR peak amplitude (n = 17, r = 0.734, p = 0.0007; n = 28, r = -0.498, p = 0.0071, respectively). **(E)** Correlation matrix derived from combined standardized data of six MLIs showing significant positive correlations within the ISI, distributed across two focal areas similar to the matrix for simple spikes (Fig. 2D), with mean eyelid traces (left panel) and spike traces (bottom panel) corresponding to four cells that showed the early focal area (green box) and two that did not (purple box). **(F)** Correlation matrix that shows the temporal distribution of the negative correlations found in two interneurons, similarly accompanied by mean eyelid spike trace. **(G)** Learning curves for L7-KCC2 mutants (red, n = 9) and wild-type littermates (blue, n = 13) were computed by taking the average percentage eyelid closure right at US onset time for all trials (100 per session). Error bars denote standard error of the mean. **(H)** Learning curves, similarly computed, for L7-$\Delta\gamma$2 mutants (red, n = 14) and wild-type littermates (blue, n = 11). Percentages of eyelid closures in G and H were normalized for comparison across the mutant groups, which were derived from different backgrounds (Wulff et al., 2009; Seja et al., 2012).
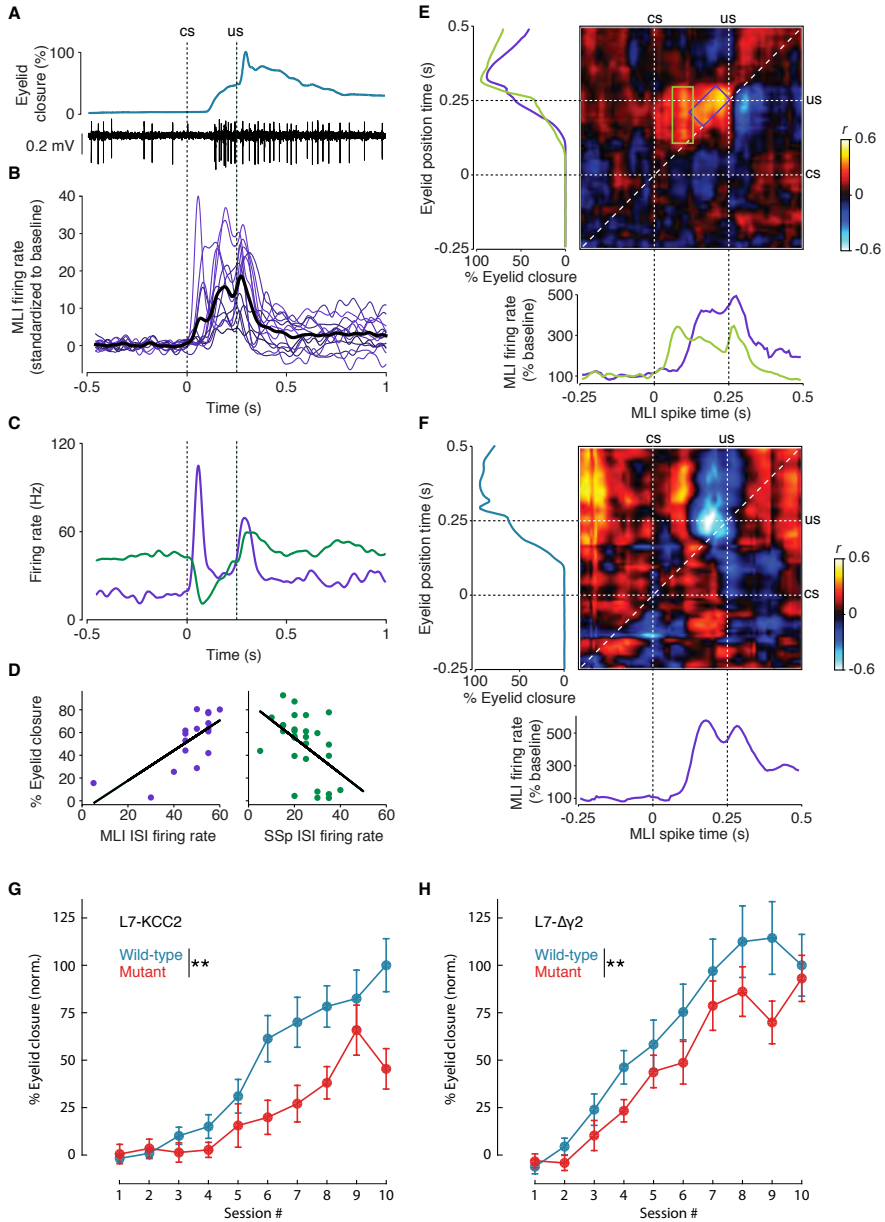
3 Discussion

This work brings together electrophysiological data of Purkinje cells selected strictly based on the presence of consistent US-complex spike responses with precise behavioral recordings in an eyeblink conditioning paradigm employing awake behaving mice. In addition to strengthening the notion that the modulation observed in eyelid-related Purkinje cells is acquired and overwhelmingly suppressive, the current data expands on this finding by providing trial-by-trial quantification of the correlations between cellular spiking activity and eyelid behavior (Fig. 5A, B). Across trials, Purkinje cell simple spike suppression correlates the strongest to conditioned eyelid behavior occurring 50 ms afterward. Importantly, we show the existence of a consistent CS-related complex spike response within the ISI, at an average of 88 ms after CS onset, that appears to be acquired and can be related to simple spike suppression and the behavioral CR. Finally, we provide evidence that there are MLIs in lobule simplex that increase their firing in the ISI and show mainly positive correlations to the amplitude of conditioned eyelid behavior, and that genetically impairing their inhibitory effect on Purkinje cells causes behavioral deficits in conditioning.

Conditioned modulations of Purkinje cell activity and eyelid behavior

The current within-trial correlational data provide direct evidence for the intimate link between conditioned Purkinje cell simple spike suppression and behavioral CR expression. Taken together with the compelling similarities observed between the ways these neuronal and behavioral CRs are generally acquired, expressed, extinguished, and reacquired (Jirenhed et al., 2007; Wetmore et al., 2014; De Zeeuw and Ten Brinke, 2015) as well as the fact that suppression of Purkinje cell simple spikes through optogenetic stimulation of MLIs in lobule simplex can effectively elicit blink responses (Heiney et al., 2014), the inference of causality between Purkinje cell CRs and behavioral CRs is becoming increasingly unavoidable. We propose to expand this relationship to include the CS-related complex spike, a phenomenon mentioned as early as in Berthier and Moore (1986; Edgley et al., 2010). Its virtual absence in naive animals suggests that it is acquired, its latency relative to the other cerebellar cortical components and conditioned eyelid behavior fits a potentially facilitating role, and its significant correlations to both eyelid behavior and simple spike suppression further support this possibility (Fig. 5). This finding is important, because acquired climbing fiber activity within the ISI emphasizes the need to consider interplay within the broader network of olivocerebellar modules in the creation of conditioned motor responses. Indeed, the relatively mild, yet significant and positive, correlations found for Trained cells on a trial-by-trial basis between CS-complex spike responses and conditioned behavior presumably present an underestimation of the actual contribution of CS-complex spikes to conditioned behavior, because the encoding of CS responses of ensembles of Purkinje cells within functional microzones usually surpasses that of individual Purkinje cells within such zones by far (Hoogland et al., 2015). The observed level of integration within the established model of cerebellar Pavlovian conditioning is also why we consider these CS-complex spike responses to be qualitatively different from the type reported in Rasmussen et al. (2014), who mention its

presence in their training paradigm in decerebrate ferrets from the naive state on out, at predominantly 10-20 ms latencies, rather than the 70-100 ms latencies we observe in awake behaving mice.
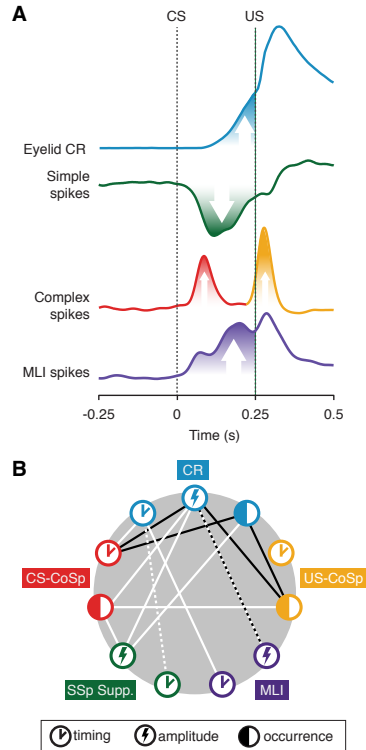
Figure 5 Cerebellar cortical activity and conditioned eyelid behavior: modulation and correlation. (A) Mean eyelid, simple spike and complex spike traces of all cells in the Trained dataset, and mean MLI spike trace of all cells in the MLI dataset, showing how the modulatory components in the cerebellar cortex relate after training. **(B)** Diagram depicting for each of the components in A the significant correlations existing between their different properties (timing, amplitude, and occurrence). White lines denote positive correlations, black lines denote negative ones. Note that the lack of connections between MLI and PC-related nodes reflects the fact that we did not record simultaneously from these types of neurons, rather than a lack of correlation between their properties. The white line connecting simple spike timing to CR timing is dashed because we could not reliably quantify onset of simple spike suppression on a per trial basis to enable robust statistical testing. We would have been remiss not to make some connection, since the correlation matrix does show a clear temporal link between the two components.

Long US-complex spike latencies did not relate to less modulation or correlation

Purkinje cells with long latency US-complex spikes should be regarded with caution, in light of the findings by Mostofi et al. (2010), who showed in rabbits that these cells

mainly originate in zone C2, which responds to more than just periocular stimulation and is unlikely to play an essential role in eyeblink conditioning (e.g. Yeo & Hesslow, 1998). In our recordings we were not able to find relevant differences based on US-complex spike latency with respect to the extent of simple spike suppression and its correlation to behavior, or the occurrence of CS-complex spikes. Our air puff US may well be responsible for an exaggerated length and spread of latencies compared to electrical periocular stimulation, obfuscating a clear distinction between the two latency groups. The resultant possibility of the inclusion of C2 cells in our dataset warrants caution with inferences regarding effect size and spread. This is also true for cells that could respond to any non-eyelid-related parts of the US, improbable as it may be. However, given the compelling correlations found, it seems unlikely we here misattribute the reported positive links with eyeblink conditioning to actual eyeblink cells from zones C1/C3/D0 while they actually correspond to non-essential C2 cells, let alone to cells that are not at all eyelid-related.

Temporal dynamics argue against a single mechanism underlying cerebellar conditioning

The temporal dynamics observed between spike activity of cerebellar cortical neurons and eyelid behavior do not suggest a single focal area around which the cells'optimal correlations are dispersed. It is clear that the acquired simple spike suppression does not only gradually deepen to maximize around US onset time. In fact, the current results hint at the possibility that there is also a particular process whose crucial window of action in the ISI is earlier on, centered around 80-100 ms after CS onset. The clear separation of these two focal areas in both the simple spike and MLI activity correlation matrix could imply differential contribution of plasticity mechanisms in cerebellar conditioning. This is certainly a plausible concept considering the variability observed in conditioned eyelid behavior in mice. Interestingly, the occurrence of CS-complex spikes strikingly overlaps with the early, but not the later, focal area in the correlation matrix, imparting this time window with remarkable significance. It is difficult to accommodate for this with a purely LTD-focused hypothesis or the notion of intrinsic plasticity at the level of single Purkinje cells. Why would an isolated time window early in the ISI show both a consistent complex spike response and particularly strong correlations between conditioned eyelid behavior and both simple spike and MLI activity?

The presence of the CS-complex spike means the CS-encoding signal has acquired the means to reach the olivary nucleus. Insofar as the eyeblink paradigm used here contains an operant component in that the CR response can reduce the aversive impact of the air puff US (Longley & Yeo, 2014), cerebral cortical involvement might possibly be involved. In any case, the strong Purkinje cell-wise link between the occurrence of CS-complex spikes and the magnitude of simple spike suppression suggests interdependent plasticity mechanisms underlying both phenomena. An interesting possibility is that loops within the olivocerebellar network could play a role. The origin of the CS-complex spike could lie in the mossy fiber collaterals to the cerebellar nuclei that are newly formed over the course of conditioning (Boele et al., 2013), which could establish a straightforward bridge to cross for CS-encoding

signals to directly hook up to the nucleo-olivary pathway (De Zeeuw et al., 1988). The resulting CS-activated olivary inhibition could then bear rebound spikes (Bazzigaluppi et al., 2012; De Gruijl et al., 2012) that return to the cerebellum to affect cortical activity in a number of ways. It could influence simple spike suppression through the climbing fiber pause (De Zeeuw et al., 2011), through non-synaptic activation of MLIs (Jorntell & Ekerot, 2003; Szapiro & Barbour, 2007; Mathews et al., 2012) as well as through several climbing fiber dependent forms of cerebellar cortical plasticity (Gao et al., 2012). Besides influencing simple spike suppression, they could play a role in higher-order conditioning, allowing the CS to be associated to novel input stimuli, preserving efficiently the same output pathway to the proper motor domain.

Molecular layer interneurons partially contribute to conditioned behavior

Our MLI data may seem at odds with the Johansson et al. (2014) study, because while the latter chemically dissociates MLI inhibition from the presence of simple spike suppression, we find strong modulation of interneuron spiking as well as correlations with behavioral CRs (Fig. 4,5). However, these findings are not mutually exclusive. The possibility of a partial contribution of MLI activity to simple spike suppression and conditioned behavior seems probable from these different findings. Our behavioral data from two independent mouse mutants with impaired MLI inhibition shows partial deficits, which is much in line with this possibility, as is the feasibility of MLI-activated blinks generated by optogenetic stimulation (Heiney et al., 2014).

Conclusion

The current study evinces the feasibility of simultaneous behavioral and neuronal recordings in awake behaving mice and strengthens the main tenet of cerebellar learning regarding suppressive modulation as a central process underlying learning (De Zeeuw et al., 2011; De Zeeuw and Ten Brinke, 2015). Although there is both theoretical and empirical support for interaction between the modulatory components of cerebellar cortical activity, they do not seem to share any strict interdependency from the perspective of individual Purkinje cells. After all, absence of CS-complex spikes alone does not necessarily prevent simple spike suppression altogether, nor does absence of feed forward inhibition through the MLIs (Johansson et al., 2014). Yet, the current findings in awake behaving mice suggest the involvement of CS-complex spikes and MLI activity in the conditioning paradigm is robust, further lending credence to the notion of distributed synergistic plasticity (Gao et al., 2012). More so, the CS-complex spike extends this notion beyond the cerebellar cortex to include recurrent activity within the whole olivocerebellar module at the level of the ISI. Of course, plasticity mechanisms intrinsic to Purkinje cells, such as those mediated by various mGluRs, phosphatases and kinases may well be a decisive factor in eyeblink conditioning (Gao et al., 2012; Johansson et al., 2014). However, the current results would at least stress caution regarding the inference of unitary localization of a plasticity process underlying conditioned simple spike suppression

within only Purkinje cells. In the same vain, we should also point out that while LTD does not seem to be essential for eyeblink conditioning (Welsh et al., 2005; Schonewille et al., 2011; Wetmore et al., 2014), we cannot exclude the possibility that it still does contribute to the observed simple spike suppression, especially since the direction of its presumptive effect appears to be in line. However, the fact that impairments in potentiation mechanisms at the level of Purkinje cells cause behavioral deficits in eyeblink conditioning (Schonewille et al., 2010) underlines how the role of plasticity mechanisms may not play out as straightforwardly as one would expect. The current results underline the importance of investigating network involvement in the acquisition and expression of Purkinje cell simple spike suppression. Specifically, unearthing the origin and function of CS-related complex spikes could further sophisticate cerebellar models of Pavlovian conditioning, and advance our understanding of the strategies implemented by the brain to achieve learning.

4   Methods

Surgery

We used 12-20 week old male wild-type C57Bl/6 mice (n = 34), L7-$\Delta\gamma$2 (mutants, n = 14; wild-type littermates, n = 11; see Wulff et al., 2009), and L7-KCC2 (mutants, n = 9; wild-type littermates, n = 11; see Seja et al., 2012), housed individually with food and water ad libitum in a normal 12:12 light/dark cycle. The experiments were approved by the institutional animal welfare committee (Erasmus MC, Rotterdam, The Netherlands). Mice were anesthetized with 2% isoflurane and body temperature was kept constant at 37řC. After fixation in a standard mouse stereotaxic alignment system (Stoelting Co., Wood Dale IL, USA), the scalp was opened to expose the skull. Membranous tissue was cleared, and the bone was surgically prepared with Optibond prime and adhesive (Kerr, Bioggio, Switzerland). A small brass pedestal was attached to the skull with Charisma (Heraeus Kulzer, Armonk NY, USA), using an xyz-manipulator, allowing for fixation to a head-bar at right angles during training and electrophysiology. For the craniotomy performed after eyeblink acquisition training, skin and muscle tissue was cleared from the left half of the interparietal bone, where, after applying a local analgesic (bupivacaine hydrochloride 2.5 mg ml-1), a roughly 1.5 mm wide craniotomy centered at -5.7 mm from bregma and 2 mm from midline was performed, exposing the left cerebellar lobule simplex. A small rim of Charisma was made around the craniotomy and anti-inflammatory (Dexamethasone 4 mg ml-1) solution was applied inside, after which the chamber was closed with a very low viscosity silicone elastomer sealant (Kwik-cast, World Precision Instruments, Sarasota FL, USA).

Training

Two days after surgery, mice were head-fixed to a brass bar suspended over a cylindrical treadmill (Chettih et al., 2011) and were placed in a sound- and light-isolating

chamber for their first habituation session, which consisted of 30 minutes during which no stimuli were presented. During a second and third habituation session on consecutive days, 10 CS-only trials were presented to acquire a baseline measurement. The next 10 days, mice received 100 paired trials daily, with an inter-trial interval of 10 ± 2 s, amounting to sessions that lasted approximately half an hour each.

The CS was a 260 ms green LED light, placed 7 cm in front of the mouse. The US was a 10 ms corneal air-puff at 40 psi delivered through a 27.5-gauge needle tip positioned 5-10 mm from the left eye, co-terminating with the CS, which amounts to an interstimulus interval (ISI) of 250 ms. TDT System 3 (Tucker Davis Technologies, Alachua FL, USA) and National Instruments NI-PXI (National Instruments, Austin TX, USA) processors were used to trigger and keep track of stimuli whilst capturing data. Eyelid movements were recorded with either the magnetic distance measurement technique (MDMT) at 1017.26 Hz or a 250-fps camera (scA640-120gc, Basler, Ahrensburg, Germany). Both methods are explained and shown to reflect eyelid movements with high accuracy (Koekkoek et al., 2002).

Electrophysiology

Before proceeding with the neuronal recordings, mice were allowed several days to get used to the electrophysiology setup, which was located in a dedicated room and contained a similar eyeblink apparatus within a light-isolated Faraday cage. During this period, trained mice received daily training sessions consisting of 100 trials for a maximum of four days to ensure at least 75% CRs. Neurons were recorded with glass capillaries (ø = 2 mm, Harvard Apparatus, Holliston MA, USA) that were heated and pulled to obtain a 2-5 μm tip, and filled with a 2M NaCl solution. The electrode was lowered into lobule simplex (Heiney et al., 2014; Van Der Giessen et al., 2008) using a one-axis hydraulic manipulator (MMO-220A, Narishige, Tokyo, Japan). The obtained electrical signal was pre-amplified and digitized at a sampling frequency of 25 kHz using a TDT System 3 electrophysiology workstation. When a recording was stable, the animal was subjected to blocks of paired trials. Purkinje cells were identified by the presence of complex spikes. When we encountered cells that were located no further than 100 μm from Purkinje cells, had relatively low firing rates, and did not show complex spikes, we would record them if they seemed to modulate within the ISI. Offline analysis was used to verify these putative MLIs (see below).

Eyeblink data analysis

For each recording, eyelid traces were normalized to the full blink range, which consisted of the minimal resting baseline value reflecting the open eye position as established visually during the experiment, and the mean of the unconditioned response peak values reflecting the closed eye position. The traces were smoothed using a 2nd degree Savitzky-Golay method. An iterative Grubbs'outlier detection test ($\alpha = 0.05$) on trial baseline standard deviations was used to remove trials that had an unstable baseline. Next, trials were considered to contain a CR when eyelid closure exceeded 10 standard deviations from the baseline mean within the ISI. CR amplitude was quantified as the maximum eyelid position within the ISI relative to

the trial baseline position, expressed as percentage of full blink range. CR onset was determined as the first time point of a continuous positive eyelid velocity leading to up to the fifth percentile of the amplitude from baseline to CR peak.

Spike analysis

Electrophysiological recordings were analyzed in Matlab (The Mathworks, Natick MA, USA) using custom-written code and SpikeTrain (Neurasmus, Rotterdam, The Netherlands). Extracellular waveforms were band-pass filtered at 150-6000 Hz. The spike threshold was set at three SDs below mean signal by default, and for Purkinje cells an additional threshold at three SDs above mean signal ensured that no complex spikes were missed. After thresholding, spike shapes were analyzed, with particular attention paid to the negative spike amplitude, spike width, amplitude of the positive inflection immediately after the spike, frequency components after the spike, and possible spikelet occurrence at specific time points. Complex and simple spike clusters were identifiable for all Purkinje cells by plotting combinations of these spike properties against each other. Manual selections of 75 simple spikes and as many complex spikes served as training sets for multilinear discriminant analysis (MLDA), which was used to label all thresholded spikes as either simple or complex spike on the basis of their spike properties. This approach provides an adequate sort while keeping the clustering procedure tied to real and intuitive variables. Clear 8-15 ms climbing fiber pauses confirmed that the sorted simple and complex spikes belonged to a single Purkinje cell. Spike density functions (SDFs) were computed for all trials by convolving simple and complex spike occurrences across 1 ms bins with a 41 ms Gaussian kernel (Supp. Fig. 2). After ascertaining whether a cell showed a clear CS-complex spike response (>20% of trials), we considered individual complex spikes to be CS-related if they occurred within the time-range in which the average complex spike SDF was more than 2.5 SDs over baseline activity. For correlational analyses involving simple spikes, the SDFs were normalized so the mean of the 500 ms baseline was 1. The first 50 ms of the ISI were excluded, as neuronal modulation was not expected to occur there (e.g. Jirenhed et al., 2007). For the last 200 ms, simple spike modulation was quantified in individual trials as the total downward or upward deviation from mean baseline, divided by the expected (mean baseline) activity in the same time range. Specifically, the 200 millisecond data points were split into the values under mean baseline (SDFunder) and those that were over (SDFover), with the following calculation resulting in the percentage of suppression and facilitation, respectively: $0.5 \sum 1 - SDF_{under(i)}$ and $0.5(\sum SDF_{over(i)} - 1)$ where i indexes the 200 ISI data points of one trial. Whether a cell modulated significantly was determined by comparing its suppression/facilitation percentages in the ISI to the deviation from baseline that occurred within the baseline itself, which was similarly computed. The non-Purkinje neurons recorded during experiments were identified as MLIs using the same process as described in Badura et al. (2013); we only appraised cells as MLIs if they passed a decision tree that incorporates various firing properties (e.g. Hz, CV, CV2, interspike interval) and is outlined in Ruigrok et al. (2011). For MLIs, the difference between ISI firing rate and baseline firing rate was used to reflect modulation.

Statistics

Significance tests were performed using MATLAB. Pearson correlations were used in all single-cell analyses involving two continuous variables, after both variables were subjected to Grubbs'test for outliers ($\alpha = 0.05$). Single-cell analyses involving one dichotomous and one continuous variable (also tested for outliers) were Wilcoxon rank-sum tests in all correlations except for the ones quantifying modulation in the ISI relative to baseline and the difference in CR amplitude between MLI mutants and wild-types across sessions, which was tested with a Wilcoxon matched-pair signed rank test. For combined analysis of multiple cells, mixed-effects linear regression was performed, with cells and animals as random effects. Visual inspection revealed no obvious deviations from normality and homoscedasticity, and helped identify extreme outliers (never more than four). Likelihood ratio tests were used to determine the appropriate random effects structure, which ended up never to include animal as a random effect. Statistical power of the mixed models was calculated using Post-hoc Monte Carlo simulations. This method takes into account the distribution of the random effects and that of the residuals present in the model, and generates simulated output data based on random sampling from these distributions, using the same sample sizes as in the original model. By reiterating this process 500 times, recording for each instance the p-values of the fixed effects (that were significant in the original model). The ratio of significant p-values indicates the probability of detecting the effect upon replication using a similar model design and similar sample sizes, and averaged 91.9% across the mixed models here presented (Supp. Table 1).

Supplementary Material
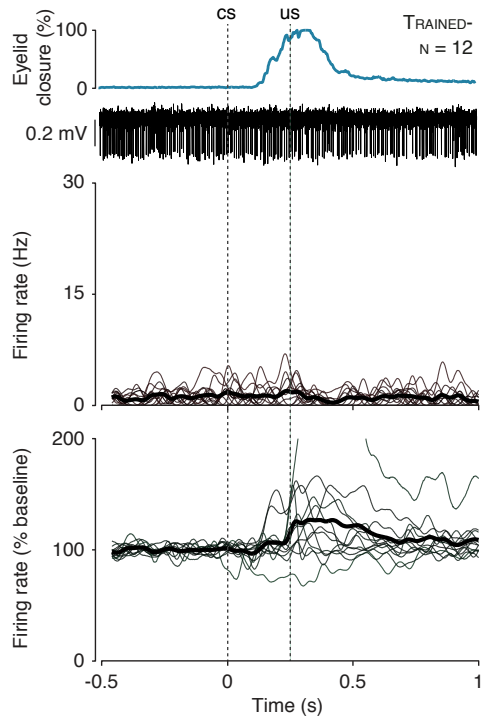
Figure S1 Purkinje cells without US-related complex spikes. Example behavioral and spike trace in the top panel, complex spike density functions for twelve Purkinje cells in the middle panel, simple spike density functions in the bottom panel. These cells did not show US-complex spike responses and were recorded in trained mice. Seven cells showed no significant simple spike modulation, one showed suppressive modulation, and three showed facilitation in the ISI. This facilitation was not observed in cells with a clear complex spike response to the US.
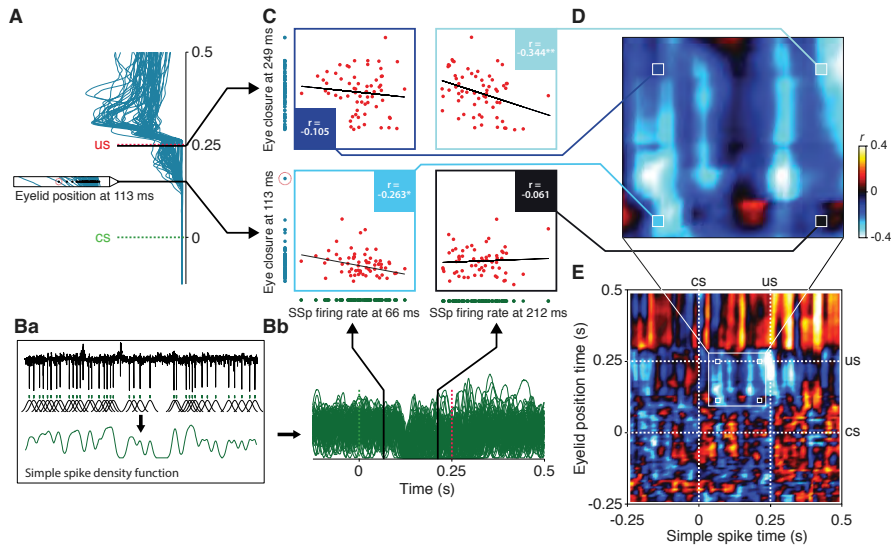
Figure S2 Construction of the simple spike-eyelid position correlation matrix. (A) The y-axis of the eventual correlation matrix, E, denotes the time at which eyelid position data is taken. Here, eyelid traces for one recording are shown, rotated 90ř counterclockwise. In the example at 113 ms after CS onset, the magnified window shows for each trial 10 datapoints, of which the means (black dots, red dashed circle indicates an outlier) are used for a correlation with spike activity. The same approach is taken to get eyelid position data at 249 ms.   **(Ba)** To create a spike density function for each trial, Purkinje cell simple spike timestamps are convolved with a 41 ms wide gaussian kernel, shown overlaid in black. The summated green trace provides a continuous measure of simple spike density. **(Bb)** The x-axis of the eventual correlation matrix, E, denotes the time at which simple spike activity is taken. Here, spike density traces for all trials of the same recording as in A are shown. Using the same approach outlined in A, 10-datapoint means are extracted for each trial at two example locations, here 66 and 212 ms after CS onset. **(C)** Between-trial correlations of eyelid position and simple spike activity data extracted at the example timepoints. Simple spike activity at 66 ms correlates more strongly to eyelid position at 113 ms, than at 249 ms. Conversely, spike activity at 212 ms relates better to eyelid position at 249 ms than at 113 ms. If these correlations were done across different recordings, their trial data would be standardized before combining them. **(D)** The r-values for each of the example correlations translate to a color and find their way into the correlation matrix at the appropriate time points on the x- (spike) and y- (eyelid position) axis. **(E)** The resultant full correlation matrix shows the temporal dynamics of the correlation between simple spike activity and eyelid position. The current cell shows negative correlation throughout the ISI, with a minor early focal point, and a major late focal point.

Supplementary Table 1. Summary of linear mixed-effects models, Related to Experimental Procedures.

A. For outcome variable **% Simple spike suppression** with random intercepts for **Purkinje cell ID**:

Fixed effect	Coefficient	F-test	P	Power*
Intercept	22.39 ± 2.53	$F_{1,972} = 78.03$	<0.0001	-
CR (yes/no)	4.4 ± 1.14	$F_{1,972} = 14.87$	0.00012	96.4%

B. For outcome variable **CR amplitude (% eyelid closure)** with random intercepts and slopes for **Purkinje cell ID**:

Fixed effect	Coefficient	F-test	P	Power
Intercept	32.69 ± 2.47	$F_{1,699} = 174.51$	<0.0001	-
% Simple spike suppression	0.334 ± 0.084	$F_{1,699} = 15.82$	<0.0001	99%

C. For outcome variable **% Simple spike suppression** with random intercepts for **Purkinje cell ID**:

Fixed effect	Coefficient	F-test	P	Power
Intercept	23.78 ± 2.3	$F_{1,972} = 107.3$	<0.0001	-
CS-Complex spike (yes/no)	4.57 ± 1.14	$F_{1,972} = 16.2$	<0.0001	86.2%

D. For outcome variable **CR amplitude (% eyelid closure)** with random intercepts for **Purkinje cell ID**:

Fixed effect	Coefficient	F-test	P	Power
Intercept	37.98 ± 3.33	$F_{1,352} = 130.04$	<0.0001	-
CS-Complex spike (yes/no)	5.20 ± 2.22	$F_{1,352} = 5.52$	0.0194	83.8%

E. For outcome variable **CR amplitude (% eyelid closure)** with random intercepts for **Purkinje cell ID**:

Fixed effect	Coefficient	F-test	P	Power
Intercept	65.28 ± 8.82	$F_{1,245} = 61.09$	<0.0001	-
CS-Complex spike latency (ms)	-0.26 ± 0.10	$F_{1,245} = 8.74$	0.0034	93.8%

F. For outcome variable **CS-Complex spike latency (ms)** with random intercepts for **Purkinje cell ID**:

Fixed effect	Coefficient	F-test	P	Power
Intercept	91.47 ± 3.31	$F_{1,345} = 764.35$	<0.0001	-
CR (yes/no)	-5.16 ± 1.29	$F_{1,345} = 15.99$	<0.0001	98.2%

G. For outcome variable **CR amplitude (% eyelid closure)** with random intercepts for **Purkinje cell ID**:

Fixed effect	Coefficient	F-test	P	Power
Intercept	29.24 ± 3.79	$F_{1,351} = 59.69$	<0.0001	-
% Simple spike suppression	0.29 ± 0.06	$F_{1,351} = 24.48$	<0.0001	99.8%
CS-Complex spike (yes/no)	3.08 ± 2.19	$F_{1,351} = 1.98$	0.1604	-

H. For outcome variable **CR amplitude (% eyelid closure)** with random intercepts for **Purkinje cell ID**:

Fixed effect	Coefficient	F-test	P	Power
Intercept	55.02 ± 8.8	$F_{1,246} = 38.83$	<0.0001	-
% Simple spike suppression	0.24 ± 0.07	$F_{1,246} = 12.94$	0.0004	94.6%
CS-Complex spike latency (ms)	-0.24 ± 0.09	$F_{1,246} = 7.65$	0.0061	79.4%

Cell #	Hz	CV	CV2	# Valid Trials	Mean CR amplitude (%)	Mean CR onset (ms)	% CRs	% Spike facilitation in ISI	ISI Spikes x CR amplitude r-value
1	6.6	0.69	0.66	25	68.1	105.6	88	673**	0.29
2	23.2	0.84	0.31	34	46.1	82.8	97.1	104**	-0.59***
3	17.8	0.84	0.58	8	53.5	91.3	100	78**	-0.24
4	8.4	0.74	0.62	10	30.7	104	100	233**	0.19
5	7.9	1.52	0.91	85	58.6	127.5	95.3	175**	0.34**
6	36.8	1.53	1.00	17	61.9	83.7	94.1	279**	0.73**
7	11.4	1.26	0.65	28	58.3	99.5	96.4	894**	-0.55**
8	26.3	0.82	0.53	15	65.6	98.2	100	192**	0.47
9	8.5	1.45	0.99	15	74.8	96.6	100	1048**	0.12
10	24.5	0.89	0.41	29	53.2	57.1	93.1	174**	0.73**
11	20.9	0.69	0.61	73	33.6	149.4	34.2	98**	0.41*
12	22.0	0.70	0.58	40	32.5	85.2	87.5	79**	0.63*
13	41.8	1.37	0.76	47	25.3	94.2	78.7	150**	0.40***
Mean	19.7	1.03	0.66	33	50.3	98.1	89.6	321.3	0.23

Supplementary Table 2. Summary of MLI Recordings, Related to Figure 4.

* p < 0.05 ** p < 0.005; *** p < 0.001

Chapter 3

More than the sum of its parts: concurrent disruption of parallel fiber to Purkinje cell long-term depression and molecular layer interneuron to Purkinje cell inhibition severely impairs cerebellar learning

Learning is associated with changes in neural activity. The neural correlate of Pavlovian eyeblink conditioning, which models cerebellar learning, involves a temporary suppression of Purkinje cell simple spike firing leading to a precisely timed eye blink. Two potential mechanisms underlying this simple spike suppression include long-term depression of the parallel fiber to Purkinje cell synapse (PF-PC LTD) and feed-forward inhibition provided by the molecular layer interneurons to the Purkinje cell (MLI-PC inhibition). Here we show that only a concurrent disruption of PF-PC LTD and MLI-PC inhibition severely impairs eyeblink conditioning, whereas elimination of these suppression mechanisms individually results in no learning impairments.

M.M. ten Brinke*, H.J. Boele*, S. Peter*, L. Verdonschot, A.H.C. Ypelaar, Z. Gao, S.K.E. Koekkoek, & C.I. De Zeeuw (Submitted)

Introduction

Motor learning involves the practice-dependent acquisition, adaptation, or extinction of movements. Learning a new motor skill usually requires extensive training, but once acquired, we perform and adapt the motor task quite smoothly ''without thinking''. In our daily life, we simply ignore the dizzying motor complexity of dressing ourselves and tying our shoelaces. In neuroscience, motor learning is often studied using Pavlovian eyeblink conditioning. During this learning task, subjects typically will hear a short beep or see an LED light (conditional stimulus, CS) followed several hundred milliseconds later by an eye puff (unconditional stimulus, US). As a result of repeated CS-US pairings, subjects will eventually learn to close their eye in response to the CS. This newly acquired movement is called the conditioned response (CR) (Fig. 1A). Importantly, the eyelid CR is not simply a reflex blink in response to the CS, but instead a precisely timed eyelid movement. This timing of the eyelid CR is determined by the time interval between CS and US, whereby maximal eyelid closure occurs exactly around the onset of the expected US eye puff. Besides this timing aspect, other fundamental features of more complex motor responses, such as strength and velocity, can be distinguished in the simple blink of an eye (Boele et al., 2015; Freeman & Steinmetz, 2011).

For many species, including humans and mice, it has been well established that during Pavlovian eyeblink conditioning, the memory formation takes place in Purkinje cells (PCs) in precisely defined areas of the cerebellar cortex (Heiney et al. 2014; Hesslow, 2011; Kotani et al., 2006; Mostofi et al., 2010; Steinmetz & Freeman, 2014; Ten Brinke et al., 2015; Thurling et al., 2015) (Fig. 1B). These PCs receive massive sensory inputs from the mossy fiber – parallel fiber system, which transmits signals that can serve as CS, and input from only one climbing fiber (CF), which transmits US signals that serve as a teaching or instructive signal. During the conditioning process, PCs learn to suppress or even completely pause their simple spike firing in response to the CS (Halverson et al., 2015; Jirenhed et al., 2007; Ten Brinke et al., 2015), thereby disinhibiting the cerebellar nuclei, leading to the eyeblink CR.

One of the major challenges for cerebellar scientists now is: How can PCs time their simple spike suppression with such millisecond precision? Most models on eyeblink conditioning assume a critical role for long-term depression of the parallel fiber to Purkinje cell synapse (PF-PC LTD) (Hansel et al., 2016; Hauge et al., 1998; Koekkoek et al. 2003; Mauk & Buonomano, 2004; Medina et al., 2000). However, more recent findings have thrown some doubt upon this hypothesis (Johansson et al., 2015; Hesslow et al., 2013; Schonewille et al., 2011; Welsch et al., 2005) , for instance by showing that mice mutants lacking PF-PC LTD have completely normal eyeblink conditioning (Schonewille et al., 2011). A second contribution to PC simple spike suppression could be provided by the inhibitory molecular layer interneurons (MLIs) (Heiney et al., 2014; Hesslow et al., 2013; Korn & Axelrad, 1980). However, removal of the MLI-PC inhibition only mildly impairs eyeblink conditioning (Johansson et al., 2014; Ten Brinke et al., 2015). Here, we ask the question whether a concurrent disruption of PF-PC LTD *and* MLI-PC inhibition will lead to more severe cerebellar learning deficits. To test this hypothesis, we developed a novel mouse line in which presumably both PF-PC LTD and MLI-PC inhibition are blocked (Fig. 1C). To this end

we crossed *GluR2Δ7* knock-in mice with *L7-Δγ2* mice. *GluR2Δ7* knock-in mice have impaired PF-PC LTD, since they lack the last seven amino acids at the intracellular C-terminus tail, thereby disrupting the interaction of GluR2 with PICK1 and GRIP1/2, in turn disturbing the internalization of AMPA receptors (Steinberg et al., 2006; Xia et al., 2000). *L7-Δγ2* mice have impaired MLI-PC feed forward inhibition, since they have a PC specific (L7) ablation of the γ2 subunit of the GABAa receptors (Wulff et al., 2009; Ten Brinke et al. 2015). Subsequently, we tested the neurophysiological characteristics of this novel mouse line *GluR2Δ7 L7-Δγ2*, both *in vivo* and *in vitro*, and subjected them to a Pavlovian eyeblink conditioning task.

Results

Eyeblink conditioning

Although there were obviously learning differences between the groups, all four showed a significant increase over the 10 acquisition session in both eyeblink CR percentage and eyeblink amplitude (Fig. 1D, E, S Table 1, all p < 0.0001 except for *GluR2Δ7 L7-Δγ2* mice amplitude which was 0.018, all one-way ANOVA). In line with previous findings (Schonewille et al., 2011), *GluR2Δ7* mice, lacking pf-PC LTD, showed normal acquisition of eyelid CRs over the course of 10 days of training. Neither the percentage, nor amplitude, nor timing of eyeblink CRs showed any abnormalities compared to wildtype control litters (Fig. 1 D-F, S Table 1; CR percentage, p = 0.977; Eye closure amplitude, p = 0.989 (RM ANOVA, Tukey HSD post hoc); amplitude at expected US, t (82.3) = -0.335, p = 0.738; latency to CR onset, t (73.3) = 0.97, p = 0.33; latency to CR peak time, t (53.2) = -0.05, p = 0.963; all linear mixed effect model (LMM)). In terms of CR percentage, *L7-Δγ2* mice show virtually normal acquisition (CR percentage p = 0.704 RM ANOVA, Tukey HSD post hoc), however their CRs do not reach the amplitude values of wildtype control mice at the end of training (Fig. 1 D-F, S Table 1, amplitude at expected US, t (80.0) = -2.44, p = 0.017, LMM). Although CR timing visually seems to be more variable, this was not significantly different from wildtype control mice (Fig. 1 D-F, S Table 1, latency to CR onset t (67.8) = -1.72, p = 0.89; latency to CR peak t (49.1) = 1.64, p = 0.107, LMM). In contrast, *GluR2Δ7 L7-Δγ2* mice, where both PF-PC LTD and MLI-PC inhibition are impaired, showed a severe learning deficit in terms of both CR percentage and CR amplitude (Fig. 1 D-F, S Table 1, CR percentage p = 0.002, RM ANOVA, HSD Tukey post hoc; eyelid amplitude at expected US t (80.1) = -3.928, p = 0.0002, LMM). Interestingly, latency to CR onset was also significantly later compared to wildtype controls (t (69.7) = 2.31, p = 0.024, LMM), whereas latency to CR peak time was not (t (52.14) = 0.89, p = 0.377). For none of the groups we could establish a significant difference between the latency to onset and peak time of the unconditioned response to the US, showing that the performance of the blink response is intact and thus the observed learning deficits are not a result of impairments in the eyelid closure.

in vitro electrophysiology

To confirm that *GluR2Δ7 L7-Δγ2* mice indeed lack both PF-PC LTD and MLI-PC inhibition, we first evoked PC EPSCs using PF stimulations of varying intensities (3 to 15 µA) to determine whether normal excitatory transmission was present. The evoked EPSCs resulted in comparable amplitudes between *GluR2Δ7 L7-Δγ2* mice and wildtype controls (Fig. 2B, S Table 2, $F_{(1,10)} = 0.059$, p = 0.8, RM ANOVA) and applying inter-stimulus intervals varying from 50 to 200 ms evoked similar levels of paired-pulse facilitation (Fig. 2C, S Table 2, $F_{(1,16)} = 0.81$, p = 0.38, RM ANOVA) indicating that baseline PF–PC synaptic transmission is unaltered in *GluR2Δ7 L7-Δγ2* mice. We evaluated the inhibitory MLI-PC input by measuring sIPSCs and found that these were practically absent in *GluR2Δ7 L7-Δγ2* mice (Fig. 2D, S Table 2, $F_{(2, 32)} = 11.39$, p=0.0001, ANOVA, Bonferroni post hoc), similar to what previously has been reported for *L7-Δγ2* mice (Wulff et al., 2000). For PF-PC LTD induction, we used a high frequency stimulation of PF in conjunction with CF stimulation, a modified protocol of (Piochon et al., 2014), see method section. Indeed, wildtype control mice showed normal PF-PC LTD (Fig. 2E, S Table 2, $t_{(5)} = -4.28$, p = 0.008, Paired t-test), whereas in *GluR2Δ7 L7-Δγ2* mice PF-PC was not inducible (Fig. 2E, S Table 2, $t_{(5)} = 0.052$, p=0.96, Paired t-test).

Figure 1 Eyeblink conditioning is severely impaired in *GluR2Δ7 L7-Δγ2* whereas the mutants that carry the mutations individually show virtually normal conditioning. (A) Experimental setup and concept of eyeblink conditioning. Mice are placed in a light and sound- and light isolating chamber with their head fixed on a freely moving foam treadmill. Unconditional stimulus (US) consisted of a weak air puff and conditional stimulus (CS) was a green LED light. Eyelid movements were recorded with magnetic distance measurement technique (MDMT). During eyeblink conditioning an association is learned between an US that elicits a reflexive eyeblink and the CS that predicts the onset of this US. Repeated pairings of CS and US with fixed time-intervals (250 ms) will lead to the acquisition of conditioned responses (CRs), i.e. mice learn to close their eye in response to the CS (see MDMT set-in). *in vivo* PC recording were performed on the same treadmill system. **(B)** The memory for eyeblink conditioning is formed in the cerebellum. Climbing fibers (red), originating in the inferior olive (IO), transmit the instructive US signal to Purkinje cells (PCs) in specific micro-zones in the cerebellar cortex and the anterior interposed cerebellar nuclei (AIN) neurons. The mossy fiber - parallel fibers system (green), originating in the various brainstem nuclei including the pontine nuclei (PN), transmits the CS signals to the same PCs and to some extent the AIN. These PCs innervate the AIN, which in turn (in)directly innervates the motoneurons (MNs) that control the eyelid musculature (purple). **(C)** Schematic representation of the different mutations: *GluR2Δ7* lack PF-PC LTD, *L7-Δγ2* lack MLI-PC inhibition, *GluR2Δ7 L7-Δγ2* have both disrupted PF-PC LTD and MLI-PC inhibition. **(D)** *GluR2Δ7 L7-Δγ2* mice have a significantly lower CR percentage compared to control mice. CR percentage is plotted for all four groups over the course of ten acquisition sessions. CR threshold was set at 10% of a full eyelid closure in the CS-US interval.
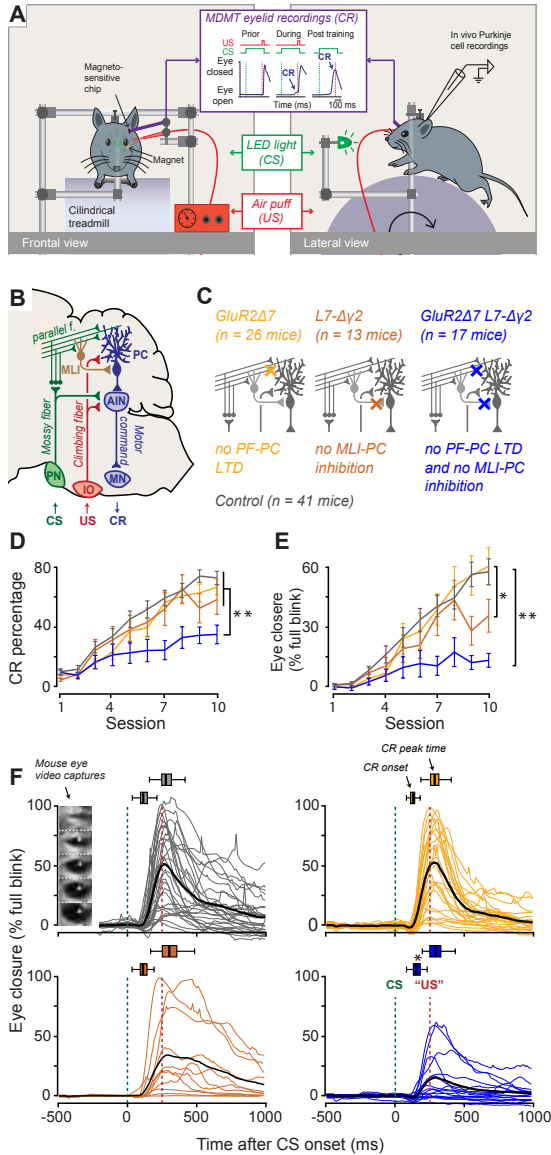
(E) *GluR2Δ7 L7-Δγ2* mice also have significantly smaller eyeblink CRs. Also, *L7-Δγ2* mice show a partial learning deficit, with smaller eyeblink CR amplitudes in the final sessions. Eyeblink amplitude value is based on all 100 paired trials per session and represents the closure at the onset of the US puff (i.e. 250 ms after CS onset, see red dashed line in panel 2A (MDMT set-in) and in panel 2F). **(F)** *GluR2Δ7 L7-Δγ2* mice have significantly smaller eyeblink CRs and the latency to CR onset is significantly increased. Each colored trace represents the average of all 30 CS only trials per mouse in the probe session; thick black line represents the average of these averages. Mouse eye video captures show eyelid closure at 0, 25, 50, 75, and 100% values of a full blink. Note that, although eyeblink conditioning is severely disrupted, in *GluR2Δ7 L7-Δγ2* mice they still do show properly timed eyeblink CRs, i.e. CRs peak at expected US onset.

In vivo PC recordings

Finally, to investigate spontaneous PC firing characteristics, we performed *in vivo* recordings in cerebellar vermis and hemispheres, differentiating between anterior (lobule I-V) and posterior (lobule IX-X) regions, which differ in terms of zebrin identity and accordingly in terms of spontaneous firing frequencies (Zhou et al., 2014). Indeed, all experimental groups showed higher simple spike firing rates in anterior lobules, which are mainly zebrin-negative, than in the predominantly zebrin-positive posterior lobules (Fig. 2F, G, H, K, S Table 2; all $p < 0.05$, LMM). First, since the removal of PF-PC LTD and MLI-PC inhibition should both constitute an increase in PC excitability, simple spike firing rates should be higher than those in the wildtype group, unless compensatory forces maintain normal firing. Our data supports the latter notion for both anterior and posterior lobules, with none of the mutant groups showing different simple spike firing rates than the wildtype control group (Fig. 2F, G, H, K, S Table 3; all $p >= 0.14$, LMM). Next, given that MLI-PC inhibition is linked to more irregular simple spike firing, we expected lower CV2 values in the *L7-$\Delta\gamma$2* and the *GluR2Δ7 L7-$\Delta\gamma$2* mutants. In both the anterior and to a lesser degree the posterior regions, this was indeed the case for the *L7-$\Delta\gamma$2* mutant (Fig. 2H, L, S Table 3; anterior: CV2, t (7.87) = -4.4, $p = 0.002$; posterior: CV2, t (15.40) = -2.2, $p = 0.04$; LMM). Interestingly, *GluR2Δ7 L7-$\Delta\gamma$2* mice partially follow this pattern, having indeed a lower anterior CV2 value, but no significantly different posterior CV2 (Fig. 2H, L, S Table 3; anterior CV2 t (9.96) = -2.50, $p = 0.031$; posterior CV2 t (15.92) = -0.95, $p = 0.36$; all LMM). Additionally, whereas in wildtypes CV2 were markedly different between anterior and posterior regions (Fig. 2H, L, S Table 3; CV2 t (38) = 2.82, $p = 0.007$; LMM), there were no significant differences in the mutant groups (Fig. 2H, L, S Table 3; all $p > 0.09$; LMM). Finally, complex spike firing rates were not different between mutant groups and wildtype mice, with wildtypes showing substantially higher rates in anterior than in posterior zones (t (38) = 4.68, $p < 0.0001$, LMM), and each mutant group showing at least a trend to that effect (Fig. 2I, M, S Table 3; all $p < 0.08$; linear mixed effects model). Thus, spontaneous *in vivo* PC simple spike and complex spike frequencies in *GluR2Δ7 L7-$\Delta\gamma$2* mice do not seem affected, and their simple spike firing regularity lies closer to that of wildtype mice than that of the *L7-$\Delta\gamma$2* mutant.

Figure 2 *GluR2Δ7 L7-$\Delta\gamma$2* **mice lack both pf-PC LTD and MLI-PC inhibition but have no gross abnormalities in spontaneous firing behavior** *in vivo.* **(A)** Schematic overview of MLI-PC inhibition and PF-PC LTD induction experiments. **(B)** PC EPSCs were evoked using PF stimulations of varying intensities (3 to 15 μA) showing that *GluR2Δ7 L7-$\Delta\gamma$2* mice do have excitatory transmission. **(C)** Applying inter-stimulus intervals varying from 50 to 200 ms evoked similar levels of paired-pulse facilitation indicating that baseline PF–PC synaptic transmission is unaltered in *GluR2Δ7 L7-$\Delta\gamma$2* mice. **(D)** *GluR2Δ7 L7-$\Delta\gamma$2* mice show significantly less spontaneous IPSPs than wildtype controls and *GluR2Δ7*, indicating that they have indeed lack MLI-PC inhibition. For PC EPCS, PPF, and sIPSC in *L7-$\Delta\gamma$2* and *GluR2Δ7* mutants, we refer to (Schonewille et al., 2011) **(E)** *GluR2Δ7 L7-$\Delta\gamma$2* show no PF-PC LTD using an induction protocol which consisted of a 100 Hz PF stimulation in 8 pulses followed by a 125 ms delay of single CF activation at 1 Hz for 5 minutes. For comparison, data of *GluR2Δ7* and *L7-$\Delta\gamma$2* mice is used with permission from Schonewille et al., (2011) and Wulff et al. (2009), respectively. **(F, J)** Raw *in vivo* PC recordings showing that for both SSp **(G, K)** and CSp **(I, M)** firing frequencies, no differences were found between wildtype controls and any of the mutant groups. SSp firing frequency is significantly higher in the anterior lobules for all groups. Control wildtype mice and *L7-$\Delta\gamma$2* mutants show complex spike (CSp) firing frequencies that are higher in the anterior lobules, whereas for groups carrying the *GluR2Δ7* mutation this is not the case.
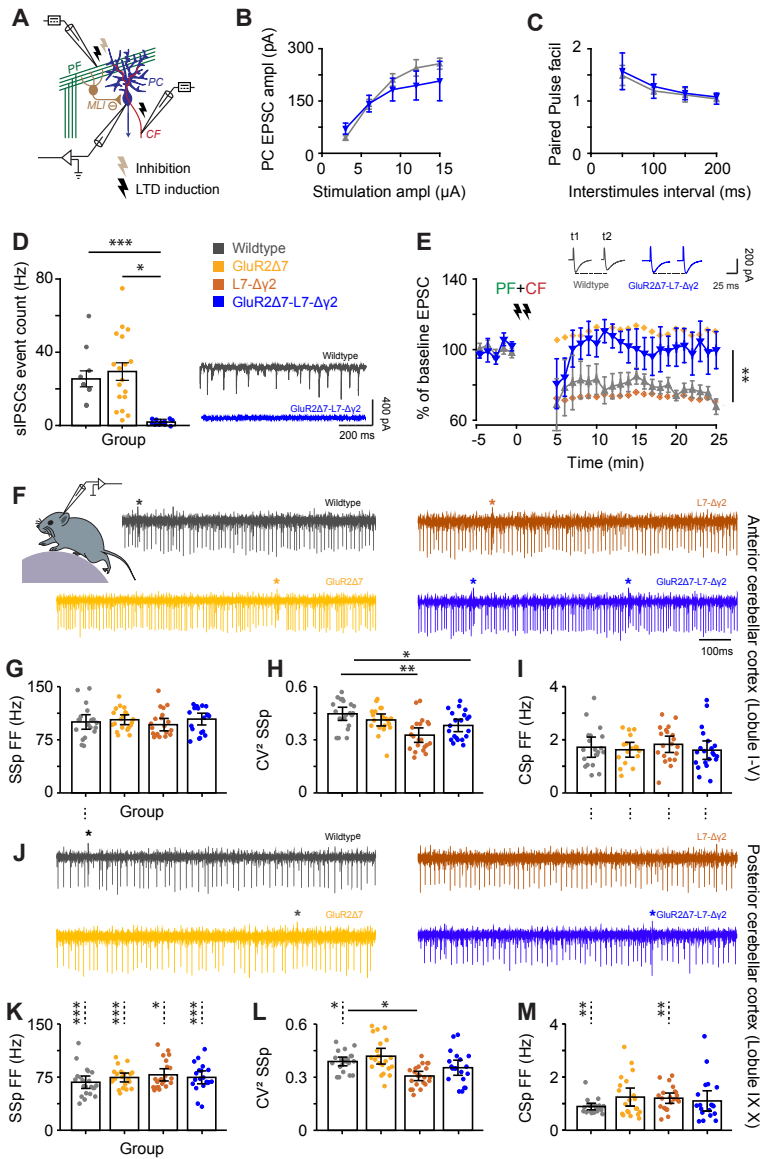
(H, L) Wildtype control mice show higher simple spike CV2 values for the anterior cerebellar lobules. None of the mutants show this pattern. *GluR2Δ7* mutants have relatively high CV2 values in both anterior and posterior lobules, *L7-Δγ2* mutants have equally low values for both zones, and *GluR2Δ7 L7-Δγ2* mutants show a hybrid pattern. Dashed vertical lines indicate differences between anterior and posterior cerebellar cortex. * p < 0.05, ** p < 0.01, *** p < 0.0001

Discussion

Here we show that a concurrent disruption of PF-PC LTD and MLI-PC inhibition results in severe cerebellar learning deficits, whereas elimination of these suppression mechanisms individually results in no or only partial learning impairments. *GluR2Δ7 L7-Δγ2* mice instead, which have proven to lack indeed both PF-PC LTD and MLI-PC inhibition (Fig. 2 A, B), acquire over the course of ten training sessions only few and small eyeblink CRs with a slightly delay in CR onset (Fig. 1D-F). Interestingly, eyeblink CR peak is properly timed around the onset of the expected US (Fig. 1F). In addition, *GluR2Δ7 L7-Δγ2* mice show normal spontaneous simple spike and complex spike firing frequencies and only a slightly reduced CV2 value compared to wildtypes, whereas *L7-Δγ2* mice show substantially more regular simple spike firing (Fig. 2C). Since *L7-Δγ2* mice have a much subtler learning deficit, it is unlikely that this lower CV2 is related to the severe learning deficit in *GluR2Δ7 L7-Δγ2* mice. In addition, in all mutants, the differential CV2 values between anterior and posterior lobes were eliminated. Since this elimination caused no learning deficits in *GluR2Δ7* and *L7-Δγ2* mice, it is unlike that this is the source of the learning impairment in *GluR2Δ7 L7-Δγ2* mice.

Our finding challenges the field of cerebellar learning in several aspects. One could simply argue that PF-PC LTD and MLI-PC inhibition are both PC suppression mechanisms and that a disruption in one of them can normally be compensated for by the other one. However, could PF-PC LTD alone indeed *pause* a PCs simple spike firing? The answer is probably no, since PC have an intrinsic spike generating mechanism (Raman & Bean,1997; Raman & Bean, 1999) and removal of excitatory inputs from the PC by the application of CNQX only has minor effects on simple spike firing rate (Cerminara & Rawson, 2004; Zhou et al., 2014). Thus, removal of PF excitation, as in PF-PC LTD, seems unable to suppress PC simple spike firing frequencies below pacemaker activity. In addition, PF-PC LTD could even not be established after eyeblink conditioning (Jirehed & Hesslow, 2011). On the other hand, MLI-PC inhibition is a potent mechanism to pause PC simple spike firing for longer periods of time (Heiney et al., 2014; Korn & Axelrad, 1980; Mittmann et al., 2005). In addition, MLIs clearly show facilitation in their firing profile, which precedes CR onset and positively correlates with CR amplitude (Ten Brinke et al., 2015). However, as shown in present study, MLI-PC inhibition alone is not essential for eyeblink conditioning. Interestingly, it has been shown *in vivo* that PF burst stimulation (= CS) followed 150 ms later by CF stimulation (= US) leads to concurrent long-term potentiation (LTP) of the PF-MLI synapse and PF-PC LTD (Jirehed et al., 2013). Based on our findings, we speculate that this concurrent PF-MLI LTP and PF-PC LTD are dependent on each other and could not take place in *GluR2Δ7 L7-Δγ2* mice, leading to cerebellar learning deficits.

Recently, is has been shown that in *GluR2Δ7* mice, PF-PC LTD can still be induced when the stimulations conditions are intensified by increasing the number of PF stimulation [PFs stimulated or PF stimulations] from 1 to 2-5 and substituting the CF stimulation with a strong PC somatic depolarization of 50 ms (Yamaguchi & Itohara; 2016), using an interval between PF and PC stimulation onset of only 0-50 ms. In current study, PF-PC LTD is induced using stimulation conditions that better

match those under which eyeblink conditioning normally occurs (Hesslow et al., 2013; Piochon et al., 2012; Titley & Hansen, 2015), i.e. 100 Hz PF stimulation (8 pulses) followed by a single CF activation after a 110 ms delay, repeated at 1 s intervals for 5 minutes.

Although eyeblink conditioning in *GluR2Δ7 L7-Δγ2* mice is severely affected, they do undeniably show eyeblink CRs at the end of training (Fig. 1F). Importantly, these eyeblink CRs are properly timed, that is, they peak around the onset of the expected US. This finding suggests additional neural mechanisms that contribute to PC simple spike suppression. In fact, it is unclear at this point whether PF-PC LTD and MLI-PC inhibition are indeed driving the PC simple spike pause or only facilitating it by optimizing the PC's inputs that transmit the CS information. In line with recent findings supporting a more neurocentric instead of exclusively synaptocentric view on learning, such a mechanism might well involve a temporal memory that is formed *in* the Purkinje cell itself and which is driven by metabotropic glutamate receptors (Johansson et al., 2014; Johansson et al., 2015; Titley et al., 2017). Such a cell intrinsic learning mechanism, however, is dependent upon optimized synaptic inputs provided by PFs and MLIs. Our finding that only a concurrent disruption of PF-PC LTD *and* MLI-PC inhibition could severely impair eyeblink conditioning, but not completely block learning, rejects the idea that a single form of neural plasticity is essential and sufficient and supports the notion that synaptic and intrinsic plasticity synergistically contribute to form a temporal memory in the cerebellum.

Methods

Subjects and generation of mice

For all experiments, we used male and female mice with a C57Bl/6 background, individually housed, food ab libitum, 12:12 light/dark cycles. For *in vitro* electrophysiology experiments we used mice aged 5-20 weeks old mice; for *in vivo* electrophysiology and eyeblink conditioning, mice were 15-25 weeks old. We made use of three different transgenic mouse lines. First, *GluR2Δ7* knock-in mice lack the last seven amino acids at the intracellular C-terminus tail, thereby disrupting the interaction of GluR2 with PICK1 and GRIP1/2, in turn disrupting the internalization of AMPA receptors, which impairs PF-PC LTD (n = 26 mice) (Steinberg et al., 2006; Xia et al., 2000). Second, *L7-Δγ2* mice have a Purkinje cell specific (L7) ablation of the γ2 subunit of the GABAa receptors resulting in impaired feed-forward inhibition provided by MLIs (Ten Brinke et al., 2015; Wulff et al., 2009) (n = 13 mice). For the *L7-Δγ2* mice we first generated *γ2I77lox* mice by flanking exon 4 of the Gabrg2 gene with *lox*P sites and changing the codon encoding F77 in exon 4 to I, which resulted in a neutral amino acid substitution. Next, homozygous *γ2I77lox* were crossed with mice hemizygous for the PC specific *L7-cre* transgene and heterozygous for *γ2I77lox* (Overdick et al., 1990; Xia et al., 2000). For experiments *L7-cre γ2I77lox/ γ2I77lox* mice (L7-Δγ2) and *γ2I77lox/ γ2I77lox* mice (controls) were used. Third, *GluR2Δ7 L7-Δγ2* mice (n = 17 mice), which both lack both pf-PC LTD and MLI feed-forward inhibition were generated by crossbreeding female mice hemizygous for *L7-cre* and homozygous

for $\gamma 2I77lox/\gamma 2I77lox$ with male homozygous $GluR2\Delta 7$ knock-in mice (= F0). Next, F1 female mice hemizygous for *L7-cre* and heterozygous for both $\gamma 2I77lox/\gamma 2I77lox$ and $GluR2\Delta 7$ were crossed with F1 male mice heterozygous for both $\gamma 2I77lox/\gamma 2I77lox$ and $GluR2\Delta 7$. This F1 breeding generated F2 mice, which were hemizygous for *L7-cre* and homozygous for both $\gamma 2I77lox/\gamma 2I77lox$ and $GluR2\Delta 7$ and F2 mice homozygous for both $\gamma 2I77lox/\gamma 2I77lox$ and $GluR2\Delta 7$. F2 mice were used in experiments. F2 mice homozygous for both $\gamma 2I77lox/\gamma 2I77lox$ and $GluR2\Delta 7$ were pooled with $GluR2\Delta 7$ knock-in mice. As controls (n = 41) we used pooled data from littermate $GluR2\Delta 7$ wildtypes and $\gamma 2I77lox/\gamma 2I77lox$ mice. All mice were genotyped by performing PCR analyses of genomic DNA at 2-3 weeks postnatal and once again post mortem. All experiments were approved by the Dutch Ethical Committee for animal experiments and were in accordance with the Institutional (Erasmus MC) Animal Care and Use Committee guidelines.

Eyeblink conditioning

Surgery   Mice were anesthetized with an isoflurane/oxygen mixture (5% for induction, 1.5-2% for maintenance) and body temperature was kept constant at 37° Celsius. Eyes were protected against drying using an eye lubricant (Duratears). After a local scalp injection of bupivacaine hydrochloride (2.5mg/ml, Bupivacaine Actavis) we made a sagittal scalp incision of 2-3 cm length. Next, we carefully removed the exposed periosteum and roughened the surface of the skull using an etchant gel (Kerr, Bioggio, Switzerland). After this, a small messing block (1.0 x 0.4 x 0.3 mm) with 1 screw thread and 2 additional pinholes was placed on the skull using Optibond primer and adhesive (Kerr, Bioggio, Switzerland) and Charisma (Heraeus Kulzer, Armonk, NY, USA). The surgical placement of this so-called pedestal and allowed for head-fixation during the eyeblink conditioning experiments.

Behavioral training   All behavioral experiments were conducted using head-fixed mice that were placed on top of a cylindrical treadmill on which they were allowed to walk freely (Fig. 1A) The treadmill consisted of a foam roller (diameter ±15cm, width ±12cm; Exervo, TeraNova EVA) with a horizontal metal rod through the axis that was connected with a ball bearing construction to two solid vertical metal poles. A horizontal messing bar was fixated to the same vertical poles at 3-5 cm above the treadmill. Mice were head-fixed to this bar using 1 screw and 2 pins, thereby ensuring perfect head-fixation (further details Chettih et al., 2011). National Instruments (NI-PXI) equipment was used to control experimental parameters and to acquire the eyelid position signal. Eyelid movements were recorded with the magnetic distance measurement technique (MDMT), which makes use of an NVE GMR magnetometer, positioned above the left upper eyelid, that measures movements of a minuscule magnet (1.5x0.7x0.5mm) that is placed on the left lower eyelid of the animal with superglue (cyanoacrylate). This way, MDMT allows high spatio-temporal detection of eyelid kinematics (further details Koekkoek et al., 2002). The conditional stimulus (CS) was a green LED light (CS duration 280 ms, LED diameter 5 mm) placed 10 cm in front of the mouse's head. Because we performed our experiments in almost complete darkness, this small LED light was a salient stimulus, which could be easily

detected by both eyes. The unconditional stimulus (US) consisted of a weak air-puff applied to the eye (30 psi, 30 ms duration), which was controlled by an API MPPI-3 pressure injector, and delivered via a 27.5-gauge needle that was perpendicularly positioned at 0.5 - 1 cm from the center of the left cornea. The training consisted of 3 daily habituation sessions, 1 baseline measurement, 5 or 10 daily acquisition sessions, and 1 probe session immediately after the last training session. During the habituation sessions, mice were placed in the setup for 30-45 minutes, during which the air puff needle (for US delivery) and green LED (for CS delivery) were positioned properly but no stimuli were presented. On the day of acquisition session 1, each animal first received 20 CS-only trials as a baseline measure, to establish that the CS did not elicit any reflexive eyelid closure. During each daily acquisition session, animals received either 100 or 200 paired CS-US trials, separated over 10 or 5 daily acquisition sessions, respectively. The interval between the onset of CS and that of US was set at 250 ms. Because of an inherent 14 ms delay in the delivery of the air puff, we triggered the air puff at 236 ms after CS onset so that it would hit the cornea exactly at 250 ms after CS onset. The inter-trial interval was set according to the following constraints: at least 10 seconds had to elapse, the eyelid had to be open below a predetermined threshold of 50% of a full eyelid closure, and eyelid position had to be stable for at least 2 seconds for a trial to begin. Immediately after acquisition session 10, we started a probe session during which we presented another 100 paired CS-US trials, but now intermingled with 30 CS-only trials. During all training sessions, the experimenter carefully inspected threshold and stability parameters and adjusted them if necessary. All experiments were performed at approximately the same time of day by the same experimenter.

Data analysis   Individual eyeblink traces were analyzed automatically with custom computer software (LabVIEW or MATLAB) in a five-step process. First, trials with significant activity in the 500 ms pre-CS period (> 6 SD) were regarded as invalid for further analysis. Second, trials were normalized by aligning the 500 ms pre-CS baselines and calculating the averaged UR amplitude in Volts per session. The voltage corresponding with a full closure was further used in the analysis of the eyeblink traces as the 100% value reflecting full eyelid closure ($\pm$ 1 mm movement), and other values like CR amplitude were expressed relative to this 100% value. Third, in the valid normalized trials, all eyelid movements larger than 10% of a full eyelid closure and with a latency to CR onset between 50-250 ms and a latency to CR peak of 100-250 ms (both relative to CS onset) were considered as conditioned responses (CRs). For CS only trials in the probe session we used the exact same criteria except that the latency to CR peak time was set at 100-500 ms after CS onset. Additionally, we determined for each individual trial the following parameters: (1) maximum/average eyelid closure (= amplitude) in the full CS-US interval; (2) eyelid closure specifically at US onset (i.e. 250 ms after CS onset); (3) latency to CR onset; (4) latency to CR peak. For 1 and 2 we used *all* valid trials, for 3 and 4 we only used the trials in which a CR was present. Fourth, based on this trial-by-trial analysis we calculated for each session per mouse the percentage of eyeblink CRs. Statistical effects of session and genotype on CR percentage were established in SPSS 24 using a repeated measures ANOVA and LSD post hoc testing. Fifth, linear mixed effect models were used in SPSS 24 to determine statistically significant effects of genotype and session on parameters 1-4.

Data was considered statistically significant if $p < 0.05$.

in vitro electrophysiology

Decapitation and preparation   Following isoflurane anaesthesia, mouse were decapitated, and the cerebellum was obtained and put in an ice-cold slicing medium, containing (in mM) 3 NMDG, 93 HCl, 2.5 KCl, 1.2 NaHPO4, 30 NaHCO3, 25 Glucose, 20 HEPES, 5 Na-ascorbate, 3 Na-pyruvate, 2 Thiourea, 10 MgSO4, 0.5 CaCl2, 5 N-acetyl-L-Cysteine that was carbogenated continuously (95% O2 and 5% CO2). Sagittal slices, 250 mm thick, of the cerebellar vermis were cut using a vibrotome (VT1200S, Leica) and put in carbogenated artificial cerebrospinal fluid (ACSF) containing (in mM): 124 NaCl, 5 KCL, 1.25 Na2HPO4, 2 MgSO4, 2 CaCl2, 26 NaHCO3 and 20 D-Glucose, for at least 1 h at 34±1 °C before the start of the experiment. All slice physiology was done at 34±1 °C in the presence of 100 mM picrotoxin except for the sIPSCs recordings. Whole-cell patch clamp recording were performed with an EPC9 amplifier (HEKA Electronics, Lambrecht, Germany). Recordings were excluded if the series (Rs) or input resistances (Ri) changed by 20% during the experiment, which was determined using a hyperpolarizing voltage step relative to the -65 mV holding potential. For whole-cell recordings PCs were visualized using an upright microscope (Axioskop 2 FS, Carl Zeiss) equipped with a 40x objective. Recording electrodes (3–5 MO, 1.65 mm outside diameter (OD) and 1.11 mm interior diameter (ID), World Precision Instruments, Sarasota, FL, USA) were filled with an intracellular solution containing (mM): 120 K-Gluconate, 9 KCL, 10 KOH, 4 NaCl, 10 HEPES, 28.5 Sucrose, 4 Na2ATP, 0.4 Na3GTP (pH 7.25–7.35 with an osmolarity of 295±5).

PF-PC transmission   For PF–PC transmission, we used various inter-stimulus intervals (50–200 ms). For recordings of spontaneously occurring IPSCs (sIPSCs), we used the previously mentioned K-based internal and recorded their occurrence during 120 s. For CF stimulation, similar electrodes (filled with ACSF) were positioned near the patched PC soma in the surrounding granule layer.

sIPSC   For the recording of spontaneous inhibitory post synaptic currents (sIPSCs), we used an intracellular solution containing (mM): 150 CsCl, 1.5 MgCl2, 0.5 EGTA, 4 Na2ATP, 0.4 Na3GTP, 10 HEPES, 5 QX314 (pH 7.25–7.35 with an osmolarity of 295±5). For extracellular stimulation of PFs, similar patch electrodes were filled with ACSF and positioned in the upper third of the molecular layer lateral to the patched PC. The stimulation intensity was set to evoke an excitatory post synaptic current (EPSC) of 200±50 pA (typically 3–5 μA stimulation intensity).

PF-PC induction   For PF-PC LTD induction we recorded from lobules 5/6. Recordings were done in voltage-clamp, except for the tetanus, which consisted of 100 Hz PF stimulation in 8 pulses followed by a 110 ms delay of single CF activation at 1 Hz for 5 minutes. We evaluated the synaptic plasticity by the change in PF-EPSC (baseline at 0.05 Hz) relative to the mean value calculated during the 5min long baseline pre-tetanus (Piochon et al., 2014).

Data analysis   Data analysis was performed using Clampfit software (Molecular Devices).

in vivo PC recordings

Surgery   Mice were surgically prepared following the same procedure as described for eyeblink conditioning. Additionally, a craniotomy (ø 2-3 mm) was performed on the occipital bone in order to perform extracellular PC recordings from both the anterior and posterior cerebellum. A small rim of Charisma was made around the craniotomy and anti-inflammatory (Dexamethasone 4 mg/ml) solution was applied inside, after which the chamber was closed with a very low viscosity silicone elastomer sealant (Kwik-cast, World Precision Instruments). After surgery mice had 5 days to recover.

Recordings   Extracellular PC recordings were conducted using head-fixed mice that were placed on top of a cylindrical treadmill system as described above. Mice were first habituated for 3 days to the treadmill. PCs were recorded from vermal lobules I–V and lobules VI-X using glass micropipettes (2.0 mm OD, 1.16 mm ID, Harvard Apparatus, MA, USA, tip 2-5 μm, impedance 2-5 MΩ. Single unit Purkinje cells were recorded for 2–5 minutes. Single-unit recording was identified online by the presence of a short SS pause (20-50 ms) after each complex spike. To verify recording locations, we made small alcian blue injections after recording sessions.

Analysis   *in vivo* recordings were analyzed offline using custom scripts in MatLab (Mathworks, Natick, MA, USA) and SPSS 24. Average simple spike and complex spike firing were calculated. Simple spike firing regularity was investigated using the CV2 value, which was calculated as $2 * \mid ISI_{n+1} - ISI_n \mid / (ISI_{n+1} - ISI_n)$.

Supplementary Material

S Table 1	CR percentage session 1-10 (10%-threshold)		Eye closure session 1-10 (% of full blink)		CR onset (ms)	CR peak time (ms)	Eyelid closure at US onset (%)
Wildtype (n = 41 mice)	9.7 (± 12.5 sd) - 73 (± 28.5 sd)	F = 58.9, p < 0.00001, ANOVA	1.7 (± 4.2 sd) - 58.1 (± 41.1 sd)	F = 37.3, p < 0.00001, ANOVA	137.8 (± 36.6 sd)	285.6 (± 42.9 sd)	64.1 (± 40.0 sd)
GluR2Δ7 (n = 26 mice)	7.2 (± 6.3 sd) - 67 (± 26.6 sd)	F = 46.4, p <0.00001, ANOVA	0.4 (± 2.0 sd) - 60.8 (±47.7)	F = 22.8, p < 0.00001, ANOVA	142.9 (± 25.5 sd)	282.0 (± 44.3 sd)	61.6 (± 49.8 sd)
L7-Δγ2 (n = 13)	4.2 (± 3.6) - 58.4 (± 36.0 sd)	F = 12.2, p <0.00001, ANOVA	1.6 (± 2.2 sd) - 36.1 (± 29.4 sd)	F = 9.4, p < 0.00001, ANOVA	118.9 (± 22.6 sd)	303.3 (± 20.2 sd)	30.7 (± 32.9 sd)
GluR2Δ7 L7-Δγ2 (n = 17)	9.3 (± 6.8 sd) - 34.9 (± 25.9 sd)	F = 5.8, p = 0.0001, ANOVA	0.7 (± 5.5 sd) - 13.9 (± 14.3 sd)	F = 3.7, p = 0.018, ANOVA	160.1 (± 26 sd)	279.0 (± 85.3 sd)	17.5 (± 21.4 sd)
Between group comparison	F (3,97) = 3.092, p < 0.00001		F (3,97) = 3.482, p < 0.0001				
Wt vs. GluR2Δ7	p = 0.518		p = 0.989		t (73.3) = 0.97, p = 0.33	t (53.2) = -0.05, p = 0.963	t (82.3) = -0.335, p = 0.738
Wt vs. L7-Δγ2	p = 0.704		p = 0.623 S9 p = 0.02, S10 p = 0.03		t(67.8) = -1.72, p = 0.89	t (49.1) = 1.64, p = 0.107	t (80.0) = -2.44, p = 0.017
Wt vs. GluR2Δ7 L7-Δγ2	p = 0.002		p = 0.007		t (69.7) = 2.31, p = 0.024	t (52.14) = 0.89, p = 0.377	t (80.1) =-3.928, p = 0.0002
Statistical test	(RM ANOVA, Tukey HSD post hoc)		(RM ANOVA, Tukey HSD post hoc)		(LMM - probe session)	(LMM - probe session)	(LMM - probe session)

PC EPSCs (pf stimulation)	Wildtype (n = 5 cells, 3 mice)	GluR2Δ7 L7-Δγ2 (n = 7 cells, 3 mice)	Statistical test	S Table 2
Stimulation Strength 3 μA	34.77 (± 17.92 sd)	83.38 (± 67.27 sd)	$F_{(1,10)}$=0.059, p=0.81 ANOVA, Repeated measures	
Stimulation Strength 6 μA	119.05 (± 37.23 sd)	166.15 (± 92.59 sd)		
Stimulation Strength 9 μA	205.26 (± 49.12 sd)	203.15 (± 116.25 sd)		
Stimulation Strength 12 μA	224.84 (± 46.64 sd)	221.79 (± 156.00 sd)		
Stimulation Strength 15 μA	257.12 (± 35.05 sd)	228.32 (± 160.55 sd)		

Paired Pulse facilitation (PPF)	Wildtype (n = 8 cells, 3 mice)	GluR2Δ7 L7-Δγ2 (n = 10 cells, 3 mice)	Statistical test	
Inter stimulus interval 50ms	1.49 (± 0.19 sd)	1.57 (± 0.35 sd)	$F_{(1,16)}$=0.81, p=0.38 ANOVA, Repeated measures	
Inter stimulus interval 100ms	1.20 (± 0.06 sd)	1.28 (± 0.23 sd)		
Inter stimulus interval 150ms	1.12 (± 0.13 sd)	1.15 (± 0.12 sd)		
Inter stimulus interval 200ms	1.04 (± 0.10 sd)	1.08 (± 0.07 sd)		

sIPSCs analysis	Wildtype (n = 6 cells, 2 mice)	GluR2Δ7 (n = 18 cells, 3 mice)	GluR2Δ7 L7-Δγ2 (n = 11 cells, 2 mice)	Statistical test
sIPSCs (Hz)	25.38 (± 10.71 sd)	29.44 (± 20.27 sd)	1.87 (± 1.42 sd)	$F_{(2, 32)}$=11.39, p=0.0001 ANOVA, post-hoc Bonferroni: Wildtype vs GluR2Δ7, p=1.00 Wildtype vs GluR2Δ7 L7-Δγ2, p=0.015 GluR2Δ7 vs GluR2Δ7 L7-Δγ2 , p=0.005

LTD analysis	Wildtype (n = 6 cells, 4 mice)	GluR2Δ7 L7-Δγ2 (n = 6 cells, 4 mice)	WT baseline vs post induction	GluR2Δ7 L7-Δγ2 baseline vs post induction	Statistical test
Baseline (pA)	192.77 (± 57.05 sd)	180.81 (± 46.08 sd)	$t_{(5)}$=-4.28, p=0.008 Paired t-test	$t_{(5)}$=0.052, p=0.96 Paired t-test	
Post induction (last 5 mins, pA)	146.60 (± 41.93 sd)	181.70 (± 52.99 sd)			

S Table 3

Wildtype (n = 6 mice)

	Posterior (n = 22 cells)	Anterior (n = 20 cells)	Ant vs. Post p-value
Complex spike firing rate (Hz)	0.89 (± 0.27)	1.72 (± 0.77)	t (38) = 4.68, p < 0.0001
Simple spike firing rate (Hz)	68.03 (± 19.74)	100.17 (± 21.93)	t (27.29) = 4.57, p < 0.0001
CV2 simple spikes	0.39 (± 0.06)	0.45 (± 0.08)	t (42) = 2.82, p = 0.007

GluR2Δ7 (n = 4 mice)

	Posterior (n = 21 cells)	Anterior (n = 20 cells)	Ant vs. Post p-value
Complex spike firing rate (Hz)	1.24 (± 0.75)	1.62 (± 0.54)	t (38) = 1.80, p = 0.08
Simple spike firing rate (Hz)	74.69 (± 13.79)	103.30 (± 14.88)	t (41) = 6.55, p < 0.0001
CV2 simple spikes	0.42 (± 0.10)	0.41 (± 0.07)	t (37.74) = -4.36, p = 0.67

L7-Δγ2 (n = 7)

	Posterior (n = 22 cells)	Anterior (n = 21 cells)	Ant vs. Post p-value
Complex spike firing rate (Hz)	1.20 (± 0.44)	1.83 (± 0.66)	t (17.76) 3.72, p = 0.002
Simple spike firing rate (Hz)	78.46 (± 19.32)	96.36 (± 19.32)	t (34.87) = 1.87, p = 0.04
CV2 simple spikes	0.31 (± 0.06)	0.33 (± 0.09)	t (41.47) = -0.75, p = 0.94

GluR2Δ7 L7-Δγ2 (n = 6)

	Posterior (n = 20 cells)	Anterior (n = 21 cells)	Anterior vs. Posterior p-value
Complex spike firing rate (Hz)	1.10 (± 0.82)	1.61 (± 0.76)	t (39.63) = 1.90, p = 0.06
Simple spike firing rate (Hz)	74.86 (± 19.40)	104.23 (± 18.27)	t (33.53) = 5.07, p < 0.0001
CV2 simple spikes	0.35 (± 0.09)	0.38 (± 0.08)	t (40.54) = 0.50, p = 0.62

Group comparison Posterior cerebellar cortex

	Wt vs. GluR2Δ7	Wt vs. L7-Δγ2	Wt vs. GluR2Δ7 L7-Δγ2
Complex spike firing rate (Hz)	t (83) = 6.69, p = 0.06	t (83) = 1.70, p = 0.09	t (76) = -0.43, p = 0.62
Simple spike firing rate (Hz)	t (11.93) = 1.02, p = 0.33	t (13.24) = 1.59, p = 0.14	t (82) = 0.54, p = 0.59
CV2 simple spikes	t (14.54) = 1.18, p = 0.26	t (15.40) = -2.2, p = 0.04	t (8.85) = -1.24, p = 0.25

Group comparison Anterior cerebellar cortex

	Wt vs. GluR2Δ7	Wt vs. L7-Δγ2	Wt vs. GluR2Δ7 L7-Δγ2
Complex spike firing rate (Hz)	t (76) = 0.50, p = 0.62	t (83) = 1.11, p = 0.27	t (61) = -0.52, p = 0.61
Simple spike firing rate (Hz)	t (82) = -0.67, p = 0.51	t (15.32) = 1.04, p = 0.32	t (82) = 0.71, p = 0.48
CV2 simple spikes	t (7.87) = -4.40, p = 0.002	t (15.92) = -0.95, p = 0.36	t (9.96) = -2.50, p = 0.031

Chapter 4

*Adaptation of whisker movements
requires cerebellar potentiation*

The ability to rapidly adapt movement patterns while exploring the world is critical for survival, yet how it comes about is unclear. Here, we developed a sensory-driven whisker movement adaptation protocol and show with trial-by-trial analyses that enhancements and accelerations of whisker behavior require increased and accelerated simple spike activity of cerebellar Purkinje cells. Blocking potentiation specifically in Purkinje cells prevents both adaptation of whisker movements and concomitant changes in simple spike patterns. The ability to express sensory-induced simple spike plasticity is set by the temporal windows in which complex spike activity is low. Our data indicate that enhancement of simple spike activity guides long-term storage of novel whisker motor patterns during learning by presenting instruction signals, whereas synchronized complex spike activity orchestrates acute stereotypic behavior, during which the simple spikes merely relay efference copy signals consistent with those needed for a fully trained internal model.

V. Romano, L. De Propris, L.W.J. Bosman, P. Warnaar, **M.M. ten Brinke**, S. Lindeman, C. Ju, A. Velauthapillai, J.K. Spanke, M. Negrello, E. D'Angelo, & C.I. De Zeeuw (Submitted)

Introduction

Active touch is important for exploring our environment, allowing us to assess the shape, substance and movements of objects and organisms around us (Prescott et al., 2011; Wolpert et al., 1998). Throughout the animal kingdom, various systems have evolved for this purpose, like the antennae of insects, the fingertips of primates and the well-developed whisker systems of rodents and sea mammals with which they actively interpret their environment (Ahl, 1986; Anjum and Brecht, 2012; Dehnhardt et al., 2001; Dere et al., 2007; Staudacher et al., 2005). Controlling and adapting movements of such systems are thus critical both in daily life and in life-threatening situations. Whereas the role of the cerebral cortex in the planning and initiation of active touch is relatively well established (Bosman et al., 2011; Brecht, 2007; Deschênes et al., 2016; Diamond and Arabzadeh, 2013; Feldmeyer et al., 2013; Guo et al., 2014; Petersen, 2014; Petreanu et al., 2012), that of the cerebellum in learning how to adapt these movements is less clear (Chen et al., 2016; Popa et al., 2012). Conceptually, the cerebellum may generate internal models to predict the sensory consequences of active control (Brooks et al., 2015; Medina and Lisberger, 2007; Wolpert et al., 1998), but with which cellular and network mechanisms it may adjust such models remains to be elucidated. Historically, long-term depression (LTD) at the parallel fiber-to-Purkinje cell (PC) synapse has been considered to be the main cellular mechanism underlying cerebellar motor learning (Albus, 1971; Ito, 2003; Konnerth et al., 1992). More recent findings though suggest that different mechanisms may prevail, dependent on the chemical identity of the cerebellar modules involved (De Zeeuw and Ten Brinke, 2015; Zhou et al., 2014). Whereas the so-called zebrin-negative modules may be dominated by plasticity mechanisms that suppress the simple spike (SS) activity of PCs, the PCs in the zebrin-positive modules may increase their SS activity during sensorimotor learning (De Zeeuw and Ten Brinke, 2015; Ten Brinke et al., 2015).

Here we set out to investigate the cellular encoding mechanisms underlying adaptation of whisker movements. Given that the cerebellar modules involved in coordination of whisker movements are largely zebrin-positive (Bosman et al., 2010; Shambes et al., 1978; Sugihara and Quy, 2007), we hypothesized that adaptation of whisker movements requires potentiation of PCs to increase their SS frequency. Moreover, given that potentiation at the parallel fiber-to-PC synapse can be most readily induced in the absence of climbing fiber activity (Coesmans et al., 2004), we predict that adaptation of whisker movements is governed by PCs in which the complex spike (CS) responses are low (De Zeeuw et al., 2011; Gao et al., 2012). As cerebellar training protocols for whisker movements had not been developed, we designed a novel paradigm. We based this on the known dynamics at the cerebellar input stage, the granular layer, which indicate that sensory stimulation at theta band frequencies may be most efficient in inducing plasticity (D'Angelo et al., 2001; Lev-Ram et al., 2002; Ramakrishnan et al., 2016). First, we established the impact of sensory stimulation on the baseline whisker movements as well as concomitant CS and SS responses of PCs in the cerebellar whisker regions crus 1 and 2 (Bosman et al., 2011; Bosman et al., 2010; Shambes et al., 1978). Next, we leveraged in our tetanic stimulation paradigm on the ability of mice to sweep their whiskers rhythmically while exploring their environment (Ahl, 1986; Voigts et al., 2015) and to adapt their

whisker movements on a cycle-by-cycle basis (Voigts et al., 2015). We show that in the naïve animal, modulatory activity of the climbing fibers precedes whisker movements, whereas that of the SSs occurs around the same time as the whisker movements. After induction of the training protocol, however, potentiated SS modulation anticipates the movements so as to instruct motor learning, highlighting a temporary accelerating shift in the internal model.

Results

Whisker responses to sensory stimulation

The large facial whiskers are a prime source of sensory information for mice. An event, such as mechanical stimulation of the whiskers, can trigger active whisking (Ferezou et al., 2007). We characterized the whisker movements around the time of air puff stimulation of the whisker pad in awake, head-restrained mice (Fig. 1A-C). It turned out that such stimulation triggers stereotypic whisker movements: a passive retraction due to the air flow followed by a large, single sweep forward. This single sweep forward could be followed by more variable whisker movement patterns. Active whisking during inter-trial intervals was relatively rare under these experimental conditions: only in 13% of all trials whisker movements of more than $10°$ happened during the 200 ms prior to an air puff to the whisker pad. The air puff initiated a stereotypic forward sweep, exceeding $10°$ in 87% of the trials. After this stereotypic stimulus-triggered forward sweep, prolonged whisker movements ($>$200 ms) were observed in 57% of the trials ($p < 0.0001$ compared to pre-stimulus interval; Fisher's exact test; Fig. 1D-H; Table S1). Thus, during most trials, there is little spontaneous whisker movement before the air puff, followed by a stereotypic forward sweep lasting until approximately 150 ms after the stimulus onset and more variable behavior afterwards.

Whisker representation in crus 1 and 2

Cerebellar Purkinje cells (PCs) receive sensory input from the whiskers via direct and indirect pathways (Bosman et al., 2011) (Fig. 2A), leading to a large heterogeneity in PC responses to whisker stimulation (Bosman et al., 2010; Chu et al., 2011). Therefore, we first made an overview of the firing properties of PCs in the ipsilateral lobules crus 1 and crus 2 in response to whisker pad air puff stimulation. Of the 53 single-unit PCs from which we recorded, 44 (83%) showed significant complex spike (CS) responses, but with large variations in latency and amplitude (Figs. 2B-D; S1A-B). Using electrolytic lesions and neural tracing, we found that the PCs with CS responses occurring within 80 ms following whisker stimulation were predominantly located around the border between crus 1 and crus 2, with the strongest responses in the lateral hemisphere, covering parts of cerebellar zones C2, C3, D1 and D2 (Figs. 2G-H; S1K-M). Cluster analysis confirmed that the lateral part of the border area between crus 1 and crus 2 was indeed the hotspot for strong CS responses to whisker pad stimulation (Fig. S1D-F, I).
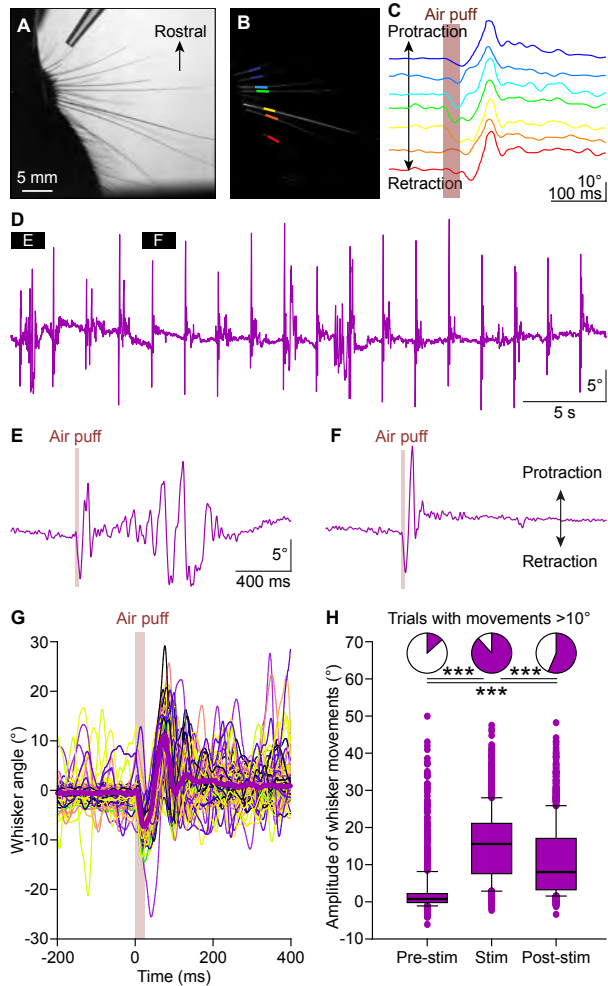
Figure 1 Whisker pad stimulation triggers stereotypic whisker behavior. (A) Mouse head with unclipped large facial whiskers and direction of the air puff (coming out of the pipette). Whisker movements were tracked (see panel b), revealing stereotypic responses to air puff stimulation: first a passive backwards movement followed by active protraction (c). The colors indicate individual whiskers. **(D)** The mean whisker angle during 0.5 Hz air puff stimulation of the whisker pad from a representative mouse. During approximately half the trials, the active protraction was only a single sweep, in the other traces multiple sweeps were observed. Prolonged periods of active whisking were rare. A trial with **(E)** and without **(F)** prolonged movements are enlarged below. **(G)** To indicate the variability in whisker behavior, 100 trials of the experiment illustrated above were superimposed. The thick line indicates the median. **(H)** Box plots showing the amplitudes (difference between maximal retraction and maximal protraction in the indicated 200 ms intervals) of individual trials of 13 mice (with approximately 100 trials per mouse). Obviously, most whisker movement was observed in the period between 0 and 200 ms after whisker pad air puff stimulation, as compared to the 200 ms intervals before and after this period. Top: Fractions of trials with movements exceeding $10°$. *** $p < 0.001$. For detailed statistics, see Table S1.

The responses of the simple spikes (SSs) were even more variable than those of the CSs, with often biphasic patterns entailing wide variations in the latencies to both troughs and peaks (Figs. 2E-F; S1C). Fifty PCs (94%) displayed a significant SS response to whisker pad stimulation. These PCs were found to be dispersed throughout crus 1 and crus 2 (Figs. 2I; S1J). The trough of the SS responses typically correlated in a reciprocal fashion with the peak of the CS responses (Figs. 2B-F; S1A-C) (Badura et al., 2013; De Zeeuw et al., 2011; Zhou et al., 2014), but the correlations between the latency and/or strength of the peak of the SS response and the strength of the CS peak response peak were poor (Fig. S1G-H). Thus, based on the CS response properties, we could define a ''whisker hotspot'' around the lateral border between crus 1 and crus 2, but also in the adjacent areas whisker-responsive PCs were abundant.

PC activity during motor performance

Next, we investigated to what extent the occurrence of CSs can have an impact on the whisker movement following an air puff. The active protraction following passive retraction was significantly stronger in trials in which a CS occurred than in trials without (on average an increase of $47 \pm 5\%$; $p = 0.0001$; Fig. 3A-D; Table S1). Remarkably, the position of the whiskers was already slightly, but significantly, more retracted before the air puff was given in trials with a CS following the air puff (a difference of $-0.18 \pm 0.05°$; $p = 0.0013$; Fig. 3B,D; Table S1), indicating that the state of the mouse at a given trial could affect its behavior. The latency between the peak in the CS response and the moment of maximal difference between trials with and without CSs was 58 ± 41 ms (median $\pm$ IQR), with the change in the whisker movement following after the CS firing (Fig. 3C-E; Table S1). Thus, indeed, CS firing was found to enhance protraction.

In view of the strong convergence between PCs and cerebellar nucleus neurons, however, we expect that CS synchrony would be required to exert motor commands (e.g., see (Hoogland et al., 2015; Mukamel et al., 2009). To study whether simultaneous CS firing by nearby PCs is indeed enhanced following whisker pad stimulation, we performed two-photon Ca^{2+} imaging in crus 1 and crus 2 (Fig. 3F). In line with earlier studies (De Gruijl et al., 2014; Mukamel et al., 2009; Ozden et al., 2009; Schultz et al., 2009), we found occasionally simultaneous Ca^{2+} events in multiple nearby PCs in the absence as well as in the presence of sensory stimulation (Fig. 3G-H). Widespread simultaneous activation was, however, much more present shortly after sensory stimulation ($p = 0.002$; Kolmogorov-Smirnov test; Fig. 3I). Thus, we conclude that coherent CS firing is substantially enhanced after whisker pad stimulation, so that indeed synchronous CS firing was present during the period in which we observed a behavioral impact of CS firing.

During spontaneous whisking, SS firing of PCs can correlate with whisker position. The large majority of PCs showed SS activity correlated to protraction and a minority with retraction (Chen et al., 2016). We studied the correlation between SS firing and whisker trajectory on a trial-by-trial basis. Of the 53 PCs of which we had simultaneous SS recordings and whisker videos, 21 (40%) showed a significant correlation during a trial-by-trial analysis (Figs. 4; S2). In all of the latter PCs, there was a positive correlation between instantaneous SS firing and whisker protraction.
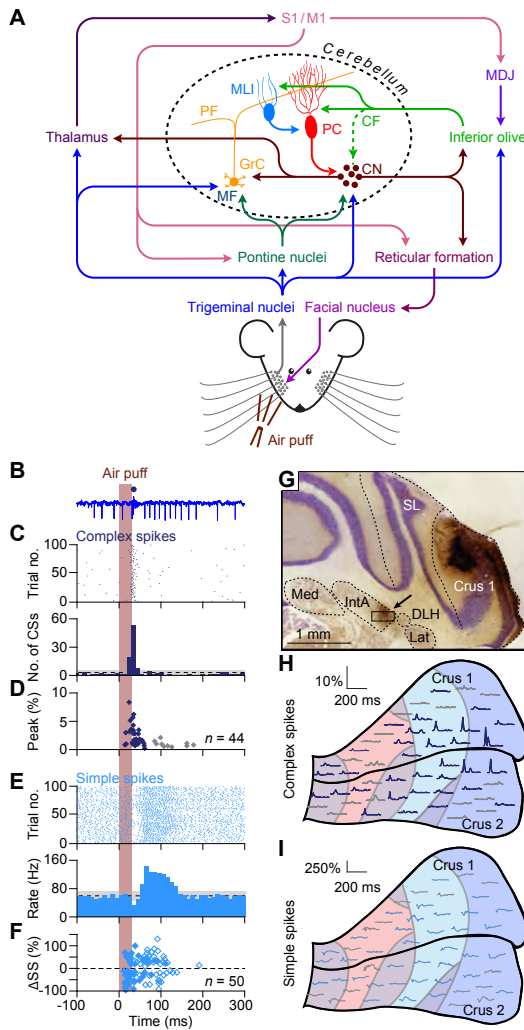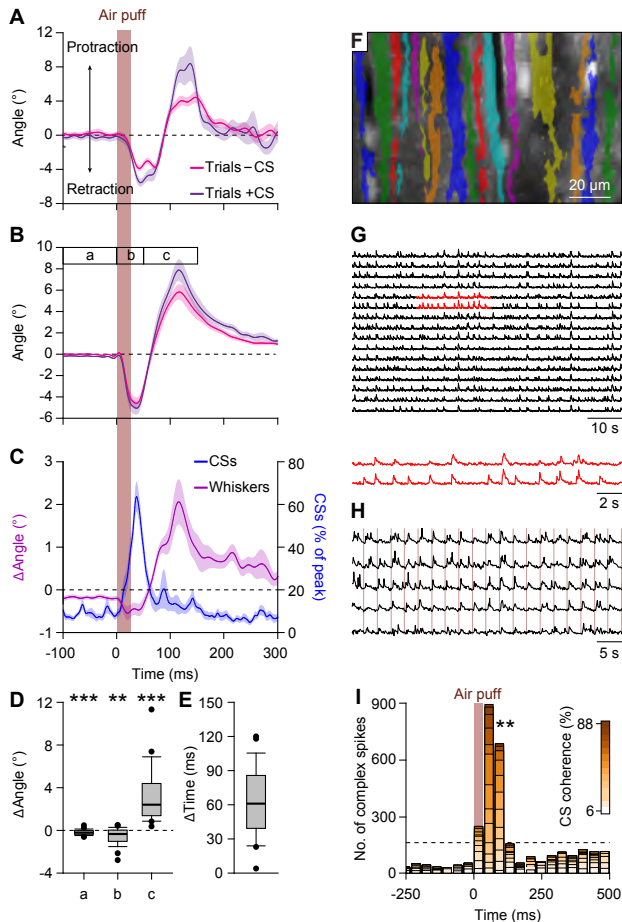
Figure 2 Heterogeneous Purkinje cell responses to whisker pad stimulation. (A) Simplified scheme of the somatosensory pathways from the whisker pad to the cerebellar Purkinje cells (PCs) and of the motor pathways directing whisker movement. The information flows from the whisker pad via the trigeminal nuclei and the thalamus to the primary somatosensory (S1) and motor cortex (M1). S1 and M1 project to the inferior olive via the nuclei of the meso-diencephalic junction (MDJ) and to the pontine nuclei. Both the inferior olive and the pontine nuclei also receive direct inputs from the trigeminal nuclei. The mossy fibers (MF) from the pontine nuclei converge with direct trigeminal MF on the cerebellar granule cells (GrC) that send parallel fibers (PF) to the PCs. The inferior olive provides climbing fibers (CF) that form extraordinarily strong synaptic connections with the PCs. Both the PFs and the CFs provide also feedforward inhibition to PCs via molecular layer interneurons (MLI). The GABAergic PCs provide the sole output of the cerebellar cortex that is directed to the cerebellar nuclei (CN). The CN sends the cerebellar output both upstream via the thalamus back to the neocortex and downstream to motor areas in the brainstem and spinal cord. The whisker pad muscles are under control of the facial nucleus which is mainly innervated via the reticular formation. Several feedback loops complement these connections. For references, see Bosman et al. (2011) and Deschênes et al. (2016). **(B)** Representative extracellular recording of a Purkinje cell in an awake mouse. A complex spike is indicated by a colored dot above the trace. **(C)** Complex spike responses of the same Purkinje cell to air puff stimulation of the whisker pad. **(D)** The latencies vs. the peak of the complex spike responses (see Methods) of all 44 Purkinje cells with a significant complex spike response. The grey symbols indicate Purkinje cells with long-latency (>80 ms) complex spike responses.

(E) Simple spike responses of the same Purkinje cell as in panels B and C. Note that the simple spike firing frequency is about 60-70 Hz. **(F)** Peak amplitudes (see Methods) and peak latency times of simple spike responses (bottom) of all 50 Purkinje cells showing a significant simple spike response to whisker pad stimulation. Simple spike responses were often found to be bi-phasic. The closed circles reflect the first and the open symbols the second phase of the simple spike response. Non-significant responses are omitted. **(G)** Purkinje cell locations could be retrieved by neural tracer injection (BDA 3000) after completion of the recording. In this example, tracer was found in the anterior interposed nucleus (IntA) (see arrow, area enlarged in Fig. S1M). SL = simple lobule, Med = medial nucleus, Lat = lateral nucleus; DLH = dorsolateral hump. **(H)** Approximate locations of the recorded Purkinje cells projected on the surface of crus 1 and crus 2. The colored bands refer to the cerebellar zones (see Fig. S1I). The kinetics of the complex spike response of each Purkinje cell is indicated as the convolved PSTH (starting from the onset of the stimulus; see Methods). **(I)** The same for the simple spike responses.

Figure 3 Complex spikes promote the initial whisker protraction after an air puff. (A) Whisker traces of a representative mouse separated according to the presence (violet) or the absence (magenta) of a complex spike produced by a simultaneously recorded Purkinje cell in the first 100 ms after stimulus onset. The trials with a complex spike tended to have a stronger protraction, which was also observed in the population (*n* = 28) **(B)**. **(C)** Averaged convolved peri-stimulus time histograms of complex spikes (blue) and the averaged difference in whisker position (purple) between trials with and without complex spikes. Complex spikes precede the observed differences in movement. Shaded areas indicate SEM. **(D)** Changes in average whisker angle before stimulation (period a; see time bar in panel B), in maximal retraction (period b) and in maximal protraction (period c) between trials with and without a complex spike in the 100 ms after an air puff. **(E)** Time intervals between the peak of the complex spike response and the maximal difference between the trials with and without complex spikes. **(F)** Field of view of a piece of crus 1 recorded using two-photon Ca^{2+} imaging in an awake mouse. The colored areas indicate 16 regions of interest, corresponding to Purkinje cell dendrites. The accompanying fluorescent traces show Ca^{2+} transients which are most likely complex spikes (**G**; see also the enlargement of the part marked in red below the traces (cf. Schultz et al. (2009)). In the absence of sensory stimulation, large-scale coherence is rare. **(H)** Following air puff stimulation of the whisker pad (brown vertical lines), complex spike coherence is largely increased. **(I)** Composite peri-stimulus time histogram of all Purkinje cells in the field of view shown in panel F. The colors represent the fraction of Purkinje cells active during each frame of 40 ms (see Methods). Complex spike synchrony is relative rare during inter-trial intervals, but strongly enhanced following air puff stimulation - i.e. during the period in which complex spike firing promoted protraction. Thus, the complex spikes measured in individual neurons (A-E) are probably largely in sync with network activity of complex spikes corresponding to the onset of the movement. *** p < 0.01; *** p < 0.001. For detailed statistics, see Table S1.*

Negative correlations, thus increased SS firing corresponding to more retraction, were also found, but never reached statistical significance (Fig. S2C). Strikingly, the correlations between SS firing and whisker protraction were most prominent around a zero lag, implying that the SS modulations occurred at the same time as the whisker movements, reminiscent of encodings required for an internal model (Brooks et al., 2015; Wolpert et al., 1998), or with a short (10-20 ms) delay respective to the whisker movement (Fig. 4D). Furthermore, the strongest correlations were found relatively late during the movement, in particular between 80 and 200 ms after the start of the air puff (Figs. 4C-D; S2D).

PC activity during motor learning

So far, we established that whisker pad stimulation induced a stereotypic motor pattern of the facial whiskers (Fig. 1). The initial protraction is preceded and promoted by synchronous CS firing (Fig. 3) and its amplitude correlates without a clear time lag with SS firing (Fig. 4). We next wondered whether the whisker movements could be enhanced following intense sensory stimulation, which would allow us to investigate correlates of PC activity with whisker movements during motor learning. We hypothesized that whisker movements might be enhanced following tetanic stimulation at 4 Hz as this frequency has been shown to be effective in recruiting SS potentiation (D'Angelo et al., 2001; Lev-Ram et al., 2002; Ramakrishnan et al., 2016). Indeed, application of this novel induction paradigm to the whiskers for only 20 seconds was sufficient to induce an increase in the level of protraction following a baseline air puff stimulation at 0.5 Hz (average increase $18.5 \pm 4.1\%$; $p < 0.001$; Fig. 5A-B; Table S1). Mice responded already during the air flow-induced retraction, leading to a reduction of the backwards movement after theta sensory stimulation ($p = 0.0211$; Table S1). Concomitantly, SS activity was significantly increased ($p < 0.001$), whereas CS activity was not significantly altered compared to baseline ($p = 0.181$; Fig. 5C-D; Table S1). Moreover, the SS response was not only increased, but also accelerated, leading to a faster and stronger SS response after induction (Fig. 5D-E). Accordingly, the correlation between instantaneous SS frequency and whisker angle, which was originally centered around a zero lag or even had a small delay relative to the whisker movement and had a relatively long latency, now occurred during a significantly earlier phase of the movement ($p = 0.0061$; Fig. 5F; Table S1). Indeed, SS modulation now preceded the whisker movement, as indicated by the large orange/red spot above the diagonal in the second correlation matrix plot of Fig. 5F. Thus, due to a relatively short period of strong sensory tetanic stimulation, SS modulation evolved from a representation of the movement to a potentially instructive signal that might contribute to the amplitude and timing of the movement.

In contrast to the effects of theta sensory stimulation on the whisker position (stronger protraction upon air puffs after theta sensory stimulation; $p < 0.0001$; Mann-Withney test), the occurrence of free whisking in between trials was not affected by theta sensory stimulation (Fig. S3A-F). Also over a longer time period, increased protraction was significant ($p = 0.024$; n = 7 mice; Friedman test). At first sight, it seemed that the increased protraction returned to baseline after approximately 25 min (Fig. S3G, L, H), but on closer inspection it turned out that over time, the
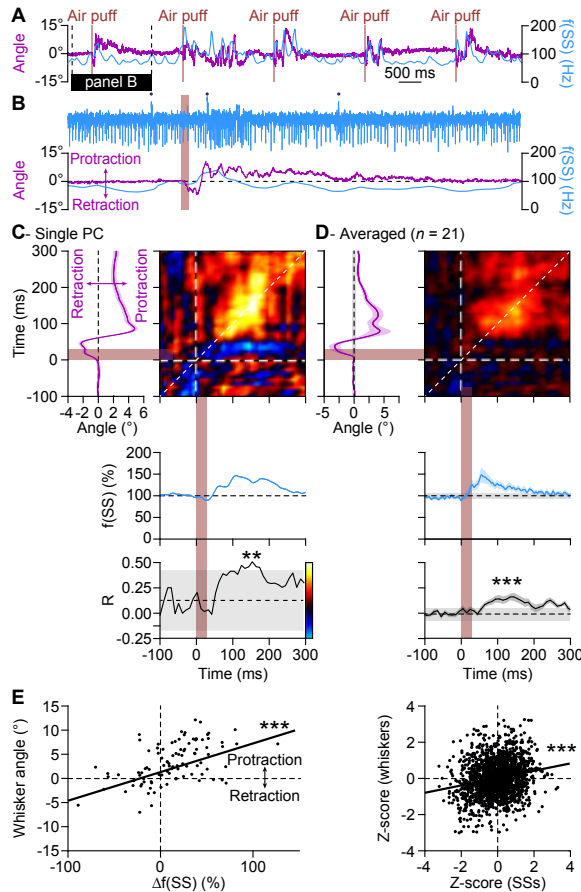
Figure 4 Increased simple spike firing correlates with whisker protraction. (A) Changes in the instantaneous SS firing rate (convolved with a 6 ms Gaussian kernel; blue) correlate roughly with whisker movement (purple). This is illustrated with a representative recording of a Purkinje cell. Vertical brown lines indicate the moments of air puff stimulation to the (ipsilateral) whisker pad. The horizontal black line designates the interval expanded in **(B)** Blue dots mark complex spikes. **(C)** Correlation matrix showing a clear positive correlation of simple spike firing (blue trace at the bottom shows convolved peri-stimulus time histogram triggered on air puff stimulation) and whisker protraction (red trace at the left; indicated is the mean ± SEM of the whisker position) based on a trial-by-trial analysis. The correlation coefficient (R) over the dashed 45° line is shown in the bottom, together with the 99% confidence interval (grey area). These data come from the example Purkinje cell shown in A-B. Averaged data from 21 Purkinje cells is shown in **(D)**. **(E)** Scatter plots with linear regression lines showing a positive correlation between whisker protraction and instantaneous SS firing (example Purkinje cell on the left and aggregated data of all 21 Purkinje cells on the right). The experiments are normalized based upon their Z-score. Data are taken from the moment with the strongest (positive) correlation (example (left): 150-160 ms (for whiskers and for simple spikes); average (right): 120-130 ms (whiskers) vs. 140-150 ms (simple spikes)). Thus, increased simple spike firing correlates with whisker protraction. ** $p < 0.01$; *** $p < 0.001$. For detailed statistics, see Table S1.

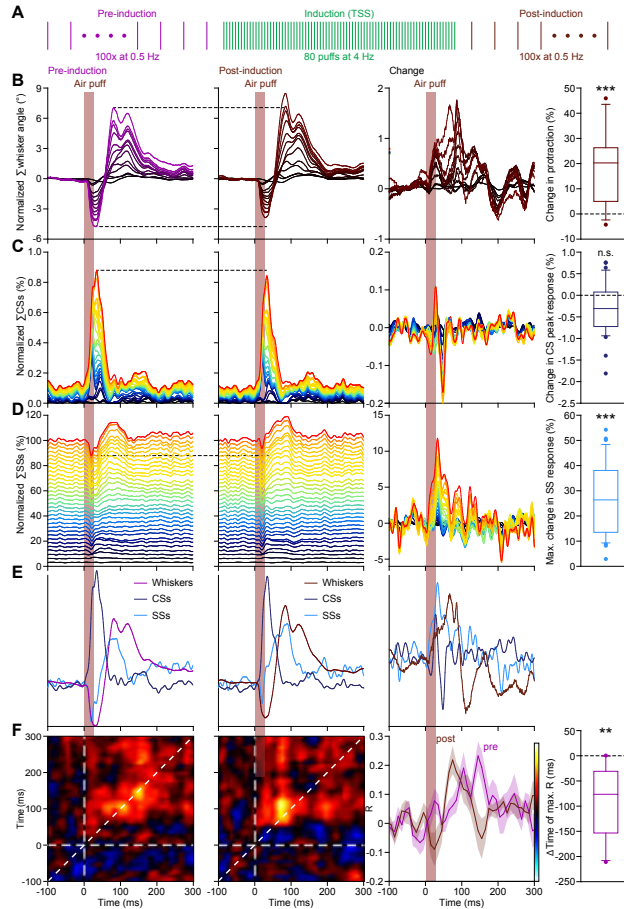**Figure 5 Sensory experience leads to anticipation of the simple spike response and stronger protraction of the whiskers. (A)** Induction protocol. Air puff stimulation at 0.5 Hz is used to characterize the impact of a brief period (20 s) of intense air puff stimulation (theta sensory stimulation at 4 Hz). **(B)** Stacked line plots (see Methods) showing the averaged whisker response before (1st column) and after (2nd column) theta sensory stimulation ($n = 13$ mice). The plots are sorted on increased protraction induced by theta sensory stimulation (3rd column). Each color depicts one mouse. Plots are normalized so that the most intense color represents the average. Theta sensory stimulation leads to a more protracted form of whisker movement (4th column). Similar plots for complex spikes (**C**, showing little change) and simple spikes (**D**, showing a clear increase in firing, especially during the early phase of the sensory response). For comparison, the averages are superimposed in **E** (for y-scaling and variations refer to B-D). Trial-by-trial analysis of 10 Purkinje cells before and after theta sensory stimulation (cf. Fig. 4C-D) highlighting the anticipation of simple spike firing **(F)**. The x-axis is based upon instantaneous simple firing and the y-axis upon whisker angle. After induction, the correlation (R) between simple spikes and whisker angle (along dashed 45° line) shifts to earlier after the air puff (3rd column; shaded areas indicate SEM). In addition, a clear correlation is found with simple spike firing leading whisker movement (yellow/red area expands above the 45° line in 2nd column as compared to the left column). Scale bar of the correlation matrices (left and middle) is at the right of the 3rd column. ** p < 0.01; *** p < 0.001. For detailed statistics, see Table S1.*

protraction started earlier, as quantified by the moment during which the whisker position passed the resting position in going from backwards to forwards ($p = 0.0252$; repeated measures ANOVA; Fig. S3G2, I). Thus, theta sensory stimulation had a long lasting effect on whisker movement that developed gradually, so that the mice reacted faster to sensory stimulation afterwards.

CS response and post-CS SS activity indicate identity of PCs involved in learning

Are the adaptation of the whisker movements and that of the SS responses following theta sensory stimulation directly due to potentiation of PCs or are both processes the consequence of plasticity elsewhere in the brain? To answer this question, we first focused on the relation between PC firing patterns and increased SS responses to sensory stimulation. We reasoned that mechanisms upstream of PCs would be likely to affect all PCs irrespective of their firing pattern during the induction period.

Long-term plasticity of the parallel fiber-to-PC synapse is known to be under control of CS firing: presence of CS activity leads to long-term depression and its absence promotes long-term potentiation (Coesmans et al., 2004). Hence, we predicted that observed SS enhancement would occur predominantly in PC cells showing a weak CS response to sensory stimulation (cf. Fig. S1D). Indeed, increased SS responses following theta sensory stimulation were prominently present in PCs with weak CS responses, but not in those with a strong CS response (Figs. 6A-B; S4A; Table S1). Hence, SS potentiation was largely absent in the ''whisker hotspot'' around the lateral part of the border between crus 1 and crus 2 (Fig. 6C). In contrast, a correlation with the SS response properties to whisker pad stimulation and the impact of theta sensory stimulation was not present (Fig. S4B). The chance in SS responsiveness lasted at least half an hour. Also over this longer timescale, the differential plasticity under control of climbing fiber activity remained intact (Fig. 6F).

A further categorization of PC firing properties according to the SS activity following the CSs into pause-only, long-pause, pause-facilitation or pause-facilitation-suppression patterns (De Zeeuw et al., 2011; Zhou et al., 2014) showed that theta sensory stimulation was mainly effective in inducing the short-latency SS increases in the PCs with a facilitation type of SS activity following the climbing fiber pause. This held true both when only analyzing the SS activity directly following the CSs (Fig. S5A-D) and when analyzing sensory SS responses (Fig. S5E-G). Thus, the strength of the CS response to whisker stimulation as well as the SS activity directly following the CSs predict to what extent the SSs of the PC will adapt to tetanic whisker stimulation and the corresponding correlations are in line with cellular induction protocols for PC potentiation (Coesmans et al., 2004). Together this is a clear indication that indeed the plasticity occurs at the level of the PCs rather than upstream.

Blockage of potentiation specifically in PCs prevents adaptation

If it is indeed plasticity at the PC level that is required for the concomitant changes in simple spike responsiveness and in increased whisker protraction, then both mod-
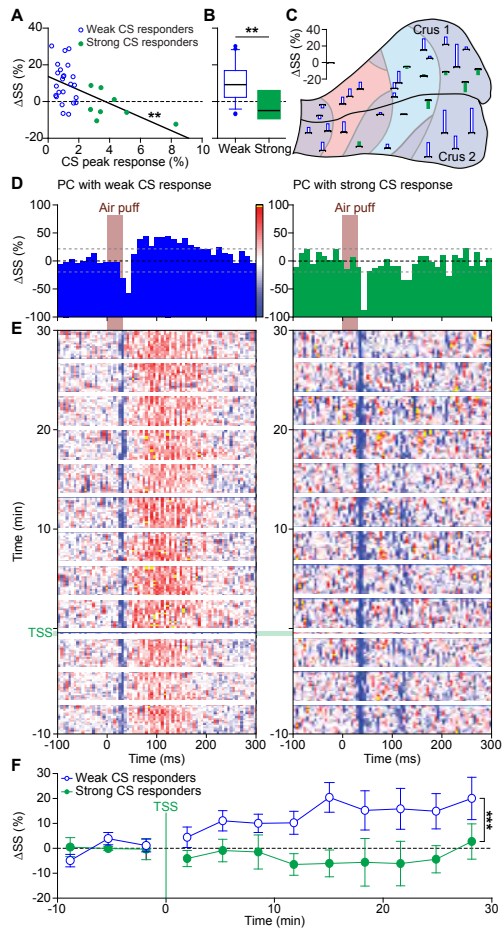
Figure 6 Whisker pad stimulation specifically potentiates PC responses with weak complex spike responses. (A) 4 Hz sensory stimulation (Fig. 5A) induced an increase in simple spike response to whisker pad stimulation, but not in all Purkinje cells. There was a clear negative correlation between the strength of the complex spike response (cf. Fig. 2D) and the potentiation of the simple spike response. Overall, there was potentiation in the Purkinje cells with weak complex spike responses (cf. Fig. S1D), but not in the strong CS responders **(B)**. **(C)** Schematic map of crus 1 and crus 2 indicating the approximate locations of Purkinje cells showing increased or decreased simple spike firing following theta sensory stimulation. Open bars indicate Purkinje cells with weak complex spike responses and the filled bars those with strong complex spike responses. These differences remained relatively stable during longer recordings. Example PSTHs of the simple spike response to whisker pad air puff stimulation of representative Purkinje cells **(D)** and how these changed over time, depicted as heat map (see Methods) **(E)**. The left column displays the data from a representative Purkinje cell with a weak complex spike response, the right column of one with a strong complex spike response. The colors of the heat map refer to the relative simple spike firing (see scale bar in D). **(F)** The number of simple spikes following an air puff stimulation increased in weakly responding WT Purkinje cells and this increase remained elevated until the end of the recording (at least 30 min). In contrast, this increase was not found in Purkinje cells with strong complex spike responses. *$p < 0.05$; ** $p < 0.01$; *** $p < 0.001$. For detailed statistics, see Table S1.
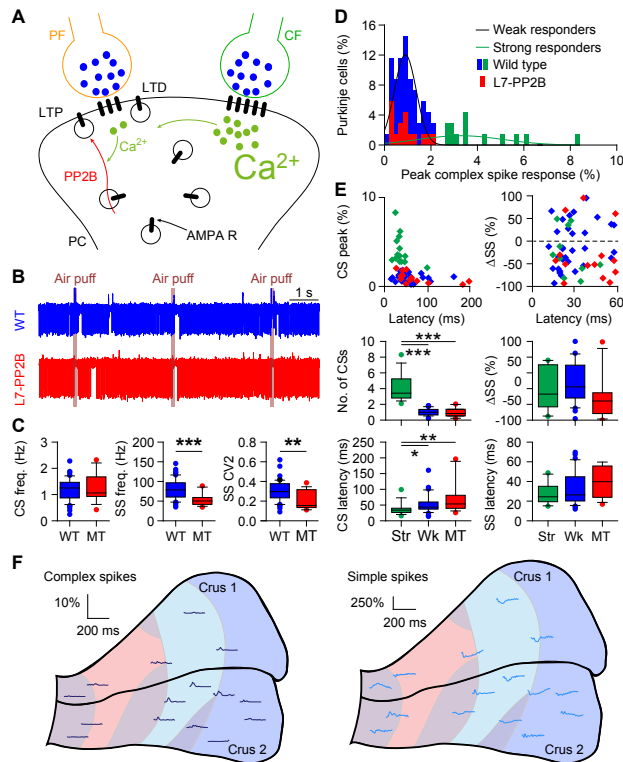
ulations should be absent in L7-PP2B mouse mutants. In these PC-specific mutant mice, the PCs display impaired intrinsic plasticity as well as an absence of LTP at their parallel fiber inputs (Schonewille et al., 2010) (Fig. 7A). Before using the same induction protocol on these mice, we first characterized the basic firing properties of their PCs. We found that PCs of L7-PP2B mice had a similar CS frequency, but a lower SS frequency than their wild-type littermates. Furthermore, SS firing was more regular than in PCs of WT littermates (Fig. 7B-C; for detailed statistics see Table S1). Since in WT mice, we showed that only PCs with weak CS responses show increased SS sensory responses after theta sensory stimulation (Fig. 6B), we focused on PCs with weak CS responses in L7-PP2B mice. These PCs had similar response properties as the WT controls (Fig. 7D-F).

Despite similar CS firing and sensory responses of their PCs, we found increased whisker protraction upon theta sensory stimulation in only three of the ten mutant mice, compared to 11 out of 13 WT littermates (p = 0.005; Fig. 8A-C). Moreover, whereas the wild-type littermates showed significantly increased SS responses during the early phase of the response period (p = 0.012), the L7-PP2B mutants did not show significant increases of their SS responses following theta stimulation (p = 0.315; Fig. 8D), which effects were stable over time (Figs. 8E; S6; Table S1). In contrast, the CS responses to sensory stimulation and their short-term impact on protraction were unaffected in the mutants (Figs. 7E, S4C-D). Thus, the PC-specific potentiation-deficient mutants were neither able to increase their SS responses in the long-term nor to adapt the protraction of their whiskers (Fig. 8), whereas their CS responses and whisker reflexes appeared normal.

Discussion

Our results show that whisker movements can be readily adjusted following a short period of sensory stimulation in the theta frequency band and that adaptive increases in SS firing of cerebellar PCs are necessary and sufficient to mediate this type of procedural memory formation. These results were observed as long as our recordings lasted (>30 min; Fig. 6E). To the best of our knowledge, this is the fastest whisker learning paradigm applied to rodents, in which a lasting effect on neuronal activity could be coupled to a change in motor behavior on a trial-by-trial basis. Presumably, similar adaptations are being used during natural object exploration (Anjum and Brecht, 2012; Bosman et al., 2011; Brecht, 2007; Voigts et al., 2015) and during go/no-go tasks involving whisker movements (Rahmati et al., 2014).

In line with the classical view on parallel fiber LTD as the prime mechanism for cerebellar plasticity (Albus, 1971; Ito, 2003; cf. Schonewille et al., 2011), some studies have shown that suppression of SS activity can indeed underlie procedural learning. For example, in eyeblink conditioning as well as in smooth pursuit learning, suppression of SSs has been shown with trial-by-trial analyses to contribute to cerebellar learning (Jirenhed et al., 2007; Ten Brinke et al., 2015; Yang and Lisberger, 2014). The current study is one of the first demonstrations in which PC-specific potentiation as well as SS enhancement, rather than LTD and SS suppression, are found to be critical for cerebellar motor learning.
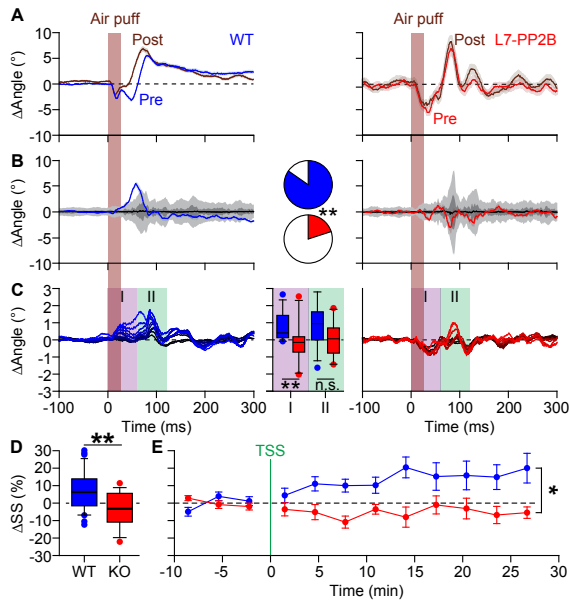
Figure 7 Purkinje cell responses to whisker pad stimulation are largely intact in L7-PP2B mice. (A) Schematic representation of the principal pathways regulating bidirectional plasticity at the parallel fiber (PF) to Purkinje cell (PC) synapses. The direction of PF-PC plasticity depends on the intracellular Ca^{2+} concentration ($[Ca^{2+}]i$) that is largely determined by climbing fiber (CF) activity. Following CF activity, $[Ca^{2+}]i$ raises rapidly and activates a phosphorylation cascade involving α-Ca^{2+}/calmodulin-dependent protein kinase II (CaMKIIA) and several other proteins eventually leading to internalization of AMPA receptors and consequently to long-term depression (LTD). PF volleys in the absence of CF activity, on the other hand, result in a moderate increase in $[Ca^{2+}]i$, activating a protein cascade involving protein phosphatase 2B (PP2B) that promotes the insertion of new AMPA receptors into the postsynaptic density, thereby leading to long-term potentiation (LTP) of the PF-PC synapse. **(B)** Example recordings of PC activity in a wild-type (WT) (top) and a L7-PP2B deficient mouse (bottom). The timing of air puffs to the whisker pad is indicated with light brown lines. **(C)** Under our experimental conditions, the CS rates were comparable between PCs from L7-PP2B KO mice (MT) and their WT littermates. However, SS firing was slower and more regular in L7-PP2B compared to the control littermates. **(D)** For further analysis, we selected only *weak CS responders* in the L7-PP2B mice (cf. Fig. S1D-F). **(E)** Comparison of the response properties showed that the peak CS responses were obviously the strongest in the strong CS responders (green), but similar between the weak CS responders of both WT (blue) and L7-PP2B (red) mice ($p = 1.000$). *Strong CS responders* had also the fastest CS responses, but the CS response latencies were not significantly different between the *weak CS responders* of both genotypes ($p = 0.643$). SS response latencies were comparable for all three groups of PCs ($p = 0.149$; Kruskal-Wallis test). **(F)** Convolved CS (left) and SS (right) response profiles plotted on the recording sites within the cerebellar cortex. The moment of the air puff is at the left side of the trace. The y axis indicates the modulation depth related to the baseline recording (see Methods). * $p < 0.05$; ** $p < 0.01$; *** $p < 0.001$. For detailed statistics, see Table S1.

Figure 8 Expression of PP2B in Purkinje cells is required for increased protraction and simple spike firing following theta sensory stimulation. (A) Example of a representative mouse with the averaged whisker movements before and after theta sensory stimulation, showing a stronger protraction afterwards, as evidenced by the differences between post- and pre-induction compared to a bootstrap analysis on the normal variation in whisker movements (b; dark shade: 95% confidence interval; light shade: 99% confidence interval). Although also differences were observed in L7-PP2B mutants, these did generally not exceed the expected variations (right). In 11 out of 13 wild-type mice more protraction than expected was observed, against in only 3 out of 10 L7-PP2B mutant mice (pie charts). **(C)** Stacked line plots (see Methods) of whisker movement differences between post- and pre-induction for all mice. The plots are normalized so that the brightest line indicates the average per genotype. The impact of theta sensory stimulation was especially different during the early phase (0-60 ms; purple), whereas similar during the later phase (60-120 ms). Box plots indicate the average differences over the indicated time intervals. **(D)** WT Purkinje cells (with weak complex spike responses) show a clear potentiation of their simple spike response to whisker pad stimulation after theta sensory stimulation (TSS), whereas Purkinje cells from L7-PP2B mice do not. This effect was stable, also during longer recordings (E). *$p < 0.05$; ** $p < 0.01$; *** $p < 0.001$. For detailed statistics, see Table S1.

Mutant mice suffering from a lack of LTP, including knock-outs of not only PP2B (Schonewille et al., 2010), but also Cav3.1 T-type calcium channels (Ly et al., 2013), Shank2 (Peter et al., 2016) or GluA3 (Gutierrez-Castellanos et al., 2017), have all been shown to suffer from impairments in adaptation of the vestibulo-ocular reflex (VOR), another common form of cerebellar motor learning, but none of these studies was able to find concomitant alterations in SS firing, let alone to demonstrate changes on a trial-by-trial basis. Still, given that VOR adaptation is mediated by the flocculus of the vestibulocerebellum, which is largely zebrin-positive (Sugihara and Quy, 2007), and that optogenetic stimulation of PCs in the flocculus can enhance both SS firing and gain increase stimulation (Voges et al., 2017), these VOR studies corroborate the current findings in that they both support the hypothesis that zebrin-positive regions may predominantly use potentiation mechanisms for learning (De Zeeuw and Ten Brinke, 2015).

Interestingly, the PCs that are responsible for the long-term adaptation in whisker movements can be distinguished from the whisker PCs that appear to mediate short-term reflexes through enhanced coherence of strong CS responses preceding the movements (De Gruijl et al., 2014). During such forms of non-adaptive motor performance, the SS modulation precisely follows the ongoing movement, as predicted by an internal model without time lag (Fig. 3D) (Brooks et al., 2015; Wolpert et al., 1998). Instead, during a training situation, SS activity accelerates and changes in SS activity precede the changes in amplitude and timing of the movements. Such a flexible coupling between SS firing and whisker movements is further emphasized by our findings that the time course of changes in SS responsiveness and increased whisker protraction are different (Fig. S3G-I). The learned signals in the whisker regions probably differentially modify the activity of the cerebellar nucleus neurons. Thus, our novel behavioral whisker learning paradigm revealed a novel pathway for fast procedural learning, in which potentiated SS signals can provide an instructive signal to the cerebellar nuclei.

Methods

Animals

The generation of mice lacking functional PP2B specifically in their Purkinje cells (PCs) (Tg(Pcp2-cre)2MPin;Ppp3r1[tm1stl]) has been described previously. Briefly, we used crossings of mice in which the gene for the regulatory subunit (CNB1) of PP2B was flanked by loxP sites with transgenic mice expressing Cre-recombinase under control of the L7 (Pcp2) promoter. L7-Cre^{+/-}-cnb1[f/f] mice ("L7-PP2B mice") were compared with L7-Cre^{-/-}-cnb1[f/f] littermate controls ("WT mice"). We used 31 WT mice (12 males and 19 females of 21 ± 10 weeks of age (average $\pm$ s.d.)) and 19 L7-PP2B mice (5 males and 14 females of 17 ± 10 weeks of age (average $\pm$ s.d.)). All mice that were used for electrophysiology received a magnetic pedestal that was attached to the skull above bregma using Optibond adhesive (Kerr Corporation, Orange, CA) and a craniotomy was made on top of crus 1 and crus 2. The surgical procedures were performed under isoflurane anaesthesia (2-4% V/V in O2). Post-surgical pain was treated with 5

mg/kg carprofen (Rimadyl, Pfizer, New York, NY), 1 μg lidocaine (Braun, Meisingen, Germany) and 1 μg bupivacaine (Actavis, Parsippany-Troy Hills, NJ, USA). After three days of recovery, mice were habituated to the recording setup during at least 2 daily sessions of approximately 45 min. In the recording setup, they were head-fixed using the magnetic pedestal. The photostimulation experiments were performed on 3 female mice (>140 days of age) expressing channelrhodopsin 2 exclusively in their PCs (Tg(Pcp2-cre)2MPin;Gt(ROSA)26Sor[tm27.1(CAG-COP4*H134R/tdTomato)Hze]) as described previously. The mice used for two-photon imaging received a head plate with a sparing on the location of the craniotomy instead of a pedestal. The head plate was attached to the skull with dental cement (Superbond C&B, Sun Medical Co., Moriyama City, Japan). To prevent the growth of scar tissue, which could affect image quality, two-photon recordings were made directly after recovery from surgical anaesthesia. For the two-photon experiments, 6 male C57Bl/6 mice (Charles Rivers, Leiden, the Netherlands) of 4-12 weeks of age were used. Mice were socially housed until the surgery and single-housed afterwards. The mice were kept at a 12/12 h light/dark cycle and had not been used for any invasive procedure (except genotyping shortly after birth) before the start of the experiment. All experimental procedures were approved a priori by an independent animal ethical committee (DEC-Consult, Soest, The Netherlands) as required by Dutch law.

Electrophysiology

Electrophysiological recordings were performed in awake mice using either glass pipettes (3-6 MΩ) or quartz-coated platinum/tungsten electrodes (2-5 MΩ), outer diameter = 80 μm, Thomas Recording, Giessen, Germany). The latter electrodes were placed in an 8x4 matrix (Thomas Recording), with an inter-electrode distance of 305 μm. Prior to the recordings, the mice were lightly anaesthetised with isoflurane to remove the dura, bring them in the setup and adjust all manipulators. Recordings started at least 60 min after termination of anaesthesia and were made in crus 1 and crus 2 ipsilateral to the side of the whisker pad stimulation at a minimal depth of 500 μm. Air puff stimulation was applied with a frequency of 0.5 Hz s at a distance of approximately 5 mm roughly perpendicular to the whisker pad. Each puff (2 bar) lasted 30 ms. During the induction period, the frequency was increased to 4 Hz and 80 puffs were given. The electrophysiological signal was digitized at 25 kHz, using a 1-6,000 Hz band-pass filter, 22x pre-amplified and stored using a RZ2 multi-channel workstation (Tucker-Davis Technologies, Alachua, FL). Spikes were detected offline using SpikeTrain (Neurasmus, Rotterdam, The Netherlands). A recording was considered to originate from a single PC when it contained both CSs (identified by the presence of stereotypic spikelets) and SSs, when the minimal inter-spike interval of SSs was 3 ms and when each CS was followed by a pause in SS firing of at least 8 ms. The regularity of SS firing was expressed as the local variation (CV2) and calculated as 2|ISIn+1-ISIn|/(ISIn+1+ISIn) with ISI = inter-SS interval. Only single-unit recordings of PCs with a minimum recording duration of 200 s were selected for further analysis. However, for the neural tracing experiments (see below), on which no quantitative analysis was performed, we accepted a minimum recording duration of 50 s.

Neural tracing & electrolytic lesions

For the neural tracing experiments, we used glass electrodes filled with 2 M NaCl for juxtacellular recordings. After a successful recording of a PC, neural tracer was pressure injected (3 x 10 ms with a pressure of 0.7 bar) either from the same pipette re-inserted at the same location or from the second barrel or a double barrel pipette. We used a gold-lectin conjugate has described previously (n = 3) or biotinylated dextran amine (BDA) 3000 (10 mg/ml in 0.9% NaCl; ThermoFisher Scientific, Waltham, MA, USA) (n = 7). Five days after the tracer injection, the mice were anaesthetised with pentobarbital (80 mg/kg intraperitoneal) and fixated by transcardial perfusion with 4% paraformaldehyde. The brains were removed and sliced (40 μm thick). The slices were processed by Nissl staining. Experiments were included in the analysis if the electrophysiology fulfilled the requirements mentioned above with a recording duration of at least 50 s and if the tracer was clearly visible. For BDA 3000 this implied that it was taken up by the PCs at the injection spot and transported to the axonal boutons a single subgroup in the cerebellar nuclei. BDA 3000 was also found in the inferior olive. For the gold-lectin conjugate the subnucleus of the inferior olive was considered. Based upon the subnuclei of the cerebellar nuclei and/or the inferior olive, the sagittal zone of the recording site was identified according to the scheme published in.

After the recordings made with the quartz/platinum electrodes, electrolytic lesions were applied to selected electrodes in order to retrieve the recording locations. To this end, we applied a DC current of 20 μA for 20 s. This typically resulted in a lesion that could be visualized after Nissl staining of 40 μm thick slices made of perfused brains (see above). We accepted a spot as a true lesion if it was visible in at least 2 consecutive slices at the same location. In total, we could retrieve 16 successful lesions. Recording locations were approximated using pictures of the entry points of the electrodes in combination with the locations of the lesions.

Characterization of sensory responses

For each PC recording, we constructed peri-stimulus time histograms (PSTHs) of CSs and SSs separately using a bin size of 10 ms for display purposes. For further quantitative analyses of the PSTHs, we used a bin size of 1 ms and convolved them with a 21 ms wide Gaussian kernel. CS responses were characterized by their peak amplitude, defined as the maximum of the convolved PSTH and expressed in percentage of trials in which a CS occurred within a 1 ms bin. Latencies were taken as the time between stimulus onset and the time of the response peak, as determined from the convolved PSTH.

For some analyses, we discriminated between the sensory response period (0-60 ms after stimulus onset) and inter-trial interval (500 to 200 ms before stimulus onset). We considered a PC responsive for sensory stimulation if the peak or trough in the PSTH in the 60 ms after the stimulus onset exceeded the threshold of 3 s.d. above or below the average of the pre-stimulus interval (1 ms bins convolved with a 21 ms Gaussian kernel, pre-stimulus interval 200 ms before stimulus onset).

Long-term stability of electrophysiological recordings was verified by heat maps of time-shifted PSTHs (e.g., see Extended Data Fig. 4B). The time-shifted PSTH is

processed by calculating the SS PSTH for 20 air puffs per row, which are shifted by 5 air puffs between neighbouring rows. The SS rates per row are calculated at 1 ms resolution and convolved with a 21 ms Gaussian kernel and colour-coded relative to baseline firing rate (-1000 to -200 ms relative to air puff time).

Cluster analysis

A principal component analysis showed that the heterogeneity among the sensory CS responses was driven almost exclusively by one parameter, the maximum amplitude peak of the convolved CS PSTH. We performed a univariate Gaussian mixture model using only that variable. The Bayesian information criterion (BIC) indicated that the model with two components with unequal variances yielded the best approximation of the data. Then we applied the function Mclust(data) in R (R Foundation, Vienna, Austria) which use the expectation-maximization algorithm in order to assert the main parameters of the resulting models (probability, mean and variance of each population).

Two-photon Ca^{2+} imaging

After the surgery (see above) during which the dura mater was preserved, the surface of the cerebellar cortex was cleaned with extracellular solution composed of (in mM) 150 NaCl, 2.5 KCl, 2 CaCl2, 1 MgCl2 and 10 HEPES (pH 7.4, adjusted with NaOH). After the surgery, the mice were allowed to recover from anaesthesia for at least 30 minutes. Subsequently, the mice were head-fixed in the recording setup and they received a bolus-loading of the cell-permeant fluorescent Ca^{2+} indicator Cal-520 AM (0.2 mM; AAT Bioquest, Sunnyvale, CA, USA). The dye was first dissolved with 10% w/V Pluronic F-127 in DMSO (Invitrogen) and diluted 20x in the extracellular solution. The dye solution was pressure injected into the molecular layer (50-80 μm below the surface) at 0.35 bar for 5 min. Finally, the brain surface was covered with 2% agarose dissolved in saline (0.9% NaCl) in order to reduce motion artefacts and prevent dehydration.

Starting at least 30 min after dye injection, in vivo two-photon Ca^{2+} imaging was performed of the molecular layer using a setup consisting of a titanium sapphire laser (Chameleon Ultra, Coherent, Santa Clara, CA), a TriM Scope II system (LaVision-BioTec, Bielefeld, Germany) mounted on a BX51 microscope with a 20x 1.0 NA water immersion objective (Olympus, Tokyo, Japan) and GaAsP photomultiplier detectors (Hamamatsu, Iwata City, Japan). A typical recording sampled 40 x 200 μm with a frame rate of approximately 25 Hz.

Image analysis was performed offline using custom made software as described and validated previously. In short, we performed independent component analysis to define the areas of individual Purkinje cell dendrites (Fig. 2D). The fluorescent values of all pixels in each region of interest were averaged per frame. These averages were plotted over time using a high-pass filter. A 8% rolling baseline was subtracted with a time window of 0.5 ms. Ca^{2+} transients were detected using template matching (Fig. 4E).

Whisker tracking and quantification

Videos of the whiskers were made from above using a bright LED panel as backlight (λ = 640 nm) at a frame rate of 1,000 Hz (480x500 pixels using an A504k camera from Basler Vision Technologies, Ahrensburg, Germany). The whiskers were not trimmed or cut. Whisker movements were tracked offline as described previously using a method based on the BIOTACT Whisker Tracking Tool. We used the average angle of all trackable large facial whiskers for further quantification of whisker behaviour.

The impact of theta-sensory stimulation on air puff-triggered whisker movement was quantified using a bootstrap method. First, we took the last 100 trials before induction and divided these randomly in two series of 50. We calculated the differences in whisker position between these two series, and repeated this 1000 times. From this distribution, we derived the expected variation after whisker pad air puff stimulation. We took the 99%-confidence interval as the threshold to which we compared the difference between 50 randomly chosen trials after and 50 randomly chosen trials before induction (Fig. 6B).

Spikes-whisker movement correlation matrix

Trial-by-trial correlation between instantaneous simple spike firing rate and whisker position was performed as described before[25]. In short: spike density functions were computed for all trials by convolving spike occurrences across 1 ms bins with an 8 ms Gaussian kernel. Both spike and whisker data were aligned to the 200 ms baseline. For cell groups, data was standardized for each cell for each correlation, and then pooled. The spike-whisker Pearson correlation coefficient R was calculated in bin of 10 ms, resulting in a 40x40 R-value matrix showing correlations for -100 to 300 ms around the air puff presentation.

Statistical analysis

Group sizes of the blindly acquired data sets were not defined a priori as the effect size and variation were not known beforehand. A post hoc power calculation based upon the results of the potentiation of the PC responses to whisker pad stimulation of the ''weak CS responders'' indicated a minimum group size of 12 PCs (α = 5%, β = 20%, Δ = 9.65%, sd = 10.59%, paired t test). This number was obtained for the ''weak CS responders'' in WT (n = 24) and L7-PP2B (n = 15) mice, but not for the relatively rare ''strong CS responders'' in WT mice (n = 8). The latter group was far from showing a significant potentiation (p = 0.547), indicating that they are not potentiated by theta sensory stimulation. This was further substantiated by other independent analyses, including ANOVA and linear regression, as described in the Results section. Variations in success rate, especially considering recordings of longer duration in combination with video tracking, explain why some groups are larger than others. Data was excluded only in case of a signal to noise ratio that was insufficient to warrant reliable analysis.

We tested whether the observed increase in coherence after sensory stimulation (Fig. 2F) was more than expected from the increased firing rate induced by the

stimulation. The expected coherence based on the firing rate was calculated from 1000 bootstrapped traces from the inhomogeneous Poisson spike trains made for each neuron. The resultant distribution was compared to the measured distribution using a two-sample Kolmogorov-Smirnov test.

Stacked line plots were generated by cumulating the values of all subjects per time point. Thus, the first line (darkest colour) represents the first subject, the second line the sum of the first two, the third line the first three, etcetera. The data are divided by the number of subjects, so that the last line (brightest colour) represents, next to the increase from the one but last value, also the population average.

Unless otherwise specified, data is represented as mean ± SEM. For normally distributed data (as evaluated using the Kolmogorov-Smirnov test) parametric tests were used. Comparisons were always made with 2-sided tests when applicable. All details on statistical tests used and their outcomes are summarized in Extended Data Fig. 7.

Supplementary Material
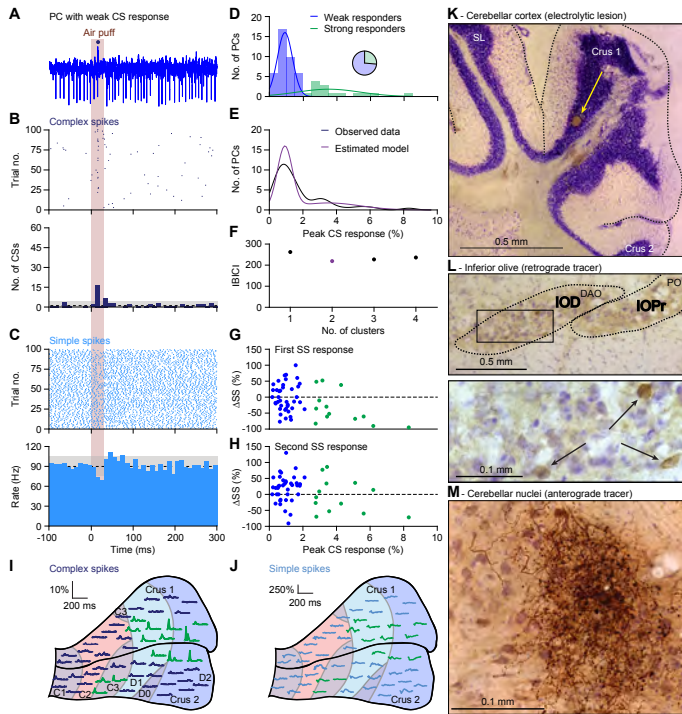
Figure S1 Anatomy of the whisker region in the cerebellar hemispheres. (A) Single trial of a Purkinje cell (PC) showing a relatively weak complex spike (CS) response to air puff stimulation of the ipsilateral whisker pad. The dark blue dot indicates a CS. **(B)** Raster plot and peri-stimulus time histogram (PSTH) of the CSs of the same neuron as in a. Note that although the initial CS response is relatively weak, being present only in about 15% of the trials, this is still much more than could be expected based on the CS frequency during the inter-trial intervals. The dashed line indicates the average CS rate in between trials with the grey area representing ± 3 sd. **(C)** The same for the simple spike (SS) response. This PC has a bimodal SS response, first a decrease and then an increase in SS response. **(D)** Based upon the peak of the CS response, defined as the maximum of the convolved PSTH (see Methods), PCs could be grouped into two clusters. The majority (73%) of the PCs could be classified as *weak CS responders* and the minority (27%) as *strong CS responders* (see pie diagram). This classification was obtained using a univariate Gaussian mixture model (see Methods). **(E)** Comparison of the distribution of the observed CS responses and that expected by our model. **(F)** Using the Bayesian information criterion (see Methods) confirmed that two clusters was indeed the optimal description of our data. **(G)** There was no good correlation between the strength of the CS response and the first peak or trough (cf. panel c) in the SS response. Only the PCs with a very strong CS response tended to have a decrease in SS response. PCs without a modulation of their SSs were set at 0% change. **(H)** The same for the second extremum of the SS response. For this later phase even less correlation between the CS and the SS responses was observed. **(I)** Map of the approximated locations of the recorded PCs based upon their CS response (green = strong CS responders; dark blue = weak CS responders). The names of the cerebellar zones are indicated. **(J)** The same for the SSs, using the color code of the CS responses. **(K)** For most of PC recordings in this study, the anatomical locations were defined by a combination of surface photographs and electrolytic lesions made after completion of the recordings. An example of such a lesion in crus 1 is shown here in combination with a Nissl staining. For a subset of experiments (*n* = 10), neural tracers were used to define the sagittal zones in which the recorded PCs were located. BDA 3000 was injected via a double barrel pipette at the recording site. After a survival period of around 1 week, retrograde staining was observed in the inferior olive **(L)** and anterograde staining in the cerebellar nuclei **(M)**. The rectangle in the top micrograph of L indicates the area enlarged in the lower micrograph. *DAO = dorsal accessory olive; PO = principal olive.*
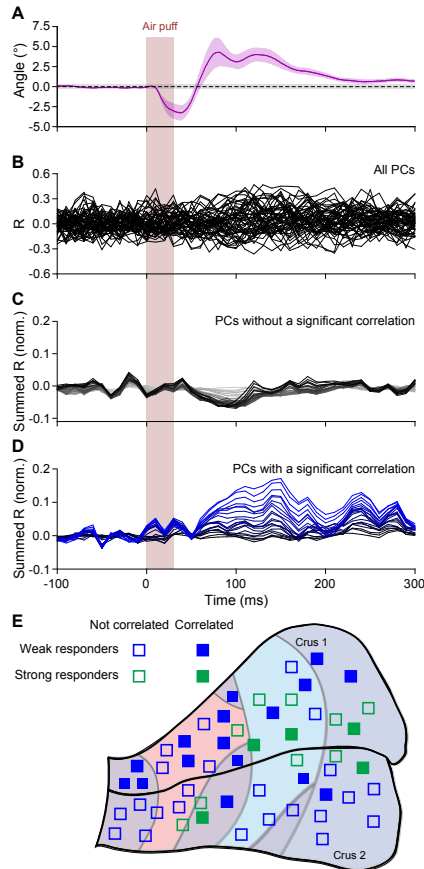
Figure S2 Simple spike firing is predominantly associated with protraction. (A) The average whisker response to air puff stimulation (for reference, copied from Fig. 4D). **(B)** Overlaid plots of the correlation between whisker angle and instantaneous simple spike frequency based on a trial-by-trial analysis of all 53 Purkinje cells (PCs) measured in this way (see Fig. 4). The correlation values are based upon the zero-lag correlation (thus along the *45° line* in Fig. 4C,D). **(C)** Stacked line plot of the 32 PCs that did not show a significant correlation between whisker angle and simple spike firing. The cells are ordered based upon their correlation value and scaled so that the darkest line corresponds to the average (see Methods). Overall, there is a negative correlation between simple spike firing and whisker position, reflecting mainly the change in whisker position without an accompanying change in simple spike firing. **(D)** The same, but for the 21 PCs showing a significant correlation between whisker angle and simple spike firing. As in panel C, the cells are ordered by their maximum correlation and scaled so that the brightest blue line corresponds to the average. A positive correlation is especially clear from around the moment that the active protraction starts. **(E)** Schematic map of crus 1 and crus 2 indicating the approximate locations of PCs that do (closed symbols) or do not (open symbols) show a significant correlation between whisker angle and simple spike firing, separated for strong (green) and weak (blue) CS responders (cf. Fig. S1D). Note that overlapping locations have been displaced minimally to increase visibility.
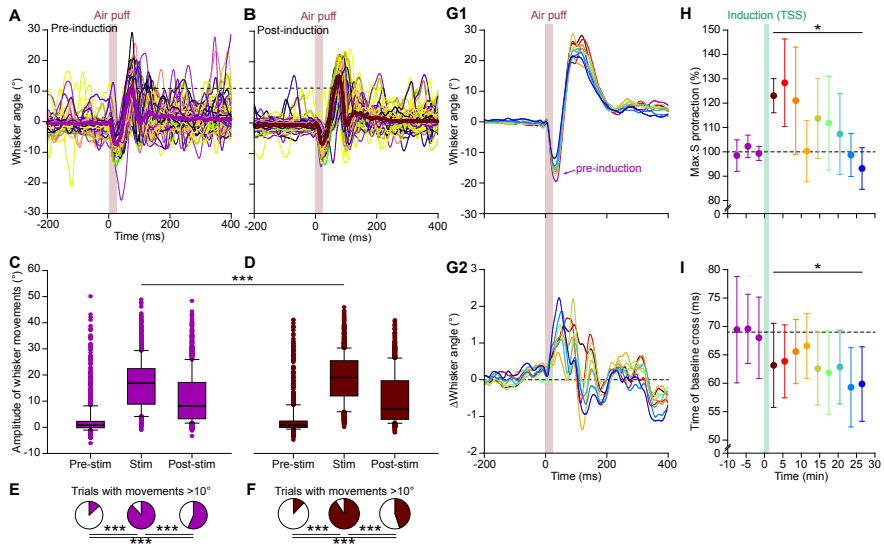
Figure S3 Theta sensory stimulation enhances stereotypic whisker protraction. (A) The variability in whisker movements is illustrated by superimposing the average whisker angle during the 100 trials before theta sensory stimulation (Fig. 5A). The thick line indicates the median. **(B)** The first 100 trials after induction of the same experiment as in panel a, showing a clear increase in whisker protraction after induction. Box plots showing the amplitudes (difference between maximal retraction and maximal protraction in the indicated 200 ms intervals) of individual trials before **(C)** and after **(D)** induction. Obviously, most whisker movement was observed in the period between 0 and 200 ms after whisker pad air puff stimulation, as compared to the 200 ms intervals before and after this period ($n = 13$ mice). Fractions of trials with movements exceeding $10°$ before **(E)** and after **(F)** induction. Especially the active protraction during the first 200 ms after the stimulus is clearly enhanced. Note that the panels A, C, and E are the same as in Fig. 1G-H and displayed here only to illustrate the impact of theta sensory stimulation on whisker movements. **(G1)** Averaged whisker traces (ordered per 100 trials) of the seven mice from which we had video data of the whole recording showing less retraction and more protraction after induction. For clarity, only the average of the last 100 trials pre-induction is plotted. Color codes as in panel h. **(G2)** Differential traces show that whiskers remain further protracted, but over time the increase gets faster. **(H)** Theta sensory stimulation (TSS) caused increased whisker protraction during approximately 20 min, after which the maximum protraction returns to pre-induction levels, although the moments during which the whiskers pass again the baseline position when going from the retraction to the protraction remain anticipated **(I)**. * $p < 0.05$; *** $p < 0.001$. For detailed statistics, see Table S1.
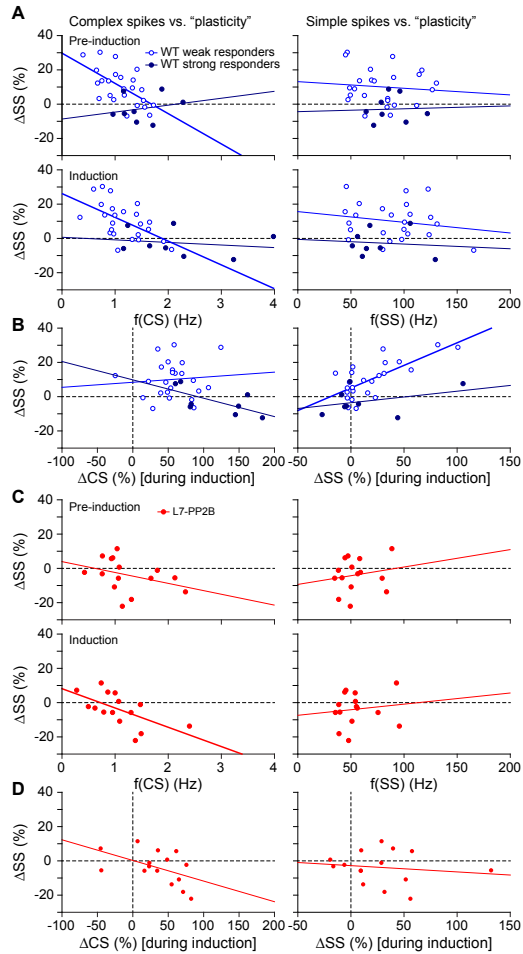
Figure S4 Complex spike rates are negatively correlated with sensory-induced potentiation. (A) Scatter plots with linear regression lines between CS (left) and SS frequency (right) during the pre-induction (top) and the induction (bottom) period with the percentage of change in SS response between post- and pre-induction. The CS firing rate was negatively correlated with the change in SS responses in the weak CS responders –both during the pre-induction and during the induction interval. However, no such significant correlation was found in the strong CS responders. The SS rate did not have a significant correlation with SS responses. **(B)** In contrast to the absolute firing rate, the difference in CS firing during the pre-induction versus the induction block did not show a clear correlation with changes in SS responsivity (left). Increased SS spike firing during the induction block, however, correlated well with increased sensory SS responses during the post-induction block, indicating that the process of potentiation already started during the induction block. **(C-D)** The same, but for PCs in L7-PP2B deficient mice. In this mutant, a correlation between CS firing (during induction) and changes in SS sensitivity were still observed. This could imply that LTD is still intact in these mice. Thick lines indicate significant linear correlations *p < 0.002. For detailed statistics, see Table S1.*
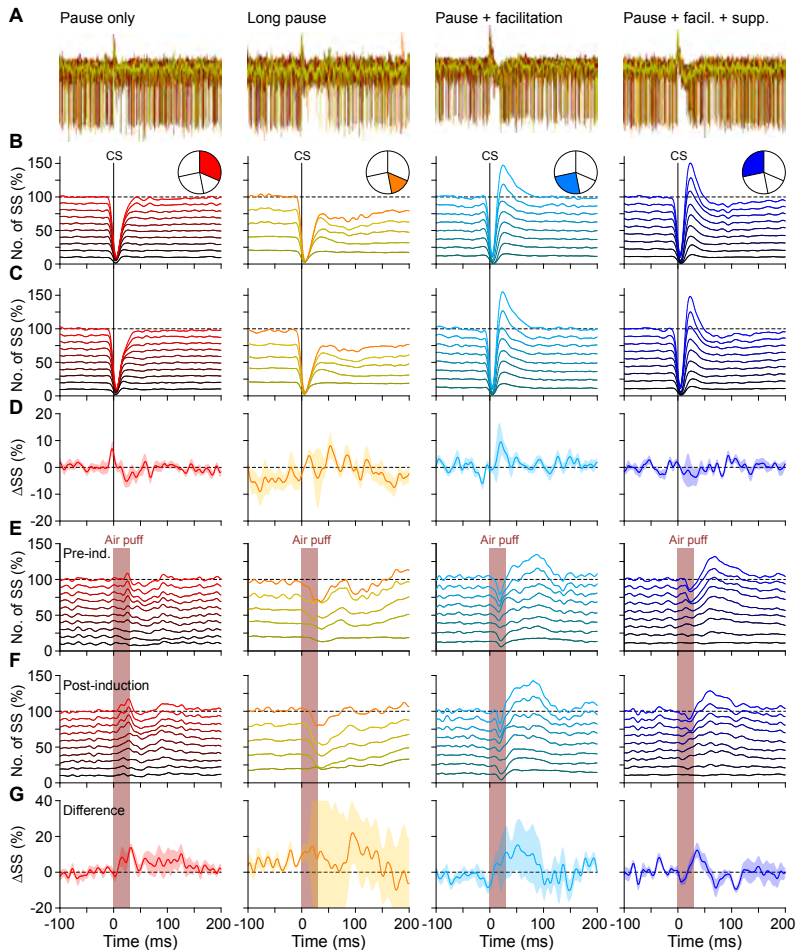
Figure S5 Theta sensory stimulation particularly affects Purkinje cells that show simple spike facilitation after a complex spike. (A) Purkinje cells (PCs) show different patterns of simple spike (SS) firing following a complex spike (CS). Some PCs (10/32 = 31%) showed only a single pause in SS firing after a CS. This is illustrated by superpositioning the first 20 CSs (for this illustration, we excluded the CS doublets firing within 150 ms after each other) of a representative PC recording. A minority of the PCs (5/32 = 16%) showed a prolonged pause in SS firing, which could last for more than 100 ms before returning to baseline firing. In 8 PCs (25%) we observed a marked increase in SS firing after the initial pause. In 9 other PCs (28%), this facilitation was followed by a period of incomplete SS suppression. **(B)** Convolved CS-triggered SS PSTHs of each of the four types illustrated as stacked line plots (see Methods). The pie diagrams in the insets illustrate the relative prevalence of each type. **(C)** Idem, but for after induction. **(D)** Averaged differences in the SS firing following a CS after theta sensory stimulation of the PCs of the four different categories. In the PCs that do not show SS suppression, the SS facilitation is enhanced. Panel D is based solely upon the Purkinje cells with weak CS responses (cf. Fig. S1D). **(E-G)**. The same, but for the air puff-induced SS patterns. Shaded areas indicate SEM.
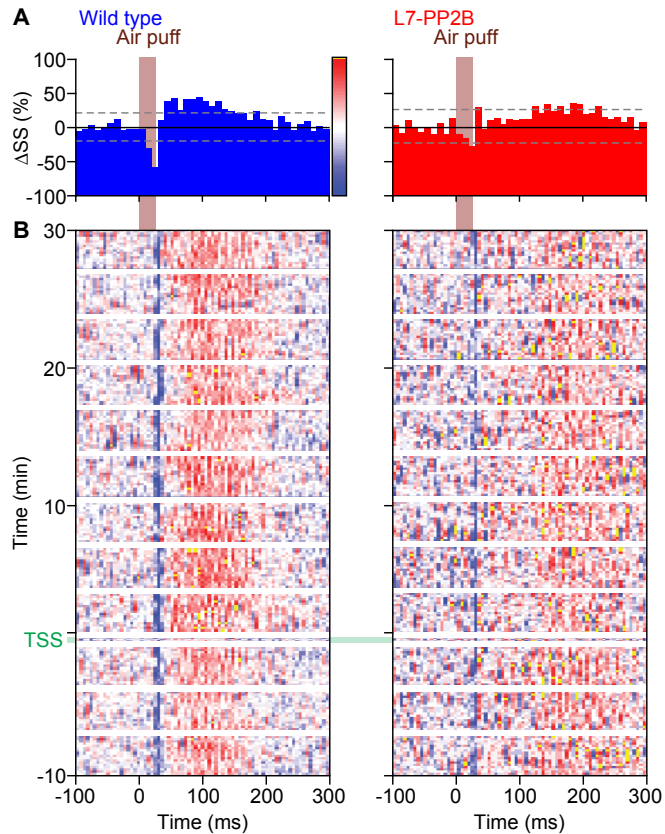
Figure S6 4 Hz whisker pad stimulation does not potentiate simple spike responses in L7-PP2B KO mice. Example PSTHs of the simple spike response to whisker pad air puff stimulation of representative Purkinje cells **(A)** and how these changed over time, depicted as heat map (see Methods) **(B)**. Both columns contain data from Purkinje cells with weak complex spike responses (cf. Fig. S1D): in the left column is data from a wild type mouse and in the right column from a L7-PP2B KO mouse. The colors of the heat map refer to the relative simple spike firing (see scale bar in A). The left column is for reference and contains the same data as shown in Fig. 6E.

Figures 1h and S3e - Fraction of trials with movements >10°		n	Fraction		p	
Pre-stimulus (-200 to 0 ms) vs. stimulus (0 to 200 ms) interval		1207 trials	13% vs 87%		<0.0001	Fisher's exact test
Pre-stimulus (-200 to 0 ms) vs. post-stimulus (200 to 400 ms) interval		(13 mice)	13% vs 57%		<0.0001 (α_{corr} = 0.0167)	
Stimulus (0 to 200 ms) vs. post-stimulus (200 to 400 ms) interval			87% vs 57%		<0.0001	

Figure 1h - Max. protraction of whiskers		n	Median	IQR		
Pre-stimulus (-200 to 0 ms) interval		1207 trials	0.78°	2.44°	<0.0001 Kruskal-Wallis test	
Stimulus (0 to 200 ms) interval		(13 mice)	16.85°	13.56°		
Post-stimulus (200 to 400 ms) interval			8.06	13.87°		

Figure 3d - Difference in whisker position between traces with CS and traces without CS		n	Median	IQR	p	
Difference in average baseline position (-200 to 0 ms interval)		28	-0.21°	0.35°	0.0013	Wilcoxon matched
Difference in maximal retraction (0 to 50 ms interval)			-0.34°	1.06°	0.0057	pairs test
Difference in maximal protraction (50 to 150 ms interval)			2.41°	3.02°	0.0001 (α_{corr} = 0.0167)	

Figure 3e - Timing of CS and whisker responses		n	Median	IQR		
Time of peak CS response (after onset of air puff)		28	36.5 ms	9.5 ms		
Time of maximal difference in whisker position between trials with and without CSs			100.0 ms	33.3 ms		
Difference in timing			58.0 ms	41.3 ms		

Inclusion criterion: PCs with significant CS response within 80 ms of the air puff (met by 28 out of 53 (53%) PCs tested).

Figure 4e - Correlation between instantaneous SS frequency and whisker position		n	R	p		
Example experiment *(left panel)*		100 trials	0.5174	<0.001		
Complete dataset *(right panel)*		21 x 100 trials	0.2229	<0.0001	Pearson correlation	

Inclusion criterion: PCs with a significant correlation between instantaneous SS frequency and whisker position (met by 21 out of 53 (40%) PCs tested).

Figure 5b - Whisker movement following air puff stimulation		n	Mean	SEM	p	t	df
Maximal retraction (pre-induction)		13	-5.71°	0.66°	0.0211	2.652	12
Maximal retraction (post-induction)		(paired)	-5.06°	0.58°	Paired t test		
Maximal protraction (pre-induction)		13	10.33°	1.32°	0.0006	4.583	12
Maximal protraction (post-induction)		(paired)	11.81°	1.37°	Paired t test		

Figure 5c - CS response to air puff stimulation		n	Median	IQR	p	
Peak (pre-induction)		32	1.096	0.984	0.1813	
Peak (post-induction)		(paired)	1.187	0.931	Wilcoxon matched pairs test	

Figure 5d - SS response to air puff stimulation		n	Mean	SEM	p	
Max. change in SS response (0-100 ms following air puff) after theta sensory stimulation		32	26.6%	2.5%	<0.0001 One sample t test (compared to 0% change)	

Figure 5f - Correlation between instantaneous SS frequency and whisker position		n	Mean	SEM	p	t	df
Time of max correlation (pre-induction)		10	161 ms	20 ms	0.0061	3.562	9
Time of max correlation (post-induction)		(paired)	77 ms	9 ms	Paired t test		

Figure 6a - CS peak response during pre-induction correlates to change in SS responsiveness		n	R	p		
WT littermates		32	0.5445	0.0013	Pearson correlation	

Figure 6b - Average change in SS firing in 0-60 ms interval after theta sensory stimulation		n	Mean	SEM	p	t	df
WT Weak CS responders		24	10.1%	2.2%	0.0022	3.639	16
WT Strong CS responders		8	-2.7%	2.8%	t test		

Figures 6f and 8e - Long-term impact of theta sensory stimulation on SS response		n	p	χ^2		
WT weak responders (comparing 10 min pre- to 30 min post-induction; 0-60 ms after onset air puff)		7	0.001	11.229		
WT strong responders pre- vs. post-induction		5	0.452	2.633		
L7-PP2B KO mice pre- vs. post-induction		8	0.241	4.200		
WT weak responders vs. WT strong responders (comparing 10 min pre- to 30 min post-induction)			<0.001	2-way ANOVA		
WT weak responders vs. L7-PP2B KO mice			0.019	Group: p = 0.001; F = 7.905		
WT strong responders vs. L7-PP2B KO mice			0.068			

Figure 7c - Firing properties of L7-PP2B KO PCs			CS freq (Hz)			SS freq (Hz)			SS CV2		
Mann-Whitney tests	n		Median	IQR	p	Median	IQR	p	Median	IQR	p
WT littermates	53		1.25	0.57	0.8360	78.49	34.97	0.0005	0.297	0.135	0.0010
L7-PP2B KO mice	15		1.06	0.55		50.22	15.62		0.155	0.124	

Figure 7e - Sensory responses in L7-PP2B KO PCs			CS peak (%)				CS peak latency (ms)		
	n		Median	IQR	p		Median	IQR	p
WT weak responders	32		1.00	0.68	<0.001		43.5	22.3	0.004
WT strong responders	14		3.42	2.06	(KW test)		34.0	9.8	(KW test)
L7-PP2B KO mice	15		0.83	0.74			54.0	30.8	
Post-hoc tests		Weak-KO: p=1.000 / Weak-strong & strong-KO: *p* <0.001				Weak-KO: p = 0.777; Weak-strong: *p* = 0.030; Strong-KO: *p* = 0.004			

Simple spike responses: amplitude: p = 0.149 (Kruskal-Wallis test); latency: p = 0.178 (Kruskal-Wallis test)

Figure 8b/c - Theta sensory stimulation does not lead to increased protraction in L7-PP2B KO		n	Median	IQR	p	
WT littermates		11 out of 13			0.0048	
L7-PP2B KO mice		3 out of 10			Fisher's exact test	
WT littermates: 0-60 ms after onset air puff		13	0.41°	1.01°	0.0099	
L7-PP2B KO mice: 0-60 ms after onset air puff		10	-0.15°	0.65°	Mann-Whitney test	
WT littermates: 60-120 ms after onset air puff		13	0.96°	1.22°	0.1151	
L7-PP2B KO mice: 60-120 ms after onset air puff		10	0.07°	1.06°	Mann-Whitney test	

Figure 8d - Theta sensory stimulation does not lead to increased protraction in L7-PP2B KO		n	Mean	SEM	p	t	df
WT littermates (all cells, comparing responses to 100 puffs pre- vs. 100 puffs post-induction)		32	6.89%	2.00%	0.0027	3.181	45
L7-PP2B KO mice		15	-3.84%	2.46%	(t test)		

[Not illustrated] - CS peak response not affected by theta sensory stimulation		n	Mean	SEM	p	
WT littermates (comparing responses to 100 puffs pre- to 100 puffs post-induction)		32	-7.37%	5.49%	0.1185	Wilcoxon
L7-PP2B KO mice		15	11.47%	8.73%	0.4212	matched pairs test

Figure S3f - Fraction of trials with movements >10° (after theta sensory stimulation)		n	Fraction		p	
Pre-stimulus (-200 to 0 ms) vs. stimulus (0 to 200 ms) interval		1208 trials	13% vs 90%		<0.0001	Fisher's exact test
Pre-stimulus (-200 to 0 ms) vs. post-stimulus (200 to 400 ms) interval		(13 mice)	13% vs 56%		<0.0001 (α_{corr} = 0.0167)	
Stimulus (0 to 200 ms) vs. post-stimulus (200 to 400 ms) interval			90% vs 56%		<0.0001	

Figure S4		Pre-induction		Pre-induction		Induction		Induction				
Pearson correlations		f(CS) vs. Δf(SS)		f(SS) vs. Δf(SS)		f(CS) vs. Δf(SS)		f(SS) vs. Δf(SS)		Δf(CS) vs. Δf(SS)		Δf(SS) vs. Δf(SS)
	n	R	p	R	p	R	p	R	p	R	p	R	p
WT weak responders	24	0.6062	0.0017	0.0971	0.6516	0.5529	0.0051	0.1897	0.3746	0.0885	0.6810	0.7111	<0.0001
WT strong responders	8	0.2269	0.5889	0.0395	0.9260	0.1877	0.6562	0.0955	0.8220	0.6639	0.0726	0.3645	0.3747
L7-PP2B KO mice	15	0.3529	0.1970	0.1793	0.5226	0.6047	0.0169	0.1284	0.6483	0.4959	0.0601	0.1445	0.6075

Supplementary Table 1 | Overview of statistical tests.
CS = complex spikes; IQR = inter-quartile range; KW = Kruskal-Wallis; PC = Purkinje cell; SS = simple spike. *p* values in bold indicate statistical significance.

Table S1 Overview of statistical tests. *CS = complex spikes; IQR = inter-quartile range; KW = Kruskal-Wallis; PC = Purkinje cell; SS = simple spike. p values in bold indicate statistical significance.*

117

Chapter 5

Dysfunctional cerebellar Purkinje cells contribute to autism-like behaviour in Shank2-deficient mice

Loss-of-function mutations in the gene encoding the postsynaptic scaffolding protein SHANK2 are a highly penetrant cause of autism spectrum disorders (ASD) including cerebellum-related motor problems. Recent studies have implicated cerebellar pathology in etiology of ASD. Here, we evaluate the possibility that cerebellar Purkinje cells represent a critical locus of ASD pathophysiology in *Shank2*-related ASD. Absence of *Shank2* impairs both Purkinje cell intrinsic plasticity and induction of long-term potentiation at the parallel fiber to Purkinje cell synapse. Moreover, inhibitory input onto Purkinje cells is significantly enhanced, most prominently in the posterior lobe where simple spike regularity is most affected. Using Purkinje cell-specific *Shank2*-knockouts, we replicate alterations of simple spike regularity *in vivo* and establish cerebellar-dependence of ASD-like behavioural phenotypes in motor learning and social interaction. These data highlight the importance of *Shank2* for Purkinje cell function, and support a model by which cerebellar pathology is prominent in certain forms of ASD.

S. Peter*, **M.M. ten Brinke***, J. Stedehouder, C.M. Reinelt, B. Wu, H. Zhou, K. Zhou, H.-J. Boele, S.A. Kushner, M. Goo Lee, M.J. Schmeisser, T.M. Boeckers, M. Schonewille, F.E. Hoebeek, & C.I. De Zeeuw (2016) **Nature Communications**

Introduction

Autism spectrum disorders (ASD) are neurodevelopmental disease entities primarily defined by deficits in social interaction and repetitive behaviour (Chen et al., 2015). In addition, individuals with autism often suffer from motor skill deficiencies (Kanner, 1943), many of which manifest early in the disease (Zwaigenbaum et al., 2013). The aetiology of ASD is complex with reported pathophysiological alterations encompassing multiple brain regions, including the cerebellum (Chen et al., 2015). Cerebellum-related motor symptoms of ASD patients have been observed by impairments in eyeblink conditioning (Oristaglio et al., 2013; Sears et al., 1994), eye movement abnormalities (Schmit et al., 2014; Takarae et al., 2004), general motor learning deficits (Marko et al., 2015; Mostofsky et al., 2000) as well as balance and postural difficulties (Memari et al., 2014; Stins et al., 2015). Patients with cerebellar lesions emerging later in development are often diagnosed with cerebellar cognitive affective syndrome, a condition characterized by deficits in language, executive function and impaired emotions which overlaps considerably with symptoms in ASD (Schmahmann, 2010). Anatomical evidence for cerebellar involvement in ASD includes a decrease in the number of Purkinje cells (PCs) by post-mortem brain histopathological examination (Allen, 2005; Bailey et al., 1998), and functional connectivity between the cerebellum, and frontoparietal and sensorimotor regions in resting-state fMRI studies of ASD (Stoodley, 2014). Moreover, the cerebellum is among the most prominent brain regions demonstrating high co-expression of ASD-associated genes (Menashe et al., 2013). Emerging data indicate that neurodevelopmental disorders including ASD result from dysfunctional synaptic networks (Grabrucker et al., 2013; Zoghbi & Bear, 2012). The postsynaptic density (PSD) in particular represents a critically important proteomic hub for a considerable proportion of neurodevelopmental disease-causing mutations, including ASD (Bourgeron, 2015). A prominent example is the Shank family of postsynaptic scaffolding proteins, which has gained wide attention because of their strong link to ASD (Berkel et al. 2010; Durand et al., 2007; Leblond et al., 2012; Mei et al., 2016; Sato et al., 2012). To date, two studies have independently reported generating *Shank2* knockout (KO) mice with ASD-like behaviour and abnormal hippocampal processing (Schmeiser et al., 2012; Won et al., 2012). However, in addition to the forebrain, *Shank2* is also highly expressed in cerebellar PCs (Boeckers et al., 1999; Boeckers et al. 2004). Moreover, patients with *Shank2*-related ASD exhibit motor impairments consistent with cerebellar dysfunction (Leblond et al., 2014). However, the causal influence of cerebellar dysfunction on *Shank2*-related ASD has never been established. We therefore used both global germ-line *Shank2* knock-out (KO; *Shank2$^{-/-}$*) and PC-specific *Shank2* KO (*L7-Shank2$^{-/-}$*) mouse models to investigate the causal influence of Shank2 on cerebellar function and ASD-related behaviours. Notably, *Shank2$^{-/-}$* mice have impairments in plasticity at the parallel fiber (PF) to PC synapse, increased inhibitory input onto PCs, and significant irregularities in PC simple spike activity. Moreover, *L7-Shank2$^{-/-}$* mice show deficits in social interaction and exhibit task-specific repetitive behaviour. Together, these results provide novel insight into the pathophysiological mechanisms by which *Shank2* mutations cause impairments in cerebellar function that may contribute to ASD.

Results

Reduction of functional cerebellar AMPAR in *Shank2*$^{-/-}$ mice

A divergent role of the *Shank2* scaffolding protein has been hypothesized for PSD function and cellular morphology (Sala et al., 2015). To evaluate the morphology of *Shank2*-deficient postsynaptic specializations along PC dendrites, we quantified the structural characteristics of dendritic spines and PSDs in the distal molecular layer of global *Shank2*$^{-/-}$ mice using Golgi-Cox staining of PC dendrites and electron microscopy (Fig. 1). Neither spine density (WT: 1.93±0.74 spines/μm dendrite; *Shank2*$^{-/-}$: 1.82±0.67 spines/μm dendrite; P=0.2, Mann-Whitney U-test (MWU-test, see Supplementary Table 1 for additional statistics), nor the length (WT: 1.34±0.77 μm; *Shank2*$^{-/-}$: 1.32±0.50 μm; P=0.4, MWU-test) or width of individual spines (WT: 0.72±0.45 μm; *Shank2*$^{-/-}$: 0.71±0.32 μm; P=0.9, MWU-test) was significantly affected (Fig. 1A). In addition, the length (WT: 313.3±97.1 nm; *Shank2*$^{-/-}$: 305.3±96.2 nm; P=0.3) and thickness of PSDs (WT: 26.2±6.0 nm; *Shank2*$^{-/-}$: 26.0±5.3 nm; P=0.9) were similar between genotypes (Fig. 1B, C). In contrast, biochemical analysis of cerebellar synaptosomes indicated that global *Shank2*$^{-/-}$ mice have lowered expression of AMPA receptor subunits GluA1 (WT: 1.00±0.37; *Shank2*$^{-/-}$: 0.63±0.23; P=0.041) (Fig. 1D, Supplementary Fig. 1) and GluA2 (WT: 1.00±0.32; *Shank2*$^{-/-}$: 0.58±0.11; P=0.014). In addition, we looked into the ASD pathology related cell adhesion molecule neuroligin 3 (Nlgn3), which has been shown to interact with Shank proteins (Bourgeron, 2015), but found no significant difference in its expression (WT: 1.00±0.37; *Shank2*$^{-/-}$ 0.84±0.33; P=0.4). Together, these findings indicate that Shank2 is not crucial for the morphological differentiation of PC dendritic spines and PSDs, but instead may play an important role in the maintenance of cerebellar GluA1 and GluA2 levels.

Normal baseline excitability in *Shank2*$^{-/-}$ Purkinje cells

Considering that we found a reduction of cerebellar AMPA receptor expression in global *Shank2*$^{-/-}$ mice, we next examined neurotransmission at the PF-PC synapse using *ex vivo* whole-cell recordings (at 21±1°C) (Fig. 2A). PF-PC EPSCs, which were obtained in WT and *Shank2*$^{-/-}$ under comparable conditions (holding current: WT: -389±102 pA; *Shank2*$^{-/-}$ -388±114 pA, P=1; PC input resistance: WT: 67.2±16.8 MΩ; *Shank2*$^{-/-}$: 69.1±12.4 MΩ; P=0.8; Fig. 2B, C), revealed no significant differences in rise time (WT: 2.1±0.7 ms; *Shank2*$^{-/-}$: 1.7±0.6 ms; P=0.2) or decay time (WT: 9.7±0.8 ms; *Shank2*$^{-/-}$: 9.3±0.3 ms; P=0.3) (Fig. 2D, E). Moreover, evoking PF-EPSCs using stimulation currents varying from 3 to 15 μA resulted in similar event amplitudes (P=0.9, repeated-measures ANOVA) (Fig. 2F, G) and applying inter-stimulus intervals varying from 50 to 200 ms evoked comparable levels of paired-pulse facilitation (P=0.2, repeated-measures ANOVA) (Fig. 2H), indicating that baseline PF-PC synaptic transmission is unaltered by the lack of Shank2.

Next, we evaluated whether the loss of Shank2 affected neurotransmission at the climbing fiber (CF) to PC synapse. CF stimulation induced PC complex spikes in WT and *Shank2*$^{-/-}$. These waveforms showed no significant differences in the amplitude of the initial Na+-spike (WT: 51.8±6.4 mV; *Shank2*$^{-/-}$: 48.5±5.9 mV, P=0.3)
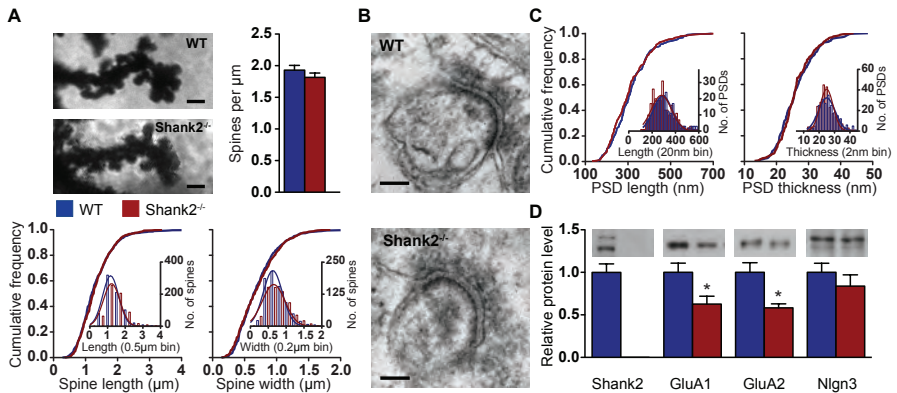
Figure 1 Reduction of AMPA receptor subunits in *Shank2*^-/- cerebellar synaptosomes, but no changes in spine and PSD morphology in the distal molecular layer (DML). (A) Representative images (Golgi-Cox staining) of distal Purkinje cell dendrites in the DML, quantification of spine density (WT, n=97/4, dendrites/mice; *Shank2*^-/-, n=89/4, P=0.2, MWU-test) and cumulative frequency plots of spine length (P=0.4, MWU-test) and thickness (P=1, MWU-test) in WT (n=748/4 spines/mice) and *Shank2*^-/- mice (n=639/4) as indicated. Scale bar: 1 μm. **(B,C)** Representative images (electron microscopy) of spine synapses in the DML and cumulative frequency plots of PSD length (WT, n=226/4, PSDs/mice; *Shank2*^-/-, n=243/4, P=0.3) and thickness (WT, n=223/4; *Shank2*^-/-, n=233/4, P=0.9) as indicated. Scale bar: 100 nm. **(D)** Biochemical analysis of Shank2 (WT, n=12 synaptosomes; *Shank2*^-/-, n=6), GluA1 (WT, n=12 synaptosomes; *Shank2*^-/-, n=6, P=0.041) GluA2 (WT, n=11; *Shank2*^-/-, n=5, P=0.014), and *Nlgn3* (WT, n=12; *Shank2*^-/-, n=6, P=0.4) in cerebellar synaptosomes from WT and *Shank2*^-/- mice as indicated. Data in bar graphs are presented as mean $\pm$ SEM; single asterisks indicates $p < 0.05$. Two-sided t-tests were used, unless stated otherwise.

and in the number of subsequent Ca^{2+}-spikelets (WT: 1.6±0.5; *Shank2$^{-/-}$*: 2.0±0.7; P=0.2) or the amplitude of Ca^{2+}-spikelets (WT: 31.8±11.9 mV; *Shank2$^{-/-}$*: 33.9±6.4 mV, P=0.7) (Supplementary Fig. 2A-C). Moreover, at P9-10 virtually all PCs of both WT and *Shank2$^{-/-}$* were innervated by multiple CFs, while at P25-35 all converted into mono-innervation (number of CF responses P9-10: WT: 2.0±0.5; *Shank2$^{-/-}$*: 2.3±0.5; P=0.2; P25-35: WT: 1.0±0.0; *Shank2$^{-/-}$*: 1.0±0.0; P=1, MWU-test) (Supplementary Fig. 2D, E). Finally, the characteristic paired-pulse depression of CF-PC synaptic transmission showed no differences throughout the tested developmental stages (P9-10: WT: 0.59±0.14; *Shank2$^{-/-}$*: 0.54±0.11; P=0.5; P25-35: WT: 0.75±0.11; *Shank2$^{-/-}$*: 0.77±0.1; P=0.6) (Supplementary Fig. 2F, G), together indicating that the CF to PC input in *Shank2$^{-/-}$* mice is not only normal in its baseline characteristics but also with respect to developmental elimination (Hashimoto & Kano, 2003).

To examine PC kinetics, we evoked action potentials (APs) using depolarizing current steps at near-physiological temperature (33±1°C) (Fig. 2I). Evoked APs showed comparable thresholds (WT: -51.4±3.9 mV; *Shank2$^{-/-}$*: -51.0±3.5 mV; P=0.8), amplitudes (WT: 39.8±5.8 mV; *Shank2$^{-/-}$*: 35.9±5.8 mV; P=0.1) and half-widths (WT: 0.29±0.02 ms; *Shank2$^{-/-}$*: 0.30±0.03 ms; P=0.7), as well as after-hyperpolarization amplitudes (WT: 6.5±1.6 mV; *Shank2$^{-/-}$*: 7.5±1.7 mV; P=0.2) (Fig. 2J-M). In addition, PC intrinsic excitability was normal (Schonewille et al., 2010) in that current step injections of increasing amplitude resulted in a linear current-to-firing frequency relationship (P=0.1, repeated-measures ANOVA) (Fig. 2N, O) with a similar slope (WT: 16.2±2.2 Hz; *Shank2$^{-/-}$*: 16.1±2.3 Hz; P=1.0) (Fig. 2O). Together, these findings indicate that both the baseline transmission at PC excitatory synapses and PC intrinsic excitability remain intact in global *Shank2$^{-/-}$* mice.

Increased sIPSCs and spiking irregularity in *Shank2$^{-/-}$* PCs

To investigate inhibition of PCs in global *Shank2$^{-/-}$* mice, we recorded spontaneous inhibitory postsynaptic currents (sIPSCs). Since PC activity can be related to the presence or absence of the glycolytic enzyme aldolase-c (referred to as zebrin) (Zhou et al., 2014), we recorded from the predominantly zebrin-negative anterior lobules I-V as well as the predominantly zebrin-positive posterior lobule X of the cerebellar cortex (Fig. 3A, B). In both regions, we observed an increase in the frequency (lobules I-V: WT: 8.3±5.9 Hz; *Shank2$^{-/-}$*: 12.2±5.4 Hz; P=0.0295; lobule X: WT: 14.2±7.0 Hz; *Shank2$^{-/-}$*: 21.5±8.8 Hz; P=0.0079) (Fig. 3C, E), but not in the amplitude (for lobules I-V, WT: 53.2±24.4 pA; *Shank2$^{-/-}$*: 65.2±29.5 pA; P=0.1; for lobule X, WT: 58.9±19.0 pA; *Shank2$^{-/-}$*: 64.0±24.7 pA; P=0.5), of sIPSCs (Fig. 3D, F). Importantly, *Shank2$^{-/-}$* sIPSC frequency was higher in lobule X than in the anterior lobe (P=0.0002). Given that inhibition decreases the firing frequency of PCs, but increases their irregularity (Haäusser & Clark, 1997; Wulff et al., 2009), we hypothesized that the increased frequency of sIPSCs in *Shank2$^{-/-}$* would translate into an overall decrease of *in vivo* simple spike (SS) activity but with an increased irregularity (Fig. 3G, H). The global *Shank2$^{-/-}$* mice did indeed exhibit a decrease in firing frequency in lobules I-V (WT: 88.2±18.7 Hz; *Shank2$^{-/-}$*: 76.3±11.8 Hz; P=0.0096) (Fig. 3I), but notably not in lobule X (WT: 52.6±12.7 Hz; *Shank2$^{-/-}$*: 50.3±12.9 Hz; P=0.6) (Fig. 3L). Conversely, and consistent with the relative magnitude of the change in sIPSC frequency, the irregularity of PC SS firing was
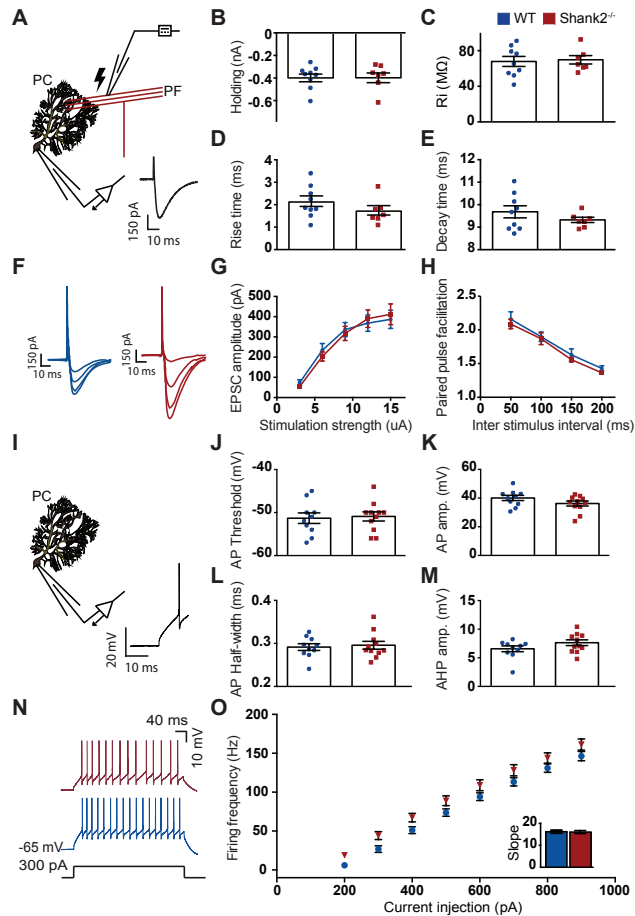
Figure 2 No changes in excited synaptic and intrinsic properties in *Shank2*^{-/-} Purkinje cells *ex vivo*. (A) Recording configuration for voltage clamp recordings of PF-PC synaptic transmission. Inset: an example PF-EPSC. **(B-E)** With comparable holding current (at -65mV) (P=1) and input resistance (Ri) (P=0.8), PC EPSC rise time (P=0.2) and EPSC decay time (P=0.3) are not different between WT (n=9/6, cells/animals) and *Shank2*^{-/-} (n=7/6). **(F)** Example EPSCs in response to 3, 6, 9, 12, and 15 μA stimulation. **(G,H)** Varying stimulation strength (P=0.9, repeated-measures ANOVA) and inter-stimulus interval (P=0.2, repeated-measures ANOVA) evoked comparable EPSC amplitude or facilitation (WT, n=11/3; *Shank2*^{-/-} 15/3). **(I)** Recording configuration for whole cell recording. Inset: an example action potential. **(J-M)** Action potential threshold (P=0.8), amplitude (P=0.1), half-width (P=0.7), and afterhyperpolarization (P=0.2) were not different (WT, n=10/6; *Shank2*^{-/-}, n=11/6). **(N)** Example traces of intrinsic Purkinje cell excitability as apparent from action potential firing evoked by 300 pA current injections. **(O)** No difference in evoked firing frequency relative to various levels of current injections (WT, n=10/5; *Shank2*^{-/-}, n=11/5, P=0.1, repeated-measures ANOVA). Inset barplot shows average slope of firing rate per current step (P=1). Data are represented as mean $\pm$ SEM. Two-sided t-tests were used, unless stated otherwise.

increased in lobule X (CV: WT, 0.30±0.08; *Shank2*^{-/-}, 0.38±0.09, P=0.0086; CV2: WT, 0.29±0.07; *Shank2*^{-/-}, 0.40±0.11, P=0.0003), but not in lobules I-V (CV: WT, 0.48±0.06; *Shank2*^{-/-}, 0.49±0.12, P=0.7; CV2: WT, 0.45±0.04; *Shank2*^{-/-}, 0.48±0.08, P=0.1) (Fig. 3J-N). The complex spike frequency and the pause in SS firing following each complex spike was similar between global *Shank2*^{-/-} mice and their WT littermates in both the anterior (WT: frequency 1.28±0.29 Hz; pause 9.11±1.98 ms; *Shank2*^{-/-}: 1.32±0.24 Hz; 10±2.9 ms; P=0.7 and P=0.2, respectively) and posterior lobules (WT: frequency 0.67±0.19 Hz; pause 19.7±5.5 ms; *Shank2*^{-/-}: frequency 0.84±0.37 Hz; pause 17.61±5.29 ms; P=0.1 and P=0.2, respectively) (Supplementary Fig. 3). Thus, in the absence of Shank2, the zebrin-positive lobule X selectively exhibits a highly irregular pattern of PC simple spike firing, which is consistent with a relative increase of inhibitory input onto lobule X PCs.

Impaired synaptic and intrinsic plasticity in *L7-Shank2*^{-/-} PCs

Given that Shank2 functions as a PSD scaffolding protein of postsynaptic receptors (Grabrucker et al., 2011; Sala et al., 2015) for which we observed decreased expression of both GluA1 and GluA2 in cerebellar synaptosomes of *Shank2*^{-/-} mice (Fig. 1), we reasoned that PC synaptic plasticity might also be affected (Schmeisser et al., 2012, Won et al., 2012). Induction of long-term potentiation (LTP) (33±1°C; 1 Hz, 5 min PF-tetanus) (Fig. 4A) reliably increased PF-EPSC amplitudes in WT PCs (121.1±19.8% at t=40 min; P=0.003, repeated-measures ANOVA), but not in those of global *Shank2*^{-/-} mice (91.8±14.2% at t=40; P=0.3, repeated-measures ANOVA) (Fig. 4B). In contrast, both WT and global *Shank2*^{-/-} mice exhibited robust long-term depression (LTD) of PF-EPSCs following co-activation (1 Hz) of PFs and CFs (WT: 71.4±14.9%; P<0.0001; *Shank2*^{-/-}: 76.9±14.6%; P=0.0009, repeated-measures ANOVA) (Fig. 4C, D). Since LTP has been reported to facilitate adaptation of intrinsic properties, driving spike activity (schonewille et al., 2010), we next examined PC intrinsic plasticity before and after PF-LTP induction (Fig. 4E). Whereas WT mice readily demonstrated a potentiation of intrinsic excitability (139.7±21.3% at t=40 min; P=0.005, repeated-measures ANOVA), intrinsic plasticity was markedly impaired in global *Shank2*^{-/-} mice (104.6±22.2% at t=40 min; P=0.5, repeated-measures ANOVA) (Fig. 4F). These results suggest that Shank2 is a critical modulator of both synaptic and intrinsic plasticity in Purkinje cells.

Expression of *Shank2* in *L7-Shank2*^{-/-} mice

To explore the behavioural impact of the lack of Shank2 in PCs, we generated a PC-specific knockout of Shank2 (see methods section) using the floxed version of the *Shank2*^{-/-} mutants (Schmeisser et al., 2012) and the L7-vector (Schonewille et al., 2010). Immunocytochemical analysis with the SA5193 rabbit primary Shank2 antibody (Boeckers et al., 1999; Schmeisser et al., 2012) confirmed that *Shank2*^{-/-} was specifically deleted in PCs in the PC-specific *L7-Shank2*^{-/-} mice, but not in WT littermates, whereas it was ubiquitously deleted in the global *Shank2*^{-/-} (Fig. 5). Importantly, PC-specific deletion of Shank2 had no discernible impact on cellular zebrin identity, or on the zonal patterns of zebrin staining across cerebellar modules (Supplementary Fig. 4).
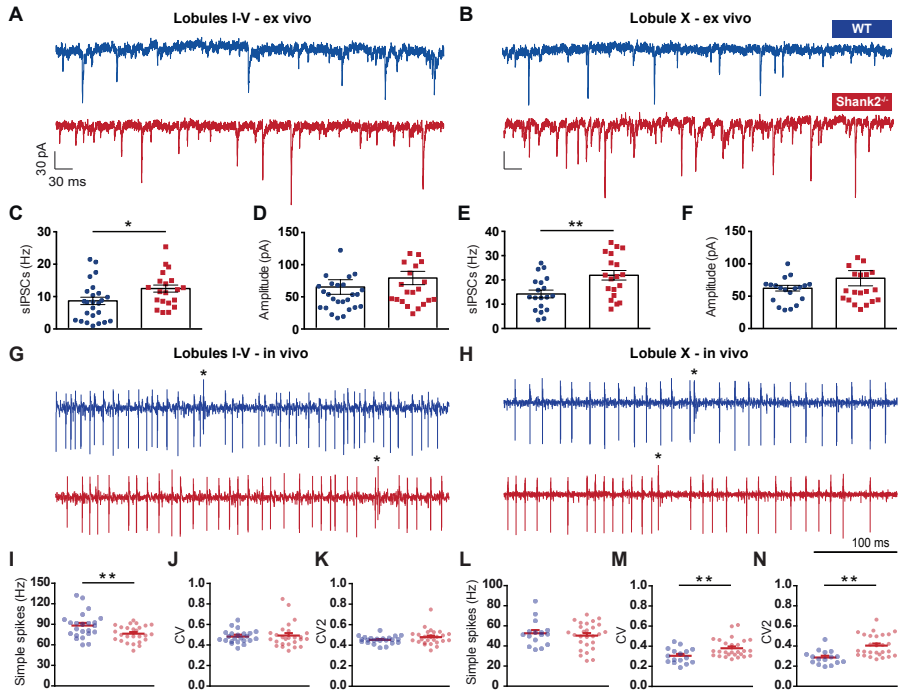
Figure 3 Increased spontaneous inhibitory events and higher simple spike irregularity in *Shank2*⁻ᐟ⁻ Purkinje cells. (A, B) Example of spontaneous firing inhibitory post synaptic currents (sIPSCs) in lobules I-V and X. **(C, E)** A higher frequency of sIPSCs is found in both anterior (I-V) (P=0.0295) and posterior (X) lobules (P=0.0079) in *Shank2*⁻ᐟ⁻ PCs (anterior: WT, n=25/3, cells/animals; *Shank2*⁻ᐟ⁻, n=20/3; posterior: WT, n=19/3; *Shank2*⁻ᐟ⁻, n=19/3). **(D, F)** There were no significant differences in sIPSC amplitudes anteriorly (P=0.1) or posteriorly (P=0.5). **(G, H)** Extracellular traces of PCs recorded in anterior (left) and posterior (right) lobules in the cerebellum, in WT and *Shank2*⁻ᐟ⁻. Asterisks denote complex spikes. **(I, J, K)** Simple spike (SS) firing frequency was significantly lower (P=0.0096) in *Shank2*⁻ᐟ⁻ (n=26/3) compared to wildtype (n = 23/3), whereas the coefficient of variation (CV) (P=0.7) and CV2 (P=0.1) did not differ. **(L, M, N)** In posterior lobule X, while SS firing frequency was similar (P=0.6), CV (P=0.0086) and CV2 (P=0.0003) were significantly higher in *Shank2*⁻ᐟ⁻ (n=27/3) compared to WT (n = 16/3). Data are represented as mean ± SEM. Single and double asterisks indicate P<0.05 and P<0.01, respectively. Two-sided t-tests were used, unless stated otherwise.
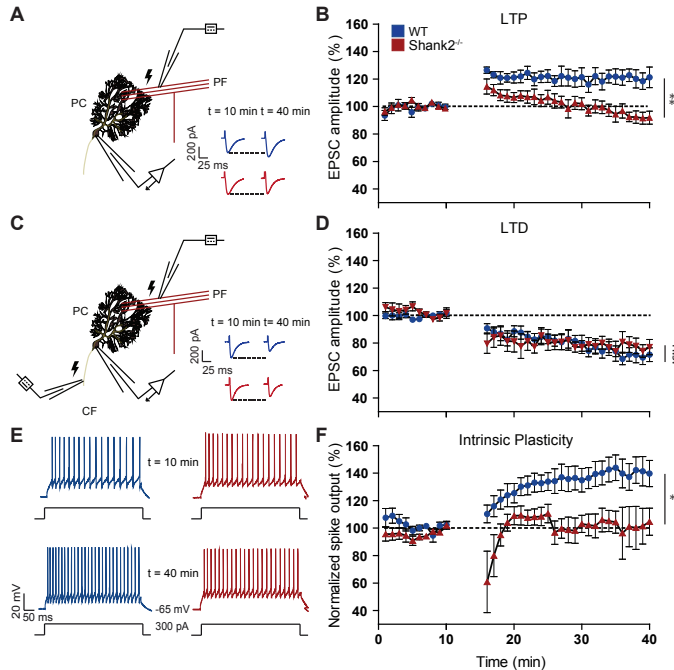
Figure 4 Impaired synaptic and intrinsic plasticity in *Shank2^-/-* ex vivo. (A) Recording configuration for PF-LTP experiments. Inset: example of 5 averaged EPSCs for WT (blue) and *Shank2^-/-* (red) before LTP induction (at 10 minutes) and after LTP induction (at 40 min). **(B)** LTP experiment with 5 min PF stimulation at 1Hz inducing LTP in WTs (n=7/6, cells/animals, P=0.0027) but not in *Shank2^-/-* PCs (n=12/6, P=0.3), which is reflected in the difference between genotypes (P=0.0066). **(C)** Recording configuration for PF-LTD experiments. Inset: example traces as in a. **(D)** LTD is induced in both WT (n=9/6, P<0.0001) and *Shank2^-/-* (n=7/6, P=0.0009) PCs, to a similar degree (P=1). **(E)** Example of traces for intrinsic plasticity with current injections of 300 pA. **(F)** LTP induction protocol induced enhanced spike output in WT PCs (n=5/4, P=0.0053), but not in *Shank2^-/-* PCs (n=5/4, P=0.5), as reflected in their difference (P=0.0201). Data are represented as mean ± SEM. Single and double asterisks indicate P<0.05 and P<0.01, respectively. All tests were repeated-measures ANOVAs.

Impaired motor learning in *L7-Shank2^-/-* mice

Given the variety of electrophysiological aberrations in PCs in the global *Shank2^-/-*, we next examined motor behavior in the PC-specific *L7-Shank2^-/-* mice. Unlike the hyperactivity exhibited by global *Shank2^-/-* mice in an open field (Schmeisser et al. 2012; Won et al., 2012), mice with PC-specific deletion of Shank2 exhibited no evidence of hyperactivity in the open field test compared to their WT littermates (velocity: WT: 12.28±2.79 cm/s; *L7-Shank2^-/-*: 13.24±2.61 cm/s ; P=0.3; distance moved: WT: 7.37±1.68 m; *L7-Shank2^-/-*: 7.94±1.57 m; P=0.3) (Supplementary Fig. 5A, B). The lack of hyperactivity was confirmed using the PhenoTyper Box (Noldus), in which free exploration was quantified over a 30 min-period in a homecage-like environment (velocity: WT: 6.7±1.1 cm/s; *L7-Shank2^-/-*: 6.3±1.3 cm/s; P=0.5, distance moved:
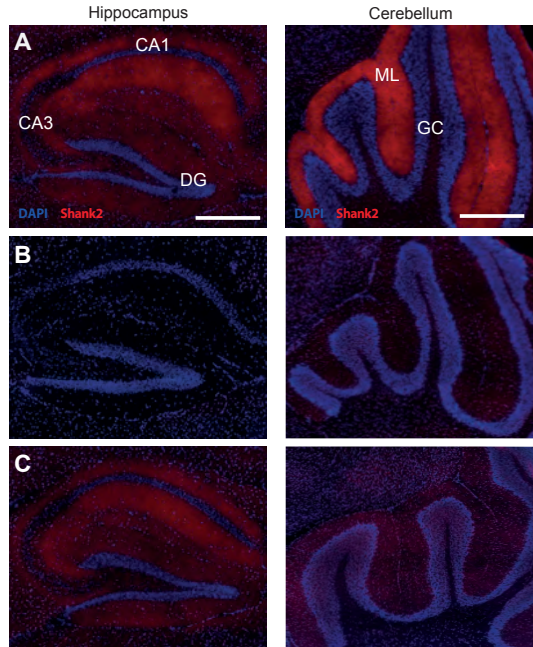
Figure 5 Immunohistological staining of the Shank2 protein in *Shank2*$^{-/-}$ and *L7-Shank2*$^{-/-}$ hippocampus and cerebellum. **(A)** Sagittal cryosection of hippocampal Shank2 (red) and nucleus staining (DAPI; blue) in a WT (left) *L7-Shank2*$^{-/-}$. Scale bar: 500 μm. Sagittal cryosection of cerebellar Shank2 staining (right). Scale bar: 200 μm. **(B)** Staining for Shank2 in the hippocampus and cerebellum of the global *Shank2*$^{-/-}$ shows absence of expression. **(C)** The *L7-Shank2*$^{-/-}$ shows expression in the hippocampus , but not in the molecular layer of the cerebellum.

WT: 384.6±68.8 cm; *L7-Shank2*$^{-/-}$: 371.7±79.7 cm; P=0.5, repeated-measures ANOVA) (Supplementary Fig. 5C, D). Moreover, during the ErasmusLadder test (Veloz et al., 2014) motor performance was similar between genotypes, including the efficiency and timing of steps (2nd day efficiency, WT: 33.1±20.0%; *L7-Shank2*$^{-/-}$: 47.1±15.4 cm; P=0.3; 2nd day timing: WT: 359.2±84.2 ms; *L7-Shank2*$^{-/-}$: 330.7±49.4 ms; P=0.8, repeated-measures ANOVA) (Supplementary Fig. 5E, F). Finally, the amplitude (gain) and timing (phase) of baseline optokinetic (OKR) (OKR gain, P=0.6, OKR phase, P=0.9, repeated-measure ANOVA) and vestibulo-ocular reflexes (VOR) (VOR gain, P=0.4, VOR phase, P=0.2, repeated-measure ANOVA) were also similar (Supplementary Fig. 5G-J), further highlighting that motor performance is normal in *L7-Shank2*$^{-/-}$ mutants.

In contrast, motor learning was consistently affected in a variety of cerebellar motor learning tasks (Fig. 6). Using a conditioning task within the ErasmusLadder, in which mice were presented with a tone preceding the elevation of an obstructive rung at a 200 ms interval (Veloz et al., 2014), *L7-Shank2*$^{-/-}$ mice were unable to successfully avoid the obstacle (*L7-Shank2*$^{-/-}$ versus WT: P=0.018, repeated-measures ANOVA) (Fig. 6A, B). Furthermore, *L7-Shank2*$^{-/-}$ mice failed to acquire the normal increase in VOR gain (*L7-Shank2*$^{-/-}$ versus WT: P=0.006, repeated-measures ANOVA) or shift in VOR

phase (2nd day; P=0.047, 3rd P=0.0013, 4th P<0.0001, 5th P=0.0003, repeated-measures ANOVA) following visuovestibular mismatch training (De Zeeuw & Ten Brinke, 2015) (Fig. 6C-F). Finally, *L7-Shank2*^{-/-} mice exhibited a significant impairment of Pavlovian eyeblink-conditioning (Ten Brinke et al., 2015) using a light pulse as the conditioning stimulus (CS) and a corneal air puff as the unconditioned stimulus at a 250 ms interval (conditioned response or CR rate: P=0.0013; CR amplitude: P=0.0009; repeated-measures ANOVA) (Fig. 6G-I). These findings indicate that *L7-Shank2*^{-/-} mice have normal baseline motor performance, but prominent impairments in motor learning.

Irregular /textitin vivo PC simple spikes in *L7-Shank2*^{-/-} mice

To investigate whether the changes in electrophysiological properties observed in PCs of the global *Shank2*^{-/-} mice may contribute to the behavioural phenotypes observed, we tested to what extent the changes in simple spike activity also occurred in the *L7-Shank2*^{-/-} mice. We first recorded extracellular single units *in vivo* from the largely zebrin-negative lobules I-V (Fig. 7A-D) and the predominantly zebrin-positive lobules IX-X (Fig. 7E-H). Importantly, the recordings in the *L7-Shank2*^{-/-} mice fully reproduced the increases in CV (WT, 0.35±0.07; *L7-Shank2*^{-/-}, 0.49±0.09; P<0.0001) and CV2 (WT, 0.36±0.06; *L7-Shank2*^{-/-}, 0.47±0.06; P<0.0001) (Fig. 7G, H) that were found in the posterior lobules of the global *Shank2*^{-/-} (Fig. 3I-N), confirming the higher SS irregularity. In addition, the *L7-Shank2*^{-/-} mice also showed signs of SS irregularity in the anterior lobules in that their CV2 was also significantly increased (WT, 0.43±0.04; *L7-Shank2*^{-/-}, 0.47±0.04; P=0.0092) (Fig. 7C, D). The *L7-Shank2*^{-/-} SS mice activity did not show higher firing frequencies in either the anterior (WT: 104.4±25.8 Hz; *L7-Shank2*^{-/-}: 101.2±19.7 Hz; P=0.6) or posterior (WT: 70.9±19.5 Hz; *L7-Shank2*^{-/-}: 76.3±23.4 Hz; P=0.4) lobules (Fig. 7B, F). Finally, we also recorded SS activity of PCs in the flocculus of the vestibulocerebellum, because they are known to directly control VOR adaptation (Wulff et al., 2009) (Fig. 7I-L). In PCs that were identified to be related to VOR-adaptation by their response to motion around the vertical axis in space, we again found a significant increase in SS irregularity (CV: WT, 0.39±0.07; *L7-Shank2*^{-/-}, 0.53±0.08; P<0.0001; CV2: WT, 0.39±0.07; *L7-Shank2*^{-/-}, 0.52±0.08; P<0.0001), while their overall firing frequency was unaffected (WT: 68.2±15.0 Hz; *L7-Shank2*^{-/-}: 69.6±18.8 Hz; P=0.8) (Fig. 7J-L). Moreover, *L7-Shank2*^{-/-} showed a bigger difference with WT in SS irregularity in the posterior lobules (40.0% and 30.6% higher CV and CV2, respectively) compared to that in the anterior lobules (4.4% and 9.3% higher CV and CV2, respectively). No significant differences were observed in the duration of the complex spike-induced simple spike pause or the complex spike firing frequency in any of the recorded lobules (P>0.2 in all cases) (Supplementary Fig. 6). Together, *L7-Shank2*^{-/-} mice demonstrate the critical importance of Shank2 in PCs for maintaining SS regularity.

Reduced cognitive functioning *L7-Shank2*^{-/-} mice

We next examined social and repetitive ASD-like behaviours in the PC-specific *L7-Shank2*^{-/-} mice. The three-chamber social interaction task is a widely used social
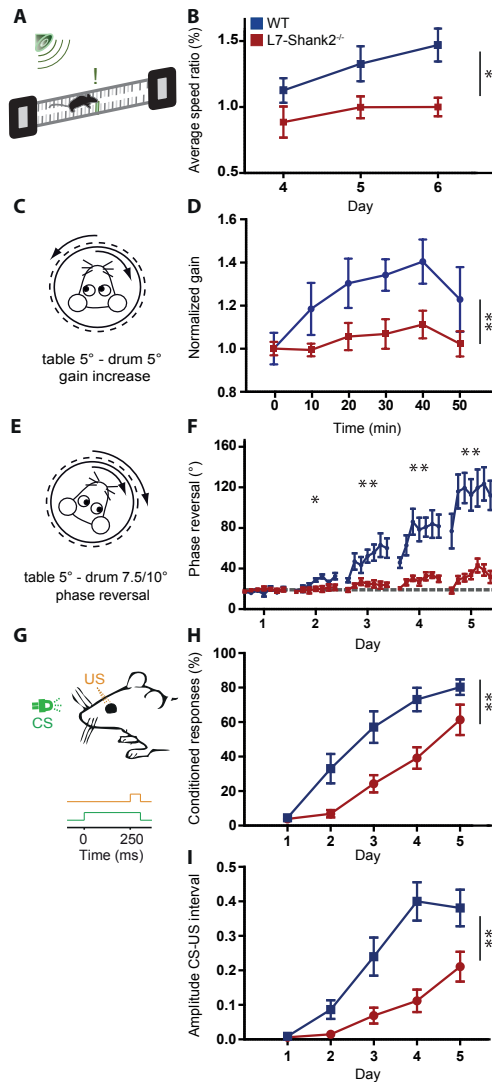
Figure 6 L7-Shank2$^{-/-}$ mice show impaired motor learning. (A, B) After three days of training, WT (n=9) but not *L7-Shank2$^{-/-}$* mice (n=6) (P=0.018) learned to increase their speed during a conditioned ErasmusLadder test using tone-cued rung displacements. **(C, D)** In vestibulo-ocular reflex (VOR) gain increase training, *L7-Shank2$^{-/-}$* mice (n=8) were not able to adapt their gain like WTs did (n=7) (P=0.006). **(E,F)** *L7-Shank2$^{-/-}$* mutants (n=9) did not adapt their VOR phase following a reversal training paradigm, whereas WT (n=9) did (2nd day, P=0.047; 3rd, P=0.0013; 4th, P<0.0001; 5th, P=0.0003). **(G,H,I)** Impaired percentage (P=0.0013) and amplitude (P=0.0009) of conditioned responses (CRs) in *L7-Shank2$^{-/-}$* mice (n=10) compared to WT (n=11) in an eyeblink conditioning paradigm (200 paired trials daily). Data are represented as mean $\pm$ SEM. Single and double asterisks indicate P<0.05 and P<0.01, respectively. All tests were repeated-measures ANOVAs.
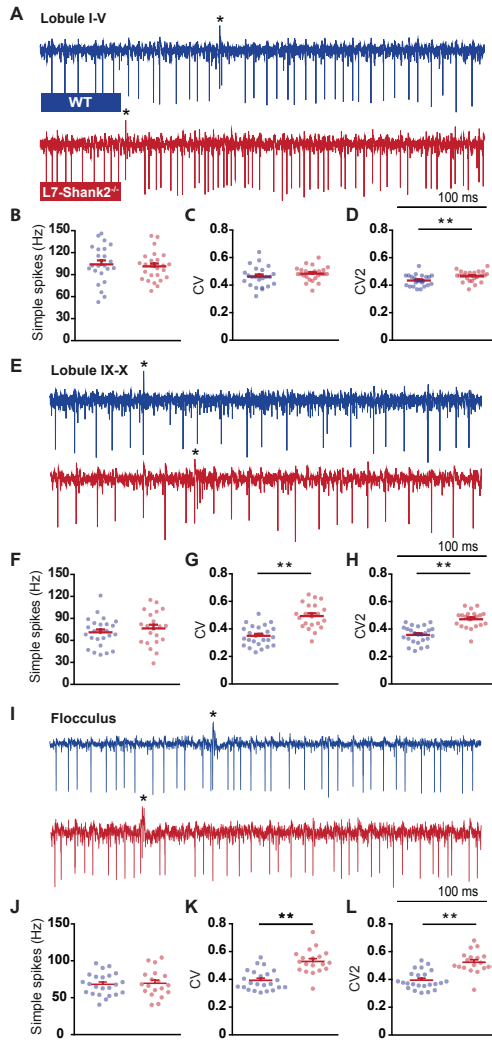
Figure 7 *in vivo* **simple spike firing characteristics in** *L7-Shank2*^{-/-} **Purkinje cells. (A)** Extracellular PC traces recorded from anterior lobules (I-V) in WT (top) and *L7-Shank2*^{-/-} (bottom) mice. **(B, C, D)** Firing characteristics in the anterior lobules reveal a difference in CV2 (P=0.0092) between *L7-Shank2*^{-/-} (n=25/3, cells/animals) and WT (n=23/3). **(E)** Example PC traces from posterior lobules (IX-X). **(F, G, H)** PCs from the posterior cerebellum in *L7-Shank2*^{-/-} (n=21/3) showed significantly higher CV (P<0.0001) and CV2 (P<0.0001) values compared to WT (n=25/3). **(I)** Example PC traces from posteriorly located flocculus, which is responsible for VOR learning. **(J, K, L)** Again, *L7-Shank2*^{-/-} (n=19/2) shows significantly higher CV (P<0.0001) and CV2 (P<0.0001) values than WT (n=23/2). Double asterisks denote P<0.01. All tests were two-sided t-tests.

131

interaction paradigm for evaluating ASD-like behaviour in mouse models of autism (Schmeisser at al., 2012; Won et al., 2012). WT mice exhibited a normal preference for the chamber in which the stranger mouse (S1) was present, compared to the empty chamber (P=0.0002, MWU-test) (Fig. 8A). In contrast, *L7-Shank2*$^{-/-}$ mice had no preference for either S1 or the empty chamber (P=0.7, MWU-test) (Fig. 8B). Comparing the preference index (stranger-empty) between WT and *L7-Shank2*$^{-/-}$ mice revealed a significantly decreased preference of *L7-Shank2*$^{-/-}$ mice for the stranger mouse (P=0.0213) (Fig. 8C), indicating their social interaction deficits. With the introduction of a second stranger in the previously empty chamber, WT mice again demonstrated an increased preference for the novel stranger (S2), this time compared to the familiar mouse (S1) (P=0.0001, MWU-test) (Fig. 8D), whereas *L7-Shank2*$^{-/-}$ mice showed no preference for either the familiar or the novel stranger mice (P=0.1, MWU-test) (Fig. 8E). Comparing the preference index (S2-S1) between WT and *L7-Shank2*$^{-/-}$ confirmed the impairment of social interaction in *L7-Shank2*$^{-/-}$ mice (P=0.0136) (Fig. 8F). Because of previously reported compulsive grooming (Schmeisser et al., 2012) and jumping (Won et al., 2012) in global *Shank2*$^{-/-}$ mice, we next examined repetitive behaviour. We observed no significant differences between WT and *L7-Shank2*$^{-/-}$ mice in the percentage of buried marbles in the marble-burying task (P=1.0) (Fig. 8G) or in the duration of grooming over a 15 min-period (P=0.054) (Fig. 8H). However, the *L7-Shank2*$^{-/-}$ mice did show an increase of repetitive behaviour in the T-maze through an increased perseveration, highlighting a reduction in cognitive flexibility (P=0.0023, MWU-test) (Fig. 8I). Finally, we observed no significant difference in anxiety (P=0.7, χ2-test) or olfactory sensitivity (P=0.6) of *L7-Shank2*$^{-/-}$ mice that could have potentially biased the social behaviour assessments (Supplementary Fig. 7). Together, these results indicate that *L7-Shank2*$^{-/-}$ mice exhibit ASD-like social impairments and task-specific repetitive behaviour.

Discussion

Severe loss-of-function mutations in SHANK2 have been firmly established as conferring a high genetic risk for ASD and intellectual disability (Berkel et al., 2010; Leblond et al., 2012; Leblond et al., 2014). Children with disruptive *SHANK2* mutations exhibit motor impairments, language delay and cerebellar dysfunction including dysmetria and dysdiadochokinesis (Leblond et al., 2014). Considering the increasing evidence for cerebellar involvement in ASD (Becker & Stoodley, 2013), we investigated anatomical, molecular and physiological consequences of global Shank2 ablation in the cerebellum. In addition, we analyzed *L7-Shank2*$^{-/-}$ mice with cerebellar PC-specific deletion of Shank2 to evaluate the extent to which the ASD-related behavioural findings in global *Shank2*$^{-/-}$ mice can be attributed to cerebellar dysfunction. In recent years, several genetic mouse models for ASD have been used for the study of cerebellar abnormalities. The first study to implement a Purkinje cell-specific model related to ASD involved the deletion of FMR1, the fragile X mental retardation 1 protein (Koekkoek et al., 2005). In this study, the authors reported eye-blink abnormalities and increased LTD in both global and Purkinje cell-specific deletion of FMR1. Furthermore, global Nlgn3-KO mutants exhibited deficits in cerebellum-related motor performance as assessed by the ErasmusLadder (Baudouin et al., 2012). A more recent model examining the 15q11-13
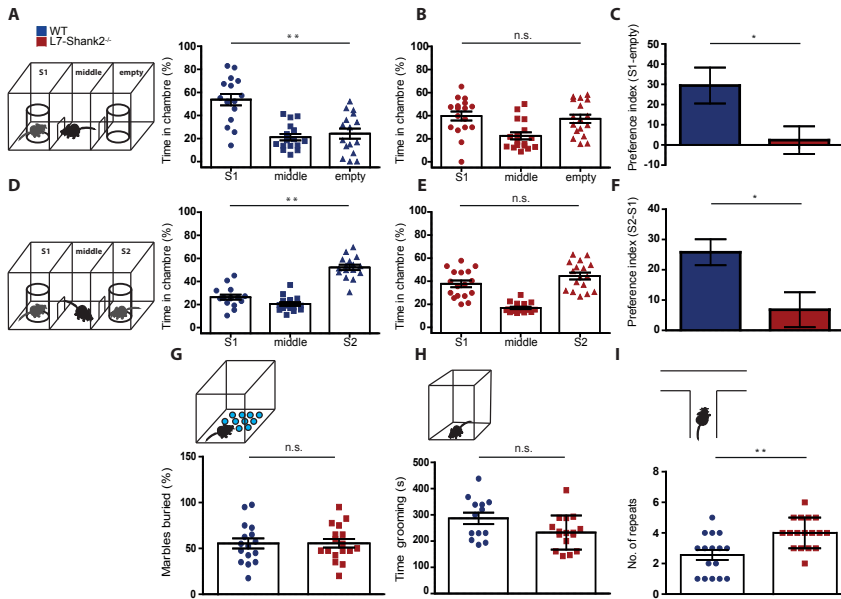
Figure 8 *L7-Shank2^{-/-}* mice show social impairment and signs of task-specific repetitive behaviour.
(A) Three-chamber social interaction evaluated by relative time spent in each chamber. WTs (n=16) prefer to spend time in the room with the stranger 1 mouse (S1), compared to the empty room (P=0.0002, MWU-test). **(B)** This was not the case for *L7-Shank2^{-/-}* (n=17) mice (P=0.7, MWU-test). **(C)** The preference index (S1-empty) confirms the difference between genotypes (P=0.021). **(D)** Following the introduction of a second stranger (S2), WTs (n=16) prefer to spend time in the chamber with S2 compared to that with S1 (P=0.0001, MWU-test). **(e)** The *L7-Shank2^{-/-}* mice (n=17) did not show a preference for newly introduced S2 (P=0.1, MWU-test). **(F)** The S1-S2 preference index indicates that WTs prefer S2 more than *L7-Shank2^{-/-}* do (P=0.013). **(G)** No difference was found in a marble burying task indicative of anxious and/or repetitive behaviour (WT, n=16; *L7-Shank2^{-/-}*, n=17, P=1.0). **(H)** *L7-Shank2^{-/-}* (n=16) seemed to trend towards less grooming than WTs (n=13) (P=0.054). **(I)** T-maze paradigm showed less consecutive alternations in *L7-Shank2^{-/-}* (n=17) compared to WT (n=16) (P=0.0023, MWU-test) indicating repetitive decision-making. Data are presented as mean ± SEM. Single and double asterisks indicate P<0.05 and P<0.01, respectively. Two-sided t-tests were used, unless stated otherwise.

duplication ASD syndrome demonstrated impaired cerebellar synaptic plasticity and motor learning deficits as assessed by eye-blink conditioning (Piochon et al., 2014). Perhaps the most definitive study implicating cerebellar dysfunction as etiologic for ASD-like behaviour involved a Purkinje cell-specific deletion of Tsc1 (Kloth et al., 2015). This study was the first to demonstrate that Purkinje cell-specific deletion of an ASD-associated gene results in ASD-like behaviour. Finally, a very recent study using multiple mouse models of syndromic ASD found a consistent pattern of impaired sensorimotor integration (Belmeguenai et a.l, 2010). These studies have established the foundation by which the cerebellar synaptic pathophysiology underlying ASD can be mechanistically investigated (Zoghbi & Bear, 2012).

Given the general importance of Shank2 in the regulation of neuronal plasticity (Schmeisser et al., 2012; Won et al., 2012), we investigated both synaptic and intrinsic plasticity of cerebellar Purkinje cells (Fig. 4). Our results indicate that Shank2 is crucial for PF-PC LTP, but not LTD. Additionally, we show that Shank2 is important for intrinsic plasticity of neuronal excitability (Belmeguenai et al., 2010). In contrast to a recent study of the 15q11-13 duplication ASD syndrome in which PC synaptic plasticity deficits were limited to LTD (Piochon et al., 2014), our results now highlight LTP impairments as a candidate mechanism underlying the cerebellar pathophysiology of ASD. Shank2 is a dedicated scaffolding protein, which has a major role in the regulation of glutamate receptor integration, synaptic transmission and plasticity (Grabrucker et al., 2011; Jiang & Ehlers, 2013). Future molecular and functional studies will have to elucidate the exact mechanisms by which Shank2 mediates plasticity in the Purkinje cell, but it may well include a suboptimal integration of GluR subunits as the expression levels of GluA1 and GluA2 were both reduced in the $Shank2^{-/-}$ mice. Since GluR subunit levels were analysed in synaptosomes from whole cerebella, it remains to be further investigated to what extent these changes are limited to the PF to PC synapse.

Because of the cerebellar physiological impairments and the previously reported motor hyperactivity in $Shank2^{-/-}$ mice (Schmeisser et al., 2012; Won et al., 2012), we examined activity levels during both baseline exploration and motor learning. To our surprise we did not find motor performance abnormalities in the PC-specific $L7$-$Shank2^{-/-}$ mice during various assessments including five separate locomotion and eye movement tests (Supplementary Fig. 2). However, we did observe substantial impairments of cerebellar motor learning including conditioning of locomotion and eyeblink responses as well as adaptation of compensatory eye movements (Fig. 6). It might seem counterintuitive that baseline motor performance can be intact while the capacity for motor learning is reduced, but this combination has been observed in many different mutant lines over the last few decades (De Zeeuw et al., 2011). Most likely, it reflects the indispensable role of PC plasticity for the acquisition of new behaviours within relatively short periods of time as occurs during the experimental training paradigms (i.e. in the order of hours) and the ability of the motor performance control system to compensate upstream and/or downstream of the affected synapse when prolonged adaptation periods are available as occurs during postnatal development (i.e. in the order of weeks) (Van Alphen & De Zeeuw, 2002). The potential causality of the identified electrophysiological abnormalities as underlying the motor learning impairments is strengthened by our independent findings in another Purkinje cell-specific mouse mutant (L7-PP2B-/-), in which also both synaptic LTP and

intrinsic plasticity were affected (Schonewille et al, 2010). Together, these phenotypes point towards a PC-dependent contribution to the behavioural motor impairments frequently observed in ASD.

In addition to changes in plasticity, we also found that inhibition of PCs was enhanced in the global *Shank2*^{-/-} mutants. Since reduced inhibition of PCs increases regularity of SS activity (Wulff et al., 2009), we hypothesized that PCs of the global *Shank2*^{-/-} mutants should have a higher level of irregularity of SS firing (Fig. 3). Indeed, this hypothesis was not only consistent with the *in vivo* extracellular recordings in lobule X of the global *Shank2*^{-/-}, but also confirmed in three different areas (Lobules I-V, Lobules IX-X and the flocculus) of the *L7-Shank2*^{-/-} mice (Fig. 7). Moreover, this correlation was also in line with the fact that the differences in sIPSCs, CV and CV2 had bigger effect sizes in the posterior lobules than the anterior lobules.

The increased frequency of inhibition in the global *Shank2*^{-/-} did not occur concomitantly with increased amplitude of sIPSCs postsynaptically at PCs, indicating that the observed effect could be of pre-synaptic origin. The PC irregularity in the *L7-Shank2*^{-/-} would then have to originate from a pre-synaptic effect of the postsynaptic absence of Shank2. Indeed, recent evidence indicates the possibility of Shank-mediated transsynaptic signalling through transmembrane proteins affecting both post and pre-synaptic processes important for vesicle release probability (Arons et al., 2012). This type of transsynaptic signalling could manipulate the inhibitory input to PCs either directly or indirectly, e.g. through altered glutamate spillover from the climbing fiber to Purkinje cell synapse (Szapiro & Barbour, 2007). Future research aimed at pinpointing the sites relevant to the effects described above should thus focus not only on Purkinje cell specific mouse mutants, but also on those in which their afferents are specifically affected (Badura et al., 2013). In doing so, important consideration in studies implementing cell-specific deletions should be given to germline analyses, given the sensitivity of the *L7*-cre (Belmeguenai et al, 2010; Barski et al., 2000) and *Shank2* lines (Supplementary Table 1) (Schmidt-Supprian & Rajewsky, 2007).

We observed a significant decrease in SS frequency in the anterior lobules of global *Shank2*^{-/-} mice, but not in their posterior lobules, nor in the anterior or posterior lobules of *L7-Shank2*^{-/-} mice. We believe that this inconsistency may reflect the fact that the spontaneous SS firing frequency of PCs is probably largely due to their intrinsic properties rather than the synaptic efficacy of their inhibitory or excitatory inputs (Zhou et al., 2014). Indeed, blocking inhibitory or excitatory synaptic input to PCs by deleting their GABA-A-γ2 receptor-subunits or abolishing voltage gated calcium channels at their parallel fiber input primarily affects the regularity of SS firing, rather than their firing frequency (Wulff et al., 2009; Galliano et al., 2013). Thus, the consistent irregularity of SS in PCs, particularly in the posterior lobe, of the *Shank2*^{-/-} mutants underlines the putative importance of precise SS regularity for behavioural output (De Zeeuw et al., 2011). Although abnormalities in the anterior and posterior lobules have both been proposed as relevant sites of cerebellar pathology in ASD (Mosconi et al., 2015), our converging data obtained in the posterior lobe suggest that the mechanisms governing the regularity of SS firing reveal a common biological vulnerability in the etiology of ASD.

Here, we report impaired social and task specific repetitive behaviour due to the Purkinje cell-specific deletion of *Shank2* (Fig. 8). This result is particularly interesting as, to our knowledge, it is the first Purkinje cell-specific mouse model for a non-

syndromic form of autism in which ASD-like behaviour has been established. The impaired social behaviour, late-onset ataxia and reduced excitability of Purkinje cells previously observed in *L7-Tsc1* mice (Tsai et al., 2012) were due to the absence of a protein that inhibits mTOR signalling through which the translation of a wide variety of proteins is regulated. In contrast, we here show that disruption of the synapse through the absence of a single postsynaptic scaffolding protein in the Purkinje cell is sufficient to show impaired ASD-related motor learning and social behavioural impairments. In addition to the social impairments, we found signs of enhanced repetitive behaviour in the T-maze paradigm, but not the marble burying task or grooming tasks. Since the T-maze task reveals the level of cognitive inflexibility following decision making over consecutive trials rather than the level of repetitious behaviour dominated by high-frequency motor activity that characterizes the other two tasks and that may well be confounded by deficits in cerebellar motor learning, these results highlight the importance of the Purkinje cell synaptic function for ASD beyond the classically ascribed motor-related behaviour. One of the main challenges remaining is to mechanistically explain the contribution of impaired Purkinje cell physiology to the observed ASD behavioural phenotypes. As previously mentioned, the Shank family of postsynaptic scaffolding proteins has many different interacting proteins in the postsynaptic density through which they could contribute to the functional establishment of regulatory mechanisms for plasticity. The translational challenge from synapse to behaviour brings about two main questions: How does an impaired Purkinje cell mediate ASD-related behaviour? And how might Purkinje cell impairments lead to abnormal brain function beyond the cerebellum with regards to neurodevelopmental critical periods? The first question has been extensively addressed by the accumulating evidence regarding the contribution of ASD-related cerebellar dysfunction to impaired motor learning, as apparent from the eye movement adaptation, ErasmusLadder, and eyeblink conditioning findings examined here and by other investigators (Kloth et al., 2015). It is indeed possible that the increased inhibition and irregularity of SS firing, in addition to impaired cerebellar plasticity mechanisms, may contribute to social and repetitive behaviour-related phenotypes in ASD. We believe that the answer to how the cerebellum can essentially contribute to socially impaired behaviour could reside in various mechanisms. The idea that disruption of a certain brain area during development could affect the development and consequently the function of other inter-connected areas, also termed developmental diaschisis, has recently been put forward as a prime mechanism for the cerebellum in its ability to influence other cortical areas in critical developmental periods (Wang et al., 2014). In the future, the latter hypothesis can for example be tested with Purkinje cell specific *Shank2* ablation at different stages during development using inducible mouse models, as has recently been employed for other ASD-related genes (Mei et al., 2016; Silva-Santos et al., 2015). These experiments will help to further elucidate the mechanisms by which differential genes, such as *Shank2*, regulate cerebellar function and ultimately ASD-like behaviour.

Methods

Experiments and analyses were performed with the experimenters blinded to the genotype. Mice used were global germ-line *Shank2*$^{-/-}$ and their littermate WTs all bred on a mixed C57BL6/N and C57BL6/J background. The generation of these mice has previously been described in detail (Schmeisser et al., 2012; Won et al., 2012). The *L7-Shank2*$^{-/-}$ was generated by crossing Purkinje specific L7(Pcp2)-Cre (Barski et al., 2000) with *Shank2*$^{flxd/flxd}$ (Schmeisser et al., 2012). Genotyping was performed on postnatal day (P)7-10 using primers 1700 S (TCCATGGTT TCGCGAGAGCG), 1842 AS (TCCCTATTGGGACGCAGTGG) and 2394 AS (CAGCATCATGACAATGTCTCCA). For all experiments we used mice from both genders, unless indicated otherwise. The mice were individually housed with food and water available ad libitum and in 12:12 hrs light/dark cycles. All experiments were approved by local and national ethical committees.

Primary antibodies

The anti-*Shank2* SA5193 antibody has been characterized previously (Schmeisser et al., 2012) the following antibodies were from commercial suppliers: anti-GluA1 (Cat. No. 182 003), anti-GluA2 (Cat. No. 182 103), anti-Nlgn3 (Cat. No. 129 113) (all Synaptic Systems, Goettingen, Germany), anti-β3-Tubulin (Cat. No. MRB-435P) (Covance, Brussels, Belgium) and Aldolase C (Cat. No. 12065) (Santa Cruz, Dallas, U.S.A.)

Golgi stainings

Adult mouse cerebella were dissected and prepared using the FD Rapid GolgiStain Kit (NeuroTechnologies, Vilnius, Lithuania). Serial coronal sections of 150 μm were collected from WTs and global *Shank2*$^{-/-}$ mice and Z-stack images were taken using an upright Axioscope (Carl Zeiss, Jena, Germany). Distal dendrites of Purkinje cells were traced for spine analysis.

Electron microscopy

Adult mice were transcardially perfused with fixative (2 % paraformaldehyde, 2.5 % glutaraldehyde, 1 % saccharose in 0.1 M cacodylate buffer, pH 7.3) and their cerebella were dissected and post-fixed overnight at 4 °C. After dehydration and staining with 2 % uranyl acetate, the material was embedded in epoxy resin. Ultrathin sections were cut using an ultramicrotome (Ultracut UCT, Leica). After lead citrate staining, sections from WTs and global *Shank2*$^{-/-}$ mice were examined using an electron microscope (JEM 1400 TEM, Jeol). For ultrastructural PSD analysis, spine synapses have been selected in the distal molecular layer where the parallel fiber-Purkinje cell (PF-PC) contacts greatly outnumber other types of synapses.

Biochemistry

Adult mouse cerebella were homogenized on ice in HEPES-buffered sucrose (320 mM sucrose, 5 mM HEPES, pH 7.4) containing protease inhibitor mixture (Roche, Mannheim, Germany). The homogenate was centrifuged (1.000 x g, 4 °C) to remove cell debris and nuclei. The supernatant was further centrifuged (12.000 x g, 4 °C) to obtain a pellet containing the cerebellar synaptosomes. Equal amounts of 10-20 μg protein per lane were separated by SDS-polyacrylamide gel electrophoresis and blotted onto polyvinylidene fluoride membranes using standard protocols. After incubation with primary antibodies (1:1.000 for anti-Shank1, anti-GluA1, anti-GluA2, anti Nlgn3; 1:10.000 for anti- β3-Tubulin), immunoreactivity was visualized on X-ray film (GE Healthcare, Freiburg, Germany) using HRP-conjugated secondary antibodies (Dako; Hamburg, Germany) and the SuperSignal detection system (Thermo Scientific). For quantification, the films were scanned, the grey value of each band was analysed by ImageJ (National Institutes of Health, Bethesda, MD, USA) and normalized to the grey value of β3-Tubulin.

Immunohistochemistry

Mouse brains were snap-frozen after removal without perfusion. Tissue was sectioned at 7 μm using a cryostat at -20°C and a knife temperature of -14°C. Sections were air-dried on superfrost glass and stored at -80°C. For staining sections were defrosted at room temperature (RT) for 60 min and subsequently washed with -20°C MeOH for 3 min followed by 3X 10 min of PBS wash. To permeabilize membranes, sections were incubated for 60 min in 0.5% Triton X-100 in PBS at RT and washed 3X in PBS for 10 min. Following a 60 min incubation in 5% BSA (in PBS) at RT and subsequent PBS washing, sections were incubated in SA5193 antibody (1:1000, dissolved in 2% bovine-serum albumin, see Boeckers et al., 1999) O/N at 4°C. The sections were then washed for 3X 10 minutes in PBS followed by 120 min of fluorescent antibody staining (1:200, Donkey anti goat-Cy3) in 2% BSA at RT. After the fluorescent antibody a wash of 3X 10 min of PBS was followed by 2X 10 min wash with PB. The sections were then put for 10 min in DAPI (200 μl in 50 ml 0.1 M PB). This was concluded by a 2x 10 min PB wash. For Zebrin (Adolase C) we used a different approach after the defrosting of sections at RT. These slices were washed with 10 min 4% PFA followed by 20 min of methanol and subsequently by 2 min PBS and 30 min 100 ml PBS (with 2 ml 30% H_2O_2 + 0.8 ml sodium azide). Here after a wash of 2 min PBS and 2X 2 min in PBS (with 1 L PBS, 5 g protifar and 1.5 g glycine, sections were incubated in the primary antibody for Adolase C (1:1000; Santa Cruz, Dallas, U.S.A., Cat. No. 12065) O/N at 4°C. The sections were then washed for 3X 10 minutes in PBS followed by 90 min of fluorescent antibody staining (1:200, donkey anti goat-Cy3; The Jackson Laboratory, Sacramento, U.S.A., Cat. No 705-165-147) in 2% BSA at RT. After the fluorescent antibody a wash of 3X 10 min of PBS was followed by 2X 10 min wash with PB. The sections were then put for 10 min in DAPI (ThermoFisher Scientific, Waltham, U.S.A., Cat. No. D3571; 200 μl in 50 ml 0.1 M PB). This was concluded by a 2X 10 min PB wash. Following PBS washing, the sections were thionin-stained and permount-covered using standard protocols. All immunohistological stainings have successfully been replicated on multiple occasions.

Ex vivo electrophysiology

Following decapitation of mice under isoflurane anaesthesia, the cerebellum was re-moved into an ice-cold 'slicing medium', containing (in mM) 240 sucrose, 2.5 KCL, 1.25 Na_2HPO_4, 2 $MgSO_4$, 1 $CaCl_2$, 26 $NaHCO_3$ and 10 D-Glucose, that was carbogenated continuously (95% O_2 and 5% CO_2). Sagittal slices, 250 m thick, of the cerebellar vermis were cut using a vibrotome (VT1200S, Leica) and put in carbogenated artificial cerebrospinal fluid (ACSF) containing (in mM): 124 NaCl, 5 KCL, 1.25 Na_2HPO_4, 2 $MgSO_4$, 2 $CaCl_2$, 26 $NaHCO_3$ and 20 D-Glucose, for at least one hour at $34\pm1^\circ$C before the start of the experiment. Slice physiology was done at room temperature $21\pm1^\circ$C or $33\pm1^\circ$C as indicated in the results section and in the presence of 100 M picrotoxin except for the sIPSCs recordings. Whole-cell patch clamp recording were performed with an EPC9 amplifier (HEKA Electronics, Lambrecht, Germany). Recordings were excluded if the series (Rs) or input resistances (Ri) changed by more than 15% during the experiment, which was determined using a hyperpolarizing voltage step relative to the -65 mV holding potential. Data analysis (rise times (10-90% for EPSC and action potentials)), decay time (tau) for EPSC and IPSC amplitudes, action potential threshold (identified by steepest slope in membrane potential prior to action potential) and AHP amplitude (minimal membrane potential relative to the action potential threshold)) was performed using Clampfit software (Molecular Devices).

For whole-cell recordings Purkinje cells (PCs) were visualized using an upright microscope (Axioskop 2 FS, Carl Zeiss) equipped with a 40X objective. Recording electrodes (3-5 MΩ, 1.65 mm OD and 1.11 mm ID, World Precision Instruments, Sarasota, FL, USA) were filled with an intracellular solution containing (mM): 120 K-Gluconate, 9 KCL, 10 KOH, 4 NaCL, 10 HEPES, 28.5 Sucrose, 4 Na_2ATP, 0.4 Na_3GTP (pH 7.25-7.35 with an osmolarity of 295 ± 5). Note that we adjusted the osmolarity using sucrose (Belmeguenai et al. 2010; Coesmans et al., 2004). For the recording of sIPSCs we used an intracellular solution containing (mM): 150 CsCl, 1.5 $MgCl_2$, 0.5 EGTA, 4 Na_2ATP, 0.4 Na_3GTP, 10 HEPES, 5 QX314 (pH 7.25-7.35 with an osmolarity of 295 ± 5). For extracellular stimulation of parallel fibers (PFs), similar patch electrodes were filled with ACSF and positioned in the upper third of the molecular layer lateral to the patched Purkinje cell. The stimulation intensity was set to evoke an EPSC of 300 ± 50 pA (typically 3-6 μA stimulation intensity). For PF-PC transmission we used various inter-stimulus intervals (50-200 ms) (see Fig. 2). For recordings of spontaneously occurring IPSCs (sIPSCs) we used the previously mentioned K+-based internal and recorded their occurrence during at least 120 s.

For climbing fiber stimulation similar electrodes (filled with ACSF) were positioned near the patched Purkinje cell soma in the surrounding granule layer. We selected those recordings in which climbing fiber stimuli elicited clear all-or-none responses and lacked the co-activation of Purkinje cell axons (identifiable by back-propagating action potentials) for further analysis. For CF elimination experimental tissue was prepared in a similar way for all age groups. We systematically scanned the granule cell layer to elicit CF responses and recorded PC responses (using an intracellular solution containing (in mM): 115 $CsMeO_3$, 20 CsCl, 2.5 $MgCl_2$ 10 HEPES, 0.6 EGTA, 4 Na_2ATP, 0.4 Na_3GTP, 10 Na-phosphocreatine) at -20 mV holding potential to prevent voltage escape during the CF-responses. For CF-PC transmission we evaluated the paired pulse ratio at 50 ms stimulus interval. To evaluate the complex

spike waveforms we analysed the amplitude of the Na^+-spike and the amplitude of the first Ca^{2+}-spikelet evoked during the LTD-tetanus (Van Woerden et al., 2009). Current clamp recordings were corrected off-line for the calculated liquid junction potential (-10.2 mV).

The synaptic (LTP, LTD) and intrinsic plasticity protocols were recorded from lobules 5/6 and conducted as described previously (Belmaguenai et al., 2010; Schonewille et al., 2010). In short, for synaptic plasticity all recordings were done in voltage-clamp, except for the tetanus, which consisted of single-pulsed PF-stimulation at 1 Hz for 5 min (LTP) or single-pulsed PF + single-pulsed CF stimulation (5 ms interval) at 1 Hz for 5 min (LTD). We evaluated the synaptic plasticity by the change in PF-EPSC (presented at 0.05 Hz) relative to the mean value calculated during the last 5 min pre-tetanus. For intrinsic plasticity we utilized the PF-LTP tetanus (but without bias currents, i.e., I=0 pA) and evaluated the impact on the number of action potentials evoked by 300 pA current injections during 500 ms (presented at 0.05 Hz).

Extracellular Purkinje cell recordings

In vivo recordings were performed as recently described (Zhou et al., 2014). An immobilizing pedestal was fixed on the skull and a craniotomy (ø 3 mm) was performed on the occipital bone. After recovery of 5 days, mice were head-fixed and body restrained for recordings. Single unit recording was identified by the presence of a short simple spike pause (>6 ms) after each complex spike. Purkinje cells were recorded from vermal lobules I-V and X using single barrel (2.0 mm OD, 1.16 mm ID, Harvard Apparatus, MA, USA) and double barrel (theta septum, 1.5 OD, 1.02 ID; World Precision Instruments) boroscilate glass pipettes. *in vivo* recordings were analysed offline using Spiketrain (Neurasmus BV, Rotterdam, The Netherlands, www.neurasmus.com) and custom scripts in MatLab (Mathworks, Natick, MA, USA). The CV is calculated by dividing the SD by the mean of the interspike intervals, whereas CV2 is calculated as 2 * |ISIn+1 - ISIn| / (ISIn+1 + ISIn).

Compensatory eye movements

Mice between 8 and 10 weeks of age were prepared for head-restrained recordings of compensatory eye movements. These types of recordings have been described in detail previously (Schonewille et al, 2010). In order to head restrain the mice during the eye movement task, a small pedestal was attached using Optibond primer and adhesive (Kerr, Bioggio, Switzerland) under isoflurane anaesthesia in O_2 (induction with 4% and maintained at 1.5% concentration). After a recovery period of two to three days, mice were head-restrained by fixation using the pedestal in the experimental setup. A round screen with a random dotted pattern ('drum') surrounded the mouse during the experiment. The optokinetic reflex (OKR), vestibulo-ocular reflex (VOR) and the light-guided vestibulo-ocular reflex (VVOR) were induced using a sinusoidal rotation of the drum in light (OKR), rotation of the table in the dark (VOR) or the rotation of the table (VVOR) in the light. The motor behaviour was assessed by rotating the table and/or drum at 0.1 to 1 Hz with a fixed 5° amplitude. In order to evaluate motor learning, a mismatch between visual and vestibular input was created.

Rotating both the visual and vestibular stimuli in phase (at the same amplitude) induced a decrease of gain; rotating the drum at greater amplitude relative to the table induced the so-called phase reversal of the VOR (day 1, 5° phase difference; day 2, 7.5°; day 3-4, 10°). Rotating the visual and vestibular stimuli out of phase (at the same amplitude) induced the VOR gain increase. All training protocols were induced at 0.6 Hz with table rotation amplitude of 5°. For eye illumination during the experiments two table-fixed infrared emitters (output 600 mW, dispersion angle 7°, peak wavelength 880 nm) and a third emitter, which produced the tracked corneal reflection (CR), were mounted to the camera and aligned horizontally with the optical axis of the camera. Eye movements were recorded with eye-tracking software (ETL-200, ISCAN systems, Burlington, NA, USA). Gain and phase values of eye movements were calculated using Matlab (MathWorks).

Eyeblink conditioning

Mice of 12-15 weeks of age were prepared for head-restrained eyeblink conditioning (Ten Brinke et al., 2015). In short, a small brass pedestal was attached to the skull using Optibond primer and adhesive (Kerr) and Charisma (Heraeus Kulzer, Armonk, NY, USA), under isoflurane anaesthesia. Three to five days after surgery, mice were habituated during two short (30-45 min) sessions on two days in a sound- and light-isolating chamber which houses the eyeblink set up. During these sessions mice were head-fixed and suspended over a foam cylindrical treadmill. While no stimuli were presented, a 27.5 gauge needle through which US air-puffs are delivered was positioned at 5 mm from the center of the left cornea, a green LED (ø 5 mm) that delivers the CS was placed 5 cm in front of the mouse, and an GMR magnetometer (NVE, Eden Prairie, MN, USA) was fixed above the left eye. During five subsequent acquisition training days, this sensor measured the distance of a miniscule magnet (1.5x0.7x0.5 mm) that was placed on the left lower eyelid with high accuracy, while 200 paired trials were presented, usually spaced 10 ± 2 s apart, plus the time needed for a sporadic unstable eyelid to stabilize in open position. Each paired trial consisted of a 280 ms green LED CS, co-terminating with a 30 ms airpuff (30 psi, through an MPPI-3 pressure injector; ASI, Eugene, OR, USA). All experiments were performed at approximately the same time of day by the same experimenter. Individual eyeblink traces were analyzed using custom LabVIEW (National Instruments, Austin, TX, USA) or MATLAB (Mathworks, Natick, MA, USA) scripts. Trials with significant activity in a 500 ms pre-CS baseline period were regarded as invalid for further analysis. Valid trials were aligned by making the mean of their baseline activity zero, and the average amplitude of all post-US unconditioned blink responses was used to denote 100% eyelid closure. From this, the average eyelid closure as a percentage from baseline to full closure at the end of the CS-US interval was calculated over all valid trials. To calculate percentage of CRs, trials were judged to contain a CR if the eye closed for more than 5% between 50-250 ms after CS and the CR reached its peak after 100 ms.

ErasmusLadder

The ErasmusLadder (Noldus, Wageningen, Netherlands) is a fully automated system consisting of a horizontal ladder between two shelter boxes. It has 37 rungs on each side, spaced 15 mm apart, and attached to custom-made pressure sensors that are continuously monitored. In order to create a left-right alternating pattern, even rungs on one side and odd rungs on the other side are elevated by 6 mm. Prototype testing revealed that optimum forepaw displacement for mice is about 6 cm in a single step at medium high velocity, which is the distance between 3 consecutive elevated rungs and is defined as efficient step in the text (for more details, see Veloz et al., 2014). It is clear from previous studies that mice improve their walking efficiency over training sessions by increasing the number of efficient steps relative to steps of lower sizes (Veloz et al., 2014). In the current study, mice (male, 15-18 weeks old) were tested in 6 daily sessions consisting of 2 unperturbed sessions, 1 session with a fixed obstacle in the middle of the ladder and 3 perturbed sessions. During the first three sessions, mice were trained to walk between two shelter boxes for 50 trials each day. In the perturbed sessions, a sudden appearance of a rising rung on the right side of the mouse was used as the unconditional stimulus (US). A 15 kHz tone was used as the conditional stimulus (CS) and preceded the US by 200 ms in CS-US paired trials. CS-only trials and paired trials were randomly distributed among 50 trials. There were twice as many paired trials as CS-only trials. Step length and step time were defined as the distance and time between two consecutive touches from the right front limb. To estimate motor adaptation in CS-only trials, we calculated step speed (step length/step time) using only the steps within 1 s before and 1 s after the CS. The speed ratio during conditioning was defined as the speed post-CS divided by the speed pre-CS.

General behavioural analyses

Behavioural experiments were performed using *L7-Shank2*^{-/-} and WT littermate controls aged 8-16 weeks during the light period of their diurnal cycle. The mice used in the general behavioural experiments described here underwent multiple tests.

For the PhenoTyper test, mice were placed in a homecage-like apparatus (Noldus) with ad libitum access to food and water, and left to explore for 30 minutes. Locomotion was recorded using the automated software Noldus Ethovision XT 11 and distance and speed were calculated.

For the open field test, mice were placed in a novel circular, brightly-lit 110-cm-diameter open arena for 10 min. Locomotion was recorded using the automated software Noldus Ethovision XT 11 and total distance travelled, as well as average speed were calculated. During analysis the arena was subdivided in three concentric zones named the inner (25 cm), middle (15 cm) and outer zone (15 cm), and percentage of time in each zone was calculated.

For the three-chamber social interaction test, age and gender-matched WT target subjects (Stranger 1 and 2) were habituated for 5 consecutive days before beginning of testing by being placed inside round metal-wired cages. On the test day, experimental mice were placed in the central chamber of a clear Plexiglas box (60 x 35 cm) divided

into three interconnected chambers. After habituation for 5 min. an unfamiliar mouse (Stranger 1; S1) was introduced into a wire cage in one of the side-chambers and an empty wire cage in the other side-chamber. The dividers were then raised and the test mouse was allowed to freely explore all three chambers over a 5-minute session. Next, the mouse remained in the chamber with stranger 1 for an additional 5-minute session. Subsequently, a novel stranger mouse (Stranger 2; S2) was placed in the previously empty wire cage and again the test mouse was left to explore for 5 min. Time spent in each chamber, as well as overall locomotion, was calculated using the automated software Noldus Ethovision XT 11. Preference indices were calculated by subtracting the time spent with the empty wire cage from the time spent with stranger 1 (S1 - E), and subtracting the time spent with stranger 1 from time spent with stranger 2 (S2 - S1).

For the T-maze spontaneous alternation test, mice were placed at the base of a T-maze (arm length 50 cm) and were given the choice to freely explore either the right or left arm of the maze for 10 consecutive trials. A choice was assumed to be made when mice stepped into an arm with all four paws. At that moment the gate to that arm was closed and the animal was allowed to explore the arm for 5 s. Then, the mouse was gently placed back at the base of the T-maze for the next trial. When the mouse chose a similar arm at two consecutive trials, this was scored as number of repeats, indicative of repetitive behaviour.

For the grooming test, mice were removed from their homecage, received a single puff of water spray and placed in clean transparent cages (15 x 15 x 20 cm) under bright light for 15 min. Behaviour was recorded with a high-speed camera (30Hz full frame rate), and time spent grooming was scored by two independent raters. All types of grooming -- paw licking, nose and head self-grooming, body grooming, leg grooming and tail/genital grooming -- were scored.

For the marble burying test, Makrolon cages (50 x 26 x 18 cm) were filled with 4 cm of bedding material and 20 glass marbles, which were arranged in an equidistant 4 x 5 grid. Animals were given access to the marbles for 30 min. Marbles 100% covered by bedding were scored as buried and marbles covered partially contributed 50% to the total score.

For the olfactory test, a piece (1.25 g) of cookie was put into the subject's cage each day for three consecutive days, and checked for complete consumption the following day. For 24 hrs before the test phase, mice were completely food-deprived. Subjects were placed in a clean Makrolon cage (50 x 26 x 18 cm) with 4 cm of clean bedding, and allowed to habituate for 5 min. Then, a piece of cookie (1.25 g) was hidden in a random corner in the cage at 1 cm depth. Latency to find the cookie was recorded for a maximum of 15 mins (900 s).

Data analysis

In the text, mean ± SD values are presented, in the figures SEM-values are reported, and p-values smaller than 0.05 are considered significantly different. Two-sided Student's t-tests were performed, unless stated otherwise. For a complete representation of the data we have included a detailed overview of all statistics in Supplementary Table 1. Additionally, since the L7-Cre line was shown to reveal germline deletions

(see also Tsai et al, 2012) and since the potential impact of cerebellar Purkinje cells on general cognitive tests is widely debated (Galliano et al., 2013; Rochefort et al., 2011), we have checked for heterozygous germline deletions in our L7-Shank2 mice and statistically excluded the possibility they could have influenced our conclusions on the non-cerebellar paradigms (Supplementary Table 1).

Supplementary Material

A full account of all statistical information (**Table S1**) is available online and is not included here.
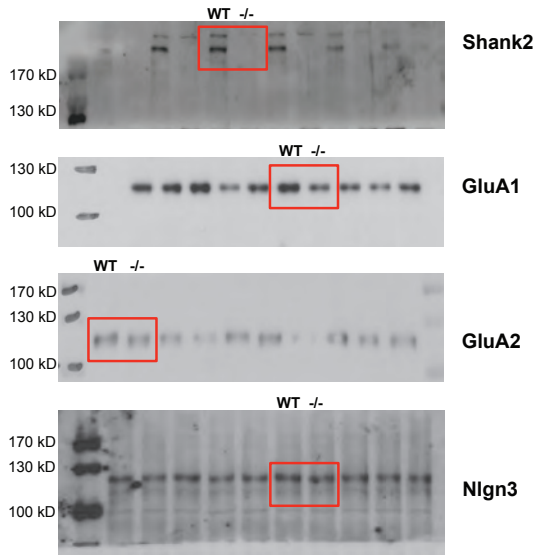
Figure S1 Full western blots with size markers related to Fig. 1D.
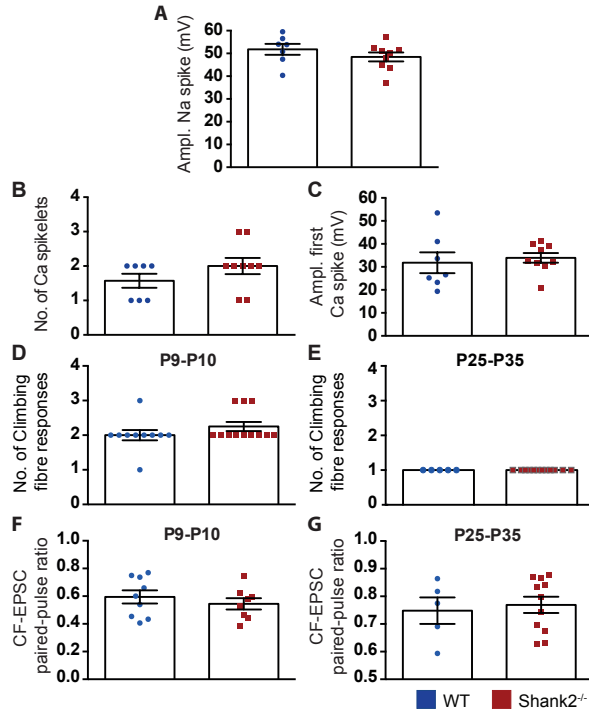
Figure S2 *Ex vivo* **climbing fibre activity shows no significant differences between** *Shank2-/-* **and WT mice.** **(A-C)** No difference in Na spike amplitude (P=0.3) **(A)**, nor in number of Ca spikelets (P=0.2) **(B)** or amplitude of the first Ca spike (P=0.7) **(C)**, between WT (n=7/6) and *Shank2-/-* (n=9/4). **(D, E)** Number of climbing fibre responses was similar between *Shank2-/-* and WT mice at P9-10 (WT, n=10/3; *Shank2-/-*, n=12/3, P=0.2)) and at P25-35 (WT, n=5/3; *Shank2-/-*, n=12/3, P=1.0). **(F, G)** Complex spike paired pulse depression was similar between *Shank2-/-* and WT mice at P9-10 (WT, n=9/3; *Shank2-/-*, n=8/3, P=0.5) and at P25-35 (WT, n=5/3; *Shank2-/-*, n=11/3, P=0.6).Statistical test used was a two-sided t-test unless stated otherwise.
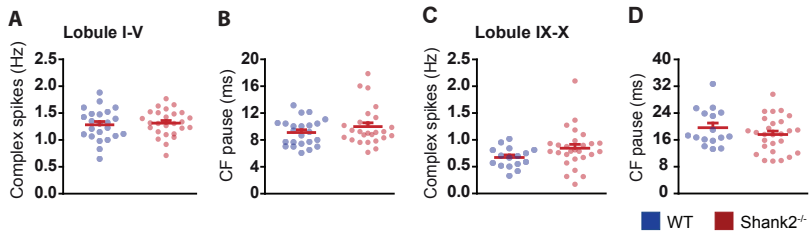
Figure S3 *In vivo* **complex spike activity shows no significant differences between** *Shank2-/-* **and WT mice.** **(A, B)** Complex spike firing frequency (P=0.7) and CF pause (P=0.2) were not different between *Shank2-/-* and WT mice in anterior lobules I-V (WT, n=23/3, cells/animals; *Shank2-/-*, n=26/3). **(C, D)** Similarly, complex spike firing rate (P=0.1) and CF pause (P=0.2) did not differ between mutant (n=27/3) and WT (n=16/3) in posterior lobules IX-X. Error bars denote SEM. Statistical test used was a two-sided t-test unless stated otherwise.
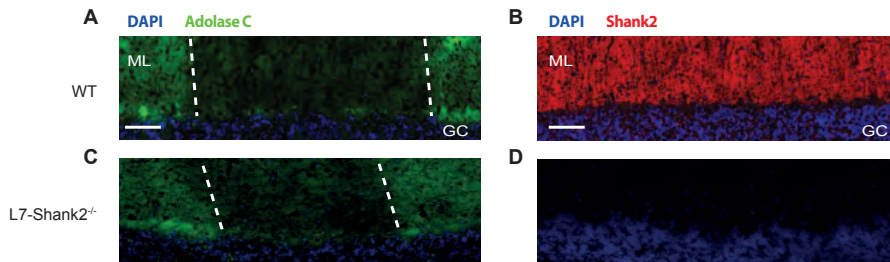
Figure S4 Cerebellar Zebrin and Shank2 immunohistology. (A, C) Coronal section of Crus 1 showing distinctive Zebrin patterning in both WT and *L7-Shank2*^{-/-}. **(B, D)** Coronal section of Crus 1 showing a uniform presence of Shank2 in WT, but a complete absence of Shank2 in *L7-Shank2*^{-/-}. Scale bar: 50 μm.
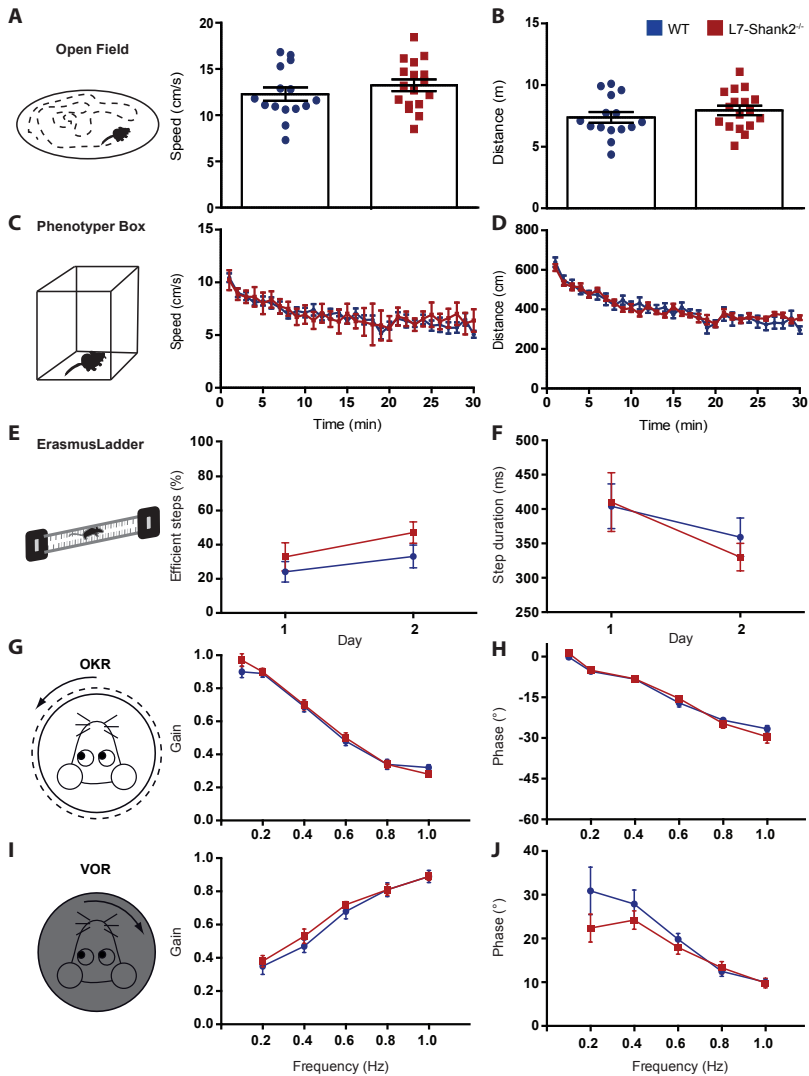
Figure S5 *L7-Shank2*$^{-/-}$ **mice have normal basic motor performance. (A)** In the open field experiment mice were allowed to move around freely. The speed of movement (P=0.3, t-test) and **(B)** distance travelled (P=0.3, t-test) during 10 min was not different (WT, n=15; *L7-Shank2*$^{-/-}$, n=17). **(C, D)** These results were confirmed in the phenotyper box for both speed (P=0.5) and distance (P=0.5) (WT, n=16; *L7-Shank2*$^{-/-}$, n=16). **(E)** ErasmusLadder revealed no difference in the percentage of efficient steps (P=0.3) or **(F)** the duration of these steps (P=0.8) over the course of two days (WT, n=10; *L7-Shank2*$^{-/-}$, n=6). **(G, H)** Optokinetic reflex (OKR) using different frequencies of drum movement revealed no differences in gain (P=0.6) or phase (P=0.9) (WT, n=9; *L7-Shank2*$^{-/-}$, n=9). **(I, J)** Similarly, the vestibulo-ocular reflex (VOR) was not affected in either gain (P=0.4) or phase (P=0.2) (WT, n=8; *L7-Shank2*$^{-/-}$, n=9). Data are represented as mean $\pm$ SEM. Statistical test used was a repeated-measures ANOVA unless stated otherwise.
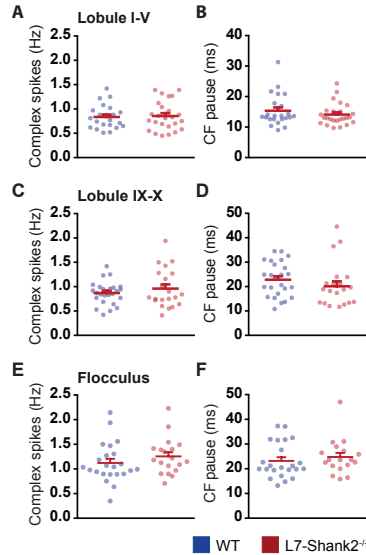
Figure S6 *In vivo* **complex spike firing characteristics in** *L7-Shank2*^{-/-} **Purkinje cells. (A, B)** No significant differences in complex spike firing frequency (P=0.6) or climbing fibre pause (P=0.3) in anterior lobules (I-V) between WTs (n = 23/3, cells/animals) and *L7-Shank2*^{-/-} mice (n = 25/3). **(C, D)** Similarly, in posterior lobules IX-X, complex spike firing frequency (P=0.3) and climbing fibre pause (P=0.3) was not different between WTs (n=25/3) and mutants (n=21/3). **(E, F)** Also located in the posterior cerebellum, Purkinje cells from flocculus showed neither firing rate (P=0.3) nor climbing fibre pause (P=0.5) differences between *L7-Shank2*^{-/-} (n=19/2) and WTs (n=23/2). Error bars denote SEM. Statistical test used was a two-sided t-test unless stated otherwise.
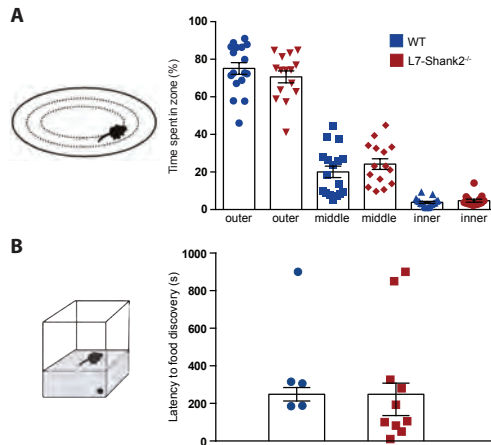
Figure S7 (A) In the open field test, WT (n=17) and *L7-Shank2*^{-/-} mice (n=15) showed no differences (P=0.7, χ^2) in time spent in the inner, middle, or outer zones. **(B)** In the olfaction test, WT (n=5) and *L7-Shank2*^{-/-} mice (n=10) showed no significant differences (P=0.6, t-test) in time taken to find buried food. Error bars denote SEM.

Part II

Cerebellar Nuclei

Chapter 6

Dynamic modulation of activity in cerebellar nuclei neurons during Pavlovian eyeblink conditioning

While research on the cerebellar cortex is crystallizing our understanding of its function in learning behavior, many questions surrounding its downstream targets remain. Here, we evaluate the dynamics of cerebellar interpositus nucleus (IpN) neurons over the course of Pavlovian eyeblink conditioning. A diverse range of learning-induced neuronal responses was observed, including increases and decreases in activity during the generation of conditioned blinks. Trial-by-trial correlational analysis and optogenetic manipulation demonstrate that facilitation in the IpN drives the eyelid movements. Adaptive facilitatory responses are often preceded by acquired transient inhibition of IpN activity that, based on latency and effect, appear to be driven by complex spikes in cerebellar cortical Purkinje cells. Likewise, during reflexive blinks to periocular stimulation, IpN cells show excitation-suppression patterns that suggest a substantial contribution of climbing fibers and their collaterals. These findings highlight the integrative properties of subcortical neurons at the cerebellar output stage mediating conditioned behavior.

M.M. ten Brinke*, S.A. Heiney*, X. Wang*, M. Proietti-Onori, H.J. Boele, J. Bakermans, J.F. Medina, Z. Gao, & C.I. De Zeeuw (Submitted)

Introduction

The cerebellar cortex, like the neocortex, is well suited for establishing new associations required during memory formation. It is becoming increasingly clear that, like cortical and subcortical structures (e.g. Constantinople and Bruno, 2013; Koralek et al., 2012; Igarashi et al., 2014; Douglas et al., 1995; Sherman and Guillery, 2004), the cerebellar cortex and nuclei exhibit complex interplay, for instance through reciprocal nucleo-cortical projections (Gao et al., 2016). Classical Pavlovian eyeblink conditioning has proven an ideal model for studying the neural mechanisms underlying associative learning, and offers a great way to address the question of how the cerebellar nuclei integrate their cerebellar cortical and extra-cerebellar input.

As a simple and quintessential behavioral manifestation of learning and memory, eyeblink conditioning depends on the cerebellar cortex and nuclei (McCormick et al., 1982; McCormick & Thompson, 1984; Yeo, Hardiman & Glickstein, 1985a, b), which are known to facilitate processes that require precise timing (Ivry & Keele, 1989; Breska & Ivry, 2016). In short, animals learn to respond to a neutral conditional stimulus (CS), such as a light, with a well-timed conditioned blink response (CR), when the CS is consistently paired at a fixed temporal interval with an unconditional blink-eliciting stimulus (US), such as a corneal air puff. Lobule HVI of the cerebellar cortex and its downstream target, the interposed nucleus (IpN), are essential for the manifestation of this conditioned eyelid behavior (McCormick et al., 1982; McCormick and Thompson, 1984; Yeo, Hardiman, and Glickstein, 1985a, b; Clark et al., 1992; Krupa and Thompson, 1997; Ohyama et al., 2006; Mostofi et al., 2010; Heiney et al., 2014b). Genetic and pharmaceutical manipulations of cerebellar cortical Purkinje cells indicate that the expression of CRs may require various cell physiological processes, including postsynaptic long-term depression and long-term potentiation at the parallel fiber to Purkinje cell synapse (Ito & Kano, 1982; Koekkoek et al., 2003; Schonewille et al., 2010), inhibition at the molecular layer interneuron to Purkinje cell synapse (Ten Brinke et al., 2015), as well as intrinsic mGluR7-mediated processes in Purkinje cells (Johansson et al., 2015). IpN neurons that can drive eyeblink behavior through the red nucleus and facial nucleus provide a feedback to the cerebellar cortex that amplifies the CR (Gao et al., 2016; Giovannucci et al., 2017). Moreover, IpN neurons receive excitatory inputs from mossy fiber and climbing fiber collaterals, which need to be integrated with the inhibitory inputs from the Purkinje cells and local interneurons and possibly even from recurrent collaterals of the nucleo-olivary neurons (Chan-Palay, 1973, 1977; De Zeeuw et al., 1988, 1997; Van Der Want et al., 1989; Uusisaari, Obata, and Knöpfel, 2007; Uusisaari and Knöpfel, 2008, 2011, 2012; Bagnall et al., 2009; Kodama et al., 2012; Witter et al., 2013; Boele et al., 2013; Najac and Raman, 2015; Canto et al., 2016).

IpN neurons and their inputs are endowed with ample forms of plasticity, all of which may in principle be implicated in eyeblink conditioning (Ohyama et al., 2006; Foscarin et al., 2011; Zheng and Raman, 2010). These include for example short-term and long-term potentiation (LTP) at the mossy fiber to IpN neuron synapse (Person and Raman, 2010), both of which may facilitate the induction of intrinsic plasticity (Aizenman and Linden, 1999 and 2000; Zheng and Raman, 2010), and learning-dependent structural outgrowth of mossy fiber collaterals in the cerebellar

nuclei, which may be directly correlated to the rate and amplitude of CRs (Boele et al., 2013). So far, extracellular recordings of neurons in the cerebellar nuclei have revealed CR-related increases in activity that lead the eyeblink movement (anterior IpN; McCormick and Thompson, 1984; Berthier and Moore, 1990; Gould and Steinmetz, 1996; Choi and Moore, 2003; Halverson et al., 2010; Heiney et al., 2014b), and CR-related increases and decreases in activity that lag the eyeblink movement (posterior IpN; Gruart et al., 2000; Delgado-Garcia & Gruart, 2005; Sanchez-Campusano et al., 2007). However, comprehensive trial-by-trial analysis of different components of IpN modulation in relation to conditioned behavior, as well as evaluation against conditioning-related modulation of activity in the cerebellar cortex and other non-cortical inputs, is lacking.

Here, we recorded conditioning-related activity in an identified blink area of the anterior interpositus nucleus of awake behaving mice, and used in-depth trial-by-trial correlational analysis, optogenetic manipulation and computationally modeled IpN output based on previously reported eyelid-related Purkinje cell modulation (Ten Brinke et al., 2015) to detail and cement the causal role of IpN activity in conditioned behavior. Our results reveal an intricate dynamic modulation of cerebellar nuclei activity during the generation of conditioned movements. We discuss how these findings shed light on a number of electrophysiological properties of the olivocerebellar network as integrated at the IpN in the normal functional context of eyeblink conditioning in awake, behaving mice. Together, our results highlight how neurons in the IpN integrate cortical and non-cortical input to establish a circuitry optimally designed to generate well-timed conditioned motor responses.

Results

Characterization of cerebellar IpN neurons

To explore the characteristics of IpN spike modulation and its relation to conditioned eyelid behavior, we made extracellular recordings across 19 mice that were trained or in training. During recordings, the mice were head-fixed on top of a cylindrical treadmill, fully awake and able to show normal eyelid behavior in response to the experimental stimuli, which included a 260 ms green LED light (CS) that co-terminated with a 10 ms corneal air puff (US), yielding a 250 ms CS-US interval (Fig. 1A).

There were 270 recordings of IpN cells that were located below Purkinje cell layers at depths between 1500-3000 μm (Fig. 1B), were recorded during at least 10 valid CS-US trials, and showed modulation in their firing rate in response to the CS and/or US. Firing frequency was similar along the depth of the IpN (r = 0.085, p = 0.16, n = 270, Pearson), averaging 67 $\pm$ 27 Hz. Within the entire dataset, 60 cells showed at least 5 Hz facilitation in the CS-US interval (22.2%, Fig. 1C, F, I), and 23 cells showed at least 5 Hz suppression (8.5%, Fig. 1D, G, J), leaving 187 cells that did not show any clear spike rate modulation within the CS-US interval (69.3%, Fig. 1E, H, K; see Methods).

In terms of eyelid behavior across the dataset (Fig. 1L), CRs were present in at least 20% of trials in 103 cells (38%); this is the criterion used throughout the paper
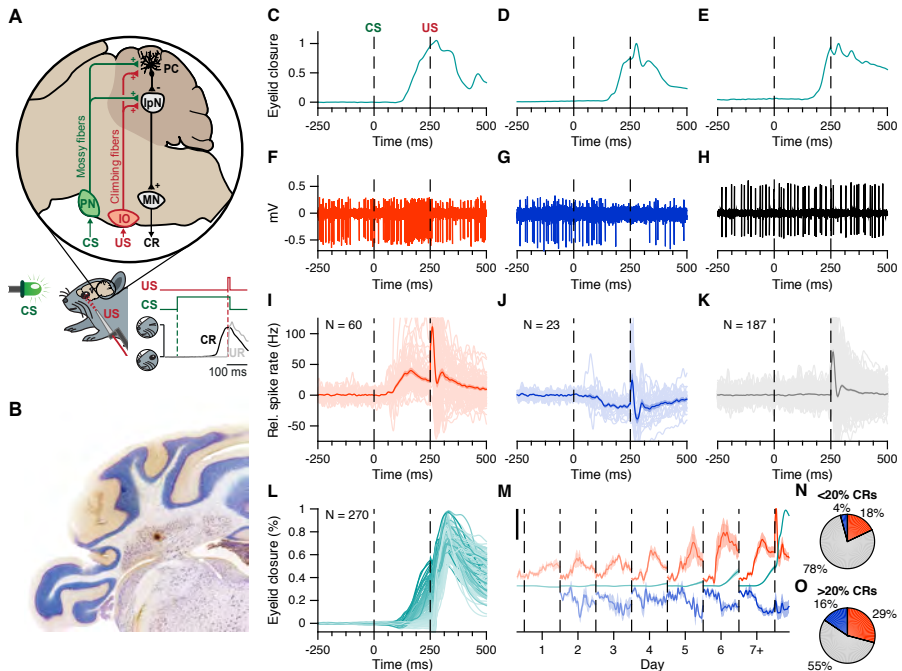
Figure 1 Interpositus nucleus electrophysiology overview. (A) CS and US signals are transmitted through mossy fibers and climbing fibers, respectively, to Purkinje cells in the simplex lobule (HVI) of the cerebellar cortex, and to the IpN, to which cortical Purkinje cells send their inhibitory projection. Combined disinhibition and excitation then lead the IpN to drive CRs. Paired trials consisted of a 260 ms LED light CS, co-terminating with a 10 ms corneal air puff. **(B)** Coronal cerebellar section showing a typical recording site in the IpN. **(C-E)** Example eyelid traces for trials where the recorded cell showed spike facilitation (C), suppression (D), or no modulation (E) in the CS-US interval. F-H Electrophysiological trace showing IpN activity corresponding to the example eyelid traces in C-E. **(I)** Spike trace averages for 60 cells showing at least 5 Hz facilitation in the CS-US interval; grand average is shown with SEM. **(J)** Same as in I, but for 23 suppressive cells. **(K)** Same as in I, but for 187 non-modulating cells. **(L)** Average traces of eyelid behavior for all 270 cells in the original dataset, color coded for average CR amplitude at US onset. **(M)** Daily CS-US interval averages of facilitatory cells (top traces, orange), suppressive cells (bottom traces, blue), and eyelid behavior for all cells showing modulation (middle traces, teal). Black scale bar denotes 25 Hz/% eyelid closure. **(N, O)** Proportion of cells showing facilitation, suppression, or no modulation, across cells with <20% CRs (n = 167), and cells with >20% CRs (n = 103). *IpN: interpositus nucleus; IO: inferior olive; MN: motor nucleus; PC: Purkinje cell; PN: pontine nuclei.*

when referring to recordings with behavior. The magnitude of spike facilitation shows a steady significant increase over the course of conditioning (r = 0.413, p = 0.001, n = 60; Spearman); spike suppression was similarly inclined (r = 0.354, p = 0.0972, n = 23; Spearman; Fig. 1M). Although both types of spike rate modulation manifested before conditioned behavior did (Fig. 1M), they were more prevalent in recordings with conditioned behavior (Fig. 1O) than in those without (Fig. 1N; facilitation: 29.1% (30/103) vs. 18% (30/167), p = 0.0463; suppression: 15.5% (16/103) vs. 4.2% (7/167), p = 0.0025, Chi-square test).

To corroborate the main findings reported below, an additional and independently obtained dataset of 102 IpN recordings was analyzed in the same way as the original

dataset and is presented alongside it (independent dataset collected at Baylor). It is important to note that this second dataset differs in the following respects from the original dataset (original dataset collected at Erasmus): i) rather than over the course of conditioning, these recordings were obtained after thorough training, and only from mice that showed at least 80% CRs; ii) the recordings were all located no more than 300 μm away from IpN sites confirmed to be eyelid-related through micro-stimulation (see Methods, and Heiney et al., 2014b); and iii) the CS was 220 ms, the US was 20 ms, resulting in a CS-US interval of 200 ms. Rather than focusing on the course of training and across-trial variability, these recordings serve to capture cerebellar nuclear dynamics in an optimally conditioned system (for an overview of the two different datasets, see Supp. Fig. 1).

In subsequent analyses, we focus on three relevant time intervals during stimulus presentation: the last 200 ms of the CS-US interval, during which broad Purkinje cell simple spike modulation takes place; 50--130 ms after the CS, during which CS-related climbing fiber activity emerges (Ohmae et al., 2015; Ten Brinke et al., 2015); and the first 60 ms after the US, during which robust climbing fiber signals take place, particularly in error trials when the mouse fails to make a CR.

IpN facilitation but not suppression can drive conditioned eyelid behavior

We first sought to characterize whether facilitation and suppression observed in IpN neurons during the last 200 ms of the CS-US interval correlates with the amplitude of eyelid closure (Fig. 2). Across the original dataset, there were 60 cells showing CS-US facilitation, with durations of 104 ± 41 ms, and magnitudes averaging 22.5 ± 20.2 Hz and correlating to both percentage CRs ($r = 0.534$, $p < 0.0001$, $n = 60$, Spearman) and CR amplitude ($r = 0.52$, $p < 0.0001$, Spearman). Out of 30 facilitation cells recorded in the presence of CRs (Fig. 2A), 17 showed significant positive trial-by-trial correlations between firing rate and CR amplitude (57%; $p = 0.0001$, bootstrap with 500 repetitions; Fig. 2B), whereas none showed negative correlations. A linear mixed model with random intercepts and slopes for these significant cells predicts 0.49% more eyelid closure at US onset per unit increase of spike facilitation in Hz (Fig. 2B, black dotted line; $p < 0.0001$, Supp. Table 1). Exploration of trial-by-trial spike-eyelid correlations across a correlation matrix reveals their temporal distribution, as explained previously (Ten Brinke et al., 2015). Here, correlations within 20 ms windows, taken at 10 ms steps across the trial timespan, show at which spike times and which eyelid times the strongest spike-eyelid correlations exist, both when taking eyelid position (Fig. 2C) and eyelid velocity (Supp. Fig. 2A) as the lead parameter. A cluster of markedly positive correlations can be seen in the upper triangle of the matrix in the second half of the CS-US interval, running parallel to the diagonal. This means the strongest across-trial correlations occurred between spiking and subsequent behavior. Indeed, temporal cross-correlations between average spike and eyelid traces confirm that spike facilitation fits best with subsequent eyelid behavior, averaging 25 ± 25.6 ms ($p = 0.0001$, Wilcoxon signed rank test; Fig. 2D).

The character and predictive power of CS-US facilitation in the IpN is strongly corroborated by the second dataset (Fig. 2E-H), with 70 cells showing facilitation
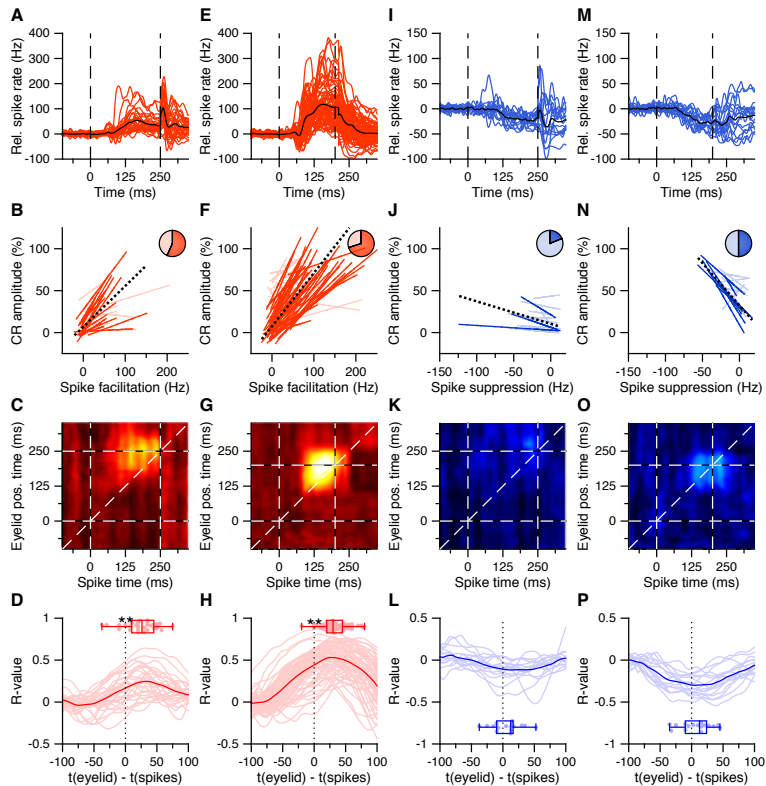
Figure 2 CS-US interval IpN modulation relates to eyelid behavior. (A) Average spike traces of 30 facilitatory neurons recorded with conditioned behavior. Black trace denotes average. Time is shown relative to CS onset. **(B)** Trial-by-trial spike-eyelid correlation lines for the cells in A, with plain red lines showing significant correlations, light red lines showing the non-significant ones, and the pie chart showing their proportionality. **(C)** Average correlation matrix showing the average temporal distribution of the spike-eyelid position correlations of the cells in A. R-values counter to the correlational direction of interest were nullified before averaging. **(D)** Temporal cross-correlations for the cells in A (light red) and their mean (plain red). Box plot shows the time of maximum correlation for all cells. **(E-H)** Same as in A-D, here for 70 facilitation cells with conditioned behavior from the independent second dataset. **(I-L)** Same as in A-D, here for 16 suppression cells recorded with conditioned behavior from the original dataset. **(M-P)** Same as in I-L, here for 16 suppression cells recorded with conditioned behavior from the second dataset.

(59.2 ± 38 Hz) in the presence of conditioned behavior (Fig. 2E), and 49 of these cells showing significant positive correlations (70%). A linear mixed model with random intercepts and slopes predicts 0.64% more eyelid closure at US onset per 1 Hz increase in facilitation (p < 0.0001, Supp. Table 1). The correlation matrices relating spike activity to eyelid position (Fig. 2G) and velocity (Supp. Fig. 2B) show hotspots of strong correlation hovering above the diagonal in the CS-US interval, with temporal cross-correlations again confirming the best fit between spike facilitation and eyelid behavior to be at significantly positive offsets (33.4 ± 19.3 ms, p < 0.0001, Wilcoxon signed rank test; Fig. 2H).

In the original dataset, in comparison with the facilitation group, CS-US suppression was less prevalent among the dataset. Within the 23 cells (8.5%) showing an average drop of at least 5 Hz in the CS-US interval (11.2 ± 6 Hz, duration: 70 ± 44 ms), the magnitude of suppression correlated to both CR percentage ($r = 0.526$, $p = 0.01$, $n = 23$, Spearman) and CR amplitude at US onset ($r = 0.443$, $p = 0.0356$, $n = 23$, Spearman). Additionally, cells with stronger suppression showed higher spike irregularity (i.e., higher CVs: $r = 0.587$, $p = 0.0038$, Spearman). Compared to facilitation, suppression had lower amplitudes (baseline z-score: 5.3 ± 1.5 vs 7.6 ± 4.7, $p = 0.0007$, Mann-Whitney U test, MWU) and lower durations (53 ± 38.4 vs 95.5 ± 36.2 ms, $p = 0.0012$, MWU), but similar onset (132 ± 21.2 vs 136.5 ± 19.9 ms, $p = 0.6$, MWU) and modulation peak times (176 ± 37.2 vs 166 ± 34.2 ms, $p = 0.6$, MWU). Relative spike suppression was further correlated to eyelid closure at US-onset relative to baseline for all recordings of suppressive cells with conditioned behavior ($n = 16$, Fig. 2I). Of these cells, 3 showed significant negative trial-by-trial correlations between firing rate and CR amplitude (19%, $p < 0.0001$, bootstrap with 500 repetitions; Fig. 2J), whereas none showed positive correlations. A linear mixed model with random intercepts and slopes for the three significant cells estimated 0.27% more eyelid closure at US onset per unitary increase of suppression in Hz ($p = 0.0272$, Supp. Table 1). The correlation matrix showed no particular concentration of the spike-eyelid correlations of suppressive cells with conditioned behavior within the CS-US interval (position: Fig. 2K; velocity: Supp. Fig. 2C), and temporal cross-correlation showed a best fit between average spike and eyelid traces at very small temporal offsets that were on average not different from zero (6.4 ± 23 ms, $p = 0.2336$, Wilcoxon signed rank test; Fig. 2L).

In the second dataset, 16 cells showed CS-US spike suppression (12.1 ± 5 Hz) in the presence of conditioned behavior (Fig. 2M), with 8 cells showing significant negative relationship between relative firing rate and CR amplitude at US onset ($p < 0.0001$, bootstrap with 500 repetitions; Fig. 2N), and a linear mixed model estimating 1.01% more eyelid closure per 1 Hz deeper suppression ($p < 0.0001$, Supp. Table 1). Although the second dataset showed stronger facilitation than the original dataset (59.2 ± 38.1 vs 30.1 ± 25.3 Hz, $p = 0.0009$, MWU), arguably due to superior CR performance (mean percentage CRs: $86.2 \pm 17.3\%$; mean CR amplitude: $43.5 \pm 17\%$ eyelid closure), the level of suppression was not different between the two datasets (11.9 ± 5 Hz vs 12.9 ± 6.4 Hz, $p = 0.864$, MWU). Moreover, the correlation matrices for eyelid position (Fig. 2O) and velocity (Supp. Fig. 2D) echo the finding that the time difference between suppressive modulation and eyelid movement is not significantly different from zero on average (6.9 ± 25 ms, $p = 0.2439$, Wilcoxon signed rank test; Fig. 2P). Together, these results, found across two independent datasets, reveal a large portion of IpN cells showing spike facilitation during the CS-US interval that predicts subsequent conditioned eyelid behavior. In contrast, there is a smaller number of suppressive neurons that are unlikely to drive eyelid movements because their activity is less correlated with CR amplitude and often lags the eyelid movement (or leads it by an insufficient amount).
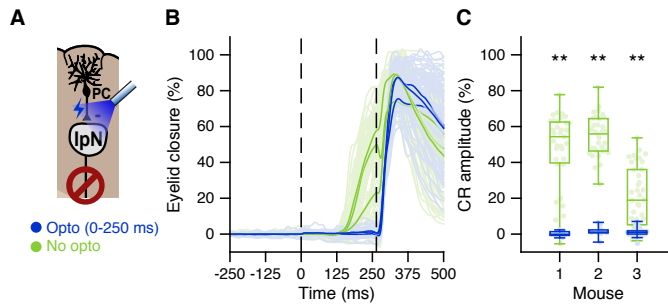
Figure 3 Optogenetic prevention of IpN facilitation eliminates CRs. **(A)** Purkinje cells in the simplex lobule that express ChR2 exert a powerful inhibitory influence on the IpN upon optogenetic stimulation (see Witter et al., 2013; Canto et al., 2016). **(B)** Average eyelid traces for trials with (dark blue) or without (green) optogenetic stimulation throughout the CS-US interval, for three mice. **(C)** Eyelid closure at US onset for the data shown in B, separated by mouse.

Optogenetic inhibition of IpN eliminates CRs

If CS-US facilitation in the IpN indeed controls eyelid closure, one would assume that inhibiting IpN activity during the CS-US interval is sufficient to abolish CRs. Pharmacological interventions suggest this is indeed so, with muscimol and/or lidocaine injections in the anterior IpN eliminating CRs completely (rabbit: Bracha et al., 1994; Ohyama et al., 2006; rat: Freeman et al., 2005; mouse: Heiney et al., 2014b). To further establish the causal role of IpN facilitation in the expression of specifically conditioned eyelid behavior, we employed optogenetic inhibition of the IpN in a set of three fully trained mice. Optic fibers were implanted near the IpN of L7-Ai27 mice in which ChR2 was expressed in all Purkinje cells (see Methods). During optogenetic excitation of Purkinje cell axon terminals, IpN neurons suppress their firing activity (Witter et al., 2013; Canto et al., 2016; Fig. 3A). If excitatory rather than suppressive modulation in the IpN plays a causal role in driving the CRs, CRs should be selectively eliminated by optogenetic stimulation. Indeed, the conditioned behavior acquired by all three mice was readily disabled in virtually all trials randomly chosen to include optogenetic stimulation (all $p < 0.0001$, MWU; Fig. 3B, C). This result expands on the observation that IpN facilitation can elicit eyeblinks (Hesslow, 1994b; Heiney et al., 2014b), by showing that it is decidedly necessary for the expression of conditioned eyelid responses.

CS-related transient spike pauses and subsequent rapid excitation in IpN neurons

Next, we examined whether and how previously reported CS-related complex spikes driven by climbing fibers in Purkinje cells (Ohmae and Medina, 2015; Ten Brinke et al., 2015) may be reflected in IpN activity. Although IpN cells do not show an identifiably distinct spike type upon climbing fiber activation, previous work characterizes a cerebellar nuclear equivalent to synchronous complex spike activity as a transient

suppression in spike rate (e.g. Hoebeek et al., 2010; Bengtsson et al., 2011; Witter et al., 2013; Bengtsson & Jörntell, 2014; Tang et al., 2016). Based on the latency of CS-related complex spikes in eyelid-related Purkinje cells (Fig. 4A, D), we looked at rapid spike deviations exceeding 4.5 baseline SDs between 50--125 ms post-CS in IpN neurons. Seven cells showed a striking transient suppression at 88 ± 12 ms (Fig. 4B, E), which we refer to as a CS pause, with five of them showing a subsequent facilitation in the CS-US interval (71.4%, vs 55/263 (21%), p = 0.0006, Fisher's test).

The presence and character of CS pauses as observed in the original dataset were strongly reflected in the second dataset, which was obtained from fully trained, high-performing mice. Out of 102 cells, 41 showed CS pauses (Fig. 4C, F), and here too cells with a CS pause were more likely to show CS-US facilitation than those without (39/41 (95%) vs 31/61 (51%) cells, p < 0.0001, Fisher's test). Importantly, there was a clear across-cell correlation between average CS pause latency and CR latency, whether looking at both datasets combined (n = 45, r = 0.582, p < 0.0001, Pearson; Fig. 4G), or just the second dataset in isolation (n = 41, r = 0.403, p = 0.0089, Pearson).

Interestingly, there were four cells in the original dataset that showed a transient increase, rather than a decrease, in firing at the same latency as the CS pause (Supp. Fig. 3A, B). Rather than showing subsequent facilitation, two of these cells showed CS-US suppression (50%, vs 21/266 (7.9%) in the other cells, p = 0.0021, Fisher's test). The suppression did not seem more enhanced in these cells compared to other suppression cells (all p > .25; Supp. Fig. 3C, D). Moreover, this transient increase in firing was not observed in any of the cells in the second dataset, which was specifically focused on eyelid-related IpN areas as identified by microstimulation-driven blinks (see Methods).

Across the original dataset, which was obtained over the course of conditioning, none of the 11 cells showing a transient spike response (CS pause or a transient increase in spikes) at the CS-related complex spike latency were recorded before day 4 of training (day 1--3, 0/99 cells; day 4+, 11/171, p = 0.0058, Fisher's test; Fig. 4H), which is consistent with the notion of an acquired CS-related climbing fiber response (Ohmae & Medina, 2015; Ten Brinke et al., 2015).

CS-US facilitation was not only more prevalent in cells with a CS pause compared to those without; between these groups (Fig. 5A, B, F, G), CS pause cells show a markedly more pronounced rapid excitatory spike profile right after the CS pause latency. In the original dataset, they show significantly higher CR-related increases in firing rate during the CS-US interval (41.5 ± 33.1 vs 15.2 ± 8.9 Hz, p = 0.0013, MWU; Fig. 5C), and they also showed distinctly higher maximum spike rate velocities (4.9 ± 1.6 vs 1.4 ± 0.5 Hz/ms, p = 0.0002, MWU; Fig. 5D). While in the second dataset, maximum facilitation was not significantly higher in facilitation cells with a CS pause (65.1 ± 39.5 Hz) compared to those without (51.7 ± 35.4 Hz, p = 0.1594, MWU; Fig. 5H), the former group did show significantly higher maximum spike rate velocities (5.6 ± 2.5 vs 3.6 ± 1.5 Hz/ms, p = 0.0004, MWU; Fig. 5I). Note that CS pause cells tended to be recorded less deeply in the nuclei than non-CS pause cells, both in the original (1840 ± 320 vs 2130 ± 350 μm, p = 0.0298, MWU; Fig. 5E) and in the second dataset (2350 ± 140 vs 2450 ± 211 μm, p = 0.0372, MWU; Fig. 5J), which had different overall recording depths due to a different point of electrode insertion.

To get an idea of the CS-US facilitation in the IpN that could follow from Purkinje cell simple spike suppression, we used simple spike profiles of 26 Purkinje cells
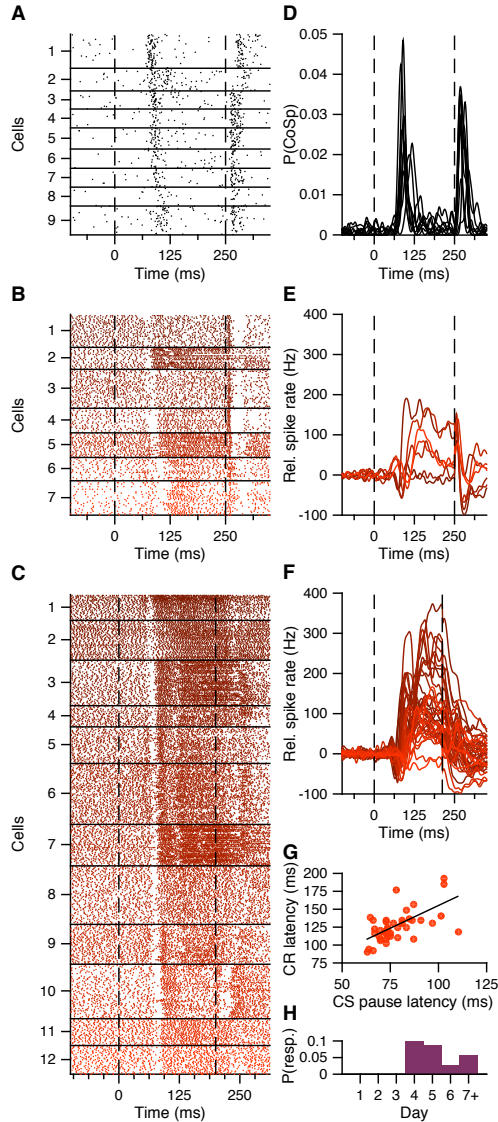
Figure 4 CS pause response reflecting CS-related Purkinje cell complex spike. (A) Combined complex spike raster plot for 9 Purkinje cells ordered by the latency of their clear CS-related complex spike response in addition to the US-related complex spike (data from ten Brinke et al., 2015). **(B)** Combined raster plot for 7 IpN neurons, ordered by the latency of their CS pause in spike activity. **(C)** Same as in B, but for 12 of the 41 IpN neurons in the second dataset that showed a CS pause. **(D-F)** Average spike traces corresponding to the cells shown in A-C, with D showing the probability of a complex spike instead of relative spike rate. **(G)** CS pause latency plotted against the latency at which the CR passes 5% eyelid closure, for all 45 cells showing both properties across the original and the second dataset. **(H)** Probability across days of finding a transient spike response at CS-complex spike latency, inhibitory (this figure) or excitatory (Supp. Fig. 3), in the original dataset.
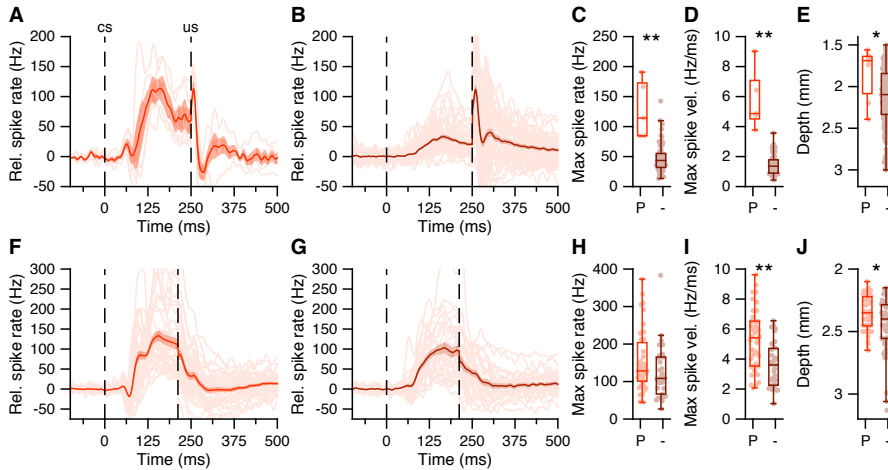
Figure 5 CS-US facilitation in IpN cells with and without CS pause. (A) Average spike traces for 5 IpN cells showing CS-US facilitation and a CS pause. Grand average shown in red, with SEM. **(B)** Same as in A, here showing 55 IpN cells with CS-US facilitation but without a CS pause. **(C)** Maximum spike rate in the CS-US interval for facilitation cells with CS pause (P) and without CS pause (-), for the data in A and B. **(D)** Same as C, here showing maximum spike rate velocity. **(E)** Same as C, here showing recording depth. **(F-J)** Same as in A-E, here showing data from the second dataset; 39 IpN cells showed CS-US facilitation and a CS pause, and 31 cells showed CS-US facilitation but not a CS pause.

reported previously (Ten Brinke et al., 2015), to model spike modulation for as many IpN neurons (Supp. Fig. 4A, B), using model parameters based on Yamazaki and Tanaka (2007) and Person and Raman (2012; Supp. Table 2). The modeled CS-US facilitation resulting from averaging the activity of all Purkinje cells together aligned better with the recorded CS-US facilitation cells without a CS pause than those with CS pause, in the original dataset (Supp. Fig. 4C-H). The model could also reproduce the much stronger and rapid excitatory response in the IpN neurons with a CS pause, but only if these IpN neurons were assumed to receive input from the Purkinje cells whose activity was suppressed the most (Supp. Fig. 4A, B, D, blue trace)

Together, these findings establish a clear reflection in the IpN of the CS-related climbing fiber response as a transient spike suppression and support its selective and acquired nature. Moreover, the link between CS pauses and the subsequent high and/or fast facilitation rates in IpN neurons across the datasets is suggestive of a potential functional role of CS-related climbing fiber activity in triggering strong excitation in the IpN, a possibility that is further explored below.

IpN responses to the US

Central to the eyeblink conditioning paradigm is the notion that the US activates climbing fibers and evokes complex spikes in eyelid-related Purkinje cells, but only if the mouse fails to make a conditioned response. Before turning to the resultant complex spike-driven transient spike suppression that is to be expected in the IpN,

we first focus on a marked increase in spikes (99 $\pm$ 59 Hz) that occurred almost immediately after US onset, at a latency of 10.6 $\pm$ 4.7 ms, and exceeded 5 baseline SDs in 211 cells (78.2%, Fig. 6A, B, see Methods). This response, here referred to as a US peak, had two important features: First, US peak amplitude, measured from baseline, diminished over the course of training, as apparent from a comparison of recordings made in the first four training days and those made subsequently (88 $\pm$ 48 vs. 29 $\pm$ 44 Hz, p < 0.0001, MWU; Fig 6C). Second, US peak amplitude correlated negatively with conditioned behavior, in terms of both CR percentage (r = -0.426, p <0.0001, n = 270, Spearman) and CR amplitude at US onset (r = -0.333, p < 0.0001, n = 270, Spearman), confirming its reduction as conditioned behavior is acquired (and also note that within the second dataset, which only contained data from well-trained mice, only 9% of cells showed a US peak, averaging only 28.1 $\pm$ 12.9 Hz). Furthermore, among 62 recordings with a US peak and CR behavior, trial-by-trial correlations reveal 13 cells in which US peak amplitude correlated negatively to CR amplitude (p < 0.0001, bootstrap with 500 repetitions; Fig. 6D). These significant recordings were twice as likely as the other 49 cells to also show significant positive correlations between CR amplitude and CS-US facilitation (69.2% (9/13) versus 36.7% (18/49), p = 0.0077, Fisher test), which itself was three times as likely to occur in cells with US peak compared to those without (26.1% (55/211) vs. 5/59, 8.5% (5/59), p = 0.007, Fisher test). Together, these results establish a substantial prevalence of US peak responses in the IpN, demonstrate their co-occurrence with conditioning-related facilitation and spike-eyelid correlations in the CS-US interval, and show cell- and trial-wide conditioning-related dynamics that are similar to those of US-related climbing fiber responses.

Interestingly, there was an additional, more counterintuitive, similarity that was observed between the US peak and US-related climbing fiber responses. Occasionally, mice tended to open their eye somewhat relative to baseline in response to the CS. Among 149 of the recordings with a US peak but without CR behavior, 17 showed positive across-trial correlations between eyelid amplitude and the US peak response (11.4%, p < 0.0001, bootstrap with 500 repetitions; Supp. Fig. 5A), i.e. more eyelid opening related to weaker US peaks. We analyzed the Purkinje cell data from Ten Brinke et al. (2015) to see if eyelid opening responses were related to US-complex spikes. Indeed, across trials where mice opened their eye further in the CS-US interval, those without a US-related complex spike showed slightly more eyelid opening (-2.65 $\pm$ 1.85 %) than those with a US-complex spike (-0.84 $\pm$ 1.86 %, p = 0.0254, MWU; Supp. Fig. 5B, C). Thus, this additional property seems to link the US peak to US-related climbing fiber activity.

In addition to US peak responses, transient suppressive responses were also observed at 28.2 $\pm$ 4.9 ms post-US in 105 IpN cells (39%), with mean magnitudes of -50 $\pm$ 24 Hz (Fig. 6F). The latency of this response, referred to as the US pause, fits with the idea of climbing fiber input inhibiting the cerebellar nuclei indirectly via Purkinje cell complex spikes (e.g. Hoebeek et al., 2010; Lu et al., 2016). Consistent with this notion, 6 out of 7 cells that showed a CS pause also showed a US pause (86%, vs. 105/263 (40%), p = 0.0012, Fisher's exact test). We found considerable overlap in the prevalence of US peaks and pauses: a third of cells showing the one response also shows the other (77 out of 239, 32.2%; Fig. 6B). Additionally, cells with only a US pause tended to be more dorsally located (1939 $\pm$ 299 μm) than cells with only a US peak (2182 $\pm$ 373 μm), and cells that showed both responses averaged an
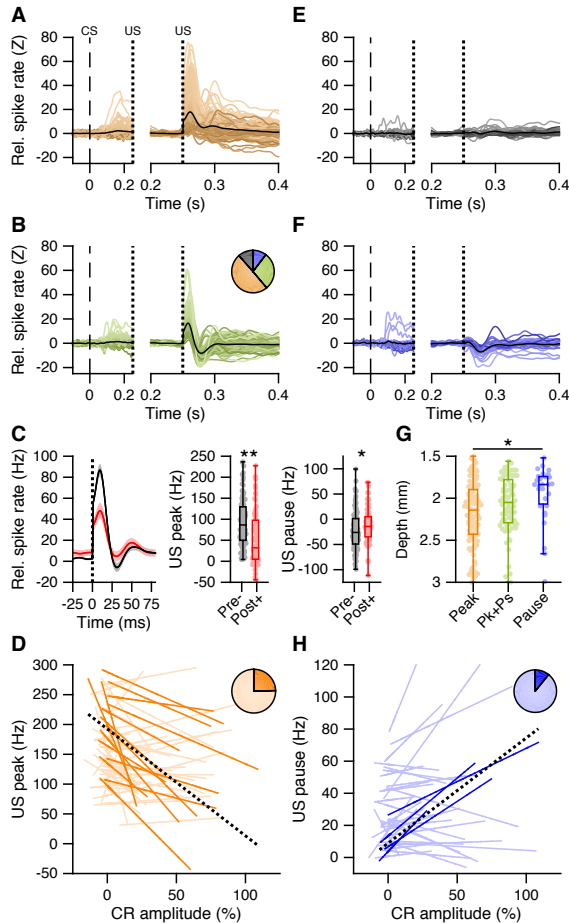
Figure 6 US peak and pause responses. (A) Average spike traces for cells showing a US peak but not a US pause response (n = 134); left panel shows activity in the CS-US interval aligned to baseline, right panel shows post-US activity aligned to the last 50 ms of the CS-US interval. **(B)** Same as in A, but for cells showing both a US peak and a US pause (n = 77). The pie chart shows the proportion of cells with a US peak (yellow), a US pause (blue), both (green), or neither (gray). **(C)** Left panel: average traces with SEM of spike activity relative to baseline for all cells recorded without conditioned behavior on days 1-4 (black), and all cells recorded after day 4 and with conditioned behavior (red). Middle panel: US peak amplitude relative to baseline was significantly higher in early recordings without conditioned behavior (pre-) than in later recordings with behavior (post+; p < 0.0001). Right panel: same as the middle panel, here showing minimum firing rate in the US pause window relative to the last 50 ms in the CS-US interval; early recordings without CR behavior show lower values than later recordings with behavior (p = 0.0312). **(D)** Significant (plain orange) and non-significant (light orange) trial-by-trial correlation lines for all cells showing conditioned behavior and a US peak (n = 62). Black dotted line shows a fit from a linear mixed model incorporating the significant cells. The pie chart inset shows the proportion of cells that were significant. **(E)** Same as in A, but for cells without a clear post-US response (n = 31). **(F)** Same as in A, but for cells with only a US pause response (n = 28). **(G)** Recording depth was different between cells separated on US responses, getting progressively less deep from cells with only a US peak (yellow, 2182 ± 373 μm), through cells showing both US peak and pause (green, 2075 ± 322 μm), to cells showing only a US pause (blue, 1939 ± 299 μm; p = 0.0025). **(H)** Similar to D, but for all cells showing conditioned behavior and a US pause (n = 37). Note that the y-axis shows the firing rate during the US pause period, with higher values implying less pronounced pauses.

intermediate depth (2075 $\pm$ 322 μm; p = 0.0025, Kruskal-Wallis; Fig. 6G). In terms of conditioning-related dynamics, the US pause shows characteristics that are similar to those of US peaks. Across the first four training days, 47.1% of cells (66/140) showed a US pause, compared to 30% (39/130) on subsequent training days in the original dataset (p = 0.0057, Chi-square test). Moreover, further into training (day 5+), the US pause showed lower magnitudes than those observed on earlier days (-13 $\pm$ 30.3 vs -28.8 $\pm$ 30.4 Hz, resp., p = 0.0018, MWU). Furthermore, on a trial-by-trial basis, 4 out of 41 recordings with a US pause and at least 20% CRs showed deeper pauses in trials with worse behavior (p = 0.0017, bootstrap with 500 repetitions; Fig. 6H). Note that, as with the US peak, US pauses were observed less frequently in the second dataset (23.5%). These findings establish a transient post-US suppressive response that is observed most reliably in conditions associated with climbing fiber-driven complex spikes in Purkinje cells.

US pauses are followed by fast excitatory responses in IpN neurons after conditioning

In addition to the US peak and pause responses, 83 IpN cells in the original dataset showed a rapid excitatory response that peaked at 46 $\pm$ 7 ms and showed magnitudes of 61.4 $\pm$ 28.3 Hz (39.4%; Fig. 7A, arrow), which we refer to as the second US peak. While the amplitudes of the first and second US peaks were correlated trial-by-trial in IpN neurons (Fig. 7D), their relation to the behavioral paradigm was different. Like the first US peak, the second peak was more prevalent in recordings with poor conditioned behavior (26 $\pm$ 32 Hz, vs 13 $\pm$ 26 Hz, p = 0.025, MWU; Fig. 7E), but it did not show a steady decline over the course of training days (r = 0.102, p = 0.13, n = 224, Spearman). To the contrary, across recordings in which CR performance was poor, the second US peak actually grew stronger over the course of conditioning days (r = 0.287, p = 0.0007, n = 138, Spearman), with maximum peak amplitudes 30-60 ms post-US of 16 $\pm$ 28.3 Hz on training days 1-4 (n = 121), and 46.5 $\pm$ 33 Hz on later training days (n = 46, p = 0.0001, MWU; Fig. 7B). Similarly, spike rate velocity was lower during the second US peak on earlier training days compared to later ones (0.55 $\pm$ 0.32 vs 0.77 $\pm$ 0.45 Hz/ms, p = 0.0072, MWU; Fig. 7C).

Consistent with the observation that US-related responses in IpN neurons tend to occur during recordings in which CR performance is poor (Fig. 6; Fig. 7E), we found that in the second dataset (in which CR performance was very high) only 9 cells (8.8%) showed a first US peak response, only 24 (23.5%) showed a US pause, and only 11 (10.8%) showed a second US peak (CR amplitude: 31.3 $\pm$ 15.9 vs 44.9 $\pm$ 16.6 % eyelid closure, p = 0.021, MWU; Fig. 7E). To examine US responses of IpN neurons in the second dataset, we interspersed US-only trials (n = 13 $\pm$ 2) during recordings of 25 cells (24.5%), of which 13 showed CS-US facilitation (Supp. Fig. 6A, B). Indeed, both the first US peak (10/25 cells, 40%) and US pause (10/25, 40%) showed a higher prevalence in US-only trials than in paired trials, but the second US peak was the most substantial, occurring in 18 cells (72%), and trumping the first US peak in terms of amplitude (94.6 $\pm$ 82.9 vs 27.8 $\pm$ 48.7 Hz, p = 0.0012, MWU). Interestingly, it was especially pronounced in US-only trials in the 12 recordings that showed clear CS pauses and CS-US facilitation in paired trials (Supp. Fig. 6A-C).
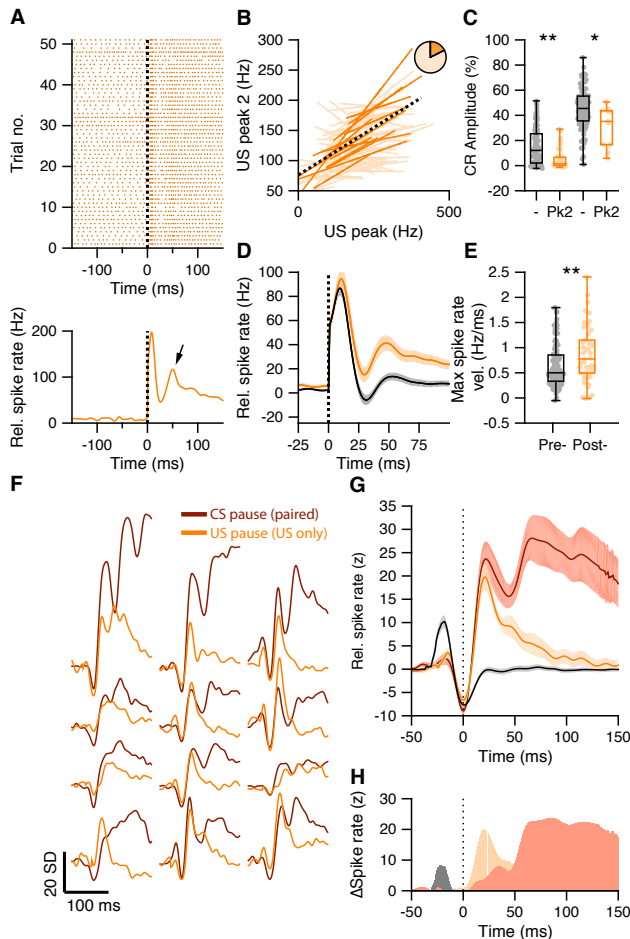
Figure 7 Second US peak response akin to rapid post-CS pause excitation. (A) Raster plot (upper panel) and average spike trace (lower panel) of an example IpN cell showing a second US peak (arrow). **(B)** Significant (plain orange) and non-significant (light orange) trial-by-trial correlation lines for cells showing both a first and a second US peak (n = 83). Pie chart shows the proportion of significant cells, black dotted line shows fit from a linear mixed model, integrating significant cells. **(C)** IpNs with a second US peak (Pk2) show lower average CR amplitudes at US onset than IpNs without (-), in both the original dataset (left boxplot pair; p < 0.0001), as well as in the second dataset (right boxplot pair; p = 0.021). **(D)** Average traces with SEM of spike activity relative to baseline for IpNs recorded without conditioned behavior on days 1-4 (black), and those recorded without conditioned behavior after day 4 (yellow). **(E)** Maximum spike rate velocity of the second US peak was significantly higher in recordings without CR behavior on day 5 and over (post-) compared to earlier recordings without behavior (pre-; p = 0.0072). **(F)** Average sike traces of paired trials, aligned by CS pause minima (brown), and of US-only trials from the corresponding IpN cell, aligned by US pause (yellow) minima, for 12 recordings from the second dataset. The traces were standardized by the activity -150 to -50 ms relative to the pause minima. **(G)** Averages of the CS pause (brown) and US pause (yellow) traces in F, with SEM. For reference, US pause-aligned traces from paired trials of IpNs from the original dataset, with US pauses, without CR behavior, and from day 1-4, are shown in black. **(H)** The difference between US-responses in US-only trials after training (yellow) and US-responses in paired trials early in training before CR behavior is acquired (gray) highlight the absence of the first US peak and the substantial presence of a second peak after the US pause, in well-trained animals. Additionally, the difference between the CS pause-aligned traces from paired trials (brown) and the US-pause aligned traces from US-only trials of the same IpN set (yellow) suggests the two profiles only start to diverge substantially approx. 50 ms after the pause response.

In fact, there is a remarkable similarity between the pause and subsequent rapid excitation observed after the US in US-only trials, and the pause and subsequent rapid excitation observed after the CS in paired trials (Fig. 7F, G), hinting at the possibility of a similar underlying mechanism.

Discussion

By quantifying neuronal responses in the cerebellar interpositus nucleus (IpN) during and after Pavlovian eyeblink conditioning, the present study sheds light on the question of how cerebellar cortical and extra-cortical afferents are integrated at the level of the cerebellar nuclei. Trial-by-trial correlations and their temporal distribution across the trial timespan, as well as optogenetic abolition of CRs, evince and characterize the causal relation between IpN facilitation and conditioned eyelid-behavior. Our findings, consistent across two independent datasets collected in two different laboratories, together characterize cerebellar cortico-nuclear integration as a multi-faceted process involving the impact of common afferents. The data suggest that the dynamic modulation of activity in the IpN during the generation of conditioned eyelid movements can be effected through a learned Purkinje cell simple spike suppression on the one hand, and through climbing fiber mediated Purkinje cell complex spike activity, possibly in tandem with activation of mossy fiber and climbing fiber collaterals, on the other (Fig. 8).

Facilitation drives the learned response

About one third of the US-responding cells recorded across the IpN over the course of conditioning showed a significant change in spiking activity within the CS-US interval, with a facilitation to suppression ratio of 2.6 (60:23). In the second dataset, recording from optimally conditioned mice in eyelid-controlling IpN regions, 85% showed CS-US spike modulation, with a facilitation to suppression ratio of 4.1 (70:17). Although facilitation also shows a clear predominance over suppression in previous work (McCormick, 1982, Berthier & Moore, 1990; Gould & Steinmetz, 1996; Freeman & Nicholson, 2000; Gruart et al., 2000; Choi & Moore, 2003; Green & Arenos, 2007; Halverson et al., 2010), its profile and relation to eyelid behavior has been characterized as lagging (posterior IpN, Gruart et al., 2000; Delgado-Garcia & Gruart, 2005) or leading (anterior IpN, Berthier & Moore, 1990; Choi & Moore, 2003; Halverson et al., 2010; Heiney et al., 2014b), and its role has been hypothesized to be only a facilitator, rather than a main driver, of CRs (Delgado-Garcia & Gruart, 2005). In all, the comprehensive trial-by-trial correlational analysis reported here confirms the leading nature of facilitation in IpN cells, in terms of the temporal profiles of modulation as well as the temporal distribution of spike-eyelid correlations. Moreover, optogenetic stimulation of Purkinje cells, which was shown to suppress the activity of cerebellar nuclei neurons (Witter et al., 2013; Canto et al., 2016), effectively abolished CRs. One potential complication would be the obstruction of CRs by the elicitation of twitches, but the inhibitory effect in the IpN that results from our protocol would only have been able to induce twitches at its offset (Witter et al., 2013), which fell
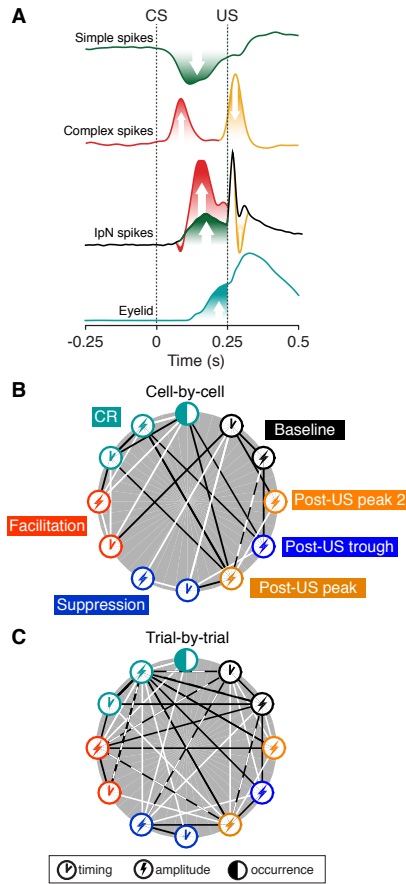
Figure 8 Eyelid-related modulation in cerebellar cortex and nuclei. (A) Mean spike traces for simple and complex spikes in Purkinje cells and IpN spike show how eyelid-related cerebellar cortical and nuclear modulation relate after training. On the one hand, simple spike suppression translates relatively straightforwardly to facilitation in the IpN. Stimulus-related complex spike input leaves a transient spike trough, with the well-timed CS-related complex spike input showing a tendency to be followed by strong rebound-like excitation. Extra-cortical afferents underlie the oft observed transient post-US excitatory response, and presumably interact with the other modulatory components. The timing component in the baseline represents the coefficient of variation (CV). **(B)** Cell-by-cell correlations between occurrence, amplitude, and timing of the different eyelid behavior and IpN spiking components. Black lines indicate negative correlations, white lines indicate positive ones. **(C)** Trial-by-trial correlations between the components also labeled in B, with lines indicating the presence of a significant number of cells showing significant correlations of the corresponding direction. For each parameter pair, recordings were included only if they were considered to show the associated phenomena. Dashed white and black lines indicate that both positive and negative correlations were significantly present among cells.

outside the CS-US interval. The opposite potential complication would be a sudden drop in muscle tone and a resulting immobility. However, this should have been reflected in reduced natural fluctuations of eyelid behavior compared to baseline, for which there was no indication in our data. Thus, while it was shown previously that

activation of IpN via optogenetic suppression of Purkinje cells is sufficient to elicit eyelid behavior (Heiney et al., 2014a), we here expand on pharmacological evidence for the necessity of facilitation in the IpN for the expression of conditioned eyelid behavior (Freeman et al., 2005; Ohyama et al., 2006; Bracha et al., 1994; Heiney et al., 2014b), by optogenetically inactivating IpN cells only during the CS-US interval, through inhibitory Purkinje cell input.

IpN neurons showing CR-related suppression of activity have previously been reported in Berthier and Moore (1990) and Gruart et al. (2000), and were hypothesized to facilitate conditioned behavior through inactivation of antagonistic muscles (Gruart et al., 2000). However, whereas the facilitation IpN cells that we recorded showed predictive trial-by-trial correlations to conditioned eyelid responses, to the modest extent that the suppressive IpN neurons showed correlations, they did only to simultaneous or past, but not future, behavior, across both datasets. While the overall minor presence of suppression in IpN neurons, and their modest, reflective correlations may be indicative of a minimal role in driving behavior, hinting perhaps at sensory feedback, the relaxation of antagonistic muscles is a secondary, passive means of facilitating CRs; its benefit would in part comprise a reduced energy cost to effect behavior, and may therefore escape proper detection in a correlational analysis focusing only on eyelid kinematics. Alternatively, although due to their small size and our electrodes being more likely to record the large projection neurons, the suppression cells might also represent inhibitory interneurons of the nuclei that in fact could serve to further shape the activity of the facilitation cells, smoothing the CR.

Stereotyped pause-excitation responses in the IpN

Many IpN neurons responded during the conditioned eyelid movement with a characteristic transient pause followed by a period of increased activity. The transient IpN spike pauses observed across datasets strikingly mirror the CS- and US-related complex spike responses found in eyelid-related Purkinje cells (Ohmae & Medina, 2015; Ten Brinke et al., 2015 and Fig. 4). The translation from complex spike input to a pause response in the IpN is supported by the findings that climbing fiber activation can trigger a prominent inhibition in the cerebellar nuclei (Hoebeek et al., 2010; Bengtsson et al., 2011; Lu et al., 2016; Tang et al., 2016) and that the strength of this inhibition can be related to the synchrony of the complex spikes (Tang et al., 2016).

The excitatory response of IpN neurons is normally attributed to learning-related suppression of Purkinje cell activity, plasticity of the excitatory mossy fiber to IpN connection, or a combination of the two (Medina et al., 2000; Ohyama et al., 2006; Longley & Yeo, 2014; Freeman, 2015). To these potential mechanisms, our results add one more: In the original dataset, the fastest and strongest cases of excitatory modulation in the IpN neurons occurred right after the CS-related spike pause (Fig. 4). Moreover, in the second dataset, a similar pattern of pause followed by strong excitation was observed in US-alone trials, which are known to trigger climbing fiber-driven complex spikes in Purkinje cells (Hesslow, 1994; Mostofi et al., 2010). This characteristic profile fits well with the notion of rebound depolarization in the cerebellar nuclei (Hoebeek et al., 2010; Bengtsson et al., 2011). This phenomenon is well established in vitro (Jahnsen, 1986; Llinás & Muhletahler, 1988; Aizenman

& Linden, 1999; Tadayonnejad et al., 2009), and can be elicited through electrical (cerebellar nuclei and inferior olive, Hoebeek et al., 2010; inferior olive and skin, Bengtsson et al., 2011) and optogenetic (inferior olive, Lu et al., 2016; cerebellar nuclei, Witter et al., 2013) stimulation. In particular, rebound-driven behavioral responses can be elicited by synchronized nuclear inhibition lasting as little as 25 ms (Witter et al., 2013). Bengtsson et al. (2011) and Hoebeek et al. (2010) report that particularly synchronized complex spike input seems fit to induce substantial rebound excitation in the cerebellar nuclei. Nevertheless, there are also stimulation studies showing less convincing rebound (Chaumont et al., 2013), and its spontaneous occurrence in vitro or in vivo seems negligible (Alviña et al., 2008, Reato et al., 2015). Given the dependence of several models of cerebellar learning on the ability of the cerebellar nuclei to use rebound depolarization to trigger mechanisms of plasticity (e.g., Kistler & van Hemmen, 1999; Steuber et al., 2007; Wetmore et al., 2008, De Zeeuw et al., 2011), the data here presented are particularly relevant in that they offer some evidence for an affirmative answer to the open question of whether rebound may occur during learning (Reato et al., 2015).

IpN neurons respond widely to unconditioned stimuli

We observed that many IpN neurons responded strongly to presentation of the US. The rapid post-US excitatory response had an average latency of 10.6 ms (25th-75th percentile: 7-12 ms), which allows for both mossy fiber and climbing fiber collateral activation as possible pathways for driving the response (Berthier & Moore, 1990; Cody & Richardson, 1979; Mostofi et al., 2010). Mostofi et al. (2010) point at latencies < 6 ms for mossy fiber activation as recorded in the cerebellar cortex in awake rabbits in response to periocular electrical stimulation, and latencies > 9 ms for climbing fiber responses, which is in line with work in cats by Cody & Richardson (1979).

The fact that we used air puff instead of electrical stimulation, which introduces a delay, and that our subjects were mice, which may introduce a small reduction in transmission time, confound proper appraisal of the pathway underlying the US peak based on its latency. Nevertheless, several properties of the US peak provide some clues as to its origin. On the one hand, one could argue that the robust and ubiquitous manifestation of the US peak across the IpN suggests mossy fiber collaterals are a more likely source than climbing fiber collaterals. IpN cells that showed eyelid-related facilitation constitute a selective subgroup of cells in the IpN, and neurons showing US pauses were more commonly observed in less deeply located IpN neurons, which agrees with the notion that the anterior IpN is the main target region for eyelid-related Purkinje cell output (Yeo et al., 1985a; Steinmetz et al., 1992; Bracha et al., 1994; Krupa & Thompson, 1997; De Zeeuw & Yeo, 2005; Freeman et al., 2005; Heiney et al., 2014b). If climbing fiber collaterals would be distributed as widely throughout the IpN as the US peak was observed to be, this would almost certainly mean they are not constrained within eyelid-related olivocerebellar modules. Therefore, mossy fiber input, which is not assumed to adhere to such a modular organization and forms a more robust input to the cerebellar nuclei (e.g. Person & Raman, 2010), may more appropriately fit the observed manifestation of the US peak. Moreover, the reduction of US peak responses over the course of conditioning may well reflect the reduced impact of the

air puff US due to protection of the eyelid, and a resultant reduced mossy fiber signal. On the other hand, there is research to suggest that climbing fiber collateral input may be more robust (Van der Want et al., 1989; Hesslow, 1994; De Zeeuw & Yeo, 2005) than the notion of ''sparse collaterals'' suggests (Chan-Palay, 1977). Moreover, stimulation of the inferior olive results in a consistent excitatory response in the cerebellar nuclei (Kitai et al., 1977; Hoebeek et al., 2010), and spontaneous complex spikes elicit a co-occurrence of excitatory and inhibitory responses in the nuclei 24% of the time (Blenkinsop & Lang, 2011), which is not very different from the percentage we observed (32%). The cell- and trial-wide correlations suggesting weaker US-peaks with better CRs may also be explained in terms of a changing level of nucleo-olivary inhibition (Medina et al., 2002), which would agree with a contribution of the climbing fiber collaterals (De Zeeuw et al., 1997). Moreover, the interesting occurrence of weaker US peaks in trials where mice opened their eyes further than baseline, agrees with Purkinje cell US-complex spike data from Ten Brinke et al. (2015), underlining another similarity between the US peak and climbing fiber activity. Thus, while these arguments suggest it is likely that climbing fibers contribute to the US peak response, its broad prevalence across the IpN suggests mossy fibers are also involved.

The question remains as to why the US-related responses were substantially more widespread than the CS-related responses. Considering the strong convergence of Purkinje cells onto IpN neurons (approx. 40:1) (Person & Raman, 2012), only a relatively small portion of the IpN neurons might evoke functional behavioral responses. As the large pool of remaining IpN neurons may show US-responses that relay general sensory information of the face, including that of the areas surrounding the eyelid region (Koekkoek et al., 2002), or feed into cognitive processes (Wagner et al., 2017, Sokolov et al., 2017), there may also be a substantial amount of redundant, yet detectable, spike responses. This would be consistent with recent findings that dense population coding during eyeblink conditioning also occurs at the cerebellar input stage, i.e. in the granule cell layer (D'Angelo et al., 2009; Giovannucci et al., 2017), which may partly result from nucleocortical feedback originating in the IpN (Houck & Person, 2015; Gao et al., 2016).

Conclusions

In the present study, we have detailed the learning-related dynamic modulation of cerebellar IpN cells and evaluated it against the previously observed modulation of Purkinje cells of the cerebellar cortex by which they are inhibited during Pavlovian eyeblink conditioning. Through the use of detailed trial-by-trial correlations with conditioned eyelid behavior as well as computational modeling and optogenetic confirmation we established the necessity of facilitation of IpN cells for the production of conditioned responses. Moreover, we have uncovered a well-timed imprint of presumptive complex spike activity in the IpN and a subsequent strong excitation. Thus, possibly in interaction with direct input to the IpN, climbing fiber input to the cerebellar cortex could provide an additional mechanism through which spike modulation may be elicited in the IpN to fine-tune the timing of CRs (De Zeeuw & Ten Brinke, 2015). These results underline the relevance of olivary climbing fibers beyond their conventional role of providing teaching signals, highlighting a unique

attribute of the olivocerebellar system relative to other networks, which generally segregate the signals that are used for inducing plasticity during learning from signals that are used for performance during memory recall.

Methods

Surgery

Subjects were 12-20-week-old wild-type C57Bl/6 mice (n = 25), housed individually with food and water ad libitum in a normal (n = 22, original dataset) or reversed (n = 6, second dataset) 12:12 light/dark cycle. For the optogenetics experiment, we used L7cre-Ai27 mice (n = 3) that express channelrhodopsin-2 in Purkinje cells. The experiments were approved by the institutional animal welfare committee (Erasmus MC, Rotterdam, The Netherlands). Mice were anesthetized with an isoflurane + oxygen mixture (5% for induction, 2% for maintenance) and body temperature was kept constant at $37°$C. After fixation in a standard mouse stereotaxic alignment system (Stoelting Co., Wood Dale IL, USA), the scalp was opened to expose the skull. Membranous tissue was cleared, and the bone was surgically prepared with Optibond prime and adhesive (Kerr, Bioggio, Switzerland). A small brass pedestal was attached to the skull with Charisma (Heraeus Kulzer, Armonk NY, USA), using an xyz-manipulator, allowing for fixation to a head bar at right angles during training and electrophysiology. For the craniotomy performed after training, skin and muscle tissue was cleared from the left half of the occipital bone, where, after applying a local analgesic (bupivacainehydrochloride 2.5 mg ml-1), a roughly 1 mm wide craniotomy was performed, 1.5 mm from midline. A small rim of Charisma was made around the craniotomy and anti-inflammatory (Dexamethasone 4 mg ml-1) solution was applied inside, after which the chamber was closed with a very low viscosity silicone elastomer sealant (Kwik-cast, World Precision Instruments, Sarasota FL, USA).

Eyeblink conditioning

Two days after surgery, mice were head-fixed to a brass bar suspended over a cylindrical treadmill (Chettih et al., 2011) and placed in the electrophysiology set-up, contained in a light-isolated Faraday cage. A first habituation session consisted of 30-45 minutes during which no stimuli were presented. During a second and third habituation session on consecutive days 10 CS-only trials were presented to allow the mice to get used to the green LED light and to acquire a baseline measurement. Eight mice were subjected to a training paradigm for five days, before the electrophysiology phase, receiving 200 paired trials daily, with an inter-trial interval of 10 ± 2 s, amounting to approximately half an hour per session. In the remaining 11 mice, electrophysiology was performed from the start of training onwards, restricting the amount of paired trials to 250 per day to ensure comparability between mice across days.

The CS was a 260 ms green LED light, placed 7 cm in front of the mouse. The US was a 10 ms corneal air-puff at 40 psi delivered through a 27.5-gauge needle tip

positioned 5-10 mm from the left eye, co-terminating with the CS, which amounts to a CS-US interval of 250 ms. National Instruments NI-PXI (National Instruments, Austin TX, USA) processors and a low-noise Axon CNS Digidata 1440a acquisition system (AutoMate Scientific Inc., Berkely CA, USA) were used to trigger and keep track of stimuli whilst capturing data. Eyelid movements were recorded with a 250-fps camera (scA640-120gm, Basler, Ahrensburg, Germany).

For each recording, eyelid traces were normalized to the full blink range, which consisted of the minimal resting baseline value reflecting the open eye position as established visually during the experiment, and the mean of the UR peak values reflecting the closed eye position. The traces were smoothed using a 2nd degree Savitzky-Golay method with a span of 10 ms. An iterative Grubbs'outlier detection test ($\alpha = 0.05$) on trial baseline standard deviations was used to remove trials that had an unstable baseline. Additionally, trials were removed if the eye was not at least halfway open. Next, CR amplitude was quantified as the maximum eyelid position within the CS-US interval relative to the trial baseline position, expressed as percentage of full blink range. Trials were considered to contain a CR when eyelid closure exceeded 5% from the baseline mean within the CS-US interval. CR onset was determined as the first time point of a continuous positive eyelid velocity leading to up to the fifth percentile of the amplitude from baseline to CR peak.

Electrophysiology

Neurons were recorded with glass capillaries (ø = 2 mm, Harvard Apparatus, Holliston MA, USA) that were heated and pulled to obtain a 2-5 μm tip, and filled with a 2M NaCl solution. The electrode was stereotactically lowered into the IpN using an electrode holder that was positioned at a 40ř angle in the caudal direction on the sagittal plane and controlled by a manipulator system (Luigs and Neumann SM7, Germany). The obtained electrical signal was pre-amplified with a computer-controlled microelectrode amplifier (Axon CNS, MultiClamp 700B, AutoMate Scientific, Inc. US) and digitized at 20 kHz using the Axon Digidata acquisition system. The IpN contains a high density of neurons that are deeper than and well separated from cortical layers, and almost always show clear, single unit spike activity. Upon encountering cells with responses to the CS and/or US, and verifying a stable recording, animals were subjected to blocks of paired trials. The trial-by-trial spike-eyelid correlations in Ten Brinke et al. (2015) showed significant r values ranging from 0.34 to 0.73, effect sizes that require 12-65 trials to be detected with the ideal statistical power of 80%. Since the same correlations for IpN neurons may be higher since their activity is located more closely to eyelid behavior, and since there was no previous information suggesting expected effect sizes for the other neuronal responses, we included all recordings with at least 10 trials. Neurons were recorded for up to 7 days, and 1% Cholera toxin B subunit (CTB, C9903, Sigma-Aldrich) was used to replace 2M saline in the electrode on the last day of electrophysiology. Eventually, 50 nL of CTB was injected after the last recoding. Electrophysiological recordings were band-pass filtered at 150-6000 Hz and spikes were thresholded in Matlab (The Mathworks, Natick MA, USA) using custom-written code and SpikeTrain (Neurasmus, Rotterdam, The Netherlands). Spike density functions (referred to as average spike traces) were computed for all

trials by convolving binary 1 ms-bin vectors containing spike occurrences with a Gaussian kernel with a 5 ms width.

Microstimulation mapping of eyeblink-controlling regions in IpN

Functional mapping of the CN was performed using 80-μm-diameter platinum iridium monopolar electrodes (100 KΩ; Alpha Omega) as in Heiney et al. (2014b). Electrodes were positioned using stereotaxic coordinates relative to a mark on the cement. Mapping was mostly confined to the anterior interpositus (IpN), dorsolateral hump (DLH), and lateral nucleus (LN). Electrodes were advanced in steps of 100 μm, and currents in the range of 1-15 μA (200 ms pulse trains; 250 μs biphasic pulses; 500 Hz) were systematically tested to identify the threshold for evoking movement. The eyeblink-controlling region of IpN was defined as the location at which discrete and sustained eyelid closure could be evoked with low currents (< 5 μA). This region was subsequently targeted for electrophysiological recordings.

Optogenetics

An optic cannula fiber (ø105 μm, 0.22NA, 2mm, Thorlabs) was vertically implanted over the IpN (AP 2.5mm, ML 2mm) and attached to the skull. In addition, a brass pedestal was attached to the skull between bregma and lambda. Animals were allowed to recover from surgery for 2 weeks. After eyeblink conditioning, mice were head-fixed on a set up that is equipped with an optogenetic blue light source (wave length 470nm, M470F3, Thorlabs) and a high-power light driver (M00283732, Thorlabs). In a 50-trial session, 10 trials were randomly presented together with a 5V optic stimulus that gave 5-ms pulses at 100Hz for the duration of the CS (260 ms), thus terminating at CS and US offset.

Spike modulation in the last 200 ms of the CS-US interval

Spike rate suppression and facilitation in the CS-US interval (Fig. 2), relative to a 500 ms baseline period, were determined separately. We chose to determine average spike modulation of cells in terms of absolute instead of relative change from the average baseline firing frequency, as we wanted to not process the data further away from actual firing frequency than necessary. Moreover, absolute change was not different across firing frequencies in terms of facilitation (r = 0.025, p = 0.68, n = 270, Spearman), and absolute suppression was only slightly deeper in faster firing cells (r = -0.131, p = 0.0308, n = 270, Spearman), whereas relative mean modulation was more clearly linked to average firing frequency (facilitation: r = -0.378, p < 0.0001; suppression: r = -0.211, p = 0.0005; n = 270, Spearman). Thus, expressing spike modulation in absolute terms thus avoids the use of a modulation criterion that is implicitly looser for cells with lower firing frequencies. We considered cells to carry CS-US facilitation if they showed an average increase of at least 5 Hz above baseline mean in the last 200 ms of the CS-US interval, after subtracting the mean above-baseline activity within the baseline itself. Similarly, cells showing an activity

of at least 5 Hz below baseline mean, correcting for below-baseline activity within the baseline itself, were considered suppressive. For both types of modulation, this threshold roughly corresponds to 3 SDs among the incidentally negatively modulating cells, i.e. cells where the baseline showed more facilitation/suppression than the CS-US interval. Duration of modulation was calculated as the sum of ms-bins exceeding 3 baseline SDs in the last 200 ms of the CS-US interval; spike firing needed to exceed this threshold for at least 10 ms during the CS-US interval.

CS-responses

To see how IpN neurons may reflect CS-related Purkinje cell complex spikes, rapid shifts in spike frequency were assessed between 50 and 125 ms post-CS in average spike traces that were standardized to baseline. A rapid drop exceeding 4.5 SDs was considered to be a CS pause if it was followed by a peak of at least 2 SDs. Similarly, an upstroke of 4.5 SDs was labeled a CS peak if it was followed by a drop of at least 2 SDs.

US-responses

First, the presence of US peak and pause responses in individual cells were quantified on the basis of their average spike traces, standardized to the 500 ms baseline. The time windows used to quantify the first US peak and pause (Fig. 6), and the second US peak (Fig. 7) were 1-30 ms, 16-45 ms, and 31-60 ms post-US, respectively. A first US peak was identified if it exceeded either 5 or 2 baseline SDs from the average of the last 50 ms of the CS-US interval, with the latter case also requiring a 5 SD difference from baseline. This way, cells that showed high facilitation in the CS-US interval were not ignored simply because they did not spare enough room for the spike increase required to meet the first criterion. Pauses were recognized if they exceeded 5 baseline SDs below the final 50 ms of the CS-US interval, and were at least 2 SDs below baseline. Alternatively, they could be 2 SDs below the end of the CS-US interval and exceed 5 SDs from baseline. This means pauses that did not dip below baseline level were not recognized as such, as it is difficult to ascertain whether they are pauses, or just the space between two peaks. Finally, second peaks were considered significant if they were still at least 2 SDs above the last 50 ms of the CS-US interval as well as 5 SDs above baseline. For both the pause and the second peak, the subsequent turnaround had to regress at least 2 SDs back to baseline, so as to avoid the inclusion of blunt, unpeak-like movements in the average spike traces. For trial-by-trial analyses, absolute firing frequency was used, taking the maximum (or, for pauses, minimum) values within 30 ms time-windows centered at the average peak- or pause-time.

Simple spike-based model of IpN neurons

A total of 26 IpN neurons were modeled (Fig. 5) using the parameters shown in Fig. 5-source data 1, with each modeled IpN neuron incorporating the simple spike

modulation of a Purkinje cell from the dataset in Ten Brinke et al. (2015). For each modeled trial of IpN modulation, 30 simple spike patterns were used as input to reflect the reported convergence rate of 20-50 Purkinje cells to 1 nuclear cell (Person & Raman, 2012). It is not known how similar or dissimilar simple spike modulation of Purkinje cells projecting to the same nuclear cell is. We here opted to take the same reference Purkinje cell for each of the thirty simple spike patterns used to model IpN activity. To avoid reusing trials, we expanded the Purkinje cell simple spike data. For each Purkinje cell, inter-spike interval distribution (ISI) characteristics (mean, SD, skewness, kurtosis) were determined across trials for each 1 ms bin in the trial timespan. By iteratively sampling a random ISI from the local ISI distribution, trials of simple spike activity are created that carry the same firing and modulation characteristics as the original Purkinje cell. The resulting set of 900 trials of simple spike activity was fed to the model, resulting in 30 trials of IpN spike activity. Spike density functions were subsequently computed for each IpN cell and parameters across the combined data were compared with actual IpN recordings.

Statistics

Significance tests were performed using MATLAB. Unless otherwise specified, mean and standard deviation were used to report central tendency and measure of deviation. Correlations between two continuous variables were made using Pearson's r if there were at least 30 data points and data was normally distributed for both variables, after a Grubbs'test for outliers (α= 0.05); otherwise, Spearman's rho was used. Group differences were assessed with Mann-Whitney U tests. For combined analysis of multiple cells, mixed-effects linear regression was performed, with random intercepts and slopes for cells included based on likelihood ratio tests. Visual inspection of residuals safeguarded adequate normality and homoscedasticity, and helped identify extreme outliers (never more than four). Bootstrap tests were used to determine the probability for a certain number of cells to be significant across a cell population, by assessing significance across 500 random datasets with similar amounts of cells and similar amounts of trials. Correlation matrices were used to explore the temporal distribution of the correlations between spike modulation and behavior (Fig. 2, Supp. Fig. 2). The procedure is identical to the one explained in Ten Brinke et al. (2015). In short, the trial timespan is divided up in 20 ms bins. Across trials, the average eyelid value within each bin is correlated to the average spike rate value within each bin, resulting in a 100x100 matrix of r-values, given the 2-second trial window. Matrices for multiple cells were subsequently compiled by taking the average r-values across matrices, after nullifying the r-values of the sign opposite to the sign of interest. Note that this constitutes a methodological tool used to assess the temporal distribution of correlations, and not to quantify their significance.
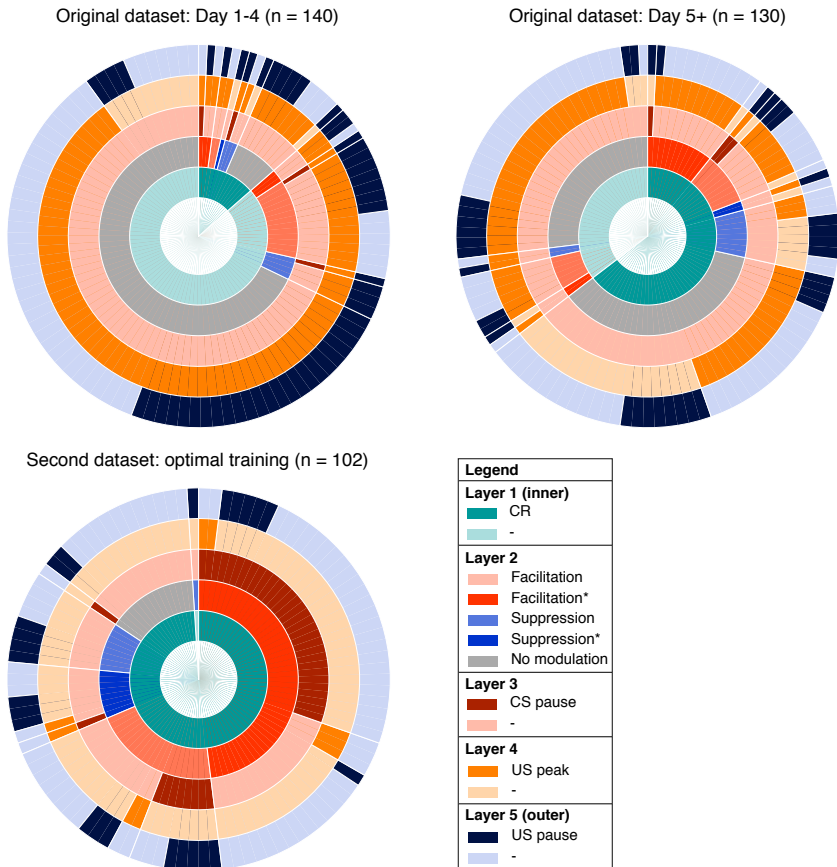
Supplementary Material

Original dataset: Day 1-4 (n = 140)

Original dataset: Day 5+ (n = 130)

Second dataset: optimal training (n = 102)

Legend	
Layer 1 (inner)	
	CR
	-
Layer 2	
	Facilitation
	Facilitation*
	Suppression
	Suppression*
	No modulation
Layer 3	
	CS pause
	-
Layer 4	
	US peak
	-
Layer 5 (outer)	
	US pause
	-

Figure S1 Overview of IpN recording datasets. The proportional prevalence of recordings with and without conditioned behavior (inner layer 1), modulation and/or significant spike-eyelid correlations (layer 2; see Fig. 2), a CS pause (layer 3; see Fig. 4), a US peak (layer 4; see Fig. 6), and a US pause (layer 5; see Fig. 6).

178
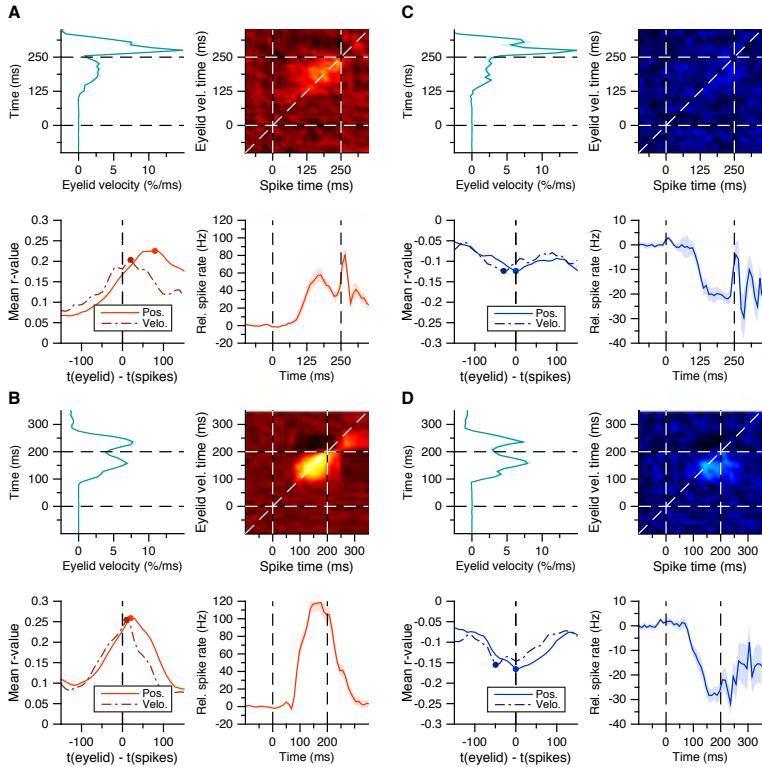
Figure S2 Spike-eyelid velocity correlation matrices. (A) Average spike-eyelid correlation matrix for the 30 facilitation cells in Fig. 2A, here using eyelid velocity instead of position (top right panel); mean eyelid velocity trace with SEM corresponding to the matrix's y-axis (top left panel); mean spike trace with SEM corresponding to the matrix's x-axis (bottom right panel); and average r-values with SEM for matrix correlations with similar temporal offset in the last 200 ms of the CS-US interval (bottom left panel). From this approach, the optimal temporal offset between spikes and eyelid position was 80 ms, and the one between spikes and eyelid velocity was 20 ms. **(B)** Same as in A, here for the 70 facilitation cells from the second dataset in Fig. 2E. The stronger correlations lie more tightly to the diagonal, as reflected in an optimal temporal offset of 20 ms for eyelid position, and 10 ms for eyelid velocity (bottom left panel). **(C)** Same as in A, but for the 16 suppression cells in Fig. 2I. As with the temporal cross-correlations in Fig. 2L, here too the optimal temporal offset suggests spikes reflecting eyelid behavior, rather than predicting it: 0 ms for eyelid position, -30 ms for velocity. **(D)** Same as in C, but for the 16 suppression cells in Fig. 2M. Again, in contrast to the facilitation cells, the optimal temporal offset reflected rather than predicted eyelid behavior: 0 ms for eyelid position, -50 ms for eyelid velocity.
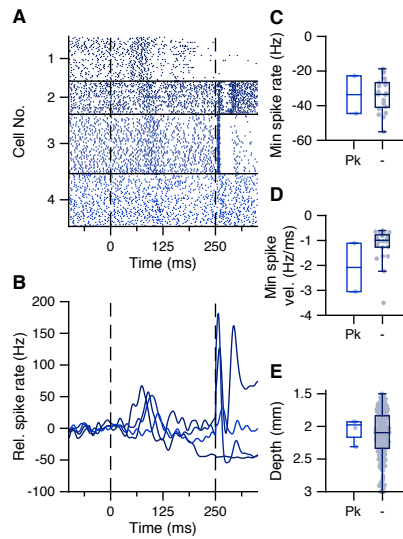
Figure S3 Transient spike increase at CS-complex spike latency. (A) Raster plot showing IpN spikes during paired trials in 4 cells that show a blunted peak response around the CS-complex spike latency. **(B)** Average spike traces for the cells in A. **(C)** Minimum spike rate in the CS-US interval did not seem more or less pronounced in suppressive cells with this blunted peak (Pk, -33.6 $\pm$ 15.4 Hz) compared to those without (-34 $\pm$ 9.6 Hz, p = 1, MWU). **(D)** Same as C, here showing no difference in spike rate velocity (-2.1 $\pm$ 1.4 vs -1.2 $\pm$ 0.7 Hz/ms, p = 0.2096, MWU). **(E)** Same as C, here showing no difference in recording depth (2048 $\pm$ 181 vs 2120 $\pm$ 36 um, p = 0.7348, MWU).
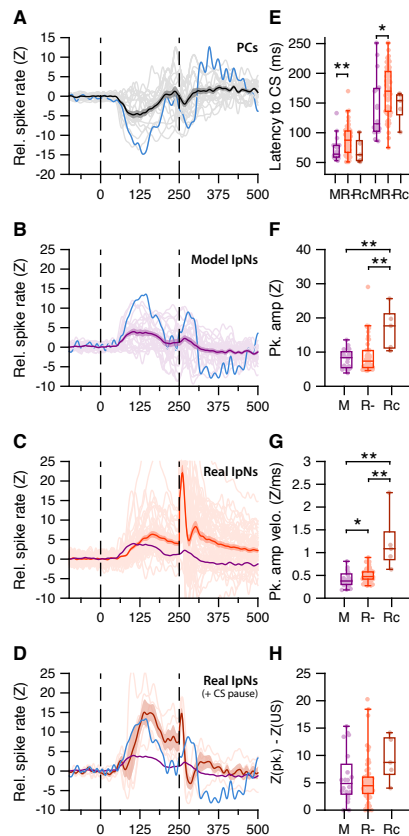
Figure S4 Modeled IpN modulation. (A) Average simple spike traces (light gray) in eyelid-related Purkinje cells that showed conditioned suppression; grand average is shown in black, with SEM. Blue trace shows the Purkinje cell with the deepest suppression. **(B)** Average traces of modeled IpN activity, with each cell containing 30 trials based on a simple spike suppression profile from the dataset in A. Blue trace shows the modeled IpN activity corresponding to the blue Purkinje cell trace in A. **(C)** Average traces of actual recordings of facilitation cells that did not show a CS pause. Purple trace denotes the average of the modeled IpN neurons in B. **(D)** Same as in C, here showing facilitation cells that did show a CS pause. Blue trace is the same as in B. **(E)** Timing of modeled (M) IpN facilitation, compared to that of real IpN neurons that did not (R-) or did (Rc) show a CS pause. The first three bars denote facilitation onset times, and the second set of bars shows peak time. The modeled IpN neurons seem to align particularly with the earlier facilitation profiles of the non-CS pause cells in terms of both onset (M: 73 ± 19 ms; R-: 88 ± 25 ms, p = 0.0098, MWU) and peak times (M: 144 ± 55 vs R-: 171 ± 43 ms, p = 0.0221, MWU). **(F)** Facilitation peak amplitude was higher in CS pause cells (Rc, 17 ± 6.3) than both modeled IpN neurons (M, 8 ± 2.8, p = 0.0039, MWU) and non-CS pause cells (R-, 9.3 ± 6, p = 0.0064, MWU). **(G)** Whereas R- cells showed slightly higher spike rate velocities than M cells (0.5 ± 0.1 vs. 0.4 ± 0.2 z/ms, 0.0198, MWU), Rc cells showed particularly high velocities (1.2 ± 0.6 z/ms) compared to both R- (p = 0.0006, MWU) and M cells (p = 0.0013, MWU). **(H)** The reduction in amplitude from peak to US onset was significantly great for Rc cells compared to R- cells (9.4 ± 4.1 vs 5.3 ± 4.3, p = 0.0283, MWU), but the comparison with M cells (6 ± 4.8, p = 0.11, MWU) failed to reach significance.

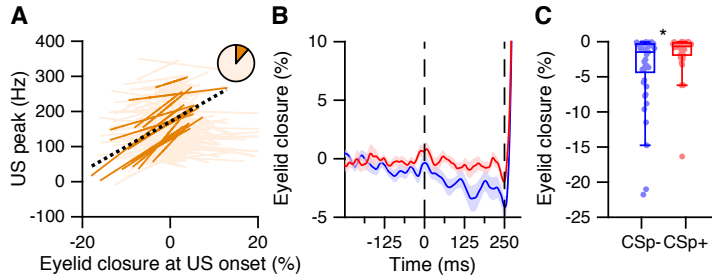**Figure S5 Eyelid opening in the CS-US interval relates to reduced US peak and absence of US-complex spike.** **(A)** Significant (plain orange) and non-significant (light orange) trial-by-trial correlation lines for cells with a US peak and without conditioned behavior (n = 149). Pie chart shows the proportion of significantly correlating cells. Black dashed line: fit line from a linear mixed model of the significant cells (Supp. Table 1). **(B)** Average eyelid traces with SEM for trials with eyelid opening responses, with (red) and without (blue) a US-related complex spike, from the Purkinje cell dataset reported in ten Brinke et al. (2015). **(C)** The eyelid was further opened at US onset in trials without a US-related complex spike (blue) than in trials with US-complex spike (red, p = 0.0218, MWU).
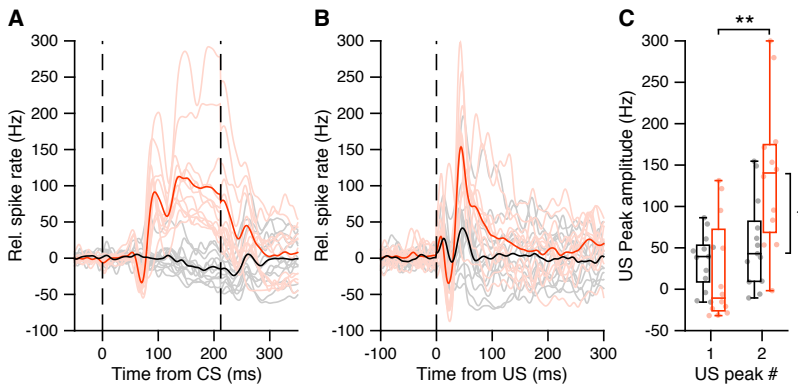
Figure S6 IpN responses in paired trials and US-only trials, after optimal conditioning. **(A)** Average spike traces during paired trials for 12 IpN cells with CS pause and CS-US facilitation (light red; average in plain red), and for 13 IpN cells that did not show both responses (gray; average in black). **(B)** Average spike traces for the same IpN cells in A, but during US-only trials. **(C)** The IpNs with CS pause and CS-US facilitation (red) showed substantially stronger post-US pause peak amplitudes (137.3 $\pm$ 89.4 Hz) than the IpNs without (black; 55 $\pm$ 53.9 Hz, p = 0.0133, MWU). The second US peak was also stronger than the first US peak within the red IpN group (137.3 $\pm$ 89.4 vs 20.3 $\pm$ 62.3 Hz; p = 0.0014, MWU), but not within the black IpN group (34.8 $\pm$ 32.8 vs 55.1 $\pm$ 53.9 Hz, p = 0.4728, MWU).

182

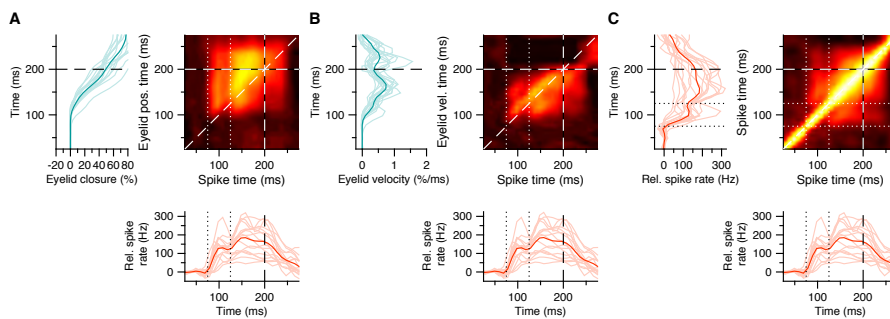**Figure S7 Rapid post-CS pause excitation relates to broader subsequent excitation and to CR behavior. A** Average trial-by-trial correlation matrix (right panel) showing positive spike-eyelid position correlations for 16 IpN neurons with a CS pause, where a hotspot of positive correlations corresponding to rapid post-CS pause excitation (straddled by dotted white lines) shows a degree of separation from the hotspot corresponding to broader subsequent excitation. Average eyelid responses (left panel) correspond to the y-axis in the matrix; average spike traces (bottom panel) correspond to its x-axis. **B** Same as in A, here showing spike-eyelid velocity correlations. **C** Same as in A, here showing the auto-correlations among spike activity, which suggest a positive relation between the rapid post-CS pause excitation and broader subsequent excitation.

Supplementary Table 1. Linear (mixed) model summaries.

Fig. 2B: For outcome variable **% Eyelid closure at US onset** with random intercepts and slopes per **IpN cell** (showing significant spike-eyelid correlations, n = 17, original dataset):

Fixed effect	Coefficient	F-test	P
Intercept	6.9 ± 2.1	$F_{1,556} = 10.7$	0.0011
Spike facilitation (Hz)	0.49 ± 0.07	$F_{1,1556} = 44.97$	<0.0001

Fig. 2F: For outcome variable **% Eyelid closure at US onset** with random intercepts and slopes per **IpN cell** (showing significant spike-eyelid correlations, n = 49, second dataset):

Fixed effect	Coefficient	F-test	P
Intercept	7.57 ± 2.47	$F_{1,2071} = 9.36$	0.0022
Spike facilitation (Hz)	0.64 ± 0.04	$F_{1,2071} = 265.12$	<0.0001

Fig. 2J: For outcome variable **% Eyelid closure at US onset** with random intercepts and slopes per **IpN cell** (showing significant spike-eyelid correlations, n = 3):

Fixed effect	Coefficient	F-test	P
Intercept	10.5 ± 5.1	$F_{1,182} = 4.29$	0.0397
Spike suppression (Hz)	-0.27 ± 0.12	$F_{1,182} = 4.96$	0.0272

Fig. 2N: For outcome variable **% Eyelid closure at US onset** with random intercepts per **IpN cell** (showing significant spike-eyelid correlations, n = 8):

Fixed effect	Coefficient	F-test	P
Intercept	32.3 ± 3.5	$F_{1,306} = 83.12$	<0.0001
Spike suppression (Hz)	-1.01 ± 0.1	$F_{1,306} = 104.19$	<0.0001

Fig. 6D. For outcome variable **Post-US peak (Hz)** with random intercepts and slopes per **IpN cell** (showing significant correlations between post-US peak and CR amplitude; n = 15):

Fixed effect	Coefficient	F-test	P
Intercept	192.5 ± 14.3	$F_{1,559} = 183.6$	<0.0001
% Eyelid closure at US onset	-1.79 ± 0.36	$F_{1,559} = 24.9$	<0.0001

Fig. 6H. For outcome variable **US peak (Hz)** across **IpN cells** (showing significant correlations between post-US trough and CR amplitude; n = 4):

Fixed effect	Coefficient	T-test	P
Intercept	8.88 ± 1.86	$T_{184} = 4.76$	<0.0001
% Eyelid closure at US onset	0.66 ± 0.06	$T_{184} = 11.03$	<0.0001

Fig. 7D. For outcome variable **2nd US peak (Hz)** with random intercepts and slopes per **IpN cell** (showing significant correlations between post-US peak and secondary post-US peak, n = 14):

Fixed effect	Coefficient	F-test	P
Intercept	76.2 ± 6.96	$F_{1,549} = 119.9$	<0.0001
Post-US peak (Hz)	0.31 ± 0.04	$F_{1,549} = 65.6$	<0.0001

Supplementary Table 2. DCN model properties*	
# PCs per CN cell	30
ϕ, firing threshold	-38.8 mV
C_m, membrane capacitance	122.3 pF
g_{leak}, max leak conductance	1.63 nS
E_{leak}, leak reversal potential	-56 mV
g_{AMPA}, max AMPA conductance	50 nS
g_{NMDA}, max NMDA conductance	25.8 nS
g_{ex_base}, baseline excitatory conductance	12 nS
E_{ex}, excitatory reversal potential	0 mV
g_{inh}, max inhibitory conductance	5 nS
E_{inh}, inhibitory reversal potential	-70 mV
g_{ahp}, max after-hyperpolarization	50 nS
E_{ahp}, after-hyperpolarization reversal potential-	-70 mV
τ_{AMPA}, AMPA time constant	9.9 ms
τ_{NMDA}, NMDA time constant	30.6 ms
τ_{inh}, inhibitory time constant	2.4 ms
τ_{ahp}, after-hyperpolarization time constant	2.5 ms
*Sources: Yamazaki and Tanaka, 2007; Person and Raman, 2012	

Excitatory cerebellar nucleocortical circuit provides internal amplification during associative conditioning

Closed-loop circuitries between cortical and subcortical regions can facilitate precision of output patterns, but the role of such networks in the cerebellum remains to be elucidated. Here, we characterize the role of internal feedback from the cerebellar nuclei to the cerebellar cortex in classical eyeblink conditioning. We find that excitatory output neurons in the interposed nucleus provide efference-copy signals via mossy fibers to the cerebellar cortical zones that belong to the same module, triggering monosynaptic responses in granule and Golgi cells and indirectly inhibiting Purkinje cells. Upon conditioning, the local density of nucleocortical mossy fiber terminals significantly increases. Optogenetic activation and inhibition of nucleocortical fibers in conditioned animals increases and decreases the amplitude of learned eyeblink responses, respectively. Our data show that the excitatory nucleocortical closed-loop circuitry of the cerebellum relays a corollary discharge of premotor signals and suggests an amplifying role of this circuitry in controlling associative motor learning.

Z. Gao, M. Proietti-Onori, Z. Lin, **M.M. ten Brinke**, H.J. Boele, J.W. Potters, T.J.H. Ruigrok, F.E. Hoebeek, & C.I. De Zeeuw (2016) **Neuron**

Introduction

Accurate execution and error correction of motor behavior requires specific neural computation and dedicated wiring of neural circuits in the brain. Cortical and subcortical regions are usually connected by closed-loop circuitries, which are thought to determine the precision of final output patterns (Ahissar and Kleinfeld, 2003; Kelly and Strick, 2003; McCormick et al., 2014; Moser et al., 2008; Shepherd, 2013; Strick et al., 2009). The cerebellum controls a variety of sensorimotor tasks with high spatial and temporal accuracy (De Zeeuw et al., 2011; Dean et al., 2010; Gao et al., 2012; Ito, 2006), but surprisingly little is known about its internal closed-loop circuitry between the cerebellar nuclei and cortex. The cerebellar cortex receives glutamatergic climbing fiber (CF) and mossy fiber (MF) inputs from inferior olive and other precerebellar nuclei, respectively, while the cerebellar nuclei receive axon collaterals of the same CF and MF inputs (Voogd and Ruigrok, 1997). In the cerebellar cortex CF and MF signals ultimately converge onto GABAergic Purkinje cells (PC), which in turn project to the cerebellar nuclei, forming the main output unit of the cerebellum.

In current learning theories on cerebellar function the CFs are thought to relay sensory error signals and provide an external feedback to the molecular layer of the cerebellar cortex during motor learning (Cerminara and Apps, 2011; De Zeeuw et al., 2011; Dean et al., 2010; Steuber and Jaeger, 2013; Voogd and Ruigrok, 1997). In contrast to models of other cortical and subcortical circuits in the brain (Ahissar and Kleinfeld, 2003; Alexander et al., 1986; McCormick et al., 2014; Nicolelis and Fanselow, 2002; Pennartz et al., 2009), it is unknown whether internal feedback mechanisms from the cerebellar nuclei onto the cerebellar cortex may also facilitate adaptive sensorimotor processing (Ankri et al., 2015; Houck and Person, 2015). In principle, cerebellar internal corollary discharges relaying an efference copy of motor signals as a feedback can be advantageous for control of movements, because preparations and predictions for new movements can be initiated ultrafast, long before sensory feedback from the periphery is provided (Hallett and Lightstone, 1976; Perrone and Krauzlis, 2008; Sperry, 1950).

In this study, we sought to examine the potential role of cerebellar nucleocortical projections (Dietrichs and Walberg, 1980; Gould and Graybiel, 1976; Hamori et al., 1981; Houck and Person, 2015; Tolbert et al., 1978; Trott et al., 1998; Umetani, 1990) as an internal corollary feedback to the granular layer during Pavlovian eyeblink conditioning (Boele et al., 2010; Gonzalez-Joekes and Schreurs, 2012; Krupa and Thompson, 1997; Morcuende et al., 2002). During eyeblink conditioning a conditional stimulus (CS), such as a tone or light, is repeatedly paired with an unconditional stimulus (US), such as an air-puff to the eye, at a fixed inter-stimulus interval of several hundred milliseconds so as to produce a conditioned response (CR) (Medina et al., 2000; Medina et al., 2002). So far, studies aimed at unraveling the mechanisms underlying the acquisition of this form of associative learning have focused mainly on the role of cerebellar cortical processes in the molecular layer, including long-term depression and long-term potentiation of the parallel fiber to PC synapse (Aiba et al., 1994; Ito et al., 2014; Schonewille et al., 2010; Schonewille et al., 2011; Welsh et al., 2005) and intrinsic plasticity of PCs (Johansson et al., 2014; Schonewille et al., 2010), most of which probably depend on the presence or absence of external feedback

provided by the CFs (Gao et al., 2012; ten Brinke et al., 2015). Here we establish that the excitatory input from the cerebellar nuclei to the cerebellar cortical eyeblink region strengthens the conditioned eyeblink response by providing an internal amplification loop, highlighting the emerging concept that the mechanisms underlying motor learning are distributed across various parts of the cerebellar modules and include an internal closed-loop circuitry (Casellato et al., 2015; Gao et al., 2012; ten Brinke et al., 2015).

Results

Morphological features of nucleocortical fibers in eyeblink region

Since the main motor route of the eyeblink paradigm is mediated by the deeper part of the primary fissure in lobule simplex (HVI), interposed nuclei (IpN) and red nucleus (RN) (Boele et al., 2010; Gonzalez-Joekes and Schreurs, 2012; Krupa and Thompson, 1997; Morcuende et al., 2002), we first investigated to what extent the nucleocortical pathway from IpN neurons to lobule simplex indeed provides an efference copy of the signals forwarded to the RN (Ruigrok and Teune, 2014). The retrograde tracers Ctb Alexa Fluor 555 and Ctb Alexa Fluor 488 were injected into the mouse cerebellar lobule simplex (HVI) and corresponding contralateral RN, respectively (n = 4). In the IpN areas where both tracers converged, we found that 52% (74/143) of the RN projecting neurons showed nucleocortical labeling and 84% (74/88) of the nucleocortical projecting neurons projected to the RN (Figs. 1A-D and Fig. S1). These data indicate that a substantial part of the nucleocortical afferents in lobule simplex relays efference copy signals of the presumptively excitatory IpN neurons that project to the RN (De Zeeuw and Ruigrok, 1994).

Next, to establish the morphology and identity of the terminals of the nucleocortical afferents in lobule simplex we injected AAV particles coding for for eYFP-tagged channelrhodopsin 2 (AAV2-hSyn-hChR2-eYFP) into the IpN and found prominent axonal labeling within and outside of cerebellum (Figs. 1E-J and Fig. S2). Within the cerebellar cortex, axonal terminals were found predominantly in the ipsilateral paravermal and hemispheric areas including lobule simplex, crus 1, crus 2, paramedian lobule and copula pyramidis (Figs. 1G and 1I). Less dense projections were found in ipsilateral (para)flocculus and contralateral vermal and paravermal regions (Fig. 1G, Fig. S2 and Table S1). The nucleocortical fiber terminals formed large rosettes with filopodia-like protrusions, manifesting the mossy fiber (MF) rosette. Notably, these MF terminals preferentially targeted the superficial granular layer (Fig. 1J). In addition, the nucleocortical MFs expressed exclusively presynaptic glutamate transporter vGlut2, whereas the majority of surrounding precerebellar MF rosettes expressed both vGlut1 and vGlut2 (Gebre et al., 2012; Hioki et al., 2003) (Fig. 1K).

When we compared the morphology of the nucleocortical MF with the precerebellar MF rosettes originating from the pontine nuclei, we found that the nucleocortical MF rosettes had a larger diameter as well as more and longer filopodia-like structures compared with precerebellar MFs from pontine nuclei (Figs. 2A and 2B). At the ultrastructural level, nucleocortical MF terminals contained higher densities of mito-
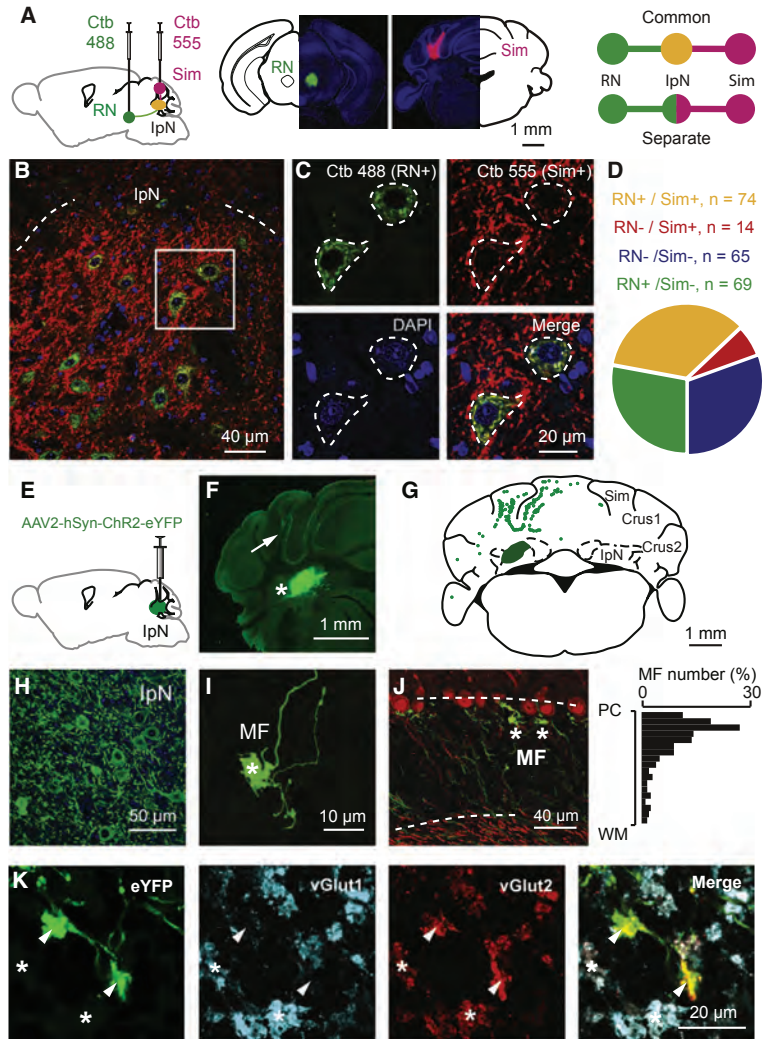
Figure 1 Nucleocortical projections from the cerebellar interposed nucleus. (A) Scheme and example of experimental setup showing retrograde labeling of IpN neurons following injection of Ctb tracers in the red nucleus (RN) and lobule simplex (Sim). Right: rationale of the experimental setup to illustrate the common (yellow) or separate (green and red) IpN neurons that project to RN and Sim. **(B)** Example image of an IpN region with labeling from RN (Ctb 488, green) and Sim (Ctb 555, red). **(C)** High magnification images showing co-labeled IpN neurons. **(D)** Summary chart of the retrogradely labeled neurons in IpN. **(E)** Schematic showing viral injection of AAV2-hSyn-ChR2-eYFP into the left interposed nucleus.**(F)** Example of AAV infected IpN (asterisk) and nucleocortical projections (arrow). **(G)** Distribution of nucleocortical MF rosettes in a coronal cerebellar section. **(H)** eYFP expressing IpN neurons and**(I)** nucleocortical MF projection with enlarged rosette and filopodia-like structure. **(J)** Example (left) and summary (right) of the nucleocortical MF (asterisks) distribution in relation to the position of the granule layer (between dashed lines); Purkinje cells are labeled in red (n = 3). **(K)** Nucleocortical MFs that express vGlut2, but not vGlut1 (arrowheads). Note the surrounding MF rosettes (asterisks) that are positive for both vGlut1 and vGlut2.
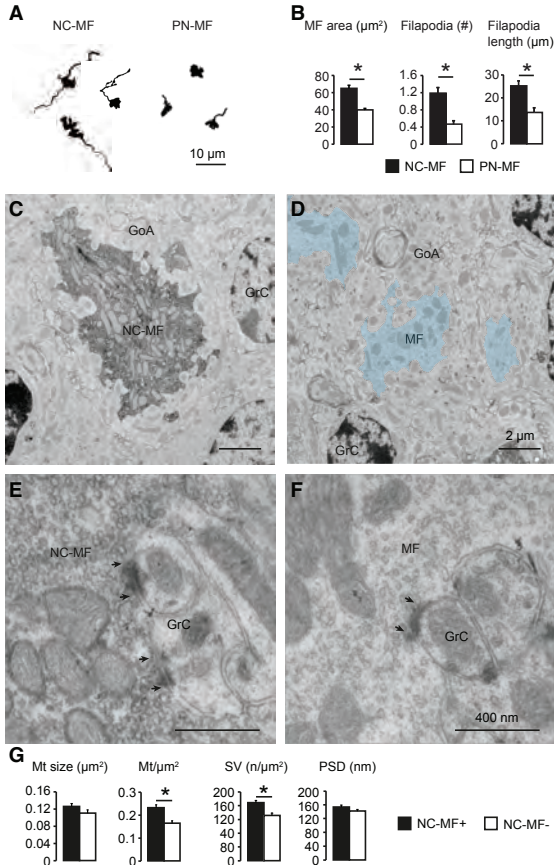
190

Figure 2 Morphological characteristics of nucleocortical mossy fibers. **(A)** Examples of nucleocortical MFs (NC-MF) and pontine nucleus MFs (PN-MF) labeled with anterograde tracer BDA 10,000 Da. **(B)** Quantitative comparison of the morphology of the nucleocortical MFs (NC-MF, n = 34) and MFs originate from the pontine nuclei (PN-MF, n = 31). NC-MFs have larger size, higher number of filopodia per rosette and longer filopodia length (all $p < 0.05$). **(C-G)** Electron micrographs of a NC-MF terminal and adjacent unlabeled MF. GrC: granule cells, GoA: Golgi cell axon. Synaptic densities are indicated with double arrows. NC-MF (n = 17) has a higher mitochondria density ($p = 0.04$) and synaptic vesicle density ($p = 0.002$), compared with adjacent unlabeled MFs (n = 21). Mt: mitochondria, SV synaptic vesicle, PSD: post synaptic density. * $p < 0.05$, Data show mean ± s.e., unpaired student's t-tests.

chondria and synaptic vesicles compared with neighboring, unlabeled MF rosettes, whereas the size of mitochondria and length of PSDs did not differ (Figs. 2C--2G). These data highlight a prominent projection of nucleocortical MFs with unique molecular and morphological features, and suggest that they carry an efference copy signal of cerebellar premotor output commands.

The organization of the olivocerebellar system is characterized by repetitive parasagittal circuits, commonly acknowledged as cerebellar modules (Apps and Hawkes, 2009; Voogd and Ruigrok, 1997). To find out whether nucleocortical MFs involved in eyeblink conditioning form an internal feedback circuitry within the borders of the relevant module, we studied the MF distribution in mice with AAV2-hSyn-ChR2-eYFP injections in the anterior IpN, a region connected with cerebellar modules negative for marker *Zebrin II* (Sugihara, 2011; Voogd and Glickstein, 1998). In line with the eyeblink regions identified in rabbit (Attwell et al., 1999; Mostofi et al., 2010), we observed that nucleocortical MFs of these animals were found predominantly in regions negative for *Zebrin II*, including the trough of lobule simplex (Figs. 3A-C).
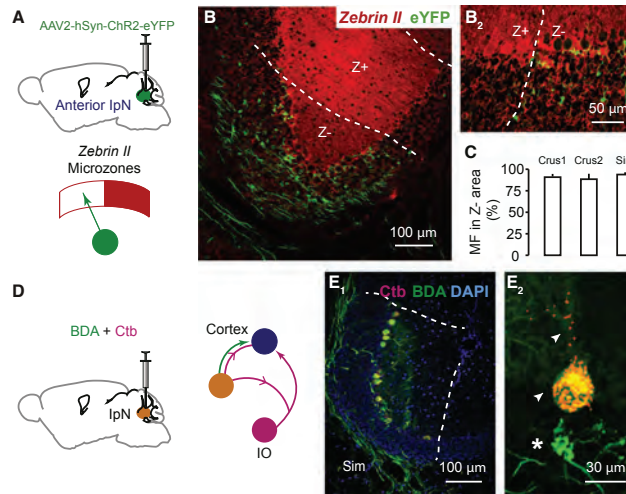
Figure 3 Modular organization of nucleocortical projections. (A) Experimental set up to investigate relation of nucleocortical afferents and zonal marker *Zebrin II*. **(B)** Distribution of nucleocortical mossy fibers (green) in relation to *Zebrin II* (red) expression at the trough of the simplex lobule **(B1)** and the border between *Zebrin II* positive (Z+) and negative (Z-) zones in Crus 1 **(B2)**. **(C)** Quantification of the nucleocortical mossy fibers terminating at the Z- zones in Crus 1 (90.5 $\pm$ 3.3%), Crus 2 (88.5 $\pm$ 6.2%) and lobule simplex (93.7 $\pm$ 2.8%), n = 4. **(D)** Experimental set up to investigate relation of nucleocortical afferents and climbing fiber zones. Arrowheads indicate the tracing directions. **(E) (E1)**: BDA 10,000 Da and Ctb 555 injection in the anterior IpN labeled cortical modules (between dashed lines) in the lobule simplex (Sim). **(E2)**: a co-localizing nucleocortical mossy fiber and PC in the same module. The PC soma and adjacent climbing fiber were labeled with CTb (yellow, arrow-heads) and the nucleocortical mossy fiber was labeled with BDA (green, asterisk).

More specifically, we observed that 90.5% ($\pm$ 3.3%), 88.5% ($\pm$ 6.2%) and 93.7% ($\pm$ 2.8%) of the nucleocortical mossy fibers originating in the anterior IpN terminated in Z- zones of Crus 1, Crus 2 and lobule simplex, respectively. This finding, which implies a modular organization of the nucleocortical pathway, was further supported by the alignment of anterogradely labeled nucleocortical MFs with retrogradely labeled PC somata and CF terminals in the same region following co-injection of Biotin Dextran Amine 10,000 Da (BDA, for nucleocortical MF labeling) and Ctb Alexa Fluor 555 (for PC soma and CF terminal labeling) into a small area of the anterior IpN (Figs. 3C and 3D). These data indicate that the regions that receive common nucleocortical MF projection also share the same CF projection and *Zebrin II* identity, consistent with the modular organization hypothesis of cerebellar functioning (Apps and Hawkes, 2009; Pijpers et al., 2006).

Electrophysiological properties of nucleocortical fibers in eyeblink region

To further characterize the cellular properties of nucleocortical IpN neurons we studied their morphological and electrophysiological properties *in vitro* (Figs. 4 and 5).

When we performed intracellular labeling following whole cell recordings on the large neurons of IpN, we found that the morphology of neurons with cerebellar cortical projections did not differ from the general population of excitatory cerebellar nuclei neurons (Aizenman et al., 2003; Uusisaari et al., 2007) in that they showed a similar soma size and number of primary dendrites (all p values > 0.31; Table S2). In addition, the electrophysiological properties of the nucleocortical cells were indistinguishable from the IpN neurons without any detectable projection to the cerebellar cortex (Table S2). Next, we characterized the electrophysiological properties of nucleocortical neurons at the level of their terminals *in vitro* with direct patch-clamp recordings of MF rosettes. Nucleocortical MFs labeled with eYFP could be readily visualized following injections of AAV-ChR2-eYFP in the IpN (Figs. 1E, 1F and 4A). The rosettes showed the electrophysiological characteristics stereotypical of MFs (Rancz et al., 2007), including a small capacitance, high input resistance and a hyperpolarization sag (Fig. 4B; Table S3). Prolonged depolarization induced only a short burst of action potential firing and a subsequent steady depolarization block. Interestingly, during spontaneous activity we observed tonic spontaneous action potential firing in 4 out of 19 recorded MF rosettes (Fig. 4C, Table S3). This activity probably reflects an intact connection to the cell body in the IpN within the slice (Fig. 5), because we did not observe any silent mossy fiber terminal that showed tonic action potential firing in response to continuous depolarization. Applying repetitive current pulses up to 500 Hz at the nucleocortical rosettes resulted in reliable action potential firing (Fig. 4D) with little adaptation in peak amplitudes, indicating that nucleocortical MFs can sustain reliable firing at extremely high frequencies, comparable to the high fidelity transmission of precerebellar MFs encoding sensory information (Chabrol et al., 2015; Rancz et al., 2007; Ritzau-Jost et al., 2014; Saviane and Silver, 2006).

To identify the cortical neurons that receive direct nucleocortical MF input from IpN we drove action potential firing specifically in the ChR2-expressing MF rosettes using optogenetics. Individual action potential firing could be reliably controlled with blue light pulses (470 nm, 1.2 mW, 1 ms pulse, onset latency 2.4 ± 0.2 ms, n = 10; Fig. 4E). We then recorded synaptic responses of neurons in the granular layer using optogenetic stimulation. Robust short latency monosynaptic EPSCs were found in both granule cells (GrCs, n = 13) and Golgi cells (GoCs, n = 9) (Figs. 4F-4I and Fig. S3). In addition, feedforward excitatory inputs from the MF-GrC-GoC pathway were detected in GoCs (Fig. 4I and Fig. S3). To further test the efficiency of eliciting action potential firing in GrCs and GoCs following nucleocortical stimulation we performed extracellular loose cell attached recordings, avoiding the potential changes in cellular excitability that can occur in the whole cell mode. Optogenetic stimulation was sufficient to entrain well-timed action potential firing in both GrCs and GoCs with high success rates (Figs. 4G and 4I). These results indicate that nucleocortical MFs originating in IpN can act as a robust and positive internal feedback to neurons in the lobule simplex in that they are configured to faithfully transmit action potential firing patterns to its granular layer.

MF afferents can control the activity of Purkinje cells (PCs) via the local cerebellar cortical circuitry comprising GrCs, GoCs and molecular layer interneurons (MLIs); they can either excite PCs via direct GrC-PC connections or inhibit PCs via feedforward GrC-MLI-PC processing (Fig. 4J). To assess the relative contribution of these two inputs (D'Angelo and De Zeeuw, 2009), we compared the inhibition/excitation (I/E)
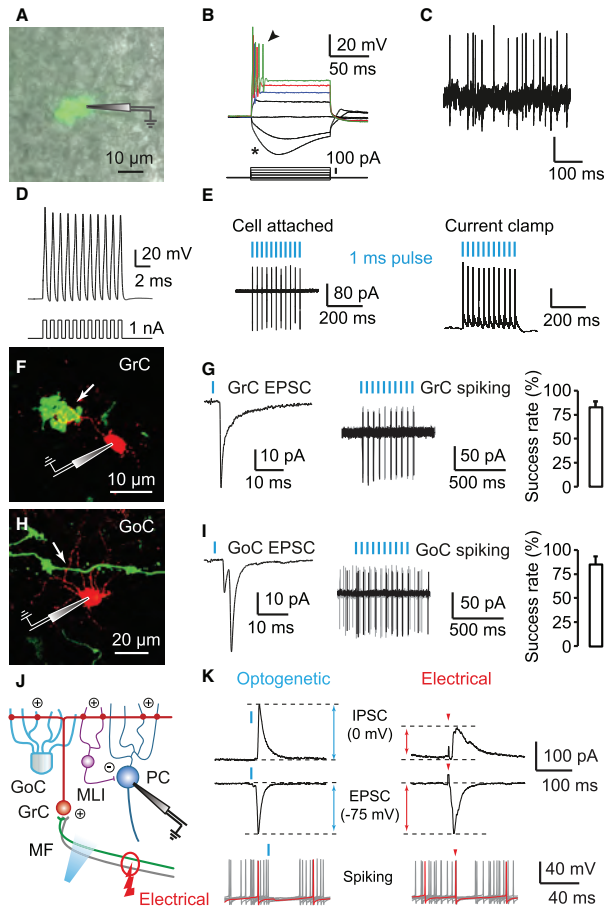
Figure 4 Nucleocortical projection imposes unique closed-loop circuit with internal feedback properties. (A) Patch-clamp recording of an eYFP labeled MF rosette visualized by overlaying epifluorescence and DIC images. **(B)** MF rosettes show current rectification, hyperpolarization sag (asterisk) and action potential firing (arrowhead) in response to steady state current injections. **(C)** Cell attached recording from a spontaneously firing nucleocortical MF. **(D)** Repetitive current pulses drive MF rosette to fire robustly at 500 Hz with little adaptation in the action potential amplitudes. **(E)** Optogenetic activation of a nucleocortical MF. Individual action potentials can be elicited with high temporal precision by a train of light pulses (1 ms 470 nm light at 30 Hz) in both cell attached and current-clamp modes. **(F)** Nucleocortical MF (green) innervates granule cell dendrite (GrC, red, arrow). **(G)** Whole cell recording of GrC-EPSC (left) and loose cell attached recording of GrC action potential firing (right) in response to 1 ms photo activation of NC-MF. High success rates of action potential firing were found in the GrC (81.7 ± 6.0%, n = 10). **(H)** Nucleocortical MF (green) innervates Golgi cell dendrite (GoC, red, arrow). **(I)** Whole cell recording of GoC-EPSC (left) and loose cell attached recording of GoC action potential firing (right) in response to 1 ms photo activation of NC-MF. High success rates of action potential firing were found in the GoC (83.8 ± 8.3%, n = 5). **(J)** Experimental setup of identifying inhibition/excitation ratio (I/E) of Purkinje cell (PC) responses. GrC axon excites (+) the molecular layer interneurons (MLIs) and PCs, and the MLI in turn inhibits (-) PCs. ChR2 expressing nucleocortical MFs (green) are selectively activated by optogenetic stimulation, while a bundle of MFs with heterogeneous sites of origin (green and grey) are activated by electrical stimulation. **(K)** Whole cell voltage clamp recordings of EPSC and IPSC elicited by optogenetic stimulation of NC-MF. EPSC and IPSC components were isolated by clamping PC at -75 mV and 0 mV, respectively. Higher IPSC to EPSC ratio (I/E ratio) from nucleocortical MFs circuits were found in PCs, compared with electrical stimulation (top). Optogenetic activation induces longer suppression of action potential firing compared with electrical stimulation (bottom).
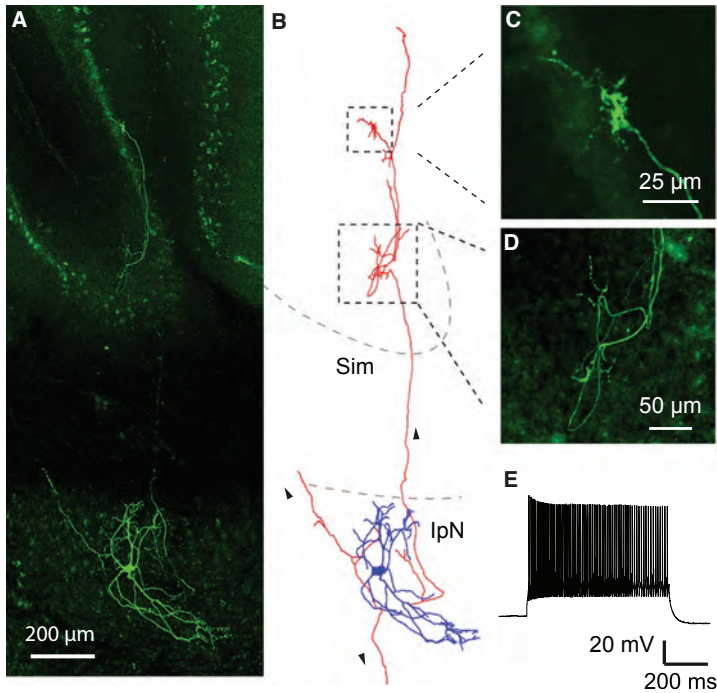
Figure 5 Physiologically identified cerebellar interposed nucleus neuron providing a nucleocortical projection. (A) Confocal image of an identified nucleocortical projecting IpN neuron recorded *in vitro*. Neuron is labeled with biocytin in the patch-clamping pipette and visualized with florescent streptavidin Alexa Fluor 488. **(B)** Neurolucida reconstruction of labeled neuron shows intact nucleocortical projection in the same sagittal plane. Arrowheads indicate the directions of extracerebellar and nucleocortical axonal projections. IpN: interposed nucleus, Sim: lobule Simplex. **(C)** High magnification image of a nucleocortical MF rosette and accompanying filopodia-like structures. **(D)** High magnification image of en passant fiber and boutons from the same neuron. **(E)** Example trace of action potential firing in response to 500 pA current injection in the neuron.

ratio of the responses of individual PCs following selective optogenetic activation of nucleocortical MF afferents with that following local electrical activation of the complete mixed group of MFs, including both nucleocortical MFs and precerebellar MFs. When the amplitudes of the excitatory components (i.e. EPSCs) were adjusted so as to be similar in the optogenetic and electrical stimulation paradigm (Fig. 4K), we observed a greater inhibitory component (i.e. IPSC) in the PC response to nucleo-cortical MF activation, resulting in a greater I/E ratio (1.09 ± 0.06 with optogenetic stimulation vs. 0.61 ± 0.09 with electrical stimulation; 6 pairs, $p = 0.006$, paired student's t-tests). Consistent with this observation, all PCs showed longer simple spike suppression upon selective activation of nucleocortical MFs (pause duration with optogenetics 71.8 ± 10.5 ms, with electrical stimulation 58.4 ± 8.5 ms; 6 pairs; $p = 0.008$, paired student's t-tests) (Fig. 4K). Thus, in effect, nucleocortical MFs convey a strong inhibitory input onto PCs, even though they directly excite GrCs.

Structural plasticity of nucleocortical fibers upon eyeblink conditioning

Although structural plasticity of MFs and their collaterals does not appear to be prominent following generally enriched but non-associative stimulation (Boele et al., 2013; Rylkova et al., 2015), it does occur during several sensorimotor learning tasks in which multiple stimuli are associated in a time-locked fashion (Boele et al., 2013; Ruediger et al., 2011). The high density of filopodia-like structures in lobule simplex (Fig. 2A and 2B) suggests that structural plasticity of the filopodia of nucleocortical MFs might also be involved in eyeblink conditioning, similar to what has been reported for extra-cerebellar MFs during other incremental learning paradigms (Ruediger et al., 2011). We first examined whether filopodia of nucleocortical MFs can in principle establish functional synapses. MF filopodial boutons labeled with eYFP consistently co-localized with vGlut2-positive endings (Fig. 6A), indicating the presence of glutamatergic synapses at these sites. On average, 44.6 ± 10.5 vGlut2-positive boutons were associated with a single nucleocortical MF rosette. To identify whether these boutons contact Golgi cells, we injected AAV encoding red marker mCherry into the IpN of the GlyT2-eGFP mice, in which the majority of Golgi cells are labeled (Zeilhofer et al., 2005). Indeed, part of the vGlut2-positive boutons was found to contact Golgi cell dendrites (Fig. S4). Next, we examined the ultrastructure of filopodial boutons using standard electron microscopy (EM). By combining serial sectioning with pre-embedding immuno-labeling of the tracer BDA (10,000 Da) and post-embedding immunogold labeling of GABA (see methods), we identified 18 filopodial boutons in two mice (Figs. 6B-D). Clear synaptic contacts were found in all 18 boutons, among which 15 contacted GrC dendrites (Fig. 6C) and 3 contacted GoC dendrites as indicated by immunogold labeling (Fig. 6D, Fig. S4). These data indicate that filopodial boutons can establish direct synaptic contacts with granule cells and Golgi cells.

We next set out to investigate whether these filopodia can undergo structural modification following eyeblink conditioning. Mice were trained to blink their eyes in a well-timed response to a light cue (CS) so as to avoid an air-puff to the eye (US) that was presented 250 ms after CS onset (Heiney et al., 2014) (Fig. 7A). The density of filopodia boutons originating from nucleocortical MFs in the deeper lobule simplex of well-trained mice was significantly increased by 69.8% (p = 0.001) compared with that in naïve mice (Figs. 7C-D). In contrast, the length of the filopodia of nucleocortical MFs was significantly reduced (p = 0.007) (Fig. 7D). This eyeblink training paradigm had no effect on the strength of nucleocortical MF synapses onto individual GrCs (p = 0.7), but further increased the I/E ratio in PCs (p = 0.02) (Figs. 7E and 7F), indicating a preferential enhancement of the feedforward inhibitory GrC-MLI-PC pathway. These data point towards hard-wired plasticity of nucleocortical MFs during associative conditioning and suggest a novel function for these afferents providing an internal feedback, triggering larger numbers of specific sets of GrCs.

Nucleocortical fibers can amplify conditioned eyeblink responses

Since simple spike suppression can be quantitatively correlated with the amplitude of conditioned eyeblink responses (ten Brinke et al., 2015), we next set out experiments to find out whether direct and selective activation of nucleocortical MFs is sufficient
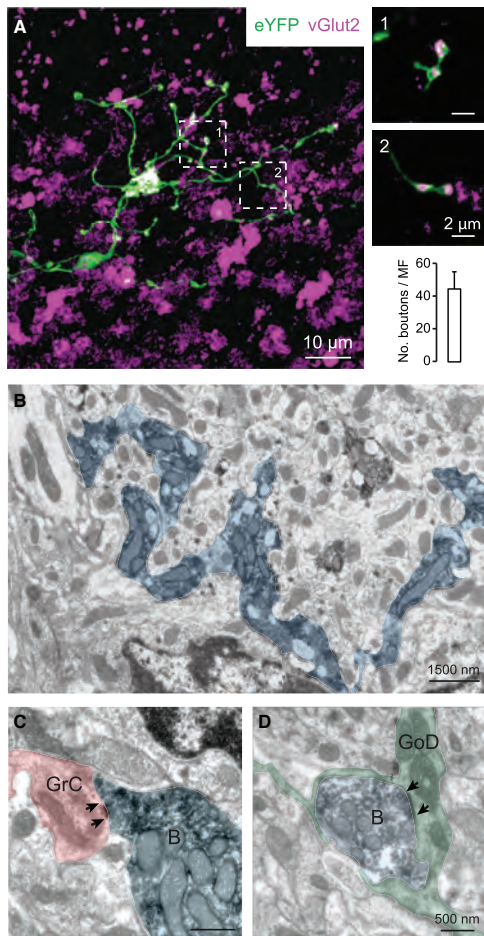
Figure 6 Filopodial boutons form functional synapses with granule and Golgi cells. (A) Representative image of a nucleocortical MF with filopodia protrusions. Insets 1 and 2 show vGlut2 positive filopodial boutons. Bar chart quantification shows the average number of vGlut2 positive filopodial boutons per MF rosette. **(B)** Representative EM image of BDA labeled filopodia traversing through the granule cell layer. Typical MF synaptic boutons (MF-B) onto granule cell (GrC) and Golgi cell dendrites (GoD) are shown in **(C)** and **(D)**, arrows indicate postsynaptic density.

to enhance conditioned eyeblink responses. We therefor trained a group of mice in which ChR2 was expressed by their nucleocortical MFs and in which an optic cannula was implanted superficially in the lobule simplex (Fig. 8A). Once the mice showed a consistent conditioned eyeblink response (see supplemental methods), we started optogenetic stimulation (for 10 ms coinciding with the CS onset) while recording the eyeblink responses as well as extracellular activity of the cerebellar nuclei and cerebellar cortex. The light intensity of the stimulus was adjusted for each mouse to make sure that it did *not* induce: 1) an instantaneous increase of action potential firing in the recorded cerebellar nuclei neurons; 2) an instantaneous eyeblink response; and 3) a detectable alteration of locomotion (Fig. S5). Optogenetic activation of nucleocortical MFs at the onset of the CS enhanced the amplitude and shortened the onset-latency of the conditioned eyeblink responses ($p = 0.0008$ and $p = 0.005$ respectively; $n = 7$; Fig. 8B). In contrast, in naïve mice optogenetic stimulation with
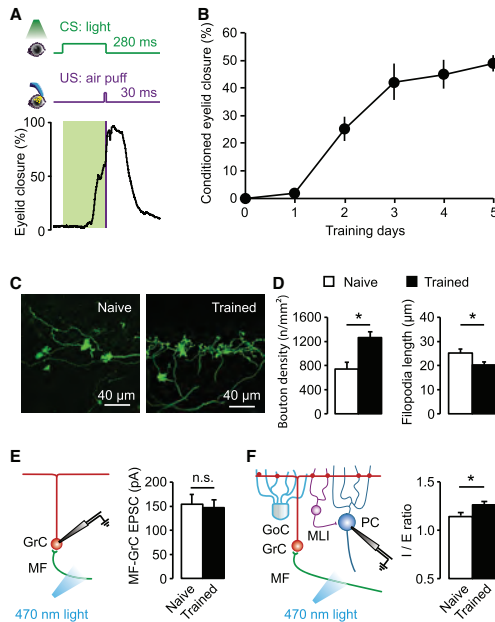
197

Figure 7 Plastic change in wiring of nucleocortical MF filopodia can be associated with classical eyeblink conditioning. (A) Scheme of eyeblink conditioning paradigm and representative trace of eyelid position in a conditioned mouse. CS and US indicate conditional stimulus and unconditional stimulus, respectively. **(B)** Development of conditioned eyeblink responses over five training days (n = 9). **(C)** Example images of nucleocortical MFs (NC-MFs) in lobule simplex (HVI) of naïve and trained mice. **(D)** Filopodial boutons in trained mice (n = 9) show a higher local density, yet a shorter length, compared with those in naïve mice (n = 8). **(E)** Summary of EPSC peak amplitudes at the nucleocortical MF to GrC synapses in naïve and eyeblink conditioning trained mice (naïve = 9, trained = 10). **(F)** The feedforward inhibition/excitation ratio was enhanced in trained mice (naïve 1.14 ± 0.03, n = 28, trained 1.26 ± 0.02, n = 20). Data show mean $\pm$ s.e., * $p < 0.05$, student's t-tests.

maximum light intensity did not induce conditioned eyeblink responses (Fig. S5), indicating that for the eyeblink conditioning paradigm, the nucleocortical loop could serve as a gain amplifier of the learned CS response. Importantly, the optogenetic stimulation confirmed an increased action potential firing (p = 0.001) of putative MLIs (Badura et al., 2013) and decreased simple spike firing (p = 0.04) in the majority of PCs in lobule simplex (Figs. 8C and 8D) *in vivo*, consistent with the GrC activation of MLIs and predominant feedforward inhibition onto PCs following nucleocortical activation, described above, as well as with the general changes in firing frequency of these neurons during eyeblink conditioning (ten Brinke et al., 2015).

If nucleocortical MFs contribute to eyeblink conditioning by providing internal amplification signals to the granular layer, one should also be able to quantify this contribution by acutely blocking these signals. We therefore tested another group of trained mice, in which the inhibitory opsin, archaerhodopsin (eArch3.0), was virally expressed in IpN neurons. Dampening the activity of their nucleocortical MFs optogenetically for 250 ms with amber light (590 nm) in lobule simplex at CS onset resulted in a significant reduction by $32 \pm 3\%$ in the amplitude of the conditioned
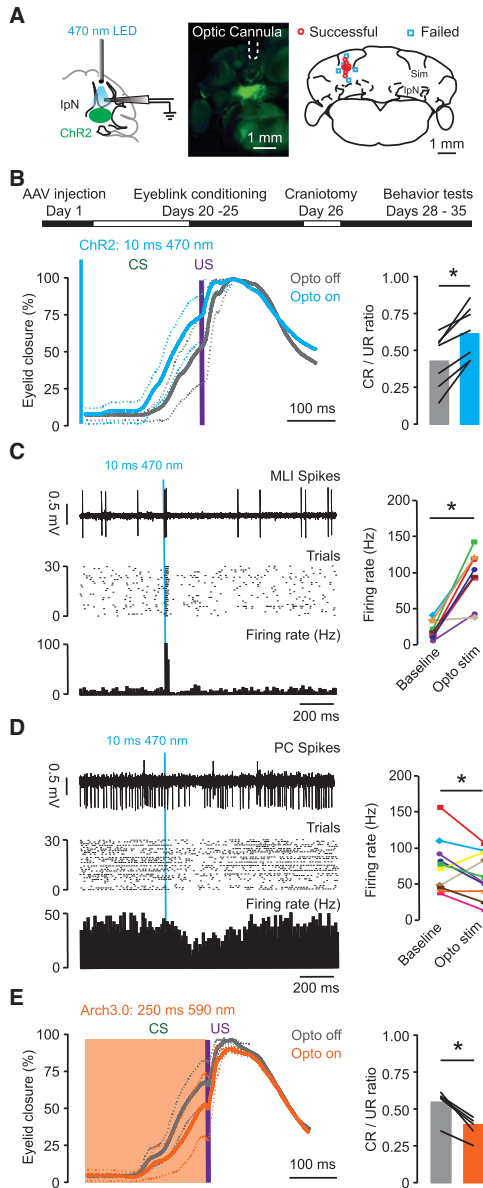
Figure 8 Nucleocortical pathway amplifies amplitudes of conditioned eyeblink response. (A) Left: experimental setup of *in vivo* recording and optogenetic stimulation. Optogenetic activation of NC-MF in the cerebellar cortex. Middle: example of location of the optic cannula in lobule simplex (dashed white line). Right: Summary of verified cannula locations in a group of successful and failed experiments. **(B)** Top: experimental setup of optogenetic manipulation during behavioral testing. Bottom left: conditioned eyeblink responses in a trained mouse, in the presence (blue) or absence (grey) of 10 ms optogenetic activation of NC-MF pathway. CS: conditional stimulus, US: unconditional stimulus. Bottom right: optogenetic activation of NC-MF pathways enhances the amplitude of conditioned eyeblink responses in trained mice. **(C)** optogenetic activation of a molecular layer interneuron. Left top: a representative trace of increased firing of a molecular layer interneuron in the eyeblink region upon optogenetic activation; 10 ms light stimulation is indicated in blue. Middle and Bottom: Raster plot and cumulative histogram of 30 consecutive trials. Right: summary of responsive MLI action potential firing upon 10 ms photo-stimulation (n = 9). **(D)** Left: suppression of Purkinje cell firing following optogenetic stimulation of NC-MFs. Top: a representative trace of decreased Purkinje cell firing upon optogenetic activation. Middle and Bottom: Raster plot and cumulative histogram of 30 consecutive trials. Right: summary of responsive Purkinje cells with both decreased (n = 7) and increased (n = 3) action potential firing upon 10 ms optogenetic stimulation. **(E)** Left: conditioned eyeblink responses in a trained eArch3.0 mouse, in the presence (orange) or absence (grey) of 250 ms eArch3.0 optogenetic dampening of NC-MF pathway (superimposed with CS). Right: optogenetic dampening of NC-MF pathways reduces the amplitude of the conditioned eyeblink response in trained mice. Data show mean $\pm$ s.e., * $p < 0.05$, student's t-tests.

199

eyeblink response (p = 0.003, n = 5; Fig. 8E). Instead, dampening nucleocortical MF activity without a CS did not induce an apparent eyeblink response or any other obvious type of motor behavior (Fig. S5), making it unlikely that the optogenetically ChR2-driven behavioral effects described above resulted from antidromic effects in nucleocortical MFs.

Discussion

The main findings of our study indicate that activity of the nucleocortical MF projection in the cerebellum contributes to gain control of learned eyeblink responses by providing internal amplification signals of an excitatory corollary discharge to the granular layer, which in turn is converted into PC inhibition via activation of MLIs. These findings corroborate the concept that increases in MLI activity and suppression of simple spikes correlate strongly with the amplitude of conditioned eyeblink responses (ten Brinke et al., 2015). Thereby, we establish for the first time a functional role for internal feedback of a corollary discharge from the cerebellar nuclei to the cerebellar cortex. To date, implications of such feedback signals have also been described in models of other major networks in sensorimotor control, such as cerebral cortex, superior colliculus, striatum and spinal cord (Hantman and Jessell, 2010; Kalinovsky et al., 2011; Sommer and Wurtz, 2008). In general, feedback of corollary discharge can facilitate the prediction of sensory consequences of movements and improve learning and preparation of movements (Crapse and Sommer, 2008; Requarth and Sawtell, 2014). For models on cerebellar learning this fast internal feedback mediated by MFs may complement the external feedback provided by the CF system (Cerminara and Apps, 2011; Llinás, 2011; Voogd and Glickstein, 1998), which is slower but better designed to reset the phase and onset of motor programs in the modules (De Zeeuw et al., 2011; ten Brinke et al., 2015; Yarom and Cohen, 2002). Indeed, since both the MF and CF systems operate within the settings of the olivocerebellar modules, together they present a rich and complementary, computational repertoire to coordinate motor learning (Fig. 9). For instance, the fast internal feedback loop appears well designed to amplify the amplitude of conditioned responses directly after the movement is initiated, whereas the external loop may reset the motor cycle and speed up the onset of subsequent trials (De Zeeuw and ten Brinke, 2015; Welsh, 2002). Interestingly, the internal and external, excitatory loops may use in part comparable mechanisms within the module(s) involved. Both feedback loops may introduce strong synchronized pauses in PC firing, which in turn can disinhibit CN premotor firing, potentially facilitated by rebound firing and activation by MF and CF collaterals (Bengtsson et al., 2011; De Zeeuw et al., 2011; Hoebeek et al., 2010; Person and Raman, 2012; cf. Alvina et al., 2008).

Given that the internal feedback loop provided by the nucleocortical MF afferents enhances simple spike suppression and that reduced PC activity in turn enhances activity in the cerebellar nuclei neurons, one should consider the possibility that signaling in this loop saturates through internally reinforcing mechanisms (Fig. 9). Although some level of reinforcement learning in the cerebellar cortex and nuclei may actually be beneficial for acquisition, consolidation and/or savings of conditioned
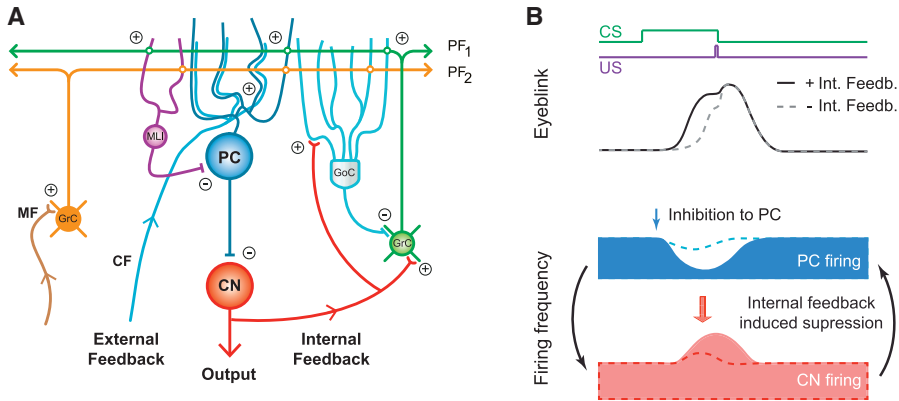
Figure 9 Circuitry and function of nucleocortical circuit. (A) Schematic illustration of a cerebellar nucleocortical circuit in which feedforward and feedbackward circuits coexist. The feedforward circuit involves mainly precerebellar mossy fiber (MF) inputs to the cerebellar cortex, whereas the feedbackward circuits entail both a well-known external system mediated by the climbing fibers (CFs) and an internal system, the function of which is described in the current paper. Excitatory and inhibitory synaptic connections are indicated by a plus- and minus-sign, respectively. GrCs, GoCs, MLI, CN and PC indicate granule cells, Golgi cells, molecular layer interneuron, cerebellar nuclei neuron and Purkinje cell, respectively. **(B)** Simplified model indicating how cerebellar cortical firing can be influenced by the nucleocortical loop that mediates the internal feedback. After the onset (blue arrow) of the increased inhibitory input from the MLIs onto the PCs the firing of CN neurons will increase (red arrow), which in turn will be fed back to neurons in the granular layer (black arrow on the right) further enhancing the interneuron activity and weakening PC firing frequency. As a consequence, such a computational loop leads to a stronger inhibition of Purkinje cells simple spike firing and higher peak amplitude of firing of cerebellar nuclei neurons (CNs), ultimately resulting in an enhanced eyelid closure. Solid and dashed lines indicate outcomes with and without internal feedback, respectively.

eyeblink responses (Campolattaro and Freeman, 2009; Medina et al., 2000; Medina et al., 2002), there are several projections in place that might prevent complete saturation. For example, there are also, next to the excitatory internal feedback loop, several types of inhibitory projections from the nuclei to the cerebellar cortex that might operate as an inhibitory internal feedback loop. Indeed, following retrograde tracing of WGA-HRP-colloidal gold complex from the cerebellar cortex to the cerebellar nuclei combined with immunocytochemistry, approximately 9% of the retrogradely labeled cells were found to be GABAergic (Batini et al., 1992). In addition, using a viral approach different from the one we applied in the current study, Uusisaari and colleagues recently showed that part of the nucleocortical afferents are glycinergic and selectively inhibit neurograinin-positive Golgi cells, which in turn could enhance granule cell activity (Ankri et al., 2015). To what extent these inhibitory projections provide similar mossy fibers with a similar tendency for structural plasticity during learning and to what extent they can prevent saturation within the excitatory internal feedback remains to be elucidated. However, it is unlikely that they operate in the exact same fashion as the corollary discharge during eyeblink conditioning described in the present study, because they will not mediate an excitatory signal to the mesodiencephalic junction and thus not mediate an efference copy to this area to control premotor activity (De Zeeuw and Ruigrok, 1994). The only inhibitory projection neurons known to leave the cerebellar anlage without targeting the inferior olive are the glycinergic neurons in the medial cerebellar nucleus, which project to vestibular and

reticular neurons in the ipsilateral brainstem (Bagnall et al., 2009), i.e. areas unlikely to be involved in eyeblink conditioning (Boele et al., 2010). So, if the inhibitory nucleo-cortical afferents prevent saturation in the excitatory nucleocortical pathway, they can strictly do so within the internal feedback loop, and not by intervening directly with the corollary discharge at the output level.

Another possible pathway that may provide homeostatic control and thus prevent saturation is formed by the GABAergic fibers that mediate the inhibitory input from the cerebellar nuclei to the inferior olive (Best and Regehr, 2009; Chen et al., 2010; de Zeeuw et al., 1988). When the simple spike activity of the PCs decreases following activation of the excitatory internal feedback loop as described above, the activity of these GABAergic neurons will increase and thus exert a stronger inhibition onto the olivary neurons, which in turn will reduce the climbing fiber signals and complex spikes in the PCs within the same olivocerebellar module (De Zeeuw et al., 2011). This reduction in complex spike activity will lead to an increase in simple spike activity, because climbing fiber activity induces various forms of short-term and long-term plasticity that will suppress simple spike activity (Gao et al., 2012). Thus, ultimately the initial decrease in simple spike activity leads to a reactive increase in simple spike activity through homeostatic activity in the external olivocerebellar feedback loop, thereby compromising the reinforcing mechanisms in the internal feedback loop that by itself could run into a state of saturation. Interestingly, it is most likely the complex spikes that depend on the GABAergic nucleo-olivary projection that contribute to the moment of onset of the CR (ten Brinke et al., 2015). Thus, this latter homeostatic mechanism appears particularly well designed to prevent the emergence of ill-timed circuits through self-reinforcing processes.

Finally, extracerebellar MF systems may also impose strong excitatory inputs to PCs. The morphological and physiological properties of the extracerebellar MF inputs are diverse (Chabrol et al., 2015; Palay and Chan-Palay, 1974) and part of these inputs may well convey strong excitatory inputs upon sensorimotor stimulation (Rancz et al., 2007). Thus, in principle this type of MF may also excite PCs via the granule cell-parallel fiber pathway and counteract the progression of the positive internal feedback.

Together, our findings on the amplifing role of the internal feedback loop provided by the excitatory nucleocortical afferents complement the well-studied olivo-cortico-nuclear modules with a robust and dynamic intra-cerebellar closed-loop architecture that allows reinforcement in a controlled manner. The data imply that feedforward as well as feedback circuitries, the two main architectures of neural computation in the brain, are orchestrated in the cerebellum to adaptively control demanding sensorimotor processing.

Methods

Animals

Male and female mice (C57BL/6) used for all the experiments were between 3 to 6 months of age and individually housed (food *ad libitum*, 12:12 light/dark cycle). All

experimental protocols were approved by the institutional animal welfare committee (Erasmus MC, Rotterdam, The Netherlands).

Stereotaxic injections   Mice were anesthetized with a mixture of isoflurane/oxygen (5% for induction, 1.5-2.0% for maintenance). Rimadyl (5 mg/kg) and buprenorphine (0.05 mg/kg) were applied intraperitoneally 30 mins prior to surgery. Body temperature was monitored and kept constant at 37°C throughout the entire surgical procedure. A patch of skin above the skull was removed and local anesthetic (lidocaine) was topically applied. The skull was prepared with Optibond prime and adhesive (Kerr, Switzerland) and a pedestal was attached with Charisma (Heraeus Kulzer, NY, USA). Mice were then positioned on a custom-made mouse stereotaxic head-holding frame. Small craniotomies (0.2 mm) were made in corresponding sites and injections were performed using glass pipettes (tip opening between 5 and 10 μm) with mechanical pressure. For AAV injections, 60-120 nl of AAV2-hSyn-hChR2(H134R)-eYFP or AAV2-hSyn-eArch3.0-eYFP (10^{12}-10^{13} infectious units per ml, packaged by the UNC Joint Vector Laboratories, RRID: SCR_002448) were injected at a speed of 10 nl/min. For tracer injections, 20-100 nl Biotin Dextran Amine 10 kDa solution (10% w/v in saline, Life Technologies) and fluorescent Cholera toxin subunit-B (Ctb Alexa Fluor 488 and Ctb Alexa Fluor 555, 5% w/v in saline, Life Technologies) were injected at a speed of 10 nl/min. After each injection, the pipette was left in place for >10 minutes before being slowly withdrawn. Coordinates used for injections into the red nucleus were: 0.5 mm to Lambda, 0.5 mm lateral to midline and -4 mm ventral; for injections into the cerebellar lobule simplex: -2.0 mm to Lambda, 2.0 mm lateral to midline and -1.5 mm ventral; for injections into the interposed nucleus: -2.5 mm to Lambda, 2.5 mm lateral to midline and -2.3 mm ventral; for injections into the pontine nucleus: -0.5 mm to Lambda, 0.5 mm lateral to midline and -5.5 mm ventral. All mice were allowed to recover for >3 days before any subsequent procedure. Mice used for the optogenetic stimulations and extracellular recordings were subjected to additional surgery. 2-3 weeks after the virus injection (see above), under the same surgical conditions described above, an optic cannula (400 μm core, 0.39 NA, Thorlabs) was implanted into the lobule simplex with coordinates: -2.0 mm to Lambda, 2.0 mm lateral to midline and -0.5 to -1.0 mm ventral. A craniotomy (1.5 mm in diameter) was placed above Crus 1 and 2 to access the lobule simplex and the interposed nuclei. Antibiotic solution (Baytril 0.5%, Enrofloxacine 5 mg/ml) was applied topically after each experiment.

Eyeblink conditioning training

Head restrained mice were placed on top of a cylindrical treadmill and allowed to walk freely, see also (Heiney et al., 2014). We used a green LED placed 5-10 cm in front of the mouse as conditioned stimulus (CS). The duration of the CS for all the experiments was kept at 280 ms. The unconditional stimulus (US) consisted of an air-puff of 30 psi, 1 cm from the animal's cornea. The onset of the puff was 250 ms after the CS onset (inter-stimulus interval) and the duration was 30 ms, resulting in a co-termination of both stimuli. National Instruments NI-PXI (National Instruments, Austin TX, USA) processor was used to trigger and keep track of stimuli whilst

capturing data. Eyelid position was illuminated by infrared LED light and recorded with a 250 fps camera (scA640-120gc, Basler, Ahrensburg, Germany) driven and acquired by custom written routines in LabVIEW. Mice were allowed to habituate on the treadmill for 2 days and followed by acquisition, in which 2 consecutive sessions were presented daily, each session consisting of 100 paired CS-US trials with inter-trial interval (ITI) 5-10 sec. The acquisition sessions were repeated for at least 5 consecutive days.

Optogenetics and electrophysiology *in vivo*

After the behavioral training and the placement of the optic cannula, we extracellularly recorded *in vivo* with or without optogenetic manipulation of the nucleocortical projecting fibers. For extracellular single-unit recordings, borosilicate glass pipettes (OD 1.5 mm, ID 0.86 mm, tip diameter 1-2 μm, Harvard Apparatus, Holliston, MA, USA) filled with 2 M NaCl were positioned stereotactically into the target regions using an electronic pipette micromanipulator (SM7; Luigs & Neumann, Ratingen, Germany). The behavioral responses and the neuronal activity were recorded in response to a brief pulse of light delivered to the brain via an optic fiber coupled with LED light sources (470 nm light for ChR2: M470F1; 590 nm light for eArch3.0 M590F1, Thorlabs). A brief pulse of 1-10 ms blue (470 nm) light or a 250 ms pulse of amber light (590 nm) was used to induce the activation or inhibition of nucleocortical mossy fibers. To avoid direct stimulation of CN soma, we only included data that met all the following criteria: 1) optic cannula were located in the superficial layer of the lobule simplex (see Fig. 8A); 2) optogenetic stimulation/inhibition was adjusted such that no instantaneous increase/decrease of action potential firing in the CN was observed; 3) optogenetic stimulation/inhibition did not result in instantaneous eyeblink responses; and 4) optogenetic stimulation/inhibition did not alter locomotion behavior (Fig. S5). Locomotion was monitored using an incremental encoder coupled to the shaft of a cylindrical treadmill (EH30, Eltra, Italy). Purkinje cells were identified by the occurrence of simple spikes and complex spikes and were confirmed to be single unit by the occurrence of climbing fiber pause (Schonewille et al., 2010). Putative molecular layer interneurons were identified as previously described (Badura et al., 2013). CN neurons were identified by their stereotactic location and the characteristic neuronal activity (Hoebeek et al., 2010). Electrophysiological recordings were acquired with a Multiclamp 700B amplifier (Molecular Devices, Sunnyvale, USA) and band-pass filtered at 100-5,000 Hz. Electrophysiological and behavioral data were digitized synchronously using Digidata 1440A (Molecular Devices, Sunnyvale, USA) at 50 kHz. All *in vivo* data were analyzed using SpikeTrain software (Neurasmus BV, Rotterdam, The Netherlands) running under Matlab (Mathworks, MA, USA). Molecular layer interneurons and Purkinje cells were considered responsive if the post-optogenetic-activation firing frequency (measured <200 ms after the offset of light) exceeded 3 times standard deviation of the pre-optogenetic-activation frequency (measured 500 ms before the onset of light).

Optogenetics and electrophysiology *in vitro*

AAV injected mice were sacrificed >3 weeks post injection for *in vitro* experiments. Mice were decapitated under anaesthetized with isoflurane. 300 μm thick cerebellar coronal slices were cut on a vibratome (VT1200s, Leica, Wetzlar, Germany) in ice-cold slicing medium containing (in mM): 240 Sucrose, 5 KCl, 1.25 Na_2HPO_4, 2 $MgSO_4$, 1 $CaCl_2$, 26 $NaHCO_3$ and 10 D-Glucose, bubbled with 95% O2 and 5% CO_2. Slices were incubated at 34°C for 1 h in the oxygenated ACSF containing (in mM): 124 NaCl, 2.5 KCl, 1.25 Na_2HPO_4, 1 $MgSO_4$, 2 $CaCl_2$, 26 $NaHCO_3$ and 25 D-Glucose and kept at room temperature (21 $\pm$ 1 °C) before use. All the experiments were performed with a constant flow of oxygenated ACSF (1.5-2.0 ml/min) at 34 $\pm$ 1 °C. Cerebellar neurons were visualized using an upright fluorescent microscope (Axioskop2 FS plus, Carl Zeiss, Jena, Germany) equipped with a 40X water immersion objective. A GFP filter was used to visualize the eYFP labeled mossy fiber terminals. Exposure time to epifuorescent light was kept short to prevent over activation of ChR2 with blue light. Acquired fluorescent images were digitally aligned with the DIC images for identifying eYFP positive mossy fiber rosettes. Whole cell and cell attached patch-clamp recordings of nucleocortical mossy fiber rosettes, granule cells, Golgi cells, Purkinje cells, and cerebellar nuclei neurons were performed under DIC visualization. Patch-clamp recordings were performed using an EPC-10 double amplifier controlled by the Patchmaster software (HEKA electronics, Lambrecht, Germany). All recordings were low-pass filtered at 5 kHz and digitized at 20 kHz. Borosilicate glass pipettes (WPI) were filled with intracellular solution containing the following (in mM): 120 K-gluconate, 9 KCl, 10 KOH, 3.48 $MgCl_2$, 4 NaCl, 10 HEPES, 4 Na_2ATP, 0.4 Na_3GTP and 17.5 sucrose (pH 7.25) and had pipette resistances of 8-10 MΩ for recording mossy fiber rosettes, 4-6 MΩ for recording granule cells and Golgi cells, and 3-4 MΩ for recording Purkinje cells and cerebellar nuclei neurons. Optogenetic stimulation was delivered via the epifluorescent light path. The light intensity was adjusted to 0.1 - 4 mW/mm^2. The light path was controlled by a mechanical shutter (LS2, Vincent Associates, USA). The shutter opening jitter was measured to be 3 ms and was subtracted from all the onset times of the EPSCs driven by optogenetic manipulation. EPSCs in granule and Golgi cells were recorded by holding cells at -70 mV in voltage-clamp mode. Action potential firing was recorded in current-clamp mode without holding current (I = 0). For comparing the inhibition/excitation (I/E) ratios following optogenetic activation of nucleocortical MFs afferents with that of the local electrical activation of a mixed group of MFs, we chose only the Purkinje cells in the lobule simplex that showed clear optogenetically induced EPSCs. For electrical stimulation, a second electrode connected with an Iso-Flex stimulus isolator (A.M.P.I., Jerusalem, Israel) was placed in the white matter adjacent to the recorded Purkinje cells. EPSC and IPSC components were isolated with intracellular solution containing: 120 Cs-gluconate, 10 CsOH, 3.48 $MgCl_2$, 4 NaCl, 10 HEPES, 4 Na_2ATP, 0.4 Na_3GTP and 17.5 sucrose (pH 7.25). EPSCs were acquired at -75 mV, close to the reversal potential of GABAA receptors. The electrical stimulation intensity was adjusted so that the EPSC amplitude was comparable to that of the optogenetic stimulation. The IPSC components were subsequently recorded with holding potential of 0 mV, close to the reversal potential of AMPA receptors. The ratio of the positive peak amplitude at 0 mV and negative peak amplitude at -75 mV was taken as a function of the I/E ratio. To compare the

electrophysiological properties of cerebellar neurons between naïve and trained mice, we repeated similar patch clamp recordings in granule cells and Purkinje cells in a group of mice that were fully trained with the eyeblink conditioning paradigm (see eyeblink conditioning section).

Immunohistochemistry and analysis

Mice were deeply anesthetized with an overdose of Nembutal (i.p.) and transcardially perfused with 20 ml saline followed by 50 ml 4% PFA. Brains were extracted and post-fixed overnight in 4% PFA at 4°C. Brains were subsequently embedded in gelatine and cryoprotected in 30% sucrose in PB, frozen on dry ice, and sectioned using a freezing microtome (40 μm thick). For light microscopy analysis of the mice injected with BDA, free-floating sections were blocked for 1h at room temperature in 10% NHS PB solution with 1% triton and visualized with the avidin-biotin-peroxidase complex method (ABC) (Vector Laboratories, Burlingame, USA,) and diaminobenzidine (DAB, 0.05%, Life Technologies) as the chromogen. For immunofluorescent staining, free-floating sections were blocked for 1 h at room temperature in PBS with 0.4% Triton X-100 and 10% NHS solution and incubation 48 hrs at 4°C in a mixture of primary antibodies diluted in PBS with 2% NHS and 0.4% Triton X-100. Sections were then washed and incubated for 2 h at room temperature in a mixture of fluorescent secondary antibodies. Primary antibodies used were rabbit anti-VGlut1 (1:1000, Synaptic Systems, RRID: AB_887876), guinea pig anti-VGlut2 (1:1000, Millipore, RRID: AB_1587626), mouse anti-Calbindin D28K (1:7000, Sigma, RRID: AB_2313712), and goat anti-*Zebrin II* (1:1000, Santa Cruz, RRID: AB_2226594). Slices were then counterstained with DAPI (1:100,000, Invitrogen) and mounted with mounting medium for fluorescence (Vectashield H-1000). All images were acquired on an upright LSM 700 confocal microscope (Carl Zeiss, Jena, Germany) and post-hoc adjusted and analyzed in FIJI software with appropriate plugins (http://pacific.mpi-cbg.de). Ctb labeled neurons were recognized as ''web-like'' Golgi apparatus labeling surrounding DAPI labeled cell nuclei, distinct from bouton-like labeling of Purkinje cell axon terminals (Fig. 1). For visualization of the granule and Golgi cell morphology after *in vitro* electrophysiological recordings, Alexa Fluor 555 or 594 (20 μM, Life Technologies) were added to the intracellular solution. For detailed quantification of CN neuron morphology, biocytin (1% w/v) was added to the intracellular solution and visualized with streptavidin Alexa Fluor 488 (1:400, Life Technologies). Immediately after recording, cerebellar slices were fixated in 4% PFA at room temperature for 2-5 hrs, washed in PBS and mounted with mounting medium for fluorescence (Vectashield H-1000). To prevent shrinkage and distortion of thick sections, special care was taken during mounting processes. Cell morphology was acquired on an upright LSM 700 confocal microscope (Carl Zeiss, Jena, Germany) and quantified with FIJI and Neurolucida (MBF bioscience, Williston, USA) software. Nucleocortical projecting IpN neurons were defined following reconstruction of the cell body and axonal projection (see Fig. 5). We consider that potential non-nucleocortical projecting neurons are the neurons of which both dendritic tree and axonal projection towards cerebellar peduncle appeared complete, yet no cortical projection was observed.

Immuno-electron microscopy

BDA injected mice were anesthetized with an overdose of nembutal (i.p.) and transcardially perfused with 10 ml saline and subsequently 50 ml 4% PFA and 0.5% glutaraldehyde in cacodylate buffer. Cerebellum was removed and post-fixed overnight in 4% PFA. 80-μm thick coronal sections were cut on a vibratome (Technical Products International, St. Louis, USA). BDA labeled MF rosettes were visualized by incubating the sections with the avidin-biotin-peroxidase complex method (ABC) for 24-48 hrs (Vector Laboratories, USA) and subsequently developed with DAB (0.05%, Life Technologies) as the chromogen. The vibratome sections were rinsed and post-fixed in 1% osmium tetroxide, stained with 1% uranyl acetate, dehydrated and embedded in araldite (Durcupan ACM; Fluka, Buchs, Switzerland). Ultrathin (50-70ănm) sections were cut on an ultramicrotome (Leica, Wetzlar, Germany), mounted on formvar-coated copper grids and contrasted with 2% uranyl acetate and 1% lead citrate (Fluka). For postGABA immunocytochemistry, the grids were rinsed in 0.5 M of Tris buffer with 0.9% NaCl and 0.1% Triton X-100, pH 7.6 (TBST), and incubated overnight at 4°C in (Sigma, 1:1500 in TBST). The grids were subsequently rinsed twice with TBST and incubated for 1 h at room temperature in goat anti-rabbit IgG labeled with 10 nm gold particles (Aurion) diluted 1:25 in TBST. Cerebellar sections containing BDA positive MFs were photographed using an electron microscope (Philips, Eindhoven, Netherlands). Electron micrographs were analyzed using FIJI software.

Statistical methods

Values are represented as mean s.e.; p values of <0.05 were considered significant and are reported in the main text. Statistical analysis was done using student's t-test, unless stated otherwise.
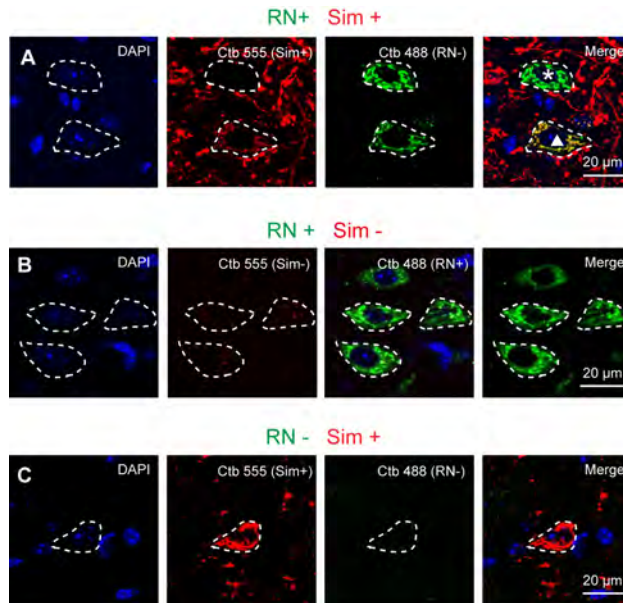
Supplementary Material

Figure S1 (Related to Fig. 1) Representative neurons in the IpN with retrograde labeling from red nucleus (RN, Ctb Alexa 488, green) and lobule simplex (Sim, Ctb Alexa 555, red). (A) Confocal images showing co-labeled IpN neurons (triangle) and a neighboring neuron with RN labeling only (asterisk). **(B)** Confocal images showing IpN neurons with retrograde labeling from RN only. **(C)** Confocal images showing an IpN neuron with retrograde labeling from Sim only.
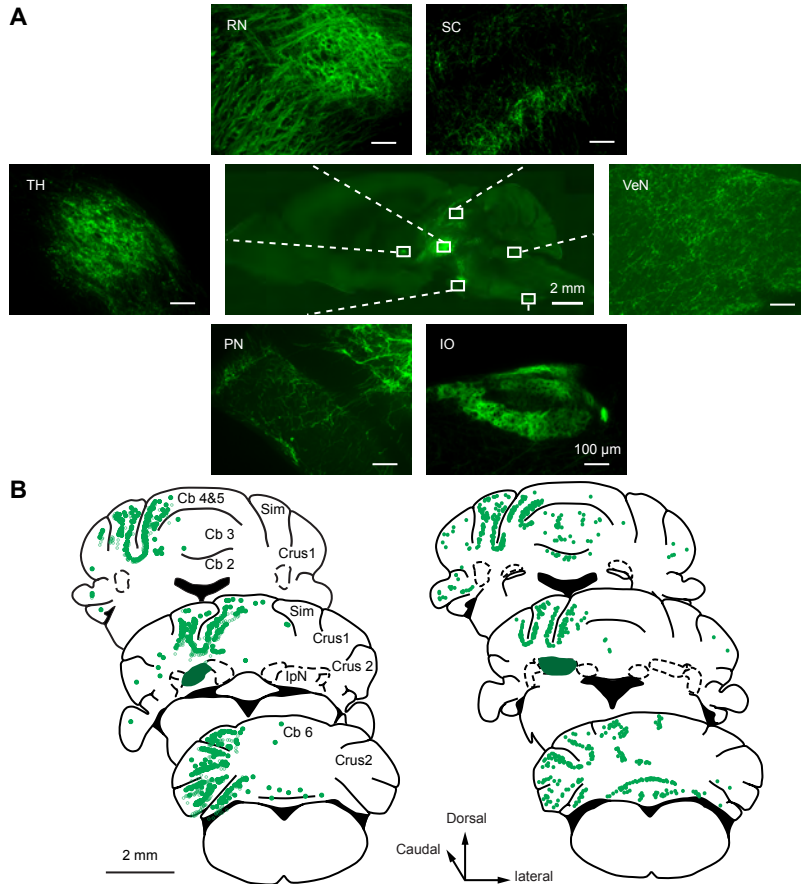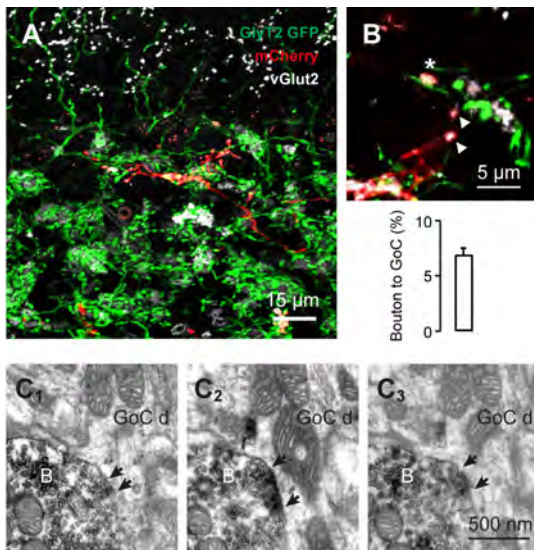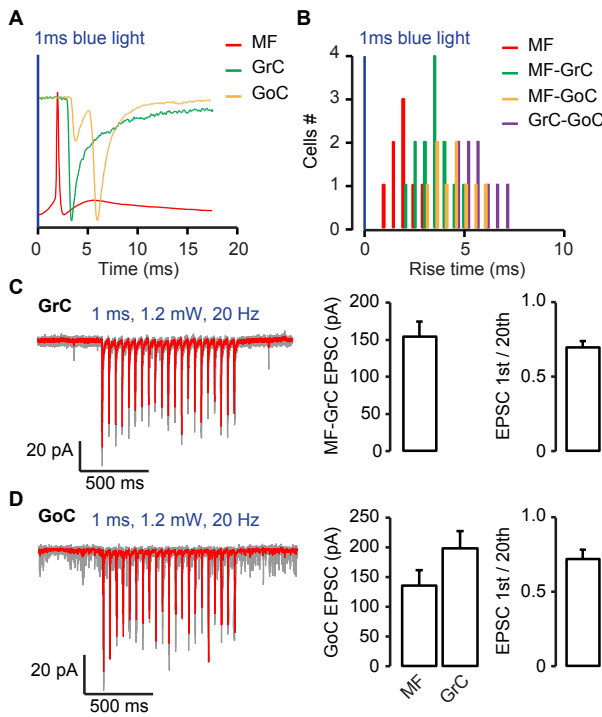
Figure S2 (Related to Fig. 1) eYFP labeled axonal projections in the IpN targeting regions. (A) Middle: Overview of axonal labeling throughout mouse brain in a sagittal section. Widespread axonal labeling can be found in the mouse in which 100 nl of AAV2-hSyn-hChR2(H134R)-eYFP was injected in the IpN nucleus. Surrounding: High magnification images indicating axonal labeling in the thalamus (TH), red nuclei (RN), superior colliculus (SC), vestibular nuclei (VeN), pontine nuclei (PN) and inferior olive (IO). **(B)** Representative distribution of nucleocortical MF rosettes in the cerebellar cortex. Schematics show coronal sections from two mice, throughout the regions in which dense nucleocortical MF labeling was observed. The initial IpN injection sites are indicated in dark green contours.
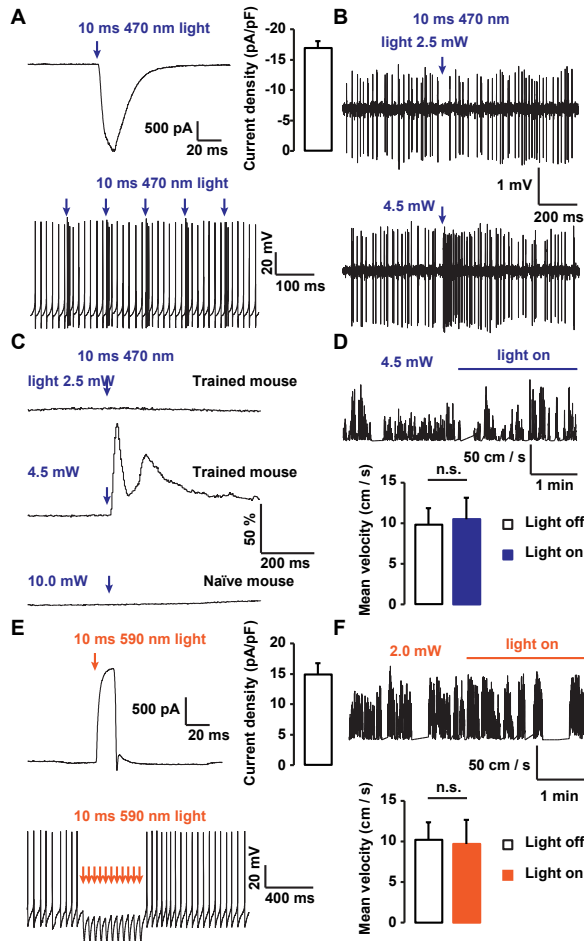
Figure S3 (Related to Fig. 4) Robust and sustained synaptic transmission between nucleocortical MF and cerebellar cortical neurons. **(A)** Monosynaptic delay between MF action potential and triggered EPSCs in GrC and GoC. Representative traces of triggered MF action potential, GrC EPSC and GoC EPSC. Traces are normalized for their amplitude and aligned to the start of light pulse. **(B)** Summary of the onset latency of the nucleocortical MF action potential (n = 10), MF-GrC EPSC (n = 13), MF-GoC and GrC-GoC EPSC (n = 9). **(C)** Sustained synaptic transmission from nucleocortical MF in response to repetitive stimulation. Left: 5 repetitive traces of MF-GrC EPSCs (gray) and the overlaying averaged trace (red) in response to an optogenetic train stimulation of 20 Hz. Right: summary of first EPSC amplitude and the ratio between the 1st and 20th EPSC during the train stimulation. **(D)** Similar to C, left: MF-GoC EPSC in response to an optogenetic train stimulation of 20 Hz. Right: summary of first EPSC amplitude and the ratio between the 1st and 20th EPSC during the train stimulation.

Figure S4 (Related to Fig. 6) Filopodial boutons form functional synapses with granule and Golgi cells. **(A)** Representative image of a nucleocortical MF with filopodia protrusions in the cerebellum of GlyT2-eGFP mice. **(B)** Inset shows a vGlut2 positive filopodial bouton contacting a GlyT2-GFP positive Golgi cell dendrite (asterisk). Note that the surrounding boutons without contacting Golgi cell dendrites are indicated with arrowheads. Bar chart quantification shows the percentage of vGlut2 positive filopodial boutons that contact Golgi cell dendrites (21 MFs, n = 2). **(C)** Representative serial EM images of a BDA labeled filopodial bouton with synaptic contacts onto Golgi cell dendrites, as visualized with immunogold labeling. Arrows indicate synaptic contacts.

Figure S5 (Related to Fig. 8) Optogenetic control of nucleocortical activity and behavioral output. (A) Top left: photo current recorded from a ChR2 expressing CN neuron in response to a brief pulse of blue light. Top right: summary of photo current density in ChR2 expressing CN neurons (n = 4). Bottom: example traces showing that five light pulses reliably drive CN cell to fire extra action potentials. **(B)** Representative CN firing pattern *in vivo*. The optogenetic light intensity was gradually adjusted to probe the threshold for CN neuron direct activation (2.5 mW sub-threshold v.s. 4.5 mW supra-threshold). For eyeblink conditioning experiments in Fig. 8, light intensity was individually adjusted such that it did not exceed the CN activation threshold *in vivo*. **(C)** Optogenetic stimulation drives eyelid closure; 10 ms 4.5 mW, but not 2.5 mW light stimulation directly drives eyelid closure in eyeblink conditioned mouse. Maximum light intensity did not induce detectable eyelid movement in naïve mice. **(D)** Prolonged subthreshold ChR2 optogenetic stimulation does not affect locomotion on the treadmill. Top: representative traces of running speed with/without optogenetic stimulation; bottom: summary of mean velocity (n = 6). **(E)** Top left: Photo current from an Arch3.0 expressing CN neuron in response to a brief pulse of amber light. Top right: summary of photo current density in Arch3.0 expressing CN neurons. Bottom: Five light pulses reliably drive CN cell to fire extra action potentials. Note the ChR2 in (A) and Arch3.0 expressing neurons in E show similar absolute current densities in our experiments. **(F)** Prolonged sub-threshold Arch3.0 optogenetic stimulation does not affect locomotion on the treadmill. Top: representative traces of running speed with/without optogenetic stimulation; bottom: summary of mean velocity (n = 5). Data show mean ± s.e., paired student's t-tests.

Supplementary Table 1 (related to Fig. 1)
Summary of nucleocortical mossy fiber distribution ipsilateral to the IpN injected with AAV vectors.

Mice	MF counted	MF per area (%)									lobules	
		Fl	PFl	PM	Cop	Crus 1	Crus 2	Sim	1-3	4-6	7-10
1	989	1.6	0.8	3.0	8.9	18.7	9.5	25.7	16.3	5.2	10.3
2	1037	1.0	0.0	0.9	7.2	12.1	3.9	25.8	27.1	17.9	4.1
3	1689	2.5	5.0	2.6	6.9	10.5	11.7	28.0	14.1	10.4	8.2
4	1100	1.2	2.5	3.0	8.9	12.1	15.2	34.2	6.1	12.0	4.9
5	1306	2.5	3.2	1.8	1.8	16.7	10.3	22.9	13.3	12.7	14.8
6	542	3.0	0.7	0.0	6.1	8.5	3.9	31.2	16.1	12.4	18.3
Mean		2.0	2.1	1.9	6.6	13.1	9.1	28.0	15.5	11.8	10.1
SD		0.8	1.9	1.2	2.6	3.9	4.5	4.1	6.8	4.1	5.6

Fl: flocculus, PFl: paraflocculus, PM: paramedian lobule, Cop: copula pyramidis, Sim: lobule simplex.

Supplementary Table 2 (related to Fig. 4)
Comparisons of electrophysiological properties between identified nucleocortical projecting neurons (NC+) and large CN neurons without detectable nucleocortical axonal projection in the IpN (NC-).

Parameter	NC + (n = 18) Mean ± s.e.	NC - (n = 14) Mean ± s.e.	t-tests
Soma size (μm^2)	359.4 ± 45.2	382.7 ± 39.2	0.31
No. Primary dendrites	4.2 ± 0.5	4.0 ± 0.3	0.60
Input resistance (MΩ)	145.5 ± 30.4	151.6 ± 25.9	0.47
Spiking threshold (mV)	-38.2 ± 1.0	-37.4 ± 1.2	0.62
Spiking amplitude (mV)	44.6 ± 0.8	44.4 ± 1.3	0.68
Rise time (ms)	1.0 ± 0.1	1.1 ± 0.1	0.56
Decay time constant (ms)	2.0 ± 0.8	2.2 ± 0.9	0.58
Spiking halfwidth (ms)	0.3 ± 0.01	0.3 ± 0.02	0.42
AHP (mV)	-12.5 ± 0.4	-13.3 ± 0.9	0.71

Supplementary Table 3 (related to Fig. 5)

Summary of the electrophysiological properties of nucleocortical MF rosettes in vitro.

	Value	n		Value	n
Spontaneous firing rate (Hz)	39.5 ± 6.0	3	Spiking threshold (mV)	41.3 ± 1.5	7
Resting potential (mV) Input	-58.3 ± 3.8	7	Spiking amplitude (mV)	40.4 ± 5.2	7
resistance (MΩ) Capacitance	387.3 ± 29.6	7	Rise time (ms)	0.3 ± 0.1	7
(pF)	3.5 ± 1.4	7	Decay time constant (ms)	0.4 ± 0.1	7
Sag ratio	0.5 ± 0.06	7	Spiking halfwidth (ms)	0.3 ± 0.1	7
1st / 10th Spike ratio	0.81 ± 0.1	7			

Part III

Olivocerebellar system

Olivary gap junction coupling facilitates formation of complex spike patterns

Olivary neurons, which provide climbing fibers to sagittal strips of Purkinje cells in the cerebellar cortex, are densely coupled by gap-junctions formed by gap-junction protein delta-2 (Gjd2). This coupling can facilitate classical conditioning and reflex movements. In addition, olivary neurons tend to oscillate due to various conductances differentially distributed across their dendritic and somatic membrane. To what extent these two properties interact at the systems level is still under debate. Here, we studied cross-correlograms of complex spike activity of Purkinje cell pairs in Crus I and Crus II using multiple single-unit recordings in awake mice. Synchronous complex spike activity happened at more constant delays in wildtype mice than in Gjd2-mutants, which lack functional gap-junctions. Moreover, only in wildtypes was there a consistent increase in these delays with medio-lateral (but not rostro-caudal) direction. Additionally, related complex spike activity in consecutive presumable oscillation cycles were less common in the mutant. Peripheral stimulation of the whisker-pad significantly altered the duration and amplitude of the cross-correlogram center-peaks and side-peaks in Gjd2 knock-outs, but less so in those of wildtypes. These data show that the presence of olivary gap junctions lead to enhanced and stabilized spatiotemporal patterning of complex spike activity in the cerebellar cortex, highlighting the impact of electrotonic coupling on oscillatory behaviour of olivary neurons.

J.K. Spanke*, C. Owens*, **M.M. ten Brinke**, K. Voges, M. Negrello, L.W.J. Bosman, & C.I. De Zeeuw (In preparation)

Introduction

The cerebellum is essential for sensorimotor coordination. Cerebellar cortex needs to integrate large amounts of data via the mossy fiber - parallel fiber pathway, modulating the simple spike activity of its sole output neuron, the Purkinje cell (Thach, 1968). One mechanism that may structure these incoming data streams are the complex spikes, which are large action potentials triggered by the other prominent cerebellar pathway, the climbing fiber input from the inferior olive (Eccles et al., 1966). Complex spike firing can act as a conductor for orchestrating simple spike activity across the cerebellar cortex, which is paramount for downstream processing at the cerebellar nuclei (Person & Raman, 2012; Atkins & Apps, 1997; Apps & Hawkes, 2009). Recent results show that phase of simple spike firing is indeed shaped by complex spike firing (Badura et al., 2013). In order for a large number of inputs from the Purkinje cell to optimally control CN firing, it has been suggested that the spatiotemporal pattern of complex spike activity of ensembles of Purkinje cells is important for both online control of movements (Welsh et al., 1995; De Zeeuw et al., 2011) as well as motor learning (Van Der Giessen et al., 2008).

The pattern of complex spike activity results from a combination of factors. First, after entering the cerebellum, single climbing fibers branch and connect with up to ten Purkinje cells within a sagittally oriented microzone, inducing synchrony in rostro-caudal direction (Armstrong et al., 1973a; Armstrong et al., 1973c; Armstrong et al., 1973b; Sugihara et al., 2001). Second, inferior olivary neurons are densely electrotonically coupled by dendrodendritic gap junctions, further enhancing the potential for synchrony (Llinás et al., 1974; Sotelo et al., 1974; De Zeeuw et al., 1995; Lang, 2002; Marshall et al., 2007). Lastly, due to a unique set of conductances, neurons of the inferior olive show sub-threshold oscillations (STO's) in their membrane potential with frequencies ranging from 1 to 3 Hz and/or 3 to 10Hz (Llinás & Yarom, 1981; Yarom Y. & Llinás, 1981; Llinás & Yarom, 1986; Khosrovani et al., 2007), on the beat of which their action potentials may ride (Llinás et al., 1974; Bloedel & Ebner, 1984; Mathy et al., 2009; Bazzigaluppi et al., 2012; Gruijl et al., 2012). To what extent the tendency to oscillate may facilitate synchronous firing remains an open question (Devor & Yarom, 2002a; Devor & Yarom, 2002b; Leznik & Llinás, 2005; Placantonakis et al., 2006; Welsh, 2002). Pharmacological blockage of gap junction coupling does not abolish olivary oscillations (Leznik & Llinás, 2005; Lang, 2002), but enhancing the oscillatory rhythm with harmaline can enhance the level of synchrony (Llinás & Sasaki, 1989; Lang et al., 1996; Jacobson et al., 2009). Intra-olivary coupling delays have not been studied in great detail and it is not quite clear at the systems electrophysiological level to what extent gap junction coupling in the olivocerebellar system can influence the oscillatory properties and related ensemble pattern formation. So far, cross-correlation studies of complex spike activity have largely focused on the zero-time bin peaks in the anesthetized or non-moving preparation, trying to tackle the mechanisms underlying synchrony (Zeeuw et al., 1996; Lang et al., 1996; Wylie et al., 1995) or restrict themselves to non-moving periods of awake recordings (Lang et al., 1999). It is also known that different phases of movement can recruit different subsets of Purkinje cells, thereby creating dynamic patterns of complex spike synchrony (Welsh et al., 1995).

218

Here, we explore the impact of olivary coupling on oscillatory pattern formation, as reflected at the cerebellar cortical level. Complex spike activity was analyzed for pairs of Purkinje cells from Crus I and II, recorded in awake mice with either functional or non-functional gap-junction protein delta-2 (Gjd2; formerly called connexin36; Long et al., 2002; De Zeeuw et al., 2003). We found that Gjd2 is essential for consistent delays between Purkinje cells'complex spike activity during the same or successive olivary oscillation cycles, highlighting the impact of coupling in the olivocerebellar system on oscillatory pattern formation in ensembles of Purkinje cells.

Results

Characterization of Gjd2 mutant and wild-type population

From simultaneous recordings made from crus I and II with a 4x8 electrode matrix (Fig. 1A, B; see Methods), 114 Purkinje cell pairs were recorded across Gjd2$^{-/-}$ mouse mutants (MT; n = 12), and 209 cell pairs were recorded across wild-type (WT) mice (n = 19; see methods). The MT and WT populations showed a similar spatial spread across medio-lateral (0.62 ± 0.39 versus 0.65 ± 0.26 mm, respectively; p = 0.33), rostro-caudal (0.51 ± 0.24 versus 0.57 ± 0.32 mm; p = 0.31) and dorso-ventral (495 ± 268 versus 526 ± 295 μm, p = 0.82) directions, and recordings had similar durations (599 ± 279 versus 598 ± 242 s; p = 0.78). However, contrary to earlier research (Van Der Giessen et al., 2008; Marshall et al., 2007), here the Gjd2 mutation resulted in significantly higher complex spike firing rates than those observed in WT's (1.41 ± 0.4 versus 1.32 ± 0.37 Hz, respectively; p = 0.03). This discrepancy may be due to the use in the current study of awake mice that were able to locomote, which has been shown to lead to increased complex spike firing rates (De Gruijl et al., 2014; Hoogland et al., 2015).

For each cell pair, cross-correlations were computed, convoluted, and significant regions were quantified in terms of strength (duration, amplitude, area) and timing (delay, asymmetry) (Fig. 1C, D; see methods). To investigate complex spikes in relation to successive olivary oscillations, we approximated the duration of a single oscillation cycle by analyzing the intervals between successive significant peaks in our WT data set. Across the whole population, there was a dominant prevalence of intervals of 100 ms between significant peaks (Fig. 1E). This value is in line with reported STO frequencies in the inferior olive, whose upper limit was reported to be around 10-12Hz (Llinás & Yarom, 1981; Yarom Y. & Llinás, 1981; Llinás & Yarom, 1986). We therefore defined 100ms time windows for complex spikes occurring in the same olivary oscillation (called the center peak time window, centered around 0ms delay) as well as in successive olivary oscillations (the side peak time windows, straddling the center peak time window; Fig. 1D).

For the WT data, 149 out of the 209 cell pairs (71.3%) showed significant correlations in their complex spike activity. In the MT data, this was the case for 92 out of 114 cell pairs (80.7%), which was not significantly different (p = 0.082, Fisher's exact test). Subsequent analyses were performed on the significant cell pairs.

The individual Purkinje cells cells presented in Fig. 2 show 10-12 Hz oscillations in their firing, as apparent from their auto-correlograms (Fig.2 B), with the WT popu-
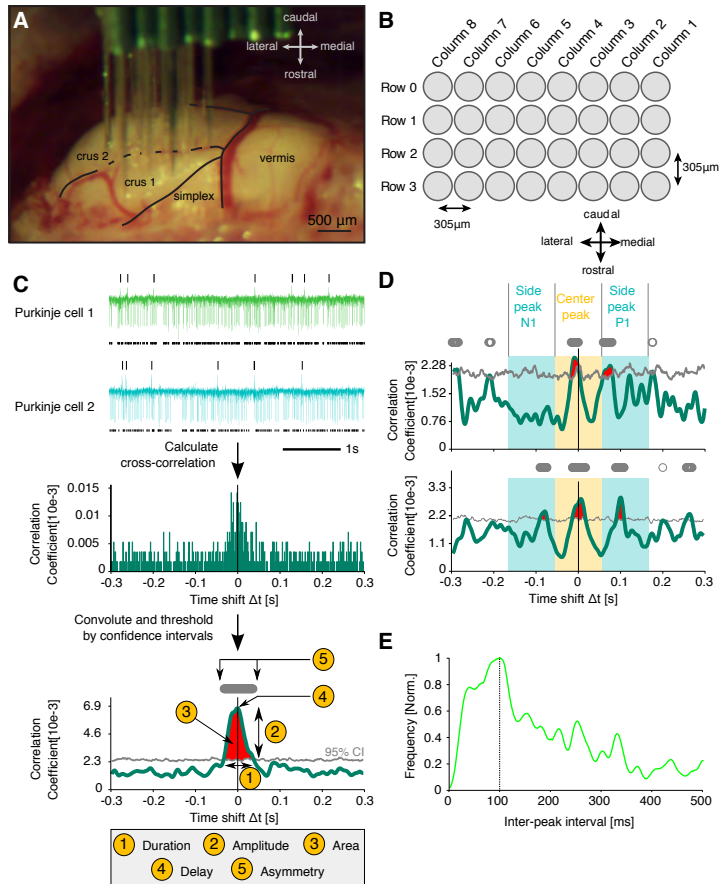
Figure 1 Electrophysiology and cross-correlation method. (A) Purkinje cell recordings are performed in Crus 1 and Crus 2 of the mouse cerebellar cortex with an electrode matrix with 32 electrodes. **(B)** Electrodes are organized in a grip pattern with four rows and eight columns, the inter-electrode distance is 305 micrometers. **(C)** Raw data traces of two exemplary Purkinje cell recordings (top graph) are analyzed and time stamps of complex (tick marks above trace) and simple spikes (tick marks below trace) extracted and binned at 1ms resolution; simple spikes are used to confirm single-unit recordings. Raw cross-correlations (middle graph) are calculated between -300ms and 300ms delays and convolved with a mixture of gaussians kernel (convolved cross-correlation, bottom graph). Resulting traces are thresholded with bootstrapped cross-correlations (grey line) and significant peaks are detected (for details see methods section). **(D)** Cross-correlograms are analyzed in time windows of 100ms, centered around 0ms delay, resulting in a center time window for the center peak and adjacent time windows for the first side peaks N1 (centered around -100ms delay) and P1 (centered around +100ms delay). The parameters in all three time windows were analyzed independently. **(E)** Histogram of inter-peak time intervals of all correlated cell pairs of the WT population, showing that the most frequent inter-peak interval is at 100ms.
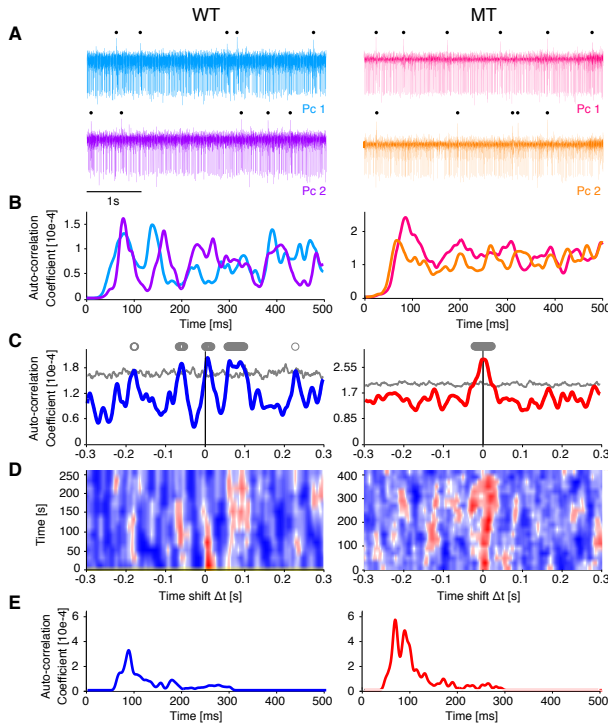
Figure 2 Representative cell pair examples of Gjd2 MT and WT mice. One cell pair for each genotype is shown in detail, wild-type (left column) and Gjd2 knock-out (right column). **(A)** Raw trace examples of both Purkinje cells of each pair, complex spikes are marked (tick marks above trace). **(B)** Auto-correlogram of both Purkinje cells between 0 and 500ms. **(C)** Typical convolved cross-correlogram between delays of -300ms and 300ms for both genotypes, wild-type typically showed lower amplitudes and asymmetric center peaks flanked by side peaks, Gjd2 knock-out showed typically stronger symmetric center peaks without side-peaks. **(D)** Time-shifted convolved cross-correlogram of both genotypes, each row represents the cross-correlogram of a 120s time window, shifted in between successive rows by 20s. It can be seen that the cross-correlograms are dynamic over time. **(E)** Population average of individual Purkinje cell complex spike auto-correlograms (like those in B).

lation average auto-correlation showing a peak at approx. 90 ms, which was more strongly present in the MT population, which showed an additional peak at approx. 70 ms (Fig. 2E). The representative WT cell-pair expresses an asymmetric center peak with clear side peaks in the cross-correlogram (Fig. 2, left column), whereas that of the MT cell-pair shows only a large, symmetric center peak (Fig. 2, right column). Note that the properties of the correlation between the complex spike activity of Purkinje cell pairs tended to fluctuate over time, which is apparent from time-shifted peri-stimulus time histograms (PSTHs, Fig. 2D).

Table 1 Center peak differences in cross-correlations of spontaneous complex spikes.

Parameter	WT (mean $\pm$ SD)	Gjd2 (mean $\pm$ SD)	p-value
Ratio [-]	91/149 = 61%	74/92 = 80%	0.0015**
Duration [ms]	25.3/ 19.8	34.6/ 18	< 0.001***
Amplitude [SD]	2.17/ 3.30	3.08/ 2.43	< 0.001***
Area [SD*ms]	54.9/ 121.8	70.3/ 70	< 0.001***
Delay [ms]	17.31/ 15.37	12.04/ 13.52	0.01*
Asymmetry [ms]	31.7/ 29.2	20.8/ 24.2	0.0095**

Stronger, less temporally precise center peaks in Gjd2-knockout complex spike cross-correlograms

We first investigated complex spike activity in what we presume to be the same olivary oscillation cycle of Purkinje cell pairs, by comparing the center peaks of the cross-correlograms, which occurred mostly between -25ms and +25ms. By including these and longer delays in our analysis, we were able to comprehensively quantify not only significant peaks that were distributed symmetrically around 0ms (Fig. 1C), but also the off-zero peaks that actually comprised the majority of the significant within-oscillatory cycle complex spike cross-correlations (Fig. 1D, upper panel).

Significant center peaks were more pronounced in MT cell pairs in terms of occurrence, duration and amplitude above the significance threshold, than in WT cell pairs (Fig. 3A, Table 1). The amplitude difference is even more apparent from the averages of the significant cross-correlation center peaks (Fig. 3B), with the mean MT center peak exceeding the significance threshold more than twice as far as the mean WT center peak (1.7 vs 0.75 SDs). In addition to being stronger, the timing of MT center peaks was closer to 0ms in terms of the delay of the maximum amplitude, and how symmetrically the area of the peak was distributed across 0ms (Fig. 3A, Table 1).

We controlled for a correlation between our cross-correlation parameters and complex spike firing rates. We found no correlation for the WT but a significant correlation between increasing firing rate and the longer durations (r=0.27, p=0.02) and a trend for bigger amplitudes (r=0.23, p=0.06) for the MT. Faster firing rates increase the odds of higher synchrony above the level of pure coincidence. This might partially explain the bigger center peak strength in the MT. We tried to approximate for how much the higher firing rate in the MT might contribute to the stronger center peak by calculating the effect of the increased firing rate on the slope of the linear correlation. An increase in firing rate of 0.09 Hz (difference between MT and WT) would account for an increase of 1.71ms in duration (0.09Hz*19ms/Hz), 0.135std in amplitude (0.09Hz*1.5 SDs/Hz). These values correspond to approx. 20% of the observed actual effect size (duration effect size: 1.71ms/(34.6ms-25.3ms) = 18.4

Less pronounced side peaks in Gjd2-knockout complex spike cross-correlograms

Next, we explored how cell pairs may behave in presumably successive olivary oscillation cycles by comparing the side peaks of the cross-correlograms. Here we
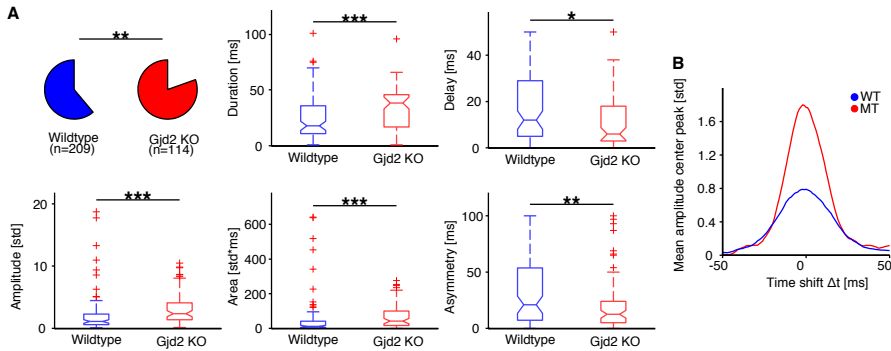
Figure 3 Center peak analysis for wild-type and Gjd2 knock-out Purkinje cell pairs. (A) The occurrence of center peaks in both groups is shown in pie charts (top left panel) showing a significantly higher ratio of MT center peaks (Fisher's exact test). The five analysis parameters of the center peaks of both populations are shown in box-plots (Mann-Whitney U tests). In summary, the duration (top middle panel), amplitude (bottom left panel) and the area (bottom middle panel) are significantly increased in MT cell pairs, while the delay (top right panel) and asymmetry (bottom right panel) are significantly increased in WT cell pairs. **(B)** Population average center peak for WT (blue) and MT (red) of all peaks in all correlated pairs that showed a center peak.

neglected the spatial arrangement of the cell pairs and only considered the largest side peak (preceding the center peak, N1, or following it, P1; see methods). The results, summarized in Fig. 4 and Table 2, show that significant side peaks did not occur more or less often in MT cell pairs than in WT cell pairs, and did not occur at different delays. However, WT side peaks were stronger in terms of duration and area, accompanied by a trend in amplitude (Fig. 4, Table 2).

Table 2 Side peak analysis.

Parameter	WT (mean $\pm$ SD)	Gjd2 (mean $\pm$ SD)	p-value
Ratio [-]	92/149 = 62%	59/92 = 64%	0.78
Duration [ms]	16.3/ 9.5	13.6/ 8.2	0.048*
Amplitude [SD]	1.08/ 0.67	0.88/ 0.59	0.065
Area [SD*ms]	13.3/ 14.3	8.9/ 9.2	0.04*
Delay [ms]	98.4/ 29.6	102.3/ 32.1	0.44

Medio-lateral distance increases timing variability in wild-type but not mutant center peaks

To investigate the influence of spatial separation between the cells on the center and the side peak, the cross-correlograms of all correlated pairs were plotted as a function of the euclidean distance between the cells of each pair. Based on this distance, irrespective of directionality, neither MT nor WT cell pairs showed any particular preference in terms of strength or timing of the center peaks (Fig. 5A, B, all $p < 0.15$). For side peaks too, cross-correlations between more proximal cells did not show more strength than those between more distal cells, for either MT or WT data. For side peaks too, WT cell pairs showed shorter delays in proximal cells (102 ± 30 ms, vs 87.4
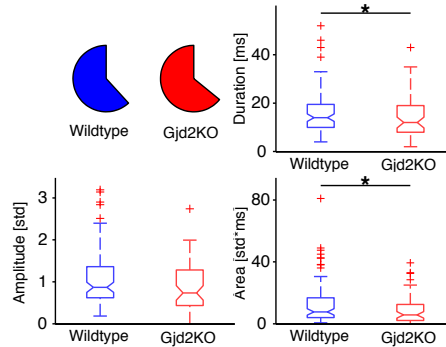
Figure 4 Side peak analysis for wild-type and Gjd2 knock-out Purkinje cell pairs. The occurrence of side peaks in both groups (top left panel) was not different between WT and MT cell pairs. Three analysis parameters of the side peaks of both populations are shown in box-plots. In summary, the duration (top right panel), amplitude (bottom left panel) and area (bottom right panel) show a slight decrease in the MT, reaching significance in the duration and area.

± 23 ms, p = 0.035; Fig. 5C, D), No differences were evident among MT cell pairs (all p > 0.25).

Next, we differentiated between distance in the coronal and parasagittal plane, as reflected in the distance in columns and in rows in the matrix of recording electrodes, respectively (Fig. 6). The index of the row and column group reflects the difference in rows or columns in between the two cells of the respective pair. Coronally, the more medial cell of each pair was used as the cross-correlation reference, and for the parasagittal plane, the more rostral cell of each pair was used as reference. This way, the N1 and P1 side peaks would reflect a consistent spacial directionality.

In line with previous work (Llinás & Sasaki, 1989; Lang et al., 1999), the clearest genotype differences were found for cell pairs that were separated on the medio-lateral plane (Fig. 6A). In terms of the timing of the center peak, both MT and WT cell pairs show complex spikes with short delays at low medio-lateral separation (column group 0 in Fig. 6A). With increasing medio-lateral separation, the WT cell pairs tend to fire with increasing delays while the MT cell pairs remain unchanged (Fig. 6A, top right panel). These differences are absent in the analysis of row groups (Fig. 6B).

Finally, in a direct comparison between WT and MT data, strength of center peaks was consistently higher in MT cell pairs, regardless of spatial distance. In terms of timing, we observed similar delays between MT and WT same-column cell pairs. While the WT data showed reduced temporal precision in off-column cell pairs, the MT data did not, suggesting a role for Gjd2 in how complex spikes are attuned between parasagittal zones. Parasagittal distance, that is distance in terms of rows, did not show an interaction with the differences in timing between MT and WT cell pairs.

We subsequently combined the euclidean distance with the separation into column groups to see where significant peaks show and found side peaks were most priminent at small medio-lateral distances in column groups 0, 1, and 2 in the WT cell pairs (Fig. 6C). Several pairs seemed to align their significant side peaks at a delay of approx. 90 ms. The more distant column groups showed a less defined center peak as well as
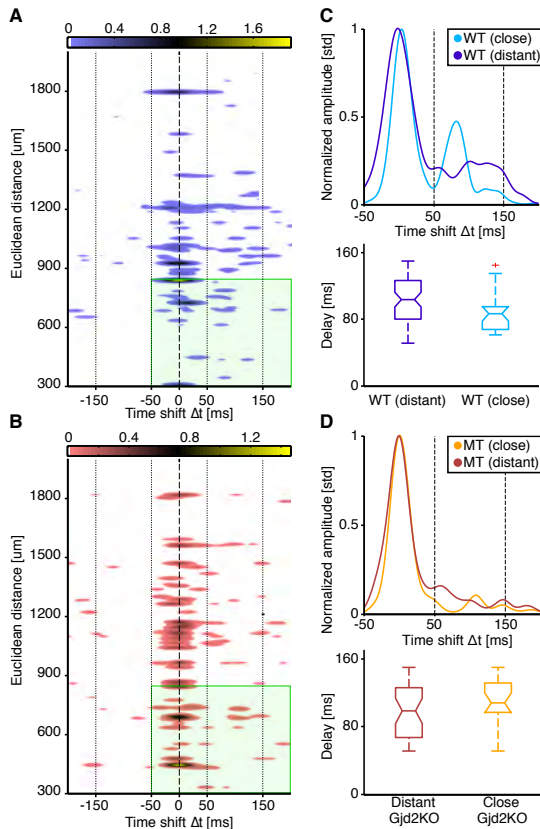
Figure 5 Cross-correlations for wild-type and Gjd2 knock-out as function of euclidean distance. **(A, B)** Single pair cross-correlograms are shown for both wild-type (A) and Gjd2 knock-out (B) in between time shifts of -200ms to +200ms (x-axis) and euclidean distances between 300μm and, 2000μm. Only significant peaks of each cell pair are inserted in a 2D matrix (oriented with the bigger side peak (N1 or P1) to positive delays) and after that the whole matrix is convolved with a 2D-kernel (details, see methods). For the wild-type the population is separated into close-by pairs (<=900μm euclidean distance) and distant (>900μm euclidean distance) pairs, the band of aligned side peaks in the close-by sub-population is indicated by a green-shaded box in Fig. 7a. **(C)** Normalized cross-correlograms of the close-by (<=900μm euclidean distance) and distant (>900μm euclidean distance) subpopulations of correlated wild-type pairs, showing a clear side peak at a delay of approx. +90ms in the close-by group (cross-correlograms of single pairs are indicated by green-shaded box in A). **(D)** As in C, but for correlated mutant cell pair, here not showing a clear side peak.

less alignment and amplitude in the side peak. Interestingly, the P1 side peak was more pronounced than the N1 side peak, suggesting a potential directional preference in which Purkinje cells fire complex spikes, i.e. from medial to lateral. The MT data (Fig. 6D) showed a clear absence of the side peak at either side while the center peak was stronger in amplitude. Those few cell pairs that showed significant side peaks seemed less aligned at fixed delays. Additionally, the amplitude of these timebins was smaller in MT than in WT cell pairs.

Stronger stimulation-evoked correlations in mutants than in wild-types

To further explore the increased complex spike synchrony in Gjd2-mutants, we calculated cross-correlograms during periods of 1 Hz air puff stimulation on the whisker pad and compared it to periods of spontaneous activity for both MT and WT mice. We analyzed recordings from 44 MT and 66 WT cell pairs that contained sufficient data for both spontaneous as well as stimulated data (Fig. 7, see methods).

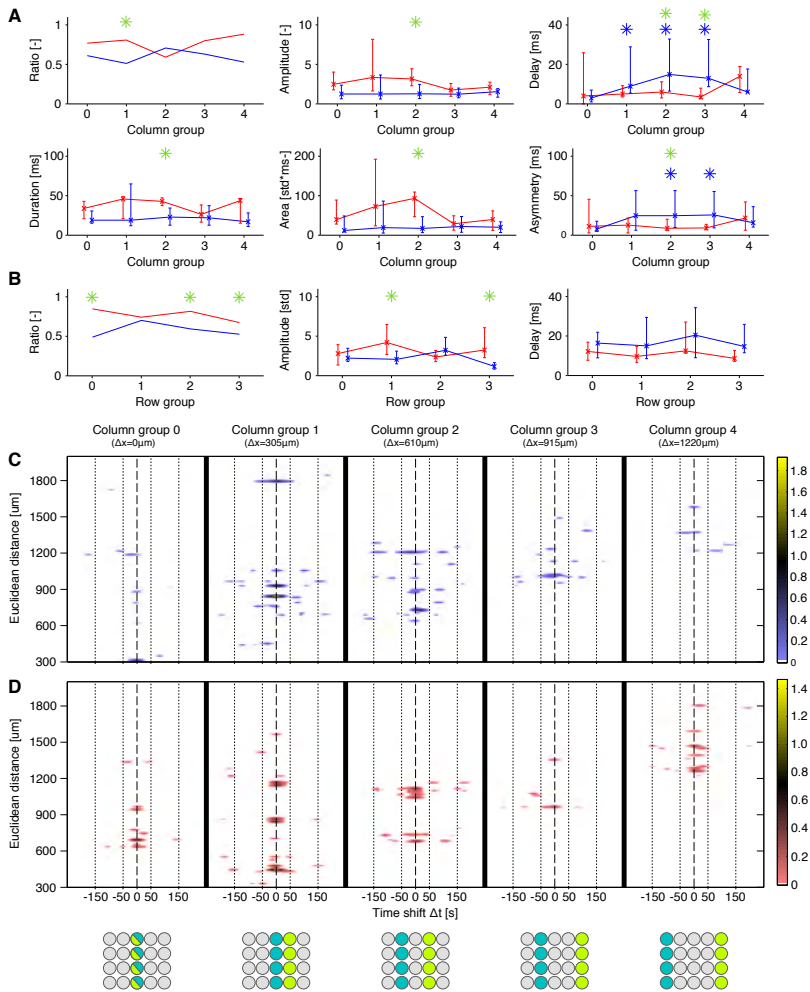In the WT data, center peaks showed no significant differences in strength and

Figure 6 Separation into column groups and row groups of MT and WT cell pairs. (A) The WT (blue) and MT (red) data are split up based on the distance between Purkinje cells in terms of electrode matrix columns, reflecting medio-lateral distance. Within genotype comparisons of center-peak properties were made between column group 0 and each other column group, with asterisks indicating significance for WT (blue) cell pairs (there were no significant differences for the MT group). Black asterisks denote between genotype comparisons at each column group. **(B)** Similar to A, here separating the data on the distance between Purkinje cells in terms of electrode matrix rows, reflecting rostrocaudal distance. **(C, D)** Single pair cross-correlograms of the column groups are shown for both WT (C) and MT (D) cell pairs, in between time shifts of -200ms to +200ms (x-axis) and euclidean distances between 300μm and, 2000μm. Only significant peaks of each cell pair are inserted in a 2D matrix and after that the whole matrix is convolved with a 2D-kernel (see methods).
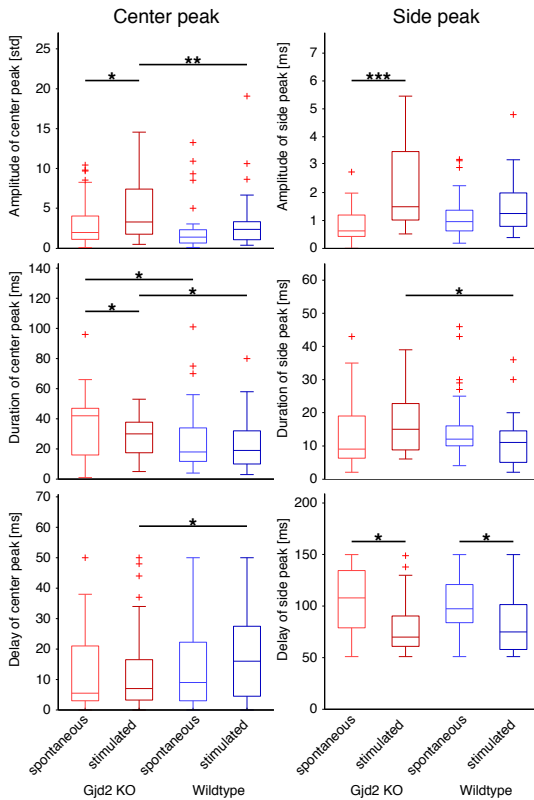
Figure 7 Correlation of spontaneous and stimulated complex spike activity for wild-type and Gjd2 knock-out cell pairs. Cross-correlograms of separate epochs of the stimulated and spontaneous condition are analyzed for both genotypes, resulting in four groups. For both center peak (left column) and side peak (right column), amplitude (top row), duration (middle row), and delay (bottom row) are shown for each of these groups. Statistical comparisons are done between the identical genotypes across conditions (Wilcoxon ranked-sum test) and between the identical conditions across genotypes (Mann-Whitney U test).

timing between spontaneous and stimulation-evoked complex spikes (Fig. 7; Table 3). However, in MT cell pairs, center peaks were more concentrated in the stimulation data, as apparent from an increase in amplitude (p = 0.039; Table 3), and a decrease in duration (p = 0.027) relative to spontaneous MT data. For the side peaks, there was a significant reduction in the delay in both the WT and MT stimulation data compared to spontaneous data. In the MT data, this effect was accompanied by a clear increase in amplitude (p < 0.001; Fig. 7; Table 3) and, together with an upward trend in duration (p = 0.074), a clear increase in area (p < 0.001). Together, these results suggest olivary responsiveness was more sharply affected by the stimulus in the MT population than in that of the WT.

In the MT but not WT data, side peaks showed substantially higher amplitudes during stimulation than during spontaneous activity (MT: p < 0.001; WT: p = 0.84; Fig. 7; Table 3). For both mouse groups, side peaks occurred at reduced delays during stimulation compared to spontaneous activity, although this difference did not reach significance for WTs (MT: p = 0.046; WT: p = 0.066, Table 3). Together, these results suggest olivary responsiveness was more sharply affected by the stimulus in the MT population than in that of the WT.

Table 3 Center and side peak properties based on spontaneous and stimulation-evoked complex spikes.

WT (median ± SD)			
Center peak	**Spont.**	**Stim.**	**p-value**
Duration [ms]	18 ± 23	21 ± 17	0.45
Amplitude [SD]	1.3 ± 3.3	2.4 ± 3.7	0.15
Delay [ms]	9.5 ± 15.4	16 ± 14.3	0.74
Side peak			
Duration [ms]	12 ± 11	9 ± 8.4	0.078
Amplitude [SD]	1.02 ± 0.99	0.85 ± 1.16	0.84
Delay [ms]	97 ± 25.3	69 ± 27.8	0.066
MT (median ± SD)			
Center peak	**Spont.**	**Stim.**	**p-value**
Duration [ms]	42 ± 20	30 ± 13	0.027*
Amplitude [SD]	2.4 ± 2.9	3.8 ± 3.5	0.039*
Delay [ms]	5 ± 13.8	5.5 ± 13.8	0.3
Side peak			
Duration [ms]	11 ± 9.4	17 ± 9.2	0.099
Amplitude [SD]	0.68 ± 0.6	1.53 ± 1.79	<0.001***
Delay [ms]	106 ± 32.7	70 ± 28.2	0.046*
MT vs WT (p-value)			
Center peak	**Spont.**	**Stim.**	
Duration [ms]	0.033*	0.049*	
Amplitude [SD]	0.059	0.007**	
Delay [ms]	0.53	0.049*	
Side peak			
Duration [ms]	0.17	0.014*	
Amplitude [SD]	0.058	0.13	
Delay [ms]	0.31	0.94	

Zero-lag Pearson correlation approach of synchrony

Previous studies exploring complex spike synchrony across the cerebellar cortex, both in anesthetized (Llinás & Sasaki, 1989; Blenkinsop & Lang, 2006) and awake non-moving preparations (Lang et al., 1999), focused on cross-correlations within a millisecond range around complex spike activity, also called zero-lag synchrony. The levels of zero-lag synchrony were calculated in the current data and compared to the results here presented. As could be expected, longer delays of the center peak maximum amplitude related to lower zero-lag synch, as did larger center peak asymmetry (Fig. 8). Importantly, these effects were more robust in WT (delay: $r = -0.38$, $p < 0.001$; asymmetry: $r = -0.39$, $p < 0.001$) than in MT data (delay: $r = -0.22$, $p = 0.068$; asymmetry: $r = -0.31$, $p = 0.01$), suggesting that particularly in WT data, zero-lag synchrony may disregard substantial relevant cross-correlation. Indeed, while in the MT there is a significant correlation between zero-lag synchrony and center peak area ($r = 0.28$, $p = 0.015$, data not shown) and a clear correlation trend with center peak amplitude ($r = 0.21$, $p = 0.079$), there was a complete lack of correlation between these parameters in the WT data (area: $r = 0.03$, $p = 0.8$; amplitude: $r = 0.07$, $p = 0.53$, data not shown). Thus, given the striking prevalence of off-zero cross-correlation in WT cell pairs, the more elaborate cross-correlation approach outlined in the current work
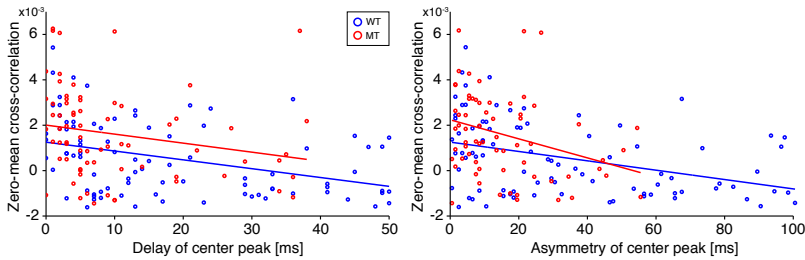
Figure 8 Comparison with a zero-lag synchrony approach. Scatterplots plotting the correlation coefficients from the zero-lag synchrony approach against the parameters from the approach in the current study are made and their correlations analyzed with a linear regression. Scatterplots with the two parameters delay (left panel; WT: Pearson r = -0.38; p<0.001, MT: Pearson r = -0.22; p=0.068) and asymmetry (right panel; (WT: Pearson r = -0.39; p<0.001; MT: Pearson r = -0.31; p=0.01) are shown, indicating significant correlations between the zero-lag synchrony correlation result and our parameters delay and asymmetry for both genotypes.

may prove a fruitful alternative to the zero-lag synchrony approach in the pursuit of a complete understanding of how two Purkinje cells synchronize their complex spike activity.

Discussion

Inferior olivary neurons heavily express Gjd2 (Condorelli et al., 1998; Belluardo et al., 2000), which is required for formation of functional gap junctions in the olivary network (De Zeeuw et al., 2003). Gap junctions in the inferior olive were discovered more than 40 years ago (Llinás et al., 1974; Sotelo et al., 1974) and their functional properties have been studied extensively ever since (Llinás & Yarom, 1981; Yarom Y. & Llinás, 1981; Llinás & Yarom, 1986). In addition, STO's have been one focus of interest; it was found that phases and amplitudes of olivary neurons can change together, but this relationship is dynamic rather that static and can change over time depending on the speed and sequence of movements (Devor & Yarom, 2002b; Jacobson et al., 2009). The absence of gap junctions leaves a relatively mild behavioral phenotype, which becomes more apparent under locomotion or demanding experimental conditions such as learning and adaptation (Kistler et al., 2002; Van Der Giessen et al., 2008; De Gruijl et al., 2014). The present study suggests that the temporal and spatial structure in complex spike signals of the cerebellar cortex (resulting from largely decoupled olivary neurons) may contribute to reduced neuroplasticity, and thereby reduced behavioral flexibility, in Gjd2 mutants. These systems level physiological findings contribute to behavioral phenotypes under demanding experimental conditions (Van Der Giessen et al., 2008; De Gruijl et al., 2014).

The present results used cross-correlograms between delays of -250ms and +250ms of wild-type and Gjd2 knock-out mice and highlighted the occurrence, shapes, and position of significant peaks. These peaks are described with the help of several parameters and statistically compared across different conditions and genotypes. Cross-correlations have been used in several studies to analyze complex spike syn-

chrony effects in the cerebellar cortex. Although many studies have focused on the 0ms timebin in cross-correlograms (investigating what happens simultaneously = $< 500\mu$s delays) in anesthetized (Llinás & Sasaki, 1989; Lang et al., 1996; Marshall et al., 2007) and awake animals (Lang et al., 1999), few studies looked at full cross-correlograms over hundreds of milliseconds (Bell & Kawasaki, 1972; Wise et al., 2010). To our knowledge, the present study is the first to quantify cross-correlation effects in detail over successive olivary oscillation cycles and as a result has captured important functional consequences.

How does Gjd2 influence temporal dynamics of complex spikes?

Here we presented data showing that, by removing Gjd2, cells act in a more independent fashion, as is expected if the Gjd2 protein is to be necessary for functional gap junctions between olivary neurons, which allows their depolarization state to spread. We observed firstly that reduced coupling between olivary neurons results in more symmetric and stronger simultaneous (center peak) correlations in the MT cell pairs. In a normally functioning olive, small consistent delays (< approx. 20ms) make different olivary neurons fire with a fixed offset in the same oscillation cycle. When this happens consistently, non-centric peaks emerge in the center peak time window. We observed this effect in the WT, but not in the MT, which implies that gap junctions may be necessary for these small but consistent delays in Purkinje cells' complex spike activity in the cerebellar cortex. This is in agreement with earlier studies that report reduced alignment and temporal precision of olivary spikes to preferred firing windows in the Gjd2 MT (Bazzigaluppi et al., 2012). We also observed shorter durations of the side peak of MT mice (accompanied by a trend for reduced amplitudes), as well as poorer temporal alignment in their distribution compared to WT cell pairs. This would suggest a reduced consistency in fixed delays of olivary spiking may also hold during successive olivary oscillation cycles.

How does Gjd2 influence excitability of olivary neurons?

Whisker stimulation responsiveness of single olivary neurons is increased in MT's compared to WT's cell pairs. A higher ratio of MT cell pairs showed center peaks, which had longer durations and higher amplitudes than WT cell pairs. These results are in line with previous studies, suggesting an increased excitability in olivary neurons lacking Gjd2 caused by increased calcium currents (De Zeeuw et al., 2003) or less gap leakage currents (De Gruijl et al., 2012). The side peak in MT cell pairs had highly increased amplitudes and a trend towards longer durations, both combined resulting in an increased area. This is in line with an earlier study that reports increased number of complex spike doublets in the MT (Van Der Giessen et al., 2008). On the other hand, these results seem to be at odds with earlier studies investigating the zero-lag synchrony in complex spikes in Gjd2 MT and WT mice, reporting reduced complex spike synchrony in the MT (Marshall et al., 2007).

We would like to emphasize that, even though the animal genotypes are identical, the recording conditions as well as the data processing steps in this article are different from the Marshall et al., paper (2007). In the latter study, animals were recorded under

anesthesia and all Purkinje cells were located in the superficial Purkinje cell layer in the cerebellar cortex. We were interested in how far their results could be translated to awake and behaving animals and how Purkinje cells within the folded cerebellar cortex would fit into the existing picture. Since both the awake state (Bengtsson & Jörntell, 2007) as well as the more complex spatial orientation of the cell pairs have most likely introduced more variability in the synchrony results, we decided to take a look at full cross-correlograms of complex spikes, accounting (and partially compensating) for temporal jitter by using a convolution kernel. In doing so, we aimed to find sequences of complex spike events across the cerebellar cortex and investigate how these sequences are influenced by olivary gap junctions.

The lack of Gjd2 could also mean that incoming current cannot flow to neighboring olivary neurons. If the input-receiving neuron is excited for a longer time it may increase the chance of firing two spikes in successive olivary oscillation cycles. Indeed, an increased occurrence of complex spike doublets in the Gjd2 MT was observed (Van Der Giessen et al., 2008).

Another result that supports increased excitability in olivary neurons lacking Gjd2 is based on the fact that the direct projection from the cerebellar nuclei to the inferior olive is inhibitory while the indirect projection (via the mesodiencephalic junction (MDJ)) is excitatory. Lesioning the direct projection removes the inhibitory input coming from the cerebellar nuclei, which results in a strongly coupled Olivary ensemble that is difficult to depolarize (de Zeeuw et al., 1989; De Zeeuw & Ruigrok, 1994; Ruigrok & Voogd, 1995). This is in line with pharmacological studies showing that inferior olivary neurons exhibit synchrony also under blockage of its inputs. While blockage of excitatory input (with the glutamate-antagonist NBQX) reduced the complex spike firing rate by 50%, it actually elevated the parasagittal stripes of synchrony in the cerebellar cortex (Lang, 2001). Blockage of inhibitory input however (with the GABA-antagonist Picrotoxin) abolished the pattern of parasagittal stripes in the cerebellar cortex, by that increasing the overall synchrony (Lang, 2002).

In combination with recent results reporting that inhibitory input to the inferior olive directly influences the coupling coefficients between olivary neurons (Lefler et al., 2014), it is plausible that inhibitory input to the olive can directly decouple ensembles of olivary neurons. An inactivation of the gap junctions could then have a similar effect of highly uncoupled olivary cells, which could lead to more easily excitable olivary neurons shown here.

How do increased complex spike firing rates in MT's influence systems level function?

We observed a significantly higher complex spike firing rate in our MT population compared to our WT population. Earlier studies found no differences between these genotypes under awake conditions (Van Der Giessen et al., 2008; De Gruijl et al., 2014) and even significantly lower firing rates in the MT under anesthesia (Marshall et al., 2007). Since the MT results correlated significantly with the firing rate, we calculated the potential influence of the firing rate on the found results. We found that the increased firing rate could explain approx. 20% of the increased effect size. We conclude that the remaining difference indeed results from structural differences

in the inferior olive, that are induced by the genetic manipulation.

Another result that supports increased excitability in olivary neurons lacking Gjd2 is based on the fact that the direct projection from the cerebellar nuclei to the inferior olive is inhibitory while the indirect projection (via the mesodiencephalic junction (MDJ)) is excitatory. Lesioning the direct projection removed the inhibitory input from the cerebellar nuclei, which resulted in a strongly coupled olivary ensemble that was difficult to depolarize (de Zeeuw et al., 1989; De Zeeuw & Ruigrok, 1994; Ruigrok & Voogd, 1995). This was in line with pharmacological studies showing that inferior olivary neurons exhibit synchrony also under blockage of its inputs. While blockage of excitatory input (with the glutamate-antagonist NBQX) reduced the complex spike firing rate by 50%, it actually elevated the parasagittal stripes of synchrony in the cerebellar cortex (Lang, 2001). Blockage of inhibitory input however (with the GABA-antagonist Picrotoxin) abolished the pattern of parasagittal stripes in the cerebellar cortex, increasing the synchrony overall (Lang, 2002). In combination with recent results reporting that inhibitory input to the inferior olive directly influences the coupling coefficients between olivary neurons (Lefler et al., 2014), it is plausible that inhibitory input to the olive can directly decouple ensembles of olivary neurons. An inactivation of the gap junctions could then have a similar effect of highly uncoupled olivary cells, which could lead to more easily excitable olivary neurons shown here.

How does distance influence the results?

We found no difference in duration, amplitude and area in the rostro-caudal nor in the medio-lateral direction when considering correlation strength. However when comparing MT and WT cell pairs, we do see stronger responses in all three parameters in the majority of comparisons. When considering the temporal precision with a coupled olive we observe increasing but consistent delays between complex spike firing in the medio-lateral direction, which become apparent from non-centered peaks. This effect is absent in the rostro-caudal direction or in the uncoupled olive.

Earlier results observed strongly increased complex spike synchrony almost exclusively in the medio-lateral direction (Llinás & Sasaki, 1989; Sasaki et al., 1989; Lang et al., 1996; Lang et al., 1999; Lang, 2001; Lang, 2002; Lang, 2003; Blenkinsop & Lang, 2006; Lang et al., 2006). We cannot confirm this effect, instead reporting a mixed picture with single coupled cell pairs at virtually all possible orientations with correlation peaks at various strengths or delays. At the population level, certain orientations do represent stronger effects than others, most of which are in line with above mentioned studies, but the effects we observed are weaker and more spread out. A number of factors may have contributed to this result. First, our recordings were made in awake behaving animals, which is likely to introduce more variability than studes done on anesthetized animals or in awake ones under exclusion of time epochs of locomotion (Lang et al., 1999). Second, our temporal region of interest was much broader than that of previous work, making comparisons with previous studies less straightforward. Third, most of the previous work focused on superficial cerebellar cortical layers, while our recordings were made across the entire depth of crus I and II, likely increasing the variability observed in our data. Lastly, our mouse preparation may have lead to larger relative distances between cell pairs, compared to most of

the previous work done in rats with comparable distances between electrodes. These factors should all be considered when drawing comparisons between the current study and previous work.

How does whisker stimulation influence complex spike firing patterns?

The increased excitability of Olivary neurons should be even more pronounced when common input is received by the inferior olive. This should happen during sensory input as well as motor output. Increased complex spike synchrony has been shown under electrical stimulation in motor cortex (Lang, 2002) as well as during spontaneous movement (Ozden et al., 2009; Hoogland et al., 2015; Tsutsumi et al., 2015). In our data we observed an increased responsiveness of olivary neurons to stimulated airpuff events especially in the MT population. A higher ratio of MT cell pairs showed center peaks, which had longer durations and higher amplitudes than WT cell pairs.

When we consider the stimulation effect on each genotype separately we see that MT center peaks get even sharper under stimulation, as can be seen from increased amplitude and decreased duration values; stimulation induced no significant differences in the WT. This effect is even stronger in the side peak: stimulation forces the MT cell pair to fire an additional spike in the successive oscillatory cycle; this spike is fired at short and consistent delays; this effect is again absent in the WT. These results are in line with previous studies, suggesting an increased excitability in olivary neurons lacking Gjd2 caused by increased calcium currents (De Zeeuw et al., 2003) or less gap leakage currents (De Gruijl et al., 2012). The side peak in MT cell pairs had highly increased amplitudes and a trend towards longer durations. This is in line with an earlier study that reports increased number of complex spike doublets in the MT (Van Der Giessen et al., 2008).

Effects outside exact synchrony

We also conclude, that the zero-lag synchrony parameter does not capture all meaningful effects of Purkinje cell function. small but consistent delays between complex spike firing of two cells cannot be detected by this approach. Beside that, small variations in response times, resulting in a temporal jitter between complex spike signals can potentially diminish the correlation. We overcame these issues by analyzing full cross-correlograms within several olivary oscillation cycles. Beside that we compensated for small variabilities by using the convolution kernel, which combines neighboring timebins. The analysis of full cross-correlograms is essential in order to capture the delays of chemical and electrical synapses, which induce delays of 1 to 5 milliseconds (Kandel et al., 2013; Goyal & Chaudhury, 2013). The delay of electrical synapses is mainly caused by the conductance of the gap junctions and the post-synaptic capacity (Bennett, 1997; Bennett & Zukin, 2004).

How does coupling influence olivary oscillations?

Single olivary neurons express subthreshold oscillations in frequencies between 1-1 OHz, which influences the probability of spiking during the rising slope and peak of the oscillation. This results in preferred firing windows in single oscillatory cycles (Llinás & Yarom, 1981 ; Yarom Y. & Llinás, 1981 ; Llinás & Yarom, 1986; Bazzigaluppi et al., 2012; De Gruijl et al., 2012). The subthreshold oscillations of neighboring olivary neurons are coupled by gap junctions, which can synchronize their individual STO's and promote synchrony in their elicited spikes (Llinás et al., 1974; Sotelo et al., 1974). It is still under debate, if these two olivary properties are independent or if they influence each other. Assuming both properties are independent, we would expect to find unaltered STO properties in the absence of gap junctions. If they are dependent on each other, we would expect to find altered STO properties. In our view, this analysis does not necessitate multiple cell analysis, but can also be investigated at the single-cell level. A coupled neuron would be influenced by its neighbors, with which it would exchange current via its gap junctions. This current flow would be likely to influence its subthreshold oscillations toward shorter or longer oscillations, by that potentially advancing or delaying an olivary spike; both seem possible depending on the filtering properties of gap junctions. We found a second auto-correlogram peak for the MT Purkinje cells at approx. 70 ms (Fig. 2E). This reflects shortened complex spike delays in the absence of gap junctions, which would correspond with faster STO frequencies. A coupled network might therefore provide a huge sink, which could absorb and distribute incoming current, by that holding back single olivary neurons from spiking and recruiting them in the network. This would also be in line with our observation of an increased peak amplitude in the MT population (Fig. 4E), and in the overall increased complex spike firing rate of our MT population. Taken together, these results hint in the direction that coupling is not essential for the expression of STO's, but STO properties do get modulated by it. It therefore seems unlikely that subthreshold oscillations and olivary coupling are completely independent phenomena.

Conclusion

It has been found that local electrical stimulation in the cerebellar cortex as well as optical stimulation in Channelrhodopsin infected Purkinje cells trigger local rebound complex spikes after short delays which support the closed-loop theory (Llinás & Sasaki, 1989; Lang et al., 1996; Jörntell et al., 2000; Chaumont et al., 2013). Different modules could be dynamically controlled based on the current state of the animal and coordinate motor output (Welsh et al., 1995; Garwicz et al., 1998; Lefler et al., 2014; Devor & Yarom, 2002a). As shown here diverging climbing fiber signals orchestrating the cerebellar cortex via complex spikes are essential to output control to the cerebellar nuclei (Lang & Blenkinsop, 2011; Person & Raman, 2011; Person & Raman, 2012) and later cerebellar output. Our data therefore supports a crucial role of Gjd2 in the synchronization of olivary neurons. It is essential for the dynamic spatiotemporal compartmentalization of olivary neurons and orchestration of consistent delays in complex spike activity.

Methods

Subjects

For the current study, 12 *Gjd2*$^{-/-}$ global knockout mutant mice (MT) were used, as well as 19 wild-type (WT) mice, of which 8 mice were *Gjd2* littermates (C57bl6 background, regularly crossed back), and 9 mice were L7-$\Delta\gamma$2 wild-type littermates (also C57bl6 background). The latter control mice were part of a separate cohort of L7-$\Delta\gamma$2 mice, in which the Purkinje cells of mutants lack a γ2-subunit of the GABA$_A$ receptor (Wulff et al., 2009). In brief, we used crossings of mice in which the gene for the regulatory subunit (γ2) was flanked by loxP sites (Zeng et al., 2001) with transgenic mice expressing Cre under control of the L7 promoter (Barski et al., 2000). All three non-mutant groups were used, i.e. L7-Cre$^{-/-}\Delta\gamma$2$^{+/+}$, L7-Cre$^{-/-}\Delta\gamma$2$^{f/f}$, and L7-Cre$^{+/+}\Delta\gamma$2$^{-/-}$ mice. We combined these groups into our wild-type groups to gain power for our analyses. A cluster algorithm was used to control for result deviations due to the mutation. We found that the majority of MT mice clustered and separated from the majority of WT mice. Both types of wild-type mice were mostly intermingled (Fig. 9). We therefore conclude that no bias is introduced due to the genetic types of our WT group. All mice were 20-25 weeks of age, were kept at a regular 12:12 hour light/dark cycle, and carried a body weight of 22-25 g during recordings. All experimental procedures were approved by the institutional animal welfare committee as required by Dutch law.

Distance

- ● Gjd2 knockout (MT)
- ● Gjd2 wild-type littermate (WT)
- ● L7 γ2 wild-type littermate (WT)
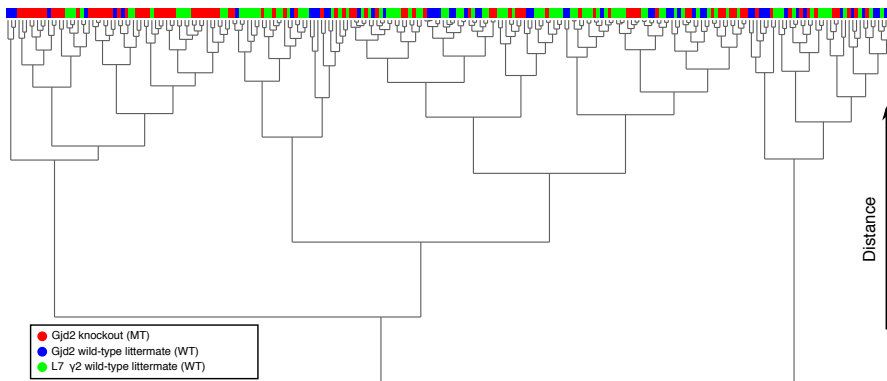
Figure 9 Cluster analysis of genotypes. A cluster analysis was applied on various parameters and results for details see methods). The resulting dendrogram presents that most MT data is separated from the WT data and that WT data of both types are mostly intermingled.

Surgery

The surgery and recovery procedure was similar to that used in Bosman et al., (2010). In brief, mice received a magnetic pedestal that was attached to the skull above bregma using Optibond adhesive (Kerr Corporation, Orange, CA) under isoflurane anesthesia

(2-4% V/V in O2). A craniotomy was performed on the occipital bone under isoflurane (4% V/V in O2) and local lidocaine (approx. 1 μg applied to the skull). Post-surgical pain was treated with carprofen (5 mg/kg, injected subcutaneously) and lidocaine (approx. 1 μg applied to the wound). After surgery, mice were allowed to recover at least three days prior to habituation to the setup and electrophysiological recordings, as described previously (Bosman et al., 2010).

Electrophysiology

Single-unit recordings were made using quartz-coated platinum/tungsten electrodes (2-5 MΩ, outer diameter = 80 μm, Thomas Recording, Giessen, Germany). The electrodes were placed in an 8x4 matrix (Thomas Recording) (Fig. 1B), with an inter-electrode distance of 305 μm over Crus 1 and Crus 2 ipsilateral to the airpuff stimulation (Fig. 1A). All recordings were made at a minimal depth of 500 μm to avoid unstable recordings. The electrophysiological signal was digitized at 25 kHz, using a 30-6,000 Hz band-pass filter, 22x pre-amplified and stored using a RZ2 multi-channel workstation (Tucker-Davis Technologies, Alachua, FL). Spikes were detected offline using SpikeTrain (Neurasmus BV, Rotterdam, The Netherlands) or a custom program written in Labview (National Instruments, Austin, TX). We identified Purkinje cell activity by the presence of both complex spikes and simple spikes. Complex spikes were recognized based on their downward (molecular layer) or upward (Purkinje cell and granular layer) deflection as well as their waveform including the presence of spikelets following the initial sodium spike. For each recording, we constructed a histogram of simple spike time stamps triggered by complex spike time stamps. We accepted a recording as a single unit if the first 7 ms following a characteristic complex spike were devoid of simple spikes. Further analysis was exclusively done on single unit Purkinje cell recordings that had a clear signal-to-noise ratio. Cross-Correlation analysis was exclusively done on cell pairs which were recorded for a period of at least 200s.

Data analysis

For the cross-correlations, the complex spike timestamps from both cells were binned into binary spike vectors at 1ms precision ("raw data"), value "1" denoting the onset of a complex spike in the respective time bin, value "0" no onset of a complex spike (Fig. 1C). Cross-correlations were calculated in Matlab (MATLAB R2011a Version 7.12 and Statistics Toolbox Version 7.5, The MathWorks, Inc., Natick, Massachusetts, United States) using the function "crosscorr", normalized by the complex spike count of both input cells [$(N_{CS\_Cell1} * N_{CS\_Cell2})^{0.5}$]. The cross-correlation was convolved with a "mixture of gaussians" kernel, consisting of three individual gaussian kernel functions having the halve widths 11ms, 16ms and 24 ms; normalized to the area 1 (*function 1a*). After the convolution, we received the convolved cross-correlogram ("conv data"), which was used for all analyses.

Significance was determined by using the bootstrap method. For this the inter-spike intervals ISI$_{CS}$ were calculated from the complex spike timestamps of each cell individually (function "diff"), their sequence randomized (function "randperm") and re-

transformed in successive timestamps (function "cumsum"). The cross-correlogram was calculated in an identical way as described above for the original data. The bootstrap was iterated 500 times per cell and the 97.5 percentile was determined individually per cross-correlogram timebin as confidence interval threshold to assess significance.

Cross-correlogram time bins were evaluated between delays of -250ms to 250ms for crossing of the threshold. If the number of significant time bins exceeded the expected number of time bins that should occur by chance (2.5% of 501 time bins = 12.53 => rounded up to 13 time bins), the cell pair was deemed as being correlated significantly. All significant time bins were combined into successive epochs; only those epochs being 5ms or longer were considered for further analysis ("peaks"). The data was separated into time windows of 100ms, because the oscillations in the inferior olive were approximated to be 10 Hz in our data (reasoning in main text). The time window of the center peak was defined between $-50ms <= delay <= 50ms$. The first side peak to both sides was defined as P1 at $50ms < delay <= 150ms$ and N1 at $-150ms <= delay < -50ms$ (Fig. 1D).

In each time window, the peaks were evaluated separately by assessing different parameters of each peak:

Duration – measured as the number of significant timebins in all peaks in the respective time window (Fig. 1C, #1). This parameter shows the span of delays at which the two cells show significantly correlated complex spikes. It can be interpreted as temporal accuracy of the correlation or stability of the coupling. A less strongly coupled pair is supposed to show less temporal accuracy in between its events and therefore tend to show a lower and wider peak.

Amplitude – measured as the maximum amplitude in the unit standard deviations (std) of all time bins in the respective time window, subtracting 1.96 stds to consider only the amplitude exceeding the threshold (Fig. 1C, #2). This parameter measures the amplitude of the peak maximum and can be interpreted as the strength of the correlation at its single strongest delay (partially accounting for temporal jitter by the convolution kernel).

Area – sums the amplitude of all significant time bins in all peaks in the respective time window (Fig. 1C, #3). This parameter represents the overall magnitude of the correlation strength in a combined fashion of parameters 1 and 2.

Delay – measures the location of the maximum amplitude peak relative to zero (Fig. 1C, #4). This parameter can be interpreted as delay of the most frequently occurring complex spike pair of the two cells.

Asymmetry – The absolute difference between the onset and the offset of the most centered peak in the respective time window (Fig. 1C, #5). This parameter measures to which extent the peak is symmetric around zero or leaning away from zero towards positive values (meaning that cell 2 leads over cell 1) or negative values (meaning that cell 2 leads over cell 1). This can be interpreted as measurement of the two cells being equally coupled in both directions or being stronger coupled from cell 1 to cell 2 than vice versa.

In a sub-set of experiments, airpuffs were delivered to the peripheral whisker field as a stimulus at fixed frequencies of 0.25Hz or as pseudo-random distributions of 0.25Hz. For all airpuff blocks of data, the data was separated into two conditions: the "stimulated conditions", comprising all complex spike events between each airpuff

stimulus and 400ms after, and the ''spontaneous condition'', comprising the remaining data. The time limit of 400ms after each airpuff stimulus was determined by testing Peri-Stimulus Time Histograms (PSTH's) for complex spike peaks of modulation, which we found reaching up to 300ms after the stimulus. Confidence intervals were calculated for both conditions separately; paying attention for the stimulated conditions that equal-sized valid time windows were correlated of the two cells. For further analysis of the stimulated condition, only cell pairs which were recorded together for at least 30 air-puffs were considered.

For the time-shifted PSTH plots (Fig. 2C), time windows of 120s were used per single row, which was pushed forward by 20s in between successive rows. For each time window the cross-correlogram was calculated individually as described above.

For the distance cross-correlograms (Fig. 5, 6C, D), we inserted all peaks (x-axis) at their respective euclidean distance (y-axis) with their respective amplitude parameter value in a matrix (resolution: x-axis 1ms, y-axis 1μm). After adding all significantly correlated cell pairs per genotype, we convolved the matrix with a two-dimensional gaussian kernel with half-width 20ms (x-axis) and 12μm (y-axis), normalized to volume 1.

Continuous variables in the notation ''x $\pm$ y'' refer to x being the population mean and y being the population standard deviation. For statistics, we used Fisher Exact Tests for dichotomous variables and Mann-Whitney tests for continuous variables if not further mentioned. Significance was determined at confidence intervals of 5% (*), 1% (**) and .1% (***).

Cluster analysis was performed using PAST software (Hammer et al., 2001). First, we normalized all quantifiable parameters (complex spike firing rate cell 1, complex spike firing rate cell 2, center peak amplitude, center peak duration, center peak area, center peak delay, center peak asymmetry, side peak amplitude, side peak duration, side peak area, side peak delay) to values between 0 and 1. Next, we performed a cluster analysis using Ward's method (with 1,000 bootstraps).

Conditioned climbing fiber responses in cerebellar cortex and nuclei

The eyeblink conditioning paradigm captures an elementary form of associative learning in a neural circuitry that is understood to an extraordinary degree. Cerebellar cortical Purkinje cell simple spike suppression is widely regarded as the main process underlying conditioned responses (CRs), through disinhibition of neurons in the cerebellar nuclei that innervate eyelid muscles downstream. However, recent work highlights the addition of a conditioned Purkinje cell complex spike response, which at the level of the interposed nucleus seems to translate to a transient spike suppression that can be followed by a rapid spike facilitation. Here, we review the characteristics of these responses at the cerebellar cortical and nuclear level, and discuss possible origins and functions.

M.M. ten Brinke, H.J. Boele, & C.I. De Zeeuw (Submitted)

The Purkinje cell CR: simple spike suppression

Over the past decades, research on Pavlovian eyeblink conditioning has established the necessity of specific regions in the cerebellar cortex and nuclei for the acquisition of well-timed conditioned behavior (Clark et al., 1984; Yeo et al., 1984, 1985a, b; McCormick & Thompson, 1984a, b; Berthier & Moore, 1986; Hesslow & Ivarsson, 1994; Yeo & Hesslow, 1998; Green & Steinmetz, 2005; Kotani et al., 2006; Jirenhed et al., 2007; Halverson et al., 2015; ten Brinke et al., 2015). As the conditioned stimulus (CS, e.g. a light or a tone) is paired with the unconditional stimulus (US, e.g. corneal air puff), the corresponding neural signals are carried to the cerebellum through mossy fiber and climbing fiber afferents and entrain cerebellar cortical Purkinje cells. Their resultant simple spike rate suppression (Fig. 1A, B) disinhibits the cerebellar nuclei in a manner that leads to the well-timed recruitment of downstream nuclei that innervate the eyelid muscles, leading to preemptive eyelid closures, i.e. conditioned responses (CRs). This simple spike suppression is also termed the Purkinje cell CR (Jirenhed et al., 2007), and constitutes a quintessential expression of the rate coding model of cerebellar learning (Walter & Khodakhah, 2006, 2009) in a zebrin-negative module (De Zeeuw & ten Brinke, 2015), where timed cortical spike rate suppression translates straightforwardly to nuclear excitation and resultant behavior.

Long term depression and potentiation at parallel fiber to Purkinje cell synapses have long been considered to adapt simple spike responses under the supervision of climbing fiber signals (Marr, 1969; Albus, 1972; Ito & Kano, 1982; Coesmans et al., 2004; Linden et al., 1991), and numerous models that build on this principle can accurately reproduce conditioned behavior while considering the translation from cerebellar cortex to nuclei to be a simple linear inversion (Buonomano & Mauk, 1994; Medina et al., 2000; Yamazaki & Tanaka, 2007; see Steuber, 2015). Nevertheless, there is an ever-growing inventory of additional sites of synaptic, intrinsic, and structural plasticity in the cerebellum (Hansel, Linden, & D'Angelo, 2001; Gao, van Beugen, & De Zeeuw, 2012; Johansson et al., 2015; Boele et al., 2013), as well as alternative neural encoding methods (Steuber et al., 2007; De Zeeuw et al., 2011; Person and Raman, 2012). In line with this rich capacity for neural communication, recent electrophysiological work expands on Purkinje cell simple spike suppression and its inverted effect in the cerebellar nuclei by highlighting some additional cerebellar neuronal responses in the eyeblink conditioning paradigm (Ohmae et al., 2015; Chapter 2: Ten Brinke et al., 2015; and Chapter 6: Ten Brinke et al., submitted).

Conditioned climbing fiber responses

Cerebellar cortical lobule HVI: CS-complex spikes

Mentioned as early as in Berthier and Moore (1986), the occurrence of a consistent complex spike response within the CS-US interval in eyelid-related Purkinje cells, here called CS-complex spikes, was reported in detail in Ohmae and Medina (2015) and ten Brinke et al. (2015), based on single unit recordings in eyeblink-conditioned mice (Fig. 1C, D). Purkinje cells were considered to be eyelid-related if they reliably
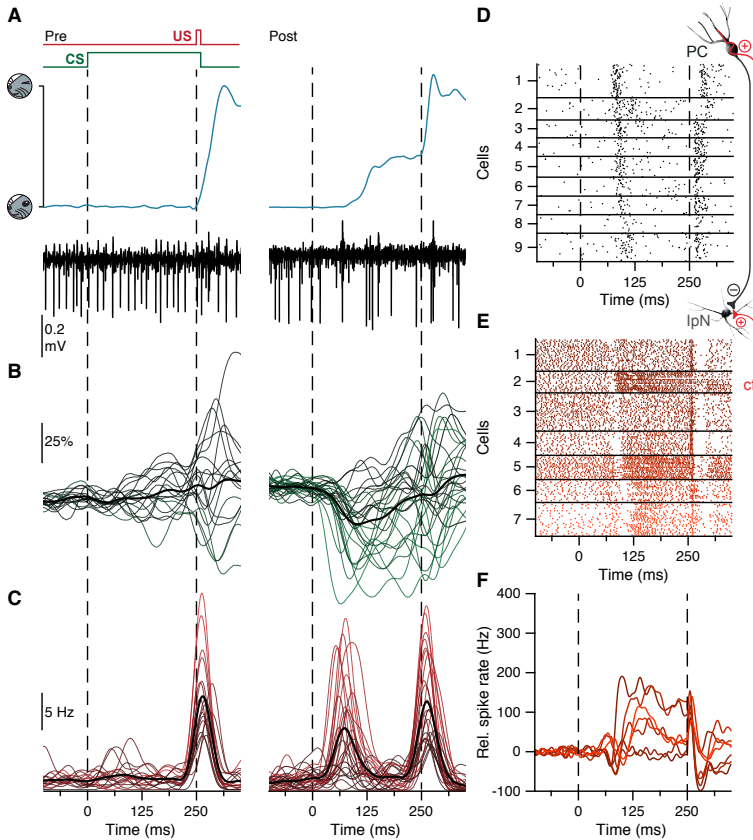
Figure 1 Conditioned responses in cerebellar cortex and nuclei. (A) Example eyelid and lobule HVI Purkinje cell trace before (left) and after (right) conditioning. **(B)** Average simple spike traces for 17 Purkinje cells before training (left), and 26 Purkinje cells after training (right), showing spike rate as percentage of baseline. **(C)** Same as in B, here showing average complex spikes traces (in Hz). **(D)** Climbing fiber (cf) evoked Purkinje cell (PC) complex spike raster plots for nine of the cells in **(C)** (each rule represents a trial), recorded after conditioning. **(E)** Spike raster plots for seven interpositus nucleus (lpN) neurons, recorded after conditioning. **(F)** Average spike traces for the lpN neurons in E. Data adapted from Chapters 2 and 6.

responded to the US with a complex spike, which indicates that their output can be adapted through perturbations of the eye. CS-complex spikes occur somewhat ahead of the typical CR onset latency, at 60-100 ms after CS onset in the case of an LED light CS, and across 220, 250, and 370 ms CS-US intervals; tone CSs elicit both earlier CRs and CS-complex spikes, Ohmae & Medina, 2015). Moreover, the response seems to be acquired over the course of conditioning, as they were virtually absent in eyelid-related Purkinje cells in naïve mice (Ohmae & Medina, 2015; Chapter 2). This agrees with one part of a dopamine neuron analogy that was put forward by Ohmae and Medina (2015), which suggests that CS-complex spikes may convey

an anticipatory signal for the impending US, a feat that should only be feasible in mice that have gone through some training. Another part of their dopamine analogy, however, suggests CS-complex spikes to reflect the novelty of the CS, which by contrast presupposes its occurrence specifically in mice that have not been previously exposed to the conditioning stimuli. Importantly, because novelty signals are not inherently related to the US, or to the eyeblink conditioning paradigm or to any specific olivo-cerebellar module in particular, any climbing fiber response they would elicit should be in itself ''naïve'', in contrast to the climbing fiber response which has developed over time in specifically eyelid-related modules. Given this qualitative difference, we shall only consider the latter, conditioned climbing fiber response relevant to the eyeblink conditioning paradigm, in this review.

There are many questions about the CS-complex spike that the currently available data is too limited to provide definitive answers to. Where does the olivary input underlying it originate and what neuronal activity mediates the plasticity leading to its emergence? Is the response in any way physiologically distinct from the climbing fiber and Purkinje cell responses that occur spontaneously or that are unconditionally elicited? Does it serve any direct or indirect purposes with regards to the conditioning paradigm, does it introduce robustness to the system through redundancy, or is it little more than a byproduct of network plasticity processes? While dedicated experiments are needed to empirically answer these questions, it is worthwhile to assess the clues that exist in the CS-complex spike data that is currently at hand.

With regards to the manifestation of CS-complex spikes, some observations would suggest the response carries some properties that may distinguish it from spontaneous complex spike activity. First, there are cases in which consecutive CS-complex spikes consistently occur within the CS-US interval (Fig. 2A, B; Chapter 2). These double responses were mirrored in the spike activity of interpositus neurons (Fig. 2C, even hinting at a third complex spike in cell 1), which are discussed further below. In the example cell in Fig. 2, the latencies of these double complex spikes relative to the CS correlated (Fig. 2D), with their interval averaging 48.8 ms (Fig. 2E). Complex spike doublets have been reported previously (Van Der Giessen et al., 2008; De Gruijl et al., 2014), and indeed with a higher incidence upon perturbation (De Gruijl et al., 2014). However, the reported latencies were more in line with olivary oscillations under 12 Hz (140 ± 12 ms, Van Der Giessen et al., 2014), in similarly awake behaving mice. This frequency seems to be an upper limit for olivary subthreshold oscillations (e.g. Van Der Giessen et al., 2008; Bazzigaluppi et al., 2012), making the observed CS-complex spike doublet intervals remarkably short. This length of time has been reported previously, however: Sedgwick and Williams found complex spike doublets spaced a similar distance apart after 0.3 ms electrical stimulation of the caudate nucleus, in cats (1967; Fig. 2A, inset). Thus, CS-complex spike doublets may reflect their stimulus-evoked nature. Moreover, given that non-functional olivary coupling through gap junctions was shown to lead to a substantially higher occurrence of doublets (Van Der Giessen et al., 2008), a dynamically decoupled state of olivary neurons could also play a role in the manifestation of CS-complex spike doublets.

Another observation potentially distinguishing CS-complex spikes from spontaneous, and even US-elicited complex spikes, relates to the complex spike waveform, which generally includes spikelets in extracellular recordings near Purkinje cell somas. Complex spikes have been shown to exhibit different spikelet characteristics,
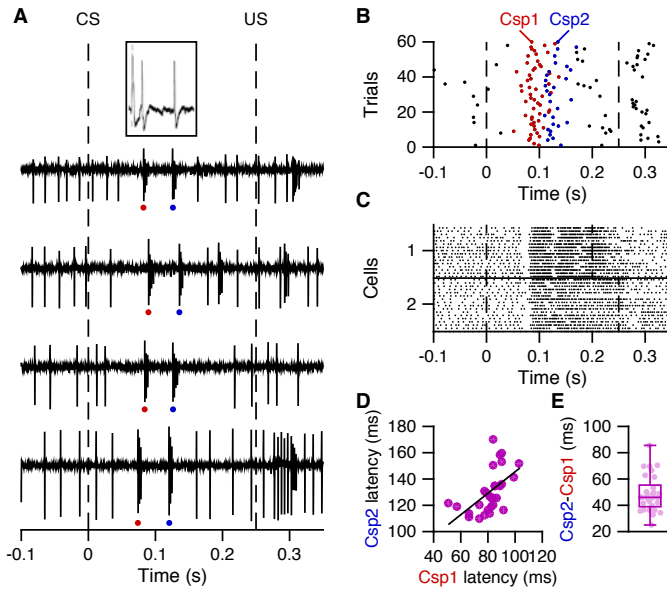
Figure 2 Double CS-complex spike responses. (A) Single unit Purkinje cell activity during four example trials that were given to a trained mouse, and show double CS-complex spike responses. Inset shows two responses in an olivary neuron after caudate stimulation (first deflexion is stimulus artefact), adapted from Sedgwick & Williams (Fig. 9; 1967). **(B)** Complex spike raster plot for the entire recording corresponding to the example trials in A. For complex spikes occurring between 50 and 170 ms post-CS, distinction was made between initial CS-complex spikes (Csp1, red), and optional second CS-complex spikes (Csp2, blue). **(C)** Rasterplots for two interpositus neurons that show hints of a second transient pause response roughly consistent with the latency of the second CS-complex spike. **(D)** Csp1 latency correlated to Csp2 latency, across 29 of the trials in Bin which both occurred (r = 0.674, p = 0.0001, Spearman). **(E)** The interval between Csp1 and Csp2 averaged 48.9 ± 13.8 ms. Data adapted from Chapters 2 and 6.

depending for instance on preceding simple spike (Servais et al., 2004) and complex spike activity (Warnaar et al., 2015) and the oscillatory phase of the source olivary cell (Mathy et al., 2009). An interesting observation among some of the Purkinje cells from Chapter 2 was that CS-complex spikes seemed inclined to exhibit an idiosyncratic waveform, as was the case in the example cell in Fig. 3. An unsupervised k-means clustering algorithm separated different clusters of complex spike waveforms (Fig. 3A), and a subsequent investigation of the proportional representation of the cluster labels among spontaneous and CS- and US-related complex spikes (Fig. 3B, C) revealed a uniquely high prevalence of one cluster among the CS-complex spikes (Fig. 3D). Given that preceding Purkinje cell activity is thought to relate to the manifestation of spikelets in complex spikes (Burroughs et al., 2016), this finding could mean that a particular transfer of conditioned neural activity is reliably in progress by the time the CS-complex spike is triggered.

Do CS-complex spikes enhance conditioned behavior? Both Ohmae and Medina (2015) and Chapter 2 report marginally better CRs in trials with a CS-complex spikes compared to those without. Additionally, among trials with a CS-complex spike, its
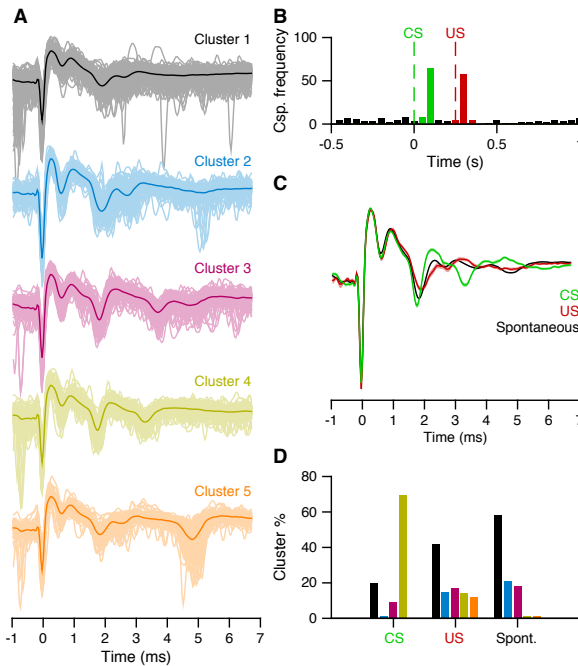
Figure 3 Idiosyncratic CS-complex spike waveform. (A) For an example eyelid-related Purkinje cell from Chapter 2, all complex spike waveforms from the recording (1 6 min.) were clustered with a k-means algorithm, minimizing squared euclidean distance. **(B)** Complex spike histogram for the trial timespan (n = 90 trials), showing the distinction between CS-complex spikes (green), US-complex spikes (red), and spontaneous complex spikes (black). **(C)** Average complex spike waveforms for the three groups in B. Note that the spontaneous complex spikes also include all occurrences outside of the trial timespan. **(D)** Proportional occurrence of complex spikes from each of the clusters separated in A, within the three groups in **(B)** and **(C)** (for each of the CS, US, and spontaneous groups, the sum of the five bars amounts to 100%). Note the uniquely high prevalence of Cluster 4 complex spikes in the CS-complex spike group.

latency seemed slightly earlier in trials with a CR compared to those without a CR (Chapter 2). However, there were no trial-by-trial correlations between CS-complex spike latency and CR onset latency (Ohmae & Medina, 2015). Compared to the substantial influence of simple spike suppression on CR expression, it would seem that CS-complex spikes may be more indirectly relevant, for instance for plasticity processes that enhance cerebellar output, or for an altogether different purpose than the expression of CRs, such as the anticipatory signal hypothesized by Ohmae & Medina (2015).

Beyond the single Purkinje cell-level, we would argue that CS-complex spikes may carry more substantial influence on conditioned cerebellar output, and thereby on conditioned behavior, at the ensemble level. While studies employing two-photon calcium imaging of strips of adjoining Purkinje cells report substantial levels of climbing fiber synchrony in response to stimuli (Ozden et al., 2009, 2012; Jacobson et al., 2009; De Gruijl et al., 2014), they are still far too low for the complex spike activity of one Purkinje cell to accurately predict that of the population on an across-trial basis. Stimulus-evoked climbing fiber synchrony ranged from 20% (De Gruijl et al., 2014) to about 40% (Ozden et al., 2012) of Purkinje cells in a 200 m window, with different dendrites responding from trial to trial (Ozden et al., 2009). Indeed, the correlation between even the most proximal pairs of Purkinje cells did not exceed 0.3 (De Gruijl et al., 2014). This suggests that rather than operating uniformly, an ensemble of olivary cells may reliably elicit specific degrees of synchronous complex spike input to the cerebellar nuclei based on the combined spike probabilities of the constituent olivary

cells. The stability of this synchrony across trials is inversely linked to the degree of correlation among olivary cells; high correlation means that on some trials many climbing fibers coactivate and on others many climbing fibers do not activate, and conversely no correlation means that the ensemble should show a similar fraction of coactive climbing fibers across trials. Given that neuronal activity should convey stimulus information stably across trials, rather than erratically, it is more likely that individual Purkinje cell complex spikes should generally only reflect a fraction of the ensemble climbing fiber input to a cerebellar nuclear neuron.

Thus, in spite of only marginal correlations with CR behavior at the individual Purkinje cell level, the CS-complex spike may still carry a substantial contribution at the ensemble level, at which it is established that Purkinje cells can transfer relevant information (Person & Raman, 2012; Hoogland et al., 2015; Tang et al., 2016). If this is the case, this should be reflected in neuronal responses in target neurons in the cerebellar interpositus nucleus, which is discussed in the next section.

Cerebellar interposed nucleus: CS pause and subsequent rapid excitation

A number of studies show that synchronized complex spike activity, spontaneous (Tang et al., 2016), elicited with optogenetic (Lu et al., 2016) or electrical (Hoebeek et al., 2010) inferior olivary stimulation, or with electrical skin stimulation (Bengtsson et al., 2011), leads to a transient spike pause in target neurons in the cerebellar nuclei. In line with these findings, single-unit recordings in the interposed nuclei confirm an increasing prevalence over the course of eyeblink conditioning of transient spike pauses at latencies similar to those of CS- and US-related complex spikes (Fig. 1E, F; Chapter 6). Particularly in regions confirmed through micro-stimulation to be eyelid-controlling, more than half of the interpositus neurons that showed facilitation in the CS-US interval also showed this so-called CS pause, in well-trained mice. The latency of minimal average firing rate in the CS-pause time window (50-125 ms after CS onset) was related to the average latency of the CR (r = 0.582, Chapter 6). This seems contradictory with the fact mentioned earlier that CS-complex spike latency was not substantially different between a 200-, 250- and a 370-ms CS-US interval, but this is not surprising given that CR onset does not show a pronounced difference across these intervals either. Note also that the link between the latencies of conditioned climbing fiber responses and the CR seems to only apply to their averages, as trials with an early CR onset did not show earlier CS-complex spikes than did trials with a late CR (Fig. 4c, f, in Ohmae and Medina, 2015).

Importantly, in many cases, the CS pause led to a rapid excitation that generally peaked within 50 ms (Chapter 6). This rapid excitation was largely unexplained by modeled IpN spike activity that was based on simple spike suppression profiles. A similar pause-excitation pattern in response to the US was apparent in IpN neurons that were recorded later in training during worse CR performance. Moreover, in 12 IpN neurons recorded during paired and US-only trials, strikingly similar pause-excitation patterns were elicited by CS and US, respectively. In fact, the profile of the excitatory component elicited in US-only trials neatly overlapped with an initial part of the CS-US facilitation, much like the part that IpN activity modeled from simple

spike suppression could not explain. Thus, within the CS-US facilitation profile, there seemed to be an initial component that seems dependent on complex spike input, called Facilcsp, and a subsequent broader facilitation component that seems dependent on simple spike suppression, Facilssp, in facilitation cells with a CS pause. The Facilcsp component fits well with neuronal response profiles found in previous work on cerebellar nuclear rebound excitation (Hoebeek et al., 2010; Bengtsson et al., 2011; Bengtsson & Jörntell, 2014). Moreover, given its prevalence decidedly later in the course of conditioning, Facilcsp likely constitutes an additional acquired neuronal response in the eyeblink conditioning paradigm. The notion of Facilcsp as an instance of acquired rebound excitation will be discussed separately further ahead.

Possible origins of conditioned climbing fiber responses

Cerebellar output

Given the acquired nature of conditioned CS-complex spikes, the inferior olivary cells that are part of eyelid-related olivocerebellar modules need to receive spike-eliciting input after training that they did not receive beforehand. The probability with which these cells elicit CS-complex spikes in their target Purkinje cells strongly related to the latter's average magnitude of simple spike suppression (r = 0.8; Chapter 2). Based on this relation, we have previously speculated that the plasticity processes underlying these reponses may lie close together (Chapter 2). One form of plasticity that was shown to occur over the course of eyeblink conditioning concerns the structural outgrowth of mossy fiber collaterals to the interposed nucleus (Fig. 4, Boele et al., 2013), which offers an interesting possibility of how CS-complex spikes can come about. These newly sprouted mossy fiber collaterals could carry CS signals to nuclear excitatory projection neurons that innervate nuclei in the mesodiencephalic junction, which has numerous excitatory projections to the inferior olive (De Zeeuw et al., 1990). Indeed, Bazzigaluppi et al. (2012) show that electrical stimulation in the cerebellar nuclei can elicit short-latency EPSPs in inferior olivary cells after 38.2 14.2 ms, and with probabilities of 43.1% and 29.1%, depending on the type of oscillations exhibited by the cell (sinusoidal subthreshold oscillations vs low-threshold oscillations, respectively). Since electrical stimulation excites both excitatory projection neurons as well as direct inhibitory nucleo-olivary projections (Hesslow & Ivarsson, 1996; De Zeeuw et al., 1997), the same experiment was able to show that nucleo-olivary inhibition takes effect after the time-window of the short-latency EPSP (Bazzigaluppi et al., 2012). Thus, even if mossy fiber collaterals also innervated nucleo-olivary cells, this should not obstruct the effect of a potential disynaptic excitatory projection to the olive.

The main problem with the idea that cerebellar output drives CS-complex spikes is that, in terms of rate coding, there do not seem to be any meaningful spike responses in the interpositus nucleus at the required latency of approximately 40 ms post-CS (given an 80 ms latency of the CS-complex spike, and a 38.15 ms delay from nuclear excitation to olivary EPSP), judging from multiple electrophysiological studies on classical conditioning in the cerebellar nuclei (Berthier & Moore, 1990; Choi and Moore, 2003; Halverson et al., 2010; Gruart et al., 2000; Delgado-Garcia & Gruart, 2005; Chapter 6).
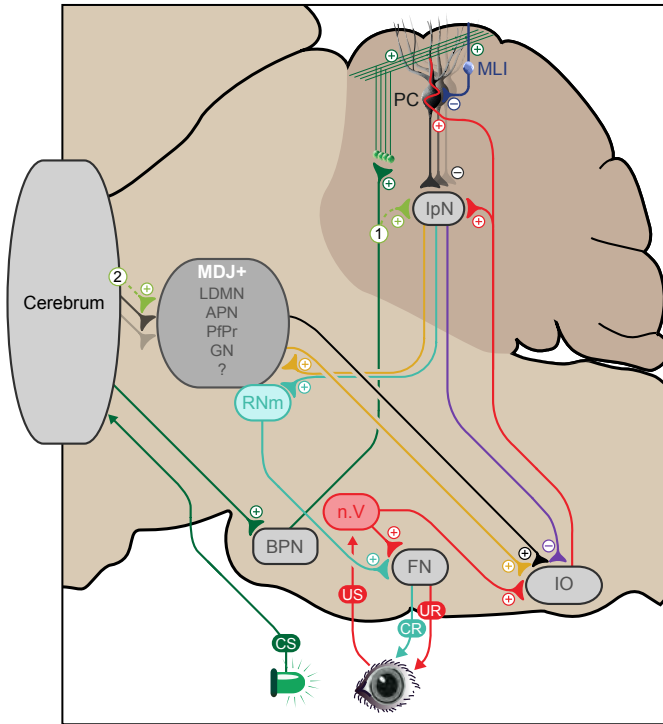
Figure 4 Neurocircuitry underlying eyeblink conditioning: possible routes to CS-complex spikes. US presentation activates a disynaptic eyeblink reflex loop, passing through the trigeminal nucleus (n. V) and the facial nucleus (FN). The trigeminal also sends US-signals to the inferior olive (10), particularly rostral dorsal accerssory olive and dorsomedial group, whose climbing fibers project to cerebellar Purkin-je cells (PC), mainly in the lobule HVI (simplex, US pathways shown in red). Since during conditioning, CS-signals consistently reach these same PCs through a mossy fiber - parallel fiber projection from the basal pontine nuclei (BPN; CS pathway shown in dark green), the climbing fiber signals condition the PCs to develop simple spike suppression in response to the CS. This causes nucleus interpositus neurons (lpN) to send excitatory signals through the magnocellular part of the red nucleus (RNm) to the facial nucleus, effecting a well-timed CR (pathway shown in teal). Toward the 10, the lpN sends a direct inhibitory projection (purple pathway), as well as a disynaptic excitatory projection through the mesodiencephalic junction and numerous other brain stem nuclei (MDJ+). Axonal outgrowth of mossy fiber collaterals to the lpN (light green, labelled with a 1) provides a possible pathway for CS signals to hook up to this excitatory projection via the MDJ. Alternatively, plasticity involving extra-cerebellar, likely cerebral sources, could send anticipatory signals evoked by the CS to the 10 via a number of possible nuclei in MDJ+ (light green, labelled with a 2). For example, the basal ganglia send efferents to the lateral deep mesencephalic nucleus (LDMN), which has a reciprocal connection with eyelid-related olivocerebellar modules. *APN, anterior pretectal nucleus; PfPr, nucleus parafasciculus prerubris; GN, gigantocellular nucleus.*

Moreover, the notion that the link between simple spike suppression strength and CS-complex spike probability implies common underlying plasticity processes may not hold in a very straightforward manner. Purkinje cells in trained mice showing CS-complex spikes did so with a probability (46.7 18%) that was comparable to the probability of eyelid-related Purkinje cells in naïve mice showing US-complex spikes (42.1 15%; p = 0.5457, Mann-Whitney U test; Chapter 2). In fact, from a

strong correlation that Ohmae and Medina (2015) report between CS-complex spike probability in paired trials and US-complex spike probability in US-only trials (r = 0.72), it seems that the responsible olivary neurons simply exhibit similar excitability to their CS- and US-related inputs. Together with the notion from central cerebellar learning theories (Marr, 1969; Albus, 1972; Ito & Kano, 1982; Coesmans et al., 2004) that modulation of Purkinje cell output is mediated by US-complex spike signals, it should logically follow that simple spike suppression be linked to the probability of CS-complex spikes. That is, higher US-complex spike probability means more instructive signals to effect conditioned Purkinje cell simple spike suppression, and comparable excitability of olivary cells to CS and US input means comparable CS- and US-complex spike probability. Thus, US-complex spike probability may be the variable mediating the link between CS-complex spike probability and simple spike suppression. Nevertheless, it could still be that downstream plasticity mediated by simple spike suppression and resultant cerebellar output tunes the level of excitation elicited by the CS at the olivary level. In conclusion, as long as the relevant olivary neurons simply respond to CS- and US-related input with a similar probability, the CS-related input could essentially come from anywhere in the brain.

Extra-cerebellar sources

If indeed the latency of CS-complex spikes precludes the reasonable inclusion of a roundtrip through the cerebellum in its route of origin, and its underlying plasticity process does not have to have any special relationship with that underlying simple spike suppression, it seems our focus should point to neural sources upstream from the cerebellum. Given the specificity of the conditioned CS-complex spike within eyelid-related Purkinje cells, these sources would have to be capable of learning to excite specifically eyelid-related olivary neurons in response to the CS. Thus, the following three aspects are important in the consideration of candidate regions: i) it should send excitatory projections to the inferior olive, including those parts that are involved in eyeblink conditioning; ii) it should receive CS-related information; and iii) it should likely receive input reflecting the eyelid-controlling olivocerebellar modules to allow for selective potentiation among their olivary efferents (Fig. 4).

The olivocerebellar modules shown to be involved in eyelid behavior are cerebellar cortical zones C1, C3 (Hesslow, 1994; Gruart et al., 1997) and D0 (Sugihara & Shinoda, 2007; Mostofi et al., 2010), which are linked to the cerebellar anterior interposed nucleus and dorsolateral hump (DLH, Morcuende et al., 2002), and in the inferior olive to mainly the ventral/rostral dorsal accessory olive (v/rDAO) and the dorsomedial group (DM; De Zeeuw et al., 1996; Sugihara & Shinoda, 2007; Sugihara, 2011; Voogd et al., 2013), respectively. Two afferents of these regions that are central to the eyeblink conditioning paradigm concern the excitatory afferents from the trigeminal nucleus (Swenson & Castro, 1982; Morcuende et al., 2002), which relay US signals from the eye, and inhibitory afferents from the corresponding cerebellar nuclear regions (De Zeeuw et al., 1988; Hesslow & Ivarsson, 1996), which may regulate olivary coupling (De Zeeuw et al., 1998; Lefler et al., 2014). Note that in the pursuit of extra-cerebellar candidate regions that could underlie conditioned climbing fiber activation, the available anatomical research dates back several decades and the employed

methods often do not permit inferences on whether projections are excitatory or inhibitory. Nevertheless, it would seem extra-cerebellar input to the olive is principally excitatory (De Zeeuw et al., 1998). Another concern is that the anatomy work is done on different species that can show substantial anatomical differences. For instance, while olivary DM and cerebellar nuclear dorsolateral hump are identifiably distinct in rodents, they are not in cats or rabbits (Voogd et al., 2013), and while the red nucleus and the nucleus of Darkschewitsch show substantial projections to the inferior olive in cats (Onodera, 1984; De Zeeuw & Ruigrok, 1994), they barely seem to in rats (Rutherford et al., 1984). Thus, work in non-rodent species should be relied on with some caution, as should the default assumption of the excitatory nature of extra-cerebellar projections to the inferior olive. Several extra-cerebellar inputs to rDAO and/or DM arise in the brainstem. Neurons in the ventral anterior pretectal nucleus and some surrounding pretectal neurons (from the dorsal pretectal nucleus and the nucleus of the posterior commissure) were shown to project to rDAO in rabbit and cat (Kitao et al., 1989; Itoh et al., 1983; Kawamura & Onodera, 1984; see Voogd et al., 2013). In addition, the prerubral parafascicular nucleus projects heavily to the inferior olive, including all subdivisions of the DAO in rats (Carlton et al., 1982). Finally, nuclei in the reticular formation, in particular the medullary gigantocellular (cats: Courville et al., 1982; rats: Swenson & Castro, 1983) and lateral deep mesencephalic nuclei (LDMN, Swenson & Castro, 1983), were shown to also project to rDAO and DM (although Swenson and Castro did not identify DM as such).

The LDMN has some interesting afferents; retrograde horse-radish peroxidase (HRP) tracers injected in rat mesencephalic reticular formation revealed pronounced labelling in cerebellar nuclear DLH (Shammah-Lagnado et al., 1983). Additionally, motor and somatosensory cortex, entopeduncular nucleus, zona incerta, substantia nigra, and superior colliculus project to LDMN in rat (Veazey & Severin, 1982). The LDMN's reciprocal connections with thalamus and basal ganglia (Veazey & Severin, 1980, 1982), together with the input it receives from eyelid-related DLH (Shammah-Lagnado et al., 1983), provide potential pathways through which the salience of the CS could be modulated, and CS-related excitatory input to the eyelid-related olivary regions could be shaped.

The simultaneous involvement of multiple pathways during eyeblink conditioning is apparent from the fact that eyelid CRs can simultaneously include startle responses, short-latency responses, and conditioned responses that are timed with the onset of the US (Boele et al., 2010). Boele et al. (2010) propose an amygdala-cerebellum-dynamic-conditioning (ACDC) model, in which CS and US information converge both in the amygdala and in the cerebellum, with each pathway dynamically shaping the short-latency and well-timed eyelid response components, respectively. In a review on the involvement of prefrontal regions in the eyeblink conditioning paradigm, Weiss and Disterhoft (2011) emphasize their likely involvement in the modulation of pontine input to the cerebellum, in particular in trace conditioning and in situations where the US would not elicit enough emotional arousal for the sufficient development of conditioning through amygdala-driven pathways, e.g. when an air puff instead of a periorbital shock is used (Oswald et al., 2006). Note that this difference between air puff and shock US may in part be due to and/or confounded with a likely degree of operant conditioning that occurs with air puff-driven but not shock-driven paradigms (Longley and Yeo, 2014). White et al. (1994) show how the caudate nucleus in rabbits

showed increased spike activity during the CS-US interval (250 ms) after a delay eyelid conditioning paradigm using an air puff US. Moreover, perturbation of the caudate through haloperidol injections reduced CR behavior only when the weaker of two tone CSs was used (80 vs 90 dB; White et al., 1994). These findings lend further support to the idea that multiple may potentiate and contribute over the course of conditioning (Weiss & Disterhoft, 2011), and multiple sites of convergence of CS and US information may simultaneously effect conditioned response processes in the brain (e.g. Weinberger, 2011). This also implies there are likely myriad potential pathways in the brain that will include points at which the criteria proposed at the start of this section are sufficiently met. Given its appropriate connectivity, the involvement of the basal ganglia in delay eyeblink conditioning, and the ability of activity in the caudate to elicit olivary complex spike doublets (Fig. 2), we would propose the LDMN is one of these potential points at which CS-related signals may develop to elicit excitation of eyelid-related olivary cells (Fig. 4).

Possible functions of conditioned climbing fiber responses

Conditioned rebound excitation: a hypothesis

There is a striking similarity between the CS- and US-related pause-excitation pattern of IpN spikes in Chapter 6 (Fig. 5A-C), and those induced by electrical olivary stimulation (Hoebeek et al., 2010), and manual and electrical stimulation of skin areas that are part of IpN neurons'climbing fiber receptive fields (Fig. 5D; Bengtsson et al., 2011; Bengtsson & Jörntell, 2014). These studies were largely aimed at addressing an open question in the cerebellar field: does cerebellar nuclear rebound depolarization constitute a meaningful coding mechanism in the cerebellum? In vitro, it was shown that upon hyperpolarizing input, cerebellar nuclear neurons are capable of showing strong post-inhibitory spike responses exceeding baseline firing frequency (Jahnsen, 1986; Llinás & Mühletahler, 1988), that could last for hundreds of milliseconds, even when excitatory transmission was blocked (Aizenman & Linden, 1999; Molineux et al., 2006; Alviña et al., 2008; Zheng & Raman, 2009; Tadayonnejad et al., 2010). Rebound depolarization seems to be mediated in part by T-type calcium channels (Llinás & Mühletahler, 1988; Alviña et al., 2009; Engbers et al., 2011), hyperpolarization-gated cyclic nucleotide channels (Engbers et al., 2011), and persistent sodium channels (Sangrey & Jaeger, 2010; Steuber et al., 2016), as well as concurrent mGlur1 activation (Zheng & Raman, 2011). The capacity for rebounds seems to apply more to the large excitatory projection neurons than to the nucleo-olivary neurons in the cerebellar nuclei (Najac & Raman, 2015; Steuber, 2016). In vivo, rebound excitation in the cerebellar nuclei is not a given; while the work by Hoebeek et al. (2010) and Bengtsson et al. (2011) reports clear rebounds, the only way to do so was through stimulus-evoked highly synchronous climbing fiber activity. By contrast, Lu et al. (2016) did not report any rebound excitation upon optogenetic stimulation in the inferior olive. Similarly, while Witter et al. (2013) report clear rebound excitation after
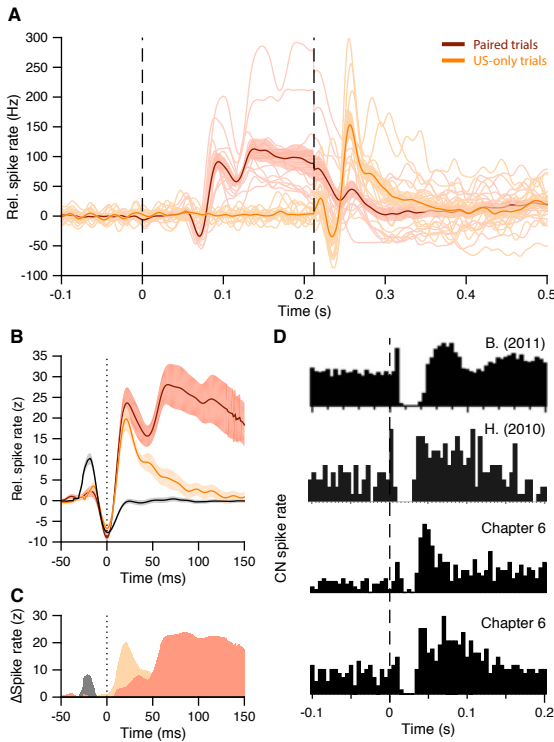
Figure 5 Rapid excitatory response following complex spike induced spike pause In lpN neurons. **(A)** Average spike traces for 12 lpN neurons recorded in well-trained mice, during paired trials, with mean and SEM (in brown and pink, respectively), and during US-only trials (orange and yellow). **(B)** Overlay of the mean traces of the paired trial data (with SEM, brown and pink) and US-only trial data (orange and yellow) in A, after standardizing by baseline. For reference, US pause-aligned traces for naïve mice receiving paired trials are shown in black and gray. **(C)** Difference plot for the mean traces in C, showing black - orange (gray), orange - black (yellow), and brown - yellow (pink). **(D)** Stacked comparison of stimulus-evoked spike responses of cerebellar nuclear cells. The top peri-stimulus time histogram (PSTH) was adapted from Bengtsson et al. (2011; Fig. BA), where the stimulus was electrical skin stimulation in the cell's climbing fiber-receptive field. The second PSTH was adapted from Hoebeek et al. (2010; Fig. 3E), where electrical stimulation of the inferior olivary was the stimulus. The bottom two PSTHs, like the other panels from this figure, were adapted from data from Chapter 6, here depicting US-only data for two of the cells in A. The stimulus was an unexpected periocular air puff of 20 ms.

optogenetic activation of Purkinje cell ensembles, Alviña et al. (2008) only observed rare occurrences of rebound after electrical stimulation of Purkinje cell afferents to cerebellar nuclear cells.

While empirical evidence has still not resolved the normal functional expression of cerebellar nuclear rebound excitation, numerous models and mechanisms of coding and plasticity presume its contribution (Kistler & Van Hemmen, 1999; Steuber et al., 2007; Pugh & Raman, 2008; Wetmore et al., 2008; Jaeger, 2011; De Zeeuw et al., 2011). Although the involvement of rebound in the performance of movement is contested, there seems to be some agreement that rebound excitation may play a role in cerebellar learning (De Zeeuw et al., 2011; Bengtsson et al., 2011; Reato et al., 2016), perhaps particularly in zebrin-negative zones (De Zeeuw & ten Brinke, 2015; Steuber, 2016). Given this suggestion, and given the striking similarity between the rebound excitation in previous work (Hoebeek et al., 2010; Bengtsson et al., 2011), and the CS- and US-related pause-excitation patterns reported in Chapter 6, we propose that rebound excitation may manifest in cerebellar nuclear neurons in the behavioral context of classical conditioning.

The post-inhibitory rebound state in the cerebellar nuclei may augment the effects of simple spike suppression by virtue of its occurrence after the conditioned CS-related climbing fiber input (Ohmae & Medina, 2015; Chapter 2), it may mediate

potentiation of CS-carrying mossy fiber input to the nuclei through its inhibition-excitation dynamic (Pugh & Raman, 2008), and it may provide feedback signals to upstream targets, such as the pons (Clark et al., 1997) or the cerebellar cortex (Gao et al., 2016), to further tune the neuronal circuitry to CS signals and amplify cerebellar conditioned output (e.g. Giovannucci et al., 2017). Of course, future research needs to establish whether the post-pause excitation as reported in Chapter 6 in fact concerns rebound, for instance by establishing its abolition upon injection of T-type calcium channel blocker TTA-P2 (Boehme et al., 2011), or NNC 55-0396 (Alviña et al., 2009). Moreover, to explore a possible interaction with mGluR activity elicited by mossy/climbing fiber collaterals, competitive mGluR antagonist CPCCOEt could be used (Zheng & Raman, 2011). Reductions in conditioned behavior as a result of these pharmacological interventions will simultaneously shed light on the weight of the contribution of rebound excitation to cerebellar eyeblink conditioning. Finally, it should be noted that the rebound excitation-like responses in Chapter 6 seemed to develop over the course of conditioning, and that the plastic modification of the intensity of rebound may be mediated by climbing fiber synchrony (De Zeeuw et al., 1998; Tang et al., 2016; Bengtsson et al., 2011). The potential absence of post-pause excitation responses in mice that lack gap junctions, such as the Gjd2-mutant, would provide compelling evidence for the functional role of gap junctions in mediating nuclear rebound excitation during cerebellar learning.

Second order conditioning

Beyond the conventional eyeblink conditioning paradigm, the CS-related complex spike imparts the CS with the crucial US-related property of eliciting error signals in the eyelid-related modules of the cerebellum. Like the US, the CS could, after conditioning, be paired with a novel neutral stimulus, which could then develop its own conditioned simple spike suppression under the instruction of CS-related complex spikes. This principle is called second order conditioning (Gewirtz & Davis, 2000; Rizley & Rescorla, 1972), and was shown to work approximately half as well as the original, first order conditioning paradigm (Pavlov, 1927). Second order eyeblink conditioning in mice, where the second CS is only paired with the first CS but never with the US, has so far not led to successful secondary CR behavior (De Zeeuw group, unpublished results). While similar future experiments may result in an effective second order conditioning paradigm, it is very much the question whether cerebellar control of movement, which hinges on accurate timing, has any benefit from transferring conditioned responses to the space between a second order and a first order CS. By contrast, types of conditioning not so dependent on timing, such as fear conditioning, may be more suited for the transference of behavioral responses from one CS to another by a process of association.

Toward an exhaustive inventory of synergistic plasticity mechanisms underlying associative learning

It is perhaps no surprise that the expanding body of research on the cerebellar system is bound to tear into monolithic models of cerebellar learning. Given the notion of synergistic interaction of multiple plasticity processes, the challenge now is to actually inventory these different processes, and determine the magnitude of their contributions, their interdependencies, and the degree of redundancy they introduce. Recent advancements contributing to this aim underline graded mediation of Purkinje cell plasticity based on complex spike duration (Yang & Lisberger, 2014; Rasmussen et al., 2013), molecular layer interneuronal inhibition (Chapter 2), intrinsic Purkinje cell mechanisms (Johansson et al., 2015), dense coding at the granule cell level (Giovannucci et al., 2017), and internal amplification through cerebellar nucleo-cortical feedback (Gao et al., 2016). The present review evaluates evidence for two additional contributors to specifically cerebellar classical conditioning. First, over the course of conditioning, an acquired climbing fiber response to the CS is reflected in complex spikes in eyelid-related Purkinje cells in mainly lobule HVI in the cerebellar cortex (Ohmae & Medina, 2015; Chapter 2). Second, in the cerebellar interpositus nucleus, this conditioned climbing fiber response, as well as a similar response to the US, are reflected as transient spike pauses (Chapter 6). Lastly, after conditioning, these complex spike-related spike pauses lead to strong excitatory responses in the cerebellar interpositus nucleus. Given that the circumstances and temporal profile of this pause-excitation pattern strikingly fits the reported post-inhibitory rebound excitation reported in Hoebeek et al. (2010) and Bengtsson et al. (2011; Fig. 5), we hypothesize the development of climbing fiber activation and subsequent rebound excitation in the cerebellar nuclei as additional conditioned cerebellar responses. Together, they could complement established conditioned simple spike suppression so as to enhance conditioned behavior, as well as mediate plasticity within the cerebellar nuclei (Pugh & Raman, 2008) as well as possibly outside of the cerebellum. In all, the conditioned responses here reviewed provide support for the idea that the inferior olive may drive timed cerebellar output (Llinás, 2009; Lefler et al., 2013) in a fashion that is not explained by rate coding mechanisms.

Chapter 10

Motor learning and the cerebellum

Whereas our capacity for declarative memory formation can nowadays be readily surpassed by that of simple personal computers, our ability to retrieve and express procedural memories still outperforms that of the most advanced robots controlled by a supercomputer. To a large extent our procedural memories are formed in the cerebellum, which embodies more than two thirds of all neurons in our brain. In this review we will focus on the emerging view that different modules of the cerebellum employ different encoding schemes to form and express their respective memories. More specifically, zebrin-positive zones in the cerebellum, such as those controlling adaptation of the vestibu-lo-ocular reflex, appear to predominantly form their memories by potentiation mechanisms and express their memories via rate coding, whereas zebrin-negative zones, such as those controlling eyeblink conditioning, appear to predominantly form their memories by suppression mechanisms and express their memories in part by temporal coding employing rebound bursting. Together, the different types of modules offer a rich repertoire to acquire and control senso-rimotor processes with specific challenges in the spatiotemporal domain.

Introduction

In the formation of procedural memories, the cerebellum shows at least two types of information coding within its massive neuronal networks (De Zeeuw et al., 2011; Person and Raman, 2012; Heck et al., 2013; Yang and Lisberger, 2013). Modulation of the average firing rate of neuronal spikes or ''rate coding'' is most often proposed as the predominant mechanism of information coding used for motor learning (Boyden et al., 2004; Lisberger, 2009; Walter and Khodakhah, 2009). However, spikes occur at millisecond precision, and their actual timing or ''temporal coding'' can increase the information content of spike trains and facilitate the entrainment of postsynaptic activity (Markram et al., 1997; De Zeeuw et al., 2011). To a large extent, the coding mechanisms used in the cerebellum for learning and expressing a particular form of motor learning depend on the specific cerebellar module that is controlling the type of behavior involved. The existence of cerebellar modules was discovered half a century ago by Jan Voogd (1964). Simply by studying the thickness of myelinated Purkinje cell axons in the white matter of the cerebellar cortex, Voogd observed distinct differences that were consistently organized in sagittal zones (Fig. 1).

Subsequent tracing and immunocytochemical experiments showed that each of these Purkinje cell zones provides an inhibitory projection to a distinct part of the cerebellar nuclei, which in turn inhibits a specific olivary subnucleus (Fig. 2). (Groenewegen and Voogd, 1977; De Zeeuw et al., 1994, 2011; Ruigrok and Voogd, 2000; Ito, 2002; Schonewille et al., 2006a). Because the climbing fibers originating from each olivary subnucleus project back to the Purkinje cells of the corresponding cerebellar cortical zone, these circuitries form precisely topographically organized three-element loops (Fig. 3A, B). They are referred to as the olivocerebellar modules and constitute the fundamental building blocks of the cerebellar system. The mossy fiber –parallel fiber system is superimposed in a largely orthogonal fashion on top of the sagittally oriented Purkinje cell zones (Fig. 3C); individual mossy fibers innervate multiple granule cells usually situated in multiple zones and the parallel fibers originating from these granule cells consistently traverse multiple zones in the molecular layer.

Over the past decades, it has gradually become clear that each module is concerned with control of specific tasks, such as execution of limb and finger movements, of trunk movements for balance, of compensatory eye movements about particular axes in space, reflexes of facial musculature, homeostasis of particular autonomic processes, and probably even specific cognitive tasks, such as time-sensitive decision making (De Zeeuw et al., 1994; Ito, 2008; Jörntell et al., 2000; Apps and Hawkes, 2009; Rahmati et al., 2014). However, it was not until recently that the specific intrinsic properties of different categories of modules emerged (Zhou et al., 2014). Here, we review the intrinsic differences of cerebellar modules and the implications for the coding mechanisms involved in cerebellar motor learning.

The sagittal zones of Purkinje cells in the cerebellar cortex can be identified based on the alternating presence and absence of expression of proteins, such as 5'-nucleotidase, zebrin I (i.e., mabQ113 antigen) and zebrin II (i.e., aldolase C), phospholipase Cb3 and b4, excitatory amino acid transporter 4 (EAAT4), $GABA_{B2}$ receptors, and splice variant b of the metabotropic glutamate receptor 1 (mGluR1b) (Brochu et al., 1990; Leclerc et al., 1990; Dehnes et al., 1998; Mateos et al., 2001; Wadiche and
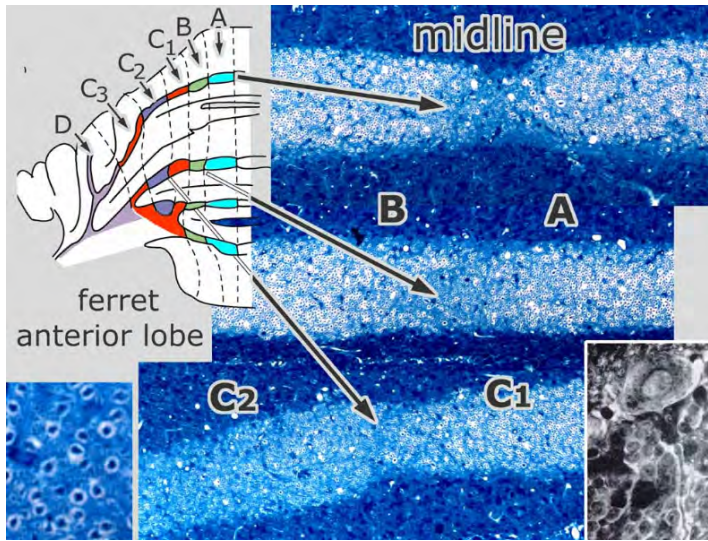
Figure 1 Original identification of Purkinje cell zones in the cerebellar cortex of ferrets using Haggquist staining (based on data from Voogd, 1964).

Jahr, 2005; Apps and Hawkes, 2009). These zebra-like patterns of protein distribution appear to be present in the cerebellum of all birds and mammals (Brochu et al., 1990; Sillitoe et al., 2003; Chung et al., 2007; Apps and Hawkes, 2009; Graham and Wylie, 2012), and in many cases. they largely correspond to the organization of the olivo-cerebellar modules (Figs. 2,3A –C) (Sugihara and Shinoda, 2004, 2007; Voogd and Ruigrok, 2004; Pijpers et al., 2006; Sugihara et al., 2009; Sugihara, 2011). For example, zebrin II, EAAT4, and $GABA_{B2}$ receptors are distributed in Purkinje cells of zones C2, D1, and D2, whereas mGluR1b is prominently expressed in zones B, C1, C3, and D0, providing a complementary pattern (Mateos et al., 2001; Chung et al., 2007; Apps and Hawkes, 2009). Importantly, Zhou and colleagues (2014) recently showed that these distribution patterns determine the intrinsic simple spike activity of Purkinje cells (Fig. 3B, C).

During sensorimotor stimulation and natural behavior, the simple spikes can modulate as a consequence of excitation via the mossy fiber–parallel fiber pathway and inhibition via the molecular layer interneurons, but at-rest Purkinje cells show a relatively high level of intrinsic activity, which can reach levels up to 120 Hz. In Purkinje cell zones positive for zebrin II and EAAT4 (referred to as zebrin-positive zones), simple spike firing approximates 60 Hz, whereas in those zones positive for mGluR1b (referred to as zebrin-negative zones), the average firing rate reaches 90 Hz (Zhou et al., 2014). The intrinsic nature of this difference in simple spike activity at rest cannot be inferred only from the fact that it can be correlated with differential protein expression inside Purkinje cells, but also from the fact that this difference holds when excitatory or inhibitory inputs to Purkinje cells are blocked (Wulff et al., 2009; Galliano et al., 2013a; Zhou et al., 2014). The molecular mechanisms that determine

the differences in firing frequencies in the zebrin-positive and zebrin-negative zones have been only partly resolved. Blocking transient receptor potential cation channel type C3 (TRPC3), which can be associated with zebrinnegative Purkinje cells and is required for the mGluR1-mediated slow excitatory postsynaptic currents (EPSCs) (Mateos et al., 2001; Hartmann et al., 2008; Chanda and Xu-Friedman, 2011; Kim et al., 2012a,b; Nelson and Glitsch, 2012), reduces simple spike activity of Purkinje cells in zebrinnegative, but not zebrin-positive Purkinje cells (Zhou et al., 2014). Thus, tonic activation of mGluR1b by ambient glutamate in zebrin-negative Purkinje cells might lead to opening of their TRPC3-channels and thereby to a relatively high level of simple spike activity (Yamakawa and Hirano, 1999; Coesmans et al., 2003; Chanda and Xu-Friedman, 2011). In contrast, similar glutamate-dependent increases may be prevented in zebrin-positive Purkinje cells, in which EAAT4 might help to keep glutamate concentrations relatively low (Dehnes et al., 1998; Auger and Attwell, 2000; Wadiche and Jahr, 2005; cf. Zhou et al., 2014). Downstream from mGluR1, proteins, such as the IP3-receptor (TRPC3 modulator), PLC-β3/4 (TRPC3 activator), protein kinase C (PKC)-δ, and NCS-1, play key roles in calcium release from intracellular calcium stores and consequently have electrophysiological impact in line with that of TRPC3. Because several of these proteins are expressed in zebrin-like bands (Barmack et al., 2000; Jinno et al., 2003; Sarna et al., 2006; Hartmann et al., 2008; Becker et al., 2009; Furutama et al., 2010; Wang et al., 2011; Kim et al., 2012a,b), it is possible that this entire pathway contributes to the high simple spike activity of zebrin-negative Purkinje cells. To what extent zebrin itself (i.e., zebrin II or aldolase C) contributes to this pathway is yet unknown, as the impact of its reaction products on simple spike firing is unclear (Zhou et al., 2014).

Figure 2 Olivocerebellar modules in mammals. The three-element modules of the olivocerebellar system are formed by a sagittal strip of Purkinje cells in the cerebellar cortex **(A)**, which converge onto a particular set of cerebellar and/or vestibular nuclei **(B-D)**, which, in turn, innervate the subnucleus in the inferior olive **(E,F)** that provides the climbing fibers to the corresponding strip of Purkinje cells, forming a closed triangular loop. **(A)** The left part of the cerebellar cortex indicates the original zones described by Voogd (1964), whereas the right part indicates the zebrin related groups described by Sugihara (2011). The color coding used in panels **B-F** is the same as that used for describing Sugihara's groups in **A** (i.e., right half), and together they reflect which parts within a particular olivocerebellar module are connected. For reference, we indicated the zebrin-positive strips with dark shading in Voogd's zones on the left. **(A)** 1-6(a/b/-/+) (see Sugihara and Shinoda, 2004, 2007); I-X, lobules I − X; CP, copula pyramidis; Cr I/II, crus I/II of ansiform lobule; FL, flocculus; Par, paramedian lobule; PFL, paraflocculus; Sim, lobulus simplex. **(B,C)** AICG, anterior interstitial cell group; AIN, anterior interposed nucleus; CP, copula pyramidis; DLH, dorsolateral hump; DLP, dorsolateral protuberance; DMC, dorsomedial crest; (v)DN, (ventral) dentate nucleus; FN, fastigial nucleus; ICG, interstitial cell group; PIN, posterior interposed nucleus. (D) DVN, descending vestibular nucleus; dY, dorsal group Y; MVN, medial vestibular nucleus; PrH, prepositus hypoglossal nucleus; SVN, superior vestibular nucleus. (E,F) β, subnucleus β; (c/v)DAO, (central/ventral) dorsal accessory olive; dc, dorsal cap; DM, dorsomedial group; DMCC, dorsomedial cell column; MAO, medial accessory olive; (d/v)PO, (dorsal/ventral) principal olive; VLO, ventrolateral outgrowth. Note that the X/CX-zones have only been found at the electrophysiological level (Ekerot and Larson, 1982).
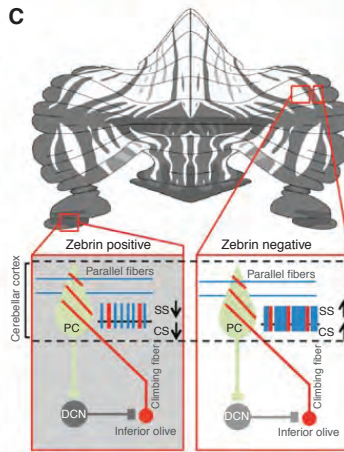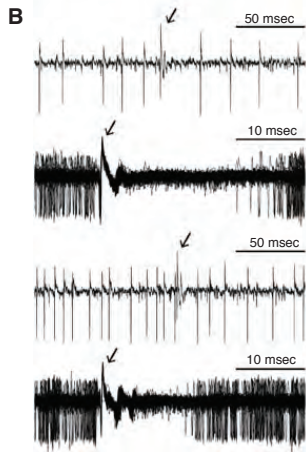
Intrinsic differences among cerebellar modules

Whereas the simple spikes are to a large extent determined by the intrinsic activity of Purkinje cells, the all-or-none complex spike activity directly reflects activity in the afferent climbing fibers derived from neurons in the inferior olive (De Zeeuw et al., 2011; Albergaria and Carey, 2014; Zhou et al., 2014). Interestingly, at rest, the firing frequency of the complex spikes is aligned with that of the simple spikes in that their firing frequency is also significantly higher in zebrin-negative zones compared with that in zebrin-positive zones (Fig. 3B, C). Thus, even though the complex spike activity copies perfectly the activity of olivary neurons at rest, it still follows the trend of simple spike activity, which is determined by the intrinsic activity of Purkinje cells. How can this come about? This alignment presumably results from a network effect within the olivocerebellar modules engaging the GABAergic neurons in the cerebellar nuclei (Chen et al., 2010; De Zeeuw et al., 2011). Enhanced simple spike activity, as observed in the zebrin-negative modules, will lead to reduced firing of these cerebellar nuclei neurons that inhibit the inferior olivary neurons leading to an increase in complex spike activity (De Zeeuw et al., 1988). Because an increase in complex spike activity suppresses simple spike frequency through cerebellar cortical interneurons in the molecular layer (Mathews et al., 2012; Coddington et al., 2013), this network effect ultimately provides an excellent way to mediate homeostasis of activity within the olivocerebellar modules (Fig. 3B, C).

Figure 3 Olivocerebellar modules and Purkinje cell activity in relation to zebrin (II) distribution. (A) The VZ and SG rows refer to the zones and groups of Purkinje cells described by Voogd (1964; VZ) and Sugihara (2011; SG), respectively. The Zeb row indicates which zones and groups are zebrin positive (grey) and zebrin negative (white). The inferior olive (IO) row indicates which subnucleus of the IO is providing climbing fibers to a particular zone/group of Purkinje cells in the cerebellar cortex and collaterals to a particular part of the cerebellar nucleus, depicted in the same column. The CN and VN row indicates the parts of the cerebellar nuclei (CN) and vestibular nuclei (VN) that are innervated by the strip of Purkinje cells, depicted in the same column. It should be noted that only those vestibular nuclei are indicated that both receive a Purkinje cell input and provide a feedback projection to the inferior olive; because, for example, medial and superior vestibular nuclei do not project to the IO, they are not incorporated in this scheme. In addition, it should be noted that this overview is also incomplete in that some nuclei, such as the dorsomedial cell column (DMCC), may receive inhibitory feedback from multiple hindbrain regions. CL indicates the color legends used for Figure 2. AICG, anterior interstitial cell group; AIN, anterior interposed nucleus; β, subnucleus β; c/rMAO, caudal/rostral medial accessory olive; dc, dorsal cap; DLH, dorsolateral hump; DLP, dorsolateral protuberance; DM, dorsomedial group; DMC, dorsomedial crest; d/vDAO, dorsal/ventral dorsal accessory olive; DVN, descending vestibular nucleus; d/vPO, dorsal/ventral principal olive; dY, dorsal group Y; floc, flocculus; FN, fastigial nucleus; ICG, interstitial cell group; LVN, lateral vestibular nucleus; nod, nodulus; PIN, posterior interposed nucleus; PrH, prepositus hypoglossal nucleus; vDN, ventral dentate nucleus; and VLO, ventrolateral outgrowth. **(B)** Examples of raw traces of Purkinje cell activity from zebrin-positive (*top* panels) and zebrin-negative (*bottom* panels) zones. Arrows indicate complex spike. (From Zhou et al., 2014; reprinted, with permission from the authors.) **(C)** Intramodular connections via deep cerebellar nuclei (DCN) explaining why the complex spike (CS) activity within a module follows the intrinsic differences in simple spike (SS) activity of Purkinje cells (PC). PC and DCN are inhibitory, whereas climbing fibers are excitatory. (From Albergaria and Carey, 2014; reprinted under the terms of the Creative Commons Attribution License, which permits unrestricted use and redistribution provided that the original author and source are credited.)

Together, the intrinsically determined simple spike and complex spike activity at rest provide the baseline values around which the Purkinje cells are modulated during natural sensory stimulation, such as that used to induce motor learning. This raises the question as to whether motor learning in the different olivocerebellar modules is also dominated by different plasticity rules mechanisms. Given the baseline firing frequencies, one might expect that zebrin-positive modules with relatively low firing frequencies have ample room for mechanisms of potentiation, whereas zebrin-negative modules showing high simple spike activity could be more prone to suppression. Indeed, Wang and colleagues (2011) found *in vivo* that the activity of zebrin-positive, but not zebrin-negative, Purkinje cells can be readily enhanced, whereas Wadiche and Jahr (2005) found that, *in vitro*, the induction of long-term depression (LTD) at the parallel fiber to Purkinje cell synapse can be readily induced in zebrin-negative Purkinje cells in lobule III, but not in zebrin-positive cells in lobule X. Below we will review the dominant learning rules for both a zebrin-positive region, that is, the flocculus of the vestibulocerebellum controlling adaptation of the vestibulo-ocular reflex (Lisberger, 1988; Ito, 2002; De Zeeuw and Yeo, 2005), and a zebrin-negative region, that is, hemispheral lobule VI controlling classical eyeblink conditioning (Hesslow, 1994a,b; Thompson and Steinmetz, 2009; Boele et al., 2010; Mostofi et al., 2010).

Motor learning in a zebrin-positive module: Adaptation of the vestibulo-ocular reflex

The flocculus, like the nodulus of the vestibulocerebellum, is virtually completely zebrin positive, and indeed its Purkinje cells fire at an average of approximately 60 Hz at rest (Fig. 3B). It contains five zones, one for controlling compensatory head movements (extension of the C2 zone) and four for controlling compensatory eye movements about different axes in space (extension of D1 –D2 zones, but referred to as F zones) (Fig. 4A) (De Zeeuw et al., 1994; De Zeeuw and Koekkoek, 1997; Schonewille et al., 2006a; Voogd et al., 2012). The vestibulo-ocular reflex translates head movement into compensatory eye movement so as to keep the observed image in the center of the visual field. By experimentally moving a subject's head while also moving the visual environment in the same or opposite direction (i.e., in or out of phase), this reflex will prove insufficient or exaggerated, until the new rules are integrated in the compensatory eye movements following a process of adaptation learning. Mechanical or genetic lesions of floccular Purkinje cells severely hamper adaptation of compensatory eye movements (Endo et al., 2009; Gao et al., 2012). Recordings of Purkinje cells in the flocculus of awake behaving mammals during a vestibulo-ocular reflex paradigm in the dark or light show simple spike modulation that correlates well with both maximum head velocity and maximum eye velocity (De Zeeuw et al., 1995). Adapting the reflex using gain-increase or phase-reversal training leads to an increment in the modulation amplitude of simple spikes (Clopath et al., 2014; K Voges and CI De Zeeuw, pers. comm.), whereas impairing the modulation amplitude of simple spikes by genetically attenuating the parallel fiber to Purkinje

cell synapse leads to a reduction in the peak of simple spike modulation as well as in the adaptation and consolidation of the reflexive compensatory eye movements (Fig. 4B –E) (Galliano et al., 2013a).

Moreover, stimulating simple spike activity of Purkinje cells either pharmacologically or optogenetically leads to an increase in the excitatory phase of the modulation amplitude of the simple spikes as well as an increase in the gain of compensatory eye movements (van der Steen and Tan, 1997; De Zeeuw et al., 2004; Nguyen-Vu et al., 2013). Thus, in line with the data obtained by Wang and colleagues (2011) and Wadiche and Jahr (2005) in other zebrinpositive areas of the cerebellum, these data suggest that strengthening the parallel fiber to Purkinje cell synapse (i.e., through long-term potentiation or LTP) or enhancing the intrinsic excitability of Purkinje cells form the dominating forms of plasticity in the zebrin-positive floccular zones controlling vestibulo-ocular reflex adaptation. Indeed, affecting both forms of potentiation simultaneously by deleting PP2B specifically in Purkinje cells results in deficits in various forms of adaptation of the reflex, such as gain increase, gain decrease, and phase-reversal adaptation (Schonewille et al., 2010). Along the same lines, enhancing Purkinje cell potentiation through an artificial or natural increase of estradiol also improves vestibulo-ocular reflex learning (Andreescu et al., 2007).

In contrast, blocking expression of LTD at the parallel fiber to Purkinje cell synapse by targeting proteins involved in late events of its signaling cascade at the level of GluRs (GluRd7 knockin and GluR2K882A knockin) or related proteins that control their trafficking (PICK1 knockout) does not lead to any obvious deficit in compensatory eye movement learning (Schonewille et al., 2011). These latter experiments indicate that LTD is not essential for vestibuloocular reflex adaptation, but they do not exclude the possibility that LTD contributes to this form of motor learning under physiological conditions. Possibly, the blockage of LTD expression at the parallel fiber to Purkinje cell synapse in the GluRd7 knockin, GluR2K882A knockin, and PICK1 knockout is compensated forbyLTPattheparallelfibertomolecularlayer interneuron synapse (Jörntell and Ekerot, 2002; Gao et al., 2012; Tanaka et al., 2013). Even though motor learning in the zebrin-positive floccular zones may be dominated by postsynaptic and intrinsic potentiation of Purkinje cell activity, the olivocerebellar system is endowed with various distributed forms of plasticity that operate in a synergistic fashion and allow for ample compensation (Gao et al., 2012). This synergy results from the fact that virtually all major forms of plasticity in the cerebellar cortex are controlled by the climbing fibers, and climbing fiber activity is phase-dependent. For example, when an optokinetic pattern moves into temporonasal direction, the subsequent activation of complex spikes in the Purkinje cells of the floccular vertical-axis zones (Fig. 4A) enhances LTD at the parallel fiber to Purkinje cell synapse as well as (on the ipsilateral side) LTP at the parallel-fiber to molecular-layer interneuron synapse and potentiation at the molecular layer interneuron to Purkinje cell synapse (Gao et al., 2014). Yet, when the optokinetic stimulus moves in the opposite direction and the climbing fibers are virtually silent (while being active on the contralateral side), it will induce LTP at the parallel fiber to Purkinje cell synapse and LTD at the parallel-fiber to molecular-layer interneuron synapse (Gao et al., 2012). Together, these climbing-fiber-driven forms of plasticity are so prominent that selectively rerouting the climbing fibers from a contralateral to an ipsilateral projection, while maintaining the laterality of the mossy fiber system, completely reverses modulation of both Purkinje cells'simple spikes and
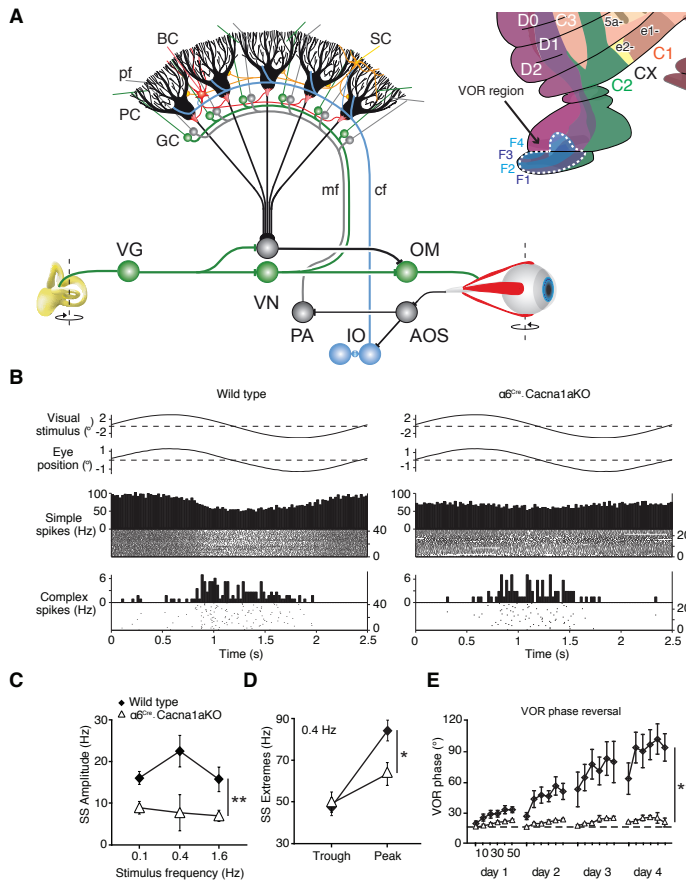
Figure 4 Circuit of the vestibulo-ocular reflex and prominent role of modulation amplitude. (A) The vestibulo-ocular reflex (VOR) is mediated by the three-neuron arc of Lorente de No in the brainstem. When the head rotates, the vestibular signals from the semicircular canals are transferred by the vestibular ganglion cells (VG) to the second-order vestibular neurons in the vestibular nuclei (VN), which in turn innervate the oculomotor neurons (OMs) driving the eyes to the opposite side. The vestibulocerebellum, which is super-imposed on this three-neuron arc, is required to compensate for the delays introduced during input-output processing. To minimize retinal slip during head movements, the accessory optic system (AOS) relays slip signals through the climbing fiber (cf) system to the zebrin-positive Purkinje cells (PC) in floccular zones F1 –F4 in the vestibulocerebellar cortex (see *inset*), where the presence and absence of the climbing fiber ac-tivity is integrated with vestibular, optokinetic, and eye movement signals mediated by the mossy fiber (mf) –granule cell (GC) –parallel fiber (pf) pathway. The Purkinje cells in turn can inject well-calibrated, acceler-ating signals into the vestibular brainstem so as to precisely compensate for the delays. **(B)** $\alpha6^{Cre}$-*Cacna1a* knockout (KO) mice, in which transmission in the vast majority, but not all, of parallel fibers is blocked, show a normal amplitude of their optokinetic reflex when a visual stimulus is given, despite a reduced modulation of their simple spike activity. **(C,D)** The modulation of the simple spike, but not the complex spike, activity in $\alpha6^{Cre}$-*Cacna1a* KO is reduced over a wide range of frequencies, and these deficiencies are caused by a reduction in the peak of the modulation. **(E)** VOR phase reversal is a form of VOR adaptation, during which the phase of the VOR is reversed by providing an in-phase optokinetic stimulus that is greater in amplitude than the vestibular stimulus; $\alpha6^{Cre}$-*Cacna1a* KO mice have severe problems reversing the phase of their eye movements indicating that mammals have their abundance of GCs and pfs to control motor learning rather than basic motor performance. PA, pontine area; BC, basket cell; SC, stellate cell. (From Galliano et al., 2013a; modified, with permission from the authors.)

molecular layer interneuron activity (Fig. 5) and induces dramatically ataxic motor behavior, which actually benefits from a cerebellectomy (Badura et al., 2013).

Downstream, it is probably the changes in simple spikes rather than the complex spikes that largely contribute to the changes in eyemovement behavior during adaptation of the vestibulo-ocular reflex (De Zeeuw et al., 2004). Comparison between recordings from floccular target neurons in the vestibular nuclei and floccular Purkinje cells indicates that it is the simple spikes that can relay the prediction signals required for this type of adaptation learning (De Zeeuw et al., 1995; Stahl and Simpson, 1995). Indeed, through pure rate coding and plasticity mechanisms in both the flocculus and vestibular nucleus neurons (Nelson et al., 2005), one can explain normal vestibulo-ocular reflex learning and consolidation in regular wild-type animals as well as the specific behavioral phenotypes and simple spike firing characteristics observed in various mutant mice in which either the excitatory or inhibitory inputs to the Purkinje cells are affected (Clopath et al., 2014).

Motor learning in a zebrin-negative module: Eyeblink conditioning

The extensions of the zebrin-negative bands are more prominent in the rostral direction of the cerebellum compared with their caudal counterparts (Sugihara and Shinoda, 2004), endowing hemispheric lobule VI, or simplex, with a substantial amount of zebrin-negative Purkinje cells that typically fire at 90 Hz, subdivided across zones C1, C3, and D0 in particular (Sugihara and Shinoda, 2004; Ten Brinke et al., 2014; Zhou et al., 2014). Together with zebrin-positive zone C2, zones C3 and D0 have been shown to respond to periocular stimulation (Hesslow, 1994a,b; Mostofi et al., 2010). Through tracer, lesion, and stimulation studies, it has become apparent that cells in C2 are more generally receptive to different kinds of stimulation, whereas C3 and D0 are specifically engaged with eyelid behavior, with their Purkinje cell output ultimately tying in to the eyelid muscle circuitry (Yeo et al., 1985a,b,c, 1986; Hesslow, 1994a,b; Attwell et al., 2001; Boele et al., 2010, 2013; Mostofi et al., 2010).

In the eyeblink-conditioning paradigm, a neutral stimulus leads to an eyeblink response on repeated pairing with a subsequent blinkinducing stimulus (McCormick and Thompson, 1984; Yeo et al., 1986; Thompson and Steinmetz, 2009; Boele et al., 2010). Eyeblink conditioning has been found to coincide with the development of a marked decrease in Purkinje cell simple spike firing with temporal characteristics similar to those of eyelid conditioned responses (CRs) (Fig. 6) (Albus, 1971; Hesslow and Ivarsson, 1994; Jirenhed et al., 2007; Ten Brinke et al., 2014). The conditioned stimulus ([CS], e.g., a light or tone) and unconditioned stimulus ([US], e.g., a corneal airpuff), in between which the CR occurs, find their respective physiological correlates in the activity of a myriad of parallel fibers and a single climbing fiber synapsing on the Purkinje cells. The repeated pairing of CS-related parallel fiber input with a subsequent climbing fiber signal, an efferent copy of the eyeblink reflex loop (Fig. 6A), sensitizes the Purkinje cells to the CS in that its simple spike activity gradually diminishes as the conditioning proceeds (Ten Brinke et al., 2014). Importantly, this
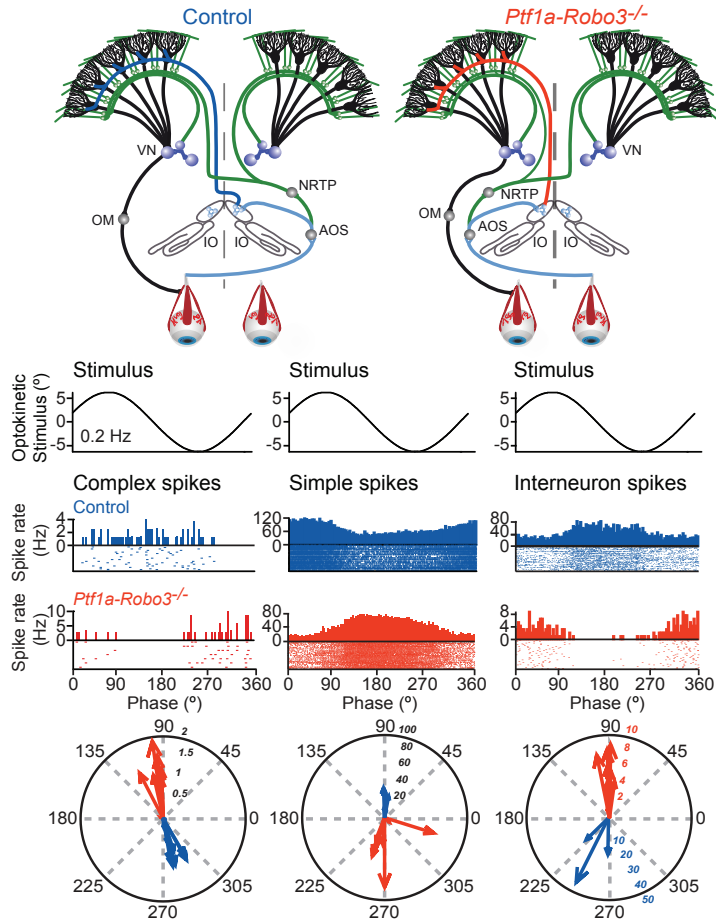
Figure 5 Climbing fibers dominate timing of simple spike firing. Although the complex spikes of Purkinje cells are modulated by activity in the climbing fiber system, the simple spikes are supposed to be largely driven by the mossy fiber system. The frequencies of these two types of spikes are often modulated reciprocally. An increase in complex spikes is associated with a decrease in simple spikes, and vice versa. This reciprocal firing is thought to be essential for motor behavior. Rerouting the climbing fiber system in *Ptf1a-Robo3* mice from a contralateral (dark blue line in *top* panel) to a predominantly ipsilateral projection (red line in *top* panel) does not only reverse the modulation of complex spike activity during natural optokinetic stimulation (see peri-stimulus time histograms (PSTHs), raster, and polar plots in *left* panel), but also that of the simple spike activity (*middle* panel). Because the laterality of the mossy fiber projection is unaffected (green lines in *top* panels), these data show that the proper timing of the climbing fiber input is essential for well-coordinated motor performance by controlling the timing of simple spike firing. The phase of molecular layer interneurons is also reversed in the mutants (*right* panel), which suggests that climbing fibers evoke their effects on simple spike activity via molecular layer interneurons. VN, Vestibular nuclei; NRTP, nucleus reticularis tegmenti pontis; OM, oculomotor neuron; IO, inferior olive; AOS, accessory optic system. (From Badura et al., 2013; modified, with permission from the authors.)

process is reversible; when the well-timed CS –US pairing is replaced with randomly paired conditioned and unconditioned stimuli, the conditioned eyeblink response and reduction in simple spike response are gradually and concomitantly extinguished (Fig. 6B, middle panel). Following this extinction, simple spike suppression reappears with a reoccurrence of the CRs in the reacquisition process (Fig. 6B, bottom panel). This suppression of simple spike activity in a zebrin-negative module, which necessitates plasticity reducing Purkinje cell activity, juxtaposes starkly with the predominantly simple spikeenhancing forms of plasticity implicated in vestibulo-ocular reflex learning that takes place in zebrin-positive areas.

Historically, the main plasticity mechanism thought to underlie the simple spike suppression during eyeblink conditioning was LTD at the parallel fiber to Purkinje cell synapse (Ito and Kano, 1982; Hauge et al., 1998; Koekkoek et al., 2003). Indeed, LTD at this synapse occurs when parallel fibers and climbing fibers are activated conjunctively (Gao et al., 2012), which corresponds well to the situation created by the paired CS –US trials of the eyeblink-conditioning paradigm. However, when parallel fiber to Purkinje cell LTD is blocked following manipulation of the GluR2-AMPA receptors described above (i.e., GluRd7 and GluR2K882A knockin), acquisition of normal CRs is not significantly impaired (Schonewille et al., 2011; see also Welsh et al., 2005). This finding is in line with the fact that most parallel fibers are probably silent to begin with (Brunel et al., 2004; van Beugen et al., 2013) and that at-rest Purkinje cells fire intrinsically at virtually the same rate with intact parallel fiber input as they do without (Cerminara and Rawson, 2004; Galliano et al., 2013a; Hesslow, 2013). In terms of rate coding, this reduces the direct impact of the few depressed CS-conveying parallel fibers on the overall simple spike suppression to negligible proportions. Along the same line, Hesslow and colleagues found that the duration of the parallel fiber activation, through which a Purkinje cell is trained, does not determine the extent and duration of the simple spike suppression (Jirenhed and Hesslow, 2011a,b).

Together, these findings suggest that there must be one or more mechanism(s) other than parallel fiber LTD that can actively suppress the simple spike activity when the conditioning signals have started to traverse across the parallel fibers. Two of these potential mechanisms include LTP at the parallel-fiber to molecular-layer interneuron synapse and potentiation at the molecular layer interneuron to Purkinje cell synapse, thereby facilitating inhibitory effects of these interneurons onto the Purkinje cells (Jörntell and Ekerot, 2002; Gao et al., 2012). Indeed, blocking both mechanisms in effect by ablating the GABA-γ2 receptor specifically in Purkinje cells (Wulff et al., 2009) significantly reduces the percentage and amplitude of CRs (Boele, 2014; Ten Brinke et al., 2014). Yet, this inhibitory effect on conditioning behavior is not complete (Boele, 2014; Ten Brinke et al., 2014), and the impact of gabazine on simple spike suppression in decerebrate ferrets is limited (Johansson et al., 2014), possibly because of extensive ephaptic inhibition at the pinceauforming terminals of the basket cells (Blot and Barbour, 2014). If the interneurons are indeed relevant for the simple spike suppression, LTD might still contribute to this process by reducing the excitation in Purkinje cells during the period in which their parallel fiber input also excites the adjacent molecular layer interneurons, evoking the active suppression. Other possibilities for active suppression include LTP at the parallel fiber to Purkinje cell synapse facilitating transmission of the CS signals and driving inhibitory intrinsic
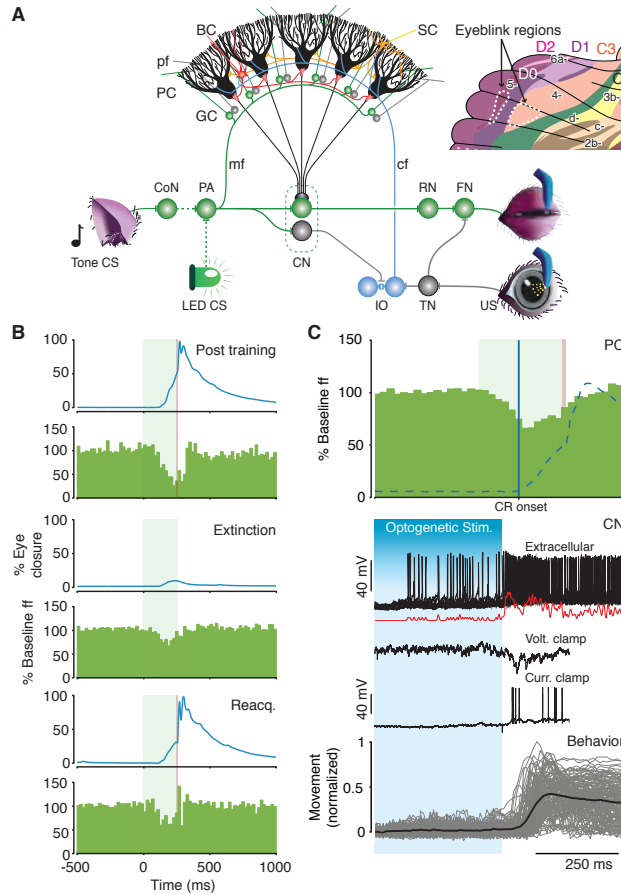
Figure 6 Eyeblink circuit and role of simple spike suppression. (A) During eyeblink conditioning, a conditioned stimulus (CS), such as a tone or LED light, is repetitively paired with an unconditioned stimuli (US), such as an airpuff, to learn a well-timed conditioned response (CR). CS and US sensory information converges at zebrin- negative Purkinje cells (PCs) in D0 and C3 (see inset) through the mossy fiber (mf) –granule cell (GC) –parallel fiber (pf) pathway and the climbing fibers (cfs) derived from the inferior olive (IO), respectively. Although the mossy fibers relay information on the CS from the pontine area (PA), the climbing fibers mediate efferent copies of signals evoked in the direct eyeblink reflex loop, which is formed by the orbital branch of the trigeminal nerve, trigeminal nucleus (TN), facial nucleus (FN), and eyelid muscle. When a fixed temporal relationship between parallel fiber and climbing fiber activation emerges, the same parallel fiber input starts to evoke a simple spike suppression that disinhibits the cerebellar nuclear (CN) cells, and consequently causes the eyelid to close before the US is about to occur. **(B)** Example of mean eyelid behavioral traces and simple spike frequency histograms of a mouse Purkinje cell from lobule HVI (zebrin-negative D0 zone) after training, extinction, and reacquisition (*top* to *bottom*). Note the concomitant changes in simple spike suppression and amplitude of the CRs. The green and red bands in the background depict CS and US duration, respectively. **(C)** (*Top*) Simple spike suppression precedes CR onset (blue line) and covaries with its course (dashed line). (*Bottom*) A rapid drop in Purkinje cell activity after stopping optogenetic stimulation elicits rebound burst activity in CN neurons (extracellular recording *in vivo*). The excitatory events in voltage and current clamp recordings of the same cell *in vivo* following optogenetic Purkinje cell stimulation show that this bursting may be facilitated by climbing and/or mossy fiber collaterals. Ultimately, CN rebound activity can reliably evoke a behavioral response. The data described under C are obtained from different experiments, but aligned at the same time scale to facilitate understanding of the course of events with respect to each other. CoN, cochlear nucleus; RN, red nucleus. (From Witter et al., 2013; modified, with permission from the authors.)

Purkinje cell mechanisms through, for example, metabotropic glutamate receptors and downstream PKC-mediated cascades and/or indirectly eliciting CSrelated complex spike activity through the nuclei, which, in turn, adds to direct activation of the molecular layer interneurons (Berthier and Moore, 1986; Angaut et al., 1996; Koekkoek et al., 2003; Schonewille et al., 2010; Johansson et al., 2014). In line with the large variety of potential mechanisms, current thoughts about cerebellar learning extend beyond the modification of mere synaptic input of CS signals and are referred to as distributed synergistic plasticity (Gao et al., 2012).

By adopting a suppressive simple spike response, Purkinje cells disinhibit cerebellar interposed nuclear cells, and the subsequent rebound activity in these cells eventually feeds via the red nucleus into the eyelid muscles, effectively closing the eye in well-timed preparation just before the US occurs (Fig. 6C) (Gauck and Jaeger, 2000; Boele et al., 2010; Witter et al., 2013). The simple spike suppression starts well before the onset of the conditioned eyeblink response (Ten Brinke et al., 2014), but the extent to which the subsequent increase in cerebellar nuclei firing determines the onset of the eyelid closure or dynamically controls the closure in an online fashion is not known (Sanchez-Campusano et al., 2011). Presumably, the rebound in the activity of cerebellar nuclei neurons following simple spike suppression is facilitated by excitatory inputs from mossy fiber and/or climbing fiber collaterals (Fig. 6C). Indeed, their excitatory inputs can be detected during whole-cell recordings *in vivo* at precisely the right moment showing coincidence with the internal rebound (Witter et al., 2013).

In contrast to the zebrin-positive modules controlling vestibulo-ocular reflex adaptation, which seem to entail predominantly rate coding, the zebrin-negative module-controlling eyeblink conditioning appears more prone to temporal coding. This is also supported by the fact that synapses of mossy fiber collaterals onto cerebellar nuclei neurons can show LTP following specific sequential activation (Pugh and Raman, 2008) and that cerebellar nuclei neurons can be entrained by periods of synchronized simple spike activity at 50 –80 Hz (De Zeeuw et al., 2008, 2011; Person and Raman, 2012), that is, the firing rate level that zebrin-negative Purkinje cells acquire during simple spike suppression controlling the conditioned eyeblink response (Fig. 6B, C). Moreover, the mossy fiber collaterals on cerebellar nuclei neurons also show structural preterminal sprouting during conditioning, the amount of which correlates well with the amplitude of the conditioned responses (Boele et al., 2013). The notion that the eyeblink-conditioning paradigm involves memory formation at both the cerebellar nuclear and cortical level may explain the considerable savings observed during reacquisition of the learned behavior after extinction (Fig. 6B) (Kehoe, 1988; Ohyama et al., 2006). Thus, even though the molecular and cellular machinery behind the active suppression central to the activity in zebrin-negative cerebellar zones still poses questions, the evidence for its functional relation to both plasticity in the cerebellar nuclei and accurate behavioral output as well as for the crucial role of climbing fiber activity at all potential plasticity sites is compelling.

271

Concluding remarks

The data reviewed here establish the differential intrinsic activity of the different sagittal Purkinje cell zones in the cerebellum and the potential consequences for motor learning. In hindsight, the recent finding by Zhou and colleagues (2014) that the intrinsic simple spike-firing frequencies of zebrin-positive and zebrin-negative Purkinje cells differ dramatically (60 Hz vs. 90 Hz) could have been predicted by the original study performed 50 years ago by Voogd (1964). Voogd used Haggquist stainings and found that the cerebellar cortex can be divided in zones of Purkinje cells with thin myelinated axons (e.g., zones C2, D1, and D2, which later turned out to be zebrin positive) and Purkinje cells with thick myelinated axons (e.g., zones B, C1, C3, and D0, which turned out to be zebrin negative) (Fig. 1). Indeed, oligodendrogenesis and the thickness of a myelination sheath appear to depend on neuronal activity and firing rate (Gibson et al., 2014). Yet, we are still only just beginning to answer the 50-year-old question as to what the functional meaning of the cerebellar zones may be. The configuration of these different zones raise the possibility that different encoding schemes are used for motor learning. Indeed the zebrin-positive zones, such as the F1 –F4 zones used for vestibulo-ocular reflex adaptation, appear well designed to use mainly potentiation to enhance simple spike firing rate and mediate motor learning through rate-coding mechanisms (Fig. 4). Instead, the zebrin-negative zones, such as the C3 and D0 zones used for eyeblink conditioning, appear optimally designed to use mainly suppression to decrease simple spike firing rate and mediate motor learning, in part, through temporal coding mechanisms downstream in the cerebellar nuclei (Fig. 6), which is supported by input from collaterals of not only mossy fibers but also climbing fibers (Van der Want et al., 1989).

Given the enormous energy consumption of high levels of neuronal activity (Sengupta et al., 2014), one may wonder why a neurobiological system like the cerebellum uses such high levels of intrinsic activity to begin with. There must be obvious benefits preserved throughout evolution (Darwin 1859). Clearly, control of motor learning is one of the prime functions of the cerebellum (Ito, 2002; De Zeeuw et al 2011; Gao et al., 2012) and exploiting diversity in intrinsic activity of its main output neurons like Purkinje cells and cerebellar nuclei neurons may benefit the execution of this function, but other regions like the cerebral cortex also have prime roles in learning, including both declarative and procedural memory formation, whereas their main output neurons, pyramidal cells, usually fire at a relatively low firing frequency at rest, preserving energy (Heck et al., 2013; Pouille et al., 2013).

What then is special about the cerebellar system in this regard? The most characteristic feature of all functions of the cerebellum is its ability to control timing at a high resolution. Across periods of hundreds of milliseconds, the cerebellum can regulate and fine-tune signal processing with a precision of approximately 5 ms (D'angelo and De Zeeuw, 2009; De Zeeuw et al., 2011). This function appears critical for controlling not only relatively simple forms of learning-dependent timing, such as for vestibulo-ocular reflex phase-reversal learning (Fig. 4) and eyeblink conditioning (Fig. 6), but probably also for more complex, timing-sensitive processes involved in cognition and episodic memory formation (Ben-Yakov and Dudai, 2011; Rahmati et al., 2014). For example, cerebellar cell-typespecific mouse mutants do not show deficits in general

cognitive tasks like Morris water maze, fear conditioning, or open field (Galliano et al., 2013b), but the very same mutants start to show phenotypes in decision making when tight temporal response windows are inserted in go/nogo tasks (Rahmati et al., 2014). Likewise, the timing function of the olivocerebellar system is essential when acute reflexes need to be engaged following perturbations (Van Der Giessen et al., 2008). Therefore, it is parsimonious to assess the potential role(s) of high and varying levels of intrinsic Purkinje cell activity in the light of the overall function of the cerebellum in timing.

If one considers the motor domains and functions controlled by the various olivo-cerebellar modules in mammals (Fig. 2), the picture emerges that slower movements, such as compensatory eye and head movements, are controlled by zebrin-positive modules (e.g., vestibulocerebellum) operating at lower firing frequencies and using rate coding downstream (Clopath et al., 2014), whereas faster movements, such as eye-blink responses or limb activity during locomotion, may depend on zebrin-negative modules (e.g., 5-region in D0 and vermal lobule V, respectively) and fast rebound activity in the cerebellar nuclei (De Zeeuw et al., 2011; Witter et al., 2013). In general, one could state that the presence of intrinsic activity as in zebrin-positive modules allows for on-line modulation in both the excitatory and inhibitory direction with ample opportunity to expand in the excitatory domain during learning (i.e., potentiation) and that an excessive amount of intrinsic activity as in zebrin-negative modules also allows for online modulation in both the excitatory and inhibitory direction, but with ample opportunity to expand in the inhibitory domain (i.e., suppression) engaging fast rebound mechanisms in the nuclei downstream. The latter condition can be considered as a pulled string maintained at a high energy level that can be released on command and evoke very fast effects when needed, such as to protect one's eye with an eyeblink when a dangerous event is approaching. The design of a system that allows for highly dynamic and precise control of temporal signal processing comes at the cost of continuous high levels of energy consumption, but apparently renders the system with a sufficiently improved survival rate. In this respect, it will be interesting to investigate the intrinsic activity of Purkinje cells during sleep. If the hypothesis described above is correct, one might expect to not waste energy during sleep and bring the cells into a down state (Loewenstein et al., 2005). These down states in Purkinje cells can indeed be induced by anesthetics, whereas they hardly occur in animals operating under physiological circumstances in the awake state (Schonewille et al., 2006b). In addition, it will be interesting to find out to what extent neighboring zebrin-positive and zebrin-negative zones can interact (see also Fig. 3). Interestingly, in the vestibulocerebellum of birds, neighboring zebrin-positive and zebrin-negative modules have been found to respond best to the same pattern of optic flow in 3D space (Graham and Wylie, 2012). One could imagine that antagonistic movements characteristic of flying may have different temporal and thereby modulational de-mands depending on their relation with gravity, engaging the zebrin-positive and -negative modules under different circumstances.

The functional concept of cerebellar modules operating in different firing fre-quency domains outlined above is based on a dichotomy found in expression of zebrin and related proteins that may control intrinsic simple spike activity. However, even though the differences in firing frequency between zebrin-positive and zebrin-negative modules are highly significant, there is considerable overlap in the ranges

of frequencies found (Zhou et al., 2014). This raises the possibility that the encoding schemes used in the various modules are more diverse than depicted here. Indeed, in some microzones, the level of zebrin expression is ambiguous (Mostofi et al., 2010), and the complete proteomics in Purkinje cells is probably sufficiently diverse to even make sagittal strips of single Purkinje cells unique (Voogd et al., 1996). Likewise, it should be noted that one cannot exclude the possibility that suppression and potentiation mechanisms may also take place in zebrin-positive and zebrin-negative modules, respectively (Yang and Lisberger, 2013, 2014) and that the concomitant encoding schemes during learning may shift accordingly, if one switches from a chronic tonic form of learning to a more acute trial-by-trial form of conditioning. In addition, it should be noted that conversion mechanisms may take place at the input stage of both types of modules in that the enhanced input from the semicircular canals to the flocculus may both have to be suppressed during ipsiversive head movements (zebrin-positive zones) and that the active input signaling the conditioned stimulus has to be turned into simple spike suppression during expression of the conditioned response (zebrin-negative zones) (De Zeeuw et al., 2004; Johansson et al., 2014). Therefore, in future studies, it will be important to determine how refined the variety of encoding schemes for cerebellar motor learning really is and to what extent these schemes are related to the dynamics of the paradigm involved. By explaining the encoding schemes for the most widely studied form of motor learning in zebrin-positive modules, that is, adaptation of the vestibulo-ocular reflex in F1–F4, as well as of that in zebrinnegative modules, that is, eyeblink conditioning in C3 –D0, this article provides a first step toward unraveling the various encoding schemes that can be used for cerebellar motor learning. Because the zebrin patterns and differences in baseline firing frequencies are consistently present throughout the cerebellar cortex, it is possible that these encoding schemes are applicable to all cerebellar learning functions.

Chapter 11

General Discussion
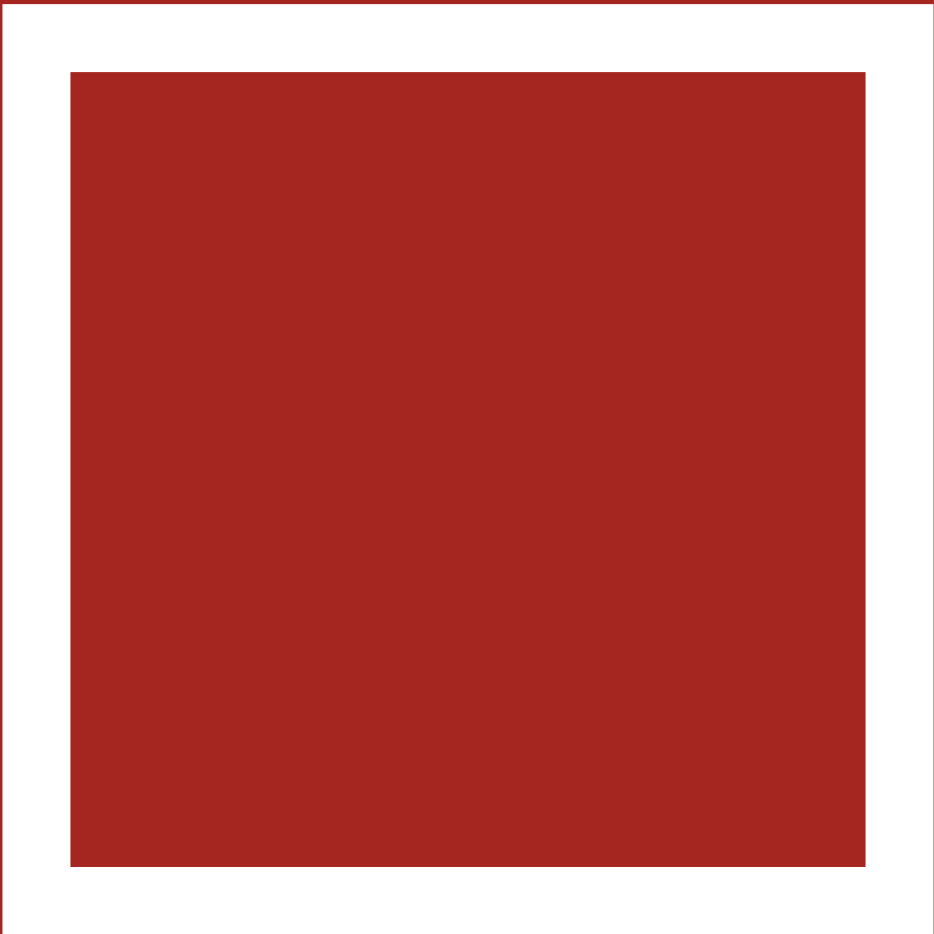
On olivocerebellar research

One could argue that the olivocerebellar system is understood to a great extent. The main components of the network and the input-output structure have been established, and multiple theories suggest sensible principles through which the physical properties of the olivocerebellar system give rise to their functional expression, predominantly in motor behavior. These conceptualizations express how this system can learn (Marr, 1969; Albus, 1971; Ito et al., 1982; Fujita, 1982; Dean & Porrill, 2008; 2011), enables timing (Braitenberg, 1967; Lamarre & Mercier, 1971; Llinás & Yarom, 1986; Ivry et al., 1988), and may generate feed-forward internal models that could be extrapolated beyond the motor domain (Wolpert, Miall, & Kawato, 1998; Ito, 2008). However, judging from spoken and written opinion across the field, it seems cerebellar understanding is deemed insufficient as often as it is deemed comprehensive, depending on the intended level of complexity of our understanding. Indeed, the existence of these opposing verdicts seems indicative of a field that has made great progress and is raising the bar ever further. Taking stock of the research in this thesis, we will find how it underlines three different ways in which the olivocerebellar field is shifting its investigative aim to higher levels of complexity. First, the establishment of different cerebellar components contributing to learned behavior concretizes the shift of focus from singular plasticity mechanisms toward network-level interplay as the physiological basis for cerebellar learning (**Chapters 2, 3, 4, 6 ,7, 8, 9**). Second, the differential ways in which zebrin-positive and -negative zones predominantly employ spike modulation to effect learning support the existence of variations on the universal computation assumed by some to hallmark olivocerebellar processing (**Chapters 2, 4, 10**). Lastly, the observation of social impairments in a Purkinje cell-specific autism-related knockout mouse joins a large body of empirical data emphasizing the need to study the olivocerebellar system beyond the context of motor behavior (**Chapter 5**). These indications affirm how far the field has come, while signaling the work that lies ahead, as explored through several suggested directions for future research.

Toward network-level interplay

Spike modulation during eyeblink conditioning

The electrophysiological work in **Chapters 2** and **6** provides an integrative picture of Pavlovian eyeblink conditioning-related spike modulation. Timed spike facilitation in molecular layer interneurons was shown to partially contribute to behavior, which it does by deepening Purkinje cell simple spike suppression, which in turn was shown to also carry predictive trial-by-trial correlations to conditioned responses, through disinhibition of neurons in the cerebellar anterior interposed nucleus. These cells, in turn, were shown to predominantly increase their spiking rate in relation to the conditioning stimuli (Fig. 1). Moreover, optogenetic stimulation of Purkinje cells, which was shown to suppress the activity of cerebellar nuclei neurons (Witter et al., 2013; Canto et al., 2016), effectively abolished CRs. Earlier work showed compelling

similarities between the acquisition, expression, extinction, and reacquisition of neu-
ronal and behavioral CRs (Jirenhed et al., 2007; Wetmore et al., 2014), as well as the
fact that suppression of Purkinje cell simple spikes through optogenetic stimulation
of molecular layer interneurons (MLIs) in lobule simplex can effectively elicit blink
responses (Heiney et al., 2014). The work in awake behaving mice presented in this
thesis shows optogenetically that cerebellar spike modulation is not only sufficient,
but necessary for the expression of conditioned eyeblink behavior. Moreover, it high-
lights how three levels of cerebellar cells receiving mossy/parallel fiber input generate
spike modulation that integrates from MLIs to Purkinje cells to cerebellar nuclear cells
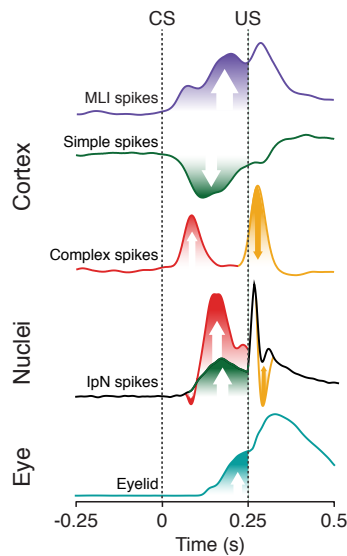(Fig. 1).

Figure 1 Schematic overview of the development of olivocerebellar neuronal responses over the course of
an eyeblink conditioning paradigm, considered in detail across Chapters 2, 6, and 9.

It is clear that the acquired simple spike suppression does not only gradually
deepen to maximize around US onset time. In fact, the elaborate analysis of the
temporal dynamics of spike-eyelid correlations hints at the possibility that there is
also a particular process with a relatively early crucial window of action in the CS-US
interval, centered around 80-100 ms after CS onset. The clear separation of this early
focal area in both the simple spike and MLI activity correlation matrices could imply
a contribution of additional plasticity mechanisms in cerebellar conditioning. This
is certainly a plausible concept considering the variability observed in conditioned
eyelid behavior in mice. However, it is difficult to accommodate for this with a purely
LTD-focused hypothesis or the notion of intrinsic plasticity at the level of single
Purkinje cells. Rather, these results would suggest a more complex interplay among
olivocerebellar components. Interestingly, the early focal area in the correlation matrix
overlaps strikingly with another phenomenon: a CS-related complex spike response.

Acquired olivary activity adds to cerebellar conditioned responses

The work in **Chapters 2** and **6**, reviewed in **Chapter 9**, revealed an interesting additional olivocerebellar phenomenon at play during the CS-US interval. A complex spike response to the CS was observed in eyelid-related Purkinje cells (mentioned before in Berthier & Moore, 1986, and Edgley et al., 2010), as well as a similarly timed transient spike suppression in a subgroup of cerebellar nuclear cells, both indicative of olivary climbing fiber activity (Hoebeek et al., 2010; Lu, Yang, and Jaeger, 2016). Only Purkinje cells that were eyelid-related by virtue of a consistent US-related complex spike response showed the CS-related complex spike. Moreover, in the independent datasets across these studies, naïve animals did not show these particular responses. Together, these findings strongly suggest that the phenomenon is acquired over the course of eyeblink conditioning.

Certain findings from the research in **Chapters 2** and **6** hint at a possible function for the CS-related olivary response. The latency of CS-related complex spikes relative to the other cerebellar cortical spike components and conditioned eyelid behavior fits a potentially facilitating role. It could influence simple spike suppression through the climbing fiber pause (De Zeeuw et al., 2011), through non-synaptic activation of MLIs (Jorntell & Ekerot, 2003; Szapiro & Barbour, 2007; Mathews et al., 2012) as well as through several climbing fiber dependent forms of cerebellar cortical plasticity (Gao et al., 2012). Indeed, modest but significant correlations to both eyelid behavior and simple spike suppression support this possibility (**Chapter 2**, Ohmae & Medina, 2015). Moreover, in many cases in the interpositus nucleus (IpN), strong excitatory responses occurred right after the CS-related spike trough. In fact, in IpN cells that showed these responses in trained animals, US-only trials yielded similar pause-excitation patterns. This makes it tempting to hypothesize that this (likely synchronized) climbing fiber activity may help to create rebound excitation in target IpN neurons, further boosting recruitment of the eyelid muscles and faciliting related plasticity in the IpN (Zheng and Raman, 2010; Person and Raman, 2010). A number of studies have established post-inhibitory rebound activity in the CN, with a link between the strength and duration of the inhibition and the strength of the rebound (Aizenman and Linden, 1999; Llinás and Mühlethaler, 1988; Tadayonnejad et al., 2009; Witter et al., 2013). With regards to climbing fiber activation specifically, Hoebeek et al., (2010) showed that olivary stimulation yielded inhibition and subsequent rebound excitation that could last up to 250 ms in 50 out of 66 IpN neurons (75%). Moreover, rebound-driven behavioral responses can be elicited by synchronized nuclear inhibition lasting as little as 25 ms (Witter et al., 2013). The fact that not all IpN cells showing CS-related spike troughs showed rebound excitation implies the existence of some qualitative requirements beyond just the transient spike suppression, e.g. in terms of olivary spike burst characteristics (Mathy et al., 2009) and/or synchrony (Tang et al., 2016). The notion that rebound excitation is not straightforwardly elicited seems consistent with the fact that T-type channels have been shown to contribute (Molineux et al., 2006, 2008), but are unlikely to account for its full breadth (Zheng and Raman, 2011). Thus, both at the level of the cerebellar cortex and in the nuclei, CS-related climbing fiber activity seems to facilitate spike modulation.

Moreover, given the role of climbing fiber activity in plasticity processes, it is quite possible that the CS-related olivary activity helps further establish procedural

memory in the longer term. This does not mean that this contribution has to relate to the conditioned spike modulation acquired in the eyeblink conditioning paradigm. Indeed, the endowment of CS-encoding signals with the same olivary teaching response as that elicited by the US could constitute a useful longer-term adaptation. After all, by the time a flash of a light has been tightly linked to subsequent perturbation of the eye with ceaseless repetition, the light carries high instructive value with relation to activation of the eyelid musculature. In this sense, the CS-related climbing fiber response constitutes experience-based expansion of the receptive field of error-signal producing olivary cells. It is thus conceivable that olivocerebellar modules receive teaching signals dynamically, with the repertoire of instructive signals adapting to the ever-changing relatedness among relevant information in and around ourselves.

The presence of CS-related complex spikes in Purkinje cells and transient spike suppression in IpN neurons necessitates that the CS-encoding signal has somehow acquired the means to reach the olivary nucleus. In resolving the origin of this response, one consideration is whether or not it involves the cerebellum (**Chapter 9**). A straightforward pathway through the cerebellum could be paved by mossy fiber collaterals to the cerebellar nuclei that are newly formed over the course of conditioning (Boele et al., 2013), which could directly hook up CS-encoding signals to the nucleo-olivary pathway (De Zeeuw et al., 1988). The resulting CS-activated nuclear activity could then bear excitatory responses in the olivary nuclei, likely through the excitatory disynaptic loop through the mesodiencephalic junction (e.g. De Zeeuw & Ruigrok, 1994), or perhaps through some rebound response to nucleo-olivary inhibition (Bazzigaluppi et al., 2012; De Gruijl et al., 2012). However, as outlined in **Chapter 9**, the latencies of even the earliest observed CS-elicited neuronal responses in the cerebellar nuclei are too long to be able to account for the CS-related climbing fiber activation. Instead, another possibility is that CS-related signals may reach olivary-projecting neurons in the brainstem, possibly being potentiated through eyelid-related cerebellar output, limiting the CS-elicited excitation of olivary cells to eyelid-related modules. One example of a brainstem site that meets these connectivity requirements is the lateral deep mesencephalic nucleus. In all, the presence of acquired climbing fiber activity within the CS-US interval emphasizes the need to consider interplay within the broader network of olivocerebellar modules in models translating physiology to behavior.

Molecular layer interneurons contribute to conditioned responses

In the cerebellar cortical microcircuit, MLIs form a relevant additional source of spike modulation that correlates with conditioned eyelid behavior. Through mouse transgenics, we were able to confirm that MLIs make a significant partial contribution to the cerebellar output that causes conditioned eyelid behavior (**Chapter 2**). Our behavioral data from two independent mouse mutants with impaired MLI inhibition show partial deficits. Moreover, the feasibility of MLI-activated blinks generated by optogenetic stimulation (Heiney et al., 2014) further supports the idea that MLIs can goad cerebellar output into behavioral expression. Severe behavioral deficits in eyeblink conditioning occur when transgenic impairment of MLI inhibition is combined with transgenically impaired parallel fiber to Purkinje cell LTD (**Chapter**

3). These results further highlight the relevance of network-level interplay in the cerebellar network.

Nucleocortical Feedback

Another additional relevant pathway in the cerebellum was shown to make a significant contribution to the expression of conditioned eyelid behavior in **Chapter 7**. Activity of the nucleocortical mossy fiber projection in the cerebellum contributes to gain control of learned eyeblink responses by providing internal amplification signals of an excitatory corollary discharge to the granular layer, which in turn is converted into Purkinje cell inhibition via activation of MLIs. These findings corroborate the concept that increases in MLI activity and suppression of simple spikes correlate strongly with the amplitude of conditioned eyeblink responses (**Chapter 2**).

In general, feedback of corollary discharge can facilitate the prediction of sensory consequences of movements and improve learning and preparation of movements (Crapse and Sommer, 2008; Requarth and Sawtell, 2014). For models on cerebellar learning, this fast internal feedback mediated by mossy fibers may complement the external feedback provided by the climbing fiber system (Cerminara and Apps, 2011; Llinás, 2011; Voogd and Glickstein, 1998), which is slower but better designed to reset the phase and onset of motor programs in the modules (De Zeeuw et al., 2011; Yarom and Cohen, 2002). Indeed, since both the mossy and climbing fiber systems operate within the setting of the olivocerebellar modules, together they present a rich and complementary computational repertoire to coordinate motor learning. For instance, the fast internal feedback loop appears well designed to amplify the amplitude of conditioned responses directly after the movement is initiated, whereas the external loop may reset the motor cycle and speed up the onset of subsequent trials (Welsh, 2002). Interestingly, the internal and external, excitatory loops may use in part comparable mechanisms within the module(s) involved. Both feedback loops may introduce strong synchronized pauses in Purkinje cell firing, which in turn can disinhibit premotor firing in the cerebellar nuclei, potentially facilitated by rebound firing and activation by mossy and climbing fiber collaterals (Bengtsson et al., 2011; De Zeeuw et al., 2011; Hoebeek et al., 2010; Person and Raman, 2012; cf. Alvina et al., 2008).

Together, our findings on the amplifying role of the internal feedback loop provided by the excitatory nucleocortical afferents complement the well-studied olivo-cortico-nuclear modules with a robust and dynamic intra-cerebellar closed-loop architecture that allows reinforcement in a controlled manner. The data imply that feedforward as well as feedback circuitries, the two main architectures of neural computation in the brain, are orchestrated in the cerebellum to adaptively control demanding sensorimotor processing.

All in all, the presence of multiple spike responses at different times within the CS-US interval across cerebellar cortical and nuclear levels, acquired climbing fiber responses to the CS, and the involvement of MLI spike modulation as well as internal nucleocortical feedback amplifying this modulation, together highlight the substantial degree of network-level interplay in the acquisition and expression of conditioned cerebellar output.

Dynamic networks within the inferior olive

Inferior olivary neurons heavily express Gjd2 (Condorelli et al., 1998; Belluardo et al., 2000), which is required for formation of functional gap junctions in the olivary network (De Zeeuw et al., 2003). Gap junctions in the inferior olive were discovered more than 40 years ago (Llinás et al., 1974; Sotelo et al., 1974) and their functional properties have been studied extensively ever since (Llinás & Yarom, 1981; Yarom Y. & Llinás, 1981; Llinás & Yarom, 1986). In addition, subthreshold oscillations (STOs) have been one focus of interest; it was found that phases and amplitudes of olivary neurons can change together, but this relationship is dynamic rather that static and can change over time depending on the speed and sequence of movements (Devor & Yarom, 2002b; Jacobson et al., 2009). The absence of gap junctions leaves a relatively mild behavioral phenotype, which becomes more apparent under locomotion or demanding experimental conditions such as learning and adaptation (Kistler et al., 2002; Van Der Giessen et al., 2008; De Gruijl et al., 2014).

The results in **Chapter 8** show that the temporal and spatial structure in complex spike signals of the cerebellar cortex (resulting from largely decoupled olivary neurons) may contribute to reduced neuroplasticity, and thereby reduced behavioral flexibility, in Gjd2 mutants. These systems level physiological findings contribute to behavioral phenotypes under demanding experimental conditions (Van Der Giessen et al., 2008; De Gruijl et al., 2014). Taken together, our observations point in the direction that coupling is not essential for the expression of STOs, but STO properties do get modulated by it.

It has been found that local electrical stimulation in the cerebellar cortex as well as optical stimulation in Channelrhodopsin infected Purkinje cells trigger local rebound complex spikes after short delays which support the closed-loop theory (Llinás & Sasaki, 1989; Lang et al., 1996; Jörntell et al., 2000; Chaumont et al., 2013). Different modules could be dynamically controlled based on the current state of the animal and coordinate motor output (Welsh et al., 1995; Garwicz et al., 1998; Lefler et al., 2014; Devor & Yarom, 2002a). As shown here diverging climbing fiber signals orchestrating the cerebellar cortex via complex spikes are essential to output control to the cerebellar nuclei (Lang & Blenkinsop, 2011; Person & Raman, 2011; Person & Raman, 2012) and later cerebellar output. The data therefore support a crucial role of Gjd2 in the synchronization of olivary neurons. It is essential for the dynamic spatiotemporal compartmentalization of olivary neurons and orchestration of consistent delays in complex spike activity.

Variations on a theme: Universal cerebellar transform

The fact that the intrinsic simple spike firing frequencies of zebrin-positive (60 Hz) and zebrin-negative (90 Hz) Purkinje cells differ dramatically raises the possibility that different encoding schemes are used for motor learning. Indeed the zebrin-positive zones, such as the F1-F4 zones used for VOR adaptation, appear well designed to use mainly potentiation to enhance simple spike firing rate and mediate motor learning through rate coding mechanisms. Instead the zebrin-negative zones, such as the C3 and D0 zones used for eyeblink conditioning, appear optimally designed to use

mainly suppression to decrease simple spike firing rate and mediate motor learning in part through temporal coding mechanisms downstream in the cerebellar nuclei (**Chapter 2, 6, 10**).

In general, one could state that the presence of intrinsic activity as in zebrin-positive modules allows for on-line modulation in both the excitatory and inhibitory direction with ample opportunity to expand in the excitatory domain during learning (i.e. potentiation) and that an excessive amount of intrinsic activity as in zebrin-negative modules also allows for on-line modulation in both the excitatory and inhibitory direction, but with ample opportunity to expand in the inhibitory domain (i.e. suppression) engaging fast rebound mechanisms in the nuclei downstream.

By explaining the encoding schemes for the most widely studied form of motor learning in zebrin-positive modules, i.e. VOR adaptation in F1-F4, as well as of that in zebrin-negative modules, i.e. eyeblink conditioning in C3-D0, **Chapter 10** provides an account of two kinds of encoding schemes that can be used for different types of cerebellar motor learning. Since the zebrin patterns and differences in baseline firing frequencies are consistently present throughout the cerebellar cortex, it is possible that these encoding schemes are applicable to all cerebellar learning functions.

In **Chapter 4**, a novel paradigm hinging on simple spike potentiation is introduced. The data show that whisker movements can be readily adjusted following a short period of air puff stimulation in the theta frequency band and that adaptive increases in SS firing of cerebellar Purkinje cells are necessary and sufficient to mediate this type of procedural memory formation. These results were observed as long as the recordings lasted (>30 min). This constitutes one of the fastest learning paradigms applied to rodents, in which a lasting effect on neuronal activity could be coupled to a change in motor behavior on a trial-by-trial basis. Moreover, these results form one of the first demonstrations in which Purkinje cell-specific potentiation and simple spike enhancement, rather than LTD and simple spike suppression, are found to be critical for cerebellar motor learning. Presumably, similar adaptations are being used during natural object exploration (Anjum & Brecht, 2012; Bosman et al., 2011; Brecht, 2007, Voigts, Herman, & Celikel, 2015) and during go/no-go tasks involving whisker movements (Rahmati et al., 2014). Impairment of Cav3.1 T-type calcium channels (Ly et al., 2013), Shank2 (**Chapter 5**) or GluA3 (Gutierrez-Castellanos et al., 2017), have all been shown to lead to deficits in adaptation of the vestibulo-ocular reflex (VOR), another common form of cerebellar motor learning, but none of these studies was able to find concomitant alterations in simple spike firing, let alone to demonstrate changes on a trial-by-trial basis. Still, given that VOR adaptation is mediated by the flocculus of the vestibulocerebellum, which is largely zebrin-positive (Sugihara & Quy, 2007), these VOR studies corroborate the findings in **Chapter 4** in that they both support the hypothesis that zebrin-positive regions may predominantly use potentiation mechanisms for learning (**Chapter 10**). Together, these chapters support the notion that insofar there is a universal cerebellar transform that is applied across the rather uniformly structured cerebellum (Cerminara et al., 2015), subtle but substantial differences across olivocerebellar modules will result in different variations on this transform, each tailored to the needs of the functionality carried by the corresponding extra-cerebellar network.

Beyond the motor domain

The work in **Chapter 5** is part of a growing focus on non-motor functionality of the olivocerebellar system. We report impaired social and task specific repetitive behavior due to Purkinje cell-specific deletion of Shank2. This result is particularly interesting as it was the first Purkinje cell-specific mouse model for a non-syndromic form of autism in which autism spectrum disorder (ASD)-like behavior has been established. Previous work in L7-Tsc1 mice (Tsai et al., 2012) reported impaired social behavior, late-onset ataxia and reduced excitability of Purkinje cells, due to the absence of a protein that inhibits mTOR signalling through which the translation of a wide variety of proteins is regulated (Tsai et al., 2012). In contrast, in **Chapter 5**, we show that disruption of the synapse through the absence of a single postsynaptic scaffolding protein in the Purkinje cell is sufficient to show impaired ASD-related motor learning and social behavioral impairments. In addition to the social impairments, we found signs of enhanced repetitive behavior in the T-maze paradigm, but not the marble burying task or grooming tasks. The T-maze task reveals the level of cognitive inflexibility following decision making over consecutive trials. In contrast, marble burying and grooming behavior reflect the level of repetitious behaviour, dominated by high-frequency motor activity, which may well be confounded by deficits in cerebellar motor learning. Thus, together, these results highlight the importance of the Purkinje cell synaptic function for ASD beyond the classically ascribed motor-related behavior.

One of the main challenges remaining is to mechanistically explain the contribution of impaired Purkinje cell physiology to the observed ASD behavioral phenotypes. As previously mentioned, the Shank family of postsynaptic scaffolding proteins has many different interacting proteins in the postsynaptic density through which they could contribute to the functional establishment of regulatory mechanisms for plasticity. The translational challenge from synapse to behavior brings about two main questions: How does an impaired Purkinje cell mediate ASD-related behavior? And how might Purkinje cell impairments lead to abnormal brain function beyond the cerebellum with regards to neurodevelopmental critical periods? The first question has been extensively addressed by the accumulating evidence regarding the contribution of ASD-related cerebellar dysfunction to impaired motor learning, as apparent from the eye movement adaptation, ErasmusLadder, and eyeblink conditioning findings examined here and by other investigators (Kloth et al, 2015). It is indeed possible that the increased inhibition and irregularity of simple spike firing, in addition to impaired cerebellar plasticity mechanisms, may contribute to social and repetitive behavior-related phenotypes in ASD. We believe that the answer to how the cerebellum can essentially contribute to socially impaired behavior could reside in various mechanisms. The idea that disruption of a certain brain area during development could affect the development and consequently the function of other inter-connected areas, also termed developmental diaschisis, has recently been put forward as a prime mechanism for the cerebellum in its ability to influence other cortical areas in critical developmental periods (Wang, Kloth, & Badura, 2014). The extent to which acute and developmental effects of the cerebellar impairments observed in Purkinje cell-specific Shank2 mouse mutants contribute to the observed non-motor

symptomatology remains to be elucidated. In all, like network-level interplay and the variable manifestation of olivocerebellar functionality, the influence of cerebellar activity needs to be determined beyond the motor domain, as challenging as it may be to establish links in the cognitive and emotive domains.

Sprezzatura

Together, the work in this dissertation provides concrete findings that are the product of a field advancing toward more complex levels of understanding. As we discover how network-level interplay within and outside of the olivocerebellar system enables, through several versions of a universal computational process, highly coordinated complex neuronal and behavioral patterns that extend beyond the motor domain, it becomes more and more clear just how much intricate work underlies the apparent effortlessness that defines the concept of sprezzatura.

One could argue that, at this point, olivocerebellar research yields a diminished return of investment, with scraps of scientific advancement requiring large effort. However, the benefit of understanding a neuronal network exceedingly well is that it offers a great territory within which to study other phenomena, such as synaptic plasticity, intrinsic plasticity, and emergent properties of network activity. This advantage is readily apparent from the eyeblink conditioning paradigm, which due to a detailed understanding of the underlying neuronal circuitry has been widely used to understand associative learning. The better our grip on the pathways, sites of plasticity, physiology, and behavioral manifestation of the olivocerebellar system, the better we can apply smart and sensible experimental designs to study and understand the learning and performing brain at all scales of magnification.

Future directions

The work in this dissertation raises at least as many questions as it answers. Among the plethora of possible avenues for future research to consider, I will outline four below.

First, to determine the origin of acquired CS-related olivary responses, a useful first step would be to determine whether the activating olivary input could come from the cerebellum. This can be investigated by recording eyelid-related Purkinje cells showing CS-related complex spikes after eyeblink conditioning, and subsequently in-activating the anterior interposed nucleus optogenetically and/or pharmocologically. A disappearance of the CS-related complex spike would assert its dependence on input from the cerebellum, whereas its persistence would suggest that it originates from pre-cerebellar sites. If indeed the CS-related olivary response depends on cerebellar output, a next step would be to determine whether this output is provided by the direct inhibitory nucleo-olivary pathway, or the indirect excitatory pathway via the mesodiencephalic junction. This could be done by similarly recording Purkinje cells that show this post-training CS-related complex spikes, and then injecting gabazine in the inferior olive, selectively disabling nucleo-olivary inhibition. Disappearance of

CS-related complex spike responses would assert its dependence on nucleo-olivary inhibition, whereas its sustenance would make the indirect excitatory loop a more likely candidate source. The determination of the function of acquired CS-related olivary responses will in part depend on more knowledge about its origin; if acquired olivary responses are qualitatively distinct from a more hard-wired brand of olivary responses, it could perhaps be possible to selectively inactivate the former response type. This could be useful to study their necessity in the acquisition and execution of more complex movements than eyeblinks, or chains of associations, such as second-order conditioning (where a novel neutral stimulus is paired with a CS).

A second approach pertaining to CS-related olivary climbing fiber responses, concerns the identity of the stimulus-evoked rapid excitatory responses observed in the IpN after transient spike pauses at typical complex spike latencies. Future research needs to establish whether the post-pause excitation as reported in **Chapter 6** in fact concerns rebound, for instance by establishing its abolition upon injection of T-type calcium channel blocker TTA-P2 (Boehme et al., 2011), or NNC 55-0396 (Alviña et al., 2009). Moreover, to explore a possible interaction with mGluR activity elicited by mossy/climbing fiber collaterals, competitive mGluR antagonist CPCCOEt could be used (Zheng & Raman, 2011). Reductions in conditioned behavior as a result of these pharmacological interventions will simultaneously shed light on the weight of the contribution of rebound excitation to cerebellar eyeblink conditioning.

Third, it should be noted that the rebound excitation-like responses in **Chapter 6** seemed to develop over the course of conditioning, and that the plastic modification of the intensity of rebound may be mediated by climbing fiber synchrony (De Zeeuw et al., 1998; Tang et al., 2016; Bengtsson et al., 2011). The potential absence of post-pause excitation responses in mice that lack gap junctions, such as the Gjd2-mutant (**Chapter 8**), would provide compelling evidence for the functional role of gap junctions in mediating complex spike synchrony to the point of carrying a meaningful influence on nuclear rebound excitation during cerebellar learning.

Lastly, to resolve the question of whether the social impairments in the Purkinje cell-specific Shank2 mutant are due to direct cerebellar or indirect developmental factors, Purkinje cell-specific Shank2 ablation should be initiated at different stages during development using inducible mouse models, as has recently been employed for other ASD-related petergenes (Mei et al., 2016; Silva-Santos et al., 2015).

There are many more questions than the ones discussed above, and many more techniques that are becoming available to tackle them, such as functional ultrasound (e.g., Tiran et al., 2017), the CRISPR/Cas9 system (Hsu, Lander, & Zhang, 2014), and perhaps magnetogenetics (although see Vogt 2016). These techniques may provide better alternatives to certain tracing methods, the use of mice for transgenic research, and invasive surgery, and may expedite the progression toward a complete model of the olivocerebellar system that can account for known cerebellar behavioral paradigms, as well as novel paradigms to be established. Moreover, for a comprehensive grasp of procedural learning, as well as its potential augmentation through whatever technological advances the future may bring, it would seem the scientific conquest of the olivocerebellar system is an essential requirement.

References

Ahissar, E., and Kleinfeld, D. (2003). Closed-loop neuronal computations: focus on vibrissa somatosensation in rat. Cerebral Cortex 53–62.

Ahl, A.S. (1986). The role of vibrissae in behavior: a status review. Vet Res Commun 245–268.

Aiba, A., Kano, M., Chen, C., Stanton, M.E., Fox, G.D., Herrup, K., Zwingman, T.A., and Tonegawa, S. (1994). Deficient cerebellar long-term depression and impaired motor learning in mGluR1 mutant mice. Cell 377–388.

Aizenman, C.D., and Linden, D.J. (1999). Regulation of the rebound depolarization and spontaneous firing patterns of deep nuclear neurons in slices of rat cerebellum. J Neurophys 82, 1697–1709.

Aizenman, C.D., and Linden, D.J. (2000). Rapid, synaptically driven increases in the intrinsic excitability of cerebellar deep nuclear neurons. Nat Neurosci 3, 109–112.

Aizenman, C.D., Huang, E.J., and Linden, D.J. (2003). Morphological correlates of intrinsic electrical excitability in neurons of the deep cerebellar nuclei. J Neurophys 1738–1747.

Aksenov, D. (2003). GABA Neurotransmission in the Cerebellar Interposed Nuclei: Involvement in Classically Conditioned Eyeblinks and Neuronal Activity. J Neurophys 91, 719–727.

Aksenov, D.P., Serdyukova, N.A., Bloedel, B., JR, and V. (2005). Glutamate neurotransmission in the cerebellar interposed nuclei: involvement in classically conditioned eyeblinks and neuronal activity. J Neurophysiol 93, 44–52.

Albergaria, C., and Carey, M. (2014). All Purkinje cells are not created equal. eLife e03285.

Albus, J.S. (1971). A theory of cerebellar function. Math Biosci 10, 25–61.

Alexander, G.E., DeLong, M.R., and Strick, P.L. (1986). Parallel organization of functionally segregated circuits linking basal ganglia and cortex. Ann Rev Neurosci 357–381.

Allen, G. (2005). The cerebellum in autism. Clin Neuropsych 321–337.

Altman, J.A., Bechterev, N.N., Radionova, E.A., Shmigidina, G.N., and Syka, J. (1976). Electrical responses of the auditory area of the cerebellar cortex to acoustic stimulation. Exp Brain Res 26, 285–298.

Alviña, K., Ellis-Davies, G., and Khodakhah, K. (2009). T-type calcium channels mediate rebound firing in intact deep cerebellar neurons. Neuroscience 158, 635–641.

Alviña, K., Walter, J.T., Kohn, A., Ellis-Davies, G., and Khodakhah, K. (2008). Questioning the role of rebound firing in the cerebellum. Nat Neurosci 11, 1256–1258.

Andersson, G., Garwicz, M., and Hesslow, G. (1988). Evidence for a GABA-mediated cerebellar inhibition of the inferior olive in the cat. Exp Brain Res 72, 450–456.

Andreasen, N.C., Paradiso, S., and O'Leary, D.S. (1998). ''Cognitive dysmetria'' as an integrative theory of schizophrenia: a dysfunction in cortical-subcortical-cerebellar circuitry? Schiz Bulletin 24, 203–218.

Andreescu, C., Milojkovic, B., Haasdijk, E., Kramer, P., De Jong, F., Krust, A., De Zeeuw, C., and De Jeu, M. (2007). Estradiol improves cerebellar memory formation by activating estrogen receptor beta. J Neurosci 10832–10839.

Angaut, P., Compoint, C., Buisseret-Delmas, C., and Batini, C. (1996). Synaptic connections of Purkinje cell axons with nucleocortical neurones in the cerebellar medial nucleus of the rat. Neurosci Res 345–348.

Anjum, F., and Brecht, M. (2012). Tactile experience shapes prey-capture behavior in Etruscan shrews. Front Behav Neurosci 6.

Ankri, L., Husson, Z., Pietrajtis, K., Proville, R., Lena, C., Yarom, Y., Dieudonne, S., and and Uusisaari, M.Y. (2015). A novel inhibitory nucleo-cortical circuit controls cerebellar Golgi cell activity. eLife.

Apps, R., and Hawkes, R. (2009). Cerebellar cortical organization: a one-map hypothesis. Nat Rev Neurosci 670–681.

Armstrong, D.M., and Schild, R.F. (1970). A quantitative study of the purkinje cells in the cerebellum of the albino rat. J Compar Neurol 139, 449–456.

Armstrong, D.M., Harvey, R.J., and Schild, R.F. (1973a). Branching of inferior olivary axons to terminate in different folia, lobules or lobes of the cerebellum. Brain Res 54, 365–371.

Armstrong, D.M., Harvey, R.J., and Schild, R.F. (1973b). Cerebello-cerebellar responses mediated via climbing fibres. Exp Brain Res 18, 19–39.

Armstrong, D.M., Harvey, R.J., and Schild, R.F. (1973c). The spatial organisation of climbing fibre branching in the cat cerebellum. Exp Brain Res 18, 40–58.

Arons, M.H. (2012). Autism-associated mutations in ProSAP2/Shank3 impair synaptic transmission and neurexin-neuroligin-mediated transsynaptic signaling. J Neurosci 14966–78.

Atkins, M.J., and Apps, R. (1997). Somatotopical organisation within the climbing fibre projection to the paramedian lobule and copula pyramidis of the rat cerebellum. J Compar Neurol 389, 249–263.

Attwell, P.J., Ivarsson, M., Millar, L., and Yeo, C.H. (2002). Cerebellar mechanisms in eyeblink conditioning. Ann N Y Acad Sci 978, 79–92.

Attwell, P.J., Rahman, S., and Yeo, C.H. (2001). Acquisition of eyeblink conditioning is critically dependent on normal function in cerebellar cortical lobule HVI. J Neurosci 21, 5715–5722.

Attwell, P.J., Rahman, S., Ivarsson, M., and Yeo, C.H. (1999). Cerebellar cortical AMPA-kainate receptor blockade prevents performance of classically conditioned nictitating membrane responses. J Neurosci RC45.

Auger, C., and Attwell, D. (2000). Fast removal of synaptic glutamate by postsynaptic transporters. Neuron 547–558.

Babinski, J. (1899). De l'asynergie cérébelleuse. Rev Neurol 7, 806–816.

Babinski, J. (1902). Sur le rôle du cervelet dans les actes volitionnels nécessitant une succession rapide de mouvements (diadococinésie). Rev Neurol 10, 1013–1015.

Badura, A., Schonewille, M., Voges, K., Galliano, E., Renier, N., Gao, Z., Witter, L., Hoebeek, F.E., Chedotal, A., and De Zeeuw, C.I. (2013). Climbing fiber input shapes reciprocity of Purkinje cell firing. Neuron 700–713.

Bagnall, M.W., Zingg, B., Sakatos, A., Moghadam, S.H., Zeilhofer, H.U., and Lac, S. d. (2009). Glycinergic Projection Neurons of the Cerebellum. J Neurosci 29, 10104–10110.

Bailey, A., Luthert, P., Dean, A., Harding, B., Janota, I., Montgomery, M., Rutter, M., and Lantos, P. (1998). A clinicopathological study of autism. Brain 121 (Pt 5), 889–905.

Bao, S., Chen, L., Kim, J.J., and Thompson, R.F. (2002). Cerebellar cortical inhibition and classical eyeblink conditioning. Proc Natl Acad Sci U S A 99, 1592–1597.

Barmack, N., Qian, Z., and Yoshimura, J. (2000). Regional and cellular distribution of protein kinase C in rat cerebellar Purkinje cells. J Comp Neurol 235–254.

Barski, J.J., Dethleffsen, K., and Meyer, M. (2000). Cre recombinase expression in cerebellar Purkinje cells. Genesis 28, 93–98.

Batini, C., Compoint, C., Buisseret-Delmas, C., Daniel, H., and Guegan, M. (1992). Cerebellar nuclei and the nucleocortical projections in the rat: retrograde tracing coupled to GABA and glutamate immunohisto-chemistry. J Compar Neurol 74–84.

Baudouin, S.J., Gaudias, J., Gerharz, S., Hatstatt, L., Zhou, K., Punnakkal, P., Tanaka, K.F., Spooren, W., Hen, R., De Zeeuw, C.I., et al. (2012). Shared synaptic pathophysiology in syndromic and nonsyndromic rodent models of autism. Science 338, 128–132.

Bazzigaluppi, P., De Gruijl, J.R., van der Giessen, R.S., Khosrovani, S., De Zeeuw, C.I., and de Jeu, M.T.G. (2012a). Olivary subthreshold oscillations and burst activity revisited. Front Neural Circuits 6, 91.

Bazzigaluppi, P., Ruigrok, T., Saisan, P., De Zeeuw, C.I., and de Jeu, M. (2012b). Properties of the Nucleo-Olivary Pathway: An In Vivo Whole-Cell Patch Clamp Study. PLOS ONE 7, e46360.

Becker, E., Oliver, P., Glitsch, M., Banks, G., Achilli, F., Hardy, A., Nolan, P., Fisher, E., and Davies, K. (2009). A point mutation in TRPC3 causes abnormal Purkinje cell development and cerebellar ataxia in moonwalker mice. Proc Natl Acad Sci U S A 6706–6711.

Becker, E.B. an. C.J.S. (2013). Autism spectrum disorder and the cerebellum. Int Rev Neurobiol 113–1.

Bell, C.C., and Kawasaki, T. (1972). Relations among climbing fiber responses of nearby Purkinje Cells. J Neurophys 35, 155–169.

Belluardo, N., Mudò, G., Trovato-Salinaro, A., Le Gurun, S., Charollais, A., Serre-Beinier, V., Amato, G., Haefliger, J.A., Meda, P., and Condorelli, D.F. (2000). Expression of connexin36 in the adult and developing rat brain. Brain Res 865, 121–138.

Belmeguenai, A., and Hansel, C. (2005). A role for protein phosphatases 1, 2A, and 2B in cerebellar long-term potentiation. J Neurosci 10768–10772.

Belmeguenai, A., Hosy, E., Bengtsson, F., Pedroarena, C.M., Piochon, C., Teuling, E., He, Q., Ohtsuki, G., De Jeu, M.T.G., Elgersma, Y., et al. (2010). Intrinsic Plasticity Complements Long-Term Potentiation in Parallel Fiber Input Gain Control in Cerebellar Purkinje Cells. J Neurosci 30, 13630–13643.

Ben-Yakov, A., and Dudai, Y. (2011). Constructing realistic engrams: Poststimulus activity of hippocampus and dorsal striatum predicts subsequent episodic memory. J Neurosci 9032–9042.

Bengtsson, F., and Jörntell, H. (2007). Ketamine and xylazine depress sensory-evoked parallel fiber and climbing fiber responses. J Neurophys 98, 1697–1705.

Bengtsson, F., and Jörntell, H. (2014). Specific Relationship between Excitatory Inputs and Climbing Fiber Receptive Fields in Deep Cerebellar Nuclear Neurons. PLOS ONE 9, e84616.

Bengtsson, F., Ekerot, C.-F., and Jörntell, H. (2011). In vivo analysis of inhibitory synaptic inputs and rebounds in deep cerebellar nuclear neurons. PLOS ONE e18822.

Bengtsson, F., Jirenhed, D.-A., Svensson, P., and Hesslow, G. (2007). Extinction of conditioned blink responses by cerebello-olivary pathway stimulation. Neuroreport 18, 1479–1482.

Bennett, M.V.L. (1997). Gap Junctions and Electrical Synapses. Encyc Neurosci 529–548.

Bennett, M.V.L., and Zukin, R.S. (2004). Electrical coupling and neuronal synchronization in the Mammalian brain. Neuron 41, 495–511.

Berger, T.W., and Thompson, R.F. (1978). Neuronal plasticity in the limbic system during classical conditioning of the rabbit nictitating membrane response. I. The hippocampus. Brain Res 145, 323–346.

Berkel, S., Marshall, C.R., Weiss, B., Howe, J., Roeth, R., Moog, U., Endris, V., Roberts, W., Szatmari, P., Pinto, D., et al. (2010). Mutations in the SHANK2 synaptic scaffolding gene in autism spectrum disorder and mental retardation. Nat Genetics 42, 489–491.

Berthier, N.E., and Moore, J.W. (1986). Cerebellar Purkinje cell activity related to the classically conditioned nictitating membrane response. Exp Brain Res 63, 341–350.

Berthier, N.E., and Moore, J.W. (1990). Activity of deep cerebellar nuclear cells during classical conditioning of nictitating membrane extension in rabbits. Exp Brain Res 83, 44–54.

Best, A.R., and Regehr, W.G. (2009). Inhibitory Regulation of Electrically Coupled Neurons in the Inferior Olive Is Mediated by Asynchronous Release of GABA. Neuron 62, 555–565.

Blankenship, M.R., Huckfeldt, R., Steinmetz, J.J., and Steinmetz, J.E. (2005). The effects of amygdala lesions on hippocampal activity and classical eyeblink conditioning in rats. Brain Res 1035, 120–130.

Blenkinsop, T., a, &, and Lang, E.J. (2006). Block of inferior olive gap junctional coupling decreases Purkinje cell complex spike synchrony and rhythmicity. J Neurosci 26, 1739–1748.

Blenkinsop, T.A., and Lang, E.J. (2011). Synaptic Action of the Olivocerebellar System on Cerebellar Nuclear Spike Activity. J Neurosci 31, 14708–14720.

Bloedel, J.R., and Ebner, T.J. (1984). Rhythmic discharge of climbing fibre afferents in response to natural peripheral stimuli in the cat. J Physiol 352, 129–146.

Blot, A., and Barbour, B. (2014). Ultra-rapid axon-axon ephaptic inhibition of cerebellar Purkinje cells by the pinceau. Nat Neurosci 17, 289–295.

Böckers, T.M., Segger-Junius, M., Iglauer, P., Bockmann, J., Gundelfinger, E.D., Kreutz, M.R., Richter, D., Kindler, S., and Kreienkamp, H.-J. (2004). Differential expression and dendritic transcript localization of Shank family members: identification of a dendritic targeting element in the 3'untranslated region of Shank1 mRNA. Mol Cell Neurosci 26, 182–190.

Boeckers, T.M., Kreutz, M.R., Winter, C., Zuschratter, W., Smalla, K.H., Sanmarti-Vila, L., Wex, H., Lang-naese, K., Bockmann, J., Garner, C.C., et al. (1999). Proline-rich synapse-associated protein-1/cortactin binding protein 1 (ProSAP1/CortBP1) is a PDZ-domain protein highly enriched in the postsynaptic density. J Neurosci 19, 6506–6518.

Boehme, R., Uebele, V.N., Renger, J.J., and Pedroarena, C. (2011). Rebound excitation triggered by synaptic inhibition in cerebellar nuclear neurons is suppressed by selective T-type calcium channel block. J Neurophys 106, 2653–2661.

Boele, H. (2014). Neural Mechanisms Underlying Motor Learning.

Boele, H.-J., Koekkoek, S.K.E., De Zeeuw, C.I., and Ruigrok, T.J.H. (2013). Axonal Sprouting and Formation of Terminals in the Adult Cerebellum during Associative Motor Learning. J Neurosci 33, 17897–17907.

Boele, H.-J., ten Brinke, M., and De Zeeuw, C. (2016). Classical Conditioning of Timed Motor Responses. In The Neuronal Codes of the Cerebellum, pp. 53–96.

Boele, H.J., Koekkoek, S.K., and De Zeeuw, C.I. (2010). Cerebellar and extracerebellar involvement in mouse eyeblink conditioning: the ACDC model. Front Cell Neurosci 19.

Bolbecker, A.R., Steinmetz, A.B., Mehta, C.S., Forsyth, J.K., Klaunig, M.J., Lazar, E.K., Steinmetz, J.E., O'Donnell, B.F., and Hetrick, W.P. (2011). Exploration of cerebellar-dependent associative learning in schizophrenia: effects of varying and shifting interstimulus interval on eyeblink conditioning. Behav Neurosci 125, 687–698.

Boneau, C.A. (1958). The interstimulus interval and the latency of the conditioned eyelid response. J Exp Psychol 56, 464–471.

Bosman, L.W.J., Houweling, A.R., Owens, C.B., Tanke, N., Shevchouk, O.T., Rahmati, N., Teunissen, W.H.T., Ju, C., Gong, W., Koekkoek, S.K.E., et al. (2011). Anatomical pathways involved in generating and sensing rhythmic whisker movements. Front Integr Neurosci 5.

Bosman, L.W.J., Koekkoek, S.K.E., Shapiro, J., Rijken, B.F.M., Zandstra, F., van der Ende, B., Owens, C.B., Potters, J.W., de Gruijl, J.R., Ruigrok, T.J.H., et al. (2010). Encoding of whisker input by cerebellar Purkinje cells. J Physiol 3757–3783.

Bostan, A.C., Dum, R.P., and Strick, P.L. (2013). Cerebellar networks with the cerebral cortex and basal ganglia. Trends Cogn Sci 17, 241–254.

Bourgeron, T. (2015). From the genetic architecture to synaptic plasticity in autism spectrum disorder. Nat Rev Neurosci 551–563.

Boyden, E., Katoh, A., and Raymond, J. (2004). Cerebellum-dependent learning: the role of multiple plasticity mechanisms. Annu Rev Neurosci 581–609.

Bracha, V., Webster, M.L., Winters, N.K., Irwin, K.B., and Bloedel, J. (1994). Effects of muscimol inactivation of the cerebellar interposed-dentate nuclear complex on the performance of the nictitating membrane response in the rabbit. Exp Brain Res 100, 453–468.

Bracha, V., Zhao, L., Irwin, K., and Bloedel, J. (2001). Intermediate cerebellum and conditioned eyeblinks. Parallel involvement in eyeblinks and tonic eyelid closure. Exp Brain Res 136, 41–49.

Braitenberg, V. (1967). Is the cerebellar cortex a biological clock in the millisecond range? Prog Brain Res 25, 334–346.

Brecht, M. (2007). Barrel cortex and whisker-mediated behaviors. Curr Opin Neurobiol 408–416.

Breska, A., and Ivry, R.B. (2016). Taxonomies of Timing: Where Does the Cerebellum Fit In? Curr Opin Beh Sci 8, 282–288.

Brochu, G., Maler, L., and Hawkes, R. (1990). Zebrin II: a polypeptide antigen expressed selectively by Purkinje cells reveals compartments in rat and fish cerebellum. J Comp Neurol 538–552.

Brodal, P., Dietrichs, E., and Walberg, F. (1986). Do pontocerebellar mossy fibres give off collaterals to the cerebellar nuclei? An experimental study in the cat with implantation of crystalline HRP-WGA. Neurosci Res 4, 12–24.

Brooks, J.X., Carriot, J., and Cullen, K.E. (2015). Learning to expect the unexpected: rapid updating in primate cerebellum during voluntary self-motion. Nat Neurosci 1310–1317.

Brown, S. (2005). The Neural Basis of Human Dance. Cerebral Cortex 16, 1157–1167.

Brunel, N., Hakim, V., Isope, P., Nadal, J., and Barbour, B. (2004). Optimal information storage and the distribution of synaptic weights: Perceptron versus Purkinje cell. Neuron 745–757.

Buchtel, H.A., Iosif, G., Marchesi, G.F., Provini, L., and Strata, P. (1972). Analysis of the activity evoked in the cerebellar cortex by stimulation of the visual pathways. Exp Brain Res 15, 278–288.

Buckner, R. (2013). The Cerebellum and Cognitive Function: 25 Years of Insight from Anatomy and Neuroimaging. Neuron 80, 807–815.

Buckner, R.L., Krienen, F.M., Castellanos, A., Diaz, J.C., and Yeo, B.T.T. (2011). The organization of the human cerebellum estimated by intrinsic functional connectivity. J Neurophys 106, 2322–2345.

Buonomano, D.V., and Mauk, M.D. (1994). Neural Network Model of the Cerebellum: Temporal Discrimination and the Timing of Motor Responses. Neural Comp 6, 38–55.

Burroughs, A., Wise, A.K., Xiao, J., Houghton, C., Tang, T., Suh, C.Y., Lang, E.J., Apps, R., and Cerminara, N.L. (2017). The dynamic relationship between cerebellar Purkinje cell simple spikes and the spikelet number of complex spikes. J Physiol 595, 283–299.

Canto, C.B., Witter, L., and Zeeuw, C.I.D. (2016). Whole-Cell Properties of Cerebellar Nuclei Neurons In Vivo. PLOS ONE 11, e0165887.

Carlton, S.M., Leichnetz, G.R., Young, E.G., and Mayer, D.J. (1983). Supramedullary afferents of the nucleus raphe magnus in the rat: a study using the transcannula HRP gel and autoradiographic techniques. J Compar Neurol 214, 43–58.

Casellato, C., Antonietti, A., Garrido, J.A., Ferrigno, G., D'Angelo, E., and Pedrocchi, A. (2015). Distributed cerebellar plasticity implements generalized multiple-scale memory components in real-robot sensorimotor tasks. Front Comp Neurosci 24.

Cason, H. (1922). The conditioned eyelid reaction. J Exp Psychol 5, 153–198.

Cerminara, N.L., and Apps, R. (2011). Behavioural significance of cerebellar modules. Cerebellum 484–494.

Cerminara, N.L., and Rawson, J.A. (2004). Evidence that climbing fibers control an intrinsic spike generator in cerebellar Purkinje cells. J Neurosci 24, 4510–4517.

Cerminara, N.L., Lang, E.J., Sillitoe, R.V., and Apps, R. (2015). Redefining the cerebellar cortex as an assembly of non-uniform Purkinje cell microcircuits. Nat Rev Neurosci 16, 79–93.

Chabrol, F.P., Arenz, A., Wiechert, M.T., Margrie, T.W., and DiGregorio, D.A. (2015). Synaptic diversity enables temporal coding of coincident multisensory inputs in single neurons. Nat Neurosci 718–727.

Chan-Palay, V. (1973). Cytology and organization in the nucleus lateralis of the cerebellum: The projections of neurons and their processes into afferent axon bundles. Zeitschrift Für Anatomie Und Entwicklungsgeschichte 141, 151–159.

Chan-Palay, V. (1977). Cerebellar dentate nucleus: Organization, cytology and transmitters. (Berlin: Springer-Verlag).

Chanda, S., and Xu-Friedman, M. (2011). Excitatory modulation in the cochlear nucleus through group I metabotropic glutamate receptor activation. J Neurosci 7450–7455.

Chapman, P.F., Steinmetz, J.E., Sears, L.L., and Thompson, R.F. (1990). Effects of lidocaine injection in the interpositus nucleus and red nucleus on conditioned behavioral and neuronal responses. Brain Res 537, 149–156.

Chaumont, J., Guyon, N., Valera, A.M., Dugue, G.P., Popa, D., Marcaggi, P., Gautheron, V., Reibel-Foisset, S., Dieudonne, S., Stephan, A., et al. (2013). Clusters of cerebellar Purkinje cells control their afferent climbing fiber discharge. Proc Natl Acad Sci U S A 110, 16223–16228.

Chen, J.A., Peñagarikano, O., Belgard, T.G., Swarup, V., and Geschwind, D.H. (2015). The emerging picture of autism spectrum disorder: genetics and pathology. Ann Rev Path 10, 111–144.

Chen, S., Augustine, G.J., and Chadderton, P. (2016). The cerebellum linearly encodes whisker position during voluntary movement. eLife.

Chen, X., Kovalchuk, Y., Adelsberger, H., Henning, H.A., Sausbier, M., Wietzorrek, G., Ruth, P., Yarom, Y., and Konnerth, A. (2010). Disruption of the olivo-cerebellar circuit by Purkinje neuron-specific ablation of BK channels. Proc Natl Acad Sci U S A 12323–12328.

Chettih, S.N., McDougle, S.D., Ruffolo, L.I., and Medina, J.F. (2011). Adaptive Timing of Motor Output in the Mouse: The Role of Movement Oscillations in Eyelid Conditioning. Front Integr Neurosci 5.

Chklovskii, D.B., Mel, B.W., and Svoboda, K. (2004). Cortical rewiring and information storage. Nature 431, 782–788.

Choi, J.-S., and Moore, J.W. (2003). Cerebellar Neuronal Activity Expresses the Complex Topography of Conditioned Eyeblink Responses. Behav Neurosci 117, 1211–1219.

Chu, C.P., Bing, Y.H., Liu, Q.R., and Qiu, D.L. (2011). Synaptic responses evoked by tactile stimuli in Purkinje cells in mouse cerebellar cortex crus II in vivo. PLOS ONE 6.

Chung, S., Zhang, Y., Van Der Hoorn, F., and Hawkes, R. (2007). The anatomy of the cerebellar nuclei in the normal and scrambler mouse as revealed by the expression of the microtubule-associated protein kinesin light chain 3. Brain Res 120–131.

Cicirata, F., Zappala, A., Serapide, M.F., Parenti, R., Panto, M.R., and Paz, C. (2005). Different pontine projections to the two sides of the cerebellum. Brain Res Rev 49, 280–294.

Clark, G.A., McCormick, D.A., Lavond, D.G., and Thompson, R.F. (1984). Effects of lesions of cerebellar nuclei on conditioned behavioral and hippocampal neuronal responses. Brain Res 291, 125–136.

Clark, R.E., Gohl, E.B., and Lavond, D.G. (1997). The learning-related activity that develops in the pontine nuclei during classical eye-blink conditioning is dependent on the interpositus nucleus. Learn Mem 3, 532–544.

Clark, R.E., Zhang, A.A., and Lavond, D.G. (1992). Reversible lesions of the cerebellar interpositus nucleus during acquisition and retention of a classically conditioned behavior. Behav Neurosci 106, 879–888.

Clopath, C., Badura, A., De Zeeuw, C., and Brunel, N. (2013). A cerebellar learning model that reproduces the behavior of vestibulo-ocular reflex adaptation in wild-type and knock-out mice. p.

Coddington, L., Rudolph, S., Vande Lune, P., Overstreet-Wadiche, L., and Wadiche, J. (2013). Spillover-mediated feedforward inhibition functionally segregates interneuron activity. Neuron 1050–1062.

Cody, F.W., and Richardson, H.C. (1979). Mossy and climbing fibre mediated responses evoked in the cerebellar cortex of the cat by trigeminal afferent stimulation. J Physiol 287, 1–14.

Coesmans, M., Smitt, P., Linden, D., Shigemoto, R., Hirano, T., Yamakawa, Y., van Alphen, A., Luo, C., van der Geest, J., Kros, J., et al. (2003). Mechanisms underlying cerebellar motor deficits due to mGluR1-autoantibodies. Ann Neurol 325–336.

Coesmans, M., Weber, J.T., De Zeeuw, C.I., and Hansel, C. (2004). Bidirectional parallel fiber plasticity in the cerebellum under climbing fiber control. Neuron 44, 691–700.

Coleman, S., and Gormezano, I. (1971). Classical conditioning of the rabbit's (Oryctolagus cuniculus) nictitating membrane response under symmetrical CS-US interval shifts. J Comp Physiol Psychol 447–455.

Colin, F., Manil, J., and Desclin, J.C. (1980). The olivocerebellar system. I. Delayed and slow inhibitory effects: an overlooked salient feature of cerebellar climbing fibers. Brain Res 187, 3–27.

Condorelli, D.F., Parenti, R., Spinella, F., Trovato Salinaro, A., Belluardo, N., Cardile, V., and Cicirata, F. (1998). Cloning of a new gap junction gene (Cx36) highly expressed in mammalian brain neurons. Eur J Neurosci 10, 1202–1208.

Constantinople, C.M., and Bruno, R.M. (2013). Deep Cortical Layers Are Activated Directly by Thalamus. Science 340, 1591–1594.

Courchesne, E. (1991). Neuroanatomic imaging in autism. Pediatrics 87, 781–790.

Courville, J. (1983). Faraco-Cantin F, Legendre A. Archives Ital Biol 121, 219–236.

Courville, J., Faraco-Cantin, F., and Legendre, A. (1983). Detailed organization of cerebello-olivary projections in the cat. An autoradiographic study. Archives Ital Biol 219–236.

Crapse, T.B., and Sommer, M.A. (2008). Corollary discharge across the animal kingdom. Nat Rev Neurosci 587–600.

D'Angelo, E., and De Zeeuw, C. (2009). Timing and plasticity in the cerebellum: focus on the granular layer. Trends Neurosci 30–40.

D'Angelo, E., and De Zeeuw, C.I. (2009). Timing and plasticity in the cerebellum: focus on the granular layer. Trends Neurosci 30–40.

D'Angelo, E., Koekkoek, S.K.E., Lombardo, P., Solinas, S., Ros, E., Garrido, J., Schonewille, M., and De Zeeuw, C.I. (2009). Timing in the cerebellum: oscillations and resonance in the granular layer. Neuroscience 162, 805–815.

D'Angelo, E., Nieus, T., Maffei, A., Armano, S., Rossi, P., Taglietti, V., Fontana, A., and Naldi, G. (2001). Theta-frequency bursting and resonance in cerebellar granule cells: experimental evidence and modeling of a slow k+-dependent mechanism. J Neurosci 759–770.

D'Mello, A.M., Crocetti, D., Mostofsky, S.H., and Stoodley, C.J. (2015). Cerebellar gray matter and lobular volumes correlate with core autism symptoms. NeuroImage: Clinical 7, 631–639.

Darwin, C. (1859). Chapter XIV. in On the Origin of Species.

De Gruijl, J.R., Bazzigaluppi, P., de Jeu, M.T.G., and De Zeeuw, C.I. (2012). Climbing fiber burst size and olivary sub-threshold oscillations in a network setting. PLoS Comput Biol 8, e1002814.

De Gruijl, J.R., Hoogland, T.M., and De Zeeuw, C.I. (2014). Behavioral correlates of complex spike synchrony in cerebellar microzones. J Neurosci 34, 8937–8947.

De Zeeuw, C., and Berrebi, A. (1995). Postsynaptic targets of Purkinje cell terminals in the cerebellar and vestibular nuclei of the rat. Eur J Neurosci 2322–2333.

De Zeeuw, C., and Koekkoek, S. (1997). Signal processing in the C2 module of the flocculus and its role in head movement control. Prog Brain Res 299–320.

De Zeeuw, C., Hansel, C., Bian, F., Koekkoek, S., van Alphen, A., Linden, D., and Oberdick, J. (1998a). Expression of a protein kinase C inhibitor in Purkinje cells blocks cerebellar LTD and adaptation of the vestibulo-ocular reflex. Neuron 495–508.

De Zeeuw, C., Hoebeek, F., and Schonewille, M. (2008). Causes and consequences of oscillations in the cerebellar cortex. Neuron 655–658.

De Zeeuw, C., Holstege, J., Calkoen, F., Ruigrok, T., and Voogd, J. (1988). A new combination of WGA-HRP anterograde tracing and GABA immunocytochemistry applied to afferents of the cat inferior olive at the ultrastructural level. Brain Res 369–375.

De Zeeuw, C., Holstege, J., Ruigrok, T., and Voogd, J. (1989). Ultrastructural study of the GABAergic, cerebellar, and mesodiencephalic innervation of the cat medial accessory olive: anterograde tracing combined with immunocytochemistry. J Comp Neurol 12–35.

De Zeeuw, C., Koekkoek, S., van Alphen, A., Luo, C., Hoebeek, F., van der Steen, J., Frens, M., Sun, J., Goossens, H., Jaarsma, D., et al. (2004). Gain and phase control of compensatory eye movements by the flocculus of the vestibulocerebellum. In The Vestibular System (Ed. SM Highstein, RR Fay and AN Popper), p.

De Zeeuw, C., Wylie, D., DiGiorgi, P., and Simpson, J. (1994). Projections of individual Purkinje cells of identified zones in the flocculus to the vestibular and cerebellar nuclei in the rabbit. J Comp Neurol 428–447.

De Zeeuw, C., Wylie, D., Stahl, J., and Simpson, J. (1995). Phase relations of Purkinje cells in the rabbit flocculus during compensatory eye movements. J Neurophysiol 2051–2064.

De Zeeuw, C.I., and Ruigrok, T.J. (1994). Olivary projecting neurons in the nucleus of Darkschewitsch in the cat receive excitatory monosynaptic input from the cerebellar nuclei. Brain Res 345–350.

De Zeeuw, C.I., and Ten Brinke, M.M. (2015). Motor Learning and the Cerebellum. Cold Spring Harb Perspect Biol 7, a021683.

De Zeeuw, C.I., and Yeo, C.H. (2005). Time and tide in cerebellar memory formation. Curr Op Neurobiol 15, 667–674.

De Zeeuw, C.I., Chorev, E., Devor, A., Manor, Y., Van Der Giessen, R.S., De Jeu, M.T., Hoogenraad, C.C., Bijman, J., Ruigrok, T.J.H., French, P., et al. (2003). Deformation of network connectivity in the inferior olive of connexin 36-deficient mice is compensated by morphological and electrophysiological changes at the single neuron level. J Neurosci 23, 4700–4711.

De Zeeuw, C.I., Hertzberg, E.L., and Mugnaini, E. (1995). The dendritic lamellar body: a new neuronal organelle putatively associated with dendrodendritic gap junctions. J Neurosci 15, 1587–1604.

De Zeeuw, C.I., Hoebeek, F.E., Bosman, L.W.J., Schonewille, M., Witter, L., and Koekkoek, S.K. (2011). Spatiotemporal firing patterns in the cerebellum. Nat Rev Neurosci 12, 327–344.

de Zeeuw, C.I., Holstege, J.C., Calkoen, F., Ruigrok, T.J., and Voogd, J. (1988). A new combination of WGA-HRP anterograde tracing and GABA immunocytochemistry applied to afferents of the cat inferior olive at the ultrastructural level. Brain Res 447, 369–375.

De Zeeuw, C.I., Holstege, J.C., Ruigrok, T.J.H., and Voogd, J. (1990). Mesodiencephalic and cerebellar terminals terminate upon the same dendritic spines in the glomeruli of the cat and rat inferior olive: An ultrastructural study using a combination of [3H]-leucine and wheat germ agglutinin coupled horseradish peroxidase anterograde tracing. Neuroscience 34, 645–655.

De Zeeuw, C.I., Hoogenraad, C.C., Koekkoek, S.K.E., Ruigrok, T.J., Galjart, N., and Simpson, J.I. (1998b). Microcircuitry and function of the inferior olive. Trends Neurosci 21, 391–400.

De Zeeuw, C.I., Lang, E.J., Sugihara, I., Ruigrok, T.J., Eisenman, L.M., Mugnaini, E., and Llinás, R. (1996). Morphological correlates of bilateral synchrony in the rat cerebellar cortex. J Neurosci 16, 3412–3426.

References

De Zeeuw, C.I., Van Alphen, A.M., Hawkins, R.K., and Ruigrok, T.J. (1997). Climbing fibre collaterals contact neurons in the cerebellar nuclei that provide a GABAergic feedback to the inferior olive. Neuroscience 80, 981–986.

Dean, P., and Porrill, J. (2008). Adaptive-filter models of the cerebellum: computational analysis. Cerebellum 7, 567–571.

Dean, P., and Porrill, J. (2011). Evaluating the adaptive-filter model of the cerebellum. J Physiol 589, 3459–3470.

Dean, P., Porrill, J., Ekerot, C.F., and Jörntell, H. (2010). The cerebellar microcircuit as an adaptive filter: experimental and computational evidence. Nat Rev Neurosci 30–43.

Dehnes, Y., Chaudhry, F., Ullensvang, K., Lehre, K., Storm-Mathisen, J., and Danbolt, N. (1998). The glutamate transporter EAAT4 in rat cerebellar Purkinje cells: a glutamate-gated chloride channel concentrated near the synapse in parts of the dendritic membrane facing astroglia. J Neurosci 3606–3619.

Dehnhardt, G., Mauck, B., Hanke, W., and Bleckmann, H. (2001). Hydrodynamic trail-following in harbor seals (Phoca vitulina). Science 102–104.

Delgado-Garcia, J., and Gruart, A. (2002). The role of interpositus nucleus in eyelid conditioned responses. Cerebellum 289–308.

Delgado-Garcia, J., and Gruart, A. (2006). Building new motor responses: eyelid conditioning revisited. Trends Neurosci 330–338.

Delgado-Garcia, J., Gruart, A., and Munera, A. (2002). Neural organization of eyelid responses. Mov Disord S33–36.

Delgado-García, J.M., and Gruart, A. (2005). Firing activities of identified posterior interpositus nucleus neurons during associative learning in behaving cats. Brain Res Rev 49, 367–376.

Delgado-Garcia, J.M., Gruart, A., and Trigo, J.A. (2003). Physiology of the eyelid motor system. Ann N Y Acad Sci 1–9.

Dere, E., Huston, J.P., and De Souza Silva, M.A. (2007). The pharmacology, neuroanatomy and neurogenetics of one-trial object recognition in rodents. Neurosci Biobehav Rev 673–704.

Deschênes, M., Kurnikova, A., Elbaz, M., and Kleinfeld, D. (2016). Circuits in the ventral medulla that phase-lock motoneurons for coordinated sniffing and whisking. Neural Plast 2016.

Desmond, J.E., and Moore, J.W. (1982). A brain stem region essential for the classically conditioned but not unconditioned nictitating membrane response. Physiol Behav 28, 1029–1033.

Devor, A., and Yarom, Y. (2002a). Electrotonic coupling in the inferior olivary nucleus revealed by simultaneous double patch recordings. J Neurophys 87, 3048–3058.

Devor, A., and Yarom, Y. (2002b). Generation and propagation of subthreshold waves in a network of inferior olivary neurons. J Neurophys 87, 3059–3069.

Diamond, M.E., and Arabzadeh, E. (2013). Whisker sensory system - From receptor to decision. Prog Neurobiol 284–240.

Dietrichs, E., and Walberg, F. (1980). The cerebellar corticonuclear and nucleocortical projections in the cat as studied with anterograde and retrograde transport of horseradish peroxidase. II. Lobulus simplex, crus I and II. Anatomy Embryol 83–103.

Dietrichs, E., and Walberg, F. (1981). The cerebellar nucleo-olivary projection in the cat. Anatomy Embryol 162, 51–67.

Dietrichs, E., and Walberg, F. (1986). The cerebellar nucleo-olivary and olivocerebellar nuclear projections in the cat as studied with anterograde and retrograde transport in the same animal after implantation of crystalline WGA-HRP. III. The interposed nuclei. Brain Res 373–383.

Dietrichs, E., Bjaalie, J.G., and Brodal, P. (1983). Do pontocerebellar fibers send collaterals to the cerebellar nuclei? Brain Res 259, 127–131.

Diño, M.R., Willard, F.H., and Mugnaini, E. (1999). Distribution of unipolar brush cells and other calretinin immunoreactive components in the mammalian cerebellar cortex. J Neurocytol 28, 99–123.

Douglas, R.J., Koch, C., Mahowald, M., Martin, K.A., and Suarez, H.H. (1995). Recurrent excitation in neocortical circuits. Science 269, 981–985.

Durand, C.M. (2007). Mutations in the gene encoding the synaptic scaffolding protein SHANK3 are associated with autism spectrum disorders. Nat Genet 25–7.

296

Dutar, P., Vu, H.M., and Perkel, D.J. (1999). Pharmacological characterization of an unusual mGluR-evoked neuronal hyperpolarization mediated by activation of GIRK channels. Neuropharm 38, 467–475.

Ebel, H., and Prokasy, W. (1963). Classical eyelid conditioning as a function of sustained and shifted interstimulus intervals. J Exp Psychol 52–58.

Eccles, J.C., Ito, M., and Szentágothai, J. (1967). The Cerebellum as a Neuronal Machine (Springer Berlin Heidelberg).

Eccles, J.C., Llinás, R., and Sasaki, K. (1966). The excitatory synaptic action of climbing fibres on the Purkinje cells of the cerebellum. J Physiol 182, 268–296.

Edgley, S.A., Mostofi, A., and Holtzman, T. (2010). Cerebellar climbing fibres are driven by extracerebellar learning in classical (eyeblink) conditioning. Poster Abstract, Society for Neuroscience, San Diego.

Ekerot, C., and Kano, M. (1985). Long-term depression of parallel fibre synapses following stimulation of climbing fibres. Brain Res 357–360.

Ekerot, C., and Larson, B. (1982). Branching of olivary axons to innervate pairs of sagittal zones in the cerebellar anterior lobe of the cat. Exp Brain Res 185–198.

Endo, S., Shutoh, F., Dinh, T., Okamoto, T., Ikeda, T., Suzuki, M., Kawahara, S., Yanagihara, D., Sato, Y., Yamada, K., et al. (2009). Dual involvement of G-substrate in motor learning revealed by gene deletion. Proc Natl Acad Sci U S A 3525–3530.

Engbers, J.D.T., Anderson, D., Tadayonnejad, R., Mehaffey, W.H., Molineux, M.L., and Turner, R.W. (2011). Distinct roles for I(T) and I(H) in controlling the frequency and timing of rebound spike responses. J Physiol 589, 5391–5413.

Fabbro, F., Tavano, A., Corti, S., Bresolin, N., De Fabritiis, P., and Borgatti, R. (2004). Long-term neuropsychological deficits after cerebellar infarctions in two young adult twins. Neuropsychologia 42, 536–545.

Feldmeyer, D., Brecht, M., Helmchen, F., Petersen, C.C.H., Poulet, J.F.A., Staiger, J.F., Luhmann, H.J., and Schwarz, C. (2013). Barrel cortex function. Prog Neurobiol 3–27.

Ferezou, I., Haiss, F., Gentet, L.J., Aronoff, R., Weber, B., and Petersen, C.C.H. (2007). Spatiotemporal dynamics of cortical sensorimotor integration in behaving mice. Neuron 907–923.

Foscarin, S., Ponchione, D., Pajaj, E., Leto, K., Gawlak, M., Wilczynski, G.M., Rossi, F., and Carulli, D. (2011). Experience-Dependent Plasticity and Modulation of Growth Regulatory Molecules at Central Synapses. PLOS ONE 6, e16666.

Fredette, B., and Mugnaini, E. (1991). The GABAergic cerebello-olivary projection in the rat. Anatomy Embryol 225–243.

Freeman, J., and Duffel, J. (2008). Eyeblink conditioning using cochlear nucleus stimulation as a conditioned stimulus in developing rats. Dev Psychobiol 640–646.

Freeman, J., Jr., C., Rabinak, and Campolattaro, M. (2005a). Pontine stimulation overcomes developmental limitations in the neural mechanisms of eyeblink conditioning. Learn Mem 255–259.

Freeman, J., Spencer, C., Skelton, R., and Stanton, M. (1993). Ontogeny of eyeblink conditioning in the rat: Effects of US intensity and interstimulus interval on delay conditioning. Psychobiology 233–242.

Freeman, J.H. (2015). Cerebellar learning mechanisms. Brain Res 1621, 260–269.

Freeman, J.H., and Nicholson, D.A. (2000). Developmental changes in eye-blink conditioning and neuronal activity in the cerebellar interpositus nucleus. J Neurosci 20, 813–819.

Freeman, J.H., and Steinmetz, A.B. (2011). Neural circuitry and plasticity mechanisms underlying delay eyeblink conditioning. Learn Mem 18, 666–677.

Freeman, J.H., Halverson, H.E., and Hubbard, E.M. (2007). Inferior colliculus lesions impair eyeblink conditioning in rats. Learn Mem 14, 842–846.

Freeman, J.H., Halverson, H.E., and Poremba, A. (2005b). Differential Effects of Cerebellar Inactivation on Eyeblink Conditioned Excitation and Inhibition. J Neurosci 25, 889–895.

Frey, W. (1969). Within and between session CS intensity performance effects in rabbit eyelid conditioning. Psychon Sci 1–2.

Fujita, M. (1982). Adaptive filter model of the cerebellum. Bio Cybernetics 45, 195–206.

Furutama, D., Morita, N., Takano, R., Sekine, Y., Sadakata, T., Shinoda, Y., Hayashi, K., Mishima, Y., Mikoshiba, K., Hawkes, R., et al. (2010). Expression of the IP3R1 promoter-driven nls-lacZ transgene in Purkinje cell parasagittal arrays of developing mouse cerebellum. J Neurosci Res 2810–2825.

Galliano, E., Gao, Z., Schonewille, M., Todorov, B., Simons, E., Pop, A.S., D'Angelo, E., van den Maagdenberg, A.M.J.M., Hoebeek, F.E., and De Zeeuw, C.I. (2013a). Silencing the majority of cerebellar granule cells uncovers their essential role in motor learning and consolidation. Cell Reports 3, 1239–1251.

Galliano, E., Potters, J.-W., Elgersma, Y., Wisden, W., Kushner, S.A., De Zeeuw, C.I., and Hoebeek, F.E. (2013b). Synaptic transmission and plasticity at inputs to murine cerebellar Purkinje cells are largely dispensable for standard nonmotor tasks. J Neurosci 33, 12599–12618.

Gallistel, C., Fairhurst, S., and Balsam, P. (2004). The learning curve: implications of a quantitative analysis. Proc Natl Acad Sci U S A 13124–13131.

Gao, Z., Proietti-Onori, M., Lin, Z., ten Brinke, M.M., Boele, H.-J., Potters, J.-W., Ruigrok, T.J.H., Hoebeek, F.E., and De Zeeuw, C.I. (2016). Excitatory Cerebellar Nucleocortical Circuit Provides Internal Amplification during Associative Conditioning. Neuron 89, 645–657.

Gao, Z., van Beugen, B.J., and De Zeeuw, C.I. (2012). Distributed synergistic plasticity and cerebellar learning. Nat Rev Neurosci 13, 619–635.

Gao, Z., van Woerden, G.M., Elgersma, Y., De Zeeuw, C.I., and Hoebeek, F.E. (2014). Distinct roles of α- and βCaMKII in controlling long-term potentiation of GABAA-receptor mediated transmission in murine Purkinje cells. Front Cell Neurosci 8.

Garcia, K., and Mauk, M. (1998). Pharmacological analysis of cerebellar contributions to the timing and expression of conditioned eyelid responses. Neuropharm 471–480.

Garcia, K., Mauk, M., Weidemann, G., and Kehoe, E. (2003). Covariation of alternative measures of responding in rabbit (Oryctolagus cuniculus) eyeblink conditioning during acquisition training and tone generalization. Behav Neurosci 292–303.

Garwicz, M., Ekerot, C.-F., and Jörntell, H. (1998). Organizational Principles of Cerebellar Neuronal Circuitry. News Phys Sci 13, 26–32.

Gauck, V., and Jaeger, D. (2000). The control of rate and timing of spikes in the deep cerebellar nuclei by inhibition. J Neurosci 3006–3016.

Gebre, S.A., Reeber, S.L., and Sillitoe, R.V. (2012). Parasagittal compartmentation of cerebellar mossy fibers as revealed by the patterned expression of vesicular glutamate transporters VGLUT1 and VGLUT2. Brain Struct Funct 165–180.

Gewirtz, J.C., and Davis, M. (2000). Using Pavlovian Higher-Order Conditioning Paradigms to Investigate the Neural Substrates of Emotional Learning and Memory. Learn Mem 7, 257–266.

Giovannucci, A., Badura, A., Deverett, B., Najafi, F., Pereira, T.D., Gao, Z., Ozden, I., Kloth, A.D., Pnevmatikakis, E., Paninski, L., et al. (2017). Cerebellar granule cells acquire a widespread predictive feedback signal during motor learning. Nat Neurosci advance online publication.

Glickstein, M., Cohen, J., Dixon, B., Gibson, A., Hollins, M., Labossiere, E., and Robinson, F. (1980). Corticopontine visual projections in macaque monkeys. J Comp Neurol 209–229.

Glickstein, M., Stein, J., and King, R. (1972). Visual input to the pontine nuclei. Science 1110–1111.

Gonzalez-Joekes, J., and Schreurs, B.G. (2012). Anatomical Characterization of a Rabbit Cerebellar Eyeblink Premotor Pathway Using Pseudorabies and Identification of a Local Modulatory Network in Anterior Interpositus. J Neurosci 32, 12472–12487.

Gormezano, I., and Kehoe, E. (1975). Classical conditioning: some methodical-conceptual issues. In: Handbook of learning and cognitive processes (Estes WK, ed), pp 143-179.

Gormezano, I., Kehoe, E., and Marshall, B. (1983). Twenty years of classical conditioning research with the rabbit.

Gormezano, I., Schneiderman, N., Deaux, E., and Fuentes, I. (1962). Nictitating Membrane: Classical Conditioning and Extinction in the Albino Rabbit. Science 138, 33–34.

Gould, B.B., and Graybiel, A.M. (1976). Afferents to the cerebellar cortex in the cat: evidence for an intrinsic pathway leading from the deep nuclei to the cortex. Brain Res 601–611.

Gould, T.J., and Steinmetz, J.E. (1996). Changes in rabbit cerebellar cortical and interpositus nucleus activity during acquisition, extinction, and backward classical eyelid conditioning. Neurobiol Learn Mem 65, 17–34.

Goyal, R.K., and Chaudhury, A. (2013). Structure activity relationship of synaptic and junctional neurotransmission. Auton Neurosci 176, 11–31.

Grabrucker, A.M., Schmeisser, M.J., Schoen, M., and Boeckers, T.M. (2011). Postsynaptic ProSAP/Shank scaffolds in the cross-hair of synaptopathies. Trends Cell Biol 21, 594–603.

Grafman, J., Litvan, I., Massaquoi, S., Stewart, M., Sirigu, A., and Hallett, M. (1992). Cognitive planning deficit in patients with cerebellar atrophy. Neurology 42, 1493–1496.

Graham, D., and Wylie, D. (2012). Zebrin-immunopositive and -immunonegative stripe pairs represent functional units in the pigeon vestibulocerebellum. J Neurosci 12769–12779.

Green, J.T., and Arenos, J.D. (2007). Hippocampal and cerebellar single-unit activity during delay and trace eyeblink conditioning in the rat. Neurobiol Learn Mem 87, 269–284.

Green, J.T., and Steinmetz, J.E. (2005). Purkinje cell activity in the cerebellar anterior lobe after rabbit eyeblink conditioning. Learn Mem 12, 260–269.

Groenewegen, H., and Voogd, J. (1977). The parasagittal zonation within the olivocerebellar projection. I. Climbing fiber distribution in the vermis of cat cerebellum. J Comp Neurol 417–488.

Gruart, A., and Delgado-Garcia, J. (1994). Discharge of identified deep cerebellar nuclei neurons related to eye blinks in the alert cat. Neuroscience 665–681.

Gruart, A., Blázquez, P., and Delgado-García, J.M. (1995). Kinematics of spontaneous, reflex, and conditioned eyelid movements in the alert cat. J Neurophys 74, 226–248.

Gruart, A., Guillazo-Blanch, G., Fernández-Mas, R., Jiménez-Díaz, L., and Delgado-García, J.M. (2000). Cerebellar posterior interpositus nucleus as an enhancer of classically conditioned eyelid responses in alert cats. J Neurophys 84, 2680–2690.

Gruart, A., Pastor, A.M., Armengol, J.A., and Delgado-García, J.M. (1997). Chapter 29 Involvement of cerebellar cortex and nuclei in the genesis and control of unconditioned and conditioned eyelid motor responses. In Prog Brain Res, C.I. De Zeeuw, P. Strata, and J. Voogd, eds. (Elsevier), pp. 511–528.

Guo, Z.V., Li, N., Huber, D., Ophir, E., Gutnisky, D., Ting, J.T., Feng, G., and Svoboda, K. (2014). Flow of cortical activity underlying a tactile decision in mice. Neuron 179–194.

Gutierrez-Castellanos, N., Da Silva-Matos, C.M., Zhou, K., Canto, C.B., Renner, M.C., Koene, L.M.C., Ozyildirim, O., Sprengel, R., Kessels, H.W., and De Zeeuw, C.I. (2017). Motor learning requires Purkinje cell synaptic potentiation through activation of AMPA-receptor subunit GluA3. Neuron 409–424.

Hallett, P.E., and Lightstone, A.D. (1976). Saccadic eye movements towards stimuli triggered by prior saccades. Vision Res 99–106.

Halverson, H., and Freeman, J. (2009). Medial auditory thalamic input to the lateral pontine nuclei is necessary for auditory eyeblink conditioning. Neurobiol Learn Mem 93, 92–98.

Halverson, H., and Freeman, J. (2010). Ventral lateral geniculate input to the medial pons is necessary for visual eyeblink conditioning in rats. Learn Mem 80–85.

Halverson, H., Poremba, A., and Freeman, J. (2008). Medial auditory thalamus inactivation prevents acquisition and retention of eyeblink conditioning. Learn Mem 532–538.

Halverson, H.E., Hubbard, E.M., and Freeman, J.H. (2009). Stimulation of the lateral geniculate, superior colliculus, or visual cortex is sufficient for eyeblink conditioning in rats. Learn Mem 16, 300–307.

Halverson, H.E., Khilkevich, A., and Mauk, M.D. (2015). Relating Cerebellar Purkinje Cell Activity to the Timing and Amplitude of Conditioned Eyelid Responses. J Neurosci 35, 7813–7832.

Halverson, H.E., Lee, I., and Freeman, J.H. (2010). Associative Plasticity in the Medial Auditory Thalamus and Cerebellar Interpositus Nucleus during Eyeblink Conditioning. J Neurosci 30, 8787–8796.

Hammer, O., Harper, D., and Ryan, P. (2001). PAST: Paleontological Statistics Software Package for Education and Data Analysis. Palaeont Elect 4, 1–9.

Hamori, J., Mezey, E., and Szentagothai, J. (1981). Electron microscopic identification of cerebellar nucleo-cortical mossy terminals in the rat. Exp Brain Res 97–100.

Hansel, C., and Linden, D. (2000). Long-term depression of the cerebellar climbing fiber–Purkinje neuron synapse. Neuron 473–482.

Hansel, C., Linden, D.J., and D'Angelo, E. (2001). Beyond parallel fiber LTD: the diversity of synaptic and non-synaptic plasticity in the cerebellum. Nat Neurosci 4, 467–475.

Hantman, A.W., and Jessell, T.M. (2010). Clarke's column neurons as the focus of a corticospinal corollary circuit. Nat Neurosci 1233–1239.

References

Hardiman, M., Ramnani, N., and Yeo, C. (1996). Reversible inactivations of the cerebellum with muscimol prevent the acquisition and extinction of conditioned nictitating membrane responses in the rabbit. Exp Brain Res 235–247.

Hartmann, J., Dragicevic, E., Adelsberger, H., Henning, H., Sumser, M., Abramowitz, J., Blum, R., Dietrich, A., Freichel, M., Flockerzi, V., et al. (2008). TRPC3 channels are required for synaptic transmission and motor coordination. Neuron 392–398.

Harvey, R., and Napper, R. (1991). Quantitative studies on the mammalian cerebellum. Prog Neurobiol 437–463.

Hashimoto, K., and Kano, M. (2003). Functional differentiation of multiple climbing fiber inputs during synapse elimination in the developing cerebellum. Neuron 38, 785–96.

Hauge, S.A., Tracy, J.A., Baudry, M., and Thompson, R.F. (1998). Selective changes in AMPA receptors in rabbit cerebellum following classical conditioning of the eyelid-nictitating membrane response. Brain Res 803, 9–18.

Häusser, M., and Clark, B.A. (1997). Tonic synaptic inhibition modulates neuronal output pattern and spatiotemporal synaptic integration. Neuron 19, 665–678.

Heck, D., De Zeeuw, C., Jaeger, D., Khodakhah, K., and Person, A. (2013). The neuronal code(s) of the cerebellum. J Neurosci 17603–17609.

Heiney, S.A., Kim, J., Augustine, G.J., and Medina, J.F. (2014a). Precise Control of Movement Kinematics by Optogenetic Inhibition of Purkinje Cell Activity. J Neurosci 34, 2321–2330.

Heiney, S.A., Wohl, M.P., Chettih, S.N., Ruffolo, L.I., and Medina, J.F. (2014b). Cerebellar-Dependent Expression of Motor Learning during Eyeblink Conditioning in Head-Fixed Mice. J Neurosci 34, 14845–14853.

Hesslow, G. (1994a). Inhibition of classically conditioned eyeblink responses by stimulation of the cerebellar cortex in the decerebrate cat. J Physiol 476, 245–256.

Hesslow, G. (1994b). Correspondence between climbing fibre input and motor output in eyeblink-related areas in cat cerebellar cortex. J Physiol 476, 229.

Hesslow, G., and Ivarsson, M. (1994). Suppression of cerebellar Purkinje cells during conditioned responses in ferrets. Neuroreport 5, 649–652.

Hesslow, G., and Ivarsson, M. (1996). Inhibition of the inferior olive during conditioned responses in the decerebrate ferret. Exp Brain Res 110, 36–46.

Hesslow, G., Jirenhed, D.-A., Rasmussen, A., and Johansson, F. (2013). Classical conditioning of motor responses: What is the learning mechanism? Neural Networks 47, 81–87.

Hesslow, G., Svensson, P., and Ivarsson, M. (1999). Learned movements elicited by direct stimulation of cerebellar mossy fiber afferents. Neuron 179–185.

Hilgard, E., and Marquis, D. (1935). Acquisition, extinction, and retention of conditioned lid responses to light in dogs. J Comp Psychol 29–58.

Hilgard, E., and Marquis, D. (1936). Conditioned eyelid responses in monkeys, with a comparison of dog, monkey, and man. Phychol Monogr 187–198.

Hioki, H., Fujiyama, F., Taki, K., Tomioka, R., Furuta, T., Tamamaki, N., and Kaneko, T. (2003). Differential distribution of vesicular glutamate transporters in the rat cerebellar cortex. Neuroscience 1–6.

Hoebeek, F.E., Witter, L., Ruigrok, T.J.H., and De Zeeuw, C.I. (2010). Differential olivo-cerebellar cortical control of rebound activity in the cerebellar nuclei. Proc Natl Acad Sci U S A 107, 8410–8415.

Hoehler, F., and Thompson, R. (1980). Effect of the interstimulus (CS-UCS) interval on hippocampal unit activity during classical conditioning of the nictitating membrane response of the rabbit (Oryctolagus cuniculus). J Comp Physiol Psychol 201–215.

Holmes, G. (1917). The symptoms of acute cerebellar injuries due to gunshot injuries. Brain 40, 461–535.

Holmes, G. (1939). The Cerebellum of Man. Brain 62, 1–30.

Holstege, G., van Ham, J., and Tan, J. (1986). Afferent projections to the orbicularis oculi motoneuronal cell group. An autoradiographical tracing study in the cat. Brain Res 306–320.

Holt, E. (1931). Animal drive and the learning proces.

Hoogland, T.M., De Gruijl, J.R., Witter, L., Canto, C.B., and De Zeeuw, C.I. (2015). Role of Synchronous Activation of Cerebellar Purkinje Cell Ensembles in Multi-joint Movement Control. Curr Biol 25, 1157–1165.

Hoppenbrouwers, S.S., Schutter, D.J.L.G., Fitzgerald, P.B., Chen, R., and Daskalakis, Z.J. (2008). The role of the cerebellum in the pathophysiology and treatment of neuropsychiatric disorders: A review. Brain Res Rev 59, 185–200.

Houck, B.D., and Person, A.L. (2015). Cerebellar premotor output neurons collateralize to innervate the cerebellar cortex. J Compar Neurol 523, 2254–2271.

Hsu, P.D., Lander, E.S., and Zhang, F. (2014). Development and Applications of CRISPR-Cas9 for Genome Engineering. Cell 157, 1262–1278.

Ichise, T., Kano, M., Hashimoto, K., Yanagihara, D., Nakao, K., Shigemoto, R., Katsuki, M., and Aiba, A. (2000). mGluR1 in cerebellar Purkinje cells essential for long-term depression, synapse elimination, and motor coordination. Science 1832–1835.

Igarashi, K.M., Lu, L., Colgin, L.L., Moser, M.-B., and Moser, E.I. (2014). Coordination of entorhinal-hippocampal ensemble activity during associative learning. Nature 510, 143–147.

Isope, P., and Barbour, B. (2002). Properties of unitary granule cell–Purkinje cell synapses in adult rat cerebellar slices. J Neurosci 9668–9678.

Ito, M. (1982). Cerebellar control of the vestibulo-ocular reflex–around the flocculus hypothesis. Ann Rev Neurosci 5, 275–296.

Ito, M. (2001). Cerebellar long-term depression: characterization, signal transduction, and functional roles. Phys Rev 81, 1143–1195.

Ito, M. (2002). Historical review of the significance of the cerebellum and the role of Purkinje cells in motor learning. Ann N Y Acad Sci 273–288.

Ito, M. (2003). Long-term depression. Ann Rev Neurosci 85–102.

Ito, M. (2006). Cerebellar circuitry as a neuronal machine. Prog Neurobiol 272–303.

Ito, M. (2008). Control of mental activities by internal models in the cerebellum. Nat Rev Neurosci 9, 304–313.

Ito, M., and Kano, M. (1982). Long-lasting depression of parallel fiber-Purkinje cell transmission induced by conjunctive stimulation of parallel fibers and climbing fibers in the cerebellar cortex. Neurosci Lett 33, 253–258.

Ito, M., Sakurai, M., and Tongroach, P. (1982). Climbing fibre induced depression of both mossy fibre responsiveness and glutamate sensitivity of cerebellar Purkinje cells. J Physiol 113–134.

Ito, M., Yamaguchi, K., Nagao, S., and Yamazaki, T. (2014). Long-term depression as a model of cerebellar plasticity. Prog Brain Res 1–30.

Itoh, K., Takada, M., Yasui, Y., Kudo, M., and Mizuno, N. (1983). Direct projections from the anterior pretectal nucleus to the dorsal accessory olive in the cat: an anterograde and retrograde WGA-HRP study. Brain Res 272, 350–353.

Ivry, R.B., and Keele, S.W. (1989). Timing functions of the cerebellum. J Cog Neurosci 1, 136–152.

Ivry, R.B., Keele, S.W., and Diener, H.C. (1988). Dissociation of the lateral and medial cerebellum in movement timing and movement execution. Exp Brain Res 73, 167–180.

Jacobson, G.A., Lev, I., Yarom, Y., and Cohen, D. (2009). Invariant phase structure of olivo-cerebellar oscillations and its putative role in temporal pattern generation. Proc Natl Acad Sci U S A 106, 3579–3584.

Jaeger, D. (2011). Mini-review: synaptic integration in the cerebellar nuclei–perspectives from dynamic clamp and computer simulation studies. Cerebellum 10, 659–666.

Jahnsen, H. (1986). Electrophysiological characteristics of neurones in the guinea-pig deep cerebellar nuclei in vitro. J Physiol 372, 129–147.

Jiang, Y.-H., and Ehlers, M.D. (2013). Modeling autism by SHANK gene mutations in mice. Neuron 78, 8–27.

Jimenez-Diaz, L. (2004). Role of Cerebellar Interpositus Nucleus in the Genesis and Control of Reflex and Conditioned Eyelid Responses. J Neurosci 24, 9138–9145.

Jimenez-Diaz, L., Gruart, A., Minano, F., and Delgado-Garcia, J. (2002). An experimental study of posterior interpositus involvement in the genesis and control of conditioned eyelid responses. Ann N Y Acad Sci 106–118.

Jinno, S., Jeromin, A., Roder, J., and Kosaka, T. (2003). Compartmentation of the mouse cerebellar cortex by neuronal calcium sensor-1. J Comp Neurol 412–424.

Jirenhed, D.-A., and Hesslow, G. (2011b). Time Course of Classically Conditioned Purkinje Cell Response Is Determined by Initial Part of Conditioned Stimulus. J Neurosci 31, 9070–9074.

Jirenhed, D.-A., Bengtsson, F., and Hesslow, G. (2007). Acquisition, Extinction, and Reacquisition of a Cerebellar Cortical Memory Trace. J Neurosci 27, 2493–2502.

Jirenhed, D.-A., Bengtsson, F., and Jörntell, H. (2013). Parallel fiber and climbing fiber responses in rat cerebellar cortical neurons in vivo. Front Sys Neurosci 7, 16.

Jirenhed, D., and Hesslow, G. (2011a). Learning stimulus intervals–adaptive timing of conditioned purkinje cell responses. Cerebellum 523–535.

Johansson, F., Carlsson, H.A.E., Rasmussen, A., Yeo, C.H., and Hesslow, G. (2015). Activation of a Temporal Memory in Purkinje Cells by the mGluR7 Receptor. Cell Reports 13, 1741–1746.

Johansson, F., Jirenhed, D.-A., Rasmussen, A., Zucca, R., and Hesslow, G. (2014). Memory trace and timing mechanism localized to cerebellar Purkinje cells. Proc Natl Acad Sci U S A 111, 14930–14934.

Jörntell, H., and Ekerot, C. (2006). Properties of somatosensory synaptic integration in cerebellar granule cells in vivo. J Neurosci 11786–11797.

Jörntell, H., and Ekerot, C.-F. (2003). Receptive field plasticity profoundly alters the cutaneous parallel fiber synaptic input to cerebellar interneurons in vivo. J Neurosci 23, 9620–9631.

Jörntell, H., Ekerot, C., Garwicz, M., and Luo, X.L. (2000). Functional organization of climbing fibre projection to the cerebellar anterior lobe of the rat. J Physiol 522 Pt 2, 297–309.

Kalinovsky, A., Boukhtouche, F., Blazeski, R., Bornmann, C., Suzuki, N., Mason, C.A., and Scheiffele, P. (2011). Development of axon-target specificity of ponto-cerebellar afferents. PLOS Biology e1001013.

Kandel, E.R., Schwartz, J.H., Jessel, T.M., Siegelbaum, S.A., and Hudspeth, A.J. (2013). Principles of neural science. New York: McGraw-Hill.

Kanner, L. (1943). Autistic disturbances of affective contact. Nervous Child 2, 217–250.

Katoh, A., Yoshida, T., Himeshima, Y., Mishina, M., and Hirano, T. (2005). Defective control and adaptation of reflex eye movements in mutant mice deficient in either the glutamate receptor delta2 subunit or Purkinje cells. Eur J Neurosci 21, 1315–1326.

Kawamura, K., and Onodera, S. (1984). Olivary projections from the pretectal region in the cat studied with horseradish peroxidase and tritiated amino acids axonal transport. Archives Ital Biol 122, 155–168.

Kehoe, E. (1988). A layered network model of associative learning: learning to learn and configuration. Psychol Rev 411–433.

Kehoe, E., and Joscelyne, A. (2005). Temporally specific extinction of conditioned responses in the rabbit (Oryctolagus cuniculus) nictitating membrane preparation. Behav Neurosci 1011–1022.

Kehoe, E., and White, N. (2002). Extinction revisited: similarities between extinction and reductions in US intensity in classical conditioning of the rabbit's nictitating membrane response. Animal Learn Behav 96–111.

Kehoe, E., Ludvig, E., Dudeney, J., Neufeld, J., and Sutton, R. (2008). Magnitude and timing of nictitating membrane movements during classical conditioning of the rabbit (Oryctolagus cuniculus). Behav Neurosci 471–476.

Kelly, R.M., and Strick, P.L. (2003). Cerebellar loops with motor cortex and prefrontal cortex of a nonhuman primate. J Neurosci 8432–8444.

Khosrovani, S., Van Der Giessen, R.S., De Zeeuw, C.I., and De Jeu, M.T.G. (2007). In vivo mouse inferior olive neurons exhibit heterogeneous subthreshold oscillations and spiking patterns. Proc Natl Acad Sci U S A 104, 15911–15916.

Kim, C., Oh, S., Lee, J., Chang, S., Kim, J., and Kim, S. (2012a). Lobule-specific membrane excitability of cerebellar Purkinje cells. J Physiol 273–288.

Kim, J., Krupa, D., and Thompson, R. (1998). Inhibitory cerebello-olivary projections and blocking effect in classical conditioning. Science 570–573.

Kim, Y., Wong, A., Power, J., Tadros, S., Klugmann, M., Moorhouse, A., Bertrand, P., and Housley, G. (2012b). Alternative splicing of the TRPC3 ion channel calmodulin/IP3 receptor-binding domain in the hindbrain enhances cation flux. J Neurosci 11414–11423.

Kimble, G. (1947). Conditioning as a function of the time between conditioned and unconditioned stimuli. J Exp Psychol 1–15.

Kishimoto, Y., Fujimichi, R., Araishi, K., Kawahara, S., Kano, M., Aiba, A., and Kirino, Y. (2002). mGluR1 in cerebellar Purkinje cells is required for normal association of temporally contiguous stimuli in classical conditioning. Eur J Neurosci 2416–2424.

Kishimoto, Y., Kawahara, S., Fujimichi, R., Mori, H., Mishina, M., and Kirino, Y. (2001). Impairment of eyeblink conditioning in GluRdelta2-mutant mice depends on the temporal overlap between conditioned and unconditioned stimuli. Eur J Neurosci 1515–1521.

Kistler, W.M., and Hemmen, J.L. van (1999). Delayed reverberation through time windows as a key to cerebellar function. Bio Cybernetics 81, 373–380.

Kistler, W.M., De Jeu, M.T.G., Elgersma, Y., Van Der Giessen, R.S., Hensbroek, R., Luo, C., Koekkoek, S.K.E., Hoogenraad, C.C., Hamers, F.P.T., Gueldenagel, M., et al. (2002). Analysis of Cx36 knockout does not support tenet that olivary gap junctions are required for complex spike synchronization and normal motor performance. Ann N Y Acad Sci 978, 391–404.

Kitai, S.T., McCrea, R.A., Preston, R.J., and Bishop, G.A. (1977). Electrophysiological and horseradish peroxidase studies of precerebellar afferents to the nucleus interpositus anterior. I. Climbing fiber system. Brain Res 122, 197–214.

Kitao, Y., Nakamura, Y., Kudo, M., Moriizumi, T., and Tokuno, H. (1989). The cerebral and cerebellar connections of pretecto-thalamic and pretecto-olivary neurons in the anterior pretectal nucleus of the cat. Brain Res 484, 304–313.

Kloth, A.D., Badura, A., Li, A., Cherskov, A., Connolly, S.G., Giovannucci, A., Bangash, M.A., Grasselli, G., Peñagarikano, O., Piochon, C., et al. (2015). Cerebellar associative sensory learning defects in five mouse autism models. eLife 4, e06085.

Knopfel, T., and Uusisaari, M. (2008). Modulation of excitation by metabotropic glutamate receptors. Results and problems in cell differentiation. 163–175.

Kobayashi, Y., and Hensch, T.K. (2013). Germline recombination by conditional gene targeting with Parvalbumin-Cre lines. Front Neural Circuits 168.

Kodama, T., Guerrero, S., Shin, M., Moghadam, S., Faulstich, M., and du Lac, S. (2012). Neuronal classification and marker gene identification via single-cell expression profiling of brainstem vestibular neurons subserving cerebellar learning. J Neurosci 32, 7819–7831.

Koekkoek, S.K.E., Hulscher, H.C., Dortland, B.R., Hensbroek, R.A., Elgersma, Y., Ruigrok, T.J.H., and Zeeuw, C.I.D. (2003). Cerebellar LTD and Learning-Dependent Timing of Conditioned Eyelid Responses. Science 301, 1736–1739.

Koekkoek, S.K.E., Ouden, W.L.D., Perry, G., Highstein, S.M., and Zeeuw, C.I.D. (2002). Monitoring Kinetic and Frequency-Domain Properties of Eyelid Responses in Mice With Magnetic Distance Measurement Technique. J Neurophys 88, 2124–2133.

Koekkoek, S.K.E., Yamaguchi, K., Milojkovic, B.A., Dortland, B.R., Ruigrok, T.J.H., Maex, R., De Graaf, W., Smit, A.E., VanderWerf, F., Bakker, C.E., et al. (2005). Deletion of FMR1 in Purkinje cells enhances parallel fiber LTD, enlarges spines, and attenuates cerebellar eyelid conditioning in Fragile X syndrome. Neuron 47, 339–352.

Koeneke, S., Lutz, K., Wüstenberg, T., and Jäncke, L. (2004). Long-term training affects cerebellar processing in skilled keyboard players: NeuroReport 15, 1279–1282.

Konnerth, A., Dreessen, J., and Augustine, G.J. (1992). Brief dendritic calcium signals initiate long-lasting synaptic depression in cerebellar Purkinje cells. Proc Natl Acad Sci U S A 7051–7055.

Koralek, A.C., Jin, X., Long Ii, J.D., Costa, R.M., and Carmena, J.M. (2012). Corticostriatal plasticity is necessary for learning intentional neuroprosthetic skills. Nature 483, 331–335.

Korn, H., and Axelrad, H. (1980). Electrical inhibition of Purkinje cells in the cerebellum of the rat. Proc Natl Acad Sci U S A 6244–6247.

Kosinski, R., Azizi, S., and Mihailoff, G. (1988). Convergence of cortico- and cuneopontine projections onto components of the pontocerebellar system in the rat: an anatomical and electrophysiological study. Exp Brain Res 541–556.

Kotani, S., Kawahara, S., and Kirino, Y. (2003). Purkinje cell activity during learning a new timing in classical eyeblink conditioning. Brain Res 994, 193–202.

Kotani, S., Kawahara, S., and Kirino, Y. (2006). Purkinje cell activity during classical eyeblink conditioning in decerebrate guinea pigs. Brain Res 1068, 70–81.

Krupa, D., and Thompson, R. (1995). Inactivation of the superior cerebellar peduncle blocks expression but not acquisition of the rabbit's classically conditioned eye-blink response. Proc Natl Acad Sci U S A 5097–5101.

Krupa, D., Thompson, J., and Thompson, R. (1993). Localization of a memory trace in the mammalian brain. Science 989–991.

Krupa, D., Weng, J., and Thompson, R. (1996). Inactivation of brainstem motor nuclei blocks expression but not acquisition of the rabbit's classically conditioned eyeblink response. Behav Neurosci 219–227.

Krupa, D.J., and Thompson, R.F. (1997). Reversible inactivation of the cerebellar interpositus nucleus completely prevents acquisition of the classically conditioned eye-blink response. Learn Mem 3, 545–556.

Lamarre, Y., and Mercier, L.A. (1971). Neurophysiological studies of harmaline-induced tremor in the cat. Canad J Phys Pharm 49, 1049–1058.

Lang, E.J. (2001). Organization of olivocerebellar activity in the absence of excitatory glutamatergic input. J Neurosci 21, 1663–1675.

Lang, E.J. (2002). GABAergic and glutamatergic modulation of spontaneous and motor-cortex-evoked complex spike activity. J Neurophys 87, 1993–2008.

Lang, E.J. (2003). Excitatory afferent modulation of complex spike synchrony. Cerebellum 2, 165–170.

Lang, E.J., Blenkinsop, &, and a., T. (2011). Control of cerebellar nuclear cells: A direct role for complex spikes? Cerebellum 10, 694–701.

Lang, E.J., Sugihara, I., and Llinás, R. (1996). GABAergic modulation of complex spike activity by the cerebellar nucleoolivary pathway in rat. J Neurophys 76, 255–275.

Lang, E.J., Sugihara, I., and Llinás, R. (2006). Olivocerebellar modulation of motor cortex ability to generate vibrissal movements in rat. J Physiol 571, 101–120.

Lang, E.J., Sugihara, I., Welsh, J.P., and Llinás, R. (1999). Patterns of spontaneous purkinje cell complex spike activity in the awake rat. J Neurosci 19, 2728–2739.

Lavond, D., and Steinmetz, J. (1989). Acquisition of classical conditioning without cerebellar cortex. Behav Brain Res 113–164.

Lavond, D., Steinmetz, J., Yokaitis, M., and Thompson, R. (1987). Reacquisition of classical conditioning after removal of cerebellar cortex. Exp Brain Res 569–593.

Leal-Campanario, R., Fairen, A., Delgado-Garcia, J., and Gruart, A. (2007). Electrical stimulation of the rostral medial prefrontal cortex in rabbits inhibits the expression of conditioned eyelid responses but not their acquisition. Proc Natl Acad Sci U S A 11459–11464.

Leblond, C.S., Heinrich, J., Delorme, R., Proepper, C., Betancur, C., Huguet, G., Konyukh, M., Chaste, P., Ey, E., Rastam, M., et al. (2012). Genetic and functional analyses of SHANK2 mutations suggest a multiple hit model of autism spectrum disorders. PLOS Gen 8, e1002521.

Leblond, C.S., Nava, C., Polge, A., Gauthier, J., Huguet, G., Lumbroso, S., Giuliano, F., Stordeur, C., Depienne, C., Mouzat, K., et al. (2014). Meta-analysis of SHANK Mutations in Autism Spectrum Disorders: A Gradient of Severity in Cognitive Impairments. PLOS Gen 10, e1004580.

Leclerc, N., Dore, L., Parent, A., and Hawkes, R. (1990). The compartmentalization of the monkey and rat cerebellar cortex: zebrin I and cytochrome oxidase. Brain Res 70–78.

Lee, T., and Kim, J. (2004). Differential effects of cerebellar, amygdalar, and hippocampal lesions on classical eyeblink conditioning in rats. J Neurosci 3242–3250.

Leergaard, T., and Bjaalie, J. (2007). Topography of the complete corticopontine projection: From experiments to principal Maps. Front Neurosci 211–223.

Lefler, Y., Torben-Nielsen, B., and Yarom, Y. (2013). Oscillatory activity, phase differences, and phase resetting in the inferior olivary nucleus. Front Sys Neurosci 7, 22.

Lefler, Y., Yarom, Y., and Uusisaari, M.Y. (2014). Cerebellar Inhibitory Input to the Inferior Olive Decreases Electrical Coupling and Blocks Subthreshold Oscillations. Neuron 81, 1389–1400.

Legg, C., Mercier, B., and Glickstein, M. (1989). Corticopontine projection in the rat: the distribution of labelled cortical cells after large injections of horseradish peroxidase in the pontine nuclei. J Comp Neurol 427–441.

Leonard, D., and Theios, J. (1967). Effect of CS-US interval shift on classical conditioning of the nictitating membrane in the rabbit. J Comp Physiol Psychol 355–358.

Lev-Ram, V., Wong, S.T., Storm, D.R., and Tsien, R.Y. (2002). A new form of cerebellar long-term potentiation is postsynaptic and depends on nitric oxide but not cAMP. Proc Natl Acad Sci U S A 8389–8393.

Levisohn, L., Cronin-Golomb, A., and Schmahmann, J.D. (2000). Neuropsychological consequences of cerebellar tumour resection in children: cerebellar cognitive affective syndrome in a paediatric population. Brain 123 (Pt 5), 1041–1050.

Lewis, J., Lo Turco, J., and Solomon, P. (1987). Lesions of the middle cerebellar peduncle disrupt acquisition and retention of the rabbit's classically conditioned nictitating membrane response. Behav Neurosci 151–157.

Leznik, E., and Llinás, R. (2005). Role of gap junctions in synchronized neuronal oscillations in the inferior olive. J Neurophys 94, 2447–2456.

Linden, D., and Connor, J. (1991). Participation of postsynaptic PKC in cerebellar long-term depression in culture. Science 1656–1659.

Linden, D.J., Dickinson, M.H., Smeyne, M., and Connor, J.A. (1991). A long-term depression of AMPA currents in cultured cerebellar Purkinje neurons. Neuron 7, 81–89.

Lisberger, S. (1988). The neural basis for motor learning in the vestibulo-ocular reflex in monkeys. Trends Neurosci 147–152.

Lisberger, S. (2009). Internal models of eye movement in the floccular complex of the monkey cerebellum. Neuroscience 763–776.

Llinás, R., and Mühlethaler, M. (1988). Electrophysiology of guinea-pig cerebellar nuclear cells in the in vitro brain stem-cerebellar preparation. J Physiol 404, 241–258.

Llinás, R., and Sasaki, K. (1989). The Functional Organization of the Olivo-Cerebellar System as Examined by Multiple Purkinje Cell Recordings. Eur J Neurosci 1, 587–602.

Llinás, R., and Welsh, J. (1993). On the cerebellum and motor learning. Curr Op Neurobiol 958–965.

Llinás, R., and Yarom, Y. (1981a). Electrophysiology of mammalian inferior olivary neurones in vitro. Different types of voltage-dependent ionic conductances. J Physiol 315, 549–567.

Llinás, R., and Yarom, Y. (1981b). Properties and distribution of ionic conductances generating electroresponsiveness of mammalian inferior olivary neurones in vitro. J Physiol 315, 569–584.

Llinás, R., and Yarom, Y. (1986). Oscillatory properties of guinea-pig inferior olivary neurones and their pharmacological modulation: an in vitro study. J Physiol 376, 163–182.

Llinás, R., Baker, R., and Sotelo, C. (1974). Electrotonic coupling between neurons in cat inferior olive. J Neurophys 37, 560–571.

Llinás, R.R. (2009). Inferior olive oscillation as the temporal basis for motricity and oscillatory reset as the basis for motor error correction. Neuroscience 162, 797–804.

Llinás, R.R. (2011). Cerebellar motor learning versus cerebellar motor timing: the climbing fibre story. J Physiol 589, 3423–3432.

Loewenstein, Y., Mahon, S., Chadderton, P., Kitamura, K., Sompolinsky, H., Yarom, Y., and Häusser, M. (2005). Bistability of cerebellar Purkinje cells modulated by sensory stimulation. Nat Neurosci 202–211.

Long, M.A., Deans, M.R., Paul, D.L., and Connors, B.W. (2002). Rhythmicity without synchrony in the electrically uncoupled inferior olive. J Neurosci 22, 10898–10905.

Longley, M., and Yeo, C.H. (2014). Distribution of Neural Plasticity in Cerebellum-Dependent Motor Learning. In Prog Brain Res, (Elsevier), pp. 79–101.

Lu, H., Yang, B., and Jaeger, D. (2016). Cerebellar Nuclei Neurons Show Only Small Excitatory Responses to Optogenetic Olivary Stimulation in Transgenic Mice: In Vivo and In Vitro Studies. Front Neural Circuits 10.

Luque, N.R., Garrido, J.A., Carrillo, R.R., Tolu, S., and Ros, E. (2011). Adaptive cerebellar spiking model embedded in the control loop: context switching and robustness against noise. J Neurosys 21, 385–401.

Ly, R., Bouvier, G., Schonewille, M., Arabo, A., Rondi-Reig, L., Léna, C., Casado, M., De Zeeuw, C.I., and Feltz, A. (2013). T-type channel blockade impairs long-term potentiation at the parallel fiber-Purkinje cell synapse and cerebellar learning. Proc Natl Acad Sci U S A 20302–20307.

Marko, M.K., Crocetti, D., Hulst, T., Donchin, O., Shadmehr, R., and Mostofsky, S.H. (2015). Behavioural and neural basis of anomalous motor learning in children with autism. Brain 138, 784–797.

Markram, H., Lubke, J., Frotscher, M., and Sakmann, B. (1997). Regulation of synaptic efficacy by coincidence of postsynaptic APs and EPSPs. Science 213–215.

Marr, D. (1969). A theory of cerebellar cortex. J Physiol 202, 437–470.

Marshall, S.P., van der Giessen, R.S., de Zeeuw, C.I., and Lang, E.J. (2007). Altered olivocerebellar activity patterns in the connexin36 knockout mouse. Cerebellum 6, 287–299.

Mateos, J., Osorio, A., Azkue, J., Benitez, R., Elezgarai, I., Bilbao, A., Diez, J., Puente, N., Kuhn, R., Knopfel, T., et al. (2001). Parasagittal compartmentalization of the metabotropic glutamate receptor mGluR1b in the cerebellar cortex. Eur J Anat 15–21.

Mathews, P., Lee, K., Peng, Z., Houser, C., and Otis, T. (2012). Effects of climbing fiber driven inhibition on Purkinje neuron spiking. J Neurosci 17988–17997.

Mathews, P.J., Lee, K.H., Peng, Z., Houser, C.R., and Otis, T.S. (2012). Effects of Climbing Fiber Driven Inhibition on Purkinje Neuron Spiking. J Neurosci 32, 17988–17997.

Mathy, A., Ho, S.S.N., Davie, J.T., Duguid, I.C., Clark, B.A., and Häusser, M. (2009). Encoding of Oscillations by Axonal Bursts in Inferior Olive Neurons. Neuron 62, 388–399.

Mauk, M., and Buonomano, D. (2004). The neural basis of temporal processing. Ann Rev Neurosci 307–340.

Mauk, M., and Ruiz, B. (1992). Learning-dependent timing of Pavlovian eyelid responses: differential conditioning using multiple interstimulus intervals. Behav Neurosci 666–681.

Mauk, M., Garcia, K., Medina, J., and Steele, P. (1998). Does cerebellar LTD mediate motor learning? Toward a resolution without a smoking gun. Neuron 359–362.

Mauk, M., Steinmetz, J., and Thompson, R. (1986). Classical conditioning using stimulation of the inferior olive as the unconditioned stimulus. Proc Natl Acad Sci U S A 5349–5353.

McAllister, W. (1953). Eyelid conditioning as a function of the CS-US interval. J Exp Psychol 417–422.

McCormick, D., and Thompson, R. (1984a). Cerebellum: essential involvement in the classically conditioned eyelid response. Science 296–299.

McCormick, D., Lavond, D., Clark, G., Kettner, R., Rising, C., and Thompson, R. (1981). The engram found? Role of the cerebellum in classical conditioning of nictitating membrane and eyelid responses. Bull Psychonom Soc 103–105.

McCormick, D., Steinmetz, J., and Thompson, R. (1985). Lesions of the inferior olivary complex cause extinction of the classically conditioned eyeblink response. Brain Res 120–130.

McCormick, D.A., and Thompson, R.F. (1984b). Neuronal responses of the rabbit cerebellum during acquisition and performance of a classically conditioned nictitating membrane-eyelid response. J Neurosci 4, 2811–2822.

McCormick, D.A., Clark, G.A., Lavond, D.G., and Thompson, R.F. (1982). Initial localization of the memory trace for a basic form of learning. Proc Natl Acad Sci U S A 79, 2731–2735.

McCormick, D.A., McGinley, M.J., and Salkoff, D.B. (2014). Brain state dependent activity in the cortex and thalamus. Curr Op Neurobiol 133–140.

McCrea, R.A., Bishop, G.A., and Kitai, S.T. (1978). Morphological and electrophysiological characteristics of projection neurons in the nucleus interpositus of the cat cerebellum. J Compar Neurol 181, 397–419.

McElligott, J.G., Beeton, P., and Polk, J. (1998). Effect of Cerebellar Inactivation by Lidocaine Microdialysis on the Vestibuloocular Reflex in Goldfish. J Neurophys 79, 1286–1294.

Medina, J. (2000). Mechanisms of cerebellar learning suggested by eyelid conditioning. Curr Op Neurobiol 10, 717–724.

Medina, J., Garcia, K., and Mauk, M. (2001). A mechanism for savings in the cerebellum. J Neurosci 4081–4089.

Medina, J.F., and Lisberger, S.G. (2007). Variation, signal, and noise in cerebellar sensory-motor processing for smooth-pursuit eye movements. J Neurosci 6832–6842.

Medina, J.F., Garcia, K.S., Nores, W.L., Taylor, N.M., and Mauk, M.D. (2000). Timing mechanisms in the cerebellum: testing predictions of a large-scale computer simulation. J Neurosci 5516–5525.

Medina, J.F., Nores, W.L., and Mauk, M.D. (2002). Inhibition of climbing fibres is a signal for the extinction of conditioned eyelid responses. Nature 416, 330–333.

Mei, Y., Monteiro, P., Zhou, Y., Kim, J.-A., Gao, X., Fu, Z., and Feng, G. (2016). Adult restoration of Shank3 expression rescues selective autistic-like phenotypes. Nature 530, 481–484.

Memari, A.H., Ghanouni, P., Shayestehfar, M., and Ghaheri, B. (2014). Postural control impairments in individuals with autism spectrum disorder: a critical review of current literature. Asian J Sports Med 5, e22963.

Menashe, I., Grange, P., Larsen, E.C., Banerjee-Basu, S., and Mitra, P.P. (2013). Co-expression profiling of autism genes in the mouse brain. PLoS Comput Biol 9, e1003128.

Mihailoff, G., Kosinski, R., Azizi, S., and Border, B. (1989). Survey of noncortical afferent projections to the basilar pontine nuclei: a retrograde tracing study in the rat. J Comp Neurol 617–643.

Mihailoff, G., Lee, H., Watt, C., and Yates, R. (1985). Projections to the basilar pontine nuclei from face sensory and motor regions of the cerebral cortex in the rat. J Comp Neurol 251–263.

Mittmann, W., Koch, U., and Häusser, M. (2005). Feed-forward inhibition shapes the spike output of cerebellar Purkinje cells. J Physiol 369–378.

Molineux, M.L., McRory, J.E., McKay, B.E., Hamid, J., Mehaffey, W.H., Rehak, R., Snutch, T.P., Zamponi, G.W., and Turner, R.W. (2006). Specific T-type calcium channel isoforms are associated with distinct burst phenotypes in deep cerebellar nuclear neurons. Proc Natl Acad Sci U S A 103, 5555–5560.

Molineux, M.L., Mehaffey, W.H., Tadayonnejad, R., Anderson, D., Tennent, A.F., and Turner, R.W. (2008). Ionic Factors Governing Rebound Burst Phenotype in Rat Deep Cerebellar Neurons. J Neurophys 100, 2684–2701.

Montarolo, P., Palestini, M., and Strata, P. (1982). The inhibitory effect of the olivocerebellar input on the cerebellar Purkinje cells in the rat. J Physiol 187–202.

Morcuende, S., Delgado-Garcia, J.-M., and Ugolini, G. (2002). Neuronal Premotor Networks Involved in Eyelid Responses: Retrograde Transneuronal Tracing with Rabies Virus from the Orbicularis Oculi Muscle in the Rat. J Neurosci 22, 8808–8818.

Mosconi, M.W., Wang, Z., Schmitt, L.M., Tsai, P., and Sweeney, J.A. (2015). The role of cerebellar circuitry alterations in the pathophysiology of autism spectrum disorders. Front Neurosci 9, 296.

Moser, E.I., Kropff, E., and Moser, M.B. (2008). Place cells, grid cells, and the brain's spatial representation system. Ann Rev Neurosci 69–89.

Mostofi, A., Holtzman, T., Grout, A.S., Yeo, C.H., and Edgley, S.A. (2010). Electrophysiological Localization of Eyeblink-Related Microzones in Rabbit Cerebellar Cortex. J Neurosci 30, 8920–8934.

Mostofsky, S.H., Goldberg, M.C., Landa, R.J., and Denckla, M.B. (2000). Evidence for a deficit in procedural learning in children and adolescents with autism: implications for cerebellar contribution. J Int Neuropsych Soc 6, 752–759.

Mower, G., Gibson, A., Robinson, F., Stein, J., and Glickstein, M. (1980). Visual pontocerebellar projections in the cat. J Neurophysiol 355–366.

Mukamel, E.A., Nimmerjahn, A., and Schnitzer, M.J. (2009). Automated analysis of cellular signals from large-scale calcium imaging data. Neuron 747–760.

Nagao, S. (1983). Effects of vestibulocerebellar lesions upon dynamic characteristics and adaptation of vestibulo-ocular and optokinetic responses in pigmented rabbits. Exp Brain Res 53, 36–46.

Najac, M., and Raman, I.M. (2015). Integration of Purkinje Cell Inhibition by Cerebellar Nucleo-Olivary Neurons. J Neurosci 35, 544–549.

Najafi, F., and Medina, J. (2013). Beyond ''all-or-nothing'' climbing fibers: graded representation of teaching signals in Purkinje cells. Front Neural Circuits 7.

Nelson, A., Gittis, A., and du Lac, S. (2005). Decreases in CaMKII activity trigger persistent potentiation of intrinsic excitability in spontaneously firing vestibular nucleus neurons. Neuron 623–631.

Nelson, C., and Glitsch, M. (2012). Lack of kinase regulation of canonical transient receptor potential 3 (TRPC3) channel-dependent currents in cerebellar Purkinje cells. J Biol Chem 6326–6335.

Neufeld, M., and Mintz, M. (2001). Involvement of the amygdala in classical conditioning of eyeblink response in the rat. Brain Res 112–117.

Ng, K., and Freeman, J. (2012). Developmental changes in medial auditory thalamic contributions to associative motor learning. J Neurosci 6841–6850.

Ng, K., and Freeman, J. (2013). Amygdala inactivation impairs eyeblink conditioning in developing rats. Dev Pyschobiol 56, 999–1007.

Nguyen-Vu, T., Kimpo, R., Rinaldi, J., Kohli, A., Zeng, H., Deisseroth, K., and Raymond, J. (2013). Cerebellar Purkinje cell activity drives motor learning. Nat Neurosci 1734–1736.

Nicholson, D., and Freeman, J. (2002). Neuronal correlates of conditioned inhibition of the eyeblink response in the anterior interpositus nucleus. Behav Neurosci 22–36.

Nicolelis, M.A., and Fanselow, E.E. (2002). Thalamocortical optimization of tactile processing according to behavioral state. Nat Neurosci 517–523.

Nordholm, A., Thompson, J., Dersarkissian, C., and Thompson, R. (1993). Lidocaine infusion in a critical region of cerebellum completely prevents learning of the conditioned eyeblink response. Behav Neurosci 882–886.

Norman, R., Buchwald, J., and Villablanca, J. (1977). Classical conditioning with auditory discrimination of the eye blink in decerebrate cats. Science 551–553.

Norman, R., Villablanca, J., Brown, K., Schwafel, J., and Buchwald, J. (1974). Classical eyeblink conditioning in the bilaterally hemispherectomized cat. Exp Neurol 363–380.

Nowak, A., Marshall-Goodell, B., Kehoe, E., and Gormezano, I. (1997). Elicitation, modification, and conditioning of the rabbit nictitating membrane response by electrical stimulation in the spinal trigeminal nucleus, inferior olive, interpositus nucleus, and red nucleus. Behav Neurosci 1041–1055.

Oakley, D., and Russell, I. (1972). Neocortical lesions and Pavlovian conditioning. Physiol Behav 915–926.

Oakley, D., and Russell, I. (1975). Role of cortex in Pavlovian discrimination learning. Physiol Behav 315–321.

Oakley, D., and Russell, I. (1976). Subcortical nature of Pavlovian differentiation in the rabbit. Physiol Behav 947–954.

Oakley, D., and Russell, I. (1977). Subcortical storage of Pavlovian conditioning in the rabbit. Physiol Behav 931–937.

Oberdick, J., Smeyne, R.J., Mann, J.R., Zackson, S., and Morgan, J.I. (1990). A promoter that drives transgene expression in cerebellar Purkinje and retinal bipolar neurons. Science 248, 223–226.

Ohmae, S., and Medina, J.F. (2015). Climbing fibers encode a temporal-difference prediction error during cerebellar learning in mice. Nat Neurosci 18, 1798–1803.

Ohyama, T., Nores, W., and Mauk, M. (2003). Stimulus generalization of conditioned eyelid responses produced without cerebellar cortex: implications for plasticity in the cerebellar nuclei. Learn Mem 346–354.

Ohyama, T., Nores, W., Medina, J., Riusech, F., and Mauk, M. (2006). Learning-induced plasticity in deep cerebellar nucleus. J Neurosci 12656–12663.

Ohyama, T., Nores, W.L., Medina, J.F., Riusech, F.A., and Mauk, M.D. (2006). Learning-Induced Plasticity in Deep Cerebellar Nucleus. J Neurosci 26, 12656–12663.

Onodera, S. (1984). Olivary projections from the mesodiencephalic structures in the cat studied by means of axonal transport of horseradish peroxidase and tritiated amino acids. J Compar Neurol 227, 37–49.

Oristaglio, J., Hyman West, S., Ghaffari, M., Lech, M.S., Verma, B.R., Harvey, J.A., Welsh, J.P., and Malone, R.P. (2013). Children with autism spectrum disorders show abnormal conditioned response timing on delay, but not trace, eyeblink conditioning. Neuroscience 248, 708–718.

Oswald, B., Knuckley, B., Mahan, K., Sanders, C., and Powell, D.A. (2006). Prefrontal control of trace versus delay eyeblink conditioning: role of the unconditioned stimulus in rabbits (Oryctolagus cuniculus). Behav Neurosci 120, 1033–1042.

Ozden, I., Dombeck, D.A., Hoogland, T.M., Tank, D.W., and Wang, S.S. (2012). Widespread state-dependent shifts in cerebellar activity in locomoting mice. PLOS ONE 7.

Ozden, I., Sullivan, M.R., Lee, H.M., and Wang, S.S.-H. (2009). Reliable Coding Emerges from Coactivation of Climbing Fibers in Microbands of Cerebellar Purkinje Neurons. J Neurosci 29, 10463–10473.

Palay, S.L., and Chan-Palay, V. (1974). Cerebellar cortex: cytology and organization (New York: Springer Berlin Heidelberg).

Palkovits, M., Mezey, E., Hamori, J., and Szentagothai, J. (1977). Quantitative histological analysis of the cerebellar nuclei in the cat. I. Numerical data on cells and on synapses. Exp Brain Res 189–209.

Parenti, R., Zappala, A., Serapide, M., Panto, M., and Cicirata, F. (2002). Projections of the basilar pontine nuclei and nucleus reticularis tegmenti pontis to the cerebellar nuclei of the rat. J Comp Neurol 115–127.

Parker, K., Zbarska, S., Carrel, A., and Bracha, V. (2009). Blocking GABAA neurotransmission in the interposed nuclei: effects on conditioned and unconditioned eyeblinks. Brain Res 25–37.

Passey, G. (1948). The influence of intensity of unconditioned stimulus upon acquisition of a conditioned response. J Exp Psychol 420–428.

Pavlov, I.P. (1927). Conditioned reflexes: an investigation of the physiological activity of the cerebral cortex. (Oxford, England: Oxford Univ. Press).

Pellegrini, J., Horn, A., and Evinger, C. (1995). The trigeminally evoked blink reflex. I. Neuronal circuits. Exp Brain Res 166–180.

Pennartz, C.M., Berke, J.D., Graybiel, A.M., Ito, R., Lansink, C.S., van der Meer, M., Redish, A.D., Smith, K.S., and Voorn, P. (2009). Corticostriatal Interactions during Learning, Memory Processing, and Decision Making. J Neurosci 12831–12838.

Perkon, I., Kosir, A., Itskov, P.M., Tasic, J., and Diamond, M.E. (2011). Unsupervised quantification of whisking and head movement in freely moving rodents. J Neurophysiol 1950–1962.

Perrett, S., Ruiz, B., and Mauk, M. (1993). Cerebellar cortex lesions disrupt learning-dependent timing of conditioned eyelid responses. J Neurosci 1708–1718.

Perrone, J.A., and Krauzlis, R.J. (2008). Vector subtraction using visual and extraretinal motion signals: a new look at efference copy and corollary discharge theories. J Vision 8.

Person, A.L., and Raman, I.M. (2010). Deactivation of L-type Ca Current by Inhibition Controls LTP at Excitatory Synapses in the Cerebellar Nuclei. Neuron 66, 550–559.

Person, A.L., and Raman, I.M. (2012a). Synchrony and neural coding in cerebellar circuits. Front Neural Circuits 6, 97.

Person, A.L., and Raman, I.M. (2012b). Purkinje neuron synchrony elicits time-locked spiking in the cerebellar nuclei. Nature 481, 502–505.

Peter, S., ten Brinke, M.M., Stedehouder, J., Reinelt, C.M., Wu, B., Zhou, H., Zhou, K., Boele, H.-J., Kushner, S.A., Lee, M.G., et al. (2016). Dysfunctional cerebellar Purkinje cells contribute to autism-like behaviour in Shank2-deficient mice. Nat Comm 7, 12627.

Petersen, C.C.H. (2014). Cortical control of whisker movement. Ann Rev Neurosci 183–203.

Petreanu, L., Gutnisky, D.A., Huber, D., Xu, N.L., O'Connor, D.H., Tian, L., Looger, L., and Svoboda, K. (2012). Activity in motor-sensory projections reveals distributed coding in somatosensation. Nature 299–303.

Pijpers, A., Apps, R., Pardoe, J., Voogd, J., and Ruigrok, T.J. (2006). Precise spatial relationships between mossy fibers and climbing fibers in rat cerebellar cortical zones. J Neurosci 12067–12080.

Pijpers, A., Voogd, J., and Ruigrok, T.J.H. (2005). Topography of olivo-cortico-nuclear modules in the intermediate cerebellum of the rat. J Compar Neurol 492, 193–213.

Piochon, C., Kloth, A.D., Grasselli, G., Titley, H.K., Nakayama, H., Hashimoto, K., Wan, V., Simmons, D.H., Eissa, T., Nakatani, J., et al. (2014). Cerebellar plasticity and motor learning deficits in a copy-number variation mouse model of autism. Nat Comm 5, 5586.

Piochon, C., Kruskal, P., Maclean, J., and Hansel, C. (2012). Non-Hebbian spike-timing-dependent plasticity in cerebellar circuits. Front Neural Circuits 6.

Placantonakis, D.G., Bukovsky, A.A., Aicher, S.A., Kiem, H.-P., and Welsh, J.P. (2006). Continuous electrical oscillations emerge from a coupled network: a study of the inferior olive using lentiviral knockdown of connexin36. J Neurosci 26, 5008–5016.

Plakke, B., Freeman, J., and Poremba, A. (2009). Metabolic mapping of rat forebrain and midbrain during delay and trace eyeblink conditioning. Neurobiol Learn Mem 335–344.

Popa, L.S., Hewitt, A.L., and Ebner, T.J. (2012). Predictive and Feedback Performance Errors Are Signaled in the Simple Spike Discharge of Individual Purkinje Cells. J Neurosci 32, 15345–15358.

Pouille, F., Watkinson, O., Scanziani, M., and Trevelyan, A. (2013). The contribution of synaptic location to inhibitory gain control in pyramidal cells. Physiol Rep e00067.

Prescott, T.J., Diamond, M.E., and Wing, A.M. (2011). Active touch sensing. Philos Trans R Soc Lond B Biol Sci 2989–2995.

Prokasy, W., and Papsdorf, J. (1965). Effects of increasing the interstimulus interval during classical conditioning of the albino rabbit. J Comp Physiol Psychol 249–252.

Prokasy, W., Ebel, H., and Thompson, D. (1963). Response shaping at long interstimulus intervals in classical eyelid conditioning. J Exp Psychol 138–141.

Pugh, J.R., and Raman, I.M. (2008). Mechanisms of Potentiation of Mossy Fiber EPSCs in the Cerebellar Nuclei by Coincident Synaptic Excitation and Inhibition. J Neurosci 28, 10549–10560.

Rahmati, N., Owens, C.B., Bosman, L.W.J., Spanke, J.K., Lindeman, S., Gong, W., Potters, J.-W., Romano, V., Voges, K., Moscato, L., et al. (2014). Cerebellar Potentiation and Learning a Whisker-Based Object Localization Task with a Time Response Window. J Neurosci 34, 1949–1962.

309

Ramakrishnan, K.B., Voges, K., De Propris, L., De Zeeuw, C.I., and D'Angelo, E. (2016). Tactile stimulation evokes long-lasting potentiation of Purkinje cell discharge in vivo. Front Cell Neurosci 10.

Raman, I., and Bean, B. (1997). Resurgent sodium current and action potential formation in dissociated cerebellar Purkinje neurons. J Neurosci 4517–4526.

Raman, I., and Bean, B. (1999). Ionic currents underlying spontaneous action potentials in isolated cerebellar Purkinje neurons. J Neurosci 1663–1674.

Rancz, E.A., Ishikawa, T., Duguid, I., Chadderton, P., Mahon, S., and Häusser, M. (2007). High-fidelity transmission of sensory information by single cerebellar mossy fibre boutons. Nature 1245–1248.

Rasmussen, A., and Hesslow, G. (2014). Feedback control of learning by the cerebello-olivary pathway. Prog Brain Res 103–119.

Rasmussen, A., Jirenhed, D.-A., and Hesslow, G. (2008). Simple and Complex Spike Firing Patterns in Purkinje Cells During Classical Conditioning. Cerebellum 7, 563.

Rasmussen, A., Jirenhed, D.-A., Wetmore, D.Z., and Hesslow, G. (2014). Changes in complex spike activity during classical conditioning. Front Neural Circuits 8.

Rasmussen, A., Jirenhed, D.-A., Zucca, R., Johansson, F., Svensson, P., and Hesslow, G. (2013). Number of Spikes in Climbing Fibers Determines the Direction of Cerebellar Learning. J Neurosci 33, 13436–13440.

Ravizza, S.M. (2005). Cerebellar damage produces selective deficits in verbal working memory. Brain 129, 306–320.

Reato, D., Tara, E., and Khodakhah, K. (2016). Deep Cerebellar Nuclei Rebound Firing In Vivo. In The Neuronal Codes of the Cerebellum, (Elsevier), pp. 27–51.

Requarth, T., and Sawtell, N.B. (2014). Plastic Corollary Discharge Predicts Sensory Consequences of Movements in a Cerebellum-Like Circuit. Neuron 82, 896–907.

Ritzau-Jost, A., Delvendahl, I., Rings, A., Byczkowicz, N., Harada, H., Shigemoto, R., Hirrlinger, J., Eilers, J., and Hallermann, S. (2014). Ultrafast action potentials mediate kilohertz signaling at a central synapse. Neuron 152–163.

Riva, D., and Giorgi, C. (2000). The neurodevelopmental price of survival in children with malignant brain tumours. Child's Nervous System 16, 751–754.

Rizley, R.C., and Rescorla, R.A. (1972). Associations in second-order conditioning and sensory preconditioning. J Compar Phys Psych 81, 1–11.

Robinson, D.A. (1976). Adaptive gain control of vestibuloocular reflex by the cerebellum. J Neurophys 39, 954–969.

Rochefort, C., Arabo, A., André, M., Poucet, B., Save, E., and Rondi-Reig, L. (2011). Cerebellum shapes hippocampal spatial code. Science 334, 385–389.

Rosenfield, M., and Moore, J. (1983). Red nucleus lesions disrupt the classically conditioned nictitating membrane response in rabbits. Behav Brain Res 393–398.

Rosenfield, M., and Moore, J. (1985). Red nucleus lesions impair acquisition of the classically conditioned nictitating membrane response but not eye-to-eye savings or unconditioned response amplitude. Behav Brain Res 77–81.

Rosenfield, M., and Moore, J. (1995). Connections to cerebellar cortex (Larsell's HVI) in the rabbit: a WGA-HRP study with implications for classical eyeblink conditioning. Behav Neurosci 1106–1118.

Ruediger, S., Vittori, C., Bednarek, E., Genoud, C., Strata, P., Sacchetti, B., and Caroni, P. (2011). Learning-related feedforward inhibitory connectivity growth required for memory precision. Nature 514–518.

Ruigrok, T. (2011). Ins and outs of cerebellar modules. Cerebellum 464–474.

Ruigrok, T., and Voogd, J. (1990). Cerebellar nucleo-olivary projections in the rat: an anterograde tracing study with Phaseolus vulgaris-leucoagglutinin (PHA-L). J Comp Neurol 315–333.

Ruigrok, T., and Voogd, J. (2000). Organization of projections from the inferior olive to the cerebellar nuclei in the rat. J Comp Neurol 209–228.

Ruigrok, T.J., and Teune, T.M. (2014). Collateralization of cerebellar output to functionally distinct brainstem areas. A retrograde, non-fluorescent tracing study in the rat. Front Sys Neurosci 23.

Ruigrok, T.J., and Voogd, J. (1995). Cerebellar influence on olivary excitability in the cat. Eur J Neurosci 7, 679–693.

Ruigrok, T.J.H., Hensbroek, R.A., and Simpson, J.I. (2011). Spontaneous Activity Signatures of Morphologically Identified Interneurons in the Vestibulocerebellum. J Neurosci 31, 712–724.

Ruigrok, T.J.H., Teune, T.M., van der Burg, J., and Sabel-Goedknegt, H. (1995). A retrograde double-labeling technique for light microscopy. A combination of axonal transport of cholera toxin B-subunit and a gold-lectin conjugate. J Neurosci Methods 127–138.

Rutherford, J.G., Anderson, W.A., and Gwyn, D.G. (1984). A reevaluation of midbrain and diencephalic projections to the inferior olive in rat with particular reference to the rubro-olivary pathway. J Compar Neurol 229, 285–300.

Rylkova, D., Crank, A.R., and Linden, D.J. (2015). Chronic In Vivo Imaging of Ponto-Cerebellar Mossy Fibers Reveals Morphological Stability during Whisker Sensory Manipulation in the Adult Rat. eNeuro 2.

Sala, C., Vicidomini, C., Bigi, I., Mossa, A., and Verpelli, C. (2015). Shank synaptic scaffold proteins: keys to understanding the pathogenesis of autism and other synaptic disorders. J Neurochem 135, 849–858.

Salafia, W., Martino, L., Cloutman, K., and Romano, A. (1979). Unconditional-stimulus locus and interstimulus-interval shift in rabbit (Oryctolagus cuniculus) nictitating membrane conditioning. Pavlovian J Bio Sci 64–71.

Sanchez-Campusano, R., Gruart, A., and Delgado-Garcia, J. (2011). Dynamic changes in the cerebellar-interpositus/red-nucleus-motoneuron pathway during motor learning. Cerebellum 702–710.

Sanchez-Campusano, R., Gruart, A., and Delgado-Garcia, J. (2011). Timing and causality in the generation of learned eyelid responses. Front Integr Neurosci 5.

Sanchez-Campusano, R., Gruart, A., and Delgado-Garcia, J.M. (2007). The Cerebellar Interpositus Nucleus and the Dynamic Control of Learned Motor Responses. J Neurosci 27, 6620–6632.

Sangrey, T., and Jaeger, D. (2010). Analysis of distinct short and prolonged components in rebound spiking of deep cerebellar nucleus neurons. Eur J Neurosci 32, 1646–1657.

Sarna, J., Marzban, H., Watanabe, M., and Hawkes, R. (2006). Complementary stripes of phospholipase Cbeta3 and Cbeta4 expression by Purkinje cell subsets in the mouse cerebellum. J Comp Neurol 303–313.

Sasaki, K., Bower, J.M., and Llinás, R. (1989). Multiple Purkinje Cell Recording in Rodent Cerebellar Cortex. Eur J Neurosci 1, 572–586.

Sato, D., Lionel, A.C., Leblond, C.S., Prasad, A., Pinto, D., Walker, S., O'Connor, I., Russell, C., Drmic, I.E., Hamdan, F.F., et al. (2012). SHANK1 Deletions in Males with Autism Spectrum Disorder. J Human Gen 90, 879–887.

Saviane, C., and Silver, R.A. (2006). Fast vesicle reloading and a large pool sustain high bandwidth transmission at a central synapse. Nature 983–987.

Schilling, K., Oberdick, J., Rossi, F., and Baader, S.L. (2008). Besides Purkinje cells and granule neurons: an appraisal of the cell biology of the interneurons of the cerebellar cortex. Histochem Cell Biol 130, 601–615.

Schmahmann, J.D. (1982). The role of the cerebellum in cognition and emotion: personal reflections since 1982 on the dysmetria of thought hypothesis, and its historical evolution from theory to therapy. Neuropsych Rev 20, 236–260.

Schmahmann, J.D. (1998). Dysmetria of thought: clinical consequences of cerebellar dysfunction on cognition and affect. Trends Cogn Sci 2, 362–371.

Schmahmann, J.D. (2000). The role of the cerebellum in affect and psychosis. J Neuroling 13, 189–214.

Schmahmann, J.D. (2010). The role of the cerebellum in cognition and emotion: personal reflections since 1982 on the dysmetria of thought hypothesis, and its historical evolution from theory to therapy. Neuropsych Rev 20, 236–260.

Schmahmann, J.D., and Sherman, J.C. (1998). The cerebellar cognitive affective syndrome. Brain 121 (Pt 4), 561–579.

Schmaltz, L., and Theios, J. (1972). Acquisition and extinction of a classically conditioned response in hippocampectomized rabbits (Oryctolagus cuniculus). J Comp Physiol Psychol 328–333.

Schmeisser, M.J., Ey, E., Wegener, S., Bockmann, J., Stempel, A.V., Kuebler, A., Janssen, A.-L., Udvardi, P.T., Shiban, E., Spilker, C., et al. (2012). Autistic-like behaviours and hyperactivity in mice lacking ProSAP1/Shank2. Nature 486, 256–260.

Schmidt-Supprian, M., and Rajewsky, K. (2007). Vagaries of conditional gene targeting. Nat Immunol 8, 665–8.

Schmitt, L.M., Cook, E.H., Sweeney, J.A., and Mosconi, M.W. (2014). Saccadic eye movement abnormalities in autism spectrum disorder indicate dysfunctions in cerebellum and brainstem. Mol Autism 5, 47.

Schneiderman, N. (1966). Interstimulus interval function of the nictitating membrane response of the rabbit under delay versus trace conditioning. J Compar Phys Psych 62, 397–402.

Schneiderman, N., and Gormezano, I. (1964). Conditioning of the Nictitating Membrane of the Rabbit as a Function of Cs-Us Interval. J Comp Physiol Psychol 188–195.

Schonewille, M., Belmeguenai, A., Koekkoek, S.K., Houtman, S.H., Boele, H.J., van Beugen, B.J., Gao, Z., Badura, A., Ohtsuki, G., Amerika, W.E., et al. (2010). Purkinje Cell-Specific Knockout of the Protein Phosphatase PP2B Impairs Potentiation and Cerebellar Motor Learning. Neuron 67, 618–628.

Schonewille, M., Gao, Z., Boele, H., Veloz, M., Amerika, W., Simek, A., De Jeu, M., Steinberg, J., Takamiya, K., Hoebeek, F., et al. (2011). Reevaluating the role of LTD in cerebellar motor learning. Neuron 43–50.

Schonewille, M., Khosrovani, S., Winkelman, B.H.J., Hoebeek, F.E., Jeu, M.T.G.D., Larsen, I.M., Burg, J.V.D., Schmolesky, M.T., Frens, M.A., and Zeeuw, C.I.D. (2006b). Purkinje cells in awake behaving animals operate at the upstate membrane potential. Nature Neuroscience 9, nn0406-459-459.

Schonewille, M., Luo, C., Ruigrok, T., Voogd, J., Schmolesky, M., Rutteman, M., Hoebeek, F., De Jeu, M., and De Zeeuw, C. (2006a). Zonal organization of the mouse flocculus: physiology, input, and output. J Comp Neurol 670–682.

Schultz, S.R., Kitamura, K., Post-Uiterweer, A., Krupic, J., and Häusser, M. (2009). Spatial pattern coding of sensory information by climbing fiber-evoked calcium signals in networks of neighboring cerebellar Purkinje cells. J Neurosci 8005–8015.

Sears, L.L., Finn, P.R., and Steinmetz, J.E. (1994). Abnormal classical eye-blink conditioning in autism. J Autism Dev Dis 24, 737–751.

Seja, P., Schonewille, M., Spitzmaul, G., Badura, A., Klein, I., Rudhard, Y., Wisden, W., Hübner, C.A., De Zeeuw, C.I., and and Jentsch, T.J. (2012). Raising cytosolic Cl- in cerebellar granule cells affects their excitability and vestibulo-ocular learning. EMBO J 1217–230.

Sengupta, B., Laughlin, S., and Niven, J. (2014). Consequences of converting graded to action potentials upon neural information coding and energy efficiency. PLoS Comput Biol e1003439.

Servais, L., Bearzatto, B., Hourez, R., Dan, B., Schiffmann, S.N., and Cheron, G. (2004). Effect of simple spike firing mode on complex spike firing rate and waveform in cerebellar Purkinje cells in non-anesthetized mice. Neurosci Lett 367, 171–176.

Shambes, G.M., Gibson, J.M., and Welker, W. (1978). Fractured somatotopy in granule cell tactile areas of rat cerebellar hemispheres revealed by micromapping. Brain Behav Evol 94–140.

Shammah-Lagnado, S.J., Ricardo, J.A., Sakamoto, N.T.M.N., and Negraõ, N. (1983). Afferent connections of the mesencephalic reticular formation: A horseradish peroxidase study in the rat. Neuroscience 9, 391–409.

Shepherd, G.M. (2013). Corticostriatal connectivity and its role in disease. Nat Rev Neurosci 278–291.

Sherman, S.M., and Guillery, R.W. Thalamus. In Synaptic Organization of the Brain, (Oxford University Press), pp. 311–359.

Shibuki, K., Gomi, H., Chen, L., Bao, S., Kim, J., Wakatsuki, H., Fujisaki, T., Fujimoto, K., Katoh, A., Ikeda, T., et al. (1996). Deficient cerebellar long-term depression, impaired eyeblink conditioning, and normal motor coordination in GFAP mutant mice. Neuron 587–599.

Shin, S.L., Hoebeek, F.E., Schonewille, M., De Zeeuw, C.I., Aertsen, A., and De Schutter, E. (2007). Regular patterns in cerebellar Purkinje cell simple spike trains. PLOS ONE 2.

Shutoh, F., Ohki, M., Kitazawa, H., Itohara, S., and Nagao, S. (2006). Memory trace of motor learning shifts transsynaptically from cerebellar cortex to nuclei for consolidation. Neuroscience 139, 767–777.

Sillitoe, R., Kunzle, H., and Hawkes, R. (2003). Zebrin II compartmentation of the cerebellum in a basal insectivore, the Madagascan hedgehog tenrec Echinops telfairi. J Anat 283–296.

Silva-Santos, S., van Woerden, G.M., Bruinsma, C.F., Mientjes, E., Jolfaei, M.A., Distel, B., Kushner, S.A., and Elgersma, Y. (2015). Ube3a reinstatement identifies distinct developmental windows in a murine Angelman syndrome model. J Clin Invest 125, 2069–2076.

Smith, M. (1968). CS-US interval and US intensity in classical conditioning of the rabbit's nictitating membrane response. J Comp Physiol Psychol 679–687.

Sokolov, A.A., Miall, R.C., and Ivry, R.B. (2017). The Cerebellum: Adaptive Prediction for Movement and Cognition. Trends Cogn Sci 21, 313–332.

Solomon, P., Blanchard, S., Levine, E., Velazquez, E., and Groccia-Ellison, M. (1991). Attenuation of age-related conditioning deficits in humans by extension of the interstimulus interval. Psychol Aging 36–42.

Sommer, M.A., and Wurtz, R.H. (2008). Brain circuits for the internal monitoring of movements. Ann Rev Neurosci 317–338.

Song, M., and Messing, R. (2005). Protein kinase C regulation of GABAA receptors. Cell Mol Life Sci 119–127.

Sotelo, C., and Llinás, R. (1972). Specialized membrane junctions between neurons in the vertebrate cerebellar cortex. J Cell Biol 271–289.

Sotelo, C., Llinás, R., and Baker, R. (1974). Structural study of inferior olivary nucleus of the cat: morphological correlates of electrotonic coupling. J Neurophys 37, 541–559.

Spence, K. (1953). Learning and performance in eyelid conditioning as a function of intensity of the UCS. J Exp Psychol 45, 57–63.

Sperry, R.W. (1950). Neural basis of the spontaneous optokinetic response produced by visual inversion. J Compar Phys Psych 482–489.

Stahl, J., and Simpson, J. (1995). Dynamics of rabbit vestibular nucleus neurons and the influence of the flocculus. J Neurophysiol 1396–1413.

Staudacher, E.M., Gebhardt, M., and Dürr, V. (2005). Antennal movements and mechanoreception: Neurobiology of active tactile sensors. Adv Insect Physiol 49–205.

Steinberg, J.P., Takamiya, K., Shen, Y., Xia, J., Rubio, M.E., Yu, S., Jin, W., Thomas, G.M., Linden, D.J., and Huganir, R.L. (2006). Targeted in vivo mutations of the AMPA receptor subunit GluR2 and its interacting protein PICK1 eliminate cerebellar long-term depression. Neuron 49, 845–860.

Steinlin, M., Styger, M., and Boltshauser, E. (1999). Cognitive impairments in patients with congenital non-progressive cerebellar ataxia. Neurology 53, 966–966.

Steinmetz, A., Buss, E., and Freeman, J. (2013). Inactivation of the ventral lateral geniculate and nucleus of the optic tract impairs retention of visual eyeblink conditioning. Behav Neurosci 690–693.

Steinmetz, A., Skosnik, P., Edwards, C., Bolbecker, A., Steinmetz, J., and Hetrick, W. (2011). Evaluation of bidirectional interstimulus interval (ISI) shift in auditory delay eye-blink conditioning in healthy humans. Learn Behav 358–370.

Steinmetz, A.B., and Freeman, J.H. (2014). Localization of the cerebellar cortical zone mediating acquisition of eyeblink conditioning in rats. Neurobiol Learn Mem 114, 148–154.

Steinmetz, J., Lavond, D., and Thompson, R. (1989). Classical conditioning in rabbits using pontine nucleus stimulation as a conditioned stimulus and inferior olive stimulation as an unconditioned stimulus. Synapse 225–233.

Steinmetz, J., Logan, C., Rosen, D., Thompson, J., Lavond, D., and Thompson, R. (1987). Initial localization of the acoustic conditioned stimulus projection system to the cerebellum essential for classical eyelid conditioning. Proc Natl Acad Sci U S A 3531–3535.

Steinmetz, J., Rosen, D., Chapman, P., Lavond, D., and Thompson, R. (1986). Classical conditioning of the rabbit eyelid response with a mossy-fiber stimulation CS: I. Pontine nuclei and middle cerebellar peduncle stimulation. Behav Neurosci 878–887.

Steinmetz, J.E., Lavond, D.G., Ivkovich, D., Logan, C.G., and Thompson, R.F. (1992). Disruption of classical eyelid conditioning after cerebellar lesions: damage to a memory trace system or a simple performance deficit? J Neurosci 12, 4403–4426.

Steuber, V. (2016). Modeling the generation of cerebellar nuclear spike output. In The Neuronal Codes of the Cerebellum, (London: Elsevier), p.

Steuber, V., and Jaeger, D. (2013). Modeling the generation of output by the cerebellar nuclei. Neural Networks 112–119.

Steuber, V., Mittmann, W., Hoebeek, F.E., Silver, R.A., De Zeeuw, C.I., Häusser, M., and De Schutter, E. (2007). Cerebellar LTD and Pattern Recognition by Purkinje Cells. Neuron 54, 121–136.

Stins, J.F., Emck, C., de Vries, E.M., Doop, S., and Beek, P.J. (2015). Attentional and sensory contributions to postural sway in children with autism spectrum disorder. Gait & Posture 42, 199–203.

Stoodley, C.J. (2014). Distinct regions of the cerebellum show gray matter decreases in autism, ADHD, and developmental dyslexia. Front Sys Neurosci 8, 92.

Strick, P.L., Dum, R.P., and Fiez, J.A. (2009). Cerebellum and nonmotor function. Ann Rev Neurosci 413–434.

Sugihara, I. (2011). Compartmentalization of the deep cerebellar nuclei based on afferent projections and aldolase C expression. Cerebellum 10, 449–463.

Sugihara, I., and Quy, P.N. (2007). Identification of aldolase C compartments in the mouse cerebellar cortex by olivocerebellar labeling. J Comp Neurol 1076–1092.

Sugihara, I., and Shinoda, Y. (2004). Molecular, topographic, and functional organization of the cerebellar cortex: a study with combined aldolase C and olivocerebellar labeling. J Neurosci 8771–8785.

Sugihara, I., and Shinoda, Y. (2007). Molecular, topographic, and functional organization of the cerebellar nuclei: analysis by three-dimensional mapping of the olivonuclear projection and aldolase C labeling. J Neurosci 27, 9696–9710.

Sugihara, I., Fujita, H., Na, J., Quy, P., Li, B., and Ikeda, D. (2009). Projection of reconstructed single Purkinje cell axons in relation to the cortical and nuclear aldolase C compartments of the rat cerebellum. J Comp Neurol 282–304.

Sugihara, I., Wu, H.S., and Shinoda, Y. (2001). The entire trajectories of single olivocerebellar axons in the cerebellar cortex and their contribution to Cerebellar compartmentalization. J Neurosci 21, 7715–7723.

Svensson, P., and Ivarsson, M. (1999). Short-lasting conditioned stimulus applied to the middle cerebellar peduncle elicits delayed conditioned eye blink responses in the decerebrate ferret. Eur J Neurosci 4333–4340.

Svensson, P., Ivarsson, M., and Hesslow, G. (1997). Effect of varying the intensity and train frequency of forelimb and cerebellar mossy fiber conditioned stimuli on the latency of conditioned eye-blink responses in decerebrate ferrets. Learn Mem 105–115.

Svensson, P., Jirenhed, D.-A., Bengtsson, F., and Hesslow, G. (2010). Effect of Conditioned Stimulus Parameters on Timing of Conditioned Purkinje Cell Responses. J Neurophys 103, 1329–1336.

Swenson, R.S., and Castro, A.J. (1983). The afferent connections of the inferior olivary complex in rats. An anterograde study using autoradiographic and axonal degeneration techniques. Neuroscience 8, 259–275.

Szapiro, G., and Barbour, B. (2007). Multiple climbing fibers signal to molecular layer interneurons exclusively via glutamate spillover. Nat Neurosci 10, 735–742.

Tadayonnejad, R., Anderson, D., Molineux, M.L., Mehaffey, W.H., Jayasuriya, K., and Turner, R.W. (2010). Rebound discharge in deep cerebellar nuclear neurons in vitro. Cerebellum 9, 352–374.

Tadayonnejad, R., Mehaffey, W.H., Anderson, D., and Turner, R.W. (2009). Reliability of triggering postinhibitory rebound bursts in deep cerebellar neurons. Channels 3, 149–155.

Takarae, Y., Minshew, N.J., Luna, B., Krisky, C.M., and Sweeney, J.A. (2004). Pursuit eye movement deficits in autism. Brain 127, 2584–2594.

Tanaka, H., Harada, M., Arai, M., and Hirata, K. (2003). Cognitive Dysfunction in Cortical Cerebellar Atrophy Correlates with Impairment of the Inhibitory System. Neuropsychobiology 47, 206–211.

Tanaka, S., Kawaguchi, S., Shioi, G., and Hirano, T. (2013). Long-term potentiation of inhibitory synaptic transmission onto cerebellar Purkinje neurons contributes to adaptation of vestibulo-ocular reflex. J Neurosci 17209–17220.

Tang, T., Suh, C.Y., Blenkinsop, T.A., and Lang, E.J. (2016). Synchrony is Key: Complex Spike Inhibition of the Deep Cerebellar Nuclei. Cerebellum 15, 10–13.

Tavano, A., Grasso, R., Gagliardi, C., Triulzi, F., Bresolin, N., Fabbro, F., and Borgatti, R. (2007). Disorders of cognitive and affective development in cerebellar malformations. Brain 130, 2646–2660.

Ten Brinke, M., Potters, J., Boele, H., and De Zeeuw, C. (2014). Linking cells to behavior: Purkinje cell electrophysiology during eyeblink conditioning in (transgenic) mice. (Milan), p.

Ten Brinke, M.M., Boele, H.-J., Spanke, J.K., Potters, J.-W., Kornysheva, K., Wulff, P., IJpelaar, A.C.H.G., Koekkoek, S.K.E., and De Zeeuw, C.I. (2015). Evolving Models of Pavlovian Conditioning: Cerebellar Cortical Dynamics in Awake Behaving Mice. Cell Reports 13, 1977–1988.

Teune, T., van der Burg, J., de Zeeuw, C., Voogd, J., and Ruigrok, T. (1998). Single Purkinje cell can innervate multiple classes of projection neurons in the cerebellar nuclei of the rat: a light microscopic and ultrastructural triple-tracer study in the rat. J Comp Neurol 164–178.

Thach, W.T. (1968). Discharge of Purkinje and cerebellar nuclear neurons during rapidly alternating arm movements in the monkey. J Neurophys 31, 785–797.

314

Thach, W.T. (1998). What is the role of the cerebellum in motor learning and cognition? Trends Cogn Sci 2, 331–337.

Thach, W.T. (2007). On the mechanism of cerebellar contributions to cognition. Cerebellum 6, 163–167.

Thompson, R., and Steinmetz, J. (2009). The role of the cerebellum in classical conditioning of discrete behavioral responses. Neuroscience 732–755.

Thompson, R.F. (1988). The neural basis of basic associative learning of discrete behavioral responses. Trends Neurosci 11, 152–155.

Thürling, M., Hautzel, H., Küper, M., Stefanescu, M.R., Maderwald, S., Ladd, M.E., and Timmann, D. (2012). Involvement of the cerebellar cortex and nuclei in verbal and visuospatial working memory: A 7T fMRI study. NeuroImage 62, 1537–1550.

Tiran, E., Ferrier, J., Deffieux, T., Gennisson, J.-L., Pezet, S., Lenkei, Z., and Tanter, M. (2017). Transcranial Functional Ultrasound Imaging in Freely Moving Awake Mice and Anesthetized Young Rats without Contrast Agent. Ultrasound Med Biol 43, 1679–1689.

Titley, H., and Hansel, C. (2015). Asymmetries in Cerebellar Plasticity and Motor Learning. Cerebellum 15, 87–92.

Titley, H.K., Brunel, N., and Hansel, C. (2017). Toward a Neurocentric View of Learning. Neuron 95, 19–32.

Tolbert, D.L., Bantli, H., and Bloedel, J.R. (1978). Organizational features of the cat and monkey cerebellar nucleocortical projection. J Compar Neurol 39–56.

Tracy, J., and Steinmetz, J. (1998). Purkinje cell responses to pontine stimulation CS during rabbit eyeblink conditioning. Physiol Behav 381–386.

Trigo, J., Gruart, A., and Delgado-Garcia, J. (1999). Discharge profiles of abducens, accessory abducens, and orbicularis oculi motoneurons during reflex and conditioned blinks in alert cats. J Neurophysiol 1666–1684.

Trott, J.R., Apps, R., and Armstrong, D.M. (1998). Zonal organization of cortico-nuclear and nucleo-cortical projections of the paramedian lobule of the cat cerebellum. 1. the C1 zone. Exp Brain Res 298–315.

Tsai, P.T., Hull, C., Chu, Y., Greene-Colozzi, E., Sadowski, A.R., Leech, J.M., Steinberg, J., Crawley, J.N., Regehr, W.G., and Sahin, M. (2012). Autistic-like behaviour and cerebellar dysfunction in Purkinje cell Tsc1 mutant mice. Nature 488, 647–651.

Tsutsumi, S., Yamazaki, M., Miyazaki, T., Watanabe, M., Sakimura, K., Kano, M., and Kitamura, K. (2015). Structure-function relationships between aldolase C/zebrin II expression and complex spike synchrony in the cerebellum. J Neurosci 35, 843–852.

Umetani, T. (1990). Topographic organization of the cerebellar nucleocortical projection in the albino rat: an autoradiographic orthograde study. Brain Res 216–224.

Uusisaari, M., and Knöpfel, T. (2008). GABAergic synaptic communication in the GABAergic and non-GABAergic cells in the deep cerebellar nuclei. Neuroscience 156, 537–549.

Uusisaari, M., and Knöpfel, T. (2011). Functional classification of neurons in the mouse lateral cerebellar nuclei. Cerebellum 10, 637–646.

Uusisaari, M., Obata, K., and Knopfel, T. (2007). Morphological and Electrophysiological Properties of GABAergic and Non-GABAergic Cells in the Deep Cerebellar Nuclei. J Neurophys 97, 901–911.

Uusisaari, M.Y., and Knöpfel, T. (2012). Diversity of neuronal elements and circuitry in the cerebellar nuclei. Cerebellum 11, 420–421.

Van Alphen, A.M., and De Zeeuw, C.I. (2002). Cerebellar LTD facilitates but is not essential for long-term adaptation of the vestibulo-ocular reflex. Eur J Neurosci 16, 486–490.

Van Alphen, A.M., Schepers, T., Luo, C., and de Zeeuw, C.I. (2002). Motor Performance and Motor Learning in Lurcher Mice. Ann N Y Acad Sci 978, 413–424.

Van Beugen, B., Gao, Z., Boele, H., Hoebeek, F., and De Zeeuw, C. (2013). High frequency burst firing of granule cells ensures transmission at the parallel fiber to purkinje cell synapse at the cost of temporal coding. Front Neural Circuits 7.

Van Der Giessen, R.S., Koekkoek, S.K., van Dorp, S., De Gruijl, J.R., Cupido, A., Khosrovani, S., Dortland, B., Wellershaus, K., Degen, J., Deuchars, J., et al. (2008). Role of Olivary Electrical Coupling in Cerebellar Motor Learning. Neuron 58, 599–612.

Van der Steen, J., and Tan, H. (1997). Cholinergic control in the floccular cerebellum of the rabbit. Prog Brain Res 335–345.

Van der Want, J.J., Wiklund, L., Guegan, M., Ruigrok, T., and Voogd, J. (1989). Anterograde tracing of the rat olivocerebellar system with Phaseolus vulgaris leucoagglutinin (PHA-L). Demonstration of climbing fiber collateral innervation of the cerebellar nuclei. J Compar Neurol 288, 1–18.

Van Ham, J., and Yeo, C. (1996a). The central distribution of primary afferents from the external eyelids, conjunctiva, and cornea in the rabbit, studied using WGA-HRP and B-HRP as transganglionic tracers. Exp Neurol 217–225.

Van Ham, J., and Yeo, C. (1996b). Trigeminal inputs to eyeblink motoneurons in the rabbit. Exp Neurol 244–257.

van Woerden, G.M., Hoebeek, F.E., Gao, Z., Nagaraja, R.Y., Hoogenraad, C.C., Kushner, S.A., Hansel, C., De Zeeuw, C.I., and Elgersma, Y. (2009). betaCaMKII controls the direction of plasticity at parallel fiber-Purkinje cell synapses. Nat Neurosci 12, 823–825.

Vinueza Veloz, M.F., Zhou, K., Bosman, L.W.J., Potters, J.-W., Negrello, M., Seepers, R.M., Strydis, C., Koekkoek, S.K.E., and De Zeeuw, C.I. (2015). Cerebellar control of gait and interlimb coordination. Brain Struct Funct 220, 3513–3536.

Vogel, E., Brandon, S., and Wagner, A. (2003). Stimulus representation in SOP: II. An application to inhibition of delay. Behav Processes 27–48.

Vogel, R.W., Amundson, J.C., Lindquist, D.H., and Steinmetz, J.E. (2009). Eyeblink conditioning during an interstimulus interval switch in rabbits (Oryctolagus cuniculus) using picrotoxin to disrupt cerebellar cortical input to the interpositus nucleus. Behav Neurosci 123, 62–74.

Voges, K., Wu, B., Post, L., Schonewille, M., and De Zeeuw, C.I. (2017). Mechanisms underlying vestibulocerebellar motor learning in mice depend on movement direction. J Physiol 5301–5326.

Vogt, N. (2016). Biophysics: Unraveling magnetogenetics. Nat Methods 13, 900–901.

Voigts, J., Herman, D.H., and Celikel, T. (2015). Tactile object localization by anticipatory whisker motion. J Neurophysiol 620–632.

Voogd, J. (1964). The cerebellum of the cat. Structure and fiber connections.

Voogd, J. (2003). The human cerebellum. J Chem Neuroanatomy 243–252.

Voogd, J., and Glickstein, M. (1998). The anatomy of the cerebellum. Trends Cogn Sci 2, 307–313.

Voogd, J., and Ruigrok, T. (2004). The organization of the corticonuclear and olivocerebellar climbing fiber projections to the rat cerebellar vermis: the congruence of projection zones and the zebrin pattern. J Neurocytol 5–21.

Voogd, J., and Ruigrok, T.J. (1997). Transverse and longitudinal patterns in the mammalian cerebellum. Prog Brain Res 21–37.

Voogd, J., Jaarsma, D., and Marani, E. (1996). The cerebellum: Chemoarchitecture and anatomy. In Handbook of Chemical Neuroanatomy, pp. 1–369.

Voogd, J., Schraa-Tam, C., van der Geest, J., and De Zeeuw, C. (2012). Visuomotor cerebellum in human and nonhuman primates. Cerebellum 392–410.

Voogd, J., Shinoda, Y., Ruigrok, T.J.H., and Sugihara, I. (2013). Cerebellar Nuclei and the Inferior Olivary Nuclei: Organization and Connections. In Handbook of the Cerebellum and Cerebellar Disorders, M. Manto, J.D. Schmahmann, F. Rossi, D.L. Gruol, and N. Koibuchi, eds. (Dordrecht: Springer Netherlands), pp. 377–436.

Wadiche, J., and Jahr, C. (2005). Patterned expression of Purkinje cell glutamate transporters controls synaptic plasticity. Nat Neurosci 1329–1334.

Wagner, M.J., Kim, T.H., Savall, J., Schnitzer, M.J., and Luo, L. (2017). Cerebellar granule cells encode the expectation of reward. Nature 544, 96–100.

Walter, J.T., and Khodakhah, K. (2006). The linear computational algorithm of cerebellar Purkinje cells. J Neurosci 26, 12861–12872.

Walter, J.T., and Khodakhah, K. (2009). The advantages of linear information processing for cerebellar computation. Proc Natl Acad Sci U S A 106, 4471–4476.

Wang, S.S.-H., Kloth, A.D., and Badura, A. (2014). The cerebellum, sensitive periods, and autism. Neuron 83, 518–532.

Wang, X., Chen, G., Gao, W., and Ebner, T. (2011). Parasagittally aligned, mGluR1-dependent patches are evoked at long latencies by parallel fiber stimulation in the mouse cerebellar cortex in vivo. J Neurophysiol 1732–1746.

Warnaar, P., Couto, J., Negrello, M., Junker, M., Smilgin, A., Ignashchenkova, A., Giugliano, M., Thier, P., and De Schutter, E. (2015). Duration of Purkinje cell complex spikes increases with their firing frequency. Front Cell Neurosci 9.

Weinberger, N.M. (2011). The medial geniculate, not the amygdala, as the root of auditory fear conditioning. Hearing Res 274, 61–74.

Weiss, C., and Disterhoft, J.F. (2011). Exploring prefrontal cortical memory mechanisms with eyeblink conditioning. Behav Neurosci 125, 318–326.

Wells, G., Hardiman, M., and Yeo, C. (1989). Visual projections to the pontine nuclei in the rabbit: orthograde and retrograde tracing studies with WGA-HRP. J Comp Neurol 629–652.

Welsh, J. (1992). Changes in the motor pattern of learned and unlearned responses following cerebellar lesions: a kinematic analysis of the nictitating membrane reflex. Neuroscience 1–19.

Welsh, J., and Harvey, J. (1989). Cerebellar lesions and the nictitating membrane reflex: performance deficits of the conditioned and unconditioned response. J Neurosci 299–311.

Welsh, J., and Harvey, J. (1991). Pavlovian conditioning in the rabbit during inactivation of the interpositus nucleus. J Physiol 459–480.

Welsh, J., and Harvey, J. (1998). Acute inactivation of the inferior olive blocks associative learning. Eur J Neurosci 3321–3332.

Welsh, J., Yamaguchi, H., Zeng, X., Kojo, M., Nakada, Y., Takagi, A., Sugimori, M., and Llinás, R. (2005). Normal motor learning during pharmacological prevention of Purkinje cell long-term depression. Proc Natl Acad Sci U S A 17166–17171.

Welsh, J.P. (2002). Functional Significance of Climbing-Fiber Synchrony. Ann N Y Acad Sci 978, 188–204.

Welsh, J.P., Lang, E.J., Suglhara, I., and Llinás, R. (1995). Dynamic organization of motor control within the olivocerebellar system. Nature 374, 453–457.

Wen, Q., Stepanyants, A., Elston, G., Grosberg, A., and Chklovskii, D. (2009). Maximization of the connectivity repertoire as a statistical principle governing the shapes of dendritic arbors. Proc Natl Acad Sci U S A 12536–12541.

Wetmore, D.Z., Jirenhed, D.-A., Rasmussen, A., Johansson, F., Schnitzer, M.J., and Hesslow, G. (2014). Bidirectional Plasticity of Purkinje Cells Matches Temporal Features of Learning. J Neurosci 34, 1731–1737.

Wetmore, D.Z., Mukamel, E.A., and Schnitzer, M.J. (2008). Lock-and-Key Mechanisms of Cerebellar Memory Recall Based on Rebound Currents. J Neurophys 100, 2328–2347.

White, I.M., Miller, D.P., White, W., Dike, G.L., Rebec, G.V., and Steinmetz, J.E. (1994). Neuronal activity in rabbit neostriatum during classical eyelid conditioning. Exp Brain Res 99, 179–190.

Wise, A.K., Cerminara, N.L., Marple-Horvat, D.E., and Apps, R. (2010). Mechanisms of synchronous activity in cerebellar Purkinje cells. J Physiol 588, 2373–2390.

Witter, L., Canto, C.B., Hoogland, T.M., de Gruijl, J.R., and De Zeeuw, C.I. (2013). Strength and timing of motor responses mediated by rebound firing in the cerebellar nuclei after Purkinje cell activation. Front Neural Circuits 7.

Wolpert, D.M., Miall, R.C., and Kawato, M. (1998). Internal models in the cerebellum. Trends Cogn Sci 2, 338–347.

Won, H., Lee, H.-R., Gee, H.Y., Mah, W., Kim, J.-I., Lee, J., Ha, S., Chung, C., Jung, E.S., Cho, Y.S., et al. (2012). Autistic-like social behaviour in Shank2-mutant mice improved by restoring NMDA receptor function. Nature 486, 261–265.

Woodruff-Pak, D., and Finkbiner, R. (1995). Larger nondeclarative than declarative deficits in learning and memory in human aging. Psychol Aging 416–426.

Wu, G., Yao, J., Hu, B., Zhang, H., Li, Y., Li, X., Li, Q., and Sui, J. (2013). Reevaluating the role of the hippocampus in delay eyeblink conditioning. PLOS ONE 8.

Wu, G., Yao, J., Zhang, L., Li, X., Fan, Z., Yang, Y., and Sui, J. (2012). Reevaluating the role of the medial prefrontal cortex in delay eyeblink conditioning. Neurobiol Learn Mem 277–288.

Wulff, P., Schonewille, M., Renzi, M., Viltono, L., Sassoè-Pognetto, M., Badura, A., Gao, Z., Hoebeek, F.E., van Dorp, S., Wisden, W., et al. (2009). Synaptic inhibition of Purkinje cells mediates consolidation of vestibulo-cerebellar motor learning. Nat Neurosci 12, 1042–1049.

Wylie, D.R., De Zeeuw, C.I., and Simpson, J.I. (1995). Temporal relations of the complex spike activity of Purkinje cell pairs in the vestibulocerebellum of rabbits. J Neurosci 15, 2875–2887.

Xia, J., Chung, H.J., Wihler, C., Huganir, R.L., and Linden, D.J. (2000). Cerebellar long-term depression requires PKC-regulated interactions between GluR2/3 and PDZ domain-containing proteins. Neuron 28, 499–510.

Xiao, J., Cerminara, N.L., Kotsurovskyy, Y., Aoki, H., Burroughs, A., Wise, A.K., Luo, Y., Marshall, S.P., Sugihara, I., Apps, R., et al. (2014). Systematic Regional Variations in Purkinje Cell Spiking Patterns. PLOS ONE 9, e105633.

Yamaguchi, K., Itohara, S., and Ito, M. (2016). Reassessment of long-term depression in cerebellar Purkinje cells in mice carrying mutated GluA2 C terminus. Proc Natl Acad Sci U S A 113, 10192–10197.

Yamakawa, Y., and Hirano, T. (1999). Contribution of mGluR1 to the basal activity of a mouse cerebellar Purkinje neuron. Neurosci Lett 103–106.

Yamamoto, T., Fukuda, M., and Llinás, R. (2001). Bilaterally synchronous complex spike Purkinje cell activity in the mammalian cerebellum. Eur J Neurosci 13, 327–339.

Yamazaki, T., and Tanaka, S. (2007). A spiking network model for passage-of-time representation in the cerebellum: Cerebellar passage-of-time representation. Eur J Neurosci 26, 2279–2292.

Yamazaki, T., and Tanaka, S. (2009). Computational models of timing mechanisms in the cerebellar granular layer. Cerebellum 423–432.

Yang, Y., and Lisberger, S.G. (2013). Interaction of plasticity and circuit organization during the acquisition of cerebellum-dependent motor learning. eLife 2.

Yang, Y., and Lisberger, S.G. (2014a). Role of Plasticity at Different Sites across the Time Course of Cerebellar Motor Learning. J Neurosci 34, 7077–7090.

Yang, Y., and Lisberger, S.G. (2014b). Purkinje-cell plasticity and cerebellar motor learning are graded by complex-spike duration. Nature 510, 529–532.

Yarom, Y., and Cohen, D. (2002). The Olivocerebellar System as a Generator of Temporal Patterns. Ann N Y Acad Sci 978, 122–134.

Yeo, C. (2004). Memory and the cerebellum. Curr Neurol Neurosci Rep 87–89.

Yeo, C., and Hardiman, M. (1992). Cerebellar cortex and eyeblink conditioning: a reexamination. Exp Brain Res 623–638.

Yeo, C., Hardiman, M., and Glickstein, M. (1986). Classical conditioning of the nictitating membrane response of the rabbit. IV. Lesions of the inferior olive. Exp Brain Res 81–92.

Yeo, C., Lobo, D., and Baum, A. (1997). Acquisition of a new-latency conditioned nictitating membrane response–major, but not complete, dependence on the ipsilateral cerebellum. Learn Mem 557–577.

Yeo, C.H., and Hesslow, G. (1998). Cerebellum and conditioned reflexes. Trends Cogn Sci 2, 322–330.

Yeo, C.H., Hardiman, M.J., and Glickstein, M. (1984). Discrete lesions of the cerebellar cortex abolish the classically conditioned nictitating membrane response of the rabbit. Behav Brain Res 13, 261–266.

Yeo, C.H., Hardiman, M.J., and Glickstein, M. (1985a). Classical conditioning of the nictitating membrane response of the rabbit. III. Connections of cerebellar lobule HVI. Exp Brain Res 60, 114–126.

Yeo, C.H., Hardiman, M.J., and Glickstein, M. (1985b). Classical conditioning of the nictitating membrane response of the rabbit. II. Lesions of the cerebellar cortex. Exp Brain Res 60, 99–113.

Yeo, C.H., Hardiman, M.J., and Glickstein, M. (1985c). Classical conditioning of the nictitating membrane response of the rabbit. I. Lesions of the cerebellar nuclei. Exp Brain Res 60, 87–98.

Yu, F., Jiang, Q., Sun, X., and Zhang, R. (2015). A new case of complete primary cerebellar agenesis: clinical and imaging findings in a living patient. Brain 138, e353–e353.

Zackowski, K.M., Thach, W.T., and Bastian, A.J. (2002). Cerebellar subjects show impaired coupling of reach and grasp movements. Exp Brain Res 146, 511–522.

Zbarska, S., Bloedel, J.R., and Bracha, V. (2008). Cerebellar Dysfunction Explains the Extinction-Like Abolition of Conditioned Eyeblinks After NBQX Injections in the Inferior Olive. J Neurosci 28, 10–20.

Zbarska, S., Holland, E., Bloedel, J., and Bracha, V. (2007). Inferior olivary inactivation abolishes conditioned eyeblinks: extinction or cerebellar malfunction? Behav Brain Res 128–138.

Zeilhofer, H.U., Studler, B., Arabadzisz, D., Schweizer, C., Ahmadi, S., Layh, B., Bosl, M.R., and Fritschy, J.M. (2005). Glycinergic neurons expressing enhanced green fluorescent protein in bacterial artificial chromosome transgenic mice. J Compar Neurol 123–141.

Zeng, H., Chattarji, S., Barbarosie, M., Rondi-Reig, L., Philpot, B.D., Miyakawa, T., Bear, M.F., and Tonegawa, S. (2001). Forebrain-specific calcineurin knockout selectively impairs bidirectional synaptic plasticity and working/episodic-like memory. Cell 617–629.

Zhang, W., and Linden, D. (2006). Long-term depression at the mossy fiber-deep cerebellar nucleus synapse. J Neurosci 6935–6944.

Zheng, N., and Raman, I.M. (2009). Ca Currents Activated by Spontaneous Firing and Synaptic Disinhibition in Neurons of the Cerebellar Nuclei. J Neurosci 29, 9826–9838.

Zheng, N., and Raman, I.M. (2010). Synaptic Inhibition, Excitation, and Plasticity in Neurons of the Cerebellar Nuclei. Cerebellum 9, 56–66.

Zheng, N., and Raman, I.M. (2011). Prolonged Postinhibitory Rebound Firing in the Cerebellar Nuclei Mediated by Group I Metabotropic Glutamate Receptor Potentiation of L-Type Calcium Currents. J Neurosci 31, 10283–10292.

Zhou, H., Lin, Z., Voges, K., Ju, C., Gao, Z., Bosman, L.W., Ruigrok, T.J., Hoebeek, F.E., De Zeeuw, C.I., and Schonewille, M. (2014). Cerebellar modules operate at different frequencies. eLife 3, e02536.

Zoghbi, H.Y., and Bear, M.F. (2012). Synaptic dysfunction in neurodevelopmental disorders associated with autism and intellectual disabilities. Cold Spring Harb Perspect Biol 4, a009886.

Zwaigenbaum, L., Bryson, S., and Garon, N. (2013). Early identification of autism spectrum disorders. Behav Brain Res 133–146.

Appendices

Summary EN

This thesis constitutes another stride in the long march toward a better understanding of how the brain employs the olivocerebellar system and its plasticity mechanisms to accommodate procedural and associative learning as well as the skillful and adaptable execution of complex movements and mental processes.

At the level of the cerebellar cortex (**Part I**), Purkinje cell simple spike suppression and facilitation in respective zebrin-negative and -positive zones are extensively correlated to learned behavior on a trial-by-trial basis. Moreover, the role of molecular layer interneurons and parallel fiber to Purkinje cell long term depression in associative learning is investigated through electrophysiology and transgenics. Lastly, Purkinje cell dysfunction resulting from ablation of the autism-related *Shank2*-gene, as well as motor and social behavioral phenotypes, are established. A subsequent focus on the cerebellar nuclei (**Part II**) elucidates the electrophysiological characteristics of interpositus neurons during eyeblink conditioning and the amplifying role of a nucleocortical projection in cortical spike modulation. Finally, the olivocerebellar system as a whole is considered (**Part III**), clarifying the role of olivary gap-junctions in the orchestration of complex spike synchrony in the cerebellar cortex; evaluating possible functions and origins of acquired stimulus-related climbing fiber activity, and their potential capacity to elicit rebound-like excitation in the interposed nuclei; and reviewing motor learning in the cerebellum, with a particular focus on potentiation and suppression of simple spikes as potentially dominant learning mechanisms in zebrin-positive and -negative zones, respectively.

Electrophysiological experiments in awake mice enabled in-depth trial-by-trial analyses of conditioned spike modulation in lobule HVI Purkinje cells, molecular layer interneurons, and interpositus nuclei neurons in the context of eyeblink conditioning (**Chapters 2 & 6**). In part through increased inhibitory input from molecular layer interneurons, Purkinje cells show a clear timed suppression in their simple spike activity, which in turn disinhibits the interposed nuclei, whose neurons show an expected timed increase in their spiking activity. The significant correlations between these types of spike modulation and subsequent eyelid movement, as well as optogenetic abolition of spike facilitation in the interposed nuclei (**Chapter 6**), provide evidence of their contribution to conditioned eyelid behavior. The relevance of molecular layer interneurons is further established through partial learning deficits in two independent mouse mutants, *L7-KCC2* and *L7-Δγ2*, with impaired interneuronal inhibition to Purkinje cells, and severe deficits in a combined mouse mutant in which also parallel fiber to Purkinje cell LTD is impaired (*GluR2Δ 7-L7-Δγ2*, **Chapter 3**).

The electrophysiology experiments in **Chapters 2 & 6**) also establish the concept of CS-related climbing fiber signals that are acquired over the course of conditioning, and may play a role in the creation of rebound-like excitation at the level of the cerebellar nuclei (**Chapter 9**).

Complementing the above-mentioned work in predominantly zebrin-negative cerebellar zones, a novel sensory stimulation paradigm was used to assess spike modulation in whisking-related Purkinje cells in zebrin-positive zones in Crus I and Crus II (**Chapter 4**). Repeated theta-band air puff stimulation of mouse whiskers leads to adaptive whisking behavior over time. This behavioral adaptation was related to

potentiation of simple spike activity in whisking-related Purkinje cells that predicted whisker protraction on a trial-by-trial basis. Together with the work on eyeblink conditioning, these results and previous work in the field lend credence to the idea that cerebellar zones show a preferred directionality of simple spike modulation, depending on whether they are zebrin-negative (suppression) or zebrin-positive (facilitation; **Chapter 10**).

A pioneering exploration of the functional role of the cerebellar nucleocortical projection establishes internal amplification of conditioned spike modulation in the context of eyeblink conditioning (**Chapter 7**). After conditioning, the density of nucle-ocortical fibers was increased in conditioning-related simplex lobule, and their activity was linked to increased inhibition of Purkinje cell activity. Moreover, conditioned responses were stronger or weaker when nucleocortical fibers were optogenetically activated or inhibited, respectively. The closed-loop internal feedback to the cerebellar cortex provided by this projection constitutes a faster, graded complement to the external feedback provided by the climbing fiber system.

At the level of the inferior olivary nuclei, gap-junctions allow for the dynamic coupling of activity across olivary neurons, under control of cerebellar nucleo-olivary inhibition. Differences in complex spike synchrony in simultaneously recorded Purkinje cells were investigated in *Gjd2*-mice, which lack functional gap-junctions (**Chapter 8**). Importantly, whereas previous work on complex spike synchrony focused on very close co-occurrence (<5 ms), we expanded the time window. In wildtypes, there were fixed temporal relationships between Purkinje cells'complex spike activity, showing intervals of up to 20 ms. Importantly, complex spike synchrony in the mutants lacking functional gap-junctions was significantly less consistent, emphasizing their importance in the production of stable spatiotemporal patterns in olivary spiking.

Extending beyond the motor domain, the olivocerebellar system has been implicated in autism. Through *in vivo* and *in vitro* electrophysiology on mice lacking the autism-related *Shank2* gene, we establish impairments in Purkinje cell intrinsic plasticity, LTP induction at the parallel fiber to Purkinje cell synapse, and simple spike regularity in predominantly zebrin-positive Purkinje cells in posterior cerebellum (**Chapter 5**). Purkinje cell-specific *Shank2*-mutants showed deficits in motor learning and even impaired social behavior, underlining the importance of cerebellar pathology in the production of autism-related symptomatology.

Samenvatting NL

Dit proefschrift vormt een volgende stap in de lange weg naar een beter begrip van hoe ons brein het olivocerebellaire systeem en diens plasticiteitsmechanismen toepast om procedureel en associatief leren en de vaardige en flexibele uitvoering van complexe bewegingen en mentale processen mogelijk te maken.

Op het niveau van de cerebellaire schors (**Deel I**) zijn er uitgebreide trial-brede correlaties vastgesteld tussen simple spike suppressie en facilitatie in Purkinje cellen in respectievelijk zebrin-negatieve en -positieve zones. Bovendien is de rol van interneuronen in de moleculaire laag (MLIs) en van long term depression (LTD) van de parallelvezel –Purkinje cell synaps in associatief leren onderzocht door middel van elektrofysiologie en transgene muislijnen. Tenslotte is Purkinje cell dysfunctie door het uitschakelen van het autisme-gerelateerde *Shank2*-gen vastgesteld, alsmede motorische en sociale gedragsafwijkingen. Daaropvolgend is de focus gelegd op de cerebellaire kernen (**Deel II**), waarbij de elektrofysiologische karakteristieken van interpositus neuronen tijdens oogblink-conditioneren zijn vastgesteld, alsook dat een nucleocorticale projectie een versterkende werking kan hebben op spike modulatie in de cerebellaire schors. Tenslotte wordt het olivocerebellaire systeem in zijn geheel overwogen (**Deel III**), waarbij de rol van olivaire gap-junctions in de orchestratie van complex spike synchroniciteit in de cerebellaire schors wordt verhelderd. Daarnaast worden mogelijke functies en origines van aangeleerde stimulus-gerelateerde klimvezel responsen geëvalueerd. Tevens wordt motorisch leren in het cerebellum beschouwd, met nadruk op potentiatie en suppressie van simple spike activiteit als potentiële leermechanismen van voorkeur in respectievelijk zerbin-positieve en -negatieve zones.

Elektrofysiologische experimenten in wakkere muizen maakten uitgebreide trial-by-trial analyses mogelijk. Deze werden toegepast op geconditioneerde spike modulatie in Purkinje cellen uit lobule HVI, interneuronen uit de moleculaire laag (MLIs), en nucleus interpositus neuronen, in de context van ooglid-conditioneren (**Hoofdstuk 2 & 6**). Deels door toename van de inhibitoire input van interneuronen, laten Purkinje cellen een duidelijke, getimede afname in hun simple spike activiteit zien, die op haar beurt de nucleus interpositus ontremt, waardoor de neuronen daar een voorspelbare toename in hun spike activiteit laten zien. De significante correlaties tussen deze typen spike modulatie en de daaropvolgende ooglid-beweging, alsook de optogenetische blokkade van spike facilitatie in de nucleus interpositus (**Hoofdstuk 6**), bieden bewijs voor hun contributie aan geconditioneerd ooglid-gedrag. De relevantie van MLIs is verder vastgesteld door gedeeltelijke leerafwijkingen in twee onafhankelijke muismutanten, *L7-KCC2* en *L7-Δγ2*, bij wie interneuronale inhibitie naar Purkinje cellen ontbreekt, en ernstige leerafwijkingen in een gecombineerde muismutant bij wie daarnaast ook long term depression (LTD) van de parallelvezel –Purkinje cel synaps mankeert (*GluR2Δ7-L7-Δγ2*, **Hoofdstuk 3**).

De elektrofysiologische experimenten in **Hoofdstuk 2 en 6** hebben ook geleid tot de vaststelling van CS-gerelateerde klimvezel-signalen die worden opgedaan over de loop van conditioneren, en een rol zouden kunnen spelen in het creëren van rebound-achtige excitatie op het niveau van de cerebellaire kernen (**Hoofdstuk 9**).

Complementair aan het hierboven genoemde werk in voornamelijk zebrin-negatieve

cerebellaire zones, is er een nieuw sensorische stimulatie-paradigma gebruikt om de modulatie van spikes te detailleren in Purkinje cellen gerelateerd aan snorhaar-beweging in zebrin-positieve zones in Crus I en II (**Hoofdstuk 4**). Herhaaldelijke luchtpuf-stimulatie, in theta-frequentie, van snorharen van muizen leidde tot aangepast snorhaar-gedrag. Deze gedragsmatige adaptatie was gerelateerd aan de potentiatie van simple spike activiteit in snorhaar-gerelateerde Purkinje cellen die de protractie van snorharen over trials konden voorspellen. Samen met het werk over oogblink-conditioneren, ondersteunen deze en eerdere resultaten in het veld het idee dat cerebellaire zones een voorkeur hebben wat betreft de directionaliteit van hun simple spike modulatie, afhankelijk van hun zebrin-negatieve (suppressie) of -positieve (facilitatie) identiteit (**Hoofdstuk 10**).

Een eerste verkenning van de functionele rol van de cerebellaire nucleocorticale verbinding bevestigt interne amplificatie van geconditioneerde spike modulatie in de context van oogblink-conditioneren (**Hoofdstuk 7**). Na het conditioneren was de dichtheid van nucleocorticale vezels groter in de aan conditioneren verwante simplex lobule, en hun activiteit was gerelateerd aan sterkere inhibitie van Purkinje cel activiteit. Bovendien waren geconditioneerde responsen sterker of zwakker wanneer nucleocorticale vezels optogenetisch werden geactiveerd of geremd, respectievelijk. De closed-loop interne feedback naar de cerebellaire schors die deze projectie mogelijk maakt creëert een snellere, graduele tegenhanger van de externe feedback die door het klimvezel-systeem geleverd wordt.

Op het niveau van de inferieure olijfkernen maken gap-junctions de dynamische koppeling van activiteit tussen olijfneuronen mogelijk, onder supervisie van cerebellaire nucleo-olivaire inhibitie. Verschillen in complex spike synchroniciteit in tegeijkertijd gemeten Purkinje cellen waren onderzocht in *Gjd2*-muizen, bij wie deze gap-junctions niet goed functioneren (**Hoofdstuk 8**). Een belangrijk verschil met eerder werk over complex spike-synchroniciteit, waar de nadruk lag op zeer dicht bij elkaar liggende latentietijden (<5 ms), is dat we in het huidige onderzoek een breder tijdsbestek bekeken. Er waren consistente tijdsrelaties tussen de complex spikes van Purkinje cellen in wild-type muizen, met intervallen tot 20 ms. Belangrijk is dat complex spike synchroniciteit significant minder consistent was in mutanten zonder functionele gap-junctions. Dit benadrukt het belang van deze koppelingen voor de productie van stabiele spatiotemporele patronen in spike activiteit in de olijfkernen.

Buiten het motorische domein is het olivocerebellaire systeem geimpliceerd in autisme. Via *in vivo* en *in vitro* elektrofysiologie in muizen bij wie het autisme-gerelateerde gen *Shank2* is uitgeschakeld, stellen we afwijkingen vast in intrinsieke plasticiteit in Purkinje cellen, de inductie van long term potentiation (LTP) in de parallel vezel – Purkinje cel synaps, en simple spike regulariteit in voornamelijk zebrin-positieve Purkinje cellen in het posteriore cerebellum (**Hoofdstuk 5**). Purkinje cel-specifieke *Shank2*-mutanten lieten afwijkingen zien in motorisch leren en zelfs in sociaal gedrag, wat het belang van cerebellaire pathologie in de productie van autisme-gerelateerde symptomatologie onderstreept.

Curriculum Vitae

Personal details

Name:	Michiel Manuel ten Brinke
Birthdate:	April 22, 1989
Birthplace:	Kampen
Nationality:	Dutch

Education & experience

2012–2017	PhD student at Erasmus MC, Dept. of Neuroscience, Rotterdam
2011–2012	Research assistant at Erasmus MC, Dept. of Neuroscience, Rotterdam
2007–2010	BSc Liberal Arts & Sciences, Honours Program (magna cum laude)
	Majors: Psychology; Cognitive Neuroscience
	Minor: Media Studies
	University College, Utrecht
2001–2007	Secondary School, VWO, at Ichthus College, Veenendaal

Teaching experience

2014–2016	Assisting with anatomy courses for medical students
2014–2016	Assisting with workshops for neuroscience master students
2013–2016	Assisting in the supervision of bachelor students of laboratory research, and a neuroscience master student

PhD Portfolio

Research

De Oude, N., **Ten Brinke, M.M.**, De Zeeuw, C.I., Hoebeek, F.E., & Boele, H.J. (in preparation). Non-invasive interruption of generalized spike-and-wave discharge occurrence through cerebellar classical eyeblink conditioning.

Wang, X., **Ten Brinke, M.M.**, De Zeeuw, C.I., & Gao, Z. (in preparation). Robust neuronal responses in cerebellar fastigial nucleus during eyeblink conditioning in mice.

Boele, H.J., **Ten Brinke, M.M.**, Hoeijmakers, J., Vermeij, W., Jaarsma, D., & De Zeeuw, C.I. (In preparation). Acquisition and retention of classically conditioned eyelid behavior in progressive Purkinje cell degeneration ERCC mouse mutants.

Ten Brinke, M.M.*, Kornysheva, K.*, Rasmussen, A., and De Zeeuw, C.I. (In preparation). In search of temporal coding of sensorimotor information in cerebellar cortex and nuclei during eyeblink conditioning in mice.

Spanke, J.K., Owens, C., **Ten Brinke, M. M.**, Voges, K., Negrello, M., Bosman, L.W.J., & De Zeeuw, C.I. (In preparation). Olivary gap junction coupling facilitates formation of complex spike patterns.

Ten Brinke, M.M., Boele, H.J., & De Zeeuw, C.I. (Submitted). Conditioned climbing fiber responses in cerebellar cortex and nuclei.

Ten Brinke, M.M.*, Boele, H.J.*, Peter, S.*, Verdonschot, L., Ypelaar, A.C., Gao, Z., Koekkoek, S.K.E., & De Zeeuw, C.I. (Submitted). More than the sum of its parts: concurrent disruption of parallel fiber to Purkinje cell long-term depression and molecular layer interneuron to Purkinje cell inhibition severely impairs cerebellar learning.

Romano, V., De Propis, L., Bosman, L.W.J., Warnaar, P., **Ten Brinke, M.M.**, Lindeman, S., Ju, C., Velauthapillai, A., Spanke, J.K., Negrello, M., D'Angelo, E., & De Zeeuw, C.I. (Submitted). Adaptation of whisker movements requires cerebellar potentiation.

Ezra, G., **Ten Brinke, M.M.**, Boele, H.J., Tsoory, M., Deussing, J., De Zeeuw, C.I., & Chen, A., (Submitted). CRFR1 depletion in cerebellar granule cells expedites associative motor learning.

Ten Brinke, M.M.*, Heiney, S.*, Wang, X.*, Prioetti-Onori, M., Boele, H.J., Bakermans, J., Medina, J.F., Gao, Z., & De Zeeuw, C.I. (Submitted). Dynamic modulation of activity in cerebellar nuclei neurons during Pavlovian eyeblink conditioning.

Peter, S.*, **Ten Brinke, M.M.***, Stedehouder, J., Reinelt, C.M., Wu, B., Zhou, H., Zhou, K., Boele, H.J., Kushner, S.A., Lee, M.G., Schmeisser, M.J., Boeckers, T.M., Schonewille, M., Hoebeek, F., & De Zeeuw, C.I., (2016). Dysfunctional Cerebellar Purkinje Cells Contribute to Autism-like behaviour in Shank2-deficient mice, *Nature Communications*, 7:12627.

Gao, Z., Proietti-Onori, M., Lin, Z., **Ten Brinke, M.M.**, Boele, H.J., Potters, J.W., Ruigrok, T.J., Hoebeek, F.E. & De Zeeuw, C.I., (2016). Excitatory Cerebellar Nucleocortical Circuit Provides Internal Amplification during Associative Conditioning, *Neuron*, 89(3), 645-57.

Ten Brinke, M.M.*, Boele, H.J.*, Spanke, J.K.*, Potters, J.W., Kornysheva, K., Wulff, P., Ypelaar, A.C., Koekkoek, S.K. & De Zeeuw, C.I., (2015). Evolving Models of Pavlovian Conditioning: Cerebellar Cortical Dynamics in Awake Behaving Mice, *Cell Reports*, 13(9), 1977-88.

Brouwer, A.M. & Neerincx, M.A., Kallen, V., van der Leer, L., & **Ten Brinke, M.M.**, (2011). EEG alpha asymmetry, heart rate variability and cortisol in response to virtual reality induced stress, *Journal of CyberTherapy and Rehabilitation*, 4 (1), 27-40.

Book chapters

Boele, H. J., **Ten Brinke, M. M.**, & de Zeeuw, C. (2015). Classical Conditioning of Timed Motor Responses: Neural Coding in Cerebellar Cortex and Cerebellar Nuclei. In: Heck, D. ed. *The Neuronal Codes of the Cerebellum*, 53-96.

De Zeeuw, C.I. & **Ten Brinke, M.M.**, (2015). Motor Learning and the Cerebellum. In: Kandel, E.R., Dudai, Y., Mayford, M. Eds. *Learning & Memory*, and *Cold Spring Harbor perspectives in biology*, 7(9), a021683.

Posters

Romano, V., De Propris, L., Bosman, L.W.J., Spanke, J.K., Warnaar, P., **Ten Brinke, M.M.**, Lindeman, S., Negrello, M. D'Angelo, E.U., & De Zeeuw, C.I. (2017). Complex Spike Activity Regulates Long-Term Plasticity of Cerebellar Purkinje Cells Induced by Repeated Sensory Stimulation in Awake Mice. *Procedural Learning Summer School*, Amsterdam, NL.

Boele, H.J., Ottenhoff, M.J., **Ten Brinke, M.M.**, Ypelaar, A.C.H., Sinan, D., Dijkhuizen, S., De Oude, N., Koekkoek, S.K.E., De Zeeuw, C.I., & Elgersma, Y. (2016). A cerebellar contribution to NF-1 motor problems? *17th European Neurofibromatosis Meeting*, Padova, Italy.

Gao, Z., Proietti-Onori, M., Lin, Z., **Ten Brinke, M.M.**, Boele, H.J., Potters, J.W., Ruigrok, T.J.H., Hoebeek, F.E., & De Zeeuw, C.I. (2015). Excitatory cerebellar nucleocortical circuit provides internal amplification during associative conditioning. *Gordon Research Conference (GRC)*, Lewiston, USA.

Boele, H.J., **Ten Brinke, M.M.**, Ypelaar, A.C.H., Bacilio, P., Van Dongen, J., Koekkoek, S.K.E., & De Zeeuw, C.I. (2015). Using mouse transgenics to affirm the importance of Purkinje cells and their input from parallel fibers and MLIs in eyeblink conditioning. *Gordon Research Conference (GRC)*, Lewiston, USA.

Broersen, R., Picard, S., Abdelgabar, A.R., **Ten Brinke, M.M.**, Keysers, C., Gazzola, V.,, & De Zeeuw, C.I. (2014). Mirror neuron system and the cerebellum. *Federation of European Neurosciences (FENS)*, Milan, Italy.

Ten Brinke, M.M., Boele, H.J., & De Zeeuw, C.I. (2013). Purkinje cell electrophysiology during eyeblink conditioning in awake mice. *Gordon Research Conference (GRC)*, New London, USA.

Ten Brinke, M.M., Boele, H.J., Koekkoek, S.K.E., & De Zeeuw, C.I. (2012). Combining in-vivo electrophysiology of Purkinje cells with classical conditioning in mice. *Federation of European Neurosciences (FENS)*, Barcelona, Spain.

Acknowledgments

I'm done! The journey down the rabbit hole has reached a conclusion. I'm frankly baffled by how I ''I don't have the patience for this'''d my way to the very end. I am immensely grateful for all the opportunities and support I've been given; even though I should and will allow myself a sliver of pride at this point, I am well aware of how every letter of this thesis is deeply dependent on forces that are external to me. I don't feel any less of a nincompoop now I'm at this point. I do feel a lot more like a masochist. Many times, my brain burned like a piece of hot iron, repeatedly bashed by whatever curveballs the data or reviewers were throwing at me. Growing pains, possibly, hopefully, but certainly also a spiraling tendency to critical evaluation that I've seen spilling a little too far beyond the data at times. I assume the mental habits and reflexes we develop determine what we notice in and around ourselves, which opens particular registers of thoughts, that in turn evoke particular moods that make us respond in particular ways that over time shape our mental habits and reflexes. In this way, I've been thoroughly ground on the academic millstone, and while I cannot imagine saying goodbye to academia, it is time for me to shift gears, regain some perspective, and loosen the reins. What a privileged position to be in! And what a great time to give thanks to the people that have helped me get there.

Mijn promotor, de onuitputtelijke Prof. Dr. Christiaan Innocentius de Zeeuw. Die doopnaam contrasteert fantastisch met de ondeugende blik in je ogen als je een vernuftig plan bedenkt. En die zijn er bij de vleet; wat een remloze impuls om mogelijkheden te zien en er mensen meesterlijk toe te mobiliseren! (Case in point: Mafer staat op stand-by om een kind voor mij te baren.) Je bent een ware conquistador, op een meesterlijk sociale manier. Je wist mij altijd precies het gevoel te geven dat mijn instemming voor jou net zo belangrijk is als dat van jezelf. Je weet meestal precies wat je wilt, en kan vervolgens anderen inpakken door ridderlijk te zijn op alle andere (ook echt zeer belangrijke) fronten. Het is fantastisch om te zien hoe effectief en betrokken je de tent runt. En vice versa, jij kan zichtbaar intens genieten van het floreren van mensen om je heen (kleine bonus als je er iets mee te maken kon hebben). Met die Caridad zit het dus ook wel goed. Chris, ik ben ontzettend dankbaar voor de mogelijkheden die je voor mij hebt kunnen zien, voor je geweldige mentorschap, en voor de vriendschap die ik uit onze vele interacties heb zien groeien. Geef Pi een dikke kus van mij.

Mijn co-promotor, de ultiem voorbeeldige Dr. Henk-Jan Boele. Je hebt gelijk hoor, promoveren doe je voor je moeder. En dat is er wellicht één uit een heel pakket van waarschijnlijk overwegend protestantse invloeden die jou wel dicht bij huis brengen voor mij, in een soort *grote broer*-hokje. En snotverdikkeme, dan ook wel gelijk een wiens master-scriptie aan studenten gegeven wordt als voorbeeld van hoe het moet. Via een weergaloze PhD fiets je met oer-Hollandse blos door naar een prachtige vrouw, een juweeltje van een zoon, en de beginselen van financiëel onafhankelijk wetenschapperen. HJ, ik dank je voor de onbetaalbare begeleiding die je me hebt gegeven, wat betreft hoe onderzoek gedaan moet worden, hoe je compromis-loos een sterke werkethos en groot plezier in je leven kunt balanceren, en hoe je voor mij een

hoge lat hebt gelegd qua ambitie, integriteit, en nuchterheid. Grote broer, ik wens jou en je gezinnetje (Philemon heeft mazzel met zulke ouders) het allerbeste in Princeton en waar dan ook, en ik hoop je niet uit het zicht te verliezen.

Prof. Dr. Javier Medina, from your friendly, down-to-earth, jocular nature it's so easy to forget just how distinguished an academic you are. I am very grateful that you put such a friendly face on my fledgling concept of the cerebellar field on the other side of the pond. I still have so much to learn; that this is true and not at all problematic was at once clear from the thoughtful, reasonable way we discussed the data from interpositus recordings the other day. Thank you very much for everything, and for your willingness to be part of my PhD committee. I wish you and your lovely wife and daughter all the best, and may you shiver with delight as you bathe in the glorious fabric of your appropriately selected robe during my defense.

Dr. Katja Kornysheva, how we have shared some high-octane periods of ploughing through various datasets and discussing analysis approaches! I've always been very impressed by your broad statistical knowledge, sharp focus, and thorough work ethic. I really hope starting up your own group in Bangor and raising little Peter at the same time does not come with joy-diminishing quantities of stress: they should both be wonderful experiences! Thanks for being in my PhD committee, and I wish you and your family all the very best, and I hope we can finish the work we still have left; just don't go drawing things on whiteboards when I'm there (my heart just skipped a beat).

Dr. Anders Rasmussen, I could have sworn I was in a Disney movie when we visited you and your family in Sweden. Such a delight, and so in line with your naturally cheerful demeanor, and that glint of child-like enthusiasm in your eyes. You are a great scientist, I have read your work with much regard, and am glad to have met you personally. Thank you for the dinners, the drinks, the quizzes, the discussions, and your participation in my PhD committee. I wish you all the best with your academic future, and send my warmest regards to your family.

Prof. Dr. Roger Adan, ik vrees dat ik u een stuk meer leeswerk heb bezorgd dan andersom, maar ik heb ''Ja dat is goed. Groet, Roger'' wel een echte page-turner gevonden. Veel dank voor uw deelname aan mijn leescommissie.

Prof. Dr. Gerard Borst, ook jij heel erg bedankt voor je last-minute aanschuiven aan mijn PhD committee. Je statuur en onschuldige blik maakte je voor mij een beetje de BFG van de afdeling, maar ik heb gemerkt hoe je kraakhelder en vlijmscherp om de hoek kan komen. Mezelf afvragen wat jij ervan zou denken heeft me nogal wel eens gepusht om voor meer data of nog betere analyses te gaan. Bedankt en het allerbeste.

Prof. Dr. Rob Willemsen, ondanks dat het aanvankelijk niet leek uit te komen, toch in mijn promotie committee! Hartelijk dank voor uw deelname, helemaal op zo een laat moment voor de datum nog.

Prof. Dr. Steven Kushner, thank you for participating in the reading committee for my thesis. Your position at the interface of clinical psychiatry and neuroscience fascinates me greatly. If your impressive academic track record and the valuable discussions we've had on the Shank2-project are any indication, I should feel a little

dismayed that the only other conversation we've had was when I was trying to think of the English translation of the word *hostie* (you said ''the Body of Christ'', I was looking for *wafer*).

Prof. Dr. Maarten Frens, erg bedankt voor het deelnemen aan de leescommissie voor mijn proefschrift. Ik ben altijd erg benieuwd geweest naar de voortgang van Erasmus University College; ik krijg opmerkelijk vaak positieve geluiden te horen van mensen die daar student blijken te zijn. Het allerbeste daar en wat er dan ook mocht volgen!

Dr. Mario Negrello, you unbelievable powerhouse of a human being, how I have rejoiced in the exhilarating G-force of the Mario, a rollercoaster ride where paradoxically the odds of falling out increase with the extent to which you try to hold on to your seat. Perhaps the inspiring friendship I have gratefully seen develop with you is partly built on this desire to capture reality in models (whether mathematical or, my much lazier preference, with slapdash analogies). Please keep enriching my life with sketchpads full of wonderful breezy exceptional conversations.

Prof. Dr. Bas Koekkoek, het maakt niet uit hoeveel klonen je zou hebben, ze zouden stuk voor stuk iets fantastisch verzinnen om te doen. Je vlijmscherpe geest laat zich nauwelijks verraden door je ontzettend broodnuchtere manier van praten; dit is wel cool, dat is wel gaaf, anders doe je gewoon dit, gebruik gewoon een dat. Je zou bijna denken dat je overlegt waar het bijzettafeltje het beste staat, maar eigenlijk zijn je suggesties superlistig en voorkomen ze veelal allerlei onnodige stappen die er anders waren geweest. Dank voor je lessen en je hulp. Het was een genot om een kijkje in de Koekkoek-keuken gehad te hebben, en ik kijk uit naar wat je allemaal nog meer zal bekokstoven. Het allerbeste voor jou en Veerle en de kinderen!

Ilja, jij pittige tante, het lab is dankzij jou compleet georganiseerd, maar ik heb jou ook een mooie ontwikkeling zien doorgaan. Je werd steeds meer ontspannen in je rol en op ten duur hing je zweep definitief aan de wilgen. Daar kwam een veel kleiner zweepje voor in de plaats, en je raakte steeds meer op je plek als een professionele lab-mamma. Nou ja, tot je er in een keer de brui aan gaf natuurlijk. Maar terecht; ik duim voor een voorspoedig resultaat van je opleiding Diergeneeskunde, en wens jouw en Bert het allerbeste in België!

Patty, thanks voor je hulp en je gezelligheid, en ik wens je een superchille baan toe (en beter fixen we die stoof-off nog)! Anne, heel veel succes met je PhD, volgens mij ga je een top-neurochirurg worden! Stephanie, wat ben je toch lekker vrolijk en enthousiast, en volgens mij is het lab in hele goede handen bij jou; veel succes! Francesca Flo, you reminded me of me when I just began at the eyeblink lab, completely new to so many aspects of the research there: I wish you all the best, enjoy your time here (and don't ever not ask questions out of fear you should know the answer! Exploit your newness to the field :). Lucas, als je knie straks is geheeld het allerbeste op het veld en in de snijzaal! Luis, heel veel succes als je straks misschien ook aan je dierenartsopleiding begint. Nina, ik hoop dat je toch die master scoort straks (en misschien zelfs...?); het allerbeste in ieder geval! Diyana, Laura, Sameha, Paul, heel veel succes met jullie stages en jullie toekomstige carrières!

Jochen, thank you for our collaborations and many discussions; hopefully when I'm done with all this thesis madness, we will finally be able to catch up! Potters, Joost, Siem, Ranjit, Jonella, Jiayi, Sanne, Mariska, Antonia, en alle andere eyeblink lab mensen die alweer verder gegaan zijn: bedankt voor alles!

Beyond the eyeblink lab, although by now at its blurry border, Gao: thank you so much for our collaborations and our many discussions, from which I've learnt a great deal. I very much admire your work and attitude, and your mastery of both hands-on experimentation and PI-like insight in the field. You deserve a bunch of grant money to continue your great research plans, and I'm pretty sure the academic world will agree. All the best for you, your lab, and your family! Xiaolu, I will forgive you for having to ask you 20 times for that opto methods section, because I know you're working your ass off doing experiments all the time. I respect your ambition, finishing two PhDs must be a great challenge! All the best. Martina, I hope you're doing great on the 14th floor, and I wish you all the very best with the remainder of your PhD, and your future afterward!

Freek, dat ging ineens wel hard aan het eind! Thanks voor je waardevolle input en ook de gezelligheid tijdens de FENS trip naar Kopenhagen. Ik wens je het allebeste en heel veel plezier straks als je een nieuw avontuur gaat beginnen in Utrecht. I'll be expecting great things! Bedankt ook voor je emergency deelname aan mijn committee! Saša, bedankt voor de mooie collaborations, ik heb goed vertrouwen dat die triple paper straks mooi terecht komt! Ik heb veel waardering voor je kritische geest en wens je een glansrijke academische carrière toe! Simona, randomly bumping into you has always managed to lighten up my mood, and opening an affordable Italian street-food cart with you sounds like an absolute dream. Consider me on stand-by for that plan. Like really, I'll be here beside my phone. Go on. Call me. Seriously. Do it. Call me. Carmen, I wish you all the best, and keep on drummin'!

Martijn, op de een of andere manier hebben we nooit aan hetzelfde project gewerkt, maar ik heb desondanks nog heel wat van je opgestoken; bedankt daarvoor, en voor de gezelligheid tijdens conferences! Bedankt ook dat je op zo'n late notice nog in mijn PhD committee wilde zitten! Bin, just a bit longer and you're also gonna have to think about putting your thesis together! All the best with your project and your future, whether in academia or in the clinic. Josh, I was pleasantly surprised to hear you were coming to Rotterdam! I hope your projects will work out according to plan, and I'm looking forward to sample some more of Jenna's culinary treats sometime when we have another crack at sjoelen. Laura, bedankt voor je geduld als ik weer eens om de genotypering van muizen kwam bakkeleien!

Laurens, die printout van dat connectiviteits-figuur die je in je kamer hebt hangen geeft me nog altijd hartkloppingen. Ik vind het wel een duidelijke indicatie van je discipline, geduld, en doortastendheid. Bedankt voor de samenwerking en de waardevolle input; ik wens je het allerbeste! Vincenzo, you're an absolute phenomenon, and I feel very lucky to have gotten to know you. It's incredible how hard-working you are, and how much you know about so many things. I wish you all the best, and I'm sure you will only get better and better at expressing your genius in the English language.

332

I can only hope to experience another party or two with you! Sander, vrolijke Frans dat je d'r bent, het was altijd een plezier om je door de gang te horen sniffelen als je weer eens met muizen had gewerkt. Bedankt voor je gezelligheid, heel veel succes met je verdediging straks, en ik wens jou en heel veel plezier en succes in Okinawa; ik heb er alle vertrouwen in dat dat helemaal gaat lukken! Lieke, helaas zitten die peukjes er niet meer in, maar we kunnen altijd nog wel biertjes pakken! Heel veel plezier met het uitbrengen van die papers die je allemaal hebt lopen, en het allerbeste met je academische toekomst! Lorenzo, thanks for everything and keep the Italian flag waving at the department! All the best with your PhD and academic future. François, from your cheerful attitude, I'm pretty sure you feel quite comfortable at the department. However, if you're ever down, remember no one can ever take that prostate conversation away from you. You'll always have the prostate conversation.

Tom, bedankt voor je tijd en expertise op momenten dat ik weer eens zomaar binnen kwam vallen met een uitgebreide vraag, en voor de kans om af en toe op de snijzaal mee te helpen met het geven van hersenanatomie-practica. Het allerbeste! Dick, ik hoop dat je nog lang mensen bij de les houdt met die eigenzinnige bijtende humor van je. Marcel, dank je voor je waardevolle input over de olijf en ik wens je heel veel succes met je onderzoek en je marathons! Christos, you're the Speedy Gonzalez of the Delft faction; I admire your immense capacities, and hope we haven't had the last of our exhilarating conversations. All the best with the grants and the plans! Devika, thank you for the great talks, and the coffees, and your hospitability when we were in Amsterdam! I hope you feel welcome at the department, and wish you all the best for your academic future! Aleksandra, we haven't ever collaborated, but I really enjoyed our discussions and wish you all the best with your academic career! Erika, Elize en andere histo-mensen die mij hebben geholpen, en Mandy, ontzettend bedankt voor alles en het allerbeste! Elise, Loes, bedankt voor het aanhoren van mijn klunzige verzoekjes en vragen, en bedankt voor jullie hulp bij mijn promotie-regelingen.

I'm also grateful to have gotten to know these people, whether still at the department or having moved on: Peter, Negah, Mafer, Elisa, Sadaf, Cullen, Martijn, Mel, Kai, Paolo, Suman, Sheena, Robert, Giorgos, Marcel, Andrius, Taf, Nouk, Oscar, Rachel, Tessa, Robin, Cathryn, Niels, and anyone I may have forgotten (forgive me, my brain is applesauce at this point).

My dear paranymphs, Caramay and Cindy, thank you so much for standing beside me during my defense. Cindy, thank you so much for your friendship, for all the laughs and our deep talks, te quiero mucho, I miss you here, and I can't wait to MC the crap out of your wedding! Caramay, schatzlein, ik hoop dat je het feit dat jij een ontzettende spil in mijn post-UC journey bent weer even tot een soort achievement voor op je prijzentafel kunt smeden. Ik heb je lief en ik hoop dat je je vernuft weet te gebruiken om net zo erg een spil te blijven, ook wanneer we straks niet elkaars woonkamer in kunnen zwaaien.

Ik ga niet eens beginnen met het bedenken van groeperingen of volgordes van vrienden en familie.

Mijn lieve familie, ik houd van jullie en ik hoop jullie weer vaker te zien nu ik klaar ben. Ma, eeuwig dank, jouw inspirerende discipline en doorzettingsvermogen hebben mij hiertoe kunnen brengen, en door je onbaatzuchtige liefde en warmte is er altijd een licht in mijn wereld. Pa, deze is natuurlijk ook voor jou, hè! Het voordeel van nooit echt zeker zijn of je de goedkeuring en trots van je vader te pakken hebt, is dat je toch net even een paar tandjes extra bijzet. Hannah, Julia, Siem, bedankt voor jullie co-auteurschap in mijn proefschrift!

Mijn lieve vrienden, hier in Rotterdam, van UCU, van de middelbare school, via via, of hoe dan ook; ontzettend bedankt voor alle afleiding, entertainment, en ondersteuning tijdens de afgelopen jaren. Ik ben gek op jullie! I know the English speaking among you know these words apply to you too (and can figure their meaning out).

De lieve mensen van de cafés waar ik het meeste van mijn schrijfwerk heb gedaan: het DE café (bedankt voor het introduceren van de flat white in mijn leven), Dudok, Bar Bistro, en bovenal mijn beste Amin van Coffee & Cakes: ontzettend bedankt voor de sloten koffie die jullie mij bezorgden tijdens mijn werk.

Als laatste, mijn allerliefste vriend, moje lásko, Michal. Wat ben je toch een ongeloofelijke Mensch. Ik heb zo ontzettend veel geluk met jou! Miluju tě strašně moc. Dankjewel voor alles. We hebben wel een vakantie verdiend, denk ik zo :)